

Determination of Human Coronary Artery Endothelial Cells Membrane Potentials for the Re-endothelialisation of Vascular Stents

by:

Nastaran Faridamin

Submitted as part of the requirement for the degree of Doctor of
Philosophy

Supervised by:

Dr Alan Reynolds

Professor Tony Anson

College of Engineering, Design and Physical Sciences

Brunel University London

August 2018

*I dedicate this thesis to my beloved parents, Reza and Zohreh Faridamin
for their great support and continuous care through all my study and life
and to my incredible sisters; Najmeh, Nargess, Nasrin and Niloofar*

Statement of Originality

I certify that the content of this thesis is my own work under supervision of: Dr Alan Reynolds and Professor Tony Anson. Any data, images and tables of others, whether published or otherwise, are fully acknowledged in my thesis.

Nastaran Faridamin

Date.....

Signature.....

Abstract

Small vessel stents have become one of the most common treatments for Coronary Artery Disease. A metal tubular mesh that is called a stent, is placed inside the blocked or narrowed artery where there is an accumulation of plaques or other disruptions that reduce luminal patency; this results in a reduction of blood flow to the heart muscle with potentially catastrophic outcomes. Deployment of the stent inside the affected artery dilates the diseased lumen, allowing normal blood flow to resume. As the stent is a foreign object, consisting of synthetic material, it can elicit an immune system reaction, leading to blood clots, vascular spasm and/or proliferation of local cells that may result in the risk of re-occurrence of blockage of the vessel lumen; this is known as restenosis.

The work undertaken in this thesis aims to reduce or eliminate the risk of restenosis by applying an oppositely polarised electrical potential onto the surface of the stent to attract vascular endothelial cells that normally inhabit arteries and veins. It has been extensively documented in the scientific literature that these specialised vascular cells play a leading role in maintaining vascular tone and stasis if continuous uninterrupted squamous endothelial cells layers populate the lumen of blood carrying vessels. Therefore, electrical attraction of vascular endothelial cells on the surface of stents generates a layer that inhibits thrombus formation and consequent in-stent restenosis. In addition, a unique approach is used to measure exactly the membrane potential of relevant human cells without interference from other electrical fields. Other techniques like di-electrophoresis and zeta potential measurements were performed to validate data of a novel direct voltage measurement technique. Cell membrane potentials were then used in a human cardiovascular bio mimicked experiment that was performed with the aim of re-endothelialisation of the stent using an external electrical field. An electrophoresis validation method was performed in a different manner, compared to gel and liquid electrophoresis methods, instead of molecular or protein species, human cell were used to determine the impact of electrical fields and polarisation status on migration and orientation of cells, specifically human coronary artery endothelial cells. To help in understanding how effective this technique would be, osteoblasts were used as a surrogate cell to support and characterise the process. Moreover, electrode passivation has been studied in this work to ensure that changes in resistance and impedance was evaluated as thin-films of oxides or other species play an important roles in electrical measurements when touching cells directly with a metal microelectrode. Experiments have been done to explore the influence of different ionic

solutions on metal electrodes and how surface changes affect their electrical profile, after immersing in different liquids that approximate biological media.

The experimental results collected in this thesis show the movements of adherent cells under the application of external electrical fields during the electrophoresis experiment. Similarly, results of a bio mimic artery experiments, describe the response of cells to externally applied electrical fields on stents, with the potential to reduce the failure rates (restenosis) after stent deployment.

Acknowledgments

First, I would like to thank my supervisors; Dr Alan Reynolds and Professor Tony Anson. Their endless support has guided me through the last four years, which have been very trying at times. They advised me in a correct direction causing my PhD comes to the end with great outcomes. They both have always been supportive and concerned about my studies and my social life until the last day of my thesis submission. Alan has always been a great supervisor because he calms me during some frustrating days. He has paid much attention to my research progress and tried to provide suitable conditions for me during my experiments. Tony has been a fantastic supervisor who listened to my problems at any time. He had always time to answer my questions which I do really appreciate. His financial support to provide equipment for my research has been acknowledged. Thanks to both of these great men who have been such incredible supervisors to me and I truly appreciate all their help from the bottom of my heart.

I would like to thank Mr Nima Taefehshokr for helping me in culturing cells for my experiments. I also like to thank Prof Michael Hughes and Dr Fatima Labeed to let me use their facilities including di-electrophoresis instruments and zeta potential measurement technique at University of Surrey.

Special thanks to Dr Homan Hadavinia for all his assistance during my PhD.

Lastly, but definitely not least, I like to thank my father and mother for their endless support through my whole life. They have always believed in me and encouraged me to go further. I also want to thank my lovely sisters who have always been supportive for me, especially during difficult situations.

Nastaran Faridamin

Table of Contents

Abstract.....	iv
Acknowledgments	vi
Table of Contents	vii
List of Figures.....	xi
List of Tables	xviii
List of Symbols & Abbreviations.....	xix
Chapter 1 Introduction	1
1.1 Introduction.....	1
1.2 Background.....	3
1.2.1 Atherosclerotic Arterial Wall.....	5
1.2.2 Artery	8
1.3 Function of Heart	10
1.4 Significance of Study	11
1.5 Aims and Objectives	14
1.6 Thesis Outline	15
Chapter 2 Literature Review	17
2.1 Introduction.....	17
2.2 Background	17
2.3 Stents.....	18
2.3.1 Types.....	19
2.4 Problems	21
2.4.1 In-stent Restenosis	21
2.4.2 Stent Thrombosis (ST).....	22
2.5 Novel Approach to Stent Development	30
2.6 Cellular Electrical Fields.....	31

2.6.1	Galvanotaxis Phenomenon (Cell Migration)	32
2.6.2	Cells Membrane Potentials	35
2.6.3	Electrical Stimulation of cells	46
2.6.4	Summary	48
Chapter 3 Experimental Method		50
3.1	Introduction.....	50
3.2	Electrodes Experiment	54
3.3	Cell Maintenance	59
3.3.1	Cell Lines	59
3.3.2	Cell Culture.....	59
3.3.3	Cell Trypsinisation.....	59
3.3.4	Cell Counting	60
3.3.5	Cell Subculture.....	61
3.3.6	Cell Freezing.....	61
3.4	Cells' Experiments.....	62
3.4.1	Direct Microelectrode Method.....	62
3.4.2	Measurement of Cell Growth Medium Voltage Behaviour.....	65
3.4.3	Di-electrophoresis Method.....	66
3.4.4	Zeta potential Method	68
3.4.5	Electrophoresis Method	69
3.4.6	Mimicked Artery Experiment	73
3.5	Section Summary	100
Chapter 4 Results		102
4.1	Introduction.....	102
4.2	Electrodes' Experiments	102
4.2.1	Electrochemical Measurements	103
4.2.2	Scanning Electron Microscopy (SEM) Results	107

4.2.3	Atomic Force Microscopic (AFM) Results	111
4.3	Cell Viability.....	120
4.4	Direct Microelectrode Method.....	121
4.4.1	Cell Growth Medium Measurement	121
4.4.2	Human Coronary Artery Endothelial Cells Measurement.....	122
4.4.3	Human Osteoblast Cells Measurement.....	128
4.5	Di-electrophoresis Method.....	133
4.6	Zeta Potential Method.....	135
4.7	Electrophoresis Method	137
4.7.1	High Range of Applied DC.....	137
4.7.2	Low Range of Applied DC	140
4.7.3	Low Range of Applied DC	144
4.8	Mimicked Artery Experiments	147
4.8.1	Bare Stent.....	148
4.8.2	Bare Stent with Cultured Endothelial Cells on its Surface	148
4.8.3	Applied Direct Current on Bare Stent.....	149
4.8.4	Applied Direct Current on Bare Stent with Extra Endothelial Cells	155
4.8.5	Applied Direct Current on Bare Stent with Extra Oxygen with Old Blood	161
4.8.6	Applied Direct Current on Bare Stent with Extra Oxygen	166
4.8.7	Applied Pulsed Direct Current on Bare Stent	169
4.9	Section Summary	171
Chapter 5 Discussion.....		173
5.1	Introduction.....	173
5.2	Electrode Experiments	173
5.3	Direct Microelectrode Method.....	175
5.4	Di-electrophoresis Method.....	180
5.5	Zeta Potential Method.....	181

5.6	Comparison of Different Methods of Cell Membrane Potential Measurements ...	181
5.7	Electrophoresis Method	182
5.8	Mimicked Artery Experiments	184
5.8.1	Comparison of Total Results of Mimicked Artery Experiments	187
5.9	Summary	189
Chapter 6 Conclusion and Future Work		191
6.1	Summary	191
6.2	Research Contribution	192
6.3	Limitations	193
6.4	Future work	193
References		195
Appendix A: Electrochemical Measurement Data		217
Appendix B: AFM Data		220
Appendix C: Direct Microelectrode Method Data		270
Appendix D: Mimicked Artery SEM Images		286
Appendix E: Publication		318

List of Figures

Figure 1.1: Premature CVD death rate by local authority for 2013/15 in the United Kingdom (British Heart Foundation, 2017b; British Heart Foundation, 2018)	2
Figure 1.2: Death rates from 2000 to 2009 (Finegold, Asaria and Francis, 2013)	3
Figure 1.3: Death rates by cardiovascular diseases in United Kingdom in 2014 (British Heart Foundation, 2015)	4
Figure 1.4: Comparison of healthy artery vs atherosclerotic artery (Drug Development, 2018)	6
Figure 1.5: Atherosclerotic progression (The Center for Prevention Heart Attack and Stroke, 2016)	7
Figure 1.6: CABG schematic (Krasopoulos, 2013)	7
Figure 1.7: Coronary stenting procedure (Britannica, 2018)	8
Figure 1.8: Arterial wall schematic (3FX Medical Animation Digital Solutions, 2012)	9
Figure 1.9: Schematic diagram of blood circulating through the heart (Texas Heart Institute, 2017)	11
Figure 1.10: Patch clamp method schematic (Veitinger, 2018)	13
Figure 2.1: Balloon angioplasty process (left) and stent angioplasty procedure (right) (University Surgical vascular, 2017).....	18
Figure 2.2: Stent Strut Cross-section can be seen in Everolimus Stent (Maktari, 2015)	20
Figure 2.3: Differences between two common types of stent, BMS and DES, can be seen (Jeudy, Waite and Chen, 2015)	21
Figure 2.4: Possibility of cardiac death in patients with ETS (51%), LST (19%) and VLST (24%) (Secemsky et al., 2015)	24
Figure 2.5: The 30 days mortality comparison in patients with EST, LST and VLST with mortality rates of 13%, 6% and 3%, respectively (Armstrong et al., 2014).	24
Figure 2.6: Incidence of stent thrombosis due to various predisposed factors: (i) continuous uncovered stent scaffold following implantation; (ii) stent malapposition (showed by arrows); (iii) formation of neoatherosclerotic plaque; (iv) intense stent incomplete expansion (Byrne, Joner and Kastrati, 2015) 27	
Figure 2.7: The risk of ST occurrence after implantation of BMS (blue), first generation of DES (G1 DES: SES, PES) (red) and second generation of DES (G2 DES: EES, ZES) (green) (Tada et al., 2013a; Byrne, Joner and Kastrati, 2015)	29
Figure 2.8: Reaction of a cell process can be seen in the above figure, when it is exposure to DCEFs effect. Cells normally have negative resting membrane potentials (a). In (b), cells with a few or no VGCCs migrate towards the cathode because anodal side is hyperpolarized because of passive influx of Ca^{2+} under effect of DCEF. In (c), depolarized cathodal part of cells with opened VGCCs cause Ca^{2+} influx causing cell movements towards the anode in the opposite direction of passive influx's effect. Then, amount of Ca^{2+} increase in both sides and net movement of cells depends on the balance of two opposing forces (Mycielska and Djamgoz, 2004).....	33
Figure 2.9: A simplified model of cell membrane	36

Figure 2.10: Ions transportation between inside and outside of a cell during different phases (Updegraff, 2017)	38
Figure 2.11: Graph of different phases of cell membrane potentials (PhysiologyWeb, 2014).....	39
Figure 2.12: Cells membrane potentials scale (Yang and Brackenbury, 2013)	40
Figure 2.13: Schematic of four electrified zones of a cell including negative central zone, inner positive zone containing dispersed ions, outer positive zone including condensed ions and negative outermost zone	42
Figure 2.14: Simplified interface of a normal cell and its surrounding (Akagi et al., 2014).....	42
Figure 2.15: Schematic representation of electrical potentials of a cell at the interface with a polar medium	44
Figure 2.16: Presentation of the energy profiles including Total Potential Energy (black), Electrostatic Repulsion Potential (green), Van der Waals Attraction Potential (blue) (DLVO Theory, 2017)	46
Figure 3.1: Overview and relation of experimental work carried out	50
Figure 3.2: Simple Voltaic Cell using Adobe Illustrator	55
Figure 3.3: Electrochemical potentials of various metals in sea water (National Physical Laboratory, 2017) .	56
Figure 3.4: Stainless steel and titanium electrodes (a), the picture of the experiment (b) and schematic diagram of the experiment (c)	57
Figure 3.5: A hemocytometer chamber (a) and counting grid detail on the glass of each chamber (b).....	60
Figure 3.6: The tungsten microelectrode (a), the titanium strip (b) and the picture of the experiment (c).....	63
Figure 3.7: Schematic diagram of the experiment when the petri dish was fully cultured with cells	63
Figure 3.8: Schematic diagram of the experiment when the petri dish was half cultured of cells	64
Figure 3.9: The picture of the experiment	65
Figure 3.10: Schematic diagram of the experiment.....	65
Figure 3.11: Disposable chips for 3DEP reader (a) and 3DEP reader (b)	68
Figure 3.12: Zeta potential cuvette	69
Figure 3.13: Schematic presentation of the electrokinetic potential of a dispensed particle (Bhattacharjee, 2016)	70
Figure 3.14: Schematic of the electrophoresis experiment	71
Figure 3.15: The electrophoresis chamber (a) and technical drawing of the electrophoresis chamber using SolidWorks (b)	71
Figure 3.16: Technical drawing of electrophoresis chamber using SolidWorks. Dimensions are in mm.....	72
Figure 3.17: Schematic of final experimental set-up using Adobe Illustrator CC.....	74
Figure 3.18: Technical drawing of a mimicked stent with a welded wire attached	75
Figure 3.19: Cutting stents in 20 mm length using a surface grinder machine (a) and final stents before welding wires to them (b).....	76
Figure 3.20: Welding machine (a) and the custom device for using welding wires on the stents (b)	76
Figure 3.21: The final designed stents	77

Figure 3.22: The custom handmade stent and its attached wire gripper device (a), measurement of the resistance of the stent and its attached wire (b) and technical concept of the measurement (c)	78
Figure 3.23: Comparison of Resistance measurements of series stents	79
Figure 3.24: Final stents before inserting in silicon tubes (a) and after inserting in silicon tubes (b)	79
Figure 3.25: Experiment picture of electrical connections to mimicked arteries within mimicked stents (a) and technical drawing of the manifold within stents using Autodesk Inventor Professional (b)	80
Figure 3.26: Electrical circuit used for providing small electrical charges for the experiments	81
Figure 3.27: A professional precious power supply and oscillator	82
Figure 3.28: Representation of visual differences between DC and pulsed DC using Autodesk Inventor Professional	82
Figure 3.29: Four 1 litre of sheep blood bottles (a) and traces of blood passing through mimicked stents (b)	85
Figure 3.30: The rotary switch from front and back view	88
Figure 3.31: Corresponding graph to water temperature rise against the time by the heat exchange system	89
Figure 3.32: Final experimental set-up	90
Figure 3.33: Systems which have to work simultaneously at the experiment	91
Figure 3.34: Schematic representation of post-experiment procedures	92
Figure 3.35: Washing each stent in an individual glass container	93
Figure 3.36: A petri dish of molecular sieve (a) and the sealed vacuum system for complete dryness of samples (b)	94
Figure 3.37: Two custom devices to open the stents: the linear wrench & holder (a) and the internal expanding gripper (b, c)	95
Figure 3.38: Comparison of mimicked stents before and after opening using handmade custom devices	96
Figure 3.39: Fully presentation of specimens mounting to use in sputter coating and SEM systems: display of an aluminium pin stub (a), show of a multi-pin stub holder (b), display of placing specimens on a multi-pin stub holder at the same time (c), set of carbon tape on an aluminium pin stub (d) , presentation of mounted specimen on an aluminum pin stub (e) and ready specimens to use in different analysing methods (f)	97
Figure 3.40: The sputter coating system (a) and the chamber of sputter coating system (b)	98
Figure 3.41: Comparison of gold coating of samples; samples before gold coating (a, c) and samples after gold coating (b, d)	99
Figure 4.1: Potential measurements in deionized water	104
Figure 4.2: Potential measurements in distilled water	105
Figure 4.3: Potential measurements in tap water	106
Figure 4.4: Potential measurements in 0.9% saline	107
Figure 4.5: SEM images from the surface of the controlled stainless steel electrode	108
Figure 4.6: SEM images from the surface of the controlled titanium electrode	108
Figure 4.7: SEM pictures taken from stainless steel electrode in deionized water	109
Figure 4.8: SEM pictures taken from titanium electrode in deionized water	109

Figure 4.9: Images from the stainless steel electrode surface after immersing in distilled water	109
Figure 4.10: Images from the titanium electrode surface after immersing in distilled water	110
Figure 4.11: SEM pictures from stainless steel electrode after the experiment with tap water	110
Figure 4.12: SEM pictures from titanium electrode after the experiment with tap water	110
Figure 4.13: SEM images from surface of stainless steel electrode after 0.9% saline experiment	111
Figure 4.14: SEM images from surface of titanium electrode after 0.9% saline experiment	111
Figure 4.15: RMS roughness values of controlled stainless steel surface obtaining by AFM	112
Figure 4.16: RMS roughness values of controlled titanium surface obtaining by AFM	113
Figure 4.17: Determined RMS roughness values from the stainless steel electrode using AFM images	114
Figure 4.18: Determined RMS roughness values from the titanium electrode using AFM images	114
Figure 4.19: Comparison of RMS roughness values of the stainless steel electrode immersing in distilled water	115
Figure 4.20: Comparison of RMS roughness values of the titanium electrode immersing in distilled water	116
Figure 4.21: Horizontal and vertical graphs of RMS roughness value for the stainless steel electrode from AFM	117
Figure 4.22: Horizontal and vertical graphs of RMS roughness value for the titanium electrode from AFM	118
Figure 4.23: Comparison of obtained RMS roughness values from the stainless steel immersing in 0.9% Saline	119
Figure 4.24: Comparison of obtained RMS roughness values from the titanium immersing in 0.9% Saline	119
Figure 4.25: Human cultured cells in both contaminated and non-contaminated conditions with magnification $\times 80$	121
Figure 4.26: Plotted potentials of both endothelial and osteoblast cell growth medium over time	122
Figure 4.27: Human coronary artery endothelial cells in different timing and magnifications for the 1 st experiment	123
Figure 4.28: Human coronary artery endothelial cells' potential measurements at different times of the 1 st experiment	124
Figure 4.29: Human coronary artery endothelial cells' potential measurements at different times of the 2 nd experiment	125
Figure 4.30: Human coronary artery endothelial cells' potential measurements at different times of the 3 rd experiment	125
Figure 4.31: 1 st experiment of potential measurements determined using direct microelectrode method	126
Figure 4.32: 2 nd experiment of potential measurements determined using direct microelectrode method	127
Figure 4.33: 3 rd experiment of potential measurements determined using direct microelectrode method	128
Figure 4.34: Cultured human osteoblast cells for direct microelectrode method for the 1 st experiment	129
Figure 4.35: Potential measurements using direct microelectrode method for the 1 st experiment	129
Figure 4.36: Potential measurements using direct microelectrode method for the 2 nd experiment	130
Figure 4.37: Potential measurements using direct microelectrode method for the 3 rd experiment	130
Figure 4.38: Different potential measurements in various time at the 1 st experiment	131

Figure 4.39: Different potential measurements in various time at the 2 nd experiment	132
Figure 4.40: Different potential measurements in various time at the 3 rd experiment.....	132
Figure 4.41: Captured images from human coronary artery endothelial cells on hemocytometer via the microscope	133
Figure 4.42: DEP spectrum of human coronary artery endothelial cells (n=5), 20 points frequency runs	134
Figure 4.43: Scattered graph of several measurement of zeta potential: human osteoblast cells' zeta potential measurements(a), human coronary artery endothelial cells' zeta potential measurements (b)	136
Figure 4.44: Corresponding graphs to Table 4.7 (human coronary artery endothelial cells (a) and human osteoblast cells (b)) illustrate the mean \pm standard deviation for each independent measurement in DEP and CCM.....	137
Figure 4.45: Comparison of cells movements' changes under high level of applied DC during a quarter of an hour.....	139
Figure 4.46: Time lapse microscopy images from cells under application of 1000 mV.....	140
Figure 4.47: Captured images using the inverted microscope from different applied DC on human cells.....	143
Figure 4.48: Time lapse microscopy images from cells changes applying 30 mV DC	144
Figure 4.49: Microscopic images illustrate the different orientation of cells under application of different applied electrical field	146
Figure 4.50: Time lapse microscopy images	147
Figure 4.51: SEM pictures with different magnification from inner surface area of the stent	148
Figure 4.52: SEM images from the inner surface of the stent that human coronary artery endothelial cells were cultured on	149
Figure 4.53: SEM pictures of the stent which underwent the application of 1V.	150
Figure 4.54: Analysis of the surface of the stent connecting to 1V.	151
Figure 4.55: SEM's images from a non-electrical connected sample which represents massive accumulation of RBCs.	151
Figure 4.56: 1 st stent which connected to 27 mV, displays adherence of endothelial cell on its surface beside presentation of RBCs.	152
Figure 4.57: Presence of biological objects on the surface of the sample	152
Figure 4.58: Presence of plenty of RBCs	153
Figure 4.59: RBCs' distributed on the surface of the stent	153
Figure 4.60: RBCs presence can be easily seen in the SEM images.	154
Figure 4.61: SEM images illustrate full coverage of the surface of the stents by presence of quiet number of RBCs.	154
Figure 4.62: SEM images presents the formation of aggregations of RBCs	155
Figure 4.63: Incidence of endothelial cells and RBCs on the surface.....	156
Figure 4.64: Presence of numbers of RBCs on the surface.....	156
Figure 4.65: SEM pictures showed RBCs attached to objects on the surface	157

Figure 4.66: SEM images showed widespread RBCs	158
Figure 4.67: SEM images showed remaining of RBCs on the surface	158
Figure 4.68: SEM image illustrated the attachment of RBCs on the item	158
Figure 4.69: Widespread existence of RBCs in the form of single layer and aggregations.....	159
Figure 4.70: High coverage of RBCs on the surface.....	159
Figure 4.71: Trapped RBCs among substances on the surface	160
Figure 4.72: SEM images showed the attraction of RBCs in form of single layers and aggregations	160
Figure 4.73: Presence of an endothelial cell	161
Figure 4.74: An endothelial cell pointed with a coloured arrow	162
Figure 4.75: A biological item on the surface	162
Figure 4.76: Focused image form the surface of the stent.....	163
Figure 4.77: Attachments of biological objects on the surface	163
Figure 4.78: Presence of biological items on the surface area	164
Figure 4.79: Accumulation of biological objects	164
Figure 4.80: Existence of biological items.....	165
Figure 4.81: Adherence of biological objects on the surface	165
Figure 4.82: Presence of a biological item	166
Figure 4.83: SEM images illustrates the surface without adherence of any particular objects	167
Figure 4.84: SEM picture shows adherence of a biological item on the surface.....	167
Figure 4.85: Accumulation of RBCs on the surface	168
Figure 4.86: Empty surface of the stent without presence of any items.....	168
Figure 4.87: SEM pictures showed attraction of biological objects on the stent's surface	169
Figure 4.88: Adherence of huge number of RBCs on the surface of the stent.....	169
Figure 4.89: Fully coverage of the surface by existence of RBCs aggregations and layers	170
Figure 4.90: Occurrence of RBCs on the surface of stent	170
Figure 4.91: Presence of RBCs plus attraction of a cell	171
Figure 4.92: Attraction of RBCs on the surface of the stent.....	171
Figure 5.1: Comparison of average potential measurements of electrodes.....	174
Figure 5.2: MEAN±SD (n=3) of each measurement of complete cultured petri dish of human coronary artery endothelial cells (blue, orange and grey spots present 0 hour, 2 hours and 10 hours, respectively) ...	176
Figure 5.3: MEAN±SD (n=3) of each measurement of half cultured petri dish of human coronary artery endothelial cells (blue, orange and grey spots present 0 hour, 2 hours and 10 hours, respectively) ...	176
Figure 5.4: MEAN±SD (n=3) of each measurement of complete cultured petri dish of human osteoblast cells (blue, orange and grey spots present 0 hour, 2 hours and 10 hours, respectively).....	177
Figure 5.5: MEAN±SD (n=3) of each measurement of half cultured petri dish of human osteoblast cells (blue, orange and grey spots present 0 hour, 2 hours and 10 hours, respectively).....	178
Figure 5.6: Comparison of human coronary artery endothelial cells (a) and human osteoblast cells (b) potential measurements in both full and half cell cultured in 0 hour.....	179

Figure 5.7: Comparison of observation of the microelectrode's tip and its shadow during experiments in three different magnifications $\times 80$, $\times 200$ and $\times 500$ 180

List of Tables

Table 1.1: Rate of mortality from CVD in the United Kingdom (British Heart Foundation, 2017b)	1
Table 2.1: Results of DES deployment	22
Table 2.2: Classification of stent thrombosis following the stent deployment (Cutlip et al., 2007; Jaffe and Strauss, 2007; Holmes et al., 2010; Claessen et al., 2014; Byrne, Joner and Kastrati, 2015; Reejhsinghani and Lotfi, 2015; Sommer and Armstrong, 2015).....	23
Table 2.3: ARC stent thrombosis definitions (Cutlip et al., 2007; Jaffe and Strauss, 2007; Holmes et al., 2010; Reejhsinghani and Lotfi, 2015).....	25
Table 2.4: Comparison of incidence of different types of stent thrombosis in patients treated by various types of stents	28
Table 2.5: Comparison of the membrane potentials of normal cells with their sick counterparts	40
Table 2.6: Presentation of the relation between magnitude of zeta potential and the stability of the colloids (Salopek, Krasic and Filipovic, 1992)	45
Table 2.7: Comparison of different types of cells direction, velocity and translocation under applied EF	47
Table 3.1: Presentation of various cells resting membrane potentials by using different methods.....	51
Table 3.2: Explanation of various conditions of electrophoresis experiments	73
Table 3.3: Records of resistance measurement of stents	78
Table 3.4: Explanation of the magnitude of small electrical charges to stents	80
Table 3.5: Stabilisation of the temperature for the experiment	89
Table 3.6: Five different conditions of mimicked artery experiment	91
Table 4.1: Corresponding table to Figure 4.1.....	104
Table 4.2: Corresponding table to Figure 4.2.....	105
Table 4.3: Corresponding table to Figure 4.3.....	106
Table 4.4: Corresponding table to Figure 4.4.....	107
Table 4.5: Human coronary artery endothelial cell parameters determined n=5, 20 point spectra	135
Table 4.6: Independent measurements of zeta potential.....	135
Table 4.7: The mean values of zeta potential of different cell lines \pm standard deviation	136
Table 5.1: Determined human coronary artery endothelial cell membrane potentials	177
Table 5.2: Determined human osteoblast cell membrane potentials	178
Table 5.3: Comparison of determined cell membrane potentials using different methods	182
Table 5.4: Comparison of impact of long term and short term applied DC on cells	183

List of Symbols & Abbreviations

ζ	Zeta
μ	Micro
2D	Two Dimensional
3D	Three Dimensional
A	Ampere
Å	Angstrom
AC	Alternative Current
AFM	Atomic Force Microscopy
ARC	Academic Research Consortium
AST	Acute Stent Thrombosis
BBVs	Blood-borne Viruses
BMS	Bare Metal Stent
bpm	Beats Per Minute
BRS	Bioresorbable Scaffold
BVS	Bioresorbable Vascular Scaffold
C	Coulomb
C	Carbon
Ca	Calcium
CABG	Coronary Artery Bypass Grafting
CAD	Coronary Artery Disease
CAS	Coronary Artery Stent
cc	Cubic Centimetre

CCM	Cell Culture Medium
CHD	Coronary Heart Disease
Cl	Chlorine
cm	Centimetre
CVD	Cardiovascular Disease
d	Distance
DAPT	Dual Antiplatelet Therapy
DC	Direct Current
DCEF	Direct Current Electric Field
DEP	Di-electrophoresis
DEP Method	Di-electrophoresis Method
DES	Drug Eluting Stent
DLVO	Derjaguin, Landau, Vervy and Overbeek
DMSO	Dimethyl Sulfoxide
EC	Endothelial Cell
EDL	Electric Double Layer
EDTA	Ethylenediaminetetraacetic Acid
EES	Everolimus-Eluting Stent
EF	Electric Field
EPC	Endothelial Progenitor Cell
EPCS	Endothelial Progenitor Cell Capturing Stent
ER	Endoplasmic Reticulum
FBS	Fetal Bovine Serum
FDA	U.S. Food & Drug Administration

FM	Freezing Medium
g	Gram
H	Hydrogen
HBV	Hepatitis B Virus
HCAEC	Human Coronary Artery Endothelial Cells
HCV	Hepatitis C Virus
HIV	Human Immunodeficiency Virus
HOb	Human Osteoblast
Hz	Hertz
ICW	Intracellular Ca ²⁺ Wave
ISR	In-stent Restenosis
j	Joule
K	Potassium
K	Kelvin
kg	Kilogram
L	Litre
LDP	Low-density Lipoprotein
LST	Late Stent Thrombosis
M	Mega
MI	Myocardial Infraction
min	Minute
ml	Millilitre
mm	Millimetre
mmHg	Millimetres of mercury

mol	Mole
mV	Millivolts
Na	Sodium
NICE	The National Institute for Clinical Excellence
nm	Nanometre
O	Oxygen
°C	Centigrade
P	Phosphorus
Pa	Pascal
PBS	Phosphate Buffered Saline
PCI	Percutaneous Coronary Intervention
PES	Paclitaxel-Eluting Stent
PM	Plasma Membrane
RMP	Resting Membrane Potential
RMS	Root Mean Square
rpm	Rotations Per Minute
s	Second
SEM	Scanning Electron Microscopy
SES	Sirolimus-Eluting Stent
SMC	Smooth Muscle Cell
SR	Sarcoplasmic Reticulum
ST	Stent Thrombosis
TEP	Transepithelial Potential
VGCC	Voltage-Gated Ca ²⁺ Channel

VLST	Very Late Stent Thrombosis
V_m	Cell Membrane Potential
V_{rest}	Cell Resting Membrane Potential
ZES	Zotarolimus-Eluting Stent
Ω	Ohm

Chapter 1 Introduction

1.1 Introduction

This chapter focuses on an overview of the human heart with reference to coronary artery disease conditions. It also contains arterial wall properties and atherosclerosis plaque formation in the arterial lumen. The therapies associated with coronary artery disease are introduced, including by-pass surgery and stenting. Moreover, the motivation and aims of this thesis and the summary of the chapters are presented in this section.

The human heart is a hardworking, complex and vital organ for the human body. A normal heart pumps and circulates over 5 litres of blood throughout the body per minute and beats between 60-80 times per minute when at rest.

Cardiovascular Disease (CVD) is a general term that describes all diseases of the heart and blood circulatory system. It includes strokes, heart attacks and congenital conditions amongst others (British Heart Foundation, 2017b). Coronary Heart Disease (CHD) relates specifically to the blood vessels associated with the heart and is one of the major causes of death in the UK, responsible for over 66,000 deaths in the UK per year (British Heart Foundation, 2017b). A recent survey by the British Heart Foundation showed that the numbers of people in the UK affected by CVD are as follows (Table 1.1).

Table 1.1: Rate of mortality from CVD in the United Kingdom (British Heart Foundation, 2017b)

Nation	Number of People Dying from CVD	Number of People Under 75 Years Old Dying from CVD	Estimated Number of People Living with CVD
England (2015)	129,147	33,662	5.9 million
Scotland (2016)	15,131	4,644	670,000
Wales (2015)	9,027	2,544	375,000
Northern Ireland (2015)	3,773	1,087	225,000
United Kingdom (2015)	158,155	42,245	7 million +

To put this data in context, 92,300 died due to coronary artery disease in England in the year 2008 (Finegold, Asaria and Francis, 2013). The map of the UK below shows that the demographics of CVD vary markedly throughout the country (Figure 1.1).

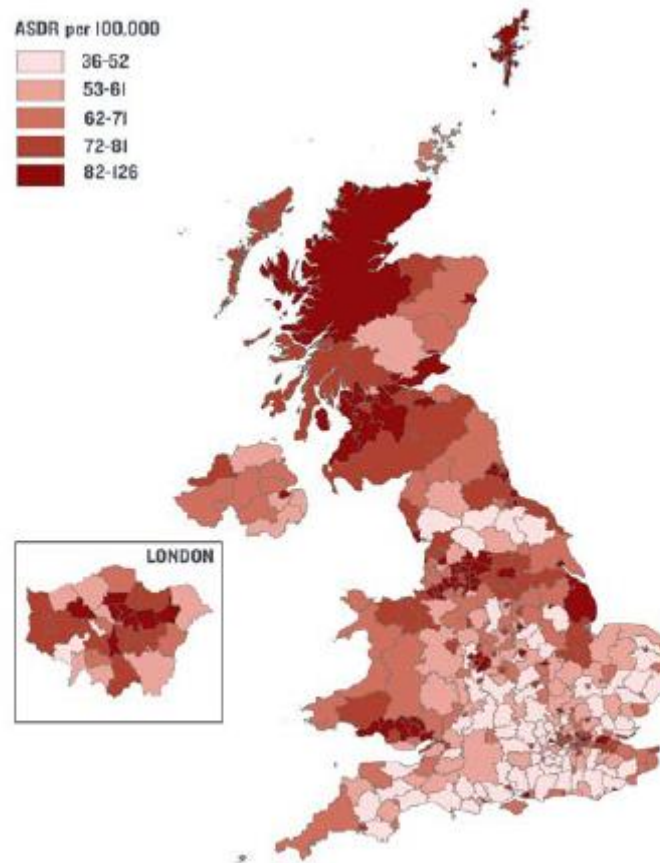


Figure 1.1: Premature CVD death rate by local authority for 2013/15 in the United Kingdom (British Heart Foundation, 2017b; British Heart Foundation, 2018)

Mortality statistics shows that heart disease has the first place among all diseases in both high-income and low-income countries with 17.1% and 10.8% deaths, respectively in year 2002 (World Health Organization, 2007). A fact sheet issued by the World Health Organisation in May 2017 shows the stark fact that, worldwide, CVD is a major cause of death throughout the world and, in particular, in the poorer countries (World Health Organization, 2018). According to World Health Organization (2018), an estimated 7.4 million out of 17.7 million people died because of coronary heart disease in 2015 which indicates 31% of deaths in the world is due to CVDs. The fact sheet reports low- and middle-income countries own over three quarters of CVD deaths.

Due to the high numbers of mortality and associated morbidity from coronary heart disease (Khalifa *et al.*, 2018), a major concern has been raised to reduce the death rate by focusing on the prevention of heart diseases, the enhancement of CAD treatments and the post treatment recovery period. This concern has resulted in a continuing but slight reduction in the number of deaths and inpatients because of coronary heart disease. According to Finegold, Asaria and Francis (2013), death rates have declined gradually in the UK (Figure 1.2). According to British Heart Foundation (2015), there is a decline of approximately 4% in the number of inpatient men from 274,816 to 264,934 from 2005/06 to 2013/14, whereas inpatient women reduced roughly 11% from 153,446 to 136,073, respectively.

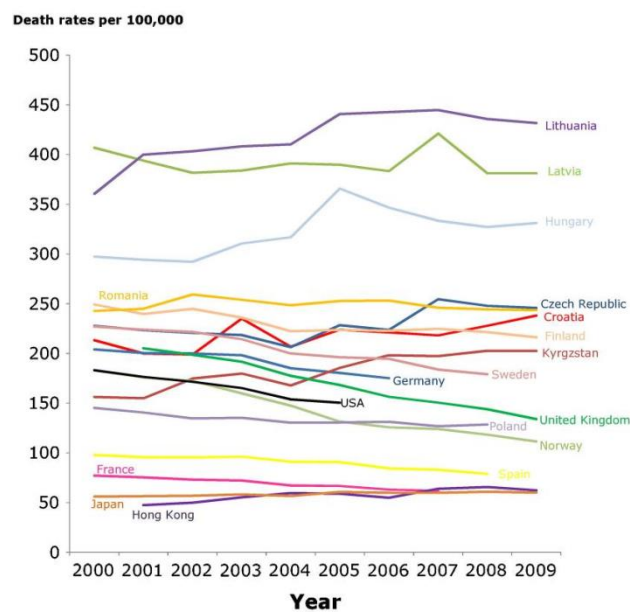


Figure 1.2: Death rates from 2000 to 2009 (Finegold, Asaria and Francis, 2013)

1.2 Background

Cardiovascular Disease (CVD) which includes all diseases of the heart and the blood circulation system, involves every disease from early stage to developed conditions. CVD includes coronary heart disease (45%), stroke (25%), valvular, venous and aortic disease, peripheral artery disease, atrial fibrillation, arrhythmia's and heart failure (17%) (British Heart Foundation, 2015). CVD plays a critical role in the death rate in the UK by causing an average of one death every three minutes that is approximately 26% of all deaths (Figure 1.3) (British Heart Foundation, 2017b). Up to £9 billion is spent for CVD health care each year in the UK (British Heart Foundation, 2017b).

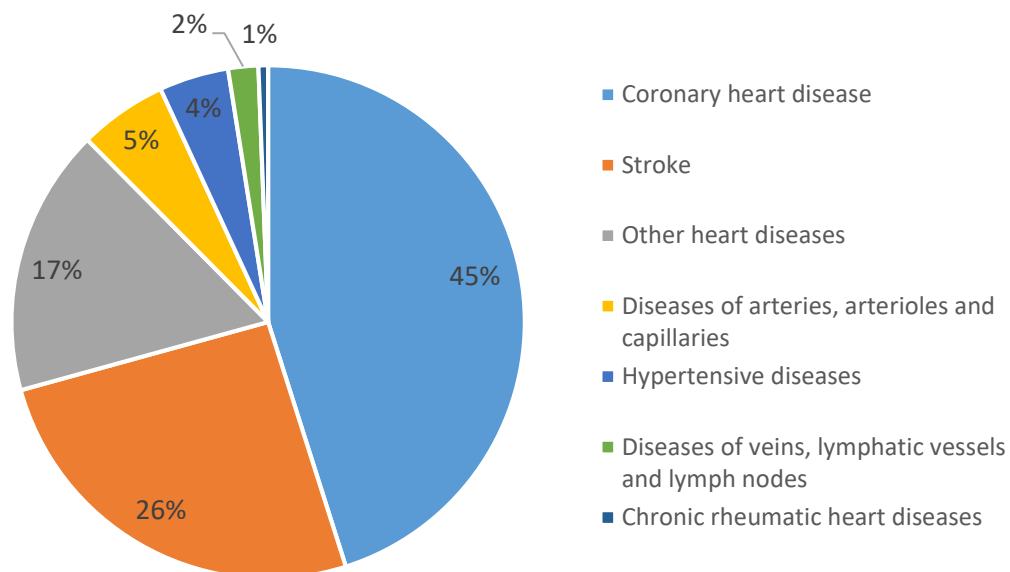


Figure 1.3: Death rates by cardiovascular diseases in United Kingdom in 2014 (British Heart Foundation, 2015)

There are number of factors that lead to cardiovascular disease with three important, independent and modifiable risk factors: hypertension, smoking and hyperlipidemia. Also, other factors such as age and gender, family history and genetics, lack of physical activity, overweight and obesity, diabetes, thrombogenic factors and air pollution are known to be important regarding the incidence of cardiovascular disease (World Health Organization, 2018).

The most common type of CVD is coronary heart disease (CHD) in which coronary arteries become narrowed or completely blocked because of a build-up of fatty materials inside their walls which causes a reduction of normal blood flow to the heart. According to British Heart Foundation (2015), CHD is the single biggest killer in the UK and causes nearly 69,000 deaths per year: approximately 15% deaths in men and 10% of deaths in women. Coronary artery occlusive disease itself comes two main outcome: heart attack and angina. Heart attack is a severe pain in the centre of the chest, when a blood clot blocks completely the coronary artery and interrupts the blood supply to the heart (Julian, Cowan and McLenachan, 1998; British Heart Foundation, 2015). Angina is a mild or severe radiating pain in the centre of the chest because of insufficient oxygen-rich blood, termed ischemia, to the heart muscle due to narrowing of the blood vessels occurring mostly during exercise. The most common reason that results in angina is coronary atherosclerosis. In most cases, usually two or three main

arteries are involved and at least the luminal diameter's of one of them is reduced by 70% or more (Julian, Cowan and McLenachan, 1998; British Heart Foundation, 2015).

Coronary artery disease (CAD) is the term used to describe the affected arteries by a pathological process in which the blood vessels become narrowed and eventually entirely blocked and stops the normal oxygen-rich blood flow to the heart. Coronary atherosclerosis is one of the major causes of CAD and is the term used to define the chronic inflammatory process in which the coronary arteries lumen harden because of accumulation of deposits consisting of focal lipids, blood and blood components, complex carbohydrate, fibrous tissue and calcium deposits (Julian, Cowan and McLenachan, 1998; Strom and Libby,2011; British Heart Foundation, 2015; British Heart Foundation, 2017a)

1.2.1 Atherosclerotic Arterial Wall

Atherosclerosis, which is associated with high level of blood cholesterol, is a physiological occurrence in the artery wall that manifests itself as a pain in the chest and leads to CVD. High level of low-density lipoprotein accelerates this common pathological progression (Ross, 1999). This inflammatory large- and medium-sized arteries' disease begins by the formation of atherosclerotic plaques that are an asymmetric, central thickening of the inner layer (tunica intima) in the arterial wall (Hansson, 2005). These lesions consist of the necrotic cores, fibrous tissue, calcium regions, lipids accumulation, blood, inflamed smooth muscle cells (SMCs), endothelial cells, leukocytes and foam cells (Julian, Cowan and McLenachan, 1998; Hansson, 2005; Strom and Libby,2011). Endothelial cells, SMCs and leukocytes play a main role in progress of this disease. These atherosclerotic plaques can progress and cause the total occlusion of the lumen as well as often being associated with hardening of the arteries (Figure 1.4). Hypertension, diabetes, smoking, male gender and high plasma cholesterol level are attributors of atherosclerosis development (Mudau *et al.*, 2012).

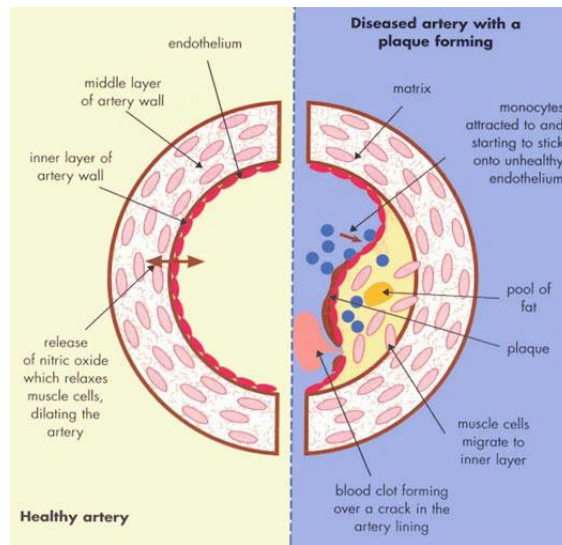


Figure 1.4: Comparison of healthy artery vs atherosclerotic artery (Drug Development, 2018)

The earliest sign of atherosclerosis is the formation of fatty streaks in the innermost layer of the vessel (Ross, 1999; Hansson, 2005). These yellow areas do not disturb the normal blood flow and do not cause symptoms, even if in some locations they return over time. Additionally, they do not make a swelling notably on the surface of the intima (Strom and Libby, 2011). These lesions are common in infants and young children (Julian, Cowan and McLenachan, 1998; Ross, 1999; Hansson, 2005). The initiation of the fatty streak's formation is not known yet, however endothelial dysfunction is considered as one of the initiating reasons of fatty streak development. Physical and chemical stressors such as hemodynamic stress change the normal endothelium which allows lipids to enter to the subendothelial space. Entered lipids act as proinflammatory mediators that result in foam cell formation and leukocyte recruitment (Hansson, 2005; Strom and Libby, 2011). Fatty streaks depend on their location and the occurrence of the related risk factors and can develop to the fibro-lipid plaques. Lipids, SMCs and their products as fibrous proteins and carbohydrates compounds are the major components of these plaques (Julian, Cowan and McLenachan, 1998). These deposits mostly occur at the bends and bifurcation of vessels resulting in heart attack in which normal blood flow is prevented through the coronary artery (Fardy, Yanowitz and Wilson, 1988; Jones and West, 1995; Julian, Cowan and McLenachan, 1998; Hansson, 2005). Figure 1.5 illustrates the atherosclerotic process in the coronary artery.

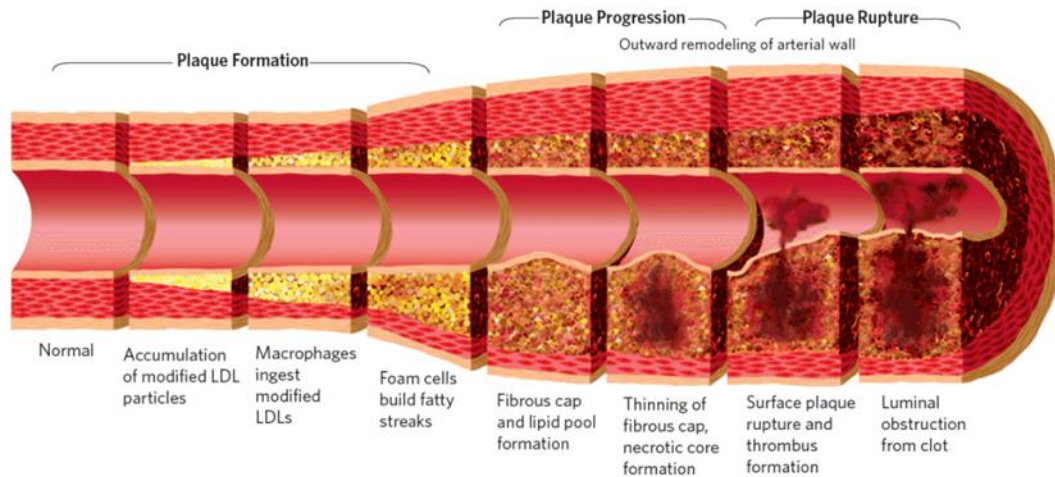


Figure 1.5: Atherosclerotic progression (The Center for Prevention Heart Attack and Stroke, 2016)

Coronary artery bypass grafting was the early approach that was used as a treatment for developed atherosclerotic disease (Perski *et al.*, 1998). In Coronary artery bypass grafting, patients undergo surgery to by-pass a blockage using an autologous graft such as the saphenous vein in the leg, the internal mammary artery in the chest or the brachial artery in the arm. This graft is sutured in place starting from a rich blood supply source, often from the coronary sinus at the root of the aorta and then sutured passed the blockage, onto the coronary artery (Figure 1.6).

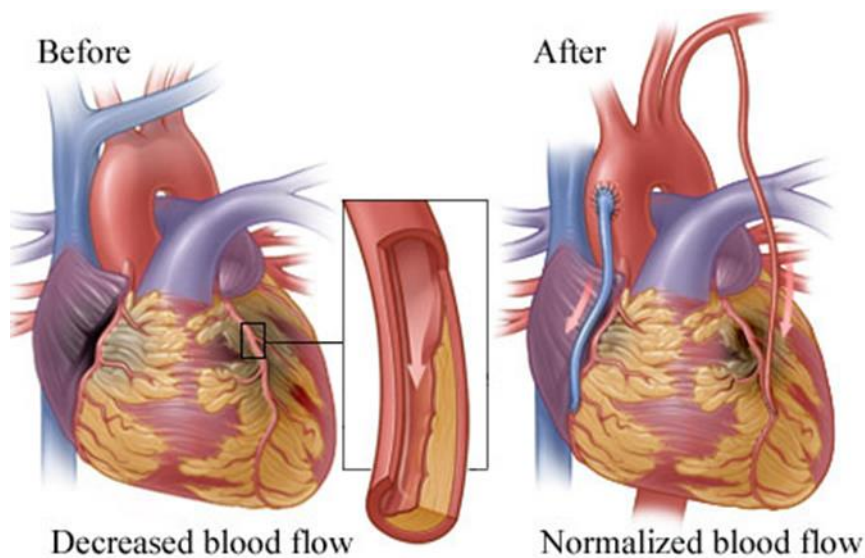


Figure 1.6: CABG schematic (Krasopoulos, 2013)

Limitations of coronary artery bypass grafting including heart failure, haemorrhage, renal failure and potential infection (Khalifa *et al.*, 2018). An alternative, minimally invasive approach to CHD, percutaneous coronary intervention (PCI) was then proposed in which a

dilatable balloon, placed inside the artery, is inflated opening the blood vessel. A further development and improvement followed by the use of a deformable, hollow cylindrical structure, called a stent: this was placed on the angioplasty balloon and dilated as the balloon was inflated. The balloon was then deflated and removed, leaving the stent in place to give radial support to the blood vessel. The stent, which is a small metal mesh tube, 6-33 mm in length, 2.25-5 mm in diameter and 0.05-0.2 mm in thickness (Colombo, Stankovic and Moses, 2002a), works as a scaffold to support the affected arterial lumen to allow normal blood flow to resume. The stenting process can be seen in Figure 1.7. The stent has developed with many different structures, geometries and materials. The first generation of stents are bare metal stents had negative consequences such as restenosis, which is reoccurrence of stenosis in arteries that results in a restricted blood flow. However, drug eluting stents have showed more efficiency than bare metal stents. Drug eluting stents are the second generation of the stents containing controlled release drugs. Despite the discovery of late thrombosis after using drug eluting stents, they have become widely used today. Stents will be presented in more details in the next chapter.

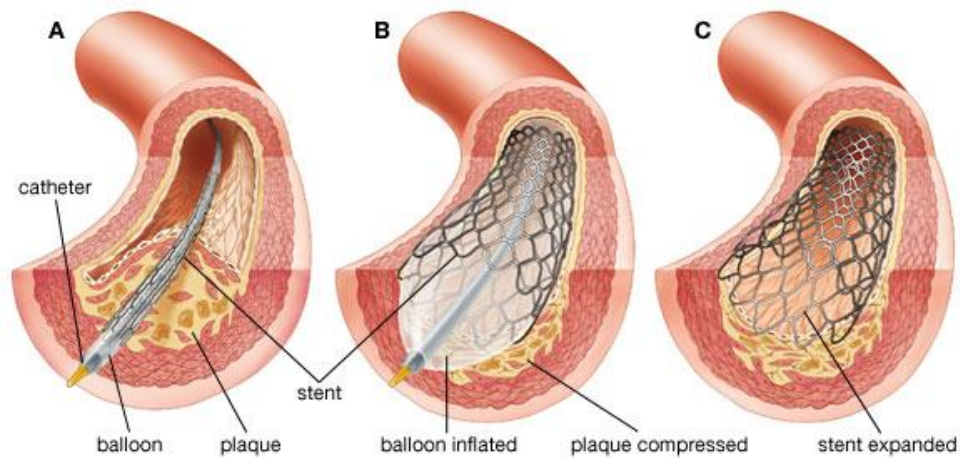


Figure 1.7: Coronary stenting procedure (Britannica, 2018)

1.2.2 Artery

Arteries are the blood vessels that circulate oxygen-rich blood from the heart to the other parts of the body, except the pulmonary artery which carries deoxygenated blood from the heart to the lungs. Normal arterial walls consist of three layers from the inside to outside as follows: tunica intima, tunica media and tunica adventitia (Figure 1.8).

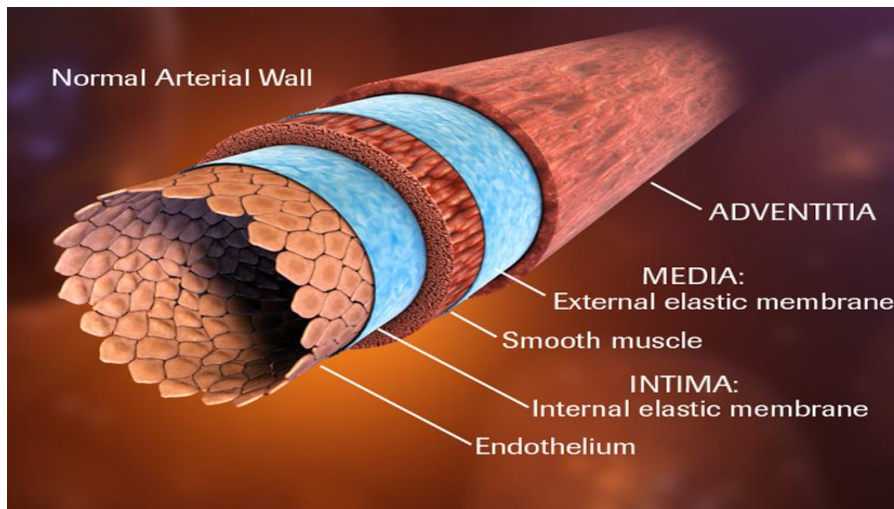


Figure 1.8: Arterial wall schematic (3FX Medical Animation Digital Solutions, 2012)

The tunica intima is a thin layer of connective tissue and comprises of a single layer of endothelial cells, which are in direct contact with blood (Levick, 2010; Strom and Libby, 2011; Chow *et al.*, 2014). This layer is the main barrier between circulating blood and the vessel wall. Endothelium is a thin single layer of endothelial cells containing of approximately $10 - 60 \times 10^{12}$ cells that is in contact with surrounding tissue and circulating blood and acts as a highly selective barrier (Mudau *et al.*, 2012). Thickness of this cell is $0.2-0.3 \mu\text{m}$ and each of them store a small amount of Ca^{2+} . A “crazy paving” format is made when these cells are adhered, edge to edge (Levick, 2010). These cells have regulatory properties and work as a non-adhesive, anti-inflammatory surface for platelets and leukocytes. Endothelium has different functions such as regulating blood-tissue exchange, initiating new blood vessel formation, maintaining homeostasis of the vessel wall, producing both anti-thrombotic and pro-thrombotic molecules (Levick, 2010; Strom and Libby, 2011; Mudau *et al.*, 2012). Thus, non-thrombogenic and anti-inflammatory surface of a normal endothelium plays a significant role in maintenance of vascular homeostasis: injury can result in the loss of the anti-thrombotic property in the vessel wall and a rapid increase in the number of damaged circulating endothelial cells, which is the first step in the formation of atheroma (Ross, 1999). Indeed, impairment of endothelium is critically important in the development of atherosclerosis. The tunica intima is separated from the media layer by an internal elastic membrane that acts as a support base for the endothelium. The tunica media is the middle and thickest layer of the arterial wall and contains smooth muscle cells and extracellular matrix. Two sheets of elastin, called the internal and external elastic laminae, are known as media boundaries. The role of this layer is to provide mechanical strength and contractile capabilities (Levick, 2010; Strom

and Libby,2011). In large arteries such as the aorta and its major branches, the contractile power of the media is responsible for stretching and recoiling the lumen during the systole and diastole, respectively. In smaller arteries like arterioles, the mechanical strength of the media is responsible for contracting or relaxing to change the resistance of the vessel (Strom & Libby, 2011). Vascular smooth muscle cells that are residents in the healthy arteries wall have contractile potencies. These types of cells have several functions including regulating the diameter of the blood vessels and providing structural integrity. Their most important role is in response to injury, they migrate and proliferate at the site of injured section (Strom and Libby,2011). Extracellular matrix is composed of fibrillary collagen, proteoglycans and elastin which are produced by vascular smooth muscle cells. The extracellular matrix mainly comprises more than half of the normal wall mass and moderates the growth of its resident cells. Structural support of the vessels and modulating cell function is the responsibility of the extracellular matrix's components (Strom and Libby,2011; Chow *et al.*, 2014). An external elastic lamina separates the tunica media from the tunica adventitia. The tunica adventitia, the outer layer of a normal blood vessel, largely consists of nerve fibres, lymphatic vessels, fibroblast cells and collagen fibres (Majesky *et al.*, 2011; Strom and Libby,2011; Chow *et al.*, 2014). This complex network inhibits artery rupture at extremely high pressures. It also nourishes the cells of the arterial wall besides controlling the lumen size by micro vessels within. This layer contributes to growth and repair of the artery wall (Majesky *et al.*, 2011; Chow *et al.*, 2014).

1.3 Function of Heart

The heart is divided into right and left parts; deoxygenated blood is pumped from the right side to the lungs and oxygenated blood is pumped from the lungs to the left side of the heart to circulate in the human body. In the pulmonary circuit, the superior and inferior vena cava veins carry deoxygenated blood to the right atrium. After contraction of the right atrium, the blood passes to the right ventricle through the tricuspid valve. After contraction of the right ventricle and opening of the pulmonary valve, the blood goes to the lungs via the pulmonary artery. Deoxygenated blood loses carbon dioxide and receives oxygen in the pulmonary artery. The pulmonary vein carries oxygenated blood into the left atrium. After contraction of the left atrium, blood then travels to the left ventricle via the mitral valve. In the systemic circuit, after contraction of the left ventricle and opening of the aorta valve, oxygenated blood goes to the arteries and capillaries via the aorta. After circulation of the blood to the tissues, deoxygenated

blood returns to the right atrium via veins (Lin *et al.*, 2011). Figure 1.9 shows the left and right sides of the heart and the valves.

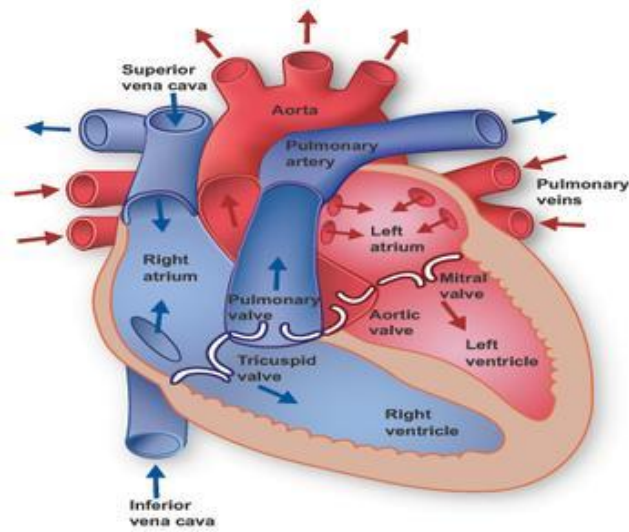


Figure 1.9: Schematic diagram of blood circulating through the heart (Texas Heart Institute, 2017)

1.4 Significance of Study

There are several important areas where this study makes an original contribution to the basic science of cell membrane potential measurement methods, cell migrations in the response to the applied electrical charges and the impact of experimental electrodes passivation.

This study first presents the heart anatomy along with human arteries, why coronary artery diseases occur and what medical treatments are provided for this problem. It mainly focuses on stenting and the negative consequences after treatment to provide a solution to reduce failure rates. Second, a new method is used to measure membrane potential of human cells to find out the optimum applied electrical charges on cells to cause cell migration on the surface of a metal.

This research explores the effect of the small electrical charges on the surface of an implanted stent. Indeed, direct current and pulsed direct current have this potential to cause the movement of cells towards the cathodically charged electrode. Migration and accumulation of human endothelial cells to the electrode (stent) can lead to a reduction of the negative consequences after the stent deployment due to the anti-thrombotic feature of an endothelium layer.

This study also provides new insights into cell's resting membrane potential measurement method. "Patch clamp technique" has been widely used in medical research, pharmaceutical studies and investigations in electrophysiology for high resolution recording of voltage and

current gates of cells. However, even though patch clamp method is known as the gold standard method for RMP measurement, there is still a lack of accuracy in the measurement of RMP as cell's membrane is ruptured during the technique causing the cell's inner voltage to influence the voltage on the outer surface of a cell. It is also a time-consuming technique. Patch clamp technique was introduced firstly by Neher and Sakmann who were awarded Nobel prize for this great success (Ypey and DeFelice,2007; Ogden and Stanfield,2011). They recorded the small ionic currents through the single channels in cell membranes by using this technique. This method can be used for two different purposes: first, a defined voltage can be applied on the membrane patch to measure the resulting current across the patch (voltage-clamp). The second one is to apply a defined current on the membrane patch to measure the flowing voltage into the patch (current-clamp). Current-clamp is hardly used for small patches of membrane. In this method, a super-clean fine glass micropipette tip is attached to the cell membrane. The micropipette is filled with an appropriate electrolyte solution (resembling the cytoplasm or the extracellular fluid) within a silver chloride coated wire connected to a highly sensitive amplifier for recordings. A gentle suction is applied in the micropipette to draw the cell membrane into the micropipette. A tight seal is made with the high electrical resistance of 10^9 (giga-Ohm sealing). The high electrical resistance is important because it not only causes less reduction in the current noise of the recordings but also increases the electrical isolation of the membrane patch. Patch clamp technique is used in 4 different configurations as: Cell-Attached Patch (CAP), Whole-Cell Patch (WC), Inside-Out Patch (IOP) and Outside-Out Patch (OOP) (Figure 1.10) (Ypey and DeFelice,2007; Sundelacruz, Levin and Kaplan, 2009; Ogden and Stanfield,2011).

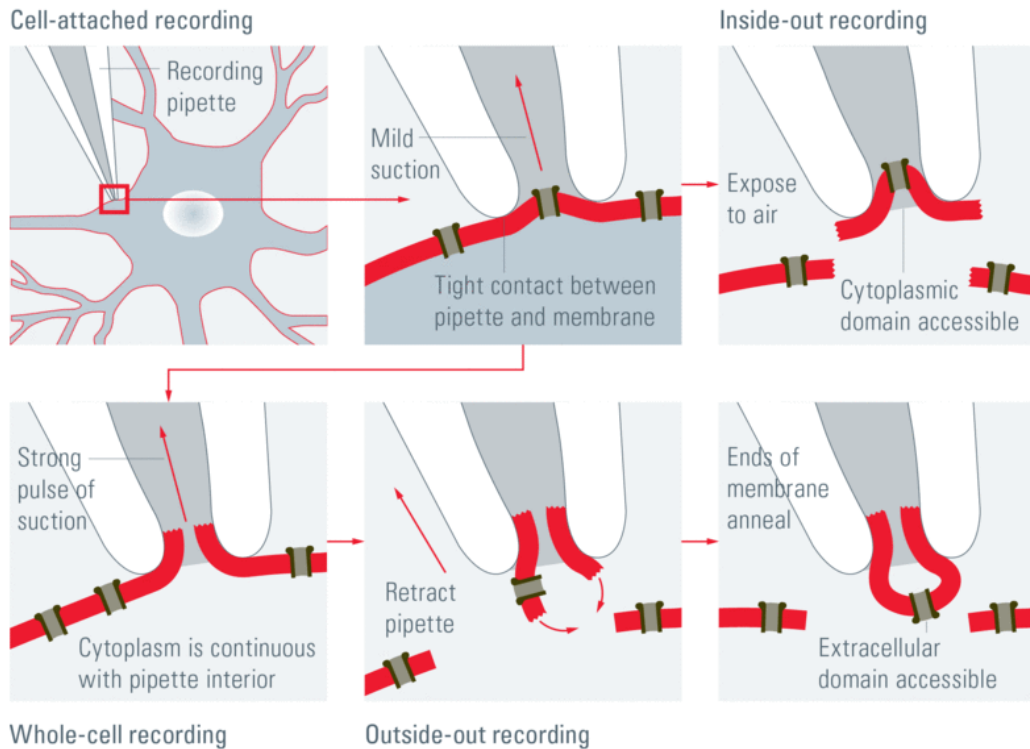


Figure 1.10: Patch clamp method schematic (Veitinger, 2018)

Considering the negative complications of patch clamp technique, “Direct Microelectrode Method (DMM)” is presented in this work and its results analysed. This method is based on the concept of battery working (movements of negative particles towards the anode through the electrolyte that produces electrical energy through ion movement) and the simplicity is the most significant point of using this technique. In this method, a tungsten microelectrode acts as a cathode and a pure titanium electrode as an anode are connected to a digital multimeter. The microelectrode is moved by using a micromanipulator for precision movement. As the microelectrode touches a cell, the cell’s voltage is recorded on the digital multimeter. Movements of ions in the cell media, complete an electrical circuit in this technique.

Moreover, touching cells using a direct microelectrode method makes a significant contribution to research on electrodes passivation which are then analysed using AFM and SEM.

This project also provided an important opportunity to advance the concept of cells movement. In electrophoresis experiments, cells are subject to DC electrical fields to illustrate the responses of adherent cells to the potential difference.

1.5 Aims and Objectives

- Aims:

The aim of this thesis has been to investigate the migration of human coronary artery endothelial cells onto the surface of implanted cardiovascular stents under application of electrical fields to reduce complications after stent deployment in an artery lumen. Migration of desired cells to the surface of the implanted stent is needed to make a covering layer that inhibits thrombus formation and in-stent restenosis in the segment of artery stented. Migration of endothelial cells towards the surface of the stent is investigated through bio-mimicked experiments.

- Objectives:

1. Measurement of cells membrane potential of cells using a novel method referred to as direct microelectrode method. This was conceived to measure cell voltage and optimize cell migration towards the stent. Various cell lines such as human osteoblast cells and human coronary artery endothelial cells membrane potentials are measured using the new technique.
2. Validating the results of the new method and comparing with other results from currently used methods such as “Di-electrophoresis method” and “Zeta potential method” are largely supportive of the new technique.
3. Measurement of cell membrane potential using zeta potential method.
In zeta potential method, the media including dispersed cells undergo an electrical field that causes cells movement with a velocity and vector. Each cell’s velocity is dependant to its zeta potential. These techniques will be introduced in more details in the third chapter.
4. Obtaining cells electrical characteristic using DEP method.
Di-electrophoresis method has been used extensively in various fields such as medical research, disease diagnosis and treatments, bioscience and biomedical developments, pharmaceutical research and cell research. DEP has strong controllability, an easy procedure, good efficiency, low cost and minimum damage to the sample. DEP is the phenomenon in which a suspended non-charged particle is set as a target for a non-uniform

electric field. A transluminal force will be applied on the dielectric particle that will be polarized into dipoles and moved towards or against the direction of the electrical field maxima under the influence of the net force. Some factors, including the frequency of the electric field, physical features and electrical properties of the particle influence the resultant force.

5. Investigation of metal electrode passivation behaviour in different solutions.

Metal electrode passivation behaviour in different solutions changes during cell membrane potential measurement using direct microelectrode technique. After examination of electrodes in different solutions and recording electrochemical measurements, the electrodes are observed in AFM and SEM.

6. Investigation of cells' movement under application of electrical fields. A modified electrophoresis method is used and compared to the common electrophoresis method, where separation of DNA and proteins under the influence of current results in movements of particles with different speed based their charge and size.

1.6 Thesis Outline

The overall structure of this thesis takes the form of six chapters, as following:

Chapter One: Thesis Overview and an introduction to the heart

In this chapter, overall view of the project and fundamental concepts are presented and aims and objectives of the project are introduced.

Chapter Two: Literature review

Main theories are explained in this section as it is the base of this thesis. It contains the various measurements of resting membrane potential of cells, different type of cells resting membrane potential, cardiovascular stenting and negative outcomes after the stent deployment. It also covers electrochemistry of metals in different solutions.

Chapter Three: Experimental method

At the beginning of the chapter, metal electrode passivation behaviours are studied. Effects of the different solutions on the surface of electrodes containing 304 stainless steel and commercially pure titanium are analysed and discussed using AFM and SEM. In addition, determination of endothelial cell membrane potential using direct microelectrode method, zeta potential method and di-electrophoresis technique are studied, and the results of each technique are compared in accuracy. Moreover, migration of endothelial cells is reviewed in electrophoresis method and in a bio-mimicked experiment.

Chapter Four: Results

Results of each experiment in the previous chapter are shown in form of graphs and tables and analysed.

Chapter Five: Discussion of the results are analysed.

Chapter Six: Conclusion and future work are presented and discussed.

Chapter 2 Literature Review

2.1 Introduction

Coronary artery disease is the most frequent type of heart disease and one of the deadliest diseases in the UK. CAD was in the second place of registered deaths with 11.5% in England and Wales in 2015 (Office for National Statistics, 2016). Due to the high rate of mortality and morbidity of CAD, massive efforts have been made on the treatments of this disease including extensive researches and technology advances.

Coronary invasive revascularizations are presented in the form of CABG and PCI. Coronary artery bypass grafting is the common performed operation for coronary heart disease, however Percutaneous Coronary Intervention (PCI) significantly has become of choice for the treatment of coronary arteries obstructive in the recent decades due to its effectiveness.

2.2 Background

Gruntzig et al introduced Percutaneous Coronary Intervention (PCI) to the world for the first time in 1977 that revolutionized the coronary artery treatments (Ashby *et al.*, 2002; Simard *et al.*, 2014; Byrne, Joner and Kastrati, 2015; Bedair *et al.*, 2017). The procedure was named balloon angioplasty in which a balloon catheter dilated in the narrowed lumen to allow normal blood flow to continue (Figure 2.1). Despite notable successful results of balloon angioplasty, there are some complications such as restenosis, re-blocking vessel and arterial dissection (Farb *et al.*, 1999; Ashby *et al.*, 2002; Byrne, Joner and Kastrati, 2015). Bedair *et al.* (2017) reported that in 30% -50% cases of balloon angioplasty needed re-vascularisation because of the restenosis. Consequently, a metallic stent was used with the balloon catheter to improve the procedure and prevent the closure (Figure 2.1). The use of coronary artery stents (CAS) was developed because of their success in diminishing restenosis rates, reducing early ischemic complications, offsetting the need for urgent coronary bypass surgery, covering arterial dissections and maintaining the expanded vessel lumen (Farb *et al.*, 1999; Ashby *et al.*, 2002; Byrne, Joner and Kastrati, 2015; Bedair *et al.*, 2017).

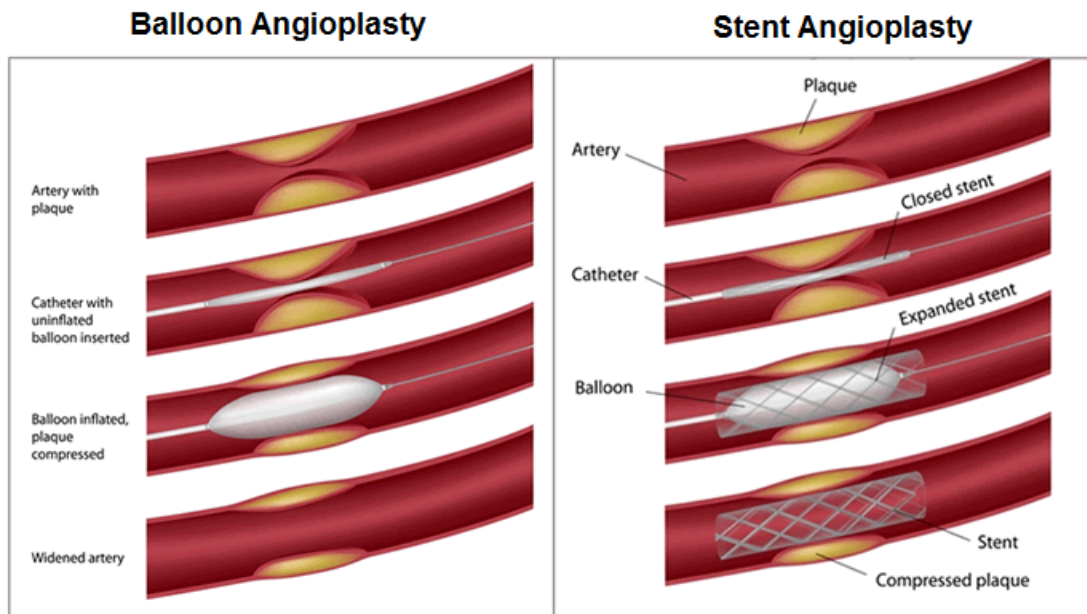


Figure 2.1: Balloon angioplasty process (left) and stent angioplasty procedure (right) (University Surgical vascular, 2017)

2.3 Stents

Coronary artery stents are small metallic tubular prosthetic meshes inserted into the affected coronary artery vessel mounted onto a collapsed balloon catheter to open the occluded or narrowed lumen to resume normal blood flow to the heart muscle. After dilation of the stent, the catheter is taken out while the stent remains in the affected segment and acts as a scaffold that prohibits either re-narrowing or re-blocking the lumen and reduces elastic recoil. Despite of initial good results of bare metal stents (BMSs), two main obstacles were identified. The first limitation was early stent thrombosis (EST) that results in the vessel closure. This happened in 25% of cases within 14 days after the stent deployment (Byrne, Joner and Kastrati, 2015). The second complication was in-stent restenosis (ISR) that was result of vascular injury due to stent implantation and happened in 30% cases (Her and Shin, 2018). Therefore, drug-eluting stents (DESs) were developed as the modification of BMSs to eliminate the problems. However, DESs markedly reduced early stent thrombosis and in-stent thrombosis incidence, some other negative outcomes emerged such as late and very late stent thrombosis (LST and VLST) after DESs implantations. Recently, more developments in DESs technologies have been focused on thinner struts, fully bioresorbable and biocompatible stents as well as duration of anti-platelet therapy (Byrne, Joner and Kastrati, 2015). Overall, an ideal stent has a short

duration of healing, does not need a long term anti-platelet therapy and lowers the risk of thrombosis and restenosis after the stent deployment.

2.3.1 Types

There are numerous types of stents that differ in structure and design and materials. Generally, stents are divided into balloon-expandable or self-expanding, coated or uncoated stents (Al Suwaidi, Berger and Holmes Jr, 2000; Ashby *et al.*, 2002; Colombo, Stankovic and Moses, 2002b). Balloon-expandable stents are the most common type in use for patients. The stents are available in various lengths and diameters, the choice of which depend on anatomical feature of the arterial lesion. Stent's length is produced from 6 mm to 38 mm with diameter of 2.25 mm to 5 mm (Al Suwaidi, Berger and Holmes Jr, 2000; Colombo, Stankovic and Moses, 2002b). The National Institute for Clinical Excellence (NICE) guidelines suggests the ideal coronary artery stents use depends on the diameter of the artery vessel. According to NICE, target arteries are divided into two categories; high and low risk of restenosis. High risk of restenosis is known when the target artery has a diameter of <3.0 mm or the lesion has a length of >15 mm in which NICE recommends to use DESs, whereas in the target artery with a diameter of ≥ 3.0 mm or the lesion has a length of ≤ 15 mm, which are known as a low risk of restenosis, NICE then recommends to use BMS. It is noteworthy to mention that these divisions are not applied for those patients who have a prior occurrence of the thrombosis in their vessels (Klomp *et al.*, 2011). Moreover, stents vary in different factors such as flexibility, radiopacity, metal composition (commonly 316L stainless steel is used), surface area coverage and metal content (Al Suwaidi, Berger and Holmes Jr, 2000). Large number of stents are commercially available or being researched that have different geometric, mechanical and material properties (Ashby *et al.*, 2002).

- Bare Metal Stents (BMSs)

BMSs reduced negative problems such as restenosis and acute occlusion in comparison to balloon angioplasty (Reejhsinghani and Lotfi, 2015). However, restenosis remains a major drawback of BMSs. It has been reported that in 20% - 30% cases of BMSs, re-narrowing of the treated vessels occurred (Martin and Boyle, 2011). Bare metal stents heal quickly and are prone to restenosis occurrence. A short term anti-platelet therapy is needed for bare metal stents.

- Drug-Eluting Stents (DESs)

Introducing the first generation of DES stents was a new era in the treatment of coronary artery disease. DESs are BMSs which are coated with a combination of drugs and polymers that reduce the risk of ISR. First generation of stents markedly reduced the risk of target vessel revascularization versus BMSs. Indeed, first generation of DESs reduced the short-term complications as early stent thrombosis and the inhibition of neointimal hyperplasia by smooth muscle cells proliferation's disruption, but they can cause late and very late stent thrombosis due to delayed re-endothelialisation (Finn *et al.*, 2007b; Nishimoto *et al.*, 2017; Torrado *et al.*, 2018). As mentioned earlier, each DES is composed of three main parts: stent platform, the stent coating and the drug-delivery mechanism (Figure 2.2).

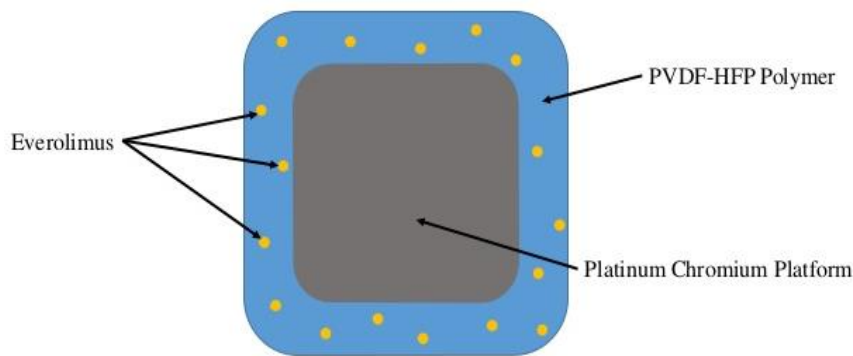


Figure 2.2: Stent Strut Cross-section can be seen in Everolimus Stent (Maktari, 2015)

First generation of DESs contains SES and PES and second generation of DESs includes ZES and EES. The main improvements in the first and second generation of DESs are the thickness of struts, polymers and drugs which leads to high successes of the second generation of DESs.

Bare metal stents heal quickly but are prone to restenosis. A short term anti-platelet therapy is needed for bare metal stents, while a long term anti-platelet therapy is required for drug-eluting stents because polymers and drugs delay the healing process. In-stent restenosis and late-stage thrombosis have a higher risk when a drug-eluting stents are used. Figure 2.3 shows the difference between BMS and DES.

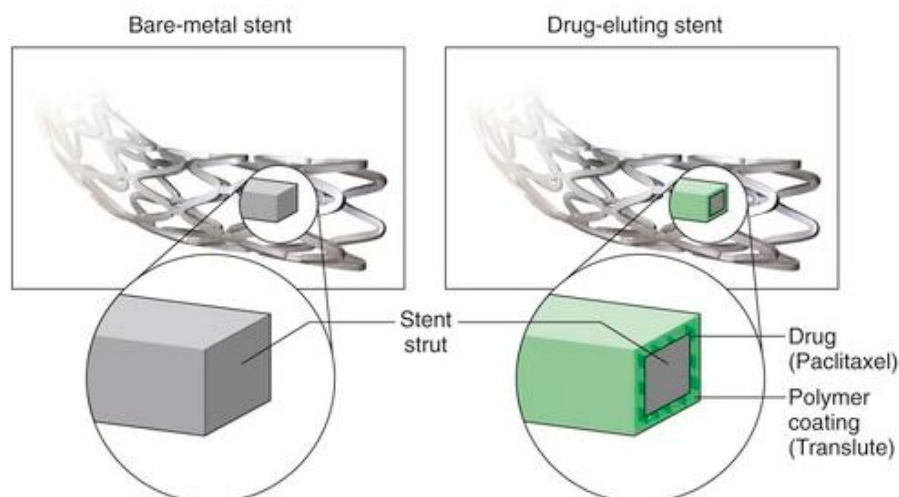


Figure 2.3: Differences between two common types of stent, BMS and DES, can be seen (Jeudy, Waite and Chen, 2015)

2.4 Problems

The most negative outcomes that patients suffer after the stent deployment are in-stent restenosis and stent thrombosis.

2.4.1 In-stent Restenosis

In-stent restenosis (ISR) still remains a recognized important obstacle after the stent implantation, however DESs notably decreased the incidence of ISR in comparison to BMSs (Farb *et al.*, 1999; Klomp *et al.*, 2011). In ISR process, the stented segment artery becomes narrowed again because of neointimal tissue proliferation, as a result of the arterial damage (Her and Shin, 2018). Smooth muscle cells proliferation, known as intimal hyperplasia is inhibited by release of the cytotoxic drugs from DESs that is the reason of the ISR reduction. Conversely, the endothelialisation process, which is important for vascular healing, is prevented by these drugs. Disturbing a normal healing procedure might increase the occurrence of stent thrombosis (Klomp *et al.*, 2011). Optimization of stents deployment and dual antiplatelet therapy (DA) probably played a significant role in the reduction in the occurrence of this issue. ISR is characterized by the diameter stenosis of $\geq 50\%$ in the stented segment of the artery (Martin and Boyle, 2011; Her and Shin, 2018). In-stent restenosis categorized angiographically into four important groups according to the development of intimal hyperplasia associated with the inserted stent (Finn *et al.*, 2007a).

- I. Pattern 1 contains focal lesions (less than 10 mm in length)

- II. Pattern 2 includes diffuse lesions larger than 10 mm inside the stent
- III. Pattern 3 includes proliferative lesions larger than 10 mm covering outside of the stent
- IV. Pattern 4 is referenced to completely occlusive in-stent restenosis

After treatment of in-stent restenosis, requiring target lesion revascularisation varies from 19% to 83%, from pattern1 to pattern 4, respectively (Finn *et al.*, 2007a; Her and Shin, 2018).

2.4.2 Stent Thrombosis (ST)

A major concern after the stent deployment is stent thrombosis (ST) which is significantly reduced by the huge improvements in stent implantation technologies, but still remains as a main cause of death after PCI (Holmes *et al.*, 2010). ST, in which a thrombus formation causing an occlusion of the stent lumen, is an unknown issue which can lead to sudden death (~20% to 40%), Myocardial Infraction (MI) (~50% to 70%) and repeat revascularization (Cutlip *et al.*, 2007; Jaffe and Strauss, 2007; Holmes *et al.*, 2010; Claessen *et al.*, 2014; Byrne, Joner and Kastrati, 2015; Reejhsinghani and Lotfi, 2015). However, improving stents design, materials and placement and effective dual antiplatelet treatments markedly declined the presence of ST complication. ST usually occurs in less than 1% of patients with BMSs within the first month of stent deployment, whereas it normally happens later than the usual 1-month timeframe in patients with DESs (Jaffe and Strauss, 2007). Notably, Sommer and Armstrong (2015) stated approximately the same possibility of incidence of ST which was around 0.5% to 1% up to one year following the stent deployment no matter which type of stents were used. Conversely, Werkum *et al.* (2009) reported that ST phenomenon occurs between 1% to 5% subsequent to stent implantation. Table 2.1 shows the consequences including death, nonfatal myocardial infraction and unstable angina rates after DES deployment.

Table 2.1: Results of DES deployment

Stent Type	Follow-Up Duration	Death	Nonfatal MI	Unstable angina
DES (Jaffe and Strauss, 2007)	9 months	24%	60%	7%
DES (Secemsky <i>et al.</i> , 2015)	4.1years	54.1%	82.0%	No data

- Stent thrombosis definitions

Two common classification; angiographic definition and clinical definition; were used historically for diagnosis of ST. But Academic Research Consortium (ARC), which is an informal association between academic research institutes in the United States and Europe, in

2007, proposed new definitions of ST rates to standardize ST diagnosis and make a consistency across different trials and researches (Cutlip *et al.*, 2007; Jaffe and Strauss, 2007; Holmes *et al.*, 2010; Claessen *et al.*, 2014; Byrne, Joner and Kastrati, 2015; Reejhsinghani and Lotfi, 2015; Sommer and Armstrong, 2015). Therefore, ST's data from trials before 2007 may be difficult to compare with data after recent ARC definition publication. The ARC definition categories of stent thrombosis is based on the level of the ST and the time of the occurrence following PCI. Classification of ST based on the time elapsed after deployment of stents include 4 categories (Table 2.2):

- I. Acute ST (AST) happens during the stenting process or within the following 24 hours after the stent implantation.
- II. Subacute ST occurs between 1st to 30th days subsequent the stent deployment.
- III. Late ST (LST) appears between 1st to 12th months after the stent placement.
- IV. Very late ST (VLST) happens after 1st year following the stent implantation.

Table 2.2: Classification of stent thrombosis following the stent deployment (Cutlip et al., 2007; Jaffe and Strauss, 2007; Holmes et al., 2010; Claessen et al., 2014; Byrne, Joner and Kastrati, 2015; Reejhsinghani and Lotfi, 2015; Sommer and Armstrong, 2015)

Term	Classification
Acute ST*	0 day after PCI < ST incidence < 1 st day after PCI
Subacute ST*	1 st day after PCI < ST occurrence < 1 st month after PCI
Late ST	1 st month after PCI < ST presence < 1 st year after PCI
Very late ST	1 st year after PCI < ST happening

* Acute and Subacute ST are subdivisions of Early Stent Thrombosis (EST).

Jaffe and Strauss (2007) also reported that degrees of acute and subacute ST phenomenon among patients using dual antiplatelet treatments, independent of the use of BMS or DES, were less than 1%. It was reported that LST rarely occurs in patients with BMSs, although incidence of LST in DESs has been focused to research recently which might be due to dual antiplatelet treatments discontinuation or the drugs in the structure of DESs that may delay the healing process and re-endothelialisation (Jaffe and Strauss, 2007; Holmes *et al.*, 2010; Reejhsinghani and Lotfi, 2015). According to Reejhsinghani and Lotfi (2015), the possibility of LST and VLST is rare to happen in BMSs treated patients (2% at 10 years following PCI). The results of the review by Reejhsinghani and Lotfi (2015) showed that in general, clinical practice the expected incidence of EST is about 1%, whereas annual rate of LST and VLST is 0.2% to 0.6%. Sommer and Armstrong (2015) also reported that the mortality rate in EST with the rate

of 7.9% is higher than LST and VLST with the rate of 3.8% and 3.6%, respectively. Likewise, Secemsky *et al.* (2015) reported that total deaths among different types of ST belonged to patients with EST (54.1%) versus LST (18.5%) and VLST (24.0%) (Figure 2.4).

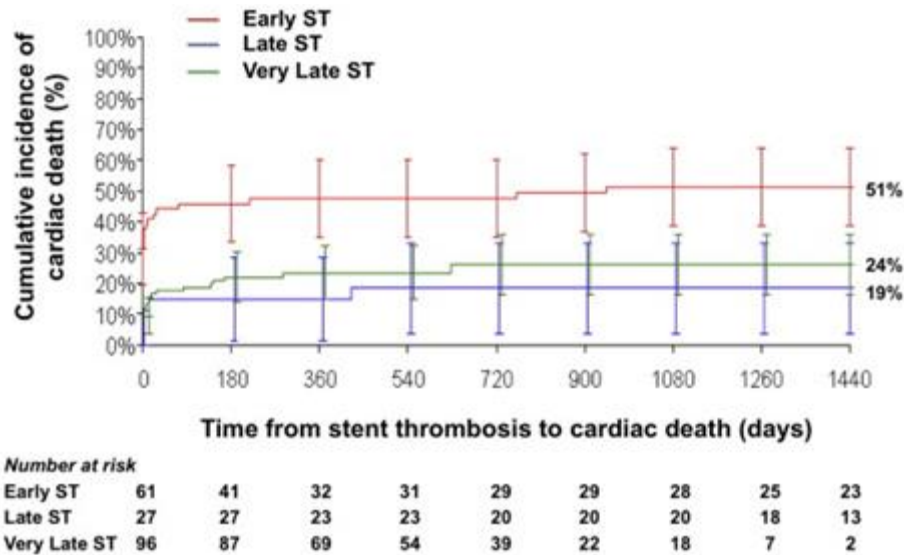


Figure 2.4: Possibility of cardiac death in patients with ETS (51%), LST (19%) and VLST (24%) (Secemsky *et al.*, 2015)

Similarly, Armstrong *et al.* (2014) reported that the 30 days mortality is significantly higher in EST versus LST and VLST with the rates of 13%, 6% and 3%, respectively (Figure 2.5). As it can be seen in Figure 2.5, the survival probability of patients with EST is less than patients with LST and VLST. Likewise, Kohn *et al.* (2013) stated that in-hospital and 30 days mortality is higher in EST versus VLST.

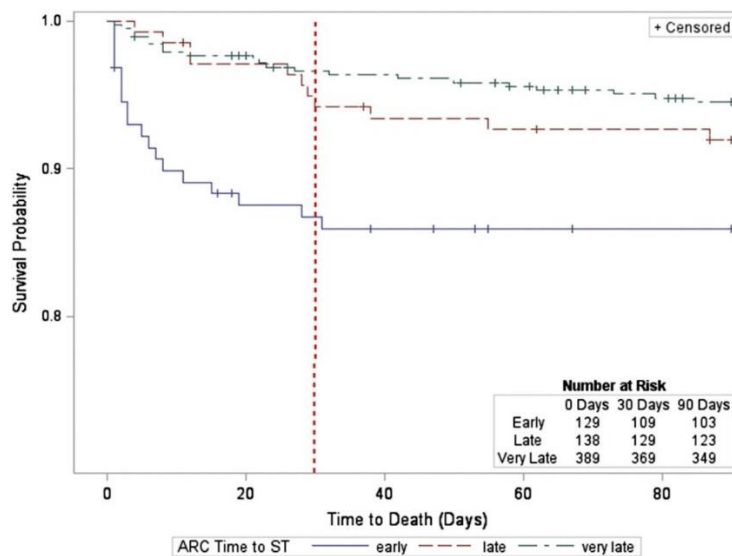


Figure 2.5: The 30 days mortality comparison in patients with EST, LST and VLST with mortality rates of 13%, 6% and 3%, respectively (Armstrong *et al.*, 2014).

Another classification of ST definitions published by ARC which is based on the level of evidence can be seen in Table 2.3. This arrangement contains three categories:

- I. Definite ST category needs angiographic or autopsy approval
- II. Probable ST is considered to have happened after PCI in the following conditions:
 - a) any unexplained death after the first 30 days following PCI
 - b) target vessel MI without angiographic confirmation
- III. Possible ST category includes any unexpected death within 30 days following PCI.

Table 2.3: ARC stent thrombosis definitions (Cutlip et al., 2007; Jaffe and Strauss, 2007; Holmes et al., 2010; Reejhsinghani and Lotfi, 2015)

Term	Definition
Definite ST	Angiographic confirmation or pathological evidence of ST
Probable ST	<ol style="list-style-type: none"> 1. Any Unexplained deaths within 30 days after PCI 2. Acute myocardial infraction involving the target vessel territory without angiographic confirmation
Possible ST	Any unexplained deaths beyond 30 days following PCI

- Mechanisms of stent thrombosis

It is now well established from a variety of studies that fundamental mechanisms of stent thrombosis contains vascular injury after stent implantation, factors influencing coagulation and platelet activity and mechanical factors leading to blood stasis (Sommer and Armstrong, 2015). Thrombus formation is a combination of thrombotic and inflammatory components containing fibrin fragments, platelet-rich thrombus and leukocytes of both neutrophil and eosinophil lineage (Byrne, Joner and Kastrati, 2015). Impairment of endothelium layer due to stent deployment is prothrombotic and play a key role in the development of stent thrombosis. Also, neo atherosclerosis is another mechanism that is associated with stent thrombosis development. Several factors including progression of atherosclerosis, prolonged inflammation and inadequate endothelial coverage may contribute in neo atherosclerosis formation (Sommer and Armstrong, 2015). The incidence of neo atherosclerosis is more in DES than BMS with the rate of 31% versus 16% (Reejhsinghani and Lotfi, 2015; Sommer and Armstrong, 2015).

- Risk factors of stent thrombosis

Collectively, data from trials and reports prove that intensity of antiplatelet treatments and amount of endothelial coverage have a significant influence on the occurrence of ST. Factors

found to be influencing ST phenomenon have been explored in quite a few studies (Jaffe and Strauss, 2007; Werkum *et al.*, 2009; Holmes *et al.*, 2010; Claessen *et al.*, 2014; Nakano *et al.*, 2014; Reejhsinghani and Lotfi, 2015). Various risk factors are divided into several groups as be heeded:

- I. Patient variables: diabetes, acute coronary syndrome (ACS), renal failure, bifurcation lesions, cardiovascular history
- II. Procedure and lesion-related factors: lesions length, malapposition of the stent (Figure 2.6: i), small vessel size, slow coronary blood flow, long stents, remaining thrombus, delayed arterial healing, in-stent restenosis, multi-vessel disease, stents incomplete expansion (Figure 2.6: iv), stent under sizing, uncovered dissection, stent fracture
- III. Antiplatelet therapy factors: inadequate intensity of treatments, premature cessation of antiplatelet therapy, under dosing, drug interactions, non-compliance, no aspirin

Some predictors play an effective role in the incidence of early stent thrombosis while some other directly lead to late and very late stent thrombosis occurrence. Stent under sizing and multi vessel disease are known as significant factors leading to early stent thrombosis happening, whereas patient related factors, neo atherosclerosis plaque formation and stent malapposition are also recognized as important predictors in LST and VLST (Byrne, Joner and Kastrati, 2015; Sommer and Armstrong, 2015). Notably, Sommer and Armstrong (2015) found that some factors of LST and VLST such as diabetes, renal disease and heart failure are associated more with LST in comparison with VLST. Some predictors such as acute coronary syndrome resulted in EST and LST, independent to type of the stents.

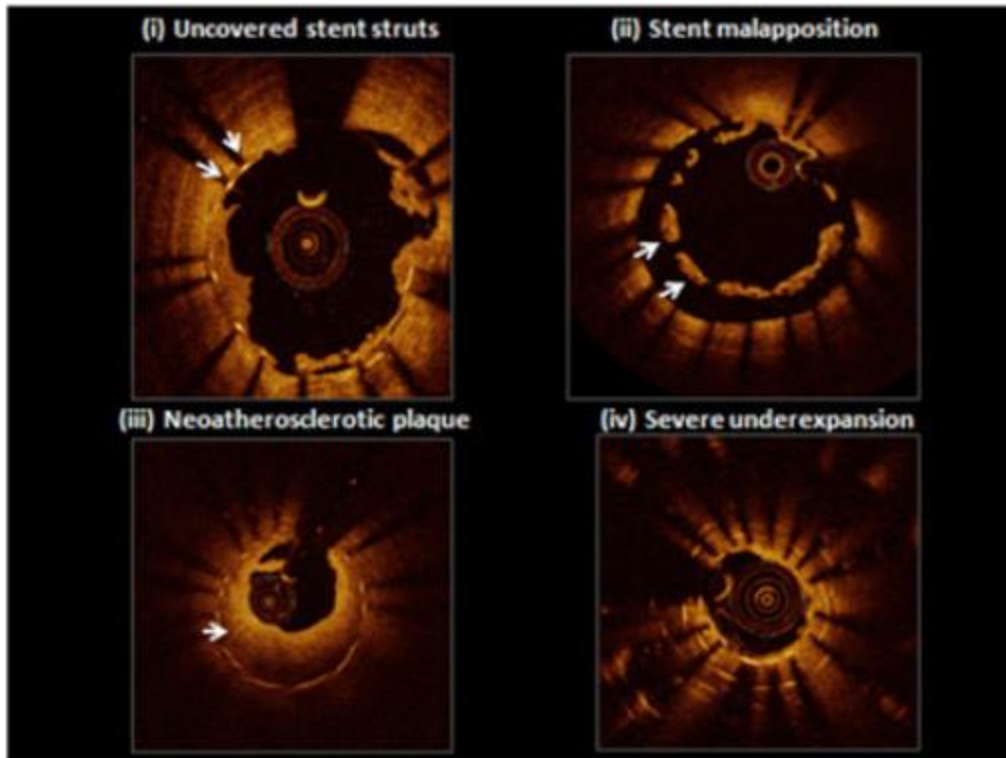


Figure 2.6: Incidence of stent thrombosis due to various predisposed factors: (i) continuous uncovered stent scaffold following implantation; (ii) stent malapposition (showed by arrows); (iii) formation of neoatherosclerotic plaque; (iv) intense stent incomplete expansion (Byrne, Joner and Kastrati, 2015)

Among multiple predictors of ST, cessation of antiplatelet therapy such as clopidogrel, aspirin and glycoprotein IIb/IIIa inhibitors is known as the most significant independent parameters that are associated with ST occurrence (Jaffe and Strauss, 2007; Werkum *et al.*, 2009; Byrne, Joner and Kastrati, 2015). Surprisingly, Werkum *et al.* (2009) highlighted that even lack of clopidogrel before 14 days after PCI considered as a ST predictor. Worth mentioning that Claessen *et al.* (2014) expressed that early cessation of DAPT, coronary artery disease' level and total length of stent were the most common factors that occurred regularly.

- Comparison of ST in BMS versus DES

Prior to significant evolution of stents, especially DESs, mortality and morbidity rates have been reduced remarkably. However, stent thrombosis phenomenon happens regularly. Despite BMS that are disposed to in-stent restenosis, the first generation of DESs; SES and PES; are prone to stent thrombosis beyond 30 days, due to delayed arterial healing that is characterized by inadequate endothelial coverage and persistent fibrin deposition and continuous vessel wall inflammation (Tada *et al.*, 2013a; Claessen *et al.*, 2014; Byrne, Joner and Kastrati, 2015; Reejhsinghani and Lotfi, 2015; Sommer and Armstrong, 2015). Several lines of evidence suggested that rate of ST is higher in PES than SES due to high smooth muscle cells death and

continuous fibrin formation within the neointima (Holmes *et al.*, 2010; Reejhsinghani and Lotfi, 2015). Table 2.4 shows stent thrombosis rates after different types of stent deployment.

Noteworthy to mention is that significant improvements in antithrombotic therapies and stent technology, like thinner strut, refined stent's platform, biocompatibility, durable or biodegradable polymer coating caused less incidence of stent failure in patients treated by second generation of DESs; EES and ZES (Tada *et al.*, 2013a; Reejhsinghani and Lotfi, 2015; Sommer and Armstrong, 2015). Recently, rates of ST occurrence became half from 3% to 1.5% (Byrne, Joner and Kastrati, 2015). As it can be seen in Figure 2.7, the risk of ST happening of second generation of DESs has become less than BMSs which proved the effectiveness of recent improvements in stent technologies.

Table 2.4: Comparison of incidence of different types of stent thrombosis in patients treated by various types of stents

Stent Type	Number of Patients	Follow-Up Duration	AST	SAST	LST	VLST
270 BMS, 152 DES, 15 both (Werkum <i>et al.</i> , 2009)	437	30.9 months	32%	41.2%	13.3%	13.5%
DES (Secemsky <i>et al.</i> , 2015)	9370	4.1years	0.6%		0.3%	1.0%
0.6% SES > 0% BMS (Jaffe and Strauss, 2007)	5261	Over 4 years	-	-	-	*
0.7% PES > 0.2% BMS (Jaffe and Strauss, 2007)	5261	Over 4 years	-	-	-	*
0.6% SES > 0.5% BMS (Jaffe and Strauss, 2007)	4958	Up to 59 months	-	-	-	*
0.7% DES > 0.1% BMS (Holmes <i>et al.</i> , 2010)	10727	Beyond 1 year	*			

*The statistics were not available.

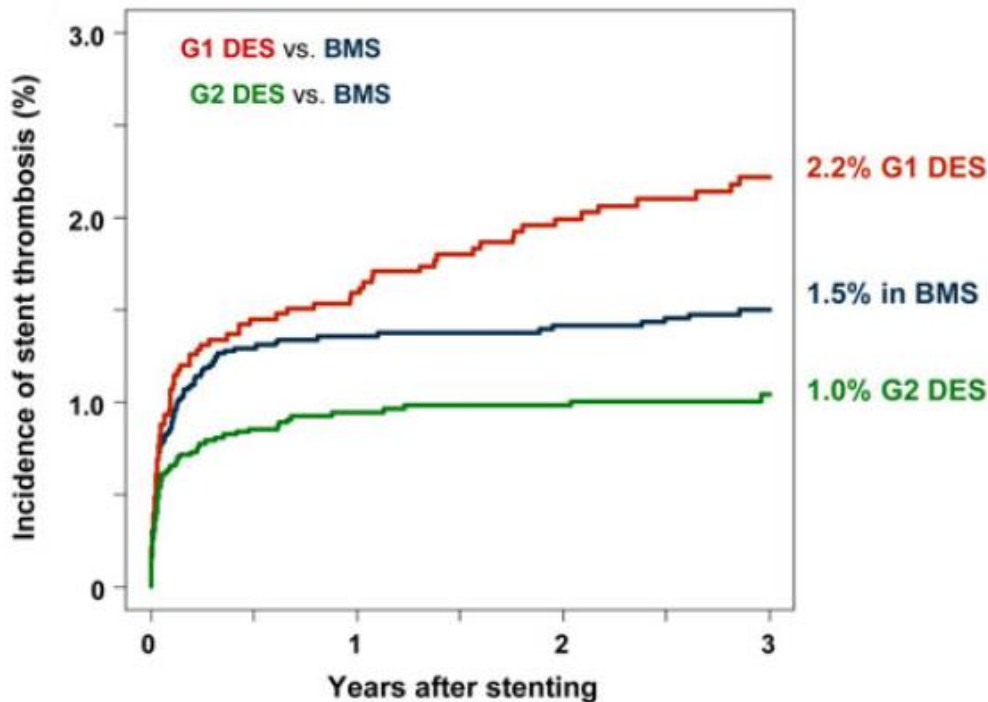


Figure 2.7: The risk of ST occurrence after implantation of BMS (blue), first generation of DES (G1 DES: SES, PES) (red) and second generation of DES (G2 DES: EES, ZES) (green) (Tada *et al.*, 2013a; Byrne, Joner and Kastrati, 2015)

- Prevention of stent thrombosis

Extensive researches have demonstrated that lengthening the duration of dual antiplatelet treatment with aspirin and a thienopyridine might be effective in reduction of LST rates of DESs (Jaffe and Strauss, 2007; Byrne, Joner and Kastrati, 2015). Similarly, Holmes *et al.* (2010) emphasized Jaffe and Strauss's (2007) view about the effect of the extended duration of aspirin and a thienopyridine causing a reduction in DES treated patients in which he reported the rate of ST was 1.76% versus 0.1% during 31 to 180 days and 2.1% versus 0.14% during 366 to 548 days in patients who stopped both aspirin and a thienopyridine versus who continued the dual antiplatelet therapy. Likewise, cessation of clopidogrel as an antiplatelet treatment is associated with the rate of ST phenomenon (Werkum *et al.*, 2009) and even more increases the possibility of death or MI occurrence (Holmes *et al.*, 2010). As Werkum *et al.* (2009) reported, subacute, late and very late stent thrombosis occurred in the patients who stopped taking clopidogrel for a median of 5, 13 and 200 days respectively. However, Subacute ST rates in BMS have declined by using triple antiplatelet therapy with aspirin, a thienopyridine and cilostazol (Jaffe and Strauss, 2007). Similarly, Holmes *et al.* (2010) stated that mortality rate and serious cardiac problems were reduced by using triple antiplatelet therapy with aspirin, a thienopyridine and cilostazol. Notably, Werkum *et al.* (2009) pointed out glycoprotein IIb/IIIa was a protective for the incidence of EST. Many recent studies showed that newer antiplatelet

therapy such prasugrel and ticagrelor significantly lead in reduction of ST. Sommer and Armstrong (2015) reviewed a trial paper in which prasugrel was used as the antiplatelet therapy and it significantly reduced the incidence of ST, independent to types of stents. He also pointed out that US guidelines currently advised treatments containing combination of aspirin and P2Y12 inhibitors like clopidogrel, ticagrelor and prasugrel for duration of at least 1 and 12 months for DES implantation in ACS patients and BMS deployment in non-ACS patients, respectively.

With the wealth of literature available, extension of dual antiplatelet therapy is recognized as one of the effective factors in reduction of the risk of ST occurrence, particularly beyond 12 months. Optimization in stents design including polymer-free and biodegradable polymers, using nonpolymeric drug delivery in DES structure, completely biodegradable DES and endothelial progenitor cell capturing stents have been known to develop as they have an adequate potential to lead a reduction in ST phenomenon (Jaffe and Strauss, 2007; Holmes *et al.*, 2010; Claessen *et al.*, 2014; Sommer and Armstrong, 2015).

2.5 Novel Approach to Stent Development

A great deal of research has been done to improve stents technologies, for example, modification of polymers, bioresorbable scaffold (BRS) and endothelial progenitor cells (Holmes *et al.*, 2010). Bioresorbable scaffold is a type of the stent that maintains the lumen open from the closure and then will disappear. Rezolve scaffold, DESolve scaffold, bioresorbable vascular scaffold (BVS) and metal alloy scaffold are currently available bioresorbable coronary scaffold types. Researches have revealed the rates of reduction in duration of dual antiplatelet therapy and late stent thrombosis after deployment of BRSs (Capodanno *et al.*, 2015; Goel *et al.*, 2017).

Directing endothelial progenitor cells (EPC) has the potential to cover the damaged segments and repair the impaired vascular sites (Klomp *et al.*, 2011; Tang *et al.*, 2016). Endothelial progenitor cell capturing stent (ECS) is a CD34+ antibodies coated stent aiming the circulating EPC to the site of damaged vascular wall (Klomp *et al.*, 2011; Pang *et al.*, 2015; Tang *et al.*, 2016). Klomp *et al.* (2011) reported a remarkable result in animal models which had full endothelial coverage on the stent strut within 48 hours after ECS deployment.

It has been suggested that rapid re-endothelialisation of the stent region could cause a reduction in thrombus formation. Various ways to improve and accelerate re-endothelialisation of a stent

has been explored, such as modification of the chemistry and topography of the stent's surface (Bedair *et al.*, 2017), surface roughening and patterning (Govindarajan and Shandas, 2014; Tan, Muhamad and Abdullah, 2017) and applying external forces like magnetic forces (Pislaru *et al.*, 2006) to cause migration of cells onto the stent area, so called electrotaxis. Research has also been performed to investigate the migration of cells onto the surface of stents using forces like an external uniform magnetic field (Polyak *et al.*, 2008).

2.6 Cellular Electrical Fields

The impact of exogenous and endogenous electric fields (EFs) on physiological processes have been studied by researchers for many years. Direct-current endogenous electric fields (DCEFs) are naturally produced pathologically and physiologically within the extracellular and sometimes intracellular spaces of human cells in the form of epithelial transcellular potentials or neural field potentials (Mycielska and Djamgoz, 2004; McCaig, Song and Rajnicek, 2009; Zhao *et al.*, 2012).

In the form of epithelial transcellular potentials; a layer of epithelial cells that covers most organs and glands produces potential electrical differences or transepithelial potentials (TEPs) that varies from a tiny value of millivolts to higher number of millivolts. As reported by Mycielska and Djamgoz (2004), the measured epithelial transcellular potentials in vivo and experimental studies differ from 50 to 500 mV/mm measuring in rat prostate (Szatkowski *et al.*, 2000) , small airways of sheep lungs (Al-Bazzaz and Gailey, 2001), guinea pig trachea (Dortch-Carnes, Van Scott and Fedan, 1999) and mouse rectum (Wang *et al.*, 2000). Although TEP value was reported between 20 to 50 mV from intact mammalian skin's regions (Nishimura, Isseroff and Nucciteili, 1996). In addition, TEP value range is reported about 15-45 mV/mm (Guo *et al.*, 2010) which is approximately near to Nishimura, Isseroff and Nucciteili's (1996) report.

EFs have been found at skin wounds and damaged tissue (Mycielska and Djamgoz, 2004; Wang and Zhao, 2010; Zhao *et al.*, 2012), embryogenesis (Mycielska and Djamgoz, 2004) and vasculature (Wang and Zhao, 2010; Zhao *et al.*, 2012).

In the form of neural field potentials; the combination of extracellular field potentials across the blood-brain barrier (Mycielska and Djamgoz, 2004) and specific transendothelial potentials (Revest, Jones and Joan Abbott, 1994) cause the presence of steady EFs in the nervous system.

Steady electrical signals (DCEFs) play a critical role in physiological processes of cells including proliferation, migration and differentiation (McCaig, Song and Rajnicek, 2009; Balint, Cassidy and Cartmell, 2013).

2.6.1 Galvanotaxis Phenomenon (Cell Migration)

The galvanotaxis phenomenon is the one of the significant results of applied DCEFs on cells where cells move in a specific direction towards a cathode (negative charged side) or an anode (positive charged side) in response to exogenous DCEFs as the same as the magnitude of endogenous DCEFs (Djamgoz *et al.*, 2001; Mycielska and Djamgoz, 2004; Wang and Zhao, 2010). The galvanotaxis mechanisms may happen in a couple of seconds to a few minutes or in a couple of minutes to a couple of hours. Galvanotaxis mechanism occurs when the concentration of the local intracellular Ca^{2+} is not even in the two anodal and cathodal sides. In fact, the local intracellular Ca^{2+} concentration on the anodal side is hyperpolarized because of the passive influx of Ca^{2+} through electrochemical diffusion. Consequently, the local intracellular Ca^{2+} concentration on the cathodal side is reduced because of passive efflux and/or intracellular redistribution. As a result, these changes cause net shift of cells towards the cathode. In addition, other factors such voltage-gated Na^+ channels, protein kinases and other properties of proteins like surface charge, growth factor and electrophoresis play a role in galvanotaxis (Mycielska and Djamgoz, 2004).

In the galvanotaxis phenomenon, the changes in the amount of Ca^{2+} is important which is stimulated by the magnitude of DCEF. However, hormonal activation and mechanical deformation can also alter the concentration of intracellular Ca^{2+} (Bootman *et al.*, 2001). The amount of Ca^{2+} can be changed by the impact of DCEFs through following ways: intracellular Ca^{2+} stores, passive influx and influx through voltage-gated Ca^{2+} channels (VGCCs).

2.6.1.1 Intracellular Ca^{2+} stores

External DCEFs can influence the release of internal Ca^{2+} stores. Normally, the concentration of internal Ca^{2+} is around 100 nM when the cells are at rest and Ca^{2+} ‘on’ and ‘off’ mechanisms are balanced, whereas the level of intracellular Ca^{2+} reaches to $\sim 1 \mu\text{M}$ or more under the effect of depolarisation of cells causing ‘on’ mechanisms to raise the level of cytosolic Ca^{2+} . The intracellular Ca^{2+} concentration is regulated by two concurrent ‘on’ and ‘off’ mechanisms. In Ca^{2+} ‘on’ mechanisms, supply of Ca^{2+} is regulated by different channels located on the

endoplasmic reticulum (ER), sarcoplasmic reticulum (SR) and plasma membrane (PM) and in Ca^{2+} 'off' mechanisms, cells remove the Ca^{2+} from the cytoplasm (Bootman *et al.*, 2001). Applying external DCEF causes the propagation of intracellular Ca^{2+} waves (ICWs) that start from the higher membrane potential side and terminate at the membrane with the lower potential as it can be seen in Figure 2.8 (b). A number of triggers such as mechanical stimulation, mechanical stretch and externally applied DCEF can stimulate the propagation of ICWs, however ICWs can be propagated without any specific trigger (Leybaert and Sanderson, 2012). For example, fast calcium waves are induced in electrotactic fish keratocytes by applying electric field pulses (Brust-Mascher and Webb, 1998). Various factors such as the nature and strength of the initiating stimulus and mechanism of propagation can influence the speed and size of ICWs (Leybaert and Sanderson, 2012). These waves are normally induced as the result of the interaction between Ca^{2+} released from the intracellular stores and Ca^{2+} influx (Bootman *et al.*, 2001; Mycielska and Djamgoz, 2004).

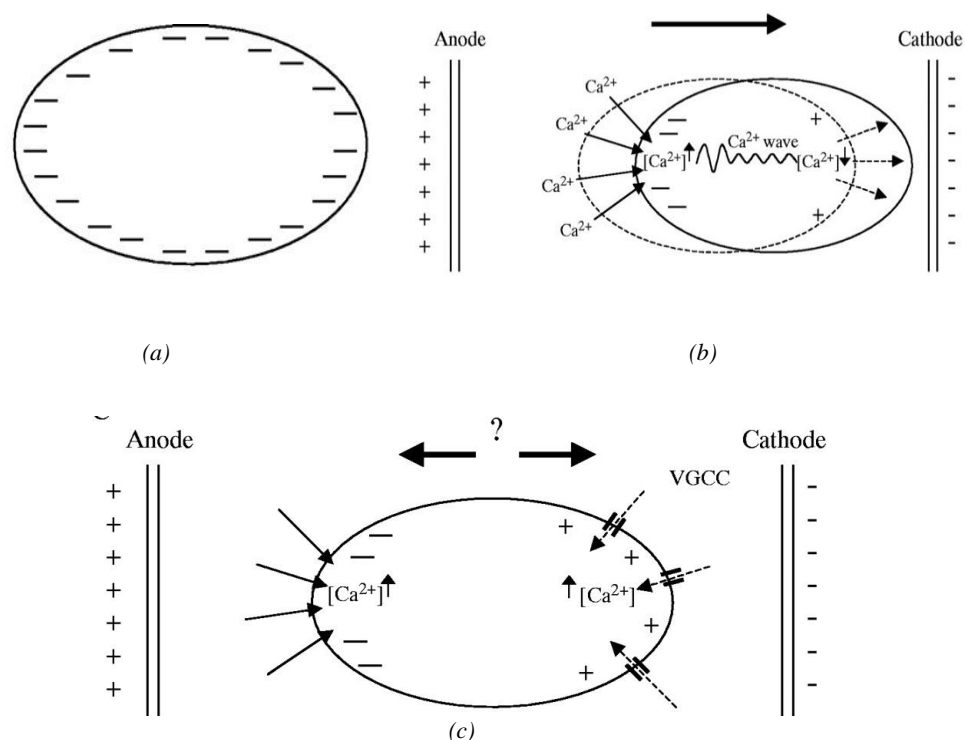


Figure 2.8: Reaction of a cell process can be seen in the above figure, when it is exposure to DCEFs effect. Cells normally have negative resting membrane potentials (a). In (b), cells with a few or no VGCCs migrate towards the cathode because anodal side is hyperpolarized because of passive influx of Ca^{2+} under effect of DCEF. In (c), depolarized cathodal part of cells with opened VGCCs cause Ca^{2+} influx causing cell movements towards the anode in the opposite direction of passive influx's effect. Then, amount of Ca^{2+} increase in both sides and net movement of cells depends on the balance of two opposing forces (Mycielska and Djamgoz, 2004).

2.6.1.2 Passive influx

In cells where VGCCs are not present or are negligible, externally applied DCEFs increase the passive influx of Ca^{2+} on the anodal face of a cell membrane and that anodal part contracts. As a consequent, the cell is pushed towards the cathode by the depolarized cathodal side Figure 2.8 (b). Applying an external DCEF hyperpolarizes the anode membrane, whereas depolarizes the cathode membrane and generates intracellular Ca^{2+} waves that begins from the hyperpolarized end and ends at the depolarized side. Measured intercellular waves in fish keratocytes (Brust-Mascher and Webb, 1998) and LNCaP human prostate cancer cell lines (Perret *et al.*, 1999) showed that the waves are induced with consistent amplitudes and average velocities of 66 $\mu\text{m/s}$ and 20 $\mu\text{m/s}$, respectively. However, it is reported that ICWs are often propagated with the average speed of $\sim 10\text{-}20 \mu\text{m/s}$ and can be continued up to tens of seconds including tens to hundreds of cells (Leybaert and Sanderson, 2012). It has also been detected that the cathode and anode facing parts of a cell 10 μm in diameter depolarized and hyperpolarized around 5 mV simultaneously under the effect of 10-100 mV/mm applied DCEFs (Poo, 1981; Patel and Poo, 1984).

2.6.1.3 Influx through voltage-gated Ca^{2+} channels (VGCCs)

In cells that possess VGCCs, the channels will be opened during depolarization of the cathodal face and allow Ca^{2+} influx which results in the movement of the cell towards the anode. The direction of this shift is in reverse to the direction of the cell's movement under the impact of passive Ca^{2+} influx alone in which the cell moves towards the cathodal side. As can be seen in Figure 2.8 (c), the final movement depends on the balance of two facing forces. Any higher force determines the direction of the cell movement.

Referring to previous researches and studies, most type of cells as human retinal pigment epithelial cells (Sulik *et al.*, 1992), endothelial progenitor cells (Zhao *et al.*, 2004), human microvascular endothelial cells (HMEC-1) (Bai *et al.*, 2004), human corneal epithelial cells (Farboud *et al.*, 2000), human keratinocytes (Nishimura, Isseroff and Nuccitelli, 1996; Sheridan, Isseroff and Nuccitelli, 1996), hippocampal neurons (Yao *et al.*, 2008), bovine corneal epithelial cells (Zhao *et al.*, 1996), bovine aortic vascular endothelial cells (Li and Kolega, 2002), fish epidermal cells (Cooper and Schliwa, 1985; Cooper and Schliwa, 1986), amphibian neural crest cells (Cooper and Keller, 1984), neural crest cells (Erickson and Nuccitelli, 1984; Stump and Robinson, 1983), avian neural crest cells (Nuccitelli and Smart,

1989), quail embryonic fibroblasts (Erickson and Nuccitelli, 1984), metastatic rat prostate cancer cells (Djamgoz *et al.*, 2001), rat osteoblast like cells (Ferrier *et al.*, 1986), National Institute of Health (NIH) 3T3 and SV101 fibroblast cell lines (Brown and Loew, 1994) and C3H/10T1/2 mouse embryo fibroblasts (Mycielska and Djamgoz, 2004) migrate towards the cathode. However, some cells move towards the anode despite of their negative membrane potential such human umbilical vein endothelial cells (HUVEC) (Bai *et al.*, 2004), metastatic human breast cancer cells (Mycielska and Djamgoz, 2004), human granulocytes (Rapp, De Boisfleury-Chevance and Gruler, 1988), human dermal fibroblasts (Guo *et al.*, 2010), mammalian granulocytes and monocytes (Gruler, 1993), murine peritoneal macrophages (Orida and Feldman, 1982), murine aorta smooth muscle cells (Bai *et al.*, 2004), rabbit osteoclast cells (Ferrier *et al.*, 1986), rabbit corneal endothelial cells (Chang *et al.*, 1996) and bovine pulmonary artery fibroblasts (BPAF) (Bai *et al.*, 2004). However, some cells like human dermal melanocytes do not migrate either to the cathode or anode under the impact of exogenous DCEF of 100 mV/mm (Grahn *et al.*, 2003). Cell origin differences influences the direction of cells migration. For instance, different types of endothelial cells might move to different charged sides as human umbilical vein endothelial cells shifted to the anode (Bai *et al.*, 2004), whereas human microvascular endothelial cells (HMEC-1) (Bai *et al.*, 2004), endothelial progenitor cells (Zhao *et al.*, 2004) and bovine aortic vascular endothelial cells (Li and Kolega, 2002) moved towards the cathode.

2.6.2 Cells Membrane Potentials

Biological membranes isolate the interior of the cells from the external environment and are semi- permeable to some distinct ions like Sodium (Na^+), Potassium (K^+), Calcium (Ca^{2+}) and Chlorine (Cl^-). Cell membranes act as an electrical capacitor between two internal and external conducting solutions and are associated with the range of cells activities such as cell signalling, cell adhesion and ion conductivity. They act as the main barrier for mass transport and the electrical insulator. Their main role is to maintain the electrolyte hemeostasis and ionic gradients. The common structure of the cell membrane includes bilayers of mobile phospholipids with accompanying proteins (Figure 2.9). This structure is known as the fluid mosaic model with width around 7 nm. Lipids compose approximately 50% of the mass of the membrane (Cooper, 2000). The head of the phospholipids are polar and hydrophilic, whereas their tails are non-polar and hydrophobic and acts as a barrier. The hydrophilic heads are in contact with the intracellular and extracellular fluids that are watery phase while hydrophobic

tails are kept far from both watery environments. Pores in the lipid bilayer is filled by the proteins. The mass of the proteins alters depending on the type of membrane and constitute 25% to 75% of the mass of the membrane (Cooper, 2000). Proteins are divided into: integral proteins which are dispersed in the lipid bilayers and peripheral proteins which are located outside of the lipid bilayer on either outside or inside the cells. Proteins function different tasks in the membranes. They can act as enzymes to accelerate chemical reactions, transport materials across the membrane and function as receptors for specific molecules. Also, short carbohydrates are attached to the outer surface of the membrane. Mostly, these carbohydrates are attached to the proteins and are called glycoproteins which help the cells to identify other cells and protect the membrane. Another component among the tails of phospholipids of animal cells are cholesterol molecules that are also hydrophobic. These cholesterol molecules, dispersed amongst the phospholipid tails, are composed of four rings of hydrogen and carbon atoms. These molecules stop the membrane from stiffening and keep the membrane as a barrier in front of some small molecules crossing.

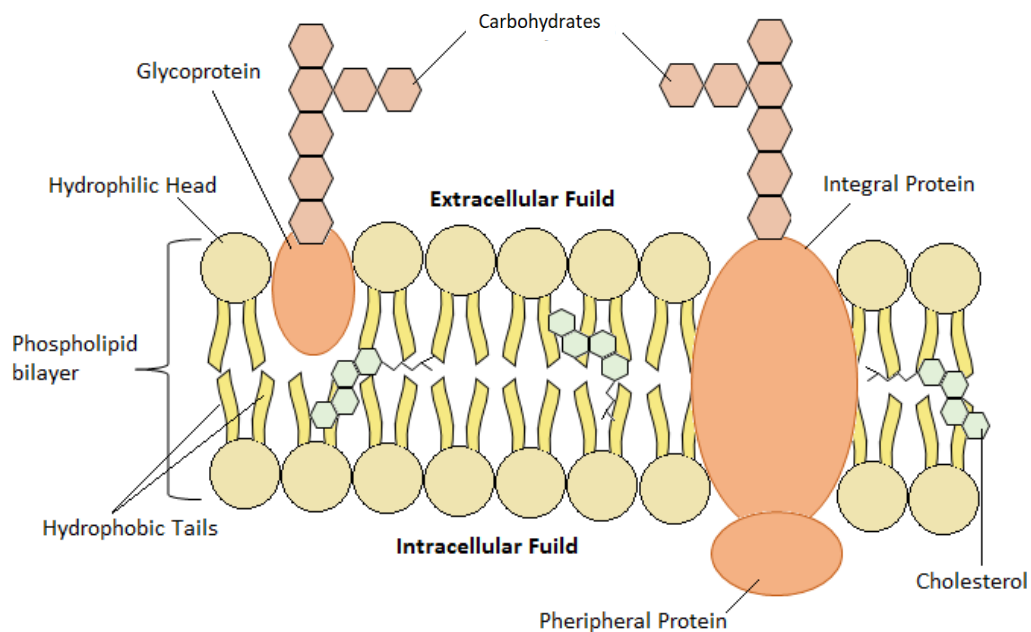


Figure 2.9: A simplified model of cell membrane

Cell membrane potential refers to a potential difference across a plasma membrane which is shown by V_m . As the membrane is selectively permeable to specific ions, a difference in concentration of various ions is on either side of the cell membrane. Consequently, a comparatively higher positive charge exists on the outer surface of the membrane than the inner membrane surface because of the different concentrations of the ionic components. The

resulting imbalance of electrical charges across the membrane occurs in all cell types. Modifications in the level of conductivity of one or more type of ions lead to alternation of V_m . In the Goldman-Hodgkin-Katz voltage equation (2.1) V_m is proportional not only to the concentration of ions inside and outside of the cells but also ions permeability (Hodgkin and Katz, 1949; Yang and Brackenbury, 2013).

$$V_m = \frac{RT}{F} \ln \left(\frac{P_{Na^+} [Na^+]_{out} + P_{K^+} [K^+]_{out} + P_{Cl^-} [Cl^-]_{in}}{P_{Na^+} [Na^+]_{in} + P_{K^+} [K^+]_{in} + P_{Cl^-} [Cl^-]_{out}} \right) \quad (2.1)$$

Where R is the ideal gas constant ($8.314 J.mol^{-1}.K^{-1}$), T is the temperature (K), F is the Faraday constant that is the magnitude of electrical charge per mole of electrons ($96485.33289(59) C.mol^{-1}$), P_{Na^+} , P_{K^+} and P_{Cl^-} are the permeability constants of each ion ($C.m.sec^{-1}$), $[Na^+]_{out}$, $[K^+]_{out}$ and $[Cl^-]_{out}$ are the extracellular concentration of each ion and $[Na^+]_{in}$, $[K^+]_{in}$ and $[Cl^-]_{in}$ are the intracellular concentration of each ion. Magnitude of permeability constant of each ion that is directly proportional to mobility and solubility of each ion in the membrane can be calculated through equation (2.2) (Hodgkin and Katz, 1949):

$$P_x = \frac{RT}{Fa} u_x b_x \quad (2.2)$$

Where R is the ideal gas constant ($8.314 J.mol^{-1}.K^{-1}$), T is the temperature (K), F is the Faraday constant that is the magnitude of electrical charge per mole of electrons ($96485.33289(59) C.mol^{-1}$), a is the thickness of membrane (nm), u_x is the mobility of the ion in the membrane ($m^2.s^{-1}.v^{-1}$) and b_x is the partition coefficient that is the ratio of concentration of an ion between the aqueous solution and membrane at equilibrium.

The term resting membrane potential (V_{rest}) refers to the cell membrane potential in the resting situation without any disturbances. Resting membrane potential changes from cell to cell and it is stated that membranes resting potentials vary from 30 mV to -300 mV in mammalian and plant cells, respectively (Pliquett *et al.*, 2007). In non-excitabile cells the membrane potentials do not change extremely over time therefore $V_m = V_{rest}$. However, in excitable cells like neurons and muscle cells the membrane potentials alter quickly within a few seconds (one second to hundred milliseconds) therefore in these types of cells the membrane potentials are not always the same as the resting membrane potentials $V_m \neq V_{rest}$.

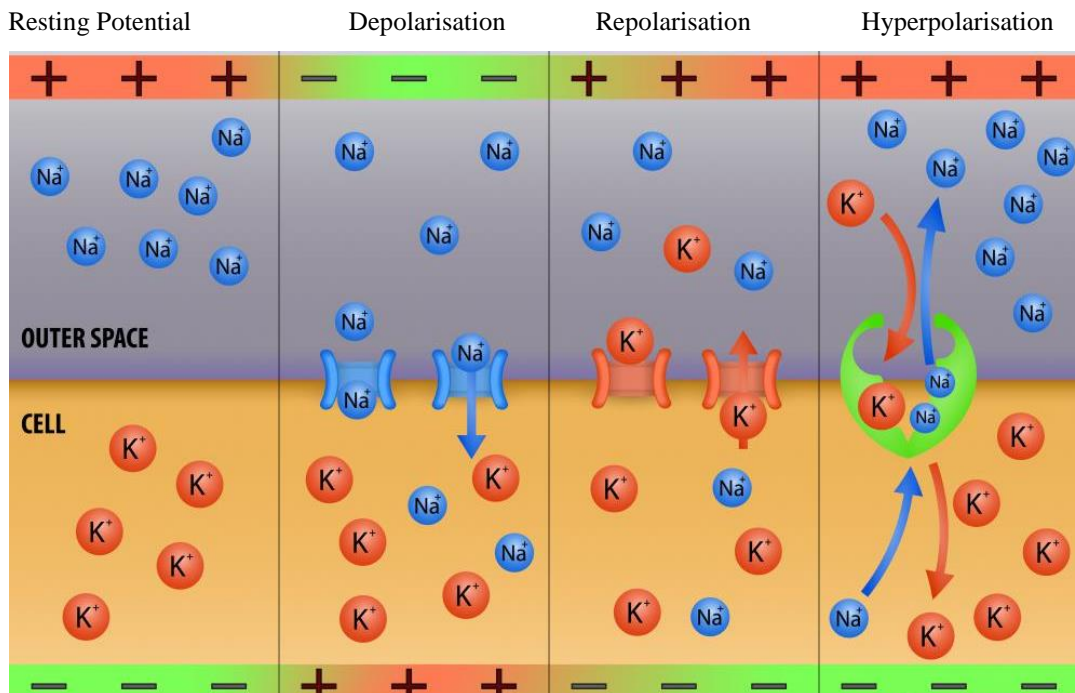


Figure 2.10: Ions transportation between inside and outside of a cell during different phases (Updegraff, 2017)

The presence of different ions migrating inside the cell through the ion channels lead to a departure from the resting membrane potential which is called depolarization where the interior of a cell has more positive membrane potential value as a result of either influx of any cations such as Na⁺ or efflux of any anions from inside the cells. The return of the membrane potential value to the resting membrane potential level from the depolarization phase is called repolarization in which Na⁺ channels become closed and K⁺ channels become opened because of the increase of the positive charged inside the cells. With opened K⁺ channels, K⁺ ions flow out of the cells and the charge inside the cell again reaches the resting membrane potential. The term hyperpolarization refers to when the interior of a cell becomes less positive as the result of either influx of Cl⁻ through Cl⁻ channels or efflux of K⁺ through K⁺ channels (Figure 2.10). In fact, influx of Na⁺ and Ca²⁺ through Na⁺ and Ca²⁺ Channels respectively inhibit the hyperpolarization. In order to return to the resting membrane potential level, K⁺ channels become opened to let K⁺ to flow in and Na⁺ is moving out from the interior of the cells. The cells have the highest voltage and much lower voltage in the depolarization and hyperpolarization phase, respectively. Figure 2.11 illustrates the membrane potential of a cell in different conditions.

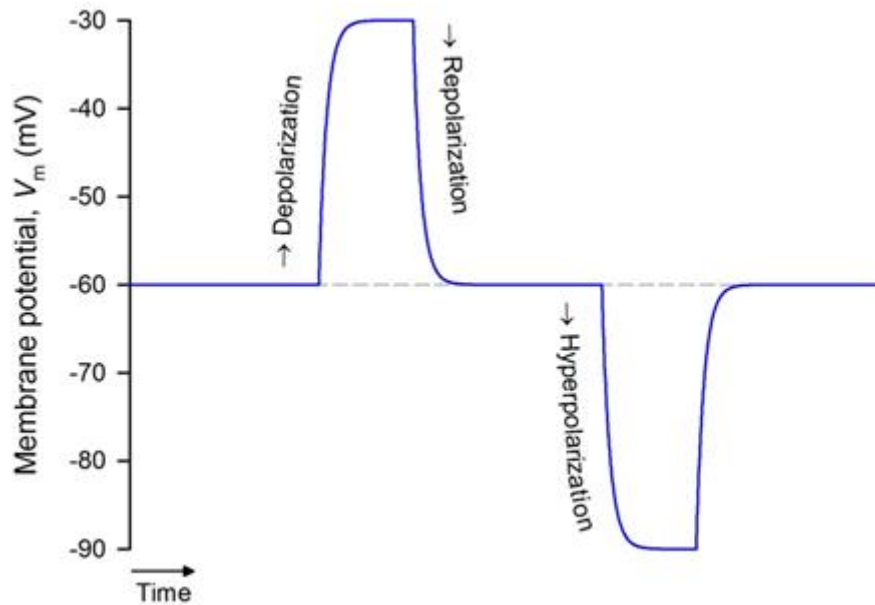


Figure 2.11: Graph of different phases of cell membrane potentials (PhysiologyWeb, 2014)

Binggeli and Weinstein (1985), Yang and Brackenbury (2013) and Pollack (2015) stated that healthy cells tend to possess higher membrane potentials than their sick counterparts as it can be seen in Figure 2.12 and Table 2.5. For instance, cancer cells such as Ehrlich mouse ascites tumor cells and HeLa cells, which is the oldest continuous cell line was derived from the cervical cancer cells (of a woman named Henrietta Lacks), possess electrical potentials of -11.2 mV (Aull, 1967) or -15 mV (Borle and Loveday, 1968) respectively, whereas the normal cells possess electrical potentials in the range of -80 to -100 mV. Taken together, all of studies proved that the depolarization of most of the sick cells in comparison to normal ones. According to Pollack (2015), any cells that falls significantly from its potential toward zero is going to die.

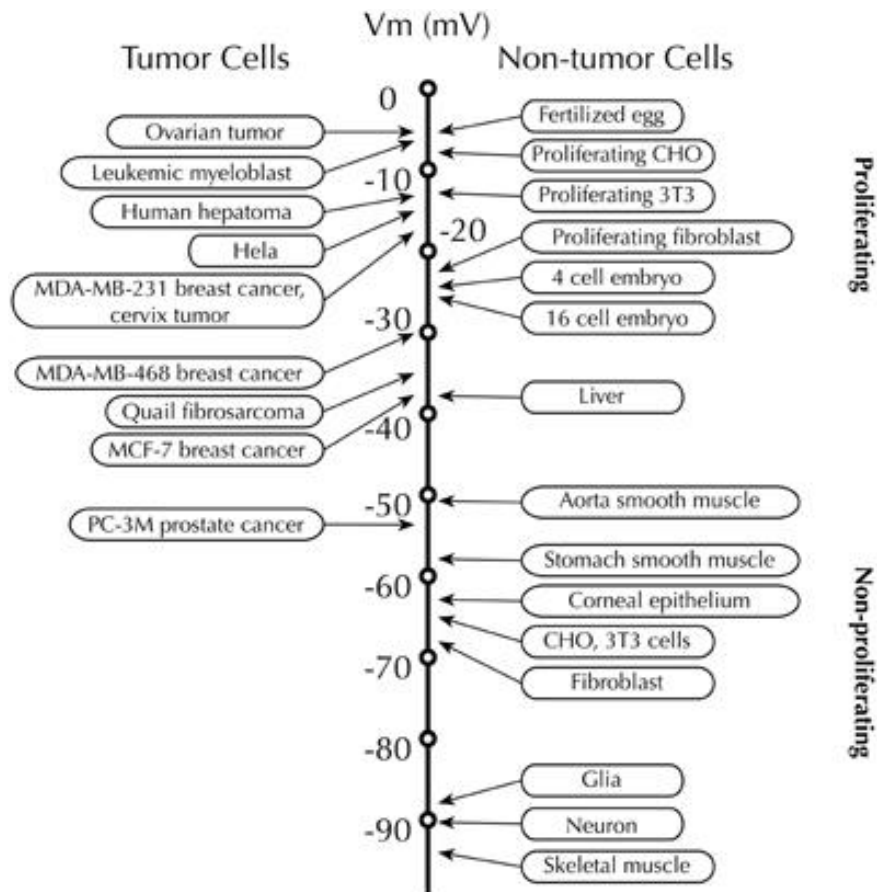


Figure 2.12: Cells membrane potentials scale (Yang and Brackenbury, 2013)

It should be noted that cancer cells not only have a higher resting membrane potential but also the concentration of the ions inside them is different from their normal counterparts. It is reported that the concentration of Na^+ in tumour cells change significantly and is higher than in non-tumour cells and the concentration of K^+ remains relatively constant (Yang and Brackenbury, 2013).

Table 2.5: Comparison of the membrane potentials of normal cells with their sick counterparts

Normal cells	Membrane potential (mV)	Sick cells	Membrane potential (mV)
Buffalo rat hepatocytes (Binggeli and Cameron, 1980)	-37.1 ± 4.3	Morris 7777 hepatoma cells	-19.8 ± 7.1
Mouse corneal fibroblasts (Binggeli and Cameron, 1980)	-42.5 ± 5.4	Mouse fibrosarcoma	-14.3 ± 5.4
Quail embryonic fibroblasts (Binggeli and Weinstein, 1985)	-40.1 ± 8.89	Quail fibrosarcoma (QT-35)	-20.7 ± 5.96

Rat kidney (Binggeli and Weinstein, 1985)	-61.9 ± 8.89	Rat fibrosarcoma	-30.7 ± 7.36
Normal skin cells (Woodrough, Canti and Watson, 1975)	-3	Basal cell carcinoma	+11

Membrane potential of healthy cells alter in the range of -50 mV to -100 mV (Haltiwanger, 2003; Pollack, 2015). As Haltiwanger (2003) reported, a cell has four distinct electrical zones depending on the locations (Figure 2.13). A central zone refers to the centre of a cell including negatively charged molecules and keeps a constant mass negativity. An inner positive zone refers to the space between the innermost of the cell membrane and the negative central zone. This zone consists a thin layer of mobile positive charged ions mostly K^+ and negligibly of Ca^{2+} . An outer positive zone refers to the outermost space on the outside of the cell membrane that contains of condensed mobile positive ions, majority of Na^+ and Ca^{2+} with minority of K^+ . Electrical potential occurs across the cell membrane due to the concentration of the positive charge on the outer surface of a cell is more than interior of the cell. An outermost negative zone refers to the tips of glycoproteins and glycolipids that are covered by negatively charged sialic acid molecules (Figure 2.14). These ubiquitous molecules possess ionized carboxylates at physiological pH. This steady negativity zone gives each cell the net negative membrane potential and each cell forms a negative electrical field around itself (Haltiwanger, 2003; Akagi *et al.*, 2014). A distance approximately 20 μm exists between the outermost negative zone and the outer positive zone.

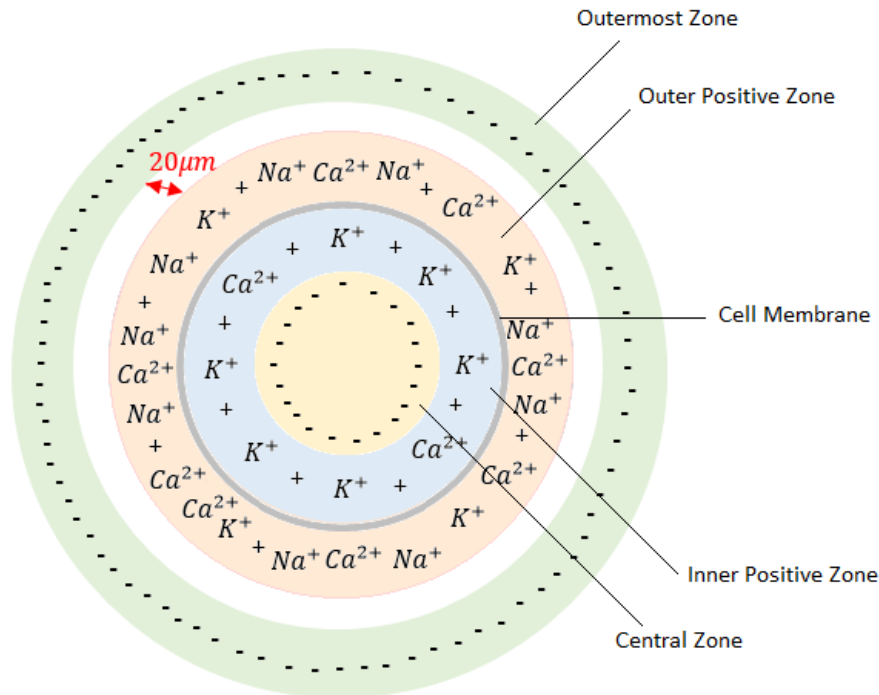


Figure 2.13: Schematic of four electrified zones of a cell including negative central zone, inner positive zone containing dispersed ions, outer positive zone including condensed ions and negative outermost zone

Two important terms; zeta potential and surface charge can be explained relating to cell electrical charges that is different to the trans-membrane potentials. Factors such as number of charged particles on the plasma membrane and the ion channel activity on the cell membrane influences the net electrical potential of the cells. As remained sialic acid molecules possessing negative charge are responsible for the negative electrical field around the cells; any factor causing increment or reduction of this type of molecule leads to the alteration of the level of the cell's negative charge. Zeta potential (ζ -potential) is a term that refers to these negatively charged sialic acid molecules on the outermost zone of a cell (Figure 2.14).

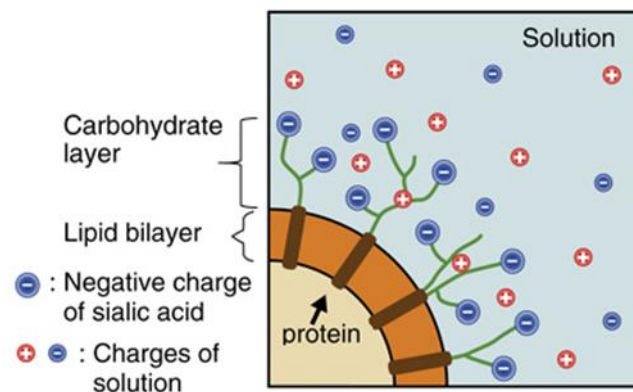


Figure 2.14: Simplified interface of a normal cell and its surrounding (Akagi et al., 2014)

Indeed, all particles that are suspended in a polar fluid possess zeta potential and cells are suspended in polar extracellular fluids. Theoretically, zeta potential is the result of different electrostatic potentials at the boundary of the dispersion fluid and the static layer of medium that is attached to the dispersed particle (Weiner, Tscharnuter and Fairhurst, 1993; particle sciences, 2012). In the other words, total electrical potential that is produced by the area bounded with slipping plane generates zeta potential. Location of the slipping plane has an impact on the magnitude of the zeta potential.

As the particle possesses the negative electrostatic surface charge which can be derived from equation (2.3), it adsorbs the positive charged particles of the polar solution on its outside surface (Mycielska and Djamgoz, 2004). These positive ions make a dense positive cloud which is known as a stern layer.

$$\sigma = \frac{q}{A} \quad (2.3)$$

Where q is the electrical charge (C) on the surface per area A (m^2) and σ is the surface charge density ($C.m^{-2}$). (Pekker and Shneider, 2014) states that the average measured cell's surface charge density is $\sigma_m = 0.3 - 0.002$ ($C.m^{-2}$). Importantly, two factors can change the surface charge of the cells: External EF can shift this charged cloud by influencing the different ions voltage-dependent gates. Also, pathophysiological state of the cell has the potential to alter the surface charge (Mycielska and Djamgoz, 2004).

A shear plane is an imaginary border which separates the stern layer with its external layer. A diffusion layer, which is an external film of the stern layer, is composed mostly of freely mobile positive charged ions and a small number of negative ions. These two layers, stern and diffusion layer, make an electrical double layer and reduce the surface potential of the negatively charged particles. The electric double layer (EDL) is a term that generally consists of two parallel layers containing charged particles surrounding an object which is exposed to a fluid. The first origin of EDL comprises of immobile compressed ions which are absorbed due to chemical attractions and the second area includes freely mobile ions which are attracted via the coulomb force that explains the force of interactions between two static electrically charged particles. A slipping plane is the edge of the diffusion layer with the bulk of solution. The electrostatic potential at the slipping plane is different with electrostatic potentials at the electrical double layer and Stern layer (Figure 2.15). The electrostatic potential is much higher at the surface of the negative particle and by increasing the distance from the bulk of the negative particle through different layers, the electrostatic potential decreases. Therefore:

Surface potential (ψ_o) > Stern potential (ψ_δ) > Zeta potential (ψ_ζ)

While the relationship of their distance from the cell is reversed such that:

$$d_o < d_\delta < d_\zeta$$

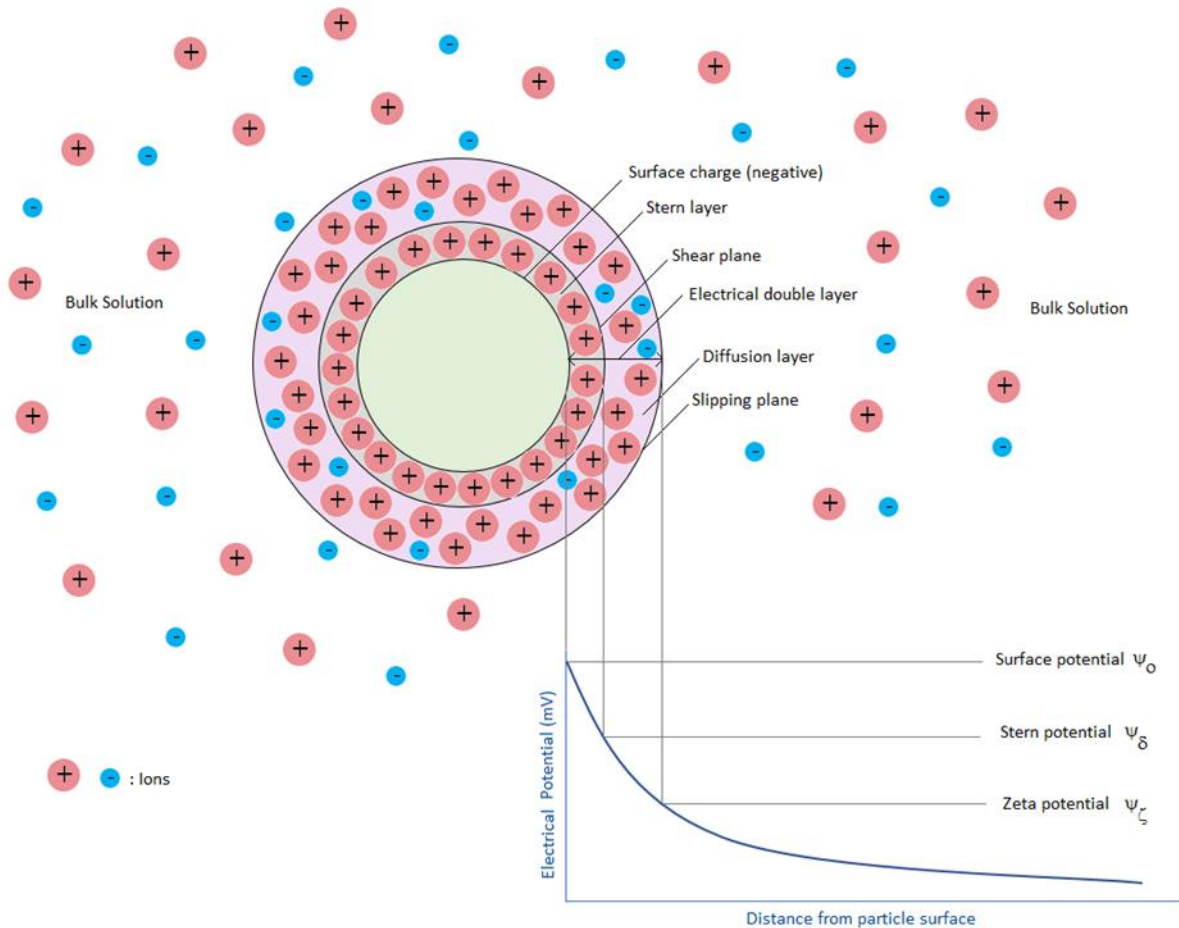


Figure 2.15: Schematic representation of electrical potentials of a cell at the interface with a polar medium

Zeta potential indicates the stability of the colloids. The magnitude of the zeta potential shows nearby similarly charged particles repulsion forces in colloidal fluids and it depends on the ions concentration of the suspension. Higher zeta potential either positive or negative, indicates that the colloids are electrically stabilized because the repulsive forces between similar charged particles are higher than attractive forces and then prohibit the aggregation of non-similar charged particles. Whilst low zeta potential indicates that the colloids are not stabilized and the attractive forces between non-similar charged particles are higher than repulsive forces causing the aggregation of particles and the dispersion may coagulate and become unstable (Table 2.6). For instance, Ayala-Torres *et al.* (2014) reported that *Mycobacterium smegmatis* mc²155 cells have a good stability which its zeta potential amount is -42.9 ± 5.9 mV.

The amount of the zeta potential depends completely on the composition of the suspended polar medium not the physical characteristics of the cells such as shape and size or the nature of the cell itself.

Table 2.6: Presentation of the relation between magnitude of zeta potential and the stability of the colloids (Salopek, Krasic and Filipovic, 1992)

Zeta Potential (mV)	Degree of stability
0 ζ-potential < +3	Maximal agglomeration and precipitation
+5 ζ-potential < -5	Region of strong agglomeration and precipitation
-10 ζ-potential < -15	Beginning of agglomeration
-16 ζ-potential < -30	Beginning of peptization
-31 ζ-potential < -40	Medium stability
-41 ζ-potential < -60	Good stability
-61 ζ-potential < -80	Very good stability
-81 ζ-potential < -100	Extremely good stability

Derjaguin, Landau, Vervy and Overbeek (DLVO) developed a theory that describes the interactions between charged particles through an ionic fluid and the aggregation behaviour of those charged particles. According to DLVO theory, which is about the stability of colloidal systems, the net potential energy (V_T) is the sum of the repulsive electrostatic potential (V_R) and the attractive potential (V_A) due to Van der Waals force ((2.4) and Figure 2.16):

$$V_T = V_R + V_A \quad (2.4)$$

DLVO theory states that if the kinetic energy of the particles does not exceed from the potential energy barrier, then aggregation of the colloids will not happen. The highest point of the potential energy barrier possesses the higher repulsive force than attractive force and the height of the potential energy barrier shows the stability of the system.

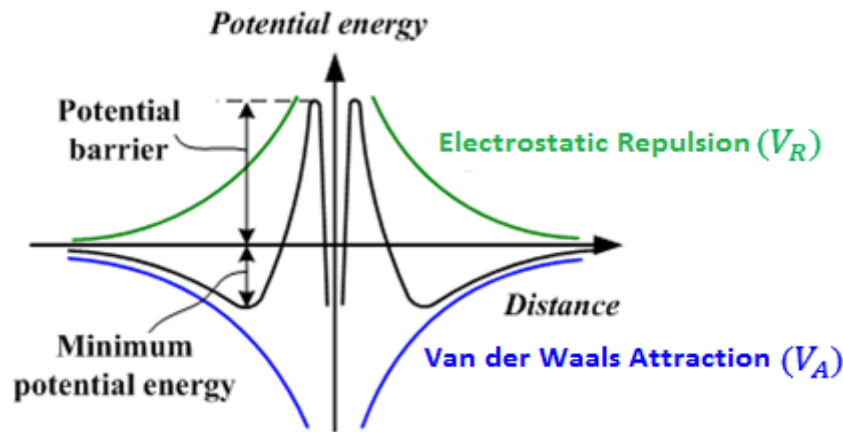


Figure 2.16. Presentation of the energy profiles including Total Potential Energy (black), Electrostatic Repulsion Potential (green), Van der Waals Attraction Potential (blue) (DLVO Theory, 2017)

2.6.3 Electrical Stimulation of cells

Applying an electric field influences the cell in two ways: first, it changes the cells membrane by causing hyperpolarization of the anodal membrane and depolarization of cathodal face of the cell. Changing the cell membrane leads to the modification ion movement across the plasma membrane. The second effect is redistribution of proteins on the surface of the cells via electrophoresis or electro-osmosis (Poo, 1981; Brust-Mascher and Webb, 1998). Protein redistribution of cell's surface is important because of its impact on various cells processes.

Applying appropriate electrical fields on cells which cause the cells migration, do not damage the appearance of cells and their shapes do not change after the electrical simulation and they are still motile (Brust-Mascher and Webb, 1998). Referring to previous reports, different patterns of externally electrical simulation lead to the increase of the intracellular (Ca_i^{2+}) concentration in cells resulting cells in cell migration. It has been detected that different cells can be influenced by different electrical signal simulations. For instance, direct current (DC) and alternative current (AC) in mouse embryo fibroblasts and human hepatoma cells (Dubé *et al.*, 2012) resulted in an increase in the level of intracellular Ca^{2+} . Interestingly, Brust-Mascher and Webb (1998) reported that changes in the intracellular (Ca_i^{2+}) concentration have not been detected in fish keratocytes under the effect of small direct current despite of migration of the cells towards the cathode.

- Steady external electrical fields
- Pulses of external electrical fields
- Alternating external electrical fields

Table 2.6 shows previous researches about migration of cells toward the positive or negative electrodes under different pattern of electrical current.

Table 2.7: Comparison of different types of cells direction, velocity and translocation under applied EF

Cells	Electric field strength (mV/mm)	Type of electrical simulation	Direction	Duration (hours)	Velocity ($\mu\text{m}/\text{min}$)	Translocation (μm)
Human keratinocytes (Nishimura, Isseroff and Nucciteili, 1996)	No EF	DC	Cathode	2	0.47 ± 0.03	63 ± 3
	10				0.40 ± 0.03	58 ± 3
	50				0.60 ± 0.04	79 ± 6
	100				0.90 ± 0.05	125 ± 7
	200				0.63 ± 0.03	89 ± 4
Bovine aortic vascular endothelial cells (Li and Kolega, 2002)	No EF	EF	**	4-8	0.27 ± 0.03	-
	1000		Cathode	0.5	1.75 ± 1.5	-
Human corneal epithelial cells (Zhao, Forrester and McCaig, 1999)	150	DC	Cathode	20	-	Perpendicular orientation most often around 90°
MAT-LyLu rat prostate cancer cells (Djamgoz <i>et al.</i> , 2001)	No EF	DC	Cathode	6	0.95 ± 1.2	40 ± 4.7
	300				1 ± 2.1	141 ± 18
AT-2 rat prostate cancer cells (Djamgoz <i>et al.</i> , 2001)	No EF	DC	Cathode	6	0.86 ± 1.2	37 ± 3.3
	300				0.95 ± 1.4	45 ± 4.6
Human microvascular endothelial cells (Bai <i>et al.</i> , 2004)	200	DC	Cathode	5	0.183	37 ± 3.3
	300					45 ± 4.6
Human bone marrow mesenchymal stem cells (Zhao <i>et al.</i> , 2011)	No EF	DC	Anode	2-10	21 ± 0.5	-
	25				-	-
	200				-	60
	300				42 ± 1	-
Human umbilical vein endothelial cells (Bai <i>et al.</i> , 2004)	200	DC	Anode	5	0.093	-
Human dermal fibroblasts (Guo <i>et al.</i> , 2010)	No EF	EF	*	-	~ 0.26	-
	50		*	5	~ 0.16	-
	≥ 100		Anode	1	~ 0.28	-

	400		Anode	1	~ 0.29	
Murine aorta smooth muscle cells (Bai <i>et al.</i> , 2004)	200	DC	Anode	5	0.053	-
Bovine pulmonary artery fibroblasts (Bai <i>et al.</i> , 2004)	200	DC	Anode	5	0.153	-
Fish epidermal cells (Cooper and Schliwa, 1986)	50-1500	DC	Cathode	0.16 - 0.5	10-30	-
Wistar rat neural stem/progenitor cells (Li <i>et al.</i> , 2008)	50 100 200	DC	Cathode	3	-	-
Rat osteoblasts RCJ 1.20 cell line (Ferrier <i>et al.</i> , 1986)	100 100 1000	EF	Cathode	17.2 17.2 -	1 st : 3.01 ± 0.55 2 nd : 20.3 ± 5.7 5-32	-
Rat osteoblasts RCB 2.2A cell line (Ferrier <i>et al.</i> , 1986)	100 1000	EF	Cathode	6 -	2.7 ± 1.0 5-32	-
Rabbit osteoclasts (Ferrier <i>et al.</i> , 1986)	100 1000	EF	Anode	3.8 1.62	72 ± 13 138 ± 16	-

*: No migration

** : Migration in all directions

It is noteworthy to mention that cells do migrate in all directions even when an external electrical field is not applied on them (Li and Kolega, 2002) but they migrate much slower in the absence of the EF (approximately 60% slower).

Gathering data proved that cells do migrate randomly and without a define destination even when they are not influenced by external electrical fields. Zhao *et al.* (2011) reported that 48% of human mesenchymal stem cells moved erratically towards one side of the dish and the rest migrated to another side of dish.

2.6.4 Summary

Despite remarkable reductions in mortality and morbidity rates after PCI, BMSs are more prone to in-stent restenosis while DESs have higher rates of thrombosis phenomenon. Occurrence of

stent thrombosis, particularly late and very late stent thrombosis in DESs treated patients, is linked to delayed arterial healing due to incomplete endothelial coverage of the stent site, persistent fibrin deposition and continuous vessel wall inflammation, however DESs remarkably reduced the rate of in-stent restenosis by prohibiting neointimal hyperplasia with their drugs. Together, early stent thrombosis happens in BMSs less than 30 days while late and very late stent thrombosis occurs with the high risk especially in first generation of DESs (SES and PES). Notably, second generation of DESs (EES and ZES) reduced the incidence of stent thrombosis.

Chapter 3 Experimental Method

3.1 Introduction

In this chapter, cells maintenance from culturing to freezing is explained step by step in full details. Cultured cell lines are used to measure cell membrane potentials using four different methods consisting of one novel technique “Direct Microelectrode Method” and three established techniques “Di-electrophoresis, Zeta potential measurement and Electrophoresis”. Human cells are used in all four methods to compare and determine the accuracy of the techniques and validation of the new technique. Electrode behavior is also studied to determine the influence of the different solutions on the voltage recording. Moreover, this section includes one of the most significant aim of this project which is “Mimicked Artery Experiment” which its initial results concluded that applying small electrical charges had an impact on cells migration. In this experiment, which is done in different modes, the human blood circulation was mimicked to determine the influence of small electrical charges on cells migration. The overview of this chapter can be seen in Figure 3.1.

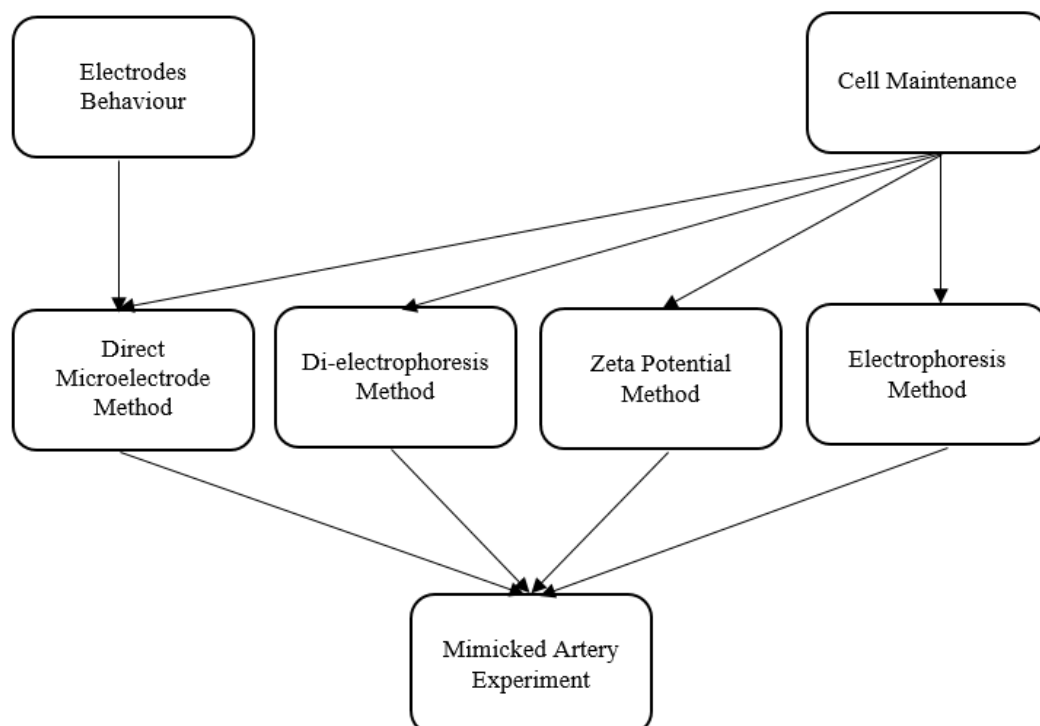


Figure 3.1: Overview and relation of experimental work carried out

Referring to previous literature surveys by other researchers, healthy human cells resting membrane potential were measured by different methods such as patch clamping, electrophoresis method, di-electrophoresis technique, microelectrode and fluorescence detecting (Table 3.1). Human cells resting membrane potential varies in the range of 0 mV to -100 mV for different types of human cells (Yang and Brackenbury, 2013).

Table 3.1: Presentation of various cells resting membrane potentials by using different methods

Cells	Resting membrane potential (mV)	Method
Human umbilical vein endothelial cells (Bregestovski <i>et al.</i> , 1988)	-27 ± 1.4	Whole cell configuration of the patch clamp
Human smooth muscle cells (Nakashima <i>et al.</i> , 1993)	-46.9 ± 0.6	Microelectrode recordings
Frog mesentery endothelial cells (HE and Curry, 1995)	-51.6 ± 4.9	Fluorescence microscopy
Bovine pulmonary artery endothelial cells (Voets, Droogmans and Nilius, 1996)	-26 ± 3	Whole cell configuration of the patch clamp
Bovine aortic endothelial cells (Trivedi, Hallock and Bergethon, 2013)	-32 ± 2	Fluorescent dyes
Glomus cells of the rabbit carotid body (Overholt <i>et al.</i> , 2000)	-48 ± 4	Whole cell current-clamp
Adult Guinea pig coronary endothelial cells (Daut <i>et al.</i> , 1988)	-33 ± 6	Whole cell current-clamp
Endothelium of intact guinea pig (Chen and Cheung, 1992)	-44 ± 0.24	Microelectrode recordings

Guinea pig mesentery smooth muscle cells (Weid and Helden, 1997)	-60.8 ± 1.1	Microelectrode recordings
Guinea pig mesentery endothelial cells (Weid and Helden, 1997)	-71.5 ± 0.5	Microelectrode recordings
Guinea pig endothelial cells (Yamamoto <i>et al.</i> , 2001)	-54 ± 1.8	Whole cell configuration of the patch clamp
Guinea pig smooth muscle cells (Yamamoto <i>et al.</i> , 2001)	-53.8 ± 1.6	Whole cell configuration of the patch clamp
Guinea pig superior mesenteric artery vascular smooth muscle cells (Harder <i>et al.</i> , 1978)	-54 ± 0.6	Microelectrode recordings
Hamster cheek pouch arterioles (Segal and Beny, 1992)	-48 ± 3	Microelectrode recordings (filled by KCl)
Hamster cheek pouch arterioles (Segal and Beny, 1992)	-52 ± 4	Microelectrode recordings (filled by Lucifer Yellow dye)
Porcine coronary artery endothelial cells (Sharma and Davis, 1994)	-42 ± 2	Whole cell current-clamp
Pig coronary artery endothelial cells (von der Weid and Beny, 1992)	-49.7 ± 1.5	Microelectrode recordings
Guinea pig coronary endothelial cells (Mehrke, Pohl and Daut, 1991)	-32 ± 8	Whole cell configuration of the patch clamp
Porcine aortic endothelial cells (Lückhoff <i>et al.</i> , 1990)	-61 ± 4	Whole cell configuration of the patch clamp

Bovine endothelial cells (Laskey <i>et al.</i> , 1990)	-66.8 ± 2.1	Whole cell current-clamp
Rabbit ileum (Rose and Schultz, 1971)	-36 ± 0.5	Microelectrode recordings
Epithelioid (Stefani and Cerejido, 1983)	-40.5 ± 1.5	Microelectrode recordings
Rat duodenum epithelial cells (Okada, Sato and Inouye, 1975)	-53	-
Wistar rat vascular smooth muscle cells (Toro, Gonzalez-Robles and Stefani, 1986)	Artery: -56 ± 5 Vein: -66 ± 3	Whole cell voltage-clamp
Rat aorta smooth muscle cells (Akaike <i>et al.</i> , 1989)	-80	Whole cell voltage-clamp
Endothelium of intact rat aorta (Marchenko and Sage, 1993)	-58 ± 8	Whole cell configuration of the patch clamp
Endothelial cells of small pulmonary artery of rat (Olschewski <i>et al.</i> , 2001)	-70.2 ± 1.5	Patch clamp

There is a strong belief that most of the cells will move towards the electrode with a positive potential because of the attraction force between negative (cells) and positive potentials. However, research showed that cells move towards either cathode or anode depending on the cell activity and the polarization status. Attracting cells by applying the electrical field on them has been commonly used for the treatment of damaged tissues and skin wound (Mycielska and Djamgoz, 2004; Zhao *et al.*, 2012). Electrical stimulation of cells has been known as one of the effective techniques for cells migration towards desired segment (Zhao *et al.*, 2012). The cells lipid membrane carries the electrical charge and the approximate voltage has to be measured to apply an optimum electrical field to affect the cells movement. Determination of the exact

voltage on the surface of the cell has been measured by various methods. Being able to select a matched cell voltage has the potential to be selective in the choice of cell that could be influenced by an applied electrical field and the more accurate the method, the more exact voltage can be gained. One issue that may influence recording of the exact voltage of cells is electrode behavior. Using metal microprobes for cell voltage measurements in a liquid, can lead to galvanic activity due to ion donation, demonstrated by minor or major differences in voltage recordings. This is particularly relevant at the millivolt ranges that cells operate at.

Coronary artery stents are commonly used for the treatment of occluded or narrowed arterial conduits instead of “stand alone” balloon angioplasty. Remarkable improvements in stent technologies have led to significant reductions in complications after stent deployment. However, stent thrombosis/restenosis still remains a main concern after stent deployment (Garg and Serruys, 2010; Watanabe *et al.*, 2018; Wang *et al.*, 2018).

As there is a link between number of coronary artery endothelial cells and stent thrombosis incidence (Wang *et al.*, 2018), attraction of human endothelial cells to the implanted stent is the target interest of this investigation. Using a synthetic process to induce a natural, therapeutic process has the potential to reduce short- or long-term stent failure. Thus, the exact human coronary artery endothelial cell voltage is needed to affect migration of vascular endothelial cells. Once the exact human endothelial cell membrane potential is obtained, an appropriate electrical potential will be applied to human endothelial cells to cause specific endothelial cells migration towards the surface of the stent, generating a layer of cells with inherent anti-thrombotic properties that leads to less formation of blood clotting. For the purposes of determining the experimental conditions for each experimental type, human osteoblasts were used to characterise cells as an analogue to the more sensitive human coronary endothelial cells. In addition, the experimental use of osteoblasts should be considered as a means to validate the unique methods used in this investigation.

3.2 Electrodes Experiment

A simple voltaic cell is produced when two electrodes are inserted into a conducting solution known as an electrolyte. Released ions from an anode move towards a cathode through the electrolyte. This transportation results in formation of current (Figure 3.2).

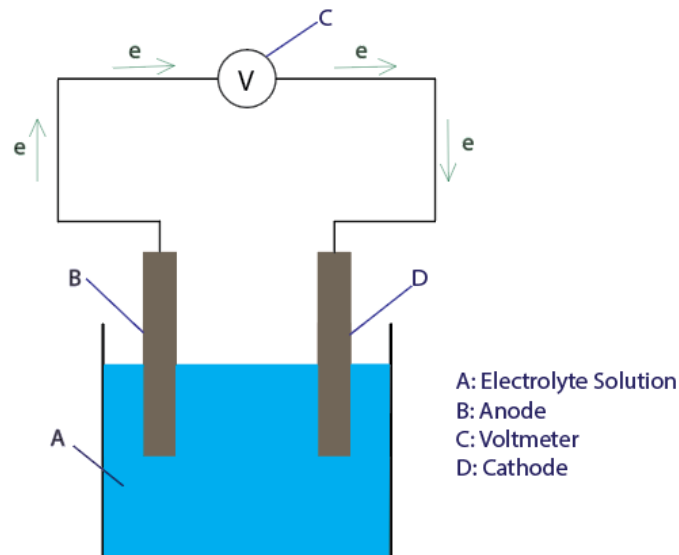


Figure 3.2: Simple Voltaic Cell using Adobe Illustrator

Different factors such as temperature, velocity and the nature of the fluid influence the potential of the electrodes (National Physical Laboratory, 2017). The chosen metal plates in this series of the experiments are commercially pure titanium and stainless steel alloy-grade 304. The electrochemical potential of some alloys in seawater are documented in Figure 3.3. However, the potentials of the electrodes will vary in different solutions. It is well known that several types of stainless steel corrode in water and its corrosion degree will be changed depending on the purity of water.

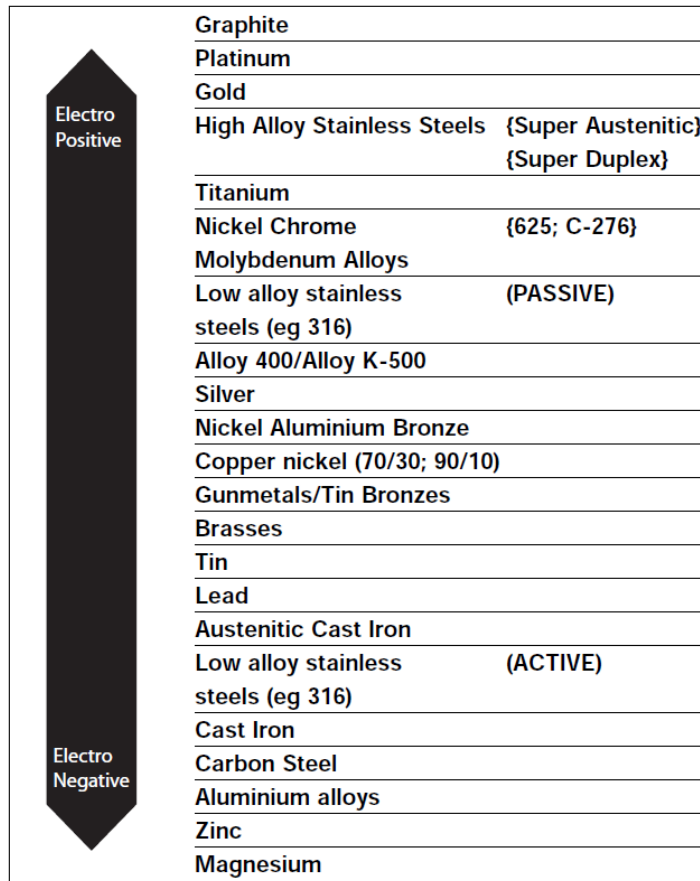
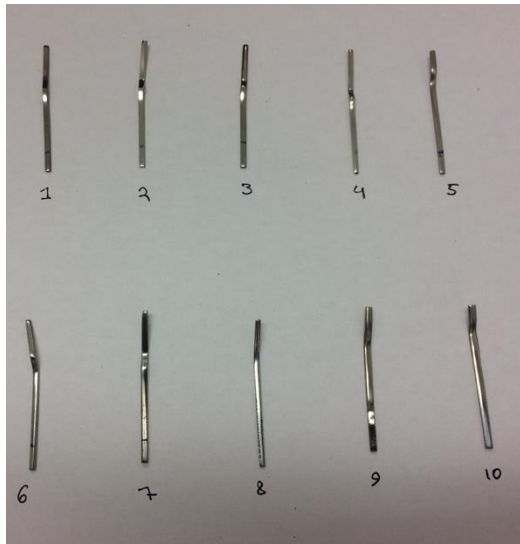


Figure 3.3: Electrochemical potentials of various metals in sea water (National Physical Laboratory, 2017)

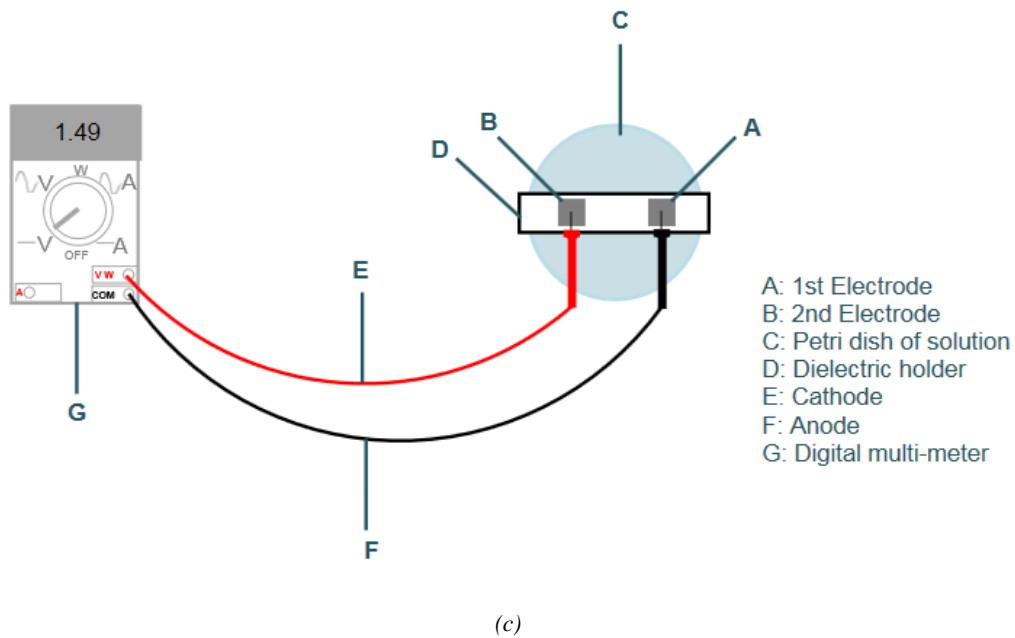
As can be seen Figure 3.3, both stainless steel and titanium are some of the highest electropositive metals.

These series of experiments were performed to show the effect of passivation layers from solutions on the electrodes, on voltage recording over a specific time. Each experiment included a glass petri dish, two 304 grade stainless steel (42.10 mm× 1.84 mm) and 99.8% pure titanium electrodes (42.28 mm × 1.61 mm), a dielectric (insulator) holder, different solutions and a digital multi-meter. The experiment set-up and electrodes can be seen in Figure 3.4.



(a)

(b)



(c)

Figure 3.4: Stainless steel and titanium electrodes (a), the picture of the experiment (b) and schematic diagram of the experiment (c)

In this method, one end of two electrodes, which were fixed in the dielectric holder, inserted into 40 ml of liquid that filled the petri dish. The other ends of the electrodes were connected to the digital multi-meter to record the voltage measurements (Figure 3.4: a). Each experiment lasted for 8 minutes in which voltage and resistance were recorded each 30 seconds. These experiments were performed in a different range of time (see below). In each experiment, a pair of electrodes, one stainless steel and one titanium were tested in different solutions. In

these series of experiments; one pair of electrodes were not tested with any solution to use as a controlled pair and each pair was dedicated to an individual solution that were:

- Deionized water
- Distilled water
- Tap water
- 0.9% Saline

All of the experiments were repeated three times for consistency. All equipment was washed with ethanol and all experiments were performed at room temperature. To determine the impact of the passivation layers on the electrodes, it was needed to analyse the electrodes surfaces. Thus, each electrode was examined in four conditions including:

- After the experiment
- One day after the experiment
- One week after the experiment
- Two weeks after the experiment

To assure that in each test, the same area of the electrodes would be examined, a datum point was marked on each electrode.

Scanning Electron Microscopy (SEM) Analysis

After each experiment, the electrodes were observed in the SEM to examine topographical changes on the surface of the electrodes. The electrodes mounted on a multi-pin stub holder and placed in a Carl Zeiss Supra 35VP SEM.

Atomic Force Microscopic (AFM)

All electrodes were examined in the atomic force microscopic (Digital Instrumentals) after the experiments to observe local properties and surface changes of the electrodes.

Results including graphs and tables are presented in the next chapter.

3.3 Cell Maintenance

3.3.1 Cell Lines

The 2nd passage adherent adult Human Osteoblast cells (HOb) (406-05A SIGMA) and Human Coronary Artery Endothelial Cells (HCAEC) (300-05A SIGMA) were obtained from SIGMA-ALDRICH (United Kingdom). The biological source of both types of cells were normal bone and coronary artery from human, respectively.

3.3.2 Cell Culture

Both types of cells in cryo-vials were stored in a liquid nitrogen vapor storage tank at a temperature of -80°C until use. On the day of culturing, vials were thawed in a 37°C water bath for 3-5 minutes until the cells were thawed. The cells were re-suspended in the vials by gently pipetting the cells 5 times with a 2 ml pipette. Then, 1 ml of the cell suspension from the vial was pipetted to a T-25 flask containing 15 ml of desired cell growth medium. The flask was agitated gently to distribute the cells evenly. HOb cell-lines and HCAEC were maintained in Human Osteoblast Growth medium (417-500 SIGMA) and MesoEndo Cell Growth medium (212-500 SIGMA) (SIGMA-ALDRICH, UK), respectively. Cells were grown as a monolayer in T-25 flasks (Sarstedt) and 100 mm tissue culture dishes (Sarstedt) for approximately two days prior to use and placed in an incubator at a temperature of 37°C and humidified atmosphere containing 5% CO₂. The cells were checked microscopically every day to ensure they grew as expected and the cells medium were changed every day to remove dead cells and nourish alive ones until the cells reach confluency of 60%. Because both types of cells were adherent, they attached to the bottom of the flasks after culturing and those cells were floating recognized as dead. Doubling time of human osteoblast cells was reported around 38.1 hours (abm, 2017). Human coronary artery endothelial cells doubling time were stated around 15-48 hours (Lonza, 2017). Cells culturing was performed under sterile conditions using class II biological safety cabinet with a vertical laminar flow hood.

3.3.3 Cell Trypsinisation

Both osteoblast cells and human coronary artery endothelial cells were adherent and attached to the bottom of the culture flasks. They were grown as a monolayer at the bottom of the flasks. A glass Pasteur pipette was used to suck the old medium in the flask. Then, the cells were

washed with 10 ml Dulbecco's calcium and magnesium free phosphate buffered saline (PBS) (Gibco, UK). Next, the PBS was aspirated and 1-2 ml Trypsin-EDTA solution (Gibco, UK) was added to the flask. Trypsin is an enzyme that breaks down the proteins causing the cells to adhere the surface and EDTA (Ethylenediaminetetraacetic Acid) interrupts proteins adherence mechanism. Combination of these two substances causes the detachment of cells from the surface of the flask. The flask was placed in the incubator at 5% CO₂ humidified air at 37°C for a duration of 5-10 minutes. After 5 minutes, the flask was checked using an inverted microscope every 2 minutes to ensure if most cells were detached or not. Then 5 ml of the fresh growth medium was added to the flask and the medium containing suspended cells was transferred to either a 15 ml falcon conical centrifuge tube (Sarstedt) for further actions or a specially made electrophoresis instrument for the experiment.

3.3.4 Cell Counting

Cell counting was performed with a hemocytometer (BRAND[®] counting chamber BLAUBRAND[®] Neubauer improved) (BR717805-1EA ALDRICH) (SIGMA-ALDRICH, UK) (Figure 3.5: a). For cell counting, first the cell lines were trypsinised and incubated in 5% CO₂ at 37°C about 5-10 minutes. Once the cells detached, they pelleted in 10 ml media. 10 µl of the cell suspension was loaded onto a glass hemocytometer and cell counting was completed.

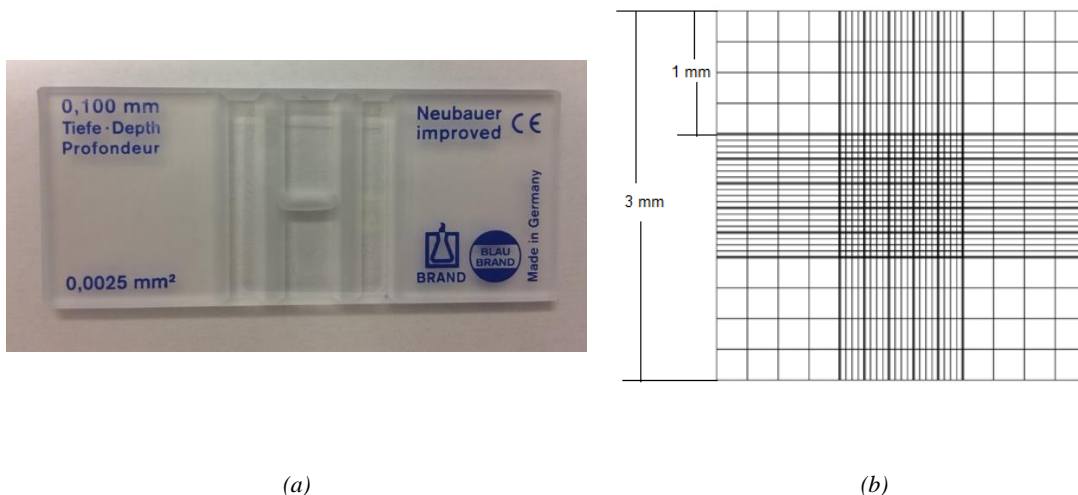


Figure 3.5: A hemocytometer chamber (a) and counting grid detail on the glass of each chamber (b)

Hemocytometer contains two chambers: upper chamber and lower chamber and one counting grid is set on the glass of each chamber. The grid which is 3 mm × 3 mm in size, has 9 large square subdivisions of width 1 mm (Figure 3.5: b). Depending on the cells size, the counting

can be done in either the central square or the four large squares in the corner. There are two square glass coverslips which are placed on the top of chambers. These coverslips make a space about 0.1 mm between the bottom of the chamber and the coverslip itself (Louis and Siegel,2011). Considering each large corner square with the area of 1 mm², then the volume will be:

$$1 \times 1 \times 0.1 = 0.1 \text{ mm}^3 = 10^{-4} \text{ ml}$$

In counting the cells, each cell inside the square and those that are over the top and right sides of the square were counted.

Average cell number (N) = Total number of cells in 4 squares / 4

So, the concentration of the sample is: $N \times 10^4$ (cell/ml)

Therefore, considering the concentration of the dilution factor (f), the concentration of whole flask is: $N \times 10^4 \times f$ (cell/ml)

3.3.5 Cell Subculture

As described, the cell lines were cultured as a monolayer in T-25 flasks. The growth medium was replaced routinely. After the cells reached the confluency of 80%, the subculture stage started. To passage the cells, the old media was removed and the cells were washed with 10 ml PBS. After aspiration of the PBS, the cells incubated in trypsin-EDTA at 37°C in 5% CO₂ humidified air atmosphere. After detaching most of the cells, 5 ml fresh media was added. Then the media with re-suspended cells was transferred into a 15 ml falcon conical centrifuge tube. Then, the tube was centrifuged at 1500 rpm for the duration of 5 minutes. Then, the media was aspirated. The cells were then re-suspended in 1 ml fresh media. A 1µm pipette was used to move up and down the media containing cells to break cells pellet and distribute the cells evenly in whole 1 ml media. After preparation of the flasks, 1 ml media containing suspended cells could be divided into several flasks or petri dishes. After division of cells between the flasks that were capped, the flasks were moved side by side to spread the cells evenly. Then, the flasks incubated at 37°C in 5% CO₂ humidified air until they reached the acceptable confluency.

3.3.6 Cell Freezing

Because of the restricted number of passages of the cells; 10 and 15 times for HOb cell-lines and HCAEC respectively, it was needed to freeze some cells to stock for further experiments.

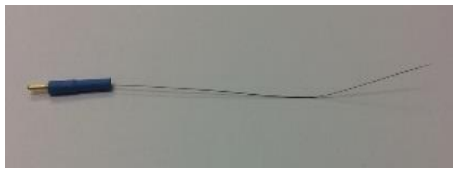
Cryo-vials were labeled first. The old media of 70-80% confluency T-25 flask of cells was removed. Cells were washed with 10 ml PBS. 1 ml trypsin-EDTA were added to the flask after aspiration of PBS. The cells incubated for 2-4 minutes. After detaching the cells from the bottom of the dish, 3 ml was added of fresh media to the flask and was transferred to the 15 ml falcon conical centrifuge tube to centrifuge at 1500 rpm about 5 minutes. After the cells pelleted, the medium was aspirated. Cells were re-suspended in 1 ml freezing medium (FM) which is made of 9 ml fetal bovine serum (FBS) and 1 ml dimethyl sulfoxide (DMSO). Pipetting up and down the cells with a 1 μ m pipette at least for 10 times. Then, the FM containing cells can be divided and transferred into pre-labeled cryo-vials. The cryo-vials containing cells must keep in temperature of -80 °C.

3.4 Cells' Experiments

This section containing two main parts; first experiments are methods exploring the cell membrane electrical potential and the second experiment is mimic human blood circulation to determine the patterns and number of migrating of endothelial cells. Three methods that were used for the measurement of the resting membrane potential of cells described as be heeded: 1-Direct Microelectrode Method, 2-Di-electrophoresis Method (DEP method), 3-Electrophoresis Method.

3.4.1 Direct Microelectrode Method

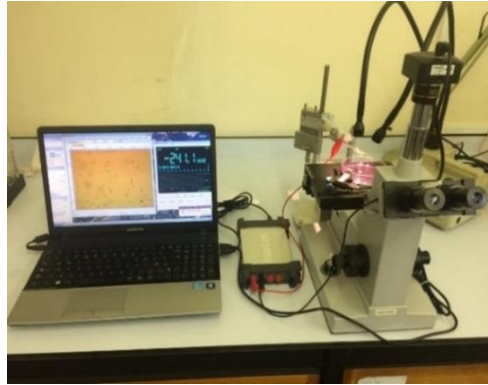
This new method was chosen as the main technique for measuring cell membrane potential to progress the main aim of this project. Both human endothelial cells and osteoblast cells measurement were done using this method. This technique was based on a very common simple electrical circuit which included the human cells (as the electric source), the cells growth medium, a 100 mm tissue culture dish (Sarstedt) of human cells, two electrodes; a tungsten microelectrode (with a tip diameter 1 μ m) (TM31A10, World Precision Instruments, Inc.) (Figure 3.6: a) and a strip of 99.8% pure titanium (50.44 mm \times 11.30 mm) (Figure 3.6: b), a conductive solution which was cell growth medium containing ions, a multi-axis micro-manipulator developed for the experiment, an inverted photo microscopy instrument (FMA050, AmScope) and a digital data logger recorder (Hantek365B, Qingdao Hantek Electronic Co., Ltd). All equipment was washed with Ethanol to remove any contamination prior to the experiment. The experimental set-up and schematic diagram of the experiments are shown in Figure 3.6: c, Figure 3.7 and Figure 3.8, respectively.



(a)



(b)



(c)

Figure 3.6: The tungsten microelectrode (a), the titanium strip (b) and the picture of the experiment (c)

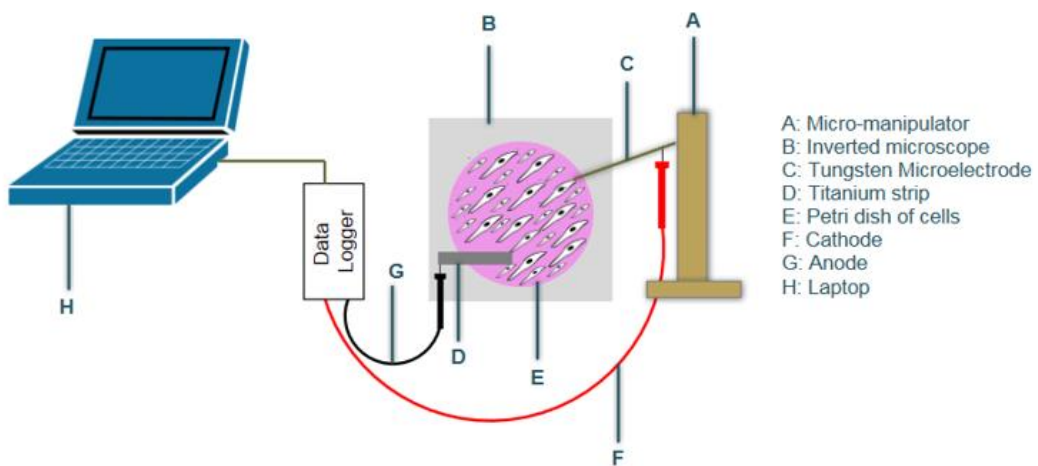


Figure 3.7: Schematic diagram of the experiment when the petri dish was fully cultured with cells

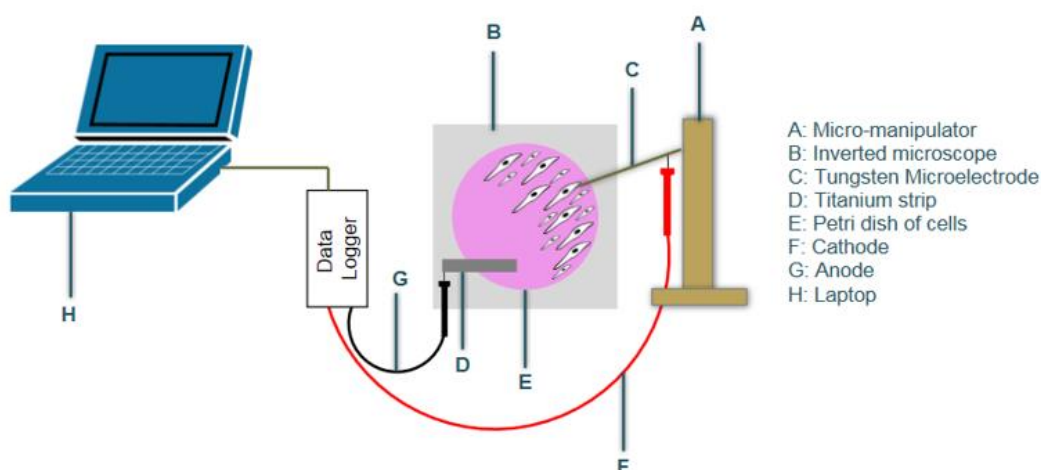


Figure 3.8: Schematic diagram of the experiment when the petri dish was half cultured of cells

In this method, the tungsten microelectrode acted as a cathode and the titanium strip, immersed in the medium, worked as an anode. The different potential between these two different metals caused ion migration, resulting in an electrical activity in the liquid which was known as the medium voltage. Released ions from the anode moved towards the cathode. The two electrodes were then connected to the digital data logger recorder to record a gained voltage. The very fine microelectrode with a tip of 1 μm was moved by the micro-manipulator for the fine movements to touch the outer surface of a cell. Precise movements were essential for the microelectrode because it's very fine tip vibrated sharply if the movements were coarse and so the sharp vibrations of the tip could cause rupture of the cell membrane. During the experiment the microelectrode was moved toward several cells to record their voltages. Using the micro-manipulator gave fine control of the microelectrode's tip. The titanium strip was placed in the petri dish of cells carefully. Noteworthy to mention, cells that were used in these experiments were cultured in two different models, some cells were cultured evenly in the whole petri dishes surfaces while in the other models the cells were cultured only in one side of the petri dishes and after 2-3 hours cell growth medium was added to the petri dishes to cover the whole surface of the petri dishes. The petri dish of cells was positioned on the inverted microscope which was connected to a lap top using AmScope software. Therefore, pictures and videos of the cell's movements could be captured by using the AmScope software. The magnifications of $\times 80$, $\times 200$, $\times 500$ and $\times 800$ were available to observe the cells and save their images. After adjusting desired magnification for cell observation, the tip of the microelectrode was inserted into the solution and touched on the cells and then the recorded voltage was shown on the

digital data logger recorder. The digital data logger recorder was set to record the voltage each 10 seconds for a duration of 15 minutes. Each petri dish of cells was examined 3 times. The experiment was done in the 25°C environment. Data of the digital data logger recorder were exported to Microsoft excel.

Results including graphs and tables are presented in the next chapter.

3.4.2 Measurement of Cell Growth Medium Voltage Behaviour

The aim of this experiment was to prove the results from human cells voltage measurement. Indeed, voltage behavior of cell growth medium could be used as a reference for the results and graphs that were concluded from human cells experiment. The experimental set-up and schematic diagram of the experiment are shown in Figure 3.9 and Figure 3.10.

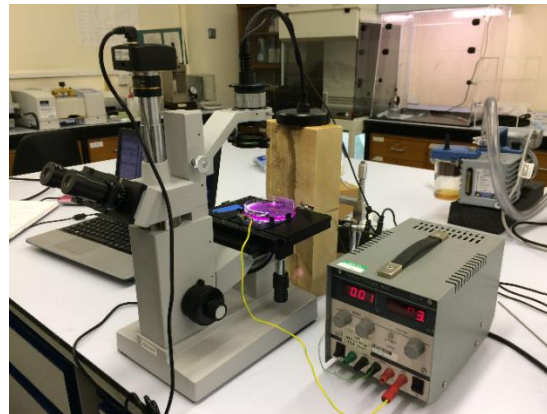


Figure 3.9: The picture of the experiment

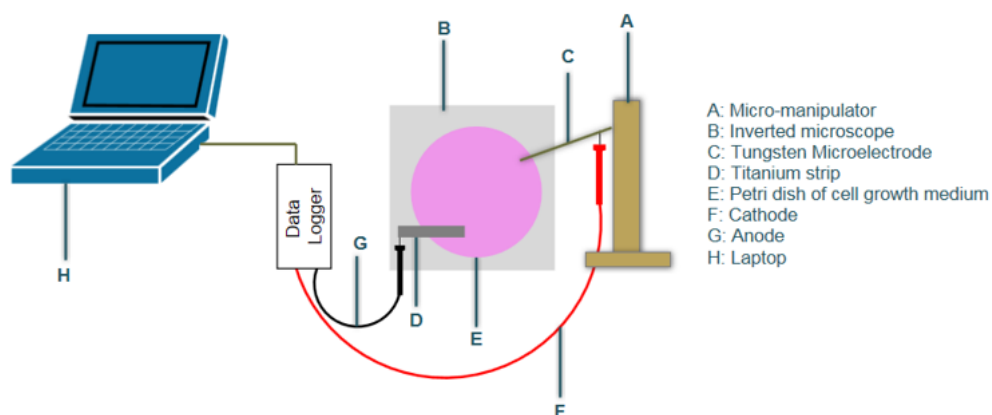


Figure 3.10: Schematic diagram of the experiment

This experiment included a 100 mm tissue culture dish (Sarstedt), 40 ml cell growth medium (either Human Osteoblast Growth medium or MesoEndo Cell Growth medium), two electrodes; a tungsten microelectrode (with a tip diameter 1 μ m) (TM31A10, World Precision Instruments, Inc.), a strip of titanium (50.44 mm \times 11.30 mm), a multi-axis micro-manipulator, an inverted microscope and a digital data logger recorder (Hantek365B, Qingdao Hantek Electronic Co., Ltd). All equipment was washed with Ethanol to remove any contamination prior to the experiment.

40 ml cell growth medium was poured inside the 100 mm tissue culture dish. Then, the titanium strip electrode was placed in the petri dish, submerged under the growth media. The tungsten microelectrode that was placed on the micromanipulator and inserted into the petri dish. As soon as the tungsten microelectrode was inserted into the solution, an electrical connection happened and the digital data logger recorder showed the voltage of the solution. The digital data logger recorder was set to record the voltage each 10 seconds for a total of 10 minutes. Recording of the digital data logger were exported to Microsoft excel shown in the next chapter. The experiments were done at a temperature of 25°C.

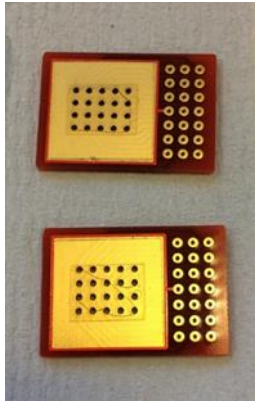
3.4.3 Di-electrophoresis Method

3D Di-electrophoresis method is a non-invasive cell analysis technique that analyses simultaneously thousands of charged particle's movements under the impact of a non-uniform applied electric fields at different frequencies and moreover determines the cells electrical properties (Broche *et al.*, 2011; Ismail *et al.*, 2015; DEP technology, 2017). Due to electrical properties of particles, they can move in different directions because the level and direction of force is dependent on frequency. Positive DEP is when cells move towards regions of high electric field, whereas negative DEP is repulsion from high electric field (Hoettges *et al.*, 2008; Broche *et al.*, 2011; Ismail *et al.*, 2015). The distance of movement can differ in a range from micrometres to millimetres (Broche *et al.*, 2011). Cells needs to be in monodispersed suspension for analysing via 3DEP (Mahabadi, Labeed and Hughes, 2015). The technique is used to measure the electric properties of cells instead of other expensive methods (Broche *et al.*, 2011).

In this system, the cells are inserted into disposables chips that are placed in the DEP reader. Each chip has 20 wells (each well is 1 mm in both height and diameter) containing a number of electrodes. 20000 cells can be analysed in 10 seconds as each electrode in each well receives a different frequency signal. The range of the frequency of the signal can be choose between 1 kHz to 45 MHz (DEP technology, 2017). Once the frequencies are applied to the wells, depending on the cells types, they may repel or be attracted to the electrodes. Positive DEP is the term when a cell attracts to the electrodes and moves from the centre of the well to the edge of it. On the other hand, if a cell repels from the electrodes, it travels to the centre of the wells.

These experiments were done in University of Surrey with help from Professor Michael P. Hughes and Dr. Fatima H. Labeed. To prepare the cells for DEP experiments, the cells were washed with PBS after sucking the old media from the flask. Once the cells become detached from the flask, after adding trypsin-EDTA and incubating the flask, 5 ml cell growth media was added to the flask to transfer the cells to a 15 ml falcon conical centrifuge tube to centrifuge. Once the media was aspirated, 4-6 ml DEP solution was added to cells for the 2nd time centrifuge at 2000 rpm for a duration of 2 minutes. DEP solution is an isotonic medium which is a combination of 8.5% sucrose and 0.3% dextrose buffer with low conductivity of 10 mS/m adjusted with PBS (Mahabadi, Labeed and Hughes, 2015). After the 2nd centrifugation, the DEP buffer was aspirated. Then, for the last time the cells were washed again with 4-6 ml DEP solution and centrifuged at 2000 rpm for the duration of 2 minutes. Once the centrifuging of cells was finished, the cells were re-suspended in 1 ml of media and transferred to a micro-centrifuge tube. After checking the viability of the suspension cells using a hemocytometer method, cells were analyzed by putting inside a DEPtech 3D Dielectrophoresis reader (DEPtech, Uckfield, UK) (Figure 3.11: b) through disposable chips with 20 parallel wells (Figure 3.11: a). Cells were analyzed simultaneously as each well received different frequency signals and the procedure had to be repeated several times. Data were analyzed using MATLAB to determine the single and mean of cells properties.

Results and graphs are presented in the next chapter.



(a)



(b)

Figure 3.11: Disposable chips for 3DEP reader (a) and 3DEP reader (b)

3.4.4 Zeta potential Method

As described before in the literature review chapter, ζ -potential is the term to describe the electrokinetic potential in colloid systems. Theoretically, the zeta potential is the electrostatic potential difference between the mobile phase of the dispersion medium and the static layer of medium that is attached to the dispersed particle (Bhattacharjee, 2016). Zeta potential's magnitude gives the information that a system will have a short- or long-term stability of emulsions.

In this technique, cells are inserted into a disposable folded capillary cell (DTS1070, MALVERN instruments, Great Britain) in order to place it in ZetaSizer Nano series (MALVERN instruments, Great Britain) (Figure 3.12). Each cell contains two gold-plated electrodes, in contact with the liquid during the measurement. ZetaSizer Nano series are used for different purposes including measurement of particle and molecular size, zeta potential and molecular weight measurements (Malvern Panalytical Ltd, 2018). The measurements were performed via Laser Doppler Micro-electrophoresis at 25°C. When the cells move under applied electric fields, the zeta potential related to the velocity of cell movement is measured.



Figure 3.12: Zeta potential cuvette

These experiments were performed in University of Surrey with help from Professor Michael P. Hughes and Dr. Fatima H. Labeed. In preparation of the cells for zeta potential measurements, firstly the cells were washed with PBS after removing the old media from the flask. After adding trypsin-EDTA and incubating the cells for couple of minutes resulting in detachment of the cells, 5 ml cell growth media was added to the flask to transfer the cells to a 15 ml falcon conical centrifuge tube to centrifuge. After centrifuging the cells and suspending cells in a micro-centrifuge tube, they were transferred to a folded capillary cell using a micropipette. After injecting the suspended cells until the marked line on the folded capillary cell, the cell should be capped by two stoppers per cell. There should not be any bubbles in the cell. If there is even tiny bubbles in the liquid either gently tap the sides of the cell or suck the liquid and refill the cell to remove the bubbles. After filling the cell, those two gold electrodes of the cell should be immersed in the injected liquid. Next, the cell is placed in ZetaSizer Nano series instrument to record the measurement.

Results and graphs are presented in the next chapter.

3.4.5 Electrophoresis Method

Electrophoresis method is the most common choice for separation of charged molecules based on their size. Using this method, when a charged particle disperses in a media, an absorbed electric double layer, which contains both same and opposite charges, develops on the surface of the particle. When an electrical field is applied on the charged particles, the relevant particles are then attracted to the oppositely polarised electrode (Bhattacharjee, 2016) (Figure 3.13).

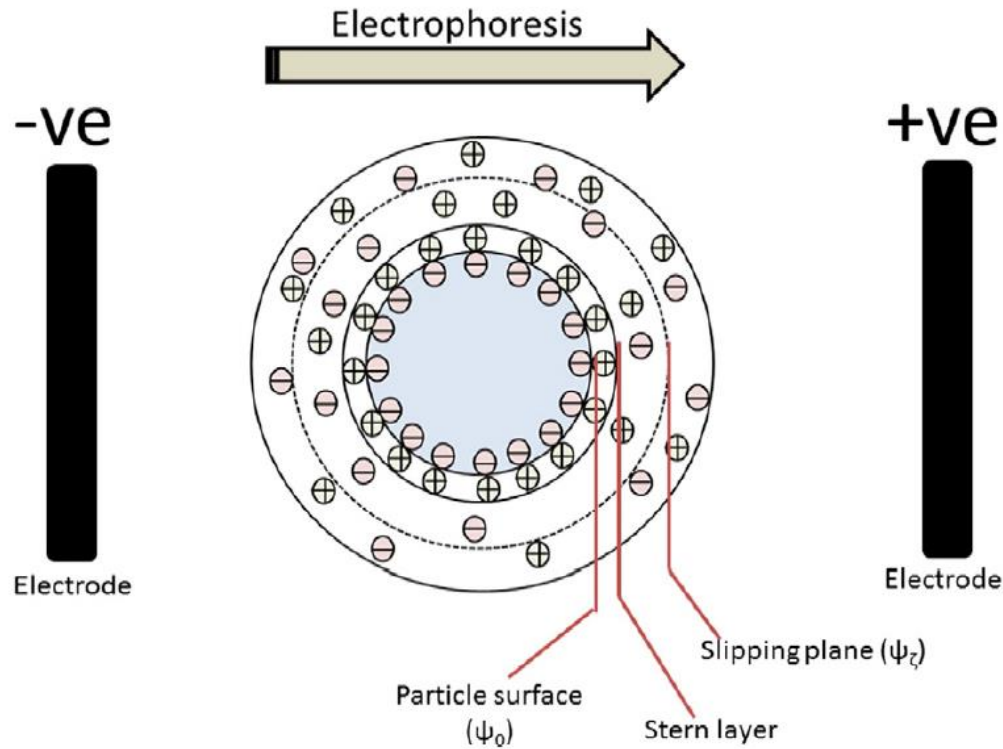


Figure 3.13: Schematic presentation of the electrokinetic potential of a dispersed particle (Bhattacharjee, 2016)

In most cases, this method consists of a standard chamber containing an agar gel, or liquid media and two electrodes (positive/negative) which are connected to an electrophoresis power supply.

Commonly, the first step in this technique was preparation of the agar gel by dissolving 37 g Luria Broth agar (LB) (MILLER) for microbiology (Merck, Germany) in 1 liter of demineralized water in a beaker. According to instructions on the LB agar container, the agar should be dissolved in demineralized water in an autoclave at 121°C for a period of 15 minutes. A microwave method is one of the preferred methods for making an agar gel. After adding the weighed LB agar to the demineralized water in a 250 ml beaker, the beaker is covered by a plastic wrap. A small hole is pierced on the plastic wrap for ventilation. Then the combination of agar and water is placed in the microwave oven on high power for heating. After the mixture comes to the boil, it is removed and swirled to check whether the agar is completely dissolved. After dissolving the agar, it is poured into the custom chamber to set. As both electrodes in the solution have contacts with the gel, a current passes through the gel causing the cells movements. Although this method is used as the common electrophoresis method for molecules, proteins and DNA, the electrophoresis method that was used in my project was

slightly altered by using cells rather than DNA or proteins. The experimental setup schematic is shown in Figure 3.14.

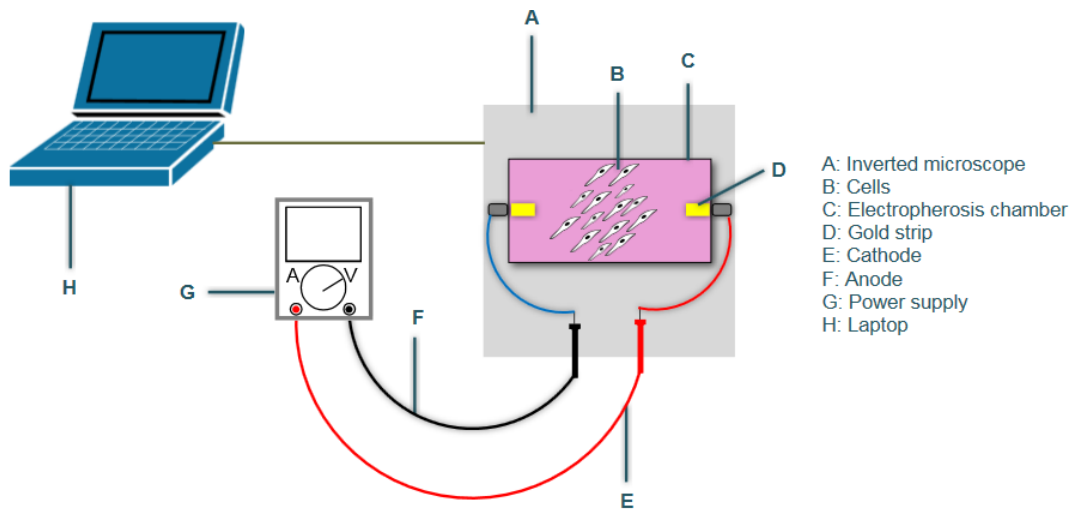


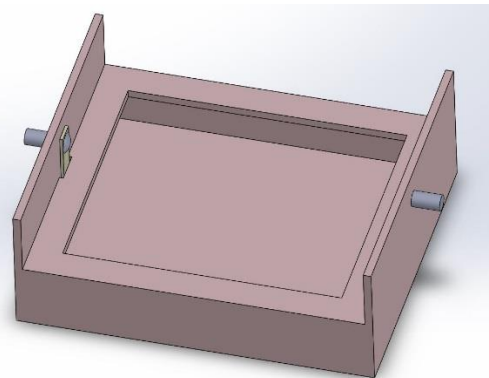
Figure 3.14: Schematic of the electrophoresis experiment

The following equipment was used in this experiment: human cells, a custom designed acrylic chamber, a power source and an inverted microscope.

The electrophoresis chamber includes two micro foil strips of gold metal which are screwed on both sides of the chamber. Each strip of gold is passed through a hole and has contact with the bottom of the chamber. Two red and blue wires were connected to each screw from one end while the other ends were connected to the power supply. The electrophoresis chamber and its design using SolidWorks can be seen in Figure 3.15 and Figure 3.16, respectively.



(a)



(b)

Figure 3.15: The electrophoresis chamber (a) and technical drawing of the electrophoresis chamber using SolidWorks (b)

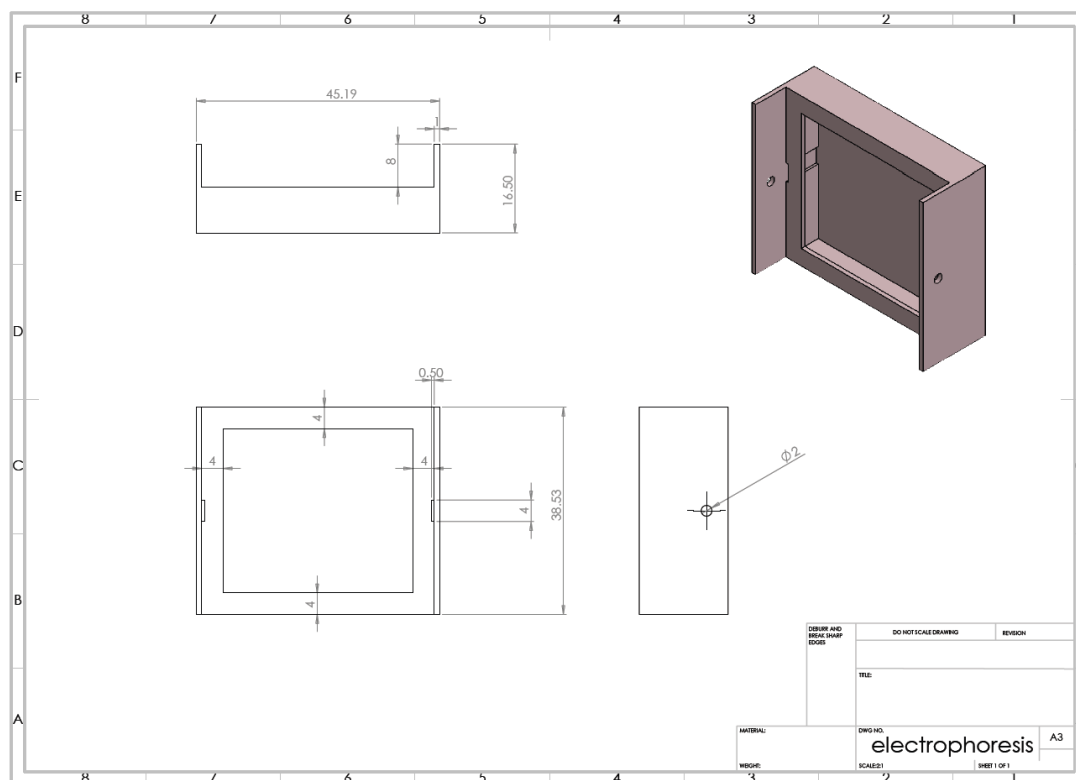


Figure 3.16: Technical drawing of electrophoresis chamber using SolidWorks. Dimensions are in mm.

The electrophoresis chamber was dipped in a beaker of ethanol 99.99% two times, each time ~15 minutes. Once it was cleaned with ethanol, it was placed under U.V. light of a vertical laminar flow cabinet PV-30/70 Telstar overnight to sterilize the chamber completely. The following day, human cells were cultured directly in the chamber. Noteworthy to mention is that in culturing the cells on the chamber, only 1 μ l of suspension of cells in the media was transferred to the centre of the chamber. The reason behind this is to give an equal chance for the cells to move freely towards either positive or negative electrode under application of current. Therefore, depending on the origin of the cells and strength of the electrical field, cells could migrate either to the positive or negative side. After 2 hours that the cells were completely adhered to the surface of the chamber, extra cell media was added to the chamber and placed in the incubator overnight. Once the chamber reached a confluency of 80%, it was taken out from the incubator and set on the inverted microscope. The chamber was placed on the inverted microscope to allow observation of cell migration. In the structure of the chamber each of the connected gold strips acted as a + or - electrode. As both electrodes had contacts with the media, the current passed through the media caused the cells to attract to either the positive or negative electrode. The chamber was connected to the power source through red and blue wires connecting to the positive and negative terminal, respectively. The power supply was adjusted

to different range of DC voltages: 30, 100, 200, 300, 400, 1000, 2000, 3000 millivolts and different range of pulsed DC voltages: 400, 1000, 1500, 2000, 3000 millivolts (Table 3.2). Once the power supply was turned on, the electrical current was applied to the cells. The experiments were run in different range of time from 15 minutes to 20 hours. The cells movements and orientation were observed and recorded by AmScope, microscope camera. All equipment was washed with Ethanol before the experiment to avoid any contamination. Results and graphs are presented in the next chapter.

Table 3.2: Explanation of various conditions of electrophoresis experiments

Type of Current	Strength of Electrical Field (mV)	Duration
Straight DC	30, 100, 200, 300, 400, 500, 1000, 2000, 3000	15 minutes
	30, 400, 1000	20 hours

3.4.6 Mimicked Artery Experiment

This experiment was very important for the project as it forms a pivotal part of this thesis. Indeed, a similar experiment was done previously in another study, which had proved the impact of the small electrical charges on the cells' movement. The initial evidence showed that specific electrical waveforms applied to electrically conductive materials, immersed in blood, was able to migrate specific cells onto an oppositely polarised electrode. The experimental set-up schematic is shown in Figure 3.17. This experimental setup was initiated by establishing and confirming that all parameters, such as temperature, pressure and frequency were suitable for a bio-mimic, in vitro experiment. Subsequent to the confirmation of the experimental parameters, the main experiment was undertaken using sheep blood and run two times under different conditions. Finally, in the post-experiment stage, the examined samples were observed with a scanning electron microscopy (SEM) to determine the endothelial cells' migration behaviour. This section includes three parts: pre-experiment, experiment and post-experiment.

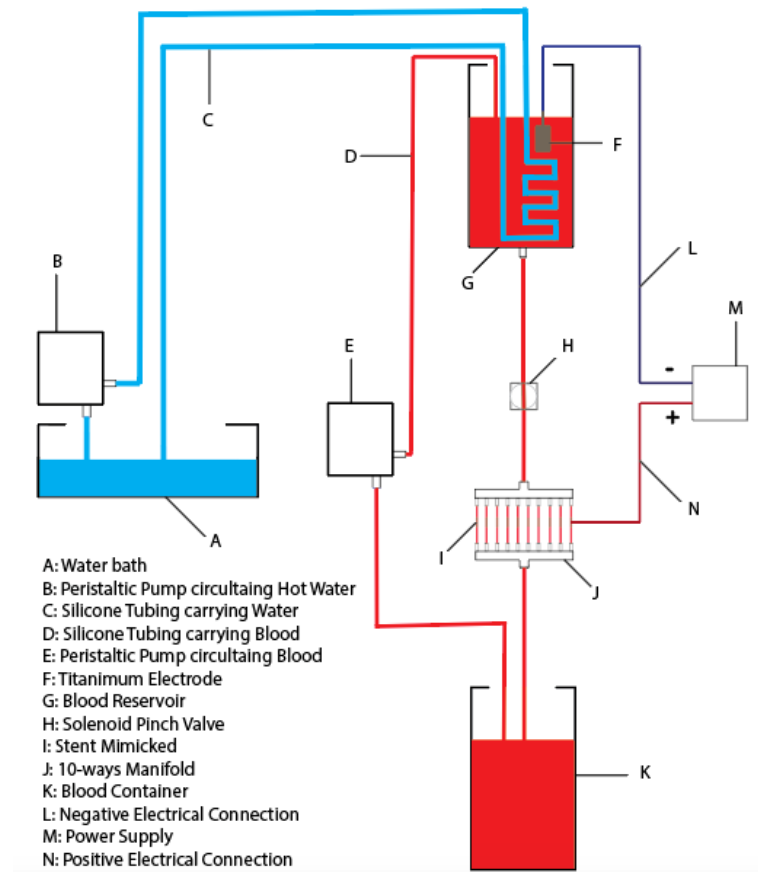


Figure 3.17: Schematic of final experimental set-up using Adobe Illustrator CC

The following items were used in the experiments: silicon tubes with 3.2 mm, 6 mm, 8 mm in diameter and 10 m, 10 m and 5 m in length, respectively (T3.2X1.6ST60, T6X1.5ST60, T8X2.ST60, silicon tubing, Polymax), 2 litre of sheep defibrinated blood (SBO55, Sheep Defibrinated Blood 500ml, TCS Biosciences LTD.), two peristaltic pumps, three power supply units, a laboratory water bath (Griffin & George Ltd), a Fixkit digital manometer with ranges ± 13.79 kPa (type TL-G1, Maplin), two, 10-ways plastic manifolds, a 1.5 litre cylindrical reservoir, a blood container, a solenoid pinch valve (series SS15 type Z230A, Sirai), a rotary switch driven by a DC motor, 12V regulated linear RS power supply unit, to control pulse frequency, three standard laboratory low voltage DC power supplies and a medical grade, high pressure oxygen cylinder with pressure regulator and metal stents. This experiment was composed of several individual parts which will be explained in the following sections.

Preparation of Metal Stents Tubes

Stent mimicks were designed as shown in Figure 3.18. The stent body was made from commercially available, 316LM stainless steel (medical grade) metal tube (Coopers Needle Works Ltd.). The stent were made from the stock material made 3 mm and 20 mm in diameter and length, respectively: the wall thickness of the tube was 0.1 mm. These dimension were chosen to approximate the size of a modern coronary artery stent. As it was planned to open the stents after the experiments in order to observe microscopically, their inner surfaces, axial slits, 0.304 mm wide, were machined along their entire length, so as not to damage the inner surface of the stent while opening the tube-like geometry to form flat areas and giving visual access to biologically relevant areas.

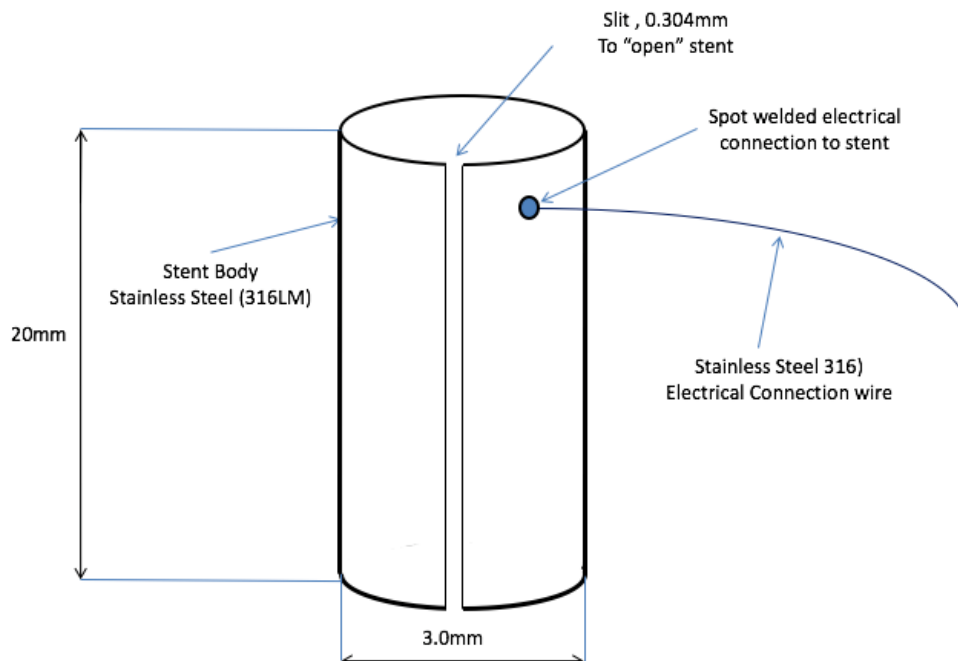


Figure 3.18: Technical drawing of a mimicked stent with a welded wire attached

Firstly, the main bulk stainless steel 316LM tube was cut into small pieces of length 20 mm using a surface grinder machine (Figure 3.19: a) with a thin abrasive slitting disk. Once the stents of 20 mm length were prepared (Figure 3.19: b), a centre grinder machine was used to make a fine cut for the stents in order to smooth the edge of the stents. Then, a slit with 0.304 mm width was made by a horizontal milling machine to enable the stent to be opened easily after the experiment. Then, the stents were inserted into a rotary abrasive polishing machine in which the abrasive went into inside and outside the stents in order to normalize and polish the surfaces.



(a)



(b)

Figure 3.19: Cutting stents in 20 mm length using a surface grinder machine (a) and final stents before welding wires to them (b)

After the stents appearance and surfaces were observed to be uniform, they were washed in ethyl alcohol and allowed to dry. Stainless steel 316L wire was then cut into small lengths of approximately 15 cm to weld onto the body of the stent. A micro spot welding machine was used to connect the wire to stent and affect a good electrical connection (Figure 3.20: a). As both wires and stents were small, it was difficult to weld the wires. This and the need for precise welding of the wires on predetermined spots led to fabrication of a custom handmade stent and wire holder device designed to hold the stents during the welding process (Figure 3.20: b). The custom device has an acrylic base with one side cut out for stent insertion. At its centre, the base has an attached metal rod holding the wire firmly in place. Once the stent and wire were placed on the custom device, the whole assembly was set under the welding machine.



(a)



(b)

Figure 3.20: Welding machine (a) and the custom device for using welding wires on the stents (b)

The final mimicked stents can be seen in Figure 3.21.

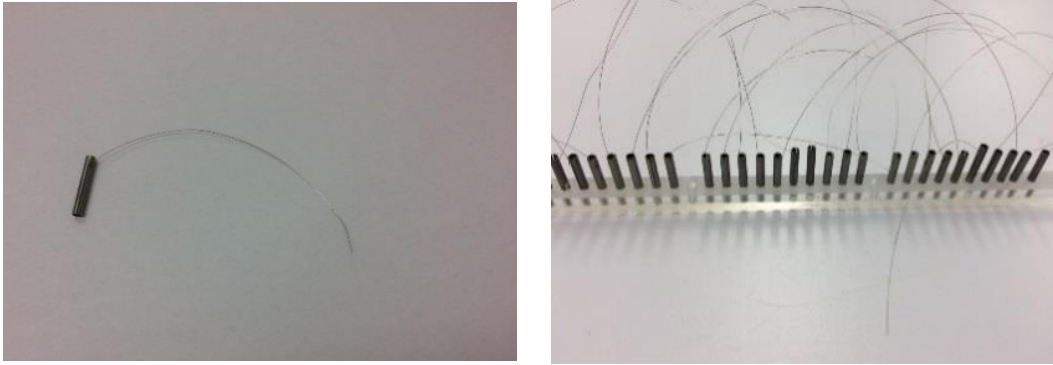
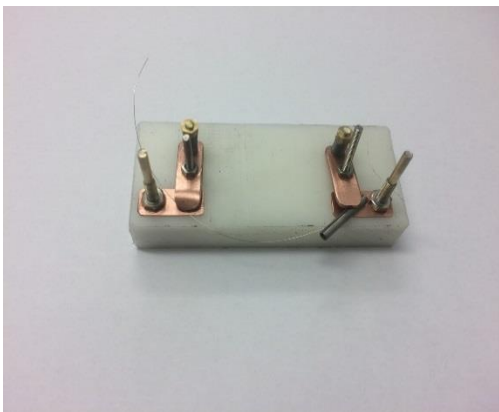


Figure 3.21: The final designed stents

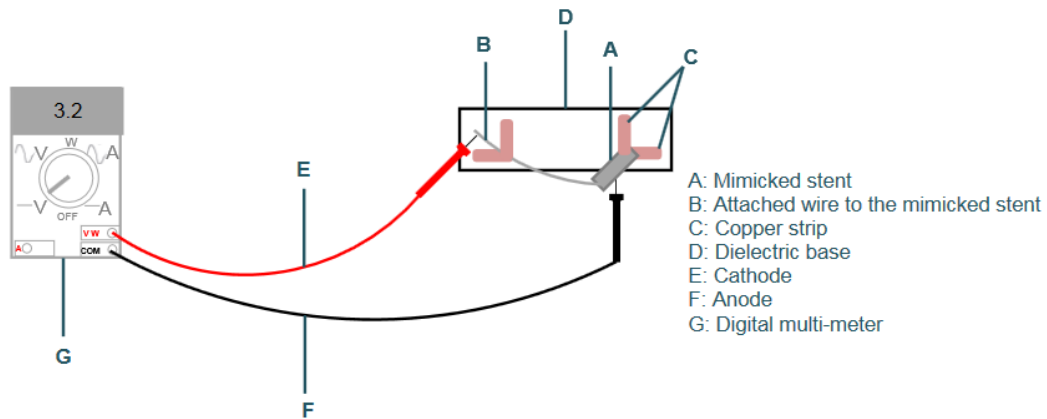
After welding the wires on the stents, resistance measurements were done to check for proper connection between the body of the stents and the welded wires. It was assumed if there was a poor connection between the wires and the stents, then the resistance would be high which would lead to inaccurate voltages on the stents. For this, a custom handmade stent and its attached wire gripper was made (Figure 3.22: a). The custom device was composed of an electrically insulating Delrin (acetyl co-polymer) base due its high resistance with two copper strips screwed on perpendicularly on each side. The top copper strips can be raised to insert the stent and its attached wire on each side. For the resistance measurements, the connections of the digital multi-meter were connected to each screw on each side as shown in Figure 3.22: b, c.



(a)



(b)



(c)

Figure 3.22: The custom handmade stent and its attached wire gripper device (a), measurement of the resistance of the stent and its attached wire (b) and technical concept of the measurement (c)

The results of the resistance measurements can be seen in Table 3.3 and the corresponding Figure 3.23. The first three experiments were performed using ten mimicked stents, while the last two experiments were done using five stents.

Table 3.3: Records of resistance measurement of stents

1 st group	Resistance (Ω)	2 nd group	Resistance (Ω)	3 rd group	Resistance (Ω)	4 th group	Resistance (Ω)	5 th group	Resistance (Ω)
1	2.9	11	4	21	6.4	31	6.2	36	4.4
2	2.8	12	4.3	22	4.9	32	5	37	5.7
3	3.2	13	4.5	23	5.1	33	6.6	38	4.8
4	2.8	14	4.7	24	4.6	34	5	39	4.5
5	2.9	15	4.1	25	6.4	35	6.9	40	4.4
6	3.7	16	3.5	26	5.1				
7	2.8	17	4.9	27	6.3				
8	2.7	18	3.9	28	6.4				
9	3.1	19	4.2	29	6.8				
10	2.4	20	3.5	30	6.6				

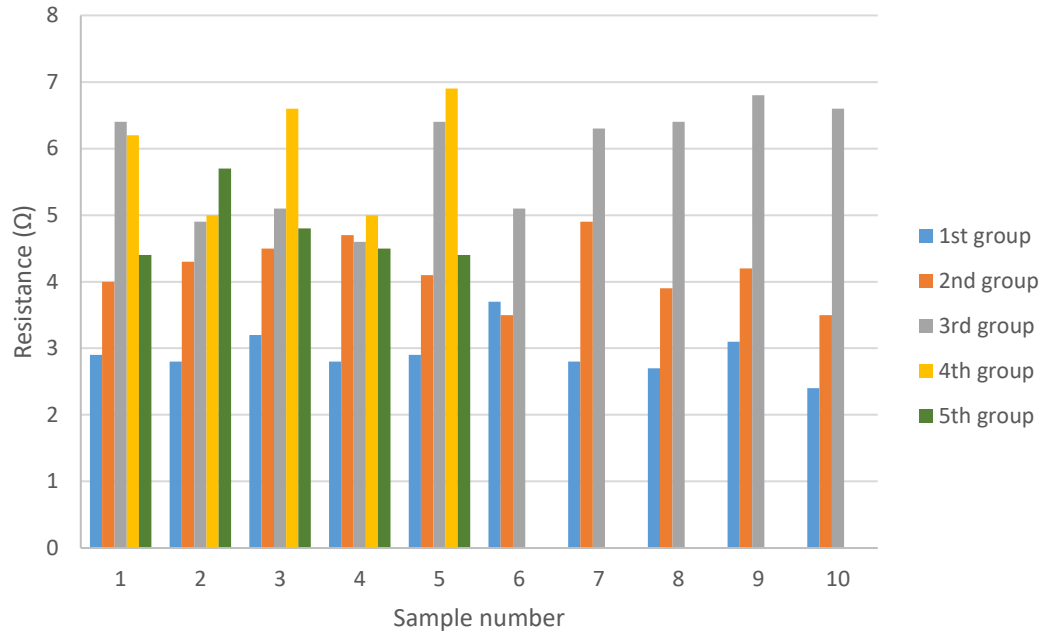


Figure 3.23: Comparison of Resistance measurements of series stents

After examination of the stents, they were washed in 99.99% Ethanol twice (Figure 3.24: a). Once they completely dried, they were inserted into the silicon tubes with 3.2 mm and 92 mm in diameter and length (Figure 3.24: b). After placement of the stents in silicon tubes, they were sterilised by autoclaving using a Prior autoclave system at 121°C for duration of 15 minutes. Then, the stents inside tubes became ready for the experiments. Each experiment required ten stents.

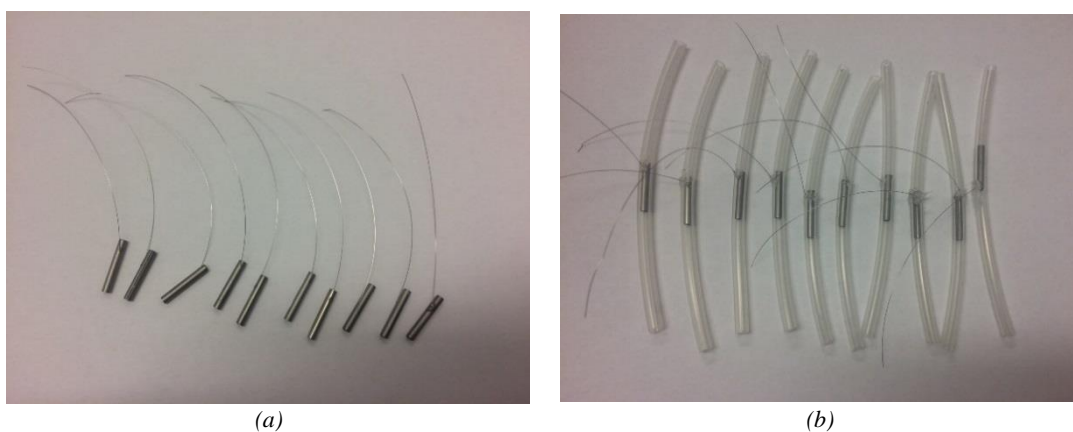
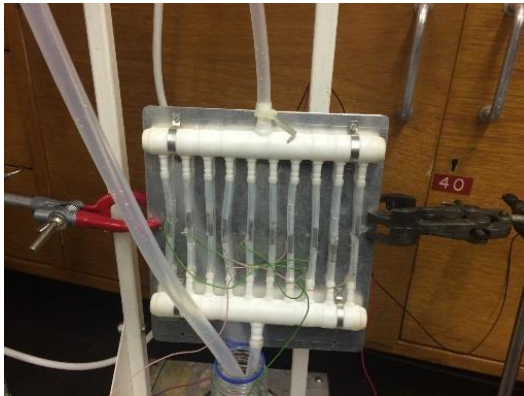


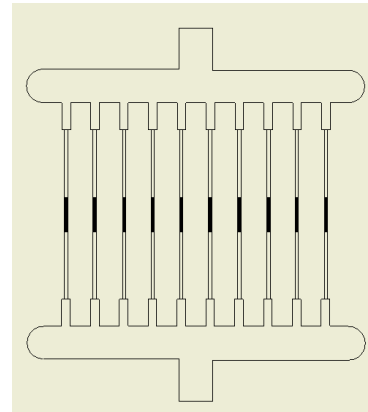
Figure 3.24: Final stents before inserting in silicon tubes (a) and after inserting in silicon tubes (b)

Electrical Connection of Mimicked Stents

In each experiment, ten sterilised mimicked stents within the artery mimicked were placed between two manifolds (Figure 3.25: a). Two manifolds were screwed on an aluminium plate. A power supply used to provide the required small electrical charges for the stents. Electrical connections occurred when coloured wires made a connection between the attached wires of the stents and the power supply as the positive pole.



(a)



(b)

Figure 3.25: Experiment picture of electrical connections to mimicked arteries within mimicked stents (a) and technical drawing of the manifold within stents using Autodesk Inventor Professional (b)

The electrical connections to the mimicked stents were mixed and not in order. As supposed two central outputs of the upper manifold had more intensity and maybe the blood flow rate was different depending the position of the outputs, therefore the connections were not in order. Three out of ten stents were control (no electrical connection), the other three were connected to 27 mV and the rest were connected to 1000 mV (Table 3.4). It must be noted that the level of voltages were the same in all experiments no matter DC or pulsed DC was applied.

Table 3.4: Explanation of the magnitude of small electrical charges to stents

Stents Numbers	Voltage (mV)	Wire colour in experiments
1, 2, 5, 8	1000	Green
3, 6, 9	0	No wire
4, 7, 10	27	Pink

The essential electrical supplies were provided differently for experiments:

- Electrical circuit for DC

As it was planned to test two different voltages simultaneously, an electrical circuit was used containing two potentiometers and one fixed resistor (Figure 3.26). The positive 1 V input from a power supply unit (model LA100, Coultant linear power supply unit single channel) became into two branches; one directly connected to the four stents providing 1 V output (green wires) and in another branch two potentiometers were adjusted and the fixed resistors acted as a dropping resistor network to provide output voltage about 27 mV (pink wires) for three stents. A straight connection providing -1 V went to the blood reservoir directly.

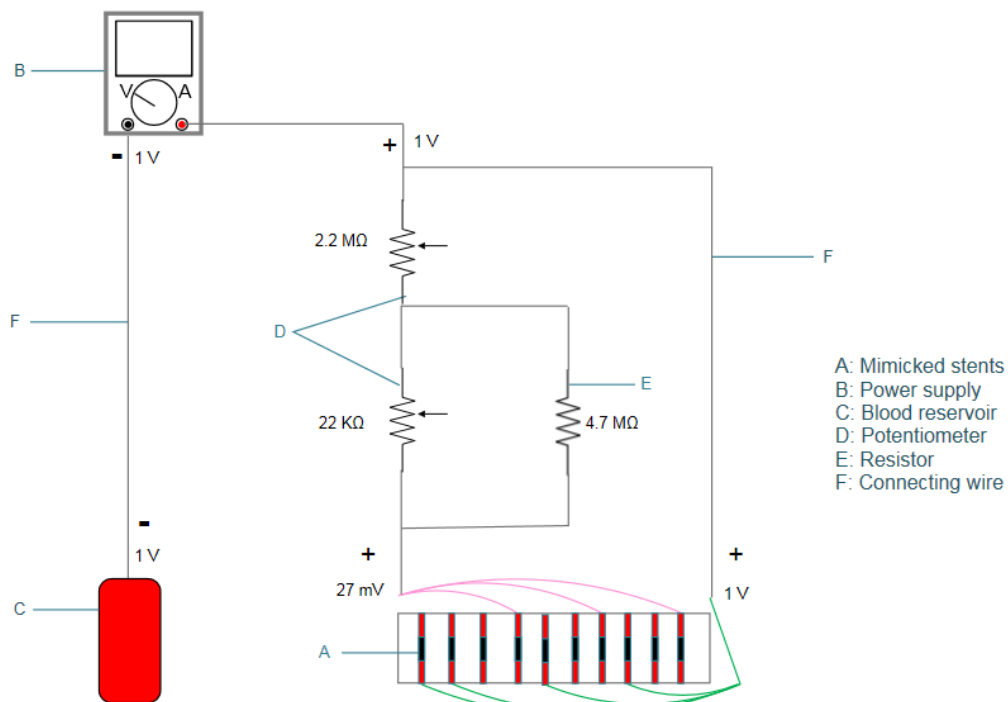


Figure 3.26: Electrical circuit used for providing small electrical charges for the experiments

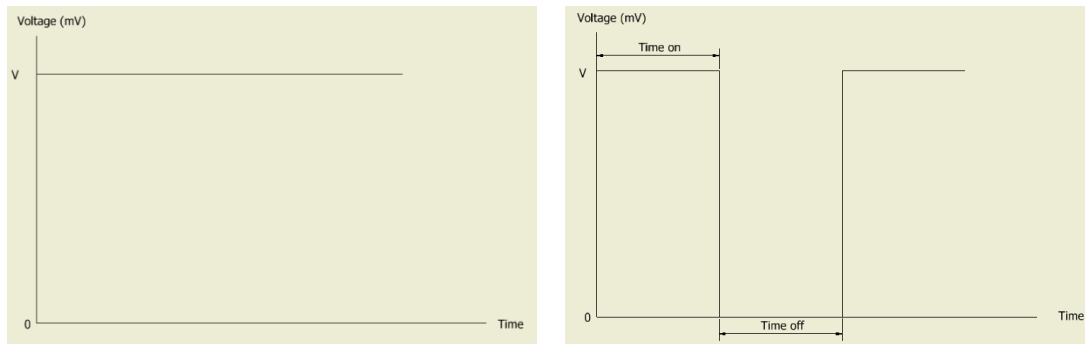
- Precision power supply and oscillator for pulsed DC

For experiment which needed pulsed DC, a professional precision power supply and oscillator was used which could be manually operated to produce square wave signals for the experiment (Figure 3.27).



Figure 3.27: A professional precision power supply and oscillator

The patterns of the electrical signals over time for both DC and pulsed DC can be seen in Figure 3.28.



(a) Direct current

(b) Pulsed direct current

Figure 3.28: Representation of visual differences between DC and pulsed DC using Autodesk Inventor Professional

Imitated Human Arteries

Medical grade (platinum cured) silicon tubing in different diameters became of choice for simulation of human arteries and were used to connect components of the loop to each other. The silicon tubing was chosen due as a blood interface material because: first, they comply with FDA guidelines for use *in-vivo* and *in-vitro* medical applications. Secondly, they were translucent which showed blood circulation perfectly and even there were any occlusion causing a stop in the blood flow, it could be seen easily and quickly to solve the problem. Thirdly, they have good thermal insulation properties and are able to perform through a wide temperature range from -40°C to 200°C with minimum heat loss or gain. Fourthly, they were flexible and could be sufficiently flexed to connect all the components of the experiment to

each other. They have enough elasticity to use in a solenoid pinch valve to turn liquid flow on or off with a desirable pulsatile profile (Polymax, 2016).

Sterilisation of the Experimental Set-up

All procedures containing living organisms have potential for infections and cross-contamination. Thus, washing all surfaces of the equipment of the experiments was done using 99.99% ethanol as a surface sterilisation technique. However, FDA has not established any mix of ethanol as a high-level disinfectant, it is fungicidal, virucidal below 50% concentration in solutions and bactericidal in concentration of 60% - 90% solutions (Rutala, Weber and the Healthcare Infection Control Practices Advisory Committee (HICPAC), 2008). As ethanol does not possess sporicidal action, another sterilisation is needed to complete sterilisation process.

To avoid any contamination including microorganisms which directly influence the results of the experiments, using a disinfectant has become the choice as an active agent against microorganisms. After initiating and testing functionality of each system, all component parts were sterilised using 30% hydrogen peroxide (diluted with H₂O) solution as a liquid sterilant: this is listed as one of the high-level disinfectants by FDA (Rutala, Weber and the Healthcare Infection Control Practices Advisory Committee (HICPAC), 2008; U.S. Food & Drug Administration, 2016). The sterilization solution mix of 500 ml hydrogen peroxide (H₂O₂) (hydrogen peroxide 30% stabilised Ph. Eur., VWR chemicals, UK) with 500 ml deionized water was circulated through the blood circulatory system for duration of 5 minutes. According to U.S. Food & Drug Administration (2016), hydrogen peroxide is established as one of the sterilisation method for medical devices. Depending on both time of exposure and concentration of hydrogen peroxide, it is can be used to inactivate microorganisms and acts as sporicidal, mycobactericidal, fungicidal, virucidal and bactericidal (Rutala, Weber and the Healthcare Infection Control Practices Advisory Committee (HICPAC), 2008). Consequently, the more concentration of hydrogen peroxide, the less time of exposure. Noteworthy to mention because hydrogen peroxide does not lead to blood coagulation, it is beneficial to choose as a liquid chemical sterilant for those experiments contacting blood (Rutala and Weber, 2004). This sterilisation method is reliable when the proper instructions such as exposure time, concentration, pH and temperature are monitored (Rutala and Weber, 2004).

Blood

Defibrinated sheep blood became the choice for this project (Figure 3.29: b) as there are many difficulties in the use of human blood as it can be the agent of diseases which even the individual infected are not aware. Blood-borne viruses (BBVs) is the main risk of using human blood because of infections. Significant concern of BBVs are Human Immunodeficiency Virus (HIV), Hepatitis B Virus (HBV) and Hepatitis C Virus (HCV) that can be transmitted easily from contaminated blood (Tarantola, Abiteboul and Rachline, 2006; University of Birmingham, 2014). Although, the blood may contain other pathogens which has to be considered. Accidental exposure to contaminated blood increase the possibility of getting infected. According to statics, health care workers have become infected to HBV, HCV and HIV with the rate of 66000, 16000 and 1000, respectively in year 2000 due accidental exposure (Deuffic-Burban *et al.*, 2011). Importantly, percutaneous injuries with a hollow-bore needle has the highest rate of these virus transmission to heath care workers (Deuffic-Burban *et al.*, 2011). Health care workers may be infected by either sharp injuries or mucocutaneous contacts (Tarantola, Abiteboul and Rachline, 2006; Yeh *et al.*, 2009). Therefore, considering the risks of working with human blood for the researcher who is this case, has to use special hand tools and other objects to open the stents and consequently, has risk of contamination.

Horse and sheep blood products are widely used instead of human blood products due to safety concerns. It has been reported that the Europe and UK commonly choose horse blood (Yeh *et al.*, 2009; EO Labs, 2017). Horse and other animal blood from a reputable supplier has to conform to national and European regulatory requirements and both animal welfare and heritage are addressed, ensuring infection free products, with assays and certificates of conformity to ISO standards. There are no additives and preservatives in animal bloods, thus they cannot be kept for a long period as it may change morphologically and biochemically during the storage (EO Labs, 2017). Thus, blood was ordered a few days prior to experiments to ensure freshness: all blood products used for experimental work was obtained from TCS Biosciences Ltd.

Also noteworthy to mention is that the supplied that animal blood, have undergone processes to remove fibrin, which are recognized as the best way to prevent formation of blood clotting (EO Labs, 2017). However, an alternative way to prevent blood clotting is to anticoagulate the blood during collection in blood bags containing citrate phosphate dextrose (Russell *et al.*,

2006; Yeh *et al.*, 2009). In commercial laboratories, animal's blood become defibrinated using magnetic stirrers during blood collection (Russell *et al.*, 2006).

Four 1 litre bottle of defibrinated sheep blood was ordered as it can be seen in Figure 3.29: a. In each experiment, 1 litre of sheep blood was used for the whole system.

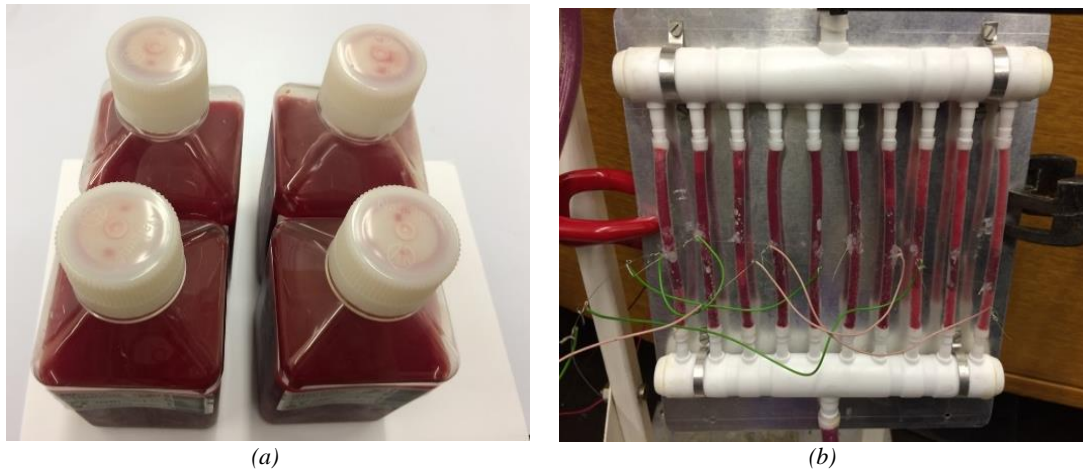


Figure 3.29: Four 1 litre of sheep blood bottles (a) and traces of blood passing through mimicked stents (b)

To imitate human blood conditions several systems were involved. A loop composed of blood circulatory system, blood pressure simulation, imitating heart pulses and heat exchange system are connected with silicone tubes leading to stent mimicks in the vascular system associated with the heart (coronary arteries). The limitation in this experiment was controlling the level of the oxygen and pH value of the blood. Although the blood for this experiment was without any infections which could affect pH value, there was a need to monitor pH level during the experiments as a factor that might play a role in migration of cells. Similarly, there was no monitoring of oxygen level during the experiments.

Blood Anti-coagulation Property

Although sterilisation method was done using hydrogen peroxide which does not cause blood coagulation, tri-sodium citrate solution was circulated through the system as an extra measure to minimise blood coagulation, particularly in small calibre tube such as the arterial mimics. According to number of studies, citrate is recognized as the most used anticoagulant to prevent blood clotting (Adcock, Kressin and Marlar, 1997; Mann *et al.*, 2007; Lahmer *et al.*, 2015). Tri-sodium citrate is used as an anticoagulant for blood causing a disruption in blood clotting

mechanism by chelating with calcium ions (Ca^{2+}) in the blood leading to calcium citrate (Lahmer *et al.*, 2015; Monchi, 2017). Calcium ions are the most significant cofactor in blood clotting mechanism (Lahmer *et al.*, 2015). However, hypocalcemia which is a decrease in the level of calcium ions, is known as the side effect of using citrate due to calcium citrate complexes (Lahmer *et al.*, 2015; Monchi, 2017).

As a matter of fact, there is a reverse relationship between the concentration of the anticoagulation and blood clotting formation. The intensity of the citrate influences directly the concentration of the calcium. Thus, the more the intensity of the anticoagulation, the less blood clotting formation (Adcock, Kressin and Marlar, 1997; Monchi, 2017). Two common sodium citrate concentration for coagulation assay are 3.2% (109 mmol.L^{-1}) and 3.8% (129 mmol.L^{-1}) (Adcock, Kressin and Marlar, 1997; Mann *et al.*, 2007). A mix of 25 g (approximately $193.75 \text{ mmol.L}^{-1}$) tri-sodium citrate $\text{Na}_3\text{C}_6\text{H}_5\text{O}_7$ (BDH[®] VWR Analytical Chemicals, UK) with 500 ml deionized water was circulated through the system for about 5 minutes. The logic behind using slightly higher concentration of tri-sodium citrate was the contact surfaces with blood mostly dried before running the blood into the loop. As a result, only traces of tri-sodium solution were left inside the mimicked arteries.

Blood Circulatory System

Blood circulatory system consisted of silicon tubes in various diameters, the manifold system, a peristaltic pump (series 683, Componenti Vending S.P.A.) connecting to a linear dc power supply (series GPS-3030, GWINSTEK), the 1.5 litre cylindrical blood reservoir, the blood receptacle/transfer container, a solenoid pinch valve and a specially constructed metal structure to contain and support all of the blood tubing, manifold, heat exchanger, receptacles and valves.

The blood was circulated, by gravity, from the top cylindrical reservoir/heat exchanger, passing through the silicon tubes to approximate human coronary arteries, the solenoid pinch valve and the manifold system, accumulating in the bottom blood container and then recirculated from the bottom blood container through silicon tubes to the top cylindrical reservoir. The continuous flow of blood, via mimic arteries was uninterrupted and stable while the experiment ran for a minimum of two hours and thirty minutes. All components were assembled on a metal structure with height adjustments, to use the hydrostatic head and pinch-valve interruption to achieve physiologically relevant systolic/diastolic pressures.

Blood Pressure Simulation

The top blood cylindrical reservoir was placed in a height which had to make conditions to provide blood hydrostatic pressure approximately 128/77 mmHg (Fox *et al.*, 2008). This would be typical of the blood pressure found in conditions of coronary artery occlusive disease. Although the normal blood pressure is 120/80 mmHg, but because the stents are normally used in patients with occlusive lumens who have typically higher blood pressure, it was fixed at 128/77 mmHg for the experiment. The hydrostatic pressure for liquids can be measured through the following equation (3.1):

$$p = \rho gh \quad (3.1)$$

Where P is the hydrostatic pressure (Pa), ρ is the density of liquid which for the blood is $1060 \text{ (kg.m}^{-3}\text{)}$, g is the gravitational acceleration and equal to $9.81 \text{ (m.s}^{-2}\text{)}$ and h is the height (m). As 130 mmHg is equal to 17065.3 Pa , then the required height from header (supply) to the manifold system should be:

$$h = \frac{17065.3}{1060 \times 9.81} = 1.64 \text{ m}$$

In addition, the pressure in the main silicon tube from the top blood reservoir up to the manifold system was measured using a Fixkit digital manometer with ranges $\pm 13.79 \text{ kPa}$ (type TL-G1, Maplin).

Blood Pulsating Characteristic

For trying to imitate human heart pulses, a solenoid pinch valve was used in which the silicon tube carrying blood was passed through. The advantage of using the solenoid pinch valve is it did not produce the turbulent flows and dead spaces (Solenoid, 2017). It also easily mounted on the metal structure in the loop of the experiment set-up. The solenoid pinch valve was electrically actuated by a rotary switch driven by a 12V DC motor (591-253, encased regulated linear RS power supply unit) and a Thurlby Thandar (PL310) power supply to control the on-off cycle (Figure 3.30). When the rotary switch started to rotate because of the connection to the linear RS power supply, it contacted the upper gold colour block during each rotation only

once because the disk is uneven. The contact times of the disk could be adjusted by increasing or decreasing voltage of the Thurlby Thandar power supply.

Despite the normal human heart beats 60 times per minute, heart rates are much greater in patients with coronary artery diseases. Notably, for each 5 bpm increase in heart rates, there is 8% increase in cardiovascular deaths (Fox *et al.*, 2008). To mimic human heart rate which is 64.1 beat per minute, the solenoid pinch valve was operated to close and open about 64.1 times per minute which meant the rotary switch should be rotated faster to have 64.1 contacts per minute (Fox *et al.*, 2008).



Figure 3.30: The rotary switch from front and back view

Heat Exchange System

As the blood was stored in a refrigerator at 4 °C temperature, it was needed to warm up the blood before the experiments. As a result, the blood was warmed up in an incubator at 37 °C temperature for duration of 45 minutes. To avoid the temperature drop of the blood during the experiment, a water bath was used to transfer sufficient heat to the blood during the experiment. The water bath began to warm its water about 1 hour sooner than inserting the blood to the experimental set-up. The stabilization of water temperature can be seen in Table 3.5 and Figure 3.31. The hot water from the water bath was circulating by a peristaltic pump (330-812, Watson Marlow peristaltic electric operated positive displacement pump) connecting to a Rapid DC power supply (series PS3025, Rapid) from the water bath, through a sterilised silicone tube to the top blood reservoir. A few coils of the silicone tube were positioned in inside the top blood container as a simple heat exchange system. The heated water then returned, via silicone tubes to the water bath. The heat from hot water could transfer to the blood in the reservoir through thermal conduction. Based on conductive heat transfer, the heat is transferred from the warmer

object to the cooler object. As the water was warmer than the blood, the heat transferred from the water to the blood. A thermometer was placed in the blood reservoir to check the temperature while the blood was receiving the heat. As the hot water temperature was greater than 37 °C, after warming up the blood, its temperature decreased. Also, there was some heat loss through silicon tubes during the water circulation. After the blood became warm in the top reservoir, it was transferred to the other parts of the experiments and after returning to the reservoir and losing temperature during the circulation, it became warm again.

Table 3.5: Stabilisation of the temperature for the experiment

Time (minute)	Temperature (°C)	Time (minute)	Temperature (°C)
0	22	35	34
5	22	40	35
10	25	45	35
15	25	50	37
20	26	55	37
25	27	60	37
30	29		

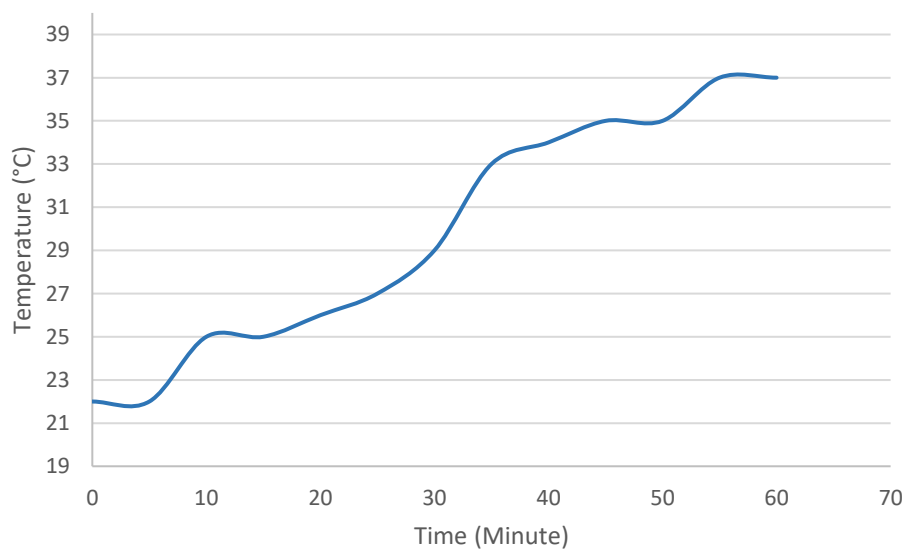


Figure 3.31: Corresponding graph to water temperature rise against the time by the heat exchange system

3.1.1.1 Pre-experiment

Once each component was positioned in the system, a pre-experiment was done with deionized water to check if everything was working satisfactorily with correct pressures, temperatures and pulse frequency. There was some leakage in the system from the mimic artery tubes due to the electrical connection passing through the tubes to the stents. The small leak was quickly fixed using silicon sealant. The temperature adjustment of the system and blood circulatory rates were tested. Once the system was examined with deionized water, the final experiments was begun.

3.1.1.2 Experiment

One litre of sheep blood was continuously circulated through silicon tubing from the upper cylindrical blood reservoir to the lower blood container (Figure 3.32).



Figure 3.32: Final experimental set-up

The procedure lasted for two hours and thirty minutes, for each experiment. The mimicked stents were connected to a selected electrical charge, according to the established protocol.

Blood temperature, blood pressure and heart pulses were monitored during the process to ensure the closest imitation to human physiological conditions (Figure 3.33).

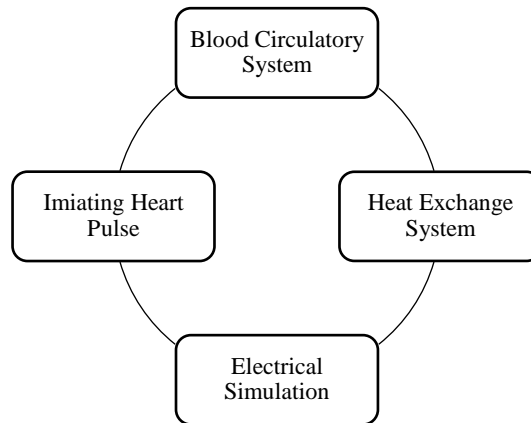


Figure 3.33: Systems which have to work simultaneously at the experiment

Noteworthy to mention that this experiment was done with five different conditions (Table 3.6).

- Only blood: two experiments were done with only sheep blood without any extra supplements. One of the experiment was performed with DC and the other one was performed with pulsed DC.
- Extra endothelial cells: in this experiment, about 500000-700000 endothelial cells were added to the sheep blood.
- Added oxygen: two experiments were performed with extra oxygen supply. One of the experiments was done using extra oxygen with an old blood which was kept for four months. The second experiment was performed with fresh blood using extra oxygen. In these experiments, a tube from oxygen cylinder was inserted to the blood reservoir with rate about 1 (cc³/min).

Table 3.6: Five different conditions of mimicked artery experiment

Number of Experiments	Blood	Electrical Pattern	Differences
1	Fresh blood	DC	-
2	Fresh blood	Pulsed DC	-

3	Fresh blood	DC	Added human coronary artery endothelial cells
4	Fresh blood	DC	Added oxygen
5	Old blood	DC	Added oxygen

It was assumed that running experiments with almost the same conditions except different blood source; one only sheep blood and another sheep blood with extra endothelial cells, would result in different numbers of attracted endothelial cells on the charged mimicked stents.

3.1.1.3 Post-experiment

After the experiments were completed a number of discreet preparatory stages were needed to examine and analyse all the samples with an electron microscope (SEM, Figure 3.34). Due to importance of inner surface of the samples, quite number of steps were done before opening the stents to examine the inner surfaces. Extreme care was needed to prevent blemishes or abrasion and accidental removal or other damage to the cells. It was also necessary to halt any biological activity of attached cells, using standard fixation methods. The procedure after the experiments can be seen in the following process pathway diagram. The described approach is one of the common acceptable and useful method for preparation of biological samples (Moran and Coats, 2012).

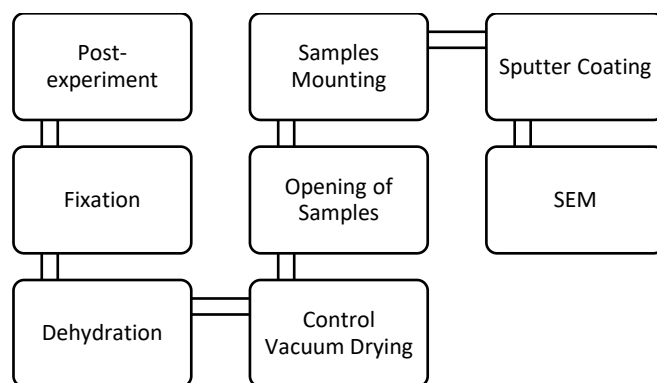


Figure 3.34: Schematic representation of post-experiment procedures

Fixation

Although there are quite number of biological samples preparation methods for scanning electron microscopy, chemical fixation is the most commonly used method for maintaining adequate cell morphology (Lešer *et al.*, 2009). The fixation phase started immediately after

the experiments finished. After carefully removing the stents from inside the silicone tubes, each stent was placed in an individual glass container and washed with phosphate buffer pH 7.4 for 10 minutes, twice (Figure 3.35). To provide phosphate buffer pH 7.4, 9.5 ml sodium dihydrogen orthophosphate dehydrate $\text{H}_2\text{NaO}_4\text{P}\cdot 2\text{H}_2\text{O}$ (Fisher chemical) and 40.5 ml di-sodium hydrogen orthophosphate dodecahydrate $\text{HNa}_2\text{O}_4\text{P}\cdot 12\text{H}_2\text{O}$ (Fisher chemical) were mixed. For pre-fixation, the stents were fixed in 2% glutaraldehyde fixative in a PO_4 buffer (pH 7.4) for one hour. Glutaraldehyde fixative is widely used due to its efficiency in cross-linking proteins and maintaining cell ultrastructure (Lešer *et al.*, 2009). In the next step, the specimens were rinsed twice in a PO_4 buffer (pH 7.4). For post-fixation, osmium tetroxide OsO_4 was used. Osmium tetroxide is a popular fixative that maintains lipids and fixes proteins (Lešer *et al.*, 2009). Next, samples were rinsed in distilled water for 15 minutes.

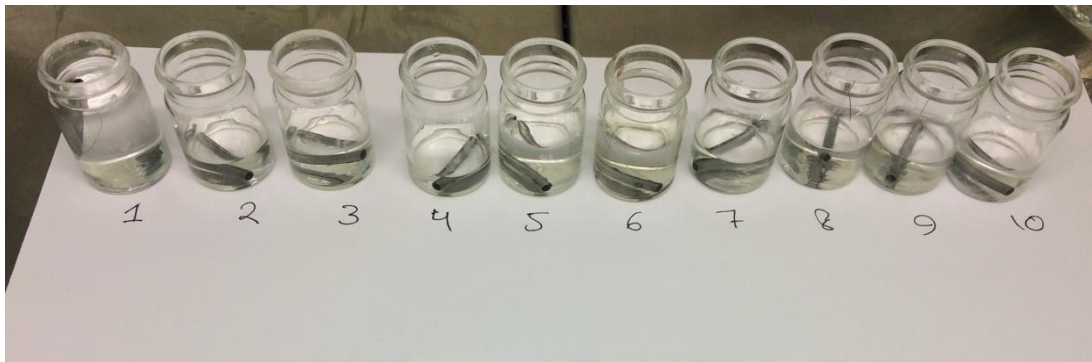


Figure 3.35: Washing each stent in an individual glass container

Dehydration

After the fixation procedure and before critical point drying process, gradual dehydration with ethanol was performed. Dehydration with a graded series of dilutions reduces surface tension properties (Moran and Coats, 2012). Specimens were dehydrated through a series of distilled water/ethanol solutions comprising 30%, 50%, 70% and 90% for 15 minutes each and dried in absolute ethanol for two changes lasting 15 minutes each.

Control Vacuum Drying

Because SEM works at high vacuum, it is needed to dry the specimens (Little *et al.*, 1991). For drying the samples, it was needed to make a vacuum environment using a high vacuum pump E2M-15 (Figure 3.36: b). In this process, the vacuum pump firstly reduced the air volume

inside the chamber, which resulted in a change of the pressure, producing the vacuum. Then, the valve was opened to vent and the pump was turned off, leading to a sealed vacuum environment. Inside the chamber, specimens were placed on molecular sieve which caused complete dryness of the samples by absorbing the water vapour inside the chamber area (Figure 3.36: a). After almost 1 hour, the samples became completely dry and were ready to observe in SEM.



(a)

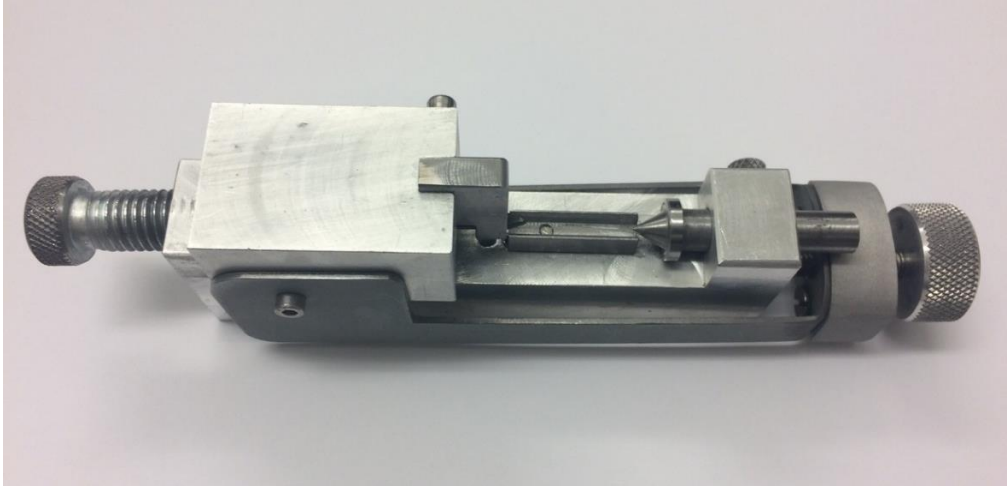


(b)

Figure 3.36: A petri dish of molecular sieve (a) and the sealed vacuum system for complete dryness of samples (b)

Opening of Samples

Once the fixation process finished, it was needed to open the stents to access easily the inner surfaces where most particles resided without exerting significant stress and pressure on the stents. Two special instruments were designed and developed to facilitate opening the stents without damaging the internal surfaces of the samples.



(a)



(b)



(c)

Figure 3.37: Two custom devices to open the stents: the linear wrench & holder (a) and the internal expanding gripper (b, c)

First, samples were placed on a custom device called linear wrench and holder (Figure 3.37: a). This device is composed of a rectangular metal base on which a holder the same size as the stent is placed between two narrow tiny tapered wedges. One wedge is fixed in position and the other one can be moved forward and backward by a screw. Once the stent was placed on the holder, from one side it had a contact with the fixed wedge and in the other side, hand the moveable wedge moved into the stent, through the slit. As the non-fixed wrench's thickness is greater than the stent's slit, the wrench expands and opens the slit. Once the slit became slightly wider greater, the second custom tool, in the form of an internal expanding gripper was used (Figure 3.37: b, c). Basically, the internal expanding gripper is composed of a round-nose plier which each its tip holds a piece of metal possessing a tiny tip to grip easily. Thus, the internal expanding gripper can go through the slit, which has been partially opened by the first tool to

completely open the stent and observe the internal area of the stent. Compared non-opened and opened stent using explained devices is shown in Figure 3.38 .



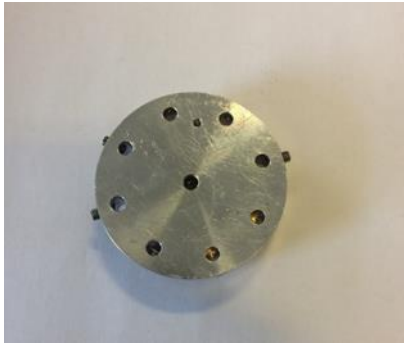
Figure 3.38: Comparison of mimicked stents before and after opening using handmade custom devices

Samples Mounting

Once the samples were opened, they are ready to mount on aluminium pin stubs which are suitable to use in both sputter coating machine and SEM (Figure 3.39: a). The samples were mounted on a double sided conductive carbon adhesive tape which is placed on a multi-pin stub holder (Figure 3.39: b, c, d and e). Electrically conductive carbon tape is widely used for secure and quick mounting of the samples on stubs. Noteworthy to mention, using the multi-pin stub holder permits to coat the samples simultaneously and observe several samples in SEM without interrupting the vacuum condition (Figure 3.39: c, f).



(a) An aluminium pin stub



(b) Multi-pin stub holder



(c) Four aluminum pin stubs placing on a multi-pin stub holder



(d) Attachment of double sided conductive carbon adhesive tape



(e) Mounting the specimen on an aluminum pin stub



(f) Prepared specimens to use in a sputter coating system and scanning electron microscopy

Figure 3.39: Fully presentation of specimens mounting to use in sputter coating and SEM systems: display of an aluminium pin stub (a), show of a multi-pin stub holder (b), display of placing specimens on a multi-pin stub holder at the same time (c), set of carbon tape on an aluminium pin stub (d), presentation of mounted specimen on an aluminum pin stub (e) and ready specimens to use in different analysing methods (f)

Sputter Coating

Coating of most biological specimens and some other materials such as plastics that are non-electrically conductive, is necessary, prior to investigation using the SEM system, (Little *et al.*, 1991). In the sputter coating process, sputtered atoms form an electrically a cathodically generated film of conductive material on the surface of the specimens. In the DC sputter coater models, the cathode material such as gold, gold-palladium, silver and platinum or carbon, are chosen to sputter onto the samples placed on the anode. The thin conductive material film leads to inhibition of electron charging, reduction thermal damage and improvement in the secondary electron emission signal for topographic visualisation and analysis (Little *et al.*, 1991; Quorum Technologies, 2002). The term charging refers to the region of scanning due to accumulation of electrons on the surface because some materials are non-conductive and become electron traps. In addition, electron beam in SEM possesses high energy and can transfer this energy in form of heat to the sample. If the samples are sensitive to heat, then they will be damaged. A layer of coating is able to reduce these issues in SEM environment.

The most common metal for sputter coating is gold due its high effective electrical conduction features, despite this, it is not the best choice for high resolution coatings because of its large grain size (Quorum Technologies, 2002).



Figure3.40: The sputter coating system (a) and the chamber of sputter coating system (b)

After preparing specimens on stubs, placing them on the multi-pin stub holder and ensuring cleanness of the work chamber, the samples were placed in the chamber, shown in (Figure3.40: b). To operate the SC7640 sputter coater (Quorum Technologies Ltd) (Figure3.40: a), the chamber's door and argon tap was closed and opened, respectively. Then, the voltage and

plasma current for gold coating were adjusted at 1.5 kV and 15 mA, respectively. The samples were coated for duration of 60 seconds. The difference between non-coated and gold-coated samples are shown in Figure 3.41 (a, c) and (b, d), respectively.



(a)



(b)



(c)



(d)

Figure 3.41: Comparison of gold coating of samples; samples before gold coating (a, c) and samples after gold coating (b, d)

The thickness of the forming film can be obtained through the following equation (3.2):

$$d = KIVt \quad (3.2)$$

Where d is thickness of the created film (\AA), K is an experimental determined constants depending on the type of metal being sputtered, the gas being used and the approximately

distance between the target and the samples which is here about 45 mm. Referring to (Quorum Technologies, 2008), K equals to approximately 0.17 when the target is gold being used with argon gas. Additionally, I is plasma current (mA), V is applied voltage (kV) and t is sputtering period (s).

Therefore, the gold film thickness that is made on the stent is

$$d = 0.17 \times 15 \times 1.5 \times 60 = 229.5 \text{ \AA} \approx 2 \frac{\text{\AA}}{s}$$

Scanning Electron Microscopy (SEM) Analysis

Once the samples were coated by a film of gold, they were ready to analyse using scanning electron microscopy. The samples mounted on the multi-pin stub holder were placed in a Carl Zeiss Supra 35VP SEM. Samples surfaces were observed using the secondary electron detector at high vacuum at 10kV. Although SEM needs some preparations procedures, it has become the method of choice for observation of inside surfaces of stents for the following beneficial reasons: first, it shows perfectly the adherence not only of cells, but also other components on the surface of the object in very high resolution. It also allows the user to count the number of adherent cells which was essential for this project. Furthermore, if re-checking of the surface of the stents is required, the process can be repeated as many times as it is needed. As Leser (2008) mentioned in his paper, SEM has been used commonly for investigation of biological samples due its applicability and advantages.

3.5 Section Summary

This chapter firstly includes an introduction to stents, cells migration and the relation between cells movement and cell membrane potentials. It also involves the methods that have been used to measure cells membrane potential.

As was needed to obtain the exact human coronary artery endothelial cell voltage for migrated cells, using a new technique “Direct Microelectrode Method” was used and described. To validate this method, it was required to measure human coronary artery endothelial cell voltage, compared to other methods. Once the endothelial cells membrane potential measurement was performed using direct microelectrode method, a mimicked human cardiovascular system

within the stents were placed and tested to prove that applying small electrical charges to facilitate migration of endothelial cells, was viable.

Chapter 4 Results

4.1 Introduction

This chapter illustrates the findings from several experiments that were fully explained in the previous chapter. The chapter presents the results of the experiments with the corresponding tables and graphs. Noteworthy to mention, other researchers' findings will be discussed and compared to the gained results in this project.

The first section of this chapter describes electrochemical reactions between titanium and stainless steel electrodes in different liquids over time plus comparison of the results of this project to others and explanation of reasons of the obtained results' occurrence. The results will represent in graphs, atomic force microscopy analysis and scanning electron microscopy observations.

The second section of results' presentation includes direct touching method results and description of how to get the cell membrane potentials using this method.

The third, fourth and fifth sections consist of the results of di-electrophoresis, zeta potential and electrophoresis method, respectively. In each section, results will be fully explained and compared to other methods findings.

The sixth and last section of this chapter presents the effect of application of electrical field in attraction of human coronary artery endothelial cells onto the surface of the stents during mimicked human physiological conditions through observation of samples using scanning electron microscopy. The novelty of this series of experiments means a comparison cannot be made with previous studies. The results of this series of experiments will be shown and described in its corresponding section.

4.2 Electrodes' Experiments

When two different metal plates are immersed into a conducting solution known as an electrolyte, it becomes a simple voltaic cell. An anode that is the metal with a higher negative electrochemical potential releases electrons which move through the electrolyte towards the metal with a lower negative electrochemical potential, is known as a cathode. This transformation of the electrons causes a current in the circuit. In another word, electrical energy

is produced because of chemical reactions. The greater potential difference between two electrodes, the greater current will occur.

As previously described, one stainless steel, grade 304 electrode and one commercially pure titanium electrode were used in electrodes experiments. Electrodes are analysed in different aspects including:

- Electrochemical measurement
- Scanning electron microscopy
- Atomic force microscopy

Each of above category will be presented later including their corresponding data.

The rationale behind these electrode experiments is to define and understand the influence of measuring electrodes immersed in an ionic solution, such as suspended cell growth media, correlated with actual cell voltage measurements. The galvanic potential has to be subtracted from the cell potential when undertaking direct cell voltage measurements.

4.2.1 Electrochemical Measurements

In the previous chapter, electrochemical measurements of each experiment were recorded and data was transferred to Microsoft Excel to obtain the graphs in order to analyse the behavior of metals in solutions.

After immersing electrodes into the liquid, voltage measurements were recorded. Behavior of each samples in different solutions varied due to electrochemical potential differences. The curves/trends of experiments will be shown and discussed later. It is noteworthy to mention that if the potential curve is descending against time, then it means there is significant redox (oxide) formation or corrosion on the electrodes. And if the potential behavior ascends against time, then a passive layer forms on the electrode and inhibits further passivation.

Measurements in Deionized Water

The curves of samples in deionized water show the formation of passivation layers on the electrodes and illustrates no tendency of electrodes to corrode (Figure 4.1). The first curve starts from a more negative potential at -210 mV and ends at a more positive potentials at -160 mV which indicates high resistance of electrodes and lower rate of corrosion. It must be noted that after the first test the rest of curves start from more negative potentials compared to the

first test which indicates the oxide layer has formed on the surface of the electrodes. However, the second, third, fourth and fifth curves start from more negative potentials (-307.5, -295.6, -253.1, -259.6 mV) and ends at more positive potentials (-251, -256.8, -196.9, -232.1 mV) which shows low rate of corrosion. The details of Figure 4.1 are shown in Table 4.1.

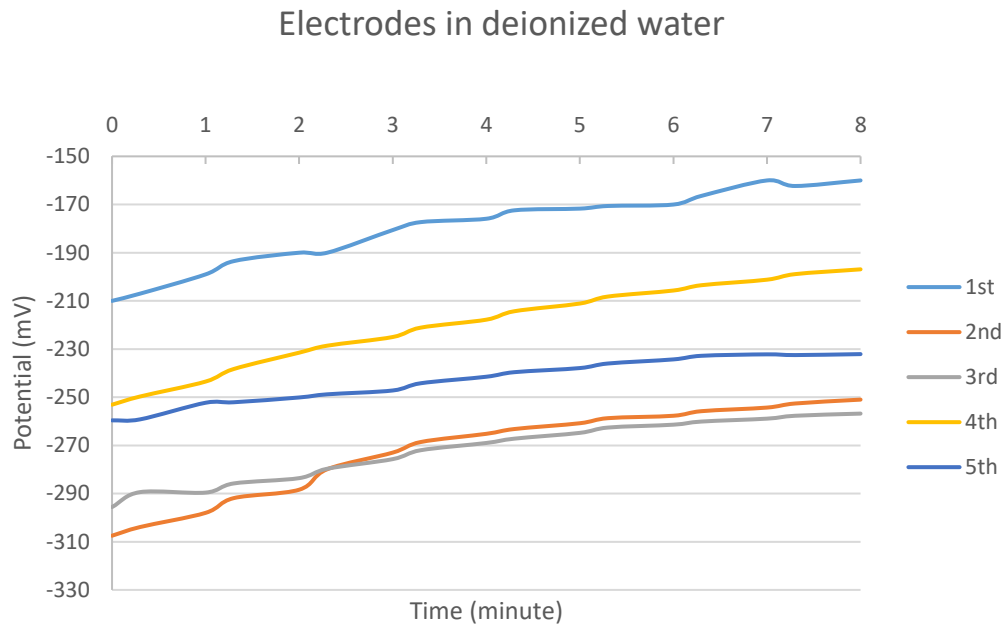


Figure 4.1: Potential measurements in deionized water

Table 4.1: Corresponding table to Figure 4.1

	1 st	2 nd	3 rd	4 th	5 th
Minimum Potential (mV)	-210	-307.5	-295.6	-253.1	-259.6
Maximum Potential (mV)	-160	-251	-256.8	-196.9	-232.1
Average (mV)	-179.80	-272.38	-272.34	-220.49	-243.08
ΔV (mV)	50	56.5	38.8	56.2	27.5
Potential _{minute=8} (mV) – Potential _{minute=0} (mV)	-50	-56.5	-38.8	-56.2	-27.5

Measurements in Distilled Water

The curve for the first experiment in distilled water shows no tendency to form an oxidation layer on the electrodes because its corresponding curve starts from a more negative potential at -70 mV and ends at a more positive potential at -4.6 mV (Figure 4.2). Considering the most negative potential belongs to the second test, it can be noticed that after the first formation of oxide layer on the electrodes after the first experiment, no more oxidation layer has been formed on the electrodes because the rest of experiments' curves start from more positive

potentials. So, the rate of corrosion for the third, fourth and fifth curve is much lower than the second one. Although formation of oxide layer after the first test caused the most negative potential for the second curve, the second curve starts from a more negative potential at -317.4 mV and ends at a more positive potential at -262.3 mV. Similarly, the third, fourth and fifth curves start from -276.1, -228.3 and -177 mV and end at -219.6, -152.1 and -131.4 mV, respectively. The determined details of Figure 4.2 are shown in Table 4.2.

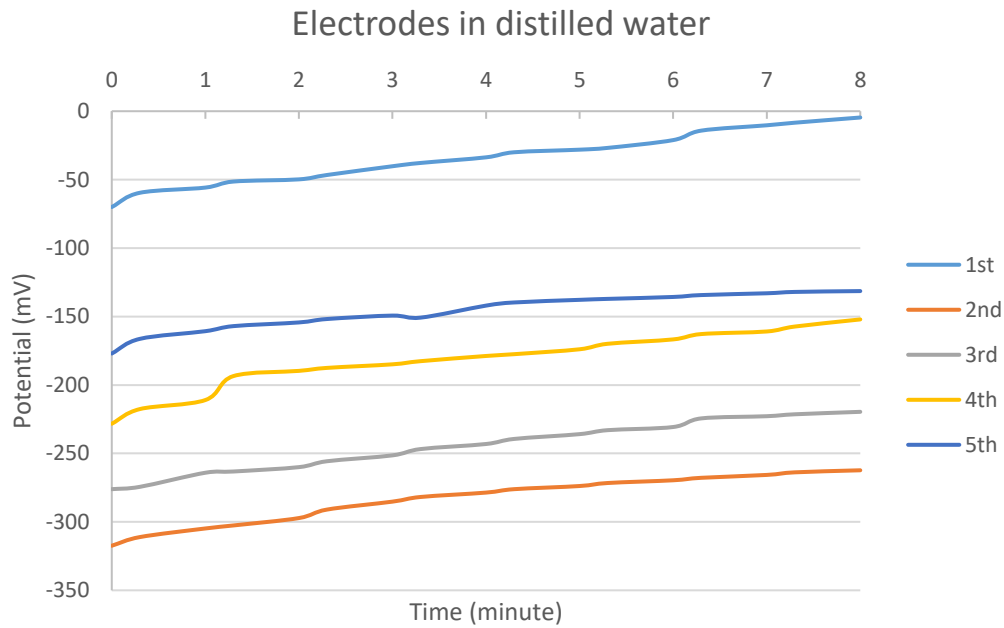


Figure 4.2: Potential measurements in distilled water

Table 4.2: Corresponding table to Figure 4.2

	1 st	2 nd	3 rd	4 th	5 th
Minimum Potential (mV)	-70	-317.4	-276.1	-228.3	-177
Maximum Potential (mV)	-4.6	-262.3	-219.6	-152.1	-131.4
Average (mV)	-34.61	-283.55	-244.82	-182.05	-146.48
ΔV (mV)	65.4	55.1	56.5	76.2	45.6
Potential _{minute=8} (mV) – Potential _{minute=0} (mV)	-65.4	-55.1	-56.5	-76.2	-45.6

Measurements in Tap Water

The curves in Figure 4.3 do not follow a trend. The first curve starts from -60 mV and after a drop until the third minute of the experiment it remains stable at -60 mV. Unlike other previous electrodes experiments in other solutions, the results from tap water indicates the formation of oxide layer on electrodes after each experiment which means curves start from more negative

potentials and the fifth curve has the most negative potential at the beginning and finishing the experiment. The second, fourth and fifth curves start from more negative potentials at -161.2, -276.7 and -310.6 mV and end at more positive potentials at -118.1, -218.7 and -289.7 mV, respectively. This indicates that the passive layer formation protects the electrodes from the corrosion. Interestingly, the third curve starts from a more positive potential at -210.8 mV and ends at a more negative potential at -218.9 mV which shows the formation of corrosion resulted in a more negative potential. The determined details of Figure 4.3 are shown in Table 4.3.

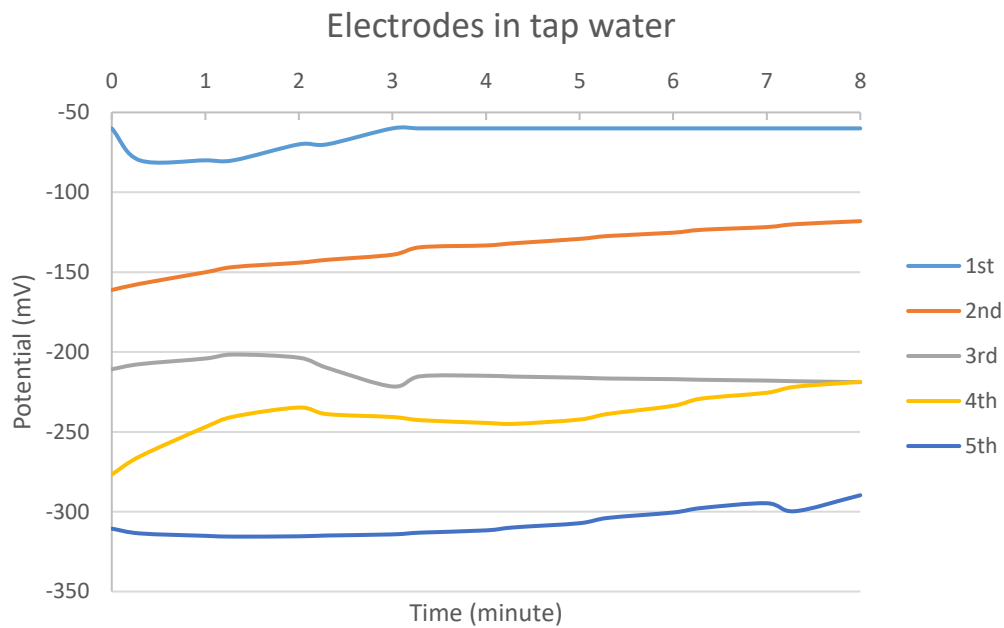


Figure 4.3: Potential measurements in tap water

Table 4.3: Corresponding table to Figure 4.3

	1 st	2 nd	3 rd	4 th	5 th
Minimum Potential (mV)	-80	-161.2	-221.6	-276.7	-315.6
Maximum Potential (mV)	-60	-118.1	-201.6	-218.7	-289.7
Average (mV)	-64.7059	-135.635	-213.347	-240.359	-307.494
ΔV (mV)	20	43.1	20	58	25.9
Potential _{minute=8} (mV) – Potential _{minute=0} (mV)	0	-43.1	8.1	-58	-20.9

Measurements in 0.9% Saline

As can be seen in Figure 4.4, all curves are noisy during the experiments. The first curve starts from a more negative potential at -69.24 mV and ends at a more positive potential at -38.7 mV which means a passivation layer has been formed on the electrodes. The second, third, fourth

and fifth curves start from more negative potentials at -199.2, -150.2, -117.9 and -204.8 mV and end at more positive potential at -171.5, -130.9, -113 and -170.9 mV respectively which shows their high resistance and low corrosion rate during their experiments. The determined details of Figure 4.3 are shown in Table 4.4.

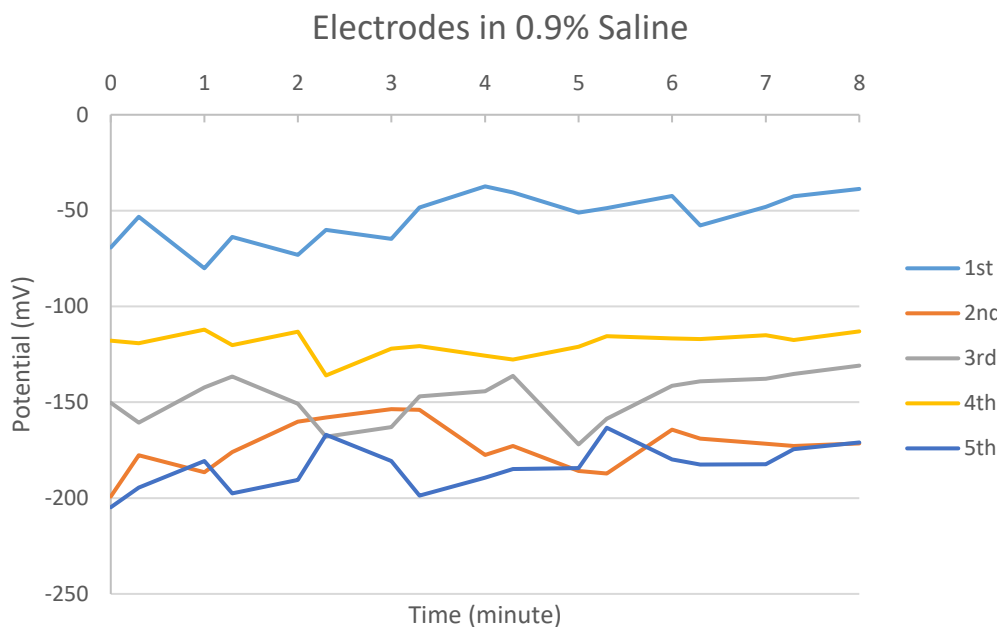


Figure 4.4: Potential measurements in 0.9% saline

Table 4.4: Corresponding table to Figure 4.4

	1 st	2 nd	3 rd	4 th	5 th
Minimum Potential (mV)	-80.1	-199.2	-172	-136	-204.8
Maximum Potential (mV)	-37.36	-153.6	-130.9	-112.1	-163.3
Average (mV)	-54.09	-172.81	-147.89	-119.47	-183.9
ΔV (mV)	42.74	45.6	41.1	23.9	41.5
Potential _{minute=8} (mV) – Potential _{minute=0} (mV)	-30.54	-27.7	-19.3	-4.9	-33.9

More information about the electrochemical measurements data can be seen in Appendix A: Electrochemical Measurement Data.

4.2.2 Scanning Electron Microscopy (SEM) Results

After running the last experiments, the surface of the electrodes were analysed in SEM. SEM observation performed in a various schedule. The purpose from observation of electrodes in the SEM was to determine whether the different solutions have sufficient potential to cause

major and significant changes on the electrodes surfaces in a short period of time, or not. In addition, it was important to determine as time passed the electrodes' topographies would alter or not even if they were not immersed in the solutions. The results of each sample will be represented in following sections. All images are taken in SEM with magnification 10k.

SEM of Controlled Sample

As can be seen in Figure 4.5 and Figure 4.6, SEM images from the surface of the controlled pair samples illustrate no topographic changes on the electrodes after exposing them to the air. Note Figure 4.5 and Figure 4.6 were used as a standard controlled only.

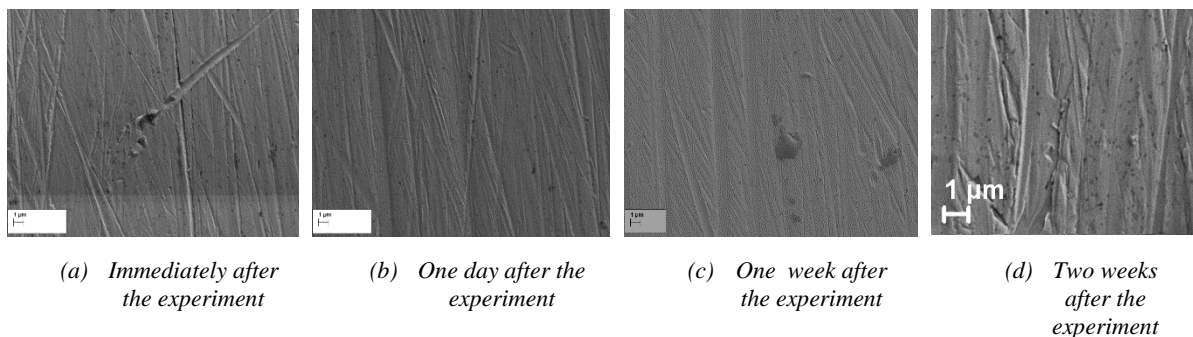


Figure 4.5: SEM images from the surface of the controlled stainless steel electrode

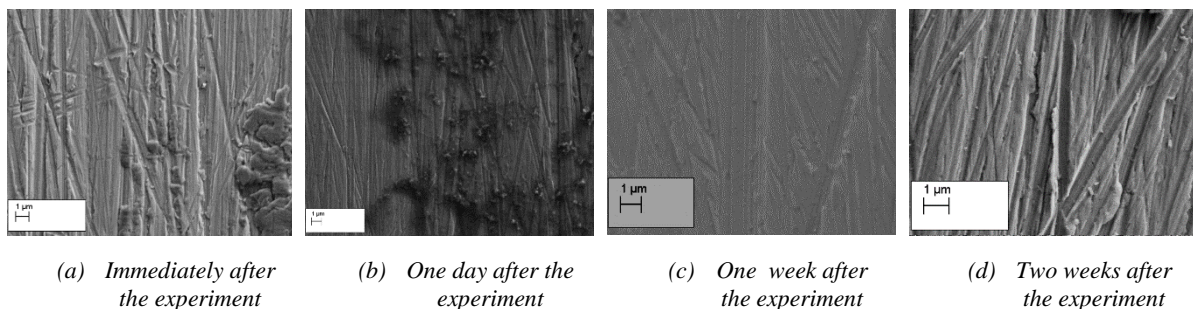


Figure 4.6: SEM images from the surface of the controlled titanium electrode

SEM of Deionized Water

Results obtained from SEM (Figure 4.7 and Figure 4.8) show the surface of the pair after immersing in deionized water do not change. Although very few particles can be seen on both electrodes, the surface do not show major differences. As all minerals including cations and

anions are removed from deionized water, there is no surprise that the pair's surface do not change.

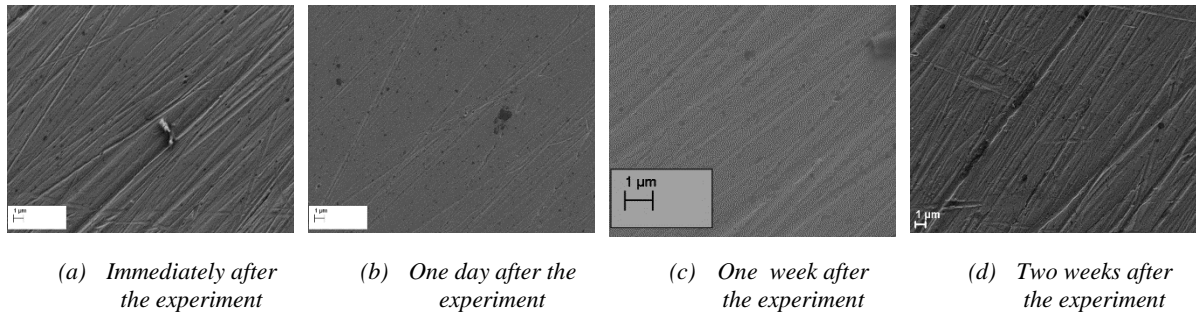


Figure 4.7: SEM pictures taken from stainless steel electrode in deionized water

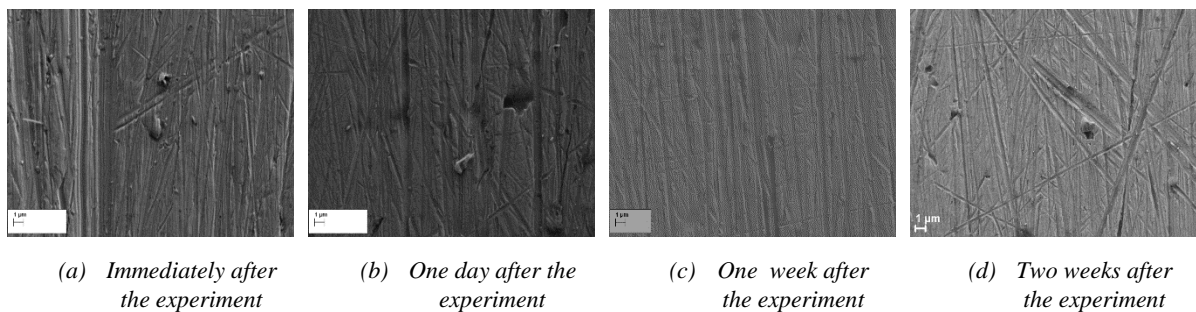


Figure 4.8: SEM pictures taken from titanium electrode in deionized water

SEM of Distilled Water

Figure 4.9 and Figure 4.10 demonstrate that the surfaces of the electrodes have not changed noticeably after performing the experiment with distilled water. Considering removal of impurities from distilled water, it does not have significant impacts leading to major changes on the surfaces.

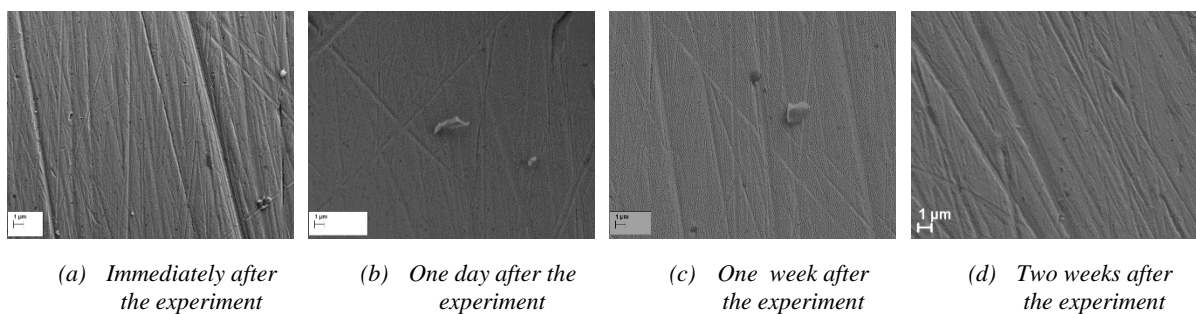


Figure 4.9: Images from the stainless steel electrode surface after immersing in distilled water

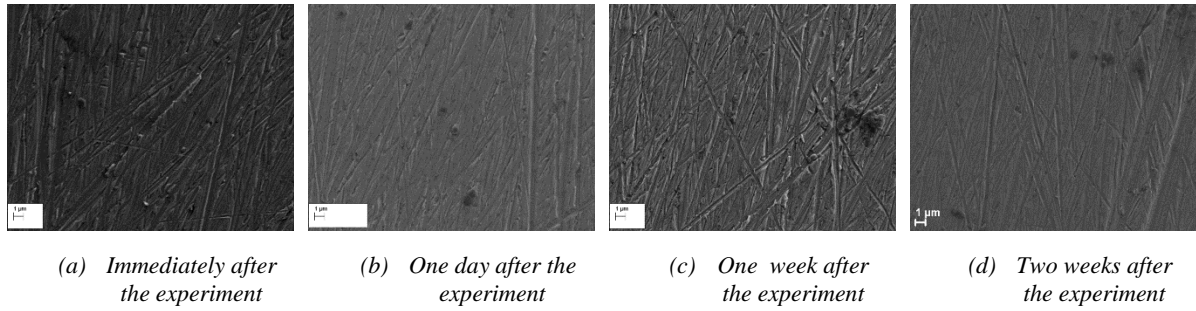


Figure 4.10: Images from the titanium electrode surface after immersing in distilled water

SEM of Tap Water

Although tap water includes minerals that result in important changes on metals, there is no significant differences in compared SEM images from surface of a pair of electrodes immersed in tap water in Figure 4.11 and Figure 4.12. However, there were unknown objects seen on the surface, possibly calcium deposits, iron or other compounds.

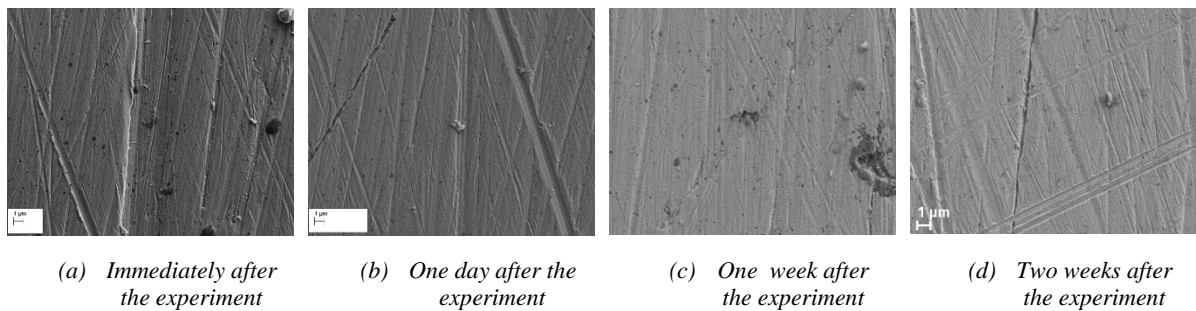


Figure 4.11: SEM pictures from stainless steel electrode after the experiment with tap water

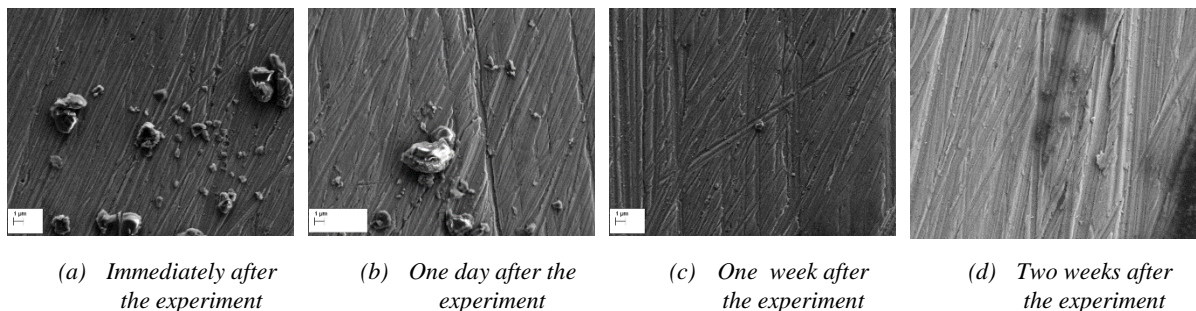


Figure 4.12: SEM pictures from titanium electrode after the experiment with tap water

SEM of 0.9% Saline

It can be seen in Figure 4.13 and Figure 4.14 that even 0.9% saline solution does not result in surface changes on the electrodes after 8 minutes in the solution.

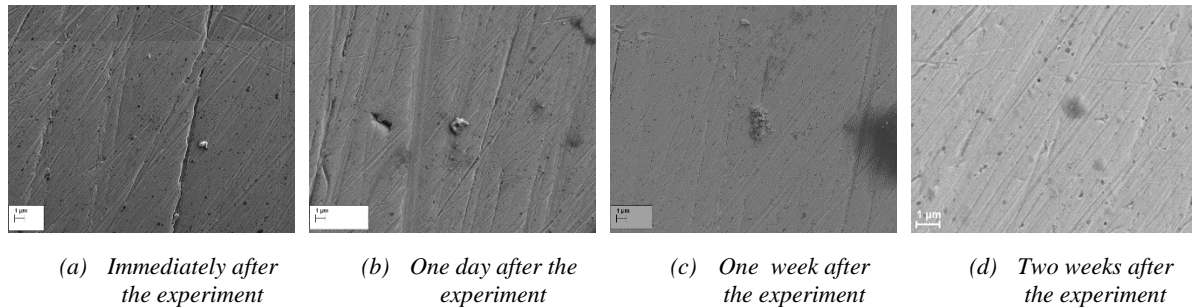


Figure 4.13: SEM images from surface of stainless steel electrode after 0.9% saline experiment

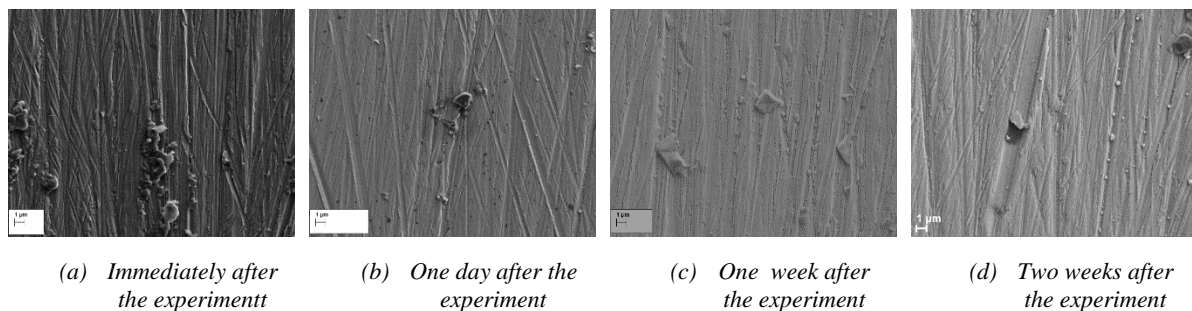


Figure 4.14: SEM images from surface of titanium electrode after 0.9% saline experiment

4.2.3 Atomic Force Microscopic (AFM) Results

Electrodes were examined in the AFM at five different time periods as described before. The AFM scanning was performed in three scan sizes from the surface as 5 μm , 20 μm and 50 μm . As the AFM results are many, therefore the AFM captured images will be presented in Appendix B: AFM Data. However, the details of images are presented in this section.

AFM of Controlled Samples:

As can be seen in Figure 4.15, RMS roughness increases over time which indicates the surface of the electrode after two weeks after the experiment is rougher than other times of analysis. Interestingly, as the scan size of the surface increases, the surface revealed higher RMS roughness which means scan size of 50 μm from the electrode is much rougher than scan size

of 5 μm and 20 μm . So, referring to Figure 4.15 the roughest surface belongs to the measurement after two weeks experiment with scan size of 50 μm .

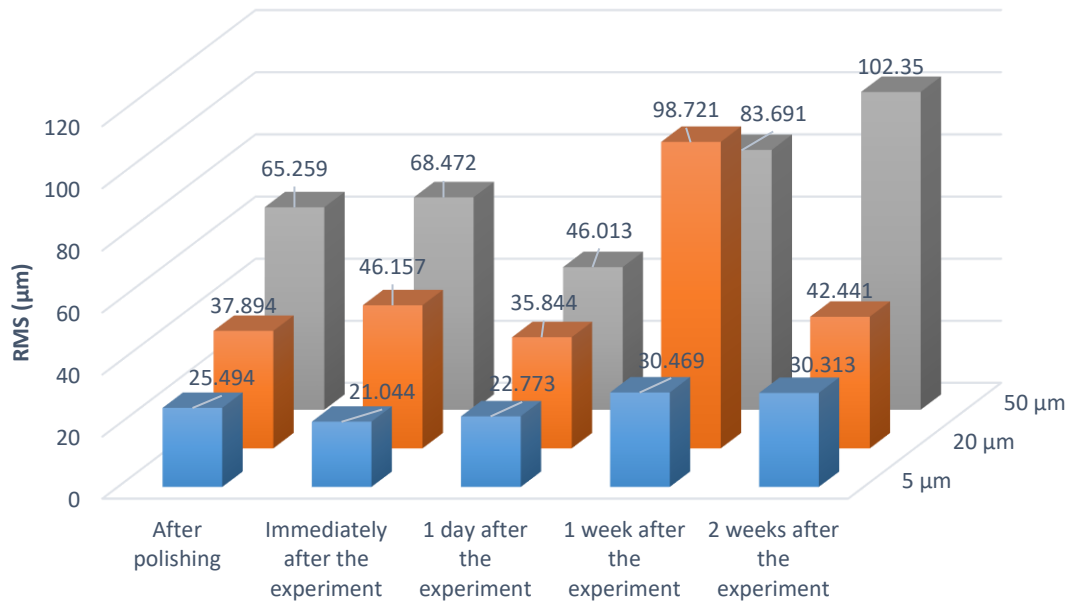


Figure 4.15: RMS roughness values of controlled stainless steel surface obtaining by AFM

Although this titanium sample was used only as a controlled, its RMS roughness value increases after exposing to the air. As can be seen in Figure 4.16, after the first exposing to the air its RMS roughness value fluctuates.

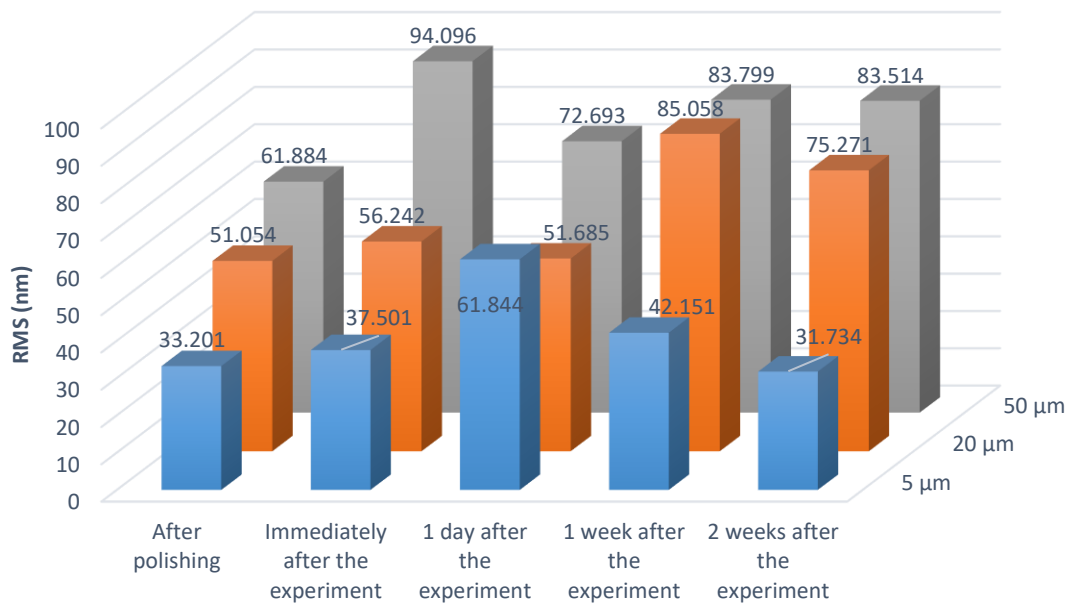


Figure 4.16: RMS roughness values of controlled titanium surface obtaining by AFM

AFM of Deionized Water:

It can be noted from Figure 4.17, the RMS roughness values from the surface of electrode immersed in deionized water fluctuate over time. Although the RMS roughness values do not follow a trend in this sample, it can be said the stainless steel electrode surface becomes smoother over time.

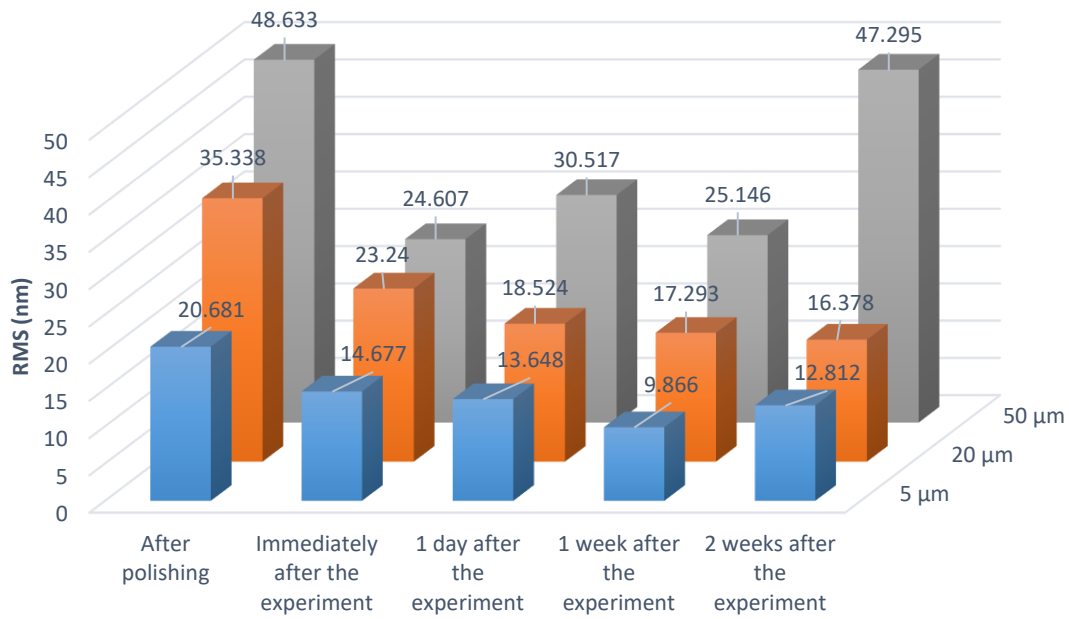


Figure 4.17: Determined RMS roughness values from the stainless steel electrode using AFM images

Figure 4.18 shows that the RMS roughness value fluctuates after the experiments. However, the RMS value increased by 44.61% in 5 μm, 11.77% 20 μm and 18.1% 50 μm of their originals. This indicates that the surface of titanium became rougher compared to before the experiment.

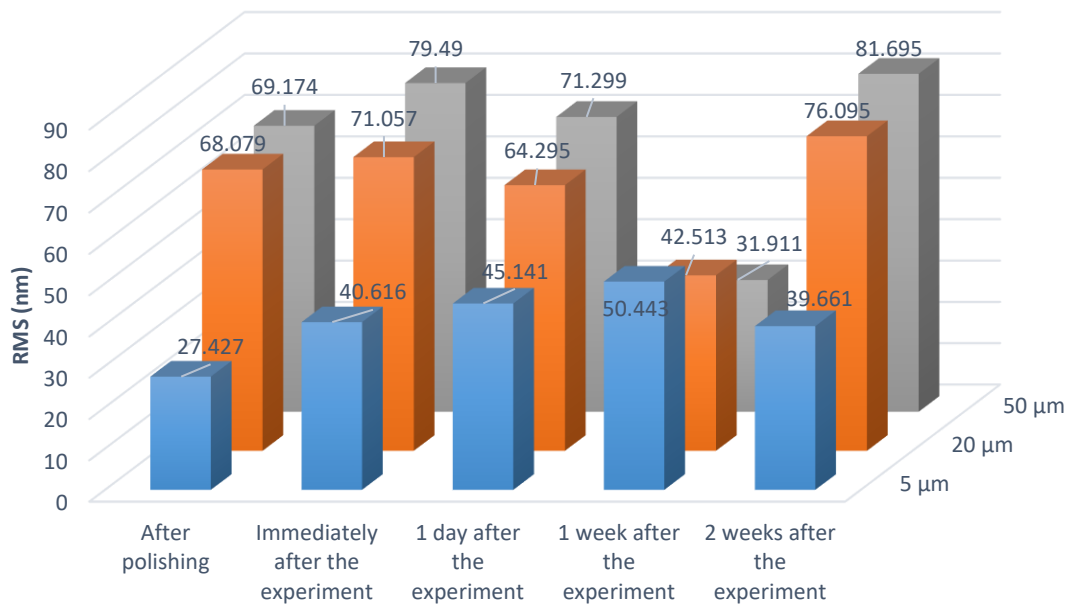


Figure 4.18: Determined RMS roughness values from the titanium electrode using AFM images

AFM of Distilled Water:

As can be noted from Figure 4.19, the RMS roughness values from the surface of stainless steel electrode immersing in distilled water has an increase of about 14.43 nm in 5 μm , 14.272 nm in 20 μm and 7.552 nm in 50 μm in the RMS value between after polishing experiment and one day after experiment which means the surface became rougher. However, this ascending behaviour stops at one day after experimental measurement. There are reductions around 1.4% in 5 μm , 43.17% in 20 μm and 33.76% in 50 μm compared the peak values to values' after two weeks after the experiment.

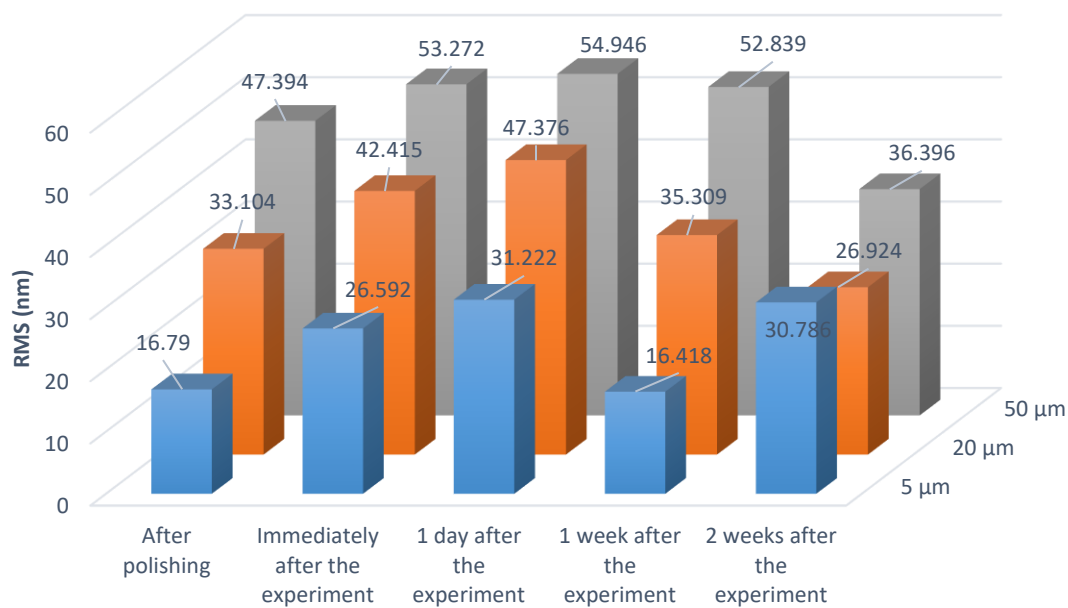


Figure 4.19: Comparison of RMS roughness values of the stainless steel electrode immersing in distilled water

The results obtained from Figure 4.20 illustrate that titanium electrodes become rougher compared to its RMS roughness value. There is an increase of 19.479 nm, 31.012 nm and 24.055 nm in RMS roughness value from their first measurements in scan sizes of 5 μm , 20 μm and 50 μm , respectively. In scan size of 5 μm , the RMS increases gradually until the last measurement. In both scan sizes of 20 μm and 50 μm , the measurement after one day after the experiment has the highest RMS roughness value which later decreases and increased again at the last measurement.

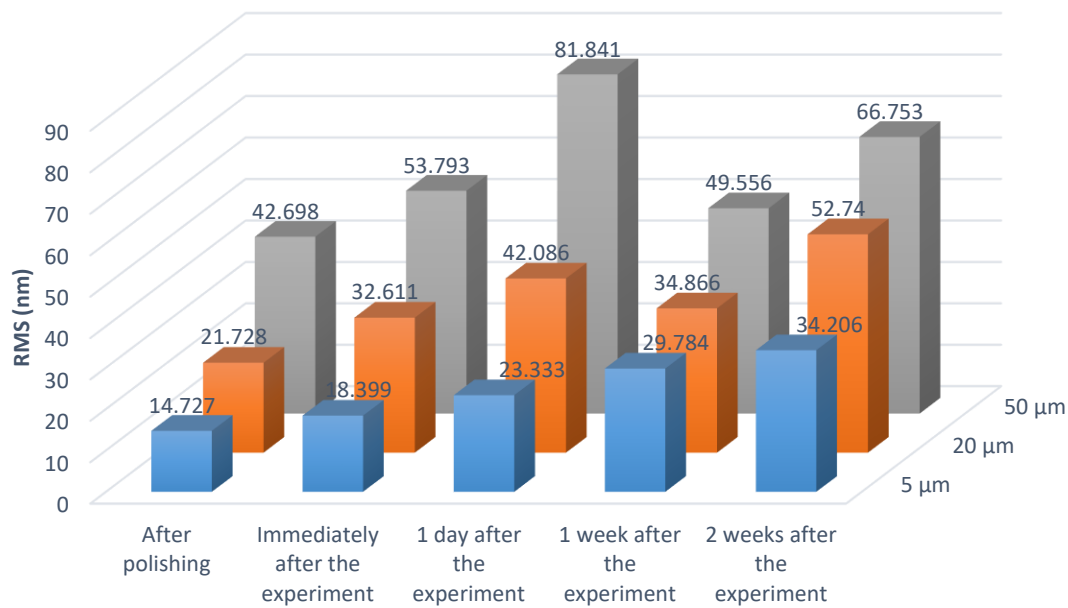


Figure 4.20: Comparison of RMS roughness values of the titanium electrode immersing in distilled water

AFM of Tap Water:

Figure 4.21 shows that the surface of the stainless steel electrode become rougher after immersing in tap water. This increase in roughness may be due to mineral deposition and ion activity acting on the surface on of the electrodes. This increasing roughness of the surface continued even one day after the experiment. The RMS values, one day after the experiment are 2.33, 2.59 and 3.15 times of the readings after polishing using scan sizes of 50 μm, 20 μm and 5 μm respectively. However, this ascending behaviour starts to decrease after one day of taking of experimental readings, to 44.5%, 45.39% and 60.7% using scan sizes of 50 μm, 20 μm and 5 μm, respectively. This significant reduction in the level of RMS roughness values reveal the surface of the stainless steel became smoother after time passed from the experiment. As a results, tap water's impact on the stainless steel cannot last for a long period of time which means it makes the surface of the electrode rougher after the experiment but only for a short period.

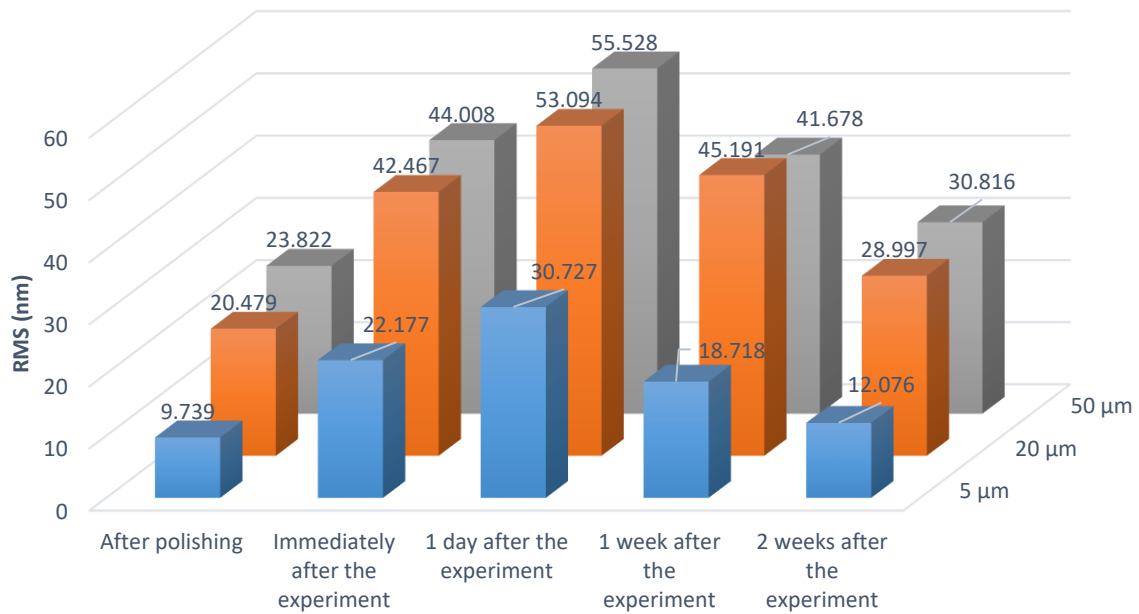


Figure 4.21: Horizontal and vertical graphs of RMS roughness value for the stainless steel electrode from AFM

It can be seen in Figure 4.22 that tap water has an impact in making titanium surfaces rougher. In scan size of 5 μm and 20 μm, there is a mild increase in the RMS roughness until one week after the experiment. Unexpectedly, there is an increase of 73.46% and 31.32% in scan sizes of 5 μm and 20 μm respectively between the RMS value of one week after the experiment and two weeks after the experiment. The RMS roughness value with scan size of 50 μm has a gradual increase until after the experimental measurement. Notably, the value increases around 40.61% at one day after the experiment. However, the RMS value increase slightly after this initial increase. As a result, it can be concluded that tap water components cause the titanium surface to become rougher.

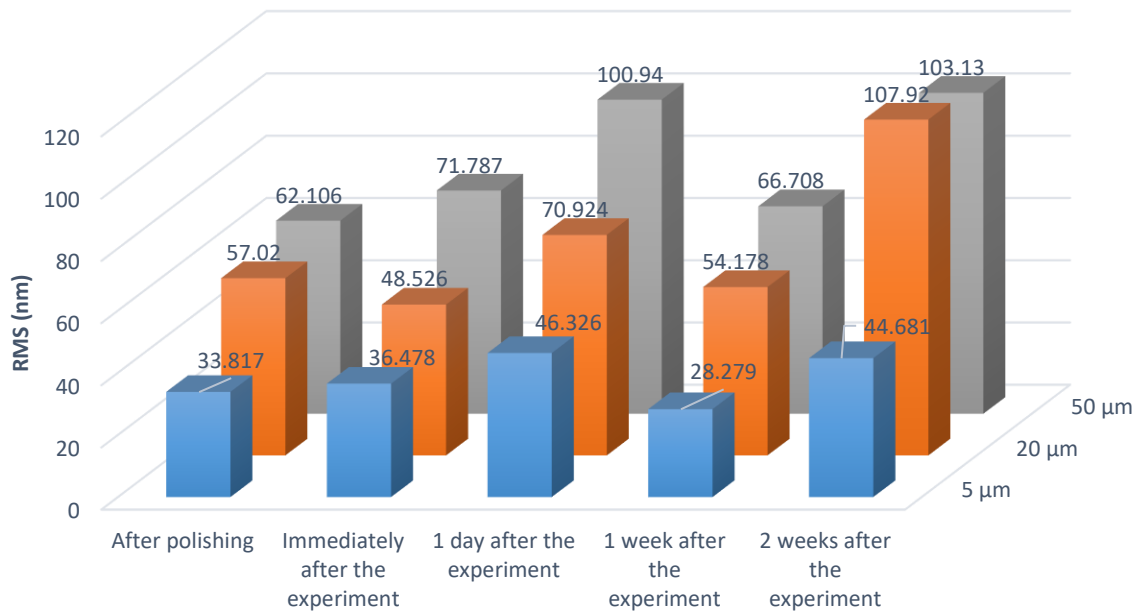


Figure 4.22: Horizontal and vertical graphs of RMS roughness value for the titanium electrode from AFM

AFM of 0.9% Saline:

As can be seen in Figure 4.23, the RMS roughness values increase gradually from the first measurements until the first day after the experiment. Values after one week after the experiment reveal an increase in roughness of the surface of the stainless steel electrode. The surface became rougher even after two weeks of immersion of the electrode in 0.9% saline with an increase of 107.89%, 96.64% and 37.83% in 5 μm, 20 μm and 50 μm scan sizes compared to the values after polishing the electrode. The obtained results indicate that 0.9% saline has great impact in making the surface of the stainless steel rougher.

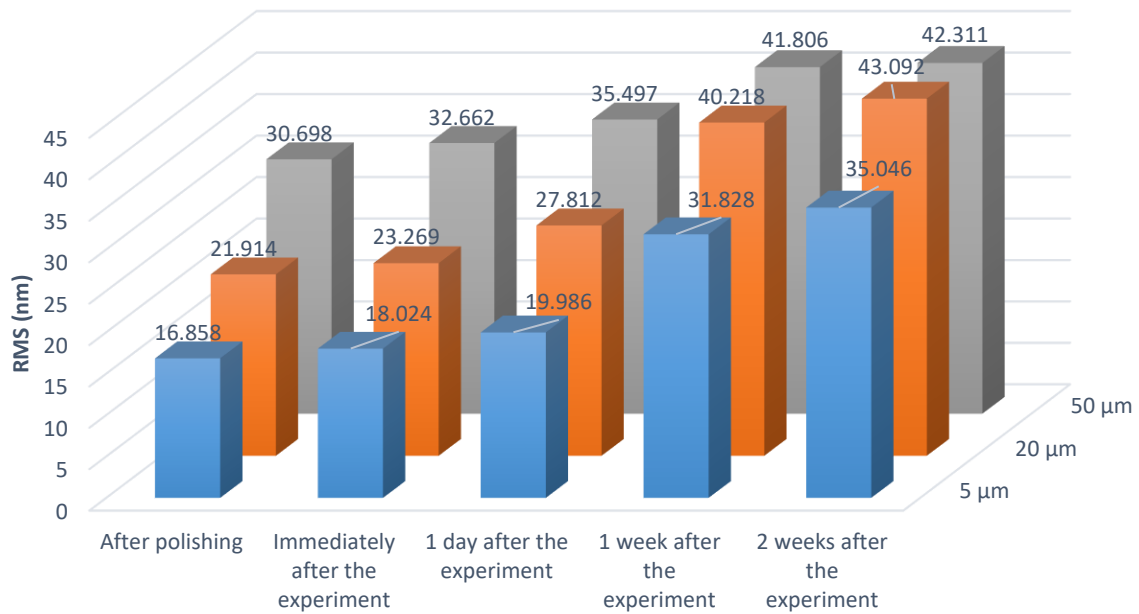


Figure 4.23: Comparison of obtained RMS roughness values from the stainless steel immersing in 0.9% Saline

Referring to Figure 4.24, it is clear that 0.9% saline results in an increase of roughness of the surface of the electrode. The RMS roughness values after the experiment reach 3.23, 1.82 and 1.89 times for 5 μm, 20 μm and 50 μm scan sizes, respectively. After these great increases, the values decline which means the roughness decreases as time passes after the experiment.

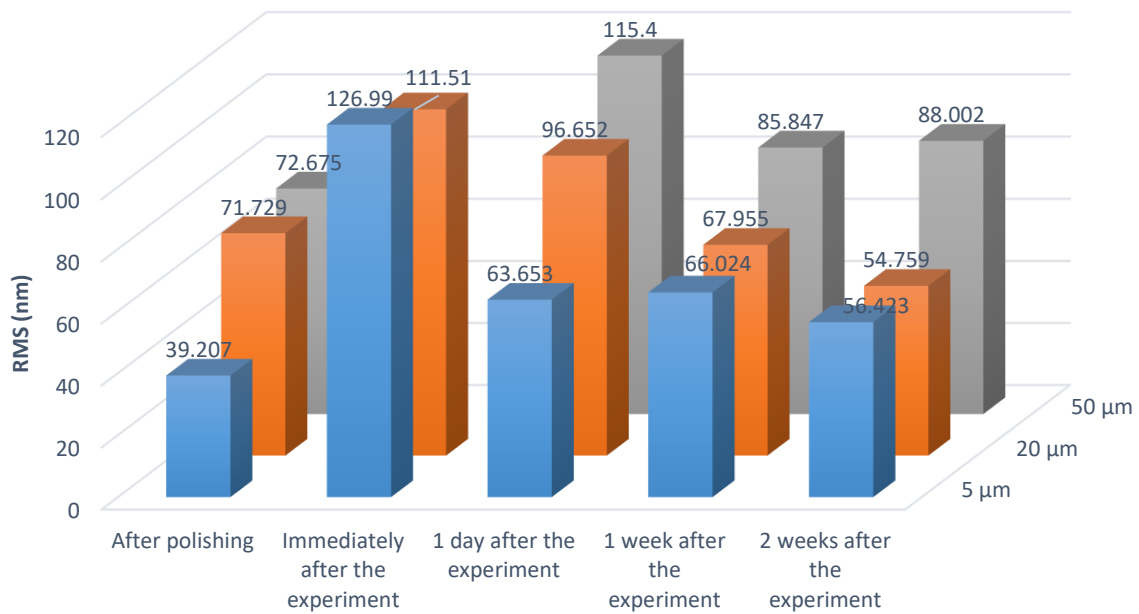


Figure 4.24: Comparison of obtained RMS roughness values from the titanium immersing in 0.9% Saline

4.3 Cell Viability

Each petri dish of cells was regularly observed using an inverted microscope to check viability of cells once, two hours after culturing and on a daily basis following days after culturing, until the cells were used. Viability of cells was recognized by morphological observation of cells. Viability of cells was determined by examining the cells, to ensure there were no bacteria, fungi or non cellular objects. Bacteria manifest themselves with alterations transparency and making whitish layer in the container and they look very active. On the other hand, fungi manifest in clumpy, filamentous shapes and grow very slowly. It can take several days for the container to show obvious signs of contamination with fungi. Fungi clumps can be easily seen without a microscope in an effected container of cells at final stages. Cell growth medium is another way to understand whether if the cells are alright or not. Cell growth medium color should be pink/salmon and transparent, if it turns to any color and becomes cloudy, it shows contamination. Sometimes, a white film is made in an infected cell container which can be due to presence of bacteria or fungi. Cells viability can be easily understood by observation via the microscope images (Figure 4.25).



Non-contaminated cultured endothelial cells



Non-contaminated cultured osteoblast cells



Contaminated cultured endothelial cells



Contaminated cultured osteoblast cells

Figure 4.25: Human cultured cells in both contaminated and non-contaminated conditions with magnification $\times 80$

After checking the viability of cells, they were counted using hemocytometer. After sufficient time, the flask of cells should reach a confluency of 70% to use for the experiments or, to subculture.

4.4 Direct Microelectrode Method

For these type of the experiments, both cells types were cultured in two different styles. First style was cultured the cells in the petri dish and distributed cells evenly in the whole surface of the petri dish by gentle shaking (known as full cell coverage). In the second style, the cells were cultured only in one side of the petri dish (known as half cell coverage). The logic behind doing these experiments in two different styles was that maybe in the full cell coverage at the moment of contact of the microelectrode's tip with the cell, the titanium anode might also be in contact with another cell, thereby influencing the total voltage measurements. However, in half cell coverage the anode electrode was positioned in the segment of the petri dish which did not include any cell adherence and the electrode was only in contact with the cell growth medium.

After checking the viability of cells following the culturing and maintenance in the incubator, they were examined at room temperature on the inverted microscope. Each experiment lasted for a maximum one hour. The measurements recorded in three different styles including immediately after taking out cells from the incubator, two hours after the first experiment and ten hours after the first experiment. During the experiments, cell voltage measurements were recorded which are presented later in this section (see Figure 4.28 to Figure 4.40), additionally, images of cells were taken with different magnifications.

4.4.1 Cell Growth Medium Measurement

Both types of cell growth medium's galvanic characteristics were recorded using voltage data logger. The data logger was set to record measurements every ten seconds. Figure 4.26 shows plotted graphs of both endothelial and osteoblast cell growth mediums over ten minutes and also the average of cell growth medium.

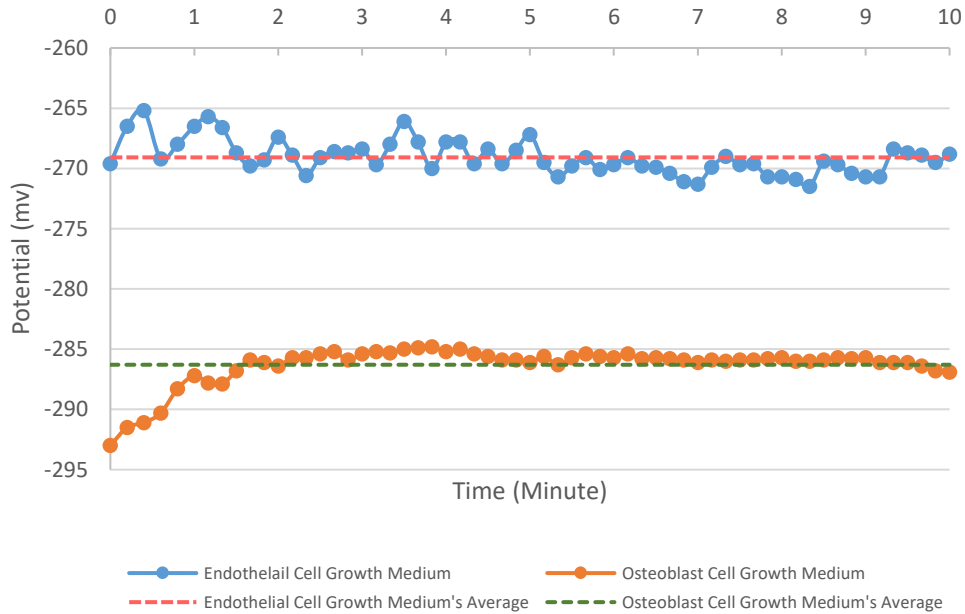


Figure 4.26: Plotted potentials of both endothelial and osteoblast cell growth medium over time

As can be seen in above graph, the blue line that indicates endothelial cell growth medium potential fluctuates in a range of -265.2 mV to -271.5 mV during one minute. The average potential for endothelial cell growth medium is -269.08 mV. It noticeable from the graph that in the first five minutes of the measurement, potential records are greater and above the average line, while for the second five minutes the measurement recordings are more negative and lower than the average line.

Interestingly, osteoblast cell growth medium recordings were completely different from endothelial cell growth medium: osteoblast cell growth medium started from lower potential and after gradually increasing in the first one minute, then they remained steady until the end of the measurement. The average potential for osteoblast cell growth medium is -286.29 mV. It is noteworthy to mention that there is about 17 mV differences between the averages of endothelial and osteoblast cell growth medium which might be due to different essential constituents for the two different cell types.

4.4.2 Human Coronary Artery Endothelial Cells Measurement

Human coronary artery endothelial cells were examined 18 times in total including both styles of full and half cell coverage measurement. Each petri dish of cells were tested three times at different times. The first experiment was done immediately after taking out cells from the incubator. The second experiment was performed about two hours after the first measurements

of cells' potential. Cells were kept in the incubator between the first and second and between the second and third measurements. The third experiment was done about ten hours after the first experiment.

Cells images before the experiments are shown only in the 1st experiment part. Cells images relating to each experiment can be seen in Appendix C: Direct Microelectrode Method Data.

Full Cell Coverage Measurement:

- 1st experiment

As can be seen in Figure 4.27, cells were viable prior to the experiments. It is obvious from the images that after 10 hours from the first experiment cells were not viable anymore and their morphologies completely changed.

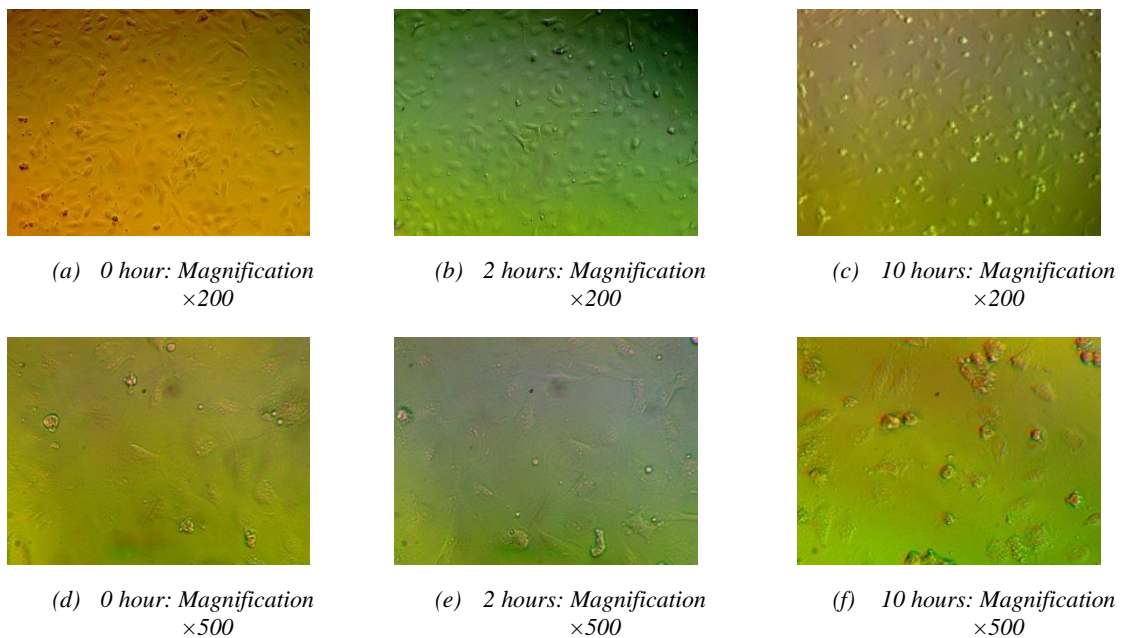


Figure 4.27: Human coronary artery endothelial cells in different timing and magnifications for the 1st experiment

As can be seen in Figure 4.28, the blue line illustrates the cell membrane potential at the beginning of the experiment which alters in the range of -218.3 mV and -273 mV. The average potential (-236.83 mV) after the deduction of the medium becomes around 32.25 mV. The second measurements of potential after 2 hours show more negative potentials in the range of -337.6 mV and -221.1 mV with the average of -256.76 mV which after the deduction of cell growth medium changes to 12.32 mV. The third measurements from these petri dish of cells were more positive than the first two measurements. The range of potential differences is

between -249.5 mV and -201.2 mV which results in an average of 61.93 mV after deduction of cell growth medium.

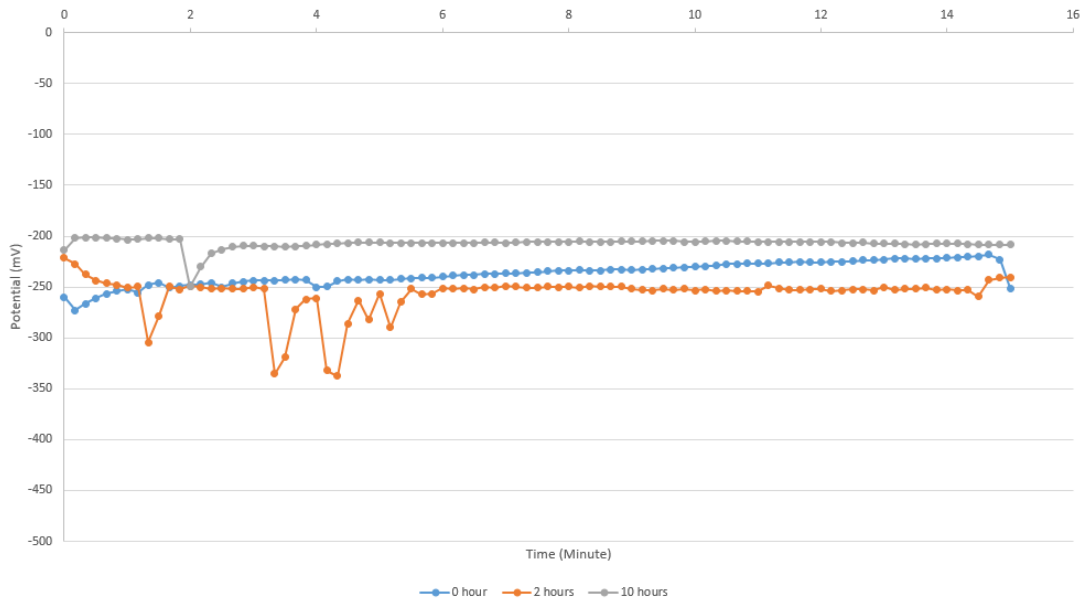


Figure 4.28: Human coronary artery endothelial cells' potential measurements at different times of the 1st experiment

- 2nd experiment

It can be seen in Figure 4.29 that the first measurements of cells potential are interestingly more positive that are between range of -336.9 mV and -198.4 mV with an average potential of -220.63 mV that after reduction of cell growth medium it changes to 48.45 mV. Similar to the first experiment, the second reading in this experiment has the same behavior which means its corresponding results are more negative than the first and third measurements. The average potential for this reading among the range of -307.2 mV and -235.3 mV is -265.47 mV that alters to 3.61 mV with the reduction of the cell growth medium. The last reading of this experiment has the lowest variation in its range which is -258.8 mV and -221.1 mV with the average of -249.93 mV before reduction of the cell growth medium.

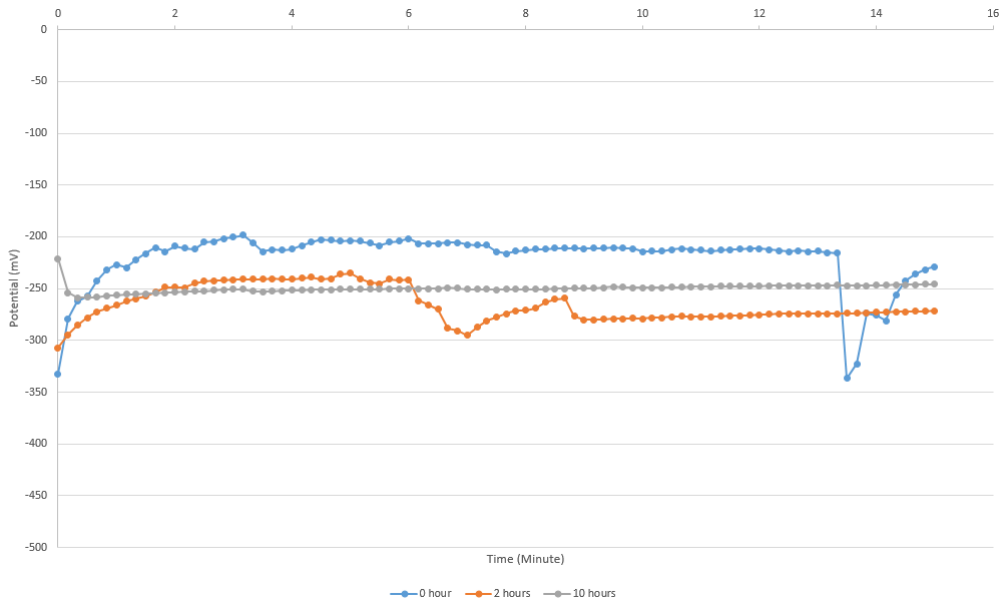


Figure 4.29: Human coronary artery endothelial cells' potential measurements at different times of the 2nd experiment

- 3rd experiment

In the Figure 4.30, the first reading varies between -272.8 mV and -244.2 mV with an average of 13.35 mV after deduction of cell growth medium. Similar to previous measurements, the second reading has the most negative potentials that varies between -387.1 mV and -317.1 mV with an average of -61.98 mV after cell growth medium deduction. The last measurement, 10 hours after the first measurement, has potentials between -283 mV and -234.4 mV with an average of 11.99 mV after decrease of cell growth medium.

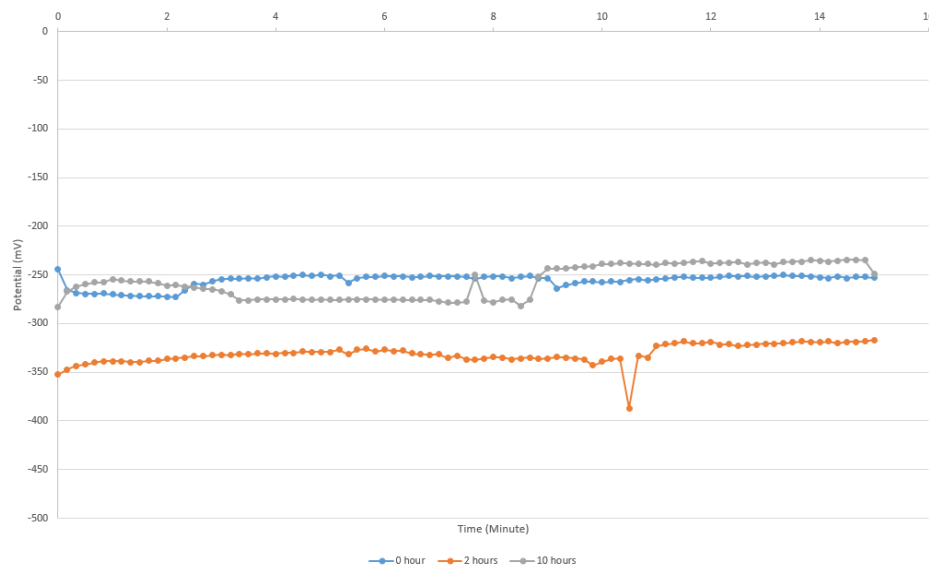


Figure 4.30: Human coronary artery endothelial cells' potential measurements at different times of the 3rd experiment

Half Cell Coverage Measurement:

- 1st experiment

It can be seen in Figure 4.31 that the blue line shows variations between -357.8 mV and -306.7 mV with average of -318.8 mV. After the deduction of the cell growth medium values, the average is -49.72 mV for human coronary artery cell. In the second attempt, the measured potentials alters in the range of -376.1 mV and -324 mV with an average of -348.51 mV that after deduction of cell growth medium, it is -79.43 mV. In the last reading of this experiment, similar to previous results the measured potentials after 10 hours is more positive and changes between -306.7 mV and -273.8 mV with an average of 10.47 mV after deduction of cell growth medium values.

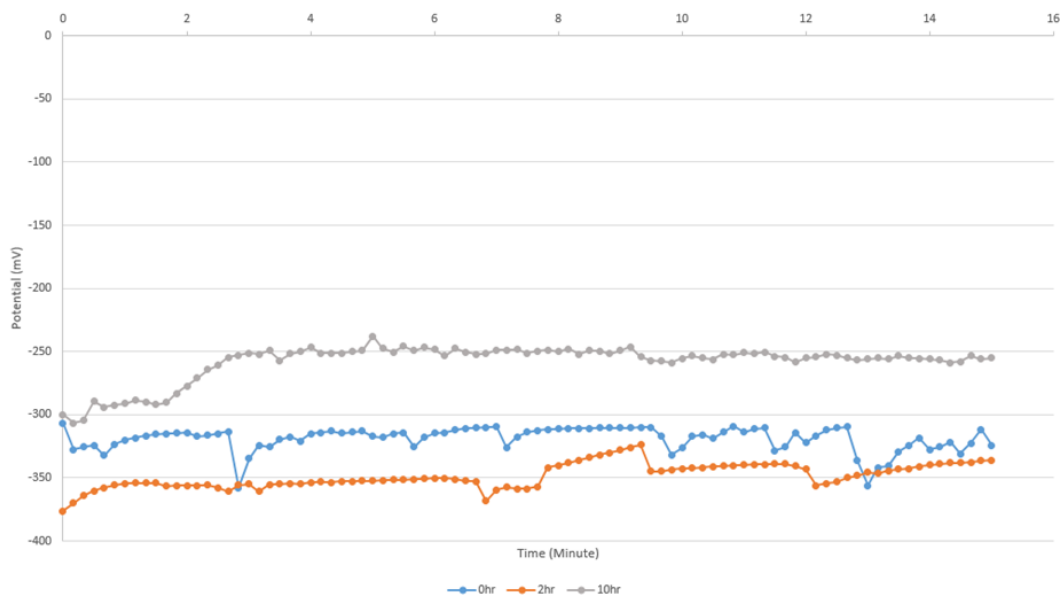


Figure 4.31: 1st experiment of potential measurements determined using direct microelectrode method

- 2nd experiment

It can be seen in Figure 4.32 that the first measurement differs from -356.7 mV and -315.3 mV with the average of -51.82 mV after the deduction of cell growth medium. The second measurements in orange line varies between -391.2 mV and -332 mV with the average of -338.72 mV that is -69.64 mV after cell medium growth deduction. And the last reading contains the most positive readings which alter between -250.3 mV and -209.7 mV with the average of 38.03 mV after deduction of the cell growth medium.

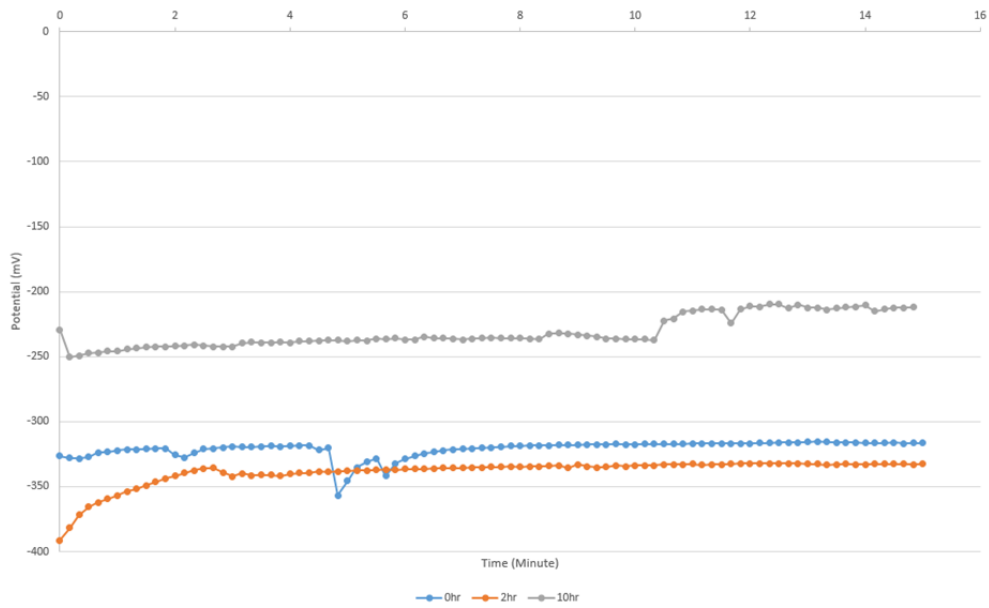


Figure 4.32: 2nd experiment of potential measurements determined using direct microelectrode method

- 3rd experiment

It can be noted from Figure 4.33 that the first measurement of cells potentials varies in the range of -317.8 mV and -292.2 mV with the average of -300.83 mV which after the deduction of cell growth medium is -31.57 mV. The second measurements of cells changes between -361.4 mV and -324.2 mV with the average of -334.88 mV that is around -65.83 mV after deduction of cells growth medium. The gray line illustrates the last measurement after 10 hours which differs from -311.1 mV and -278.7 mV with the average of -21.49 mV after the deduction of the cell growth medium values.

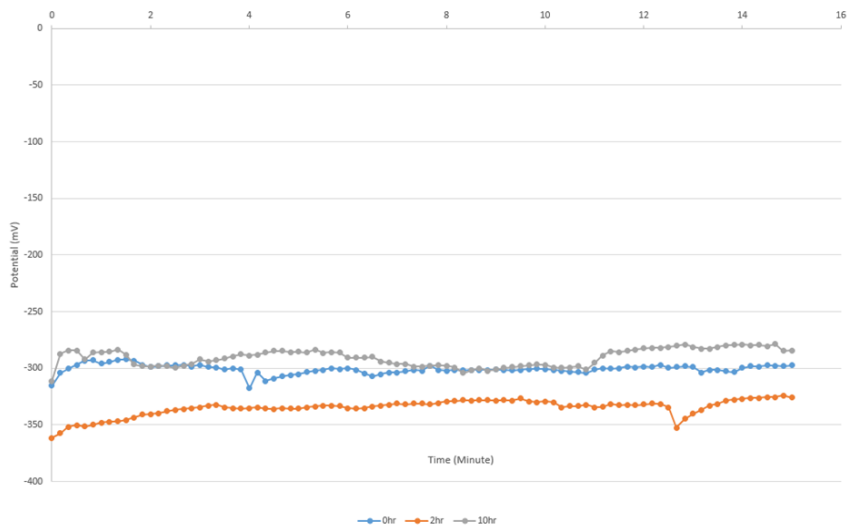


Figure 4.33: 3rd experiment of potential measurements determined using direct microelectrode method

4.4.3 Human Osteoblast Cells Measurement

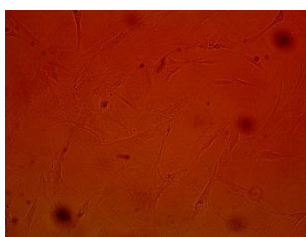
Similar procedures were applied to human osteoblast cells to obtain results for direct microelectrode method.

Cells images before the experiments are shown only in the 1st experiment section. Cells images relating to each experiment can be seen in Appendix C: Direct Microelectrode Method Data.

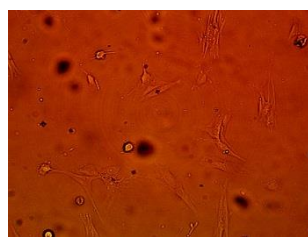
Full Cell Coverage Measurement:

- 1st experiment

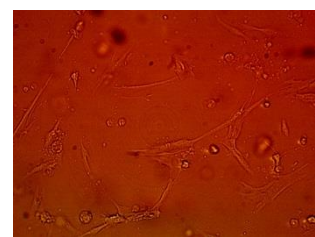
Images from 70% -80% confluency cultured human osteoblast cells can be seen in Figure 4.34.



(a) 0 hour: Magnification $\times 200$



(b) 2 hours: Magnification $\times 200$



(c) 10 hours: Magnification $\times 200$



(d) 0 hour: Magnification
×500

(e) 2 hours: Magnification
×500

(f) 10 hours: Magnification
×500

Figure 4.34: Cultured human osteoblast cells for direct microelectrode method for the 1st experiment

It can be seen in Figure 4.35 the blue line which presents the first reading of potential measurements, varies from -352 mV to -276.7 mV and its average is -296.66 mV that is -10.37 mV after the deduction of the cell growth medium. Measured potentials after 2 hours change in the range of -321.3 mV and -301.7 mV with the average of -313.14 mV that is around -26.85 mV after the deduction of cell growth medium. The last reading contains various potentials from -325.2 mV to -290.1 mV with the average of -14.57 mV after the deduction of cell growth medium value.

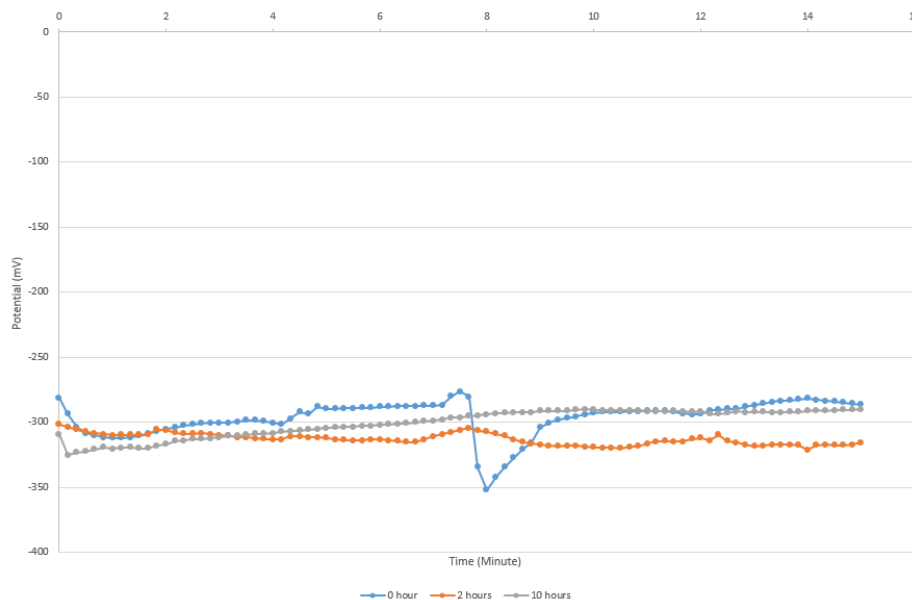


Figure 4.35: Potential measurements using direct microelectrode method for the 1st experiment

- 2nd experiment

As can be seen in Figure 4.36, the first reading fluctuates in the range of -300.3 mV and -277.9 mV with the average of 1.64 mV after the reduction of the cell growth medium. The orange line alters between -328.7 mV and -289.8 mV with the average of -302.93 mV which changes to -16.64 mV after deduction of the cell growth medium. The measurements after 10 hours differ between -287.2 mV and -256.1 mV with the average of 15.67 mV after the deduction of the cell growth medium value.

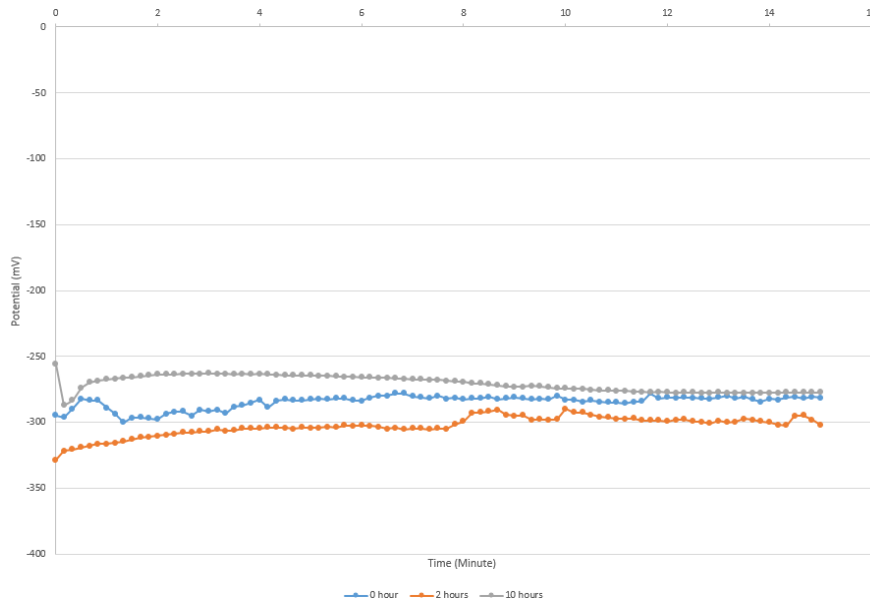


Figure 4.36: Potential measurements using direct microelectrode method for the 2nd experiment

- 3rd experiment

As can be seen in Figure 4.37, the first reading varies between -305 mV and -262.8 mV while the second reading alters between -376.5 mV and -338.7 mV. The averages after deduction of the cell growth medium are, 7.9 mV and -62.07 mV for the first and second reading, respectively. The gray line which belongs to the third reading changes in the range of -320.3 mV and -233.2 mV with the average of -253.33 mV that is 32.29 mV after the deduction of the cell growth medium values.

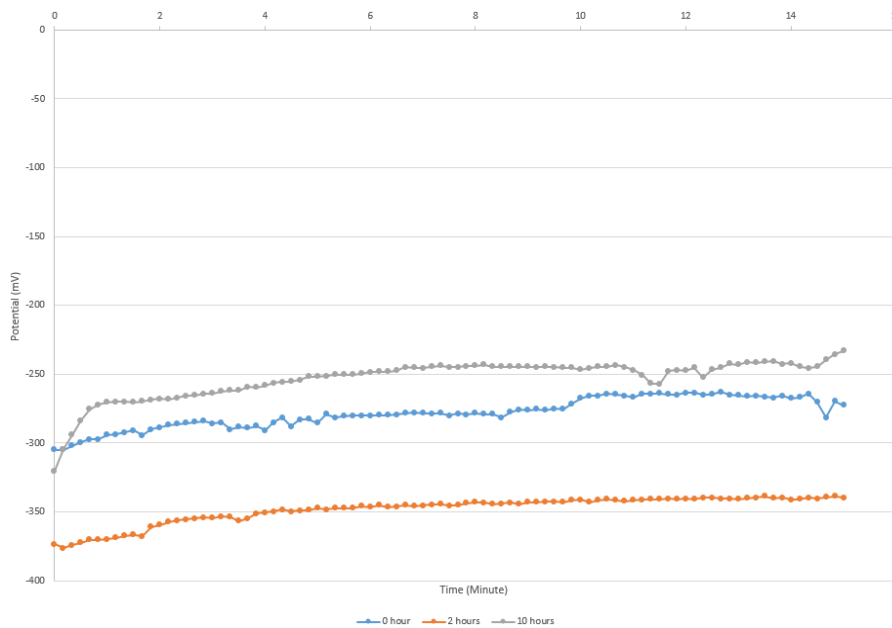


Figure 4.37: Potential measurements using direct microelectrode method for the 3rd experiment

Half Cell Coverage Measurement:

- 1st experiment

It can be seen in Figure 4.38 that the blue line varies in the range of -370.5 mV and -320.6 mV with the average of -341.87 mV which is -55.58 mV after the deduction of the cell growth medium. The second reading in this experiment changes between -414.4 mV and -371.3 mV with the average of -385.34 mV which is -99.05 mV after the deduction of the cell growth medium. The third measurements range alters between -337.8 mV and -315.3 mV with the average of -33.64 mV after the deduction of the cell growth medium.

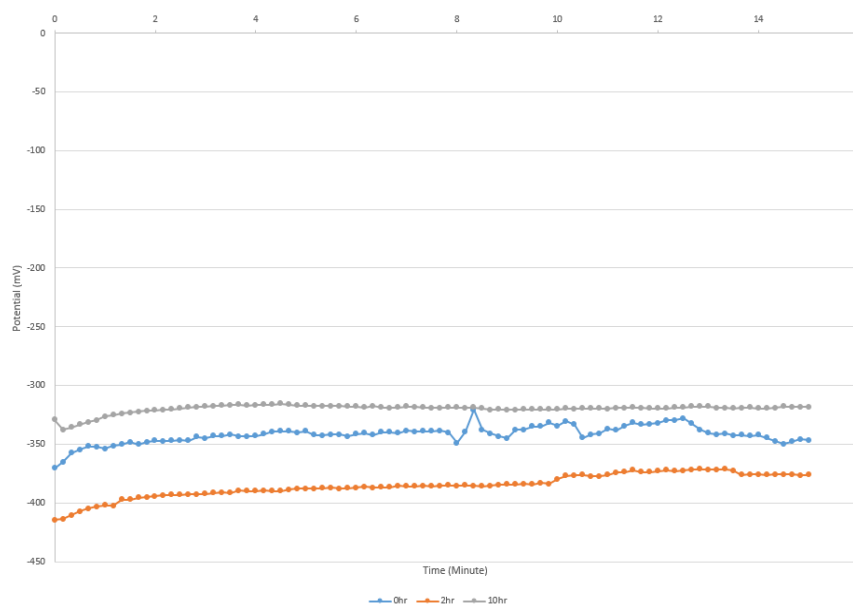


Figure 4.38: Different potential measurements in various time at the 1st experiment

- 2nd experiment

As can be noted from Figure 4.39, all three measurements in this experiment follow the same trend in which they start at a more negative potential and after a while they become more stable. The first potential measurements varies between -373 mV and -291.7 mV with the average of -322.43 mV. The corresponding average for the first measurement after the deduction of the cell growth medium is around -88.32 mV. The orange line starts with a more negative value and alters in the range of -417.7 mV and -357.9 mV with the average of -374.61 mV which is -88.32 mV after deduction of the cell growth medium. In the last reading, the potentials vary between -337.5 mV and -286.4 mV with average of -9.76 mV after the deduction of the cell growth medium values.

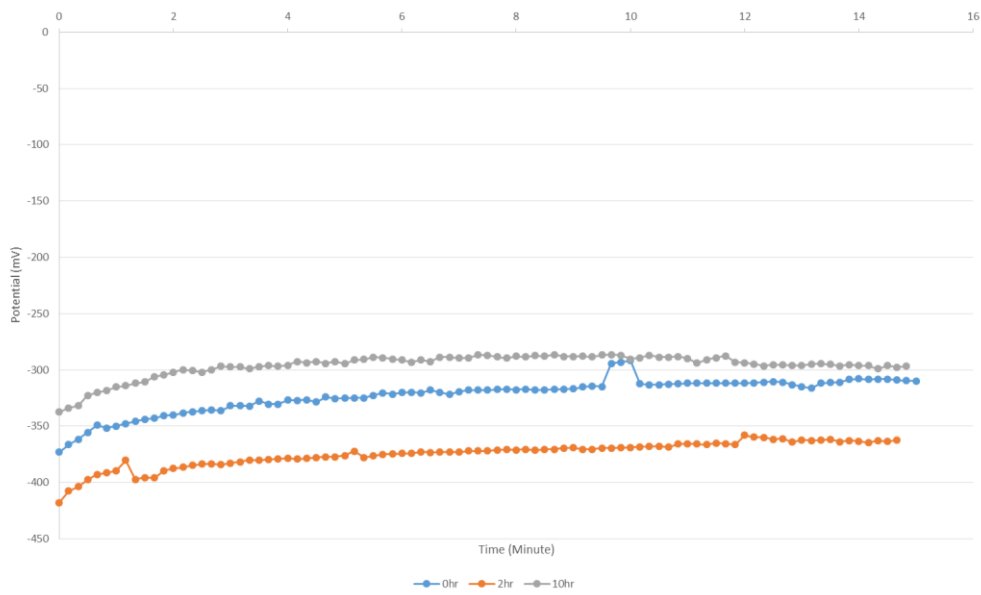


Figure 4.39: Different potential measurements in various time at the 2nd experiment

- 3rd experiment

As can be seen in Figure 4.40, the first reading range is between -343.3 mV and -289.4 mV with the average of -14.44 mV after deduction of the cell growth medium. In the second reading, potential values alters from -388.7 mV and -349.5 mV with the average of -357.79 mV which is around -71.50 mV after deduction of the cell growth medium. The gray line and last measurement of potentials, changes in the range of -266.1 mV and -219.9 mV with the average of -247.14 mV which is 39.15 mV after the deduction of the cell growth medium values.

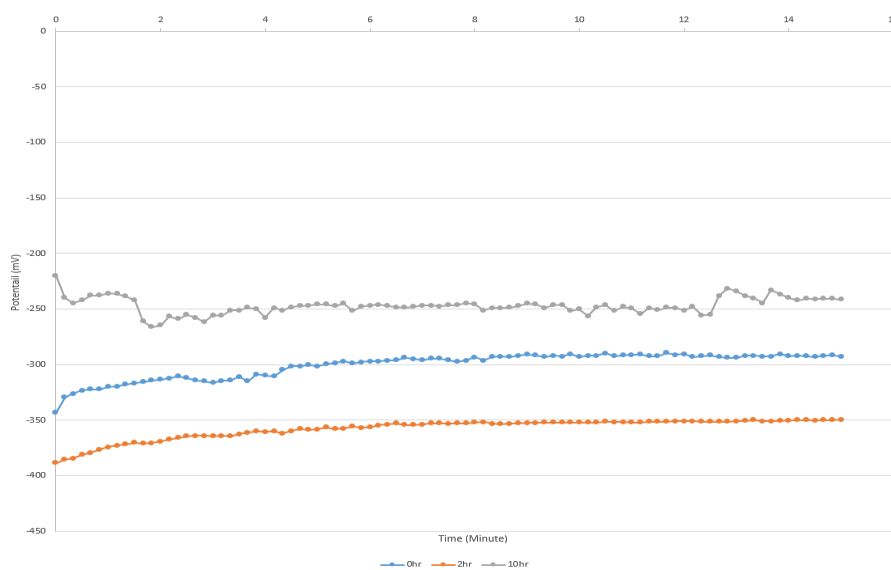


Figure 4.40: Different potential measurements in various time at the 3rd experiment

4.5 Di-electrophoresis Method

After counting and checking viability of cells, the cells were transported on the DEP chip to place in 3DEP system. Each experiments took 10 seconds and each well of the chip received a different frequency in the range of 10 kHz-20 MHz. Experiments were repeated 5 times to reduce the effect of variation in cell number.

Cells were checked through the hemocytometer for numbers and viability, before running the DEP experiment (Figure 4.41).

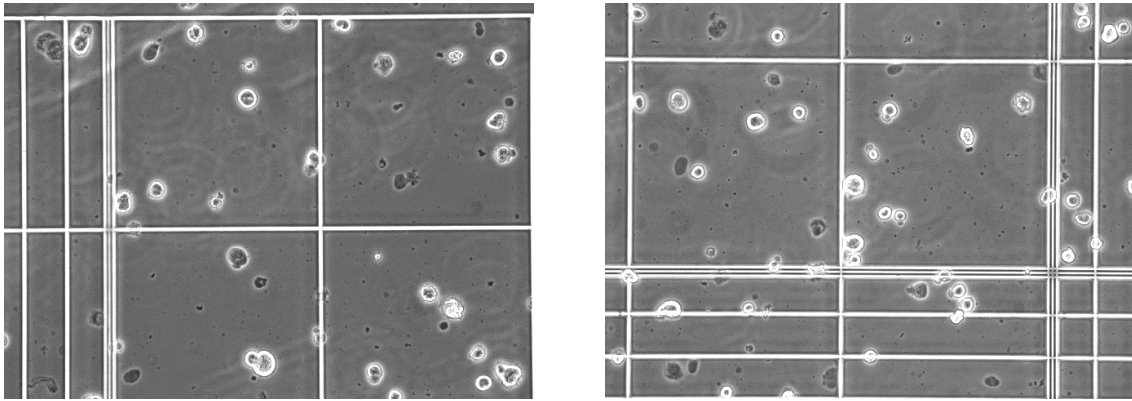
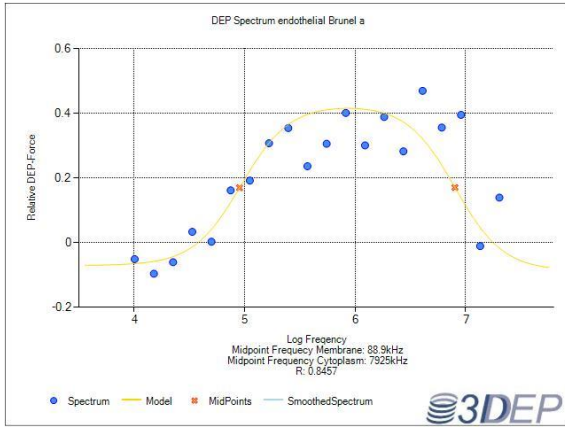


Figure 4.41: Captured images from human coronary artery endothelial cells on hemocytometer via the microscope

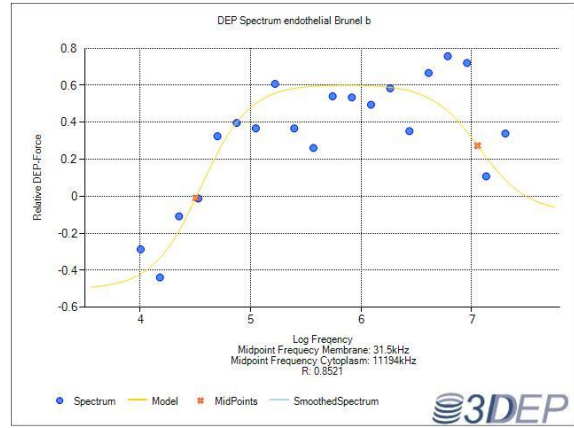
The results of di-electrophoresis experiments are shown in Figure 4.42 (a-e). The theoretical values have been derived from the equation shown below (4.1). The experimental results deviate from the theoretical values due to several variables, for example the exact dimension of the cells, their electrical properties and the properties of the media; none of these can be given in exact values, leading to differences between two theoretical and experimental data.

$$F_{Dep} = 2\pi\epsilon_m r^3 Re[f_{CM}] \nabla E_{rms}^2 \quad (4.1)$$

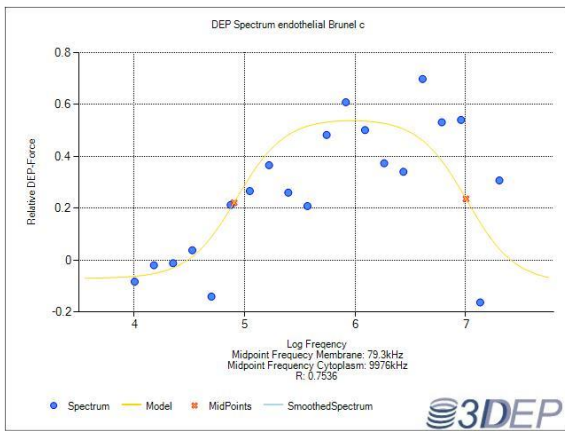
Where F_{Dep} is the relative DEP force, ϵ_m is the permittivity of the cell medium, r is the cell's radius, $Re[f_{CM}]$ is the real part of the Clausius-Mossotti factor and E_{rms}^2 is the root mean square of the electric field (Elitas *et al.*, 2017).



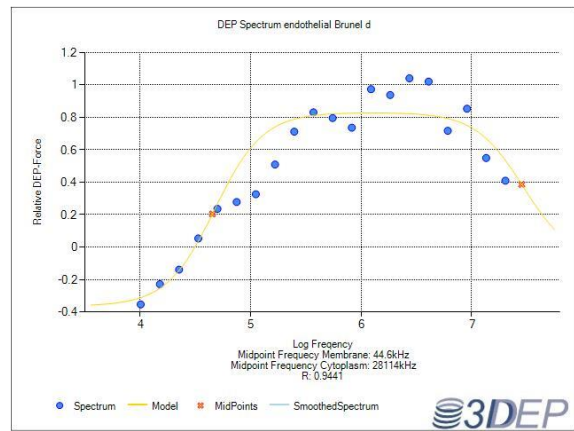
(a)



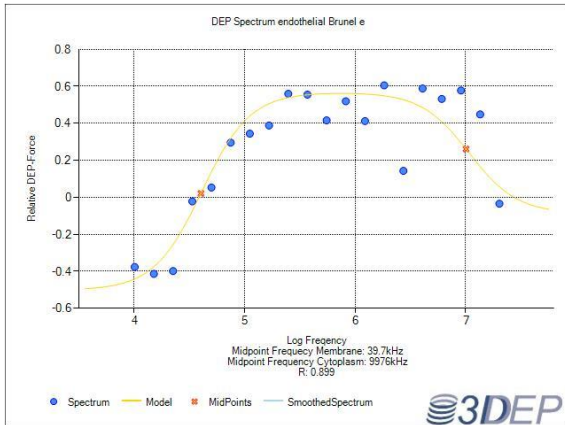
(b)



(c)



(d)



(e)

Figure 4.42: DEP spectrum of human coronary artery endothelial cells (n=5), 20 points frequency runs

Human coronary artery endothelial cells cellular characteristics after repeating five times, which determined using the DEP, is presented in the following Table 4.5:

Table 4.5: Human coronary artery endothelial cell parameters determined n=5, 20 point spectra

Cell Parameters	Mean (n=5)	± SD
Cytoplasm Conductivity (S/m)	0.130264	± 0.054887
Cytoplasm Permittivity	60	fixed
Specific Membrane Conductance (S/m ²)	1009.495	± 408.2987
Specific Membrane Capacitance (F/m ²)	0.01233	± 0.001853
Cell Radius (µm)	8	fixed
fixed Medium Conductivity (S/m)	0.018	fixed
fixed Medium Permittivity	78	fixed

4.6 Zeta Potential Method

In this experiment both cell lines including human coronary endothelial cells and human osteoblast cells were analyzed using zeta potential measurement after checking their viability. Each cell lines were tested once in its cell culture medium (CCM) and once in di-electrophoresis medium (DEP) and each measurement was repeated three times. Table 4.6 showed the zeta potential measurements of different times.

Table 4.6: Independent measurements of zeta potential

Cell type	Suspension medium	1 st measurement	2 nd measurement	3 rd measurement
Human coronary artery endothelial	Cell culture medium	-9.81	-9.91	-9.56
Human coronary artery endothelial	DEP medium	-25.2	-16.6	-22.8
Human osteoblast	Cell culture medium	-8.97	-11.6	-10.6
Human osteoblast	DEP medium	-20.6	-10.2	-9.95

The corresponding graph of independent zeta potential measurements can be seen in Figure 4.43. The measurements which were done in CCM, had much lower differences compared to the values in DEP.

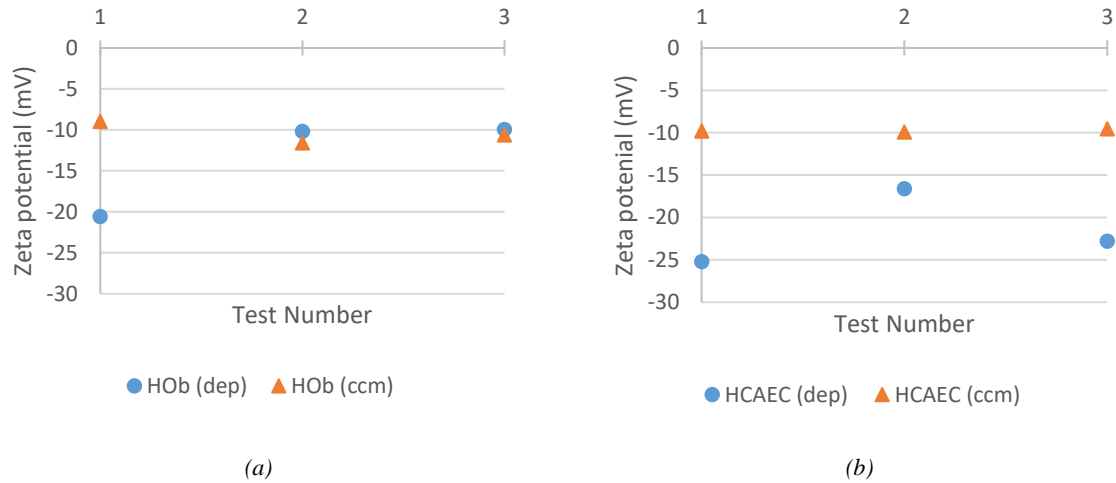


Figure 4.43: Scattered graph of several measurement of zeta potential: human osteoblast cells' zeta potential measurements(a), human coronary artery endothelial cells' zeta potential measurements (b)

Table 4.7 showed the average amounts of cells' zeta potential in different mediums.

Table 4.7: The mean values of zeta potential of different cell lines \pm standard deviation

Cell type	Suspension medium	Zeta potential (mV)
Human coronary artery endothelial	Cell culture medium	-9.76 ± 0.18
Human coronary artery endothelial	DEP medium	-21.53 ± 4.43
Human osteoblast	Cell culture medium	-10.39 ± 1.32
Human osteoblast	DEP medium	-13.58 ± 6.07

As can be seen in the corresponding graph of average of zeta potential measurement (Figure 4.44), the standard deviation from the average showed that values in CCM for both types of cells (± 0.18 for HCAEC and ± 1.32 for HOb) were greater than the observed values in DEP (± 4.43 for HCEAC and ± 6.07 for HOb). Thus, analysed results illustrated that zeta potentials measurements in CCM were more reliable than DEP ones.

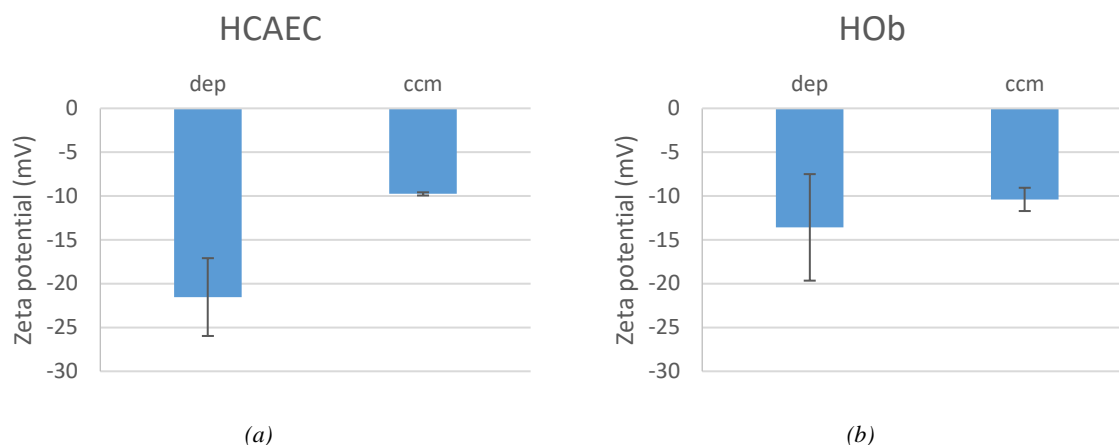


Figure 4.44: Corresponding graphs to Table 4.7 (human coronary artery endothelial cells (a) and human osteoblast cells (b)) illustrate the mean \pm standard deviation for each independent measurement in DEP and CCM.

4.7 Electrophoresis Method

Human coronary artery endothelial cells were cultured in the centre area of the cuvette in order to create equal possibilities for cells to migrate or orient towards positive and/or negative electrodes under the application of an electrical charge. It was assumed that the applied electrical fields had efficient potentials to cause migration or orientation of cells towards electrodes, specifically the cathode. Different range of electrical charges were applied with different durations. Each experiment was divided into two forms; in the first part of the experiment the cuvette of cultured cells at different voltages for the period of 15 minutes. After finishing the first part of the experiment, then the second part started in which the cuvette underwent only one choice of voltage for duration of 20 hours. Results of the first part are presented in pairs of images at minute=0 and minute=15 of the experiments. Some cells which showed changes in shapes or had displacements are marked. However, these differences may be not significant or clear due to formatting images in smaller sizes. The second part results are presented in form of four images from minute=0, hour=1, 2 and 3 of the experiment.

4.7.1 High Range of Applied DC

In this experiment, a high range of DC were selected connection.

Similarly, in the first part the range of voltages (mV) contained: 400, 1000, 1500, 2000 and 3000 for 15 minutes

Cells subjected to 400 mV showed no significant differences at minute 0 and 15 of the experiments. A few cells, shown labeled in Figure 4.45 (a, b), lengthened negligibly. Except some notable changes, the rest of the cells, subject to 1000 mV did not show spectacular changes (c, d). For example, cell A showed some elongation, one end of the cell appeared fixed while the other end moved. Cell B moved in a downward direction. Cell C was similar to cell A as it elongated. However, and somewhat contrary, cell D became shorter. No significant changes or movements were found under the application of 1500 (e, f), 2000 (g, h) and 3000 (i, j). Only a small number of cells showed slight movements with the in all last three applied electrical charges.



(a) Applied 400 mV at minute=1



(b) Applied 400 mV at minute=15



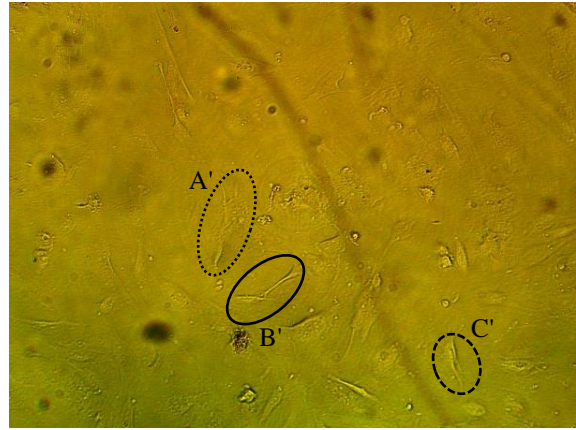
(c) Applied 1000 mV at minute=1



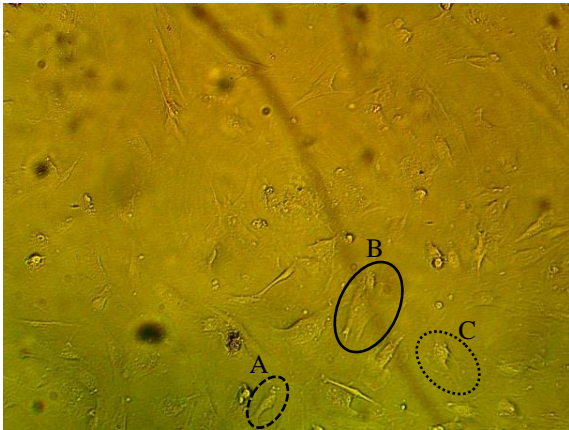
(d) Applied 1000 mV at minute=15



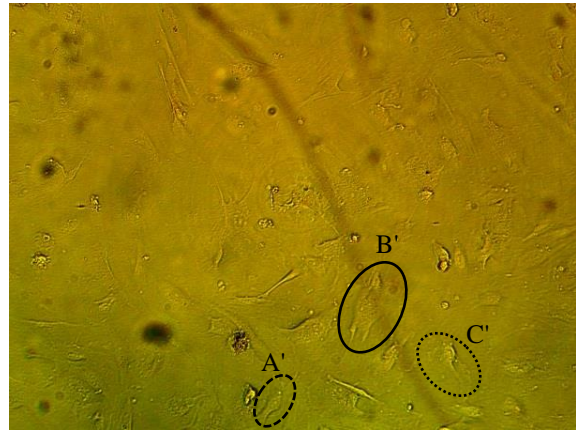
(e) Applied 1500 mV at minute=1



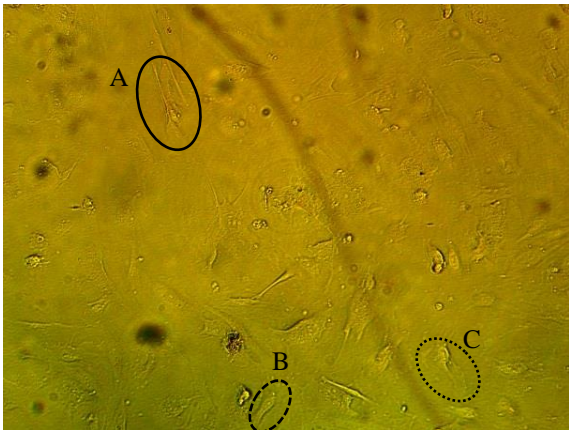
(f) Applied 1500 mV at minute=15



(g) Applied 2000 mV at minute=1



(h) Applied 2000 mV at minute=15



(i) Applied 3000 mV at minute=1



(j) Applied 3000 mV at minute=15

Figure 4.45: Comparison of cells movements' changes under high level of applied DC during a quarter of an hour

Part two included the results of applying 1000 mV for 20 hours on the cells.

From Figure 4.46 below we can see the changes of cells under application of 1000 mV over three hours. The most common trend to cells under this application is that they become thinner. However, other behavior can be seen as well among cells. For instance, cells B, C, D, F and H

became thinner during the experiment in addition cells B and C moved downward and upward, respectively and cell D moved towards right. Also, cells E and G both showed contraction.

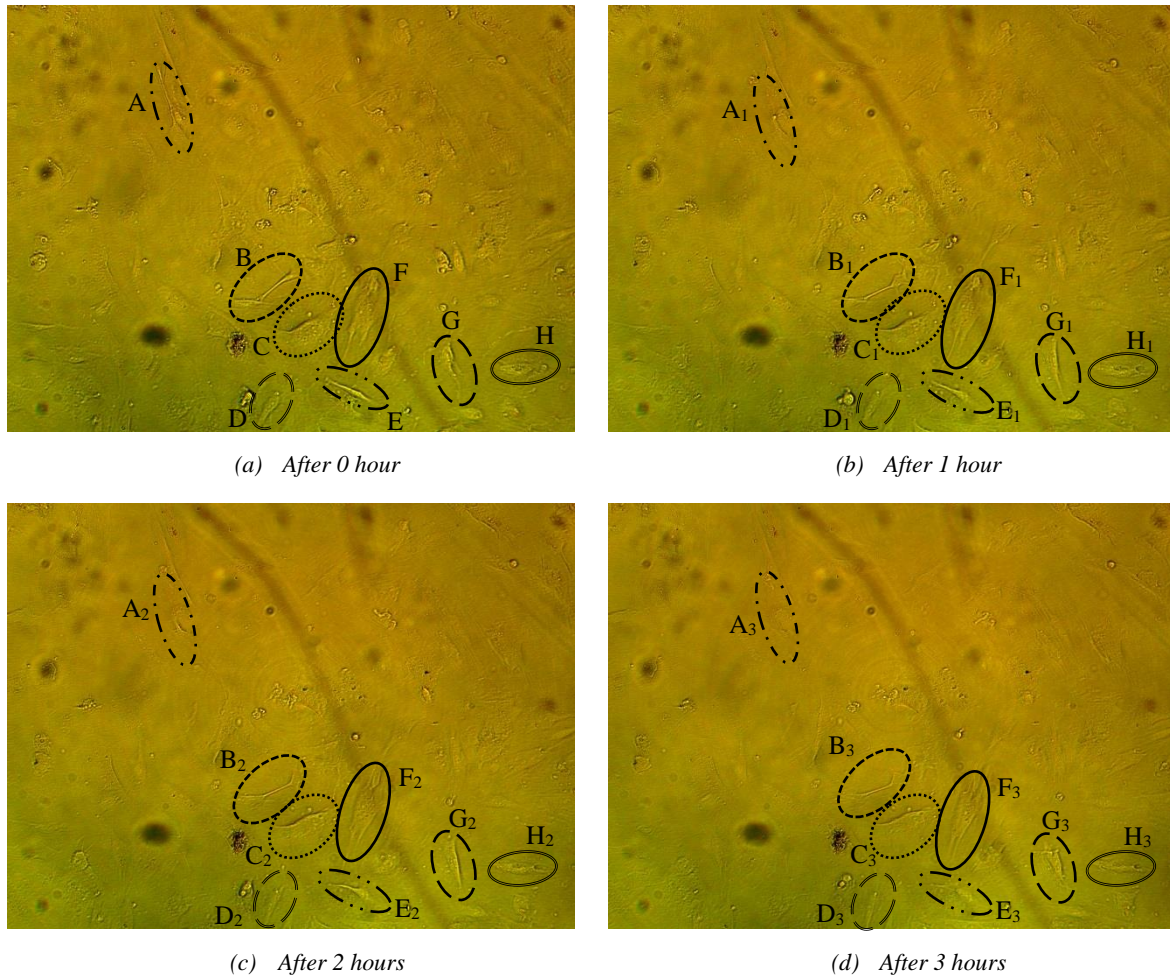


Figure 4.46: Time lapse microscopy images from cells under application of 1000 mV

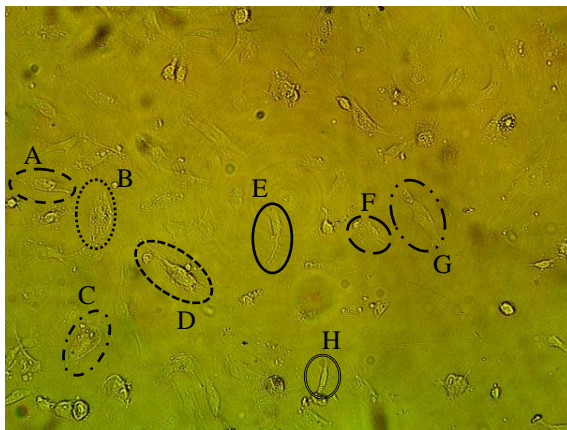
4.7.2 Low Range of Applied DC

Various range of DC was selected for the third experiment.

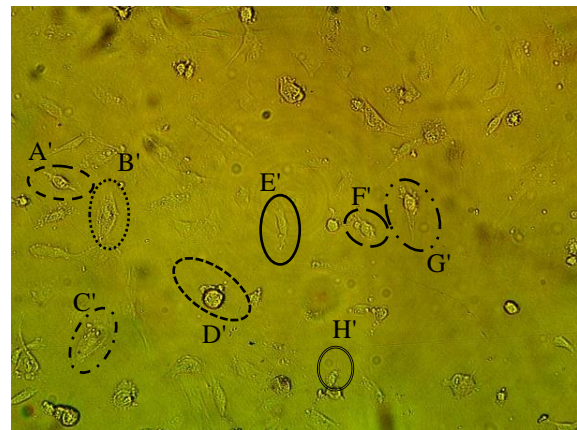
In part one of the experiment, the following amounts of electrical charges were used: 30, 100, 200, 300, 400 and 500 mV.

As can be seen in Figure 4.47, cells that are named as A, D, E, F, G and H, contracted after 15 minutes at 30 mV compared to their initial form. However, cells B and C expanded in the last minute of the experiment (a, b). In the 100 mV experiment, changes were relatively different among cells. The nucleus of cell A shifted up and became thinner, like cell B. Cell C also moved in an upwards direction. However, cell D became shorter in length by contracting from its lowest part towards its centre. Cell E moved towards the left downwards with the addition

of some stretching as well (c, d). Similar to the 100mV experiment, cells under the influence of 200 mV displayed various changes. Cell A became smaller and its nucleus shifted up and left. Both cells B and G contracted during the experiment and cells C and E moved downward. Cell D changed in dimensions by becoming thinner. Cell F stretched in a downward orientation (e, f). Cells under the application of 300 mV displayed different changes. For instance, cell A became shorter in length. Cell B became thinner and cell C contracted and became much smaller. Cell D shifted negligibly in a downward direction and cell E and cell F moved to the right and down direction, respectively (g, h). As experimentally observed when applying different electrical charges, for example 100, 200 and 300 mV, the dynamic movement and morphological changes in cells, varied again when applying 400 mV. Cell A shortened in length and cell B had an insignificant movement. However, both cell C and D again had notable movements (i, j). No significant differences were found with cell behavior during and between the first and last minute of the experiment, using 500 mV. Cells labeled in the relevant images had negligible differences during the experiment (k, l).



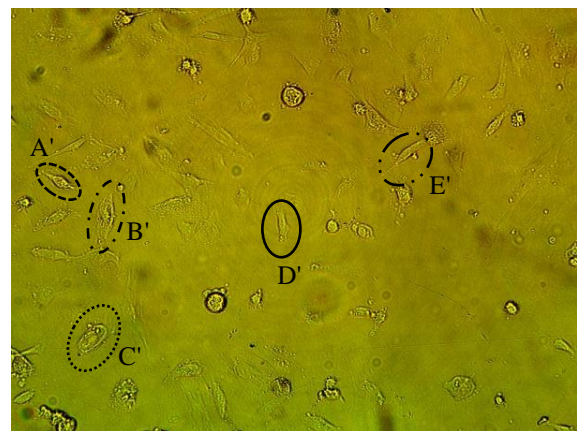
(a) Applied 30 mV at minute=1



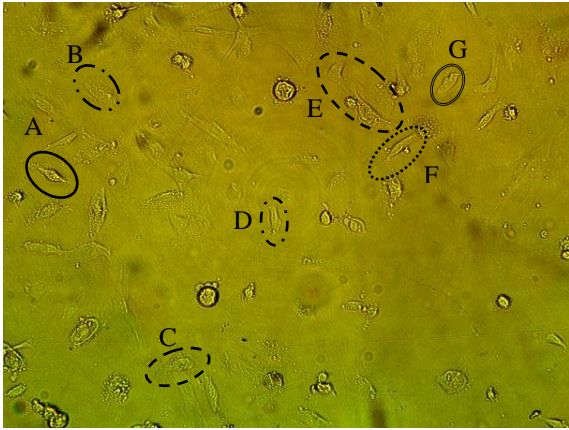
(b) Applied 30 mV at minute=15



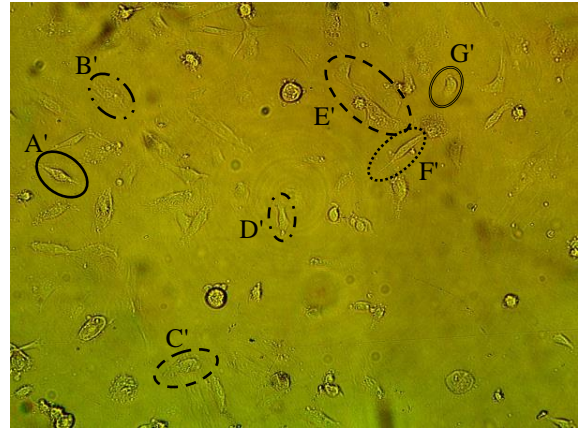
(c) Applied 100 mV at minute=1



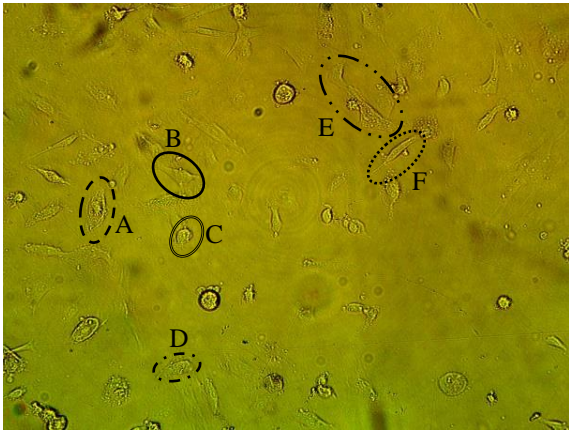
(d) Applied 100 mV at minute=15



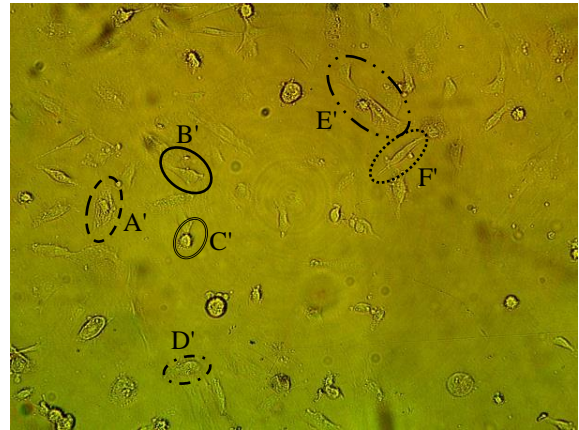
(e) Applied 200 mV at minute=1



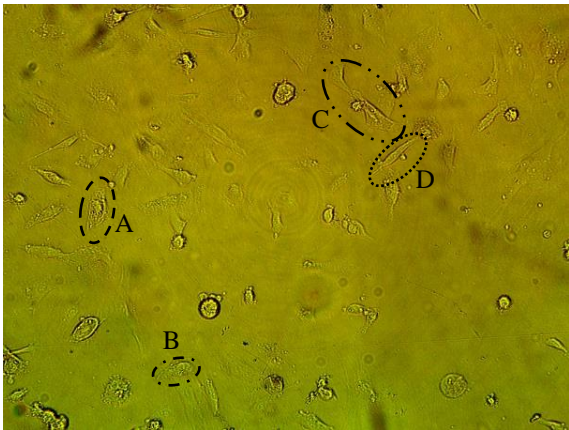
(f) Applied 200 mV at minute=15



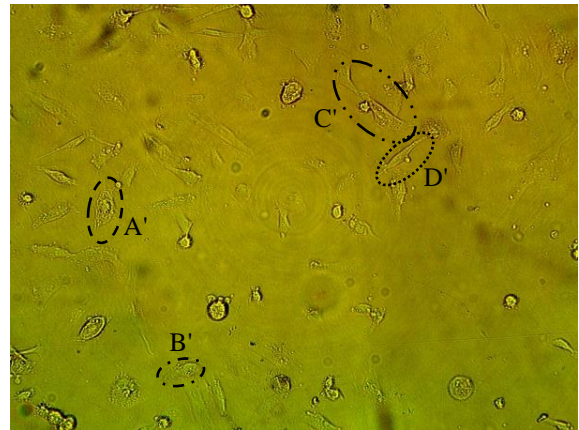
(g) Applied 300 mV at minute=1



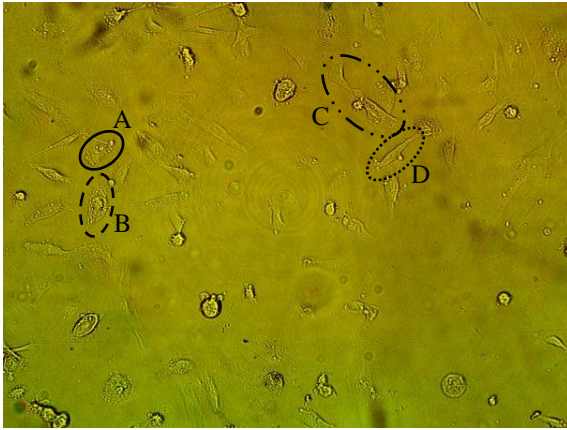
(h) Applied 300 mV at minute=15



(i) Applied 400 mV at minute=1



(j) Applied 400 mV at minute=15



(k) Applied 500 mV at minute=1

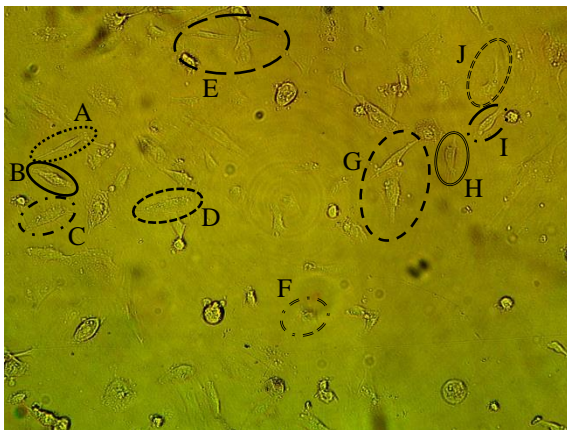


(l) Applied 500 mV at minute=15

Figure 4.47: Captured images using the inverted microscope from different applied DC on human cells

30 mV was selected to test the second part of this experiment. The 20 hours video that was recorded from this experiment converted to about 5 minutes of video using time lapse software. The images illustrate the orientation changes of cells (Figure 4.48).

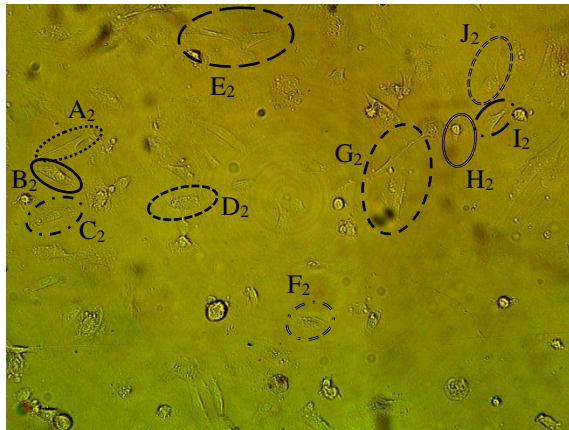
As shown in Figure 4.48, cells presented changes and movements at different times of the experiment under application of 30 mV. Some behavior was common between cells in this experiment. For instance, both cells A and F moved downward from their original positions. Likewise, the central areas of cells B and E moved upward, while cells G and H moved up in their entirety. Also some cells' dimensions were affected: cell I had an expansion so that I_3 was greater than I. however, some cells like cell C became thinner. Other behavior was found among cells such as contraction of cell J and cell D moved in the right hand direction after it contracted.



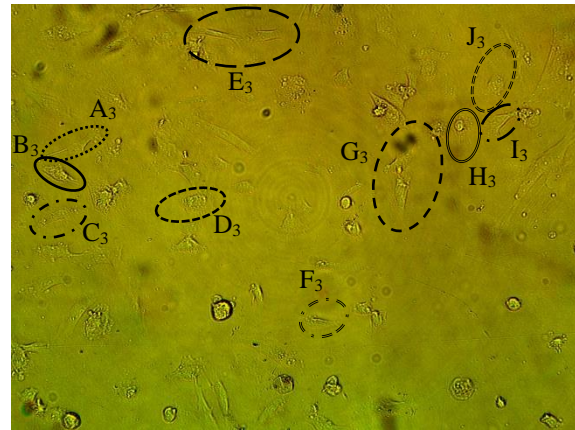
(a) After 0 hour



(b) After 1 hour



(c) After 2 hours



(d) After 3 hours

Figure 4.48: Time lapse microscopy images from cells changes applying 30 mV DC

4.7.3 Low Range of Applied DC

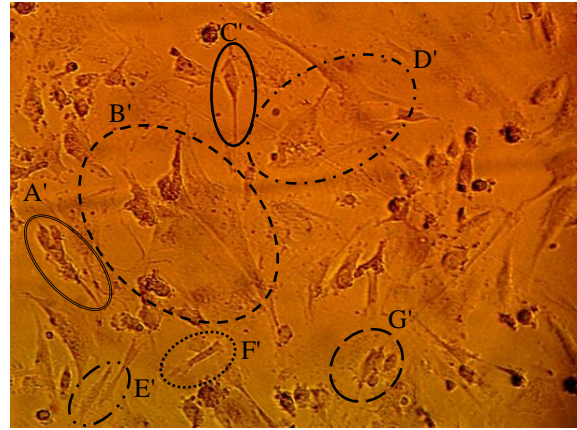
Similarly, in this experiment, chosen electrical fields was the same as the selected range in the 3rd experiment. However, in the second part there was a different.

In the first part selected electrical charges were: 100, 200, 300, 400 and 500 mV. As it can be seen in Figure 4.49, orientation of cells altered under application of some electrical voltages.

As can be easily noticed from 100 mV images (a, b), the cells were more stretched at minute 1 compared to minute 15. Indeed, the cells under application of 100 mV, after 15 minutes showed signs of contraction. For instance, the cells marked C and G, their cores became smaller after 15 minutes (C' and G'). Cell B upper side moved down and cell F became smaller. Similarly, cells contracted under the application of 200 mV (c, d). Cells' orientation was not recognizable in several images from this applied voltage. However, other changes were noticeable. Cell A became shorter in length and cell B became thinner: cells C, D, E and F became smaller. Using 300 mV, movements were very small (e, f). For instance, the cell marked A, became smaller. Most of cells did not orient at 400 mV. A few cells showed very small changes, illustrated in figure (g, h). Similar to 400 mV, the cells under application of 500 mV influence showed no significant changes (i, j).



(a) 100 mV at minute=1



(b) 100 mV at minute=15



(c) Applied 200 mV at minute=1



(d) Applied 200 mV at minute=15



(e) Applied 300 mV at minute=1



(f) Applied 300 mV at minute=15

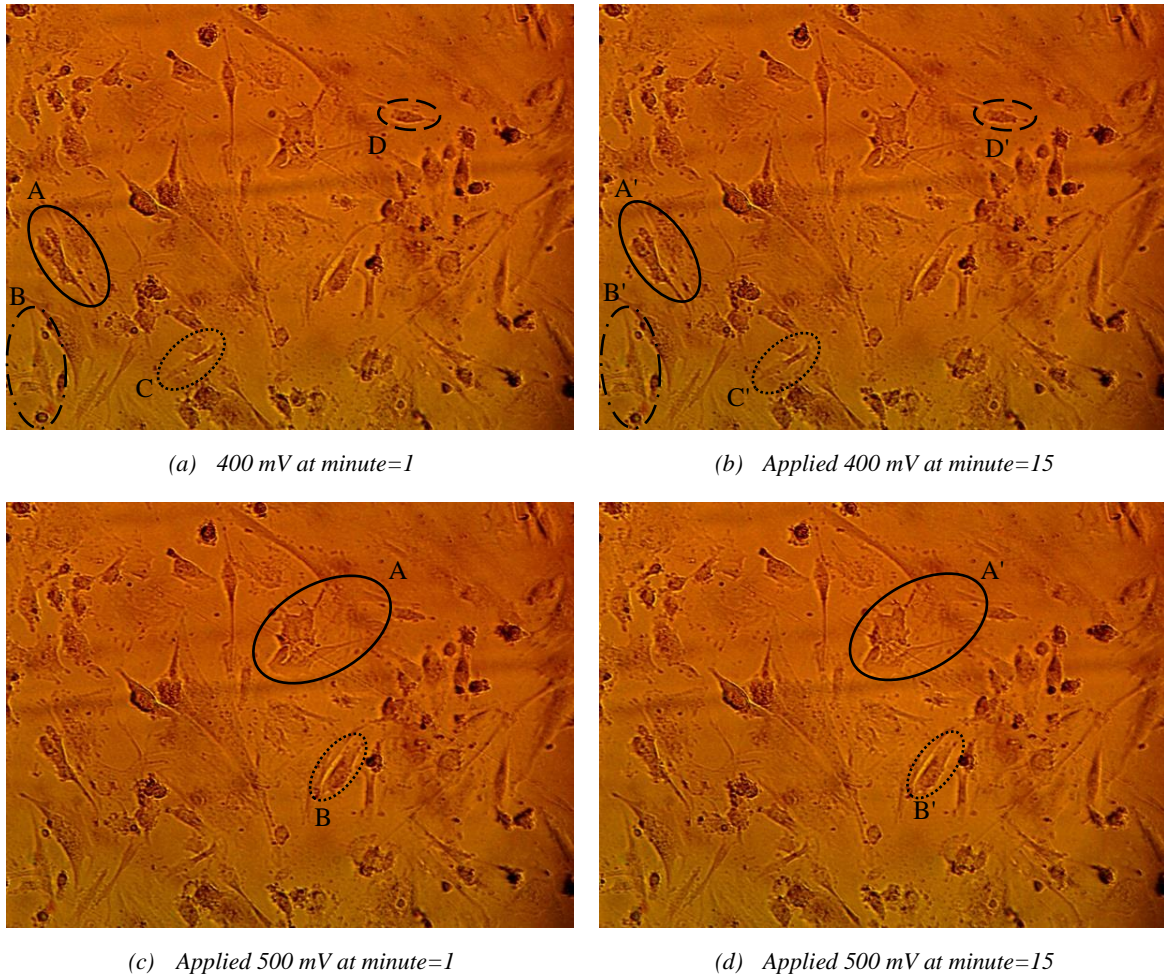


Figure 4.49: Microscopic images illustrate the different orientation of cells under application of different applied electrical field

The amount 500 mV was applied for 20 hours on cultured human coronary artery endothelial cells. Due to negligible changes and risk of dying cells after couple of hours, only images within 3 hours are represented in Figure 4.50 and will be discussed.

The cell which is marked A, has its cytoplasm aggregated up from the left side of the oval towards its nucleus A₁ (b). Then, it expanded and shifted downwards to the right of the black oval (c, d). Indeed, A₃ is greater than A₂ and A₂ is greater than A₁. The cell which is shown by small arrows B in its left side contracted, and became thicker while its right side became contracted (a, b). The left side of the cell expanded after 2 and 3 hours B₂ and B₃ (c, d). The cell labelled C also oriented towards its left side. As it can be seen, the cell is more beveled towards the left in C₃ compared to C, cell D showed small movements and cell E expanded during the experiment.

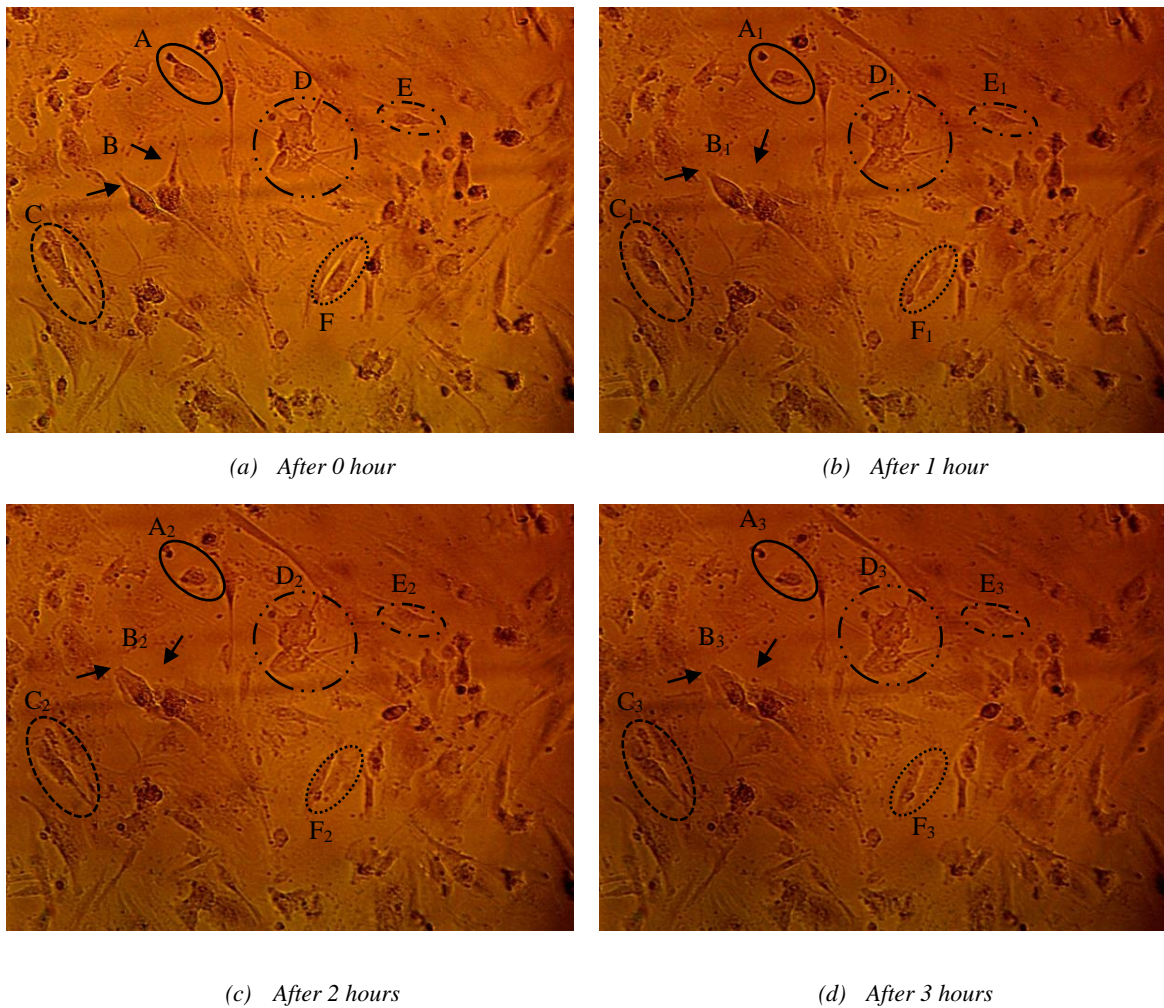


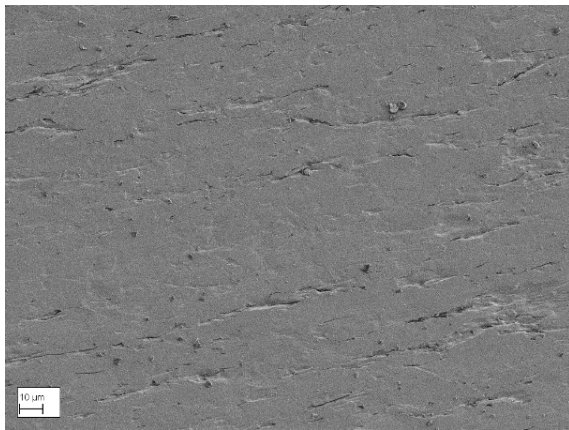
Figure 4.50: Time lapse microscopy images

4.8 Mimicked Artery Experiments

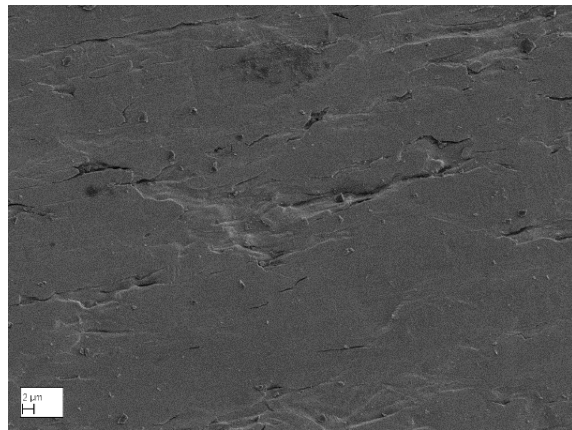
After running sheep blood through stents, in a bio-mimic apparatus, the stents were prepared and made ready to observe using SEM: this investigation explored endothelial cell numbers, morphology and other blood components onto the inner (luminal) surface of the stents. The following descriptions contain a series of results relating to the stents, which underwent 0 mV (control), 27 mV and 1 V during the experiments; plus one was used to culture endothelial cells, the second stent as a topographical control. The stents whose positions were in the middle of the manifold (numbered, 3, 4, 5, 6, 7 and 8) had greater potential to cause cell migration. Due to the large number of SEM images taken from the surface of the stents, selected, relevant image are shown in this chapter and the rest are presented in Appendix D: Mimicked Artery SEM Images.

4.8.1 Bare Stent

The following SEM images show a bare stainless steel 316LM stent. This stent is used as a reference sample without undergoing any experiments to compare with other samples that were exposed to the blood. As can be seen in both images (Figure 4.51), the inner surface of the stent has some detritus dust that was not removed consequent to abrasive polishing. It also can be noticed that the surface of the metal possesses several furrow-like features. These features may be one of the factors which have impact on capturing and aligning cells or other particulates on the stent.



Magnification $\times 1.25k$



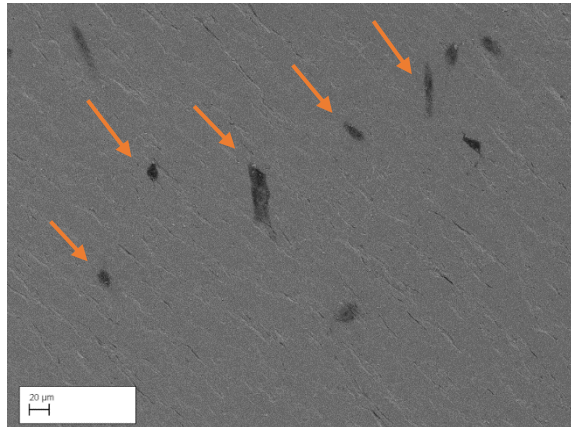
Magnification $\times 3.00k$

Figure 4.51: SEM pictures with different magnification from inner surface area of the stent

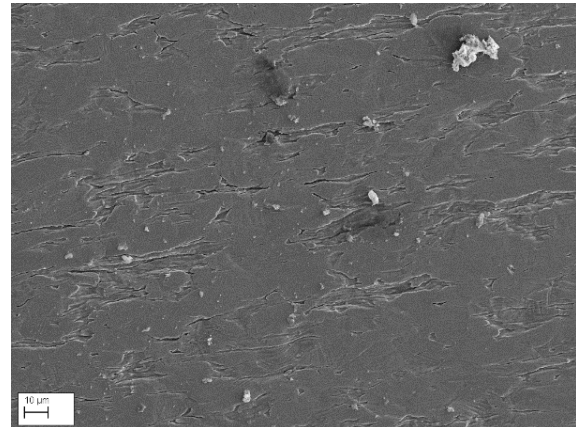
4.8.2 Bare Stent with Cultured Endothelial Cells on its Surface

Human coronary artery endothelial cells were cultured on this stent's surface. As can be seen in the SEM images (Figure 4.52), the presence of endothelial cells can be noticed in different areas of the stent's surface. However, the cells were cultured in ideal conditions to reach the confluency of 70%, a number of human coronary artery endothelial cells and these were observed in SEM pictures. One of the reasons which may influence this issue, is that some cells may not be completely adherent to the surface of the stent, thus they could not reproduce and reach the 70% confluency. Although the cells reached confluency of 70% in the petri dish before transportation to the stent, they possibly could not grow as well as in the idealised condition that are possible when cultured in the petri dish. In addition, after culturing cells on the surface of the stent, cells confluency was not able to be checked when using the required an inverted microscope. As a result, even if some cells were adherent to the surface of the stent,

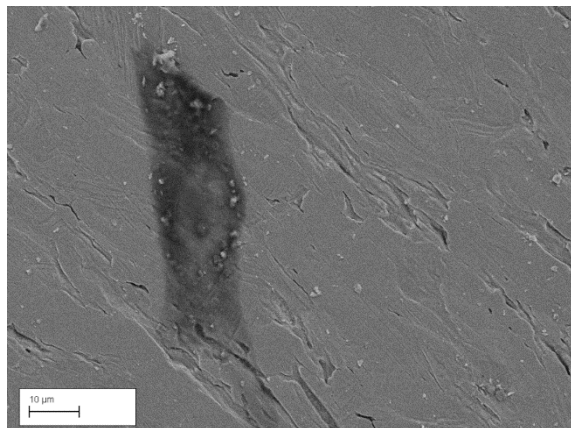
some of them were lost during fixation leading to a fewer numbers of cells being observed in SEM analysis.



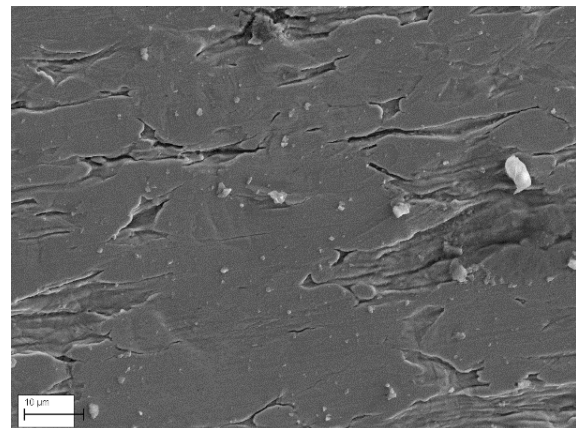
Magnification $\times 520$: Endothelial cells were showed by colored arrows.



Magnification $\times 1.25k$



Magnification $\times 2.50k$



Magnification $\times 3.00k$

Figure 4.52: SEM images from the inner surface of the stent that human coronary artery endothelial cells were cultured on

4.8.3 Applied Direct Current on Bare Stent

Different amount of direct electrical charges were applied to this series of stents. In some of the cases, electrical application was successful in attracting cells, specifically endothelial cells onto the surface of the stents.

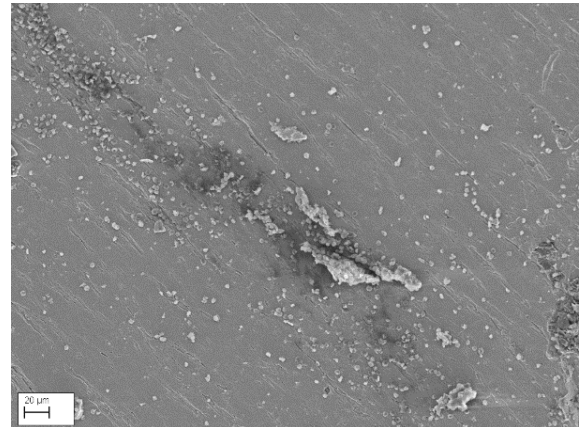
Sample 1 (1 V)

SEM images of this sample displays an endothelial cell captured on the surface (Figure 4.53), although it was one of the stents which had some interruption in blood flow during this experiment. However, this electrical charge was successful in attracting numerous red blood

cells (RBCs). Noticeably, the morphology of RBCs were ideal meaning this degree of electrical charge did not have negative impacts on RBCs attraction.



Magnification of $\times 400$: Representation of massive RBCs

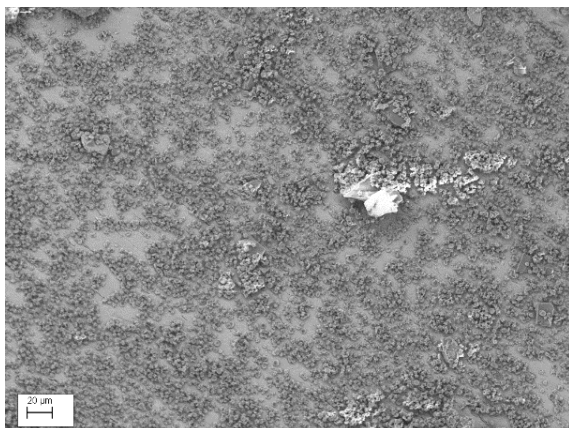


Magnification $\times 660$: An endothelial cell has been shown with a colored arrow

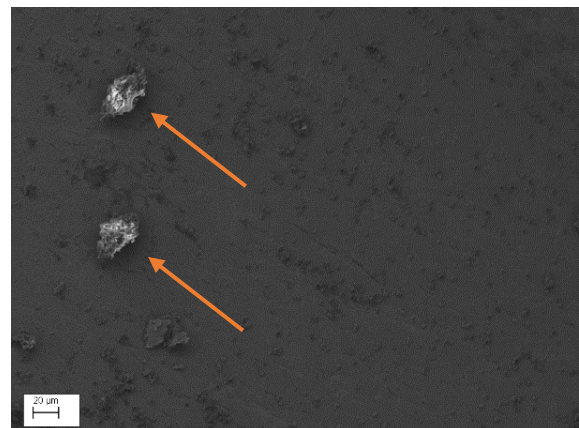
Figure 4.53: SEM pictures of the stent which underwent the application of 1V.

Sample 2 (1 V)

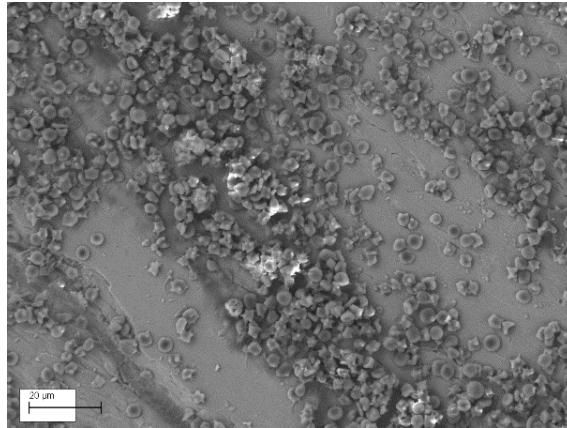
As can be seen in Figure 4.54, presence of RBCs and endothelial cells can be seen on the surface of this sample, furnished with 1V. Although the position of this stent in the manifold was tube 2, it indicated this degree of electrical charge could effect on the attraction of cells even if it did not have the ideal blood flow during the experiment, however RBCs' shape looked typical.



Magnification $\times 660$: Massive RBCs presentation



Magnification $\times 670$: Exhibition of endothelial cells

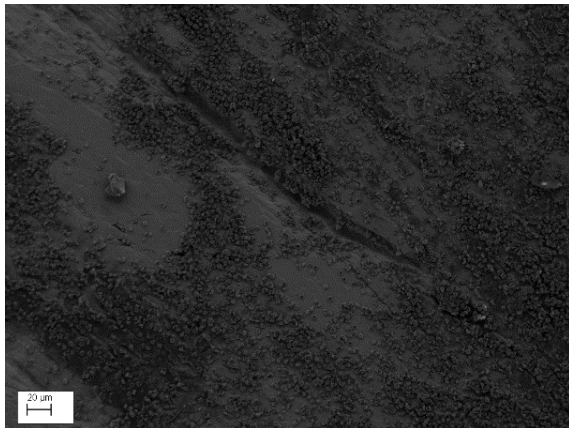


Magnification $\times 1.90k$: Presentation of RBCs

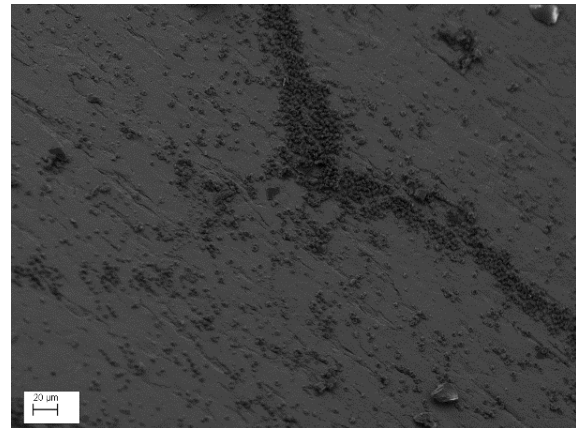
Figure 4.54: Analysis of the surface of the stent connecting to IV.

Sample 3 (non-electrical connection)

The third stent was not connected to any electrical connections and was used as the experimental control. This stent had an acceptable blood flow during the experiment as it was one of the stents positioned almost in the middle of the manifold. As shown in Figure 4.55, massive accumulation of RBCs can be seen in most segments of the stent. Although some areas were fully covered by adherence of RBCs, some other parts were shown traces of RBCs' adherence.



Magnification $\times 640$: RBCs fully covered some parts of the surface



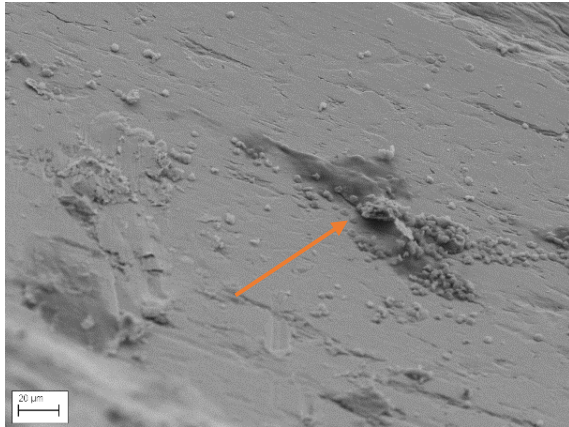
Magnification $\times 650$: Arrangement of RBCs in a line shape

Figure 4.55: SEM's images from a non-electrical connected sample which represents massive accumulation of RBCs.

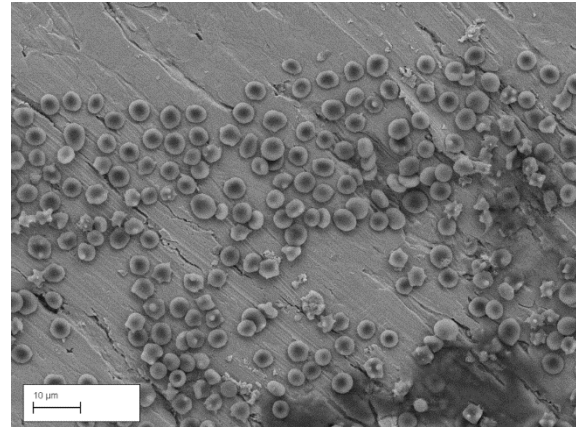
Sample 4 (27 mV)

This sample was connected to the 27 mV supply low voltage and had good blood flowing through. Distribution of RBCs can be seen in some areas of the stent (Figure 4.56). However,

this small electrical charge had the potential to attract endothelial cells on its surface. RBCs looked biconcave and round which illustrates that this amount of charge does not change the morphology of the cells.



Magnification $\times 1.00k$: An endothelial cell is adherent



Magnification $\times 2.50k$: Enormous RBCs attachments on the surface

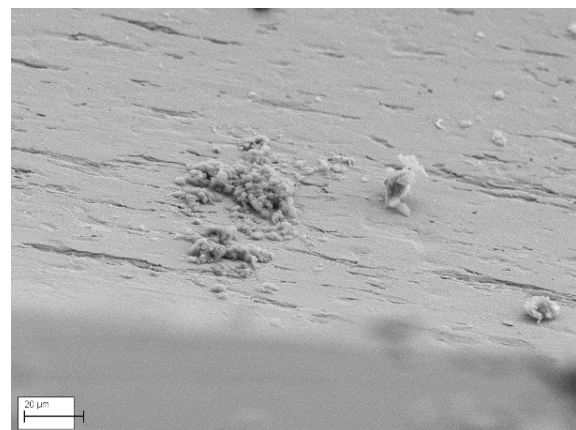
Figure 4.56: 1st stent which connected to 27 mV, displays adherence of endothelial cell on its surface beside presentation of RBCs.

Sample 5 (1 V)

Despite the ideal blood flow in this stent, desired cells were not adherent onto the surface. Although other stents which underwent the same amount of electrical charges could successfully cause presence of endothelial cells onto the surface.



Magnification $\times 1.00k$

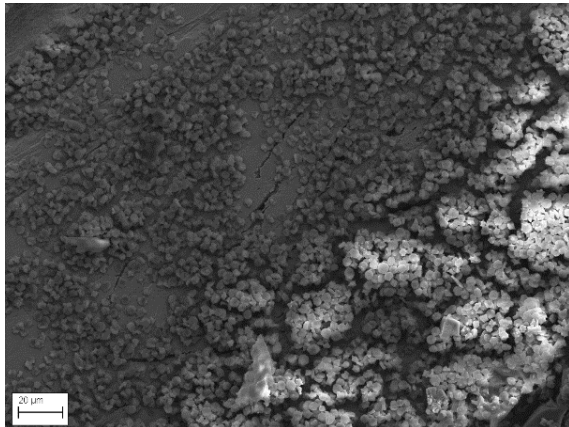


Magnification $\times 2.00$

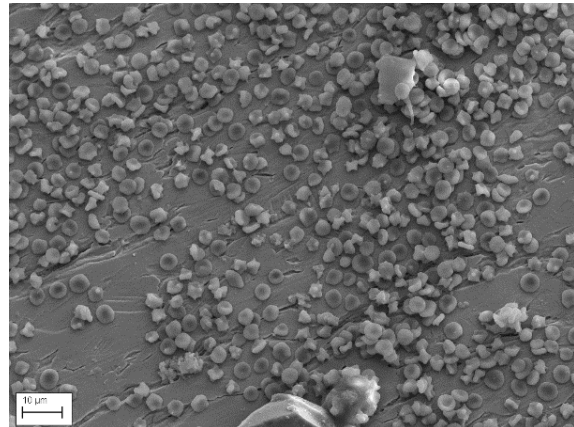
Figure 4.57: Presence of biological objects on the surface of the sample

Sample 6 (non-electrical connection)

Like stent number 3, this sample has no electrical connection and surprisingly its surface was the same as the stent number 3. As it can be seen in Figure 4.58, the surface of this stent was completely covered by RBCs. In some segments RBCs overlapped each other and made aggregations. RBCs' appearance looked normal.



Magnification $\times 1.20k$: Massive RBCs accumulation



Magnification $\times 2.10k$: Considerable incidence of RBCs

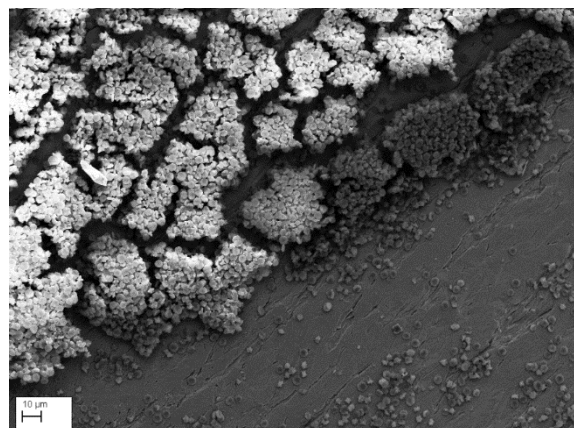
Figure 4.58: Presence of plenty of RBCs

Sample 7 (27 mV)

Observation of SEM pictures of this sample demonstrated formation of RBCs aggregations in some areas and presence of number of RBCs in some segments (Figure 4.59).



Magnification $\times 460k$: Incidence of RBCs' accumulation



Magnification $\times 1.00k$: Extensive RBCs' aggregations

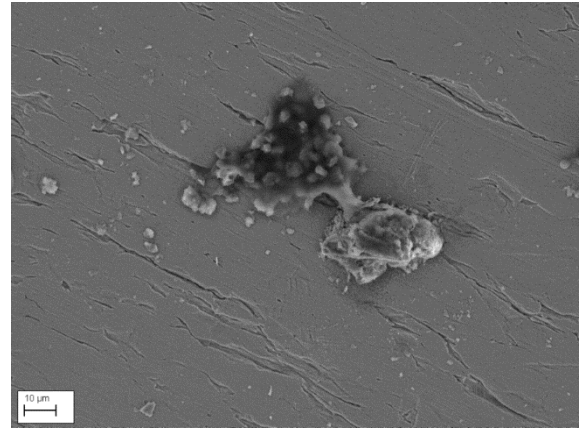
Figure 4.59: RBCs' distributed on the surface of the stent

Sample 8 (1 V)

Distribution of RBCs can be seen in Figure 4.60. Despite the observations of other stents under application of 1 V that attracted endothelial cells and extensive RBCs, few RBCs were settled on this sample stent.



Magnification ×1.00k: Dispersed adherence of RBCs.



Magnification ×1.66k

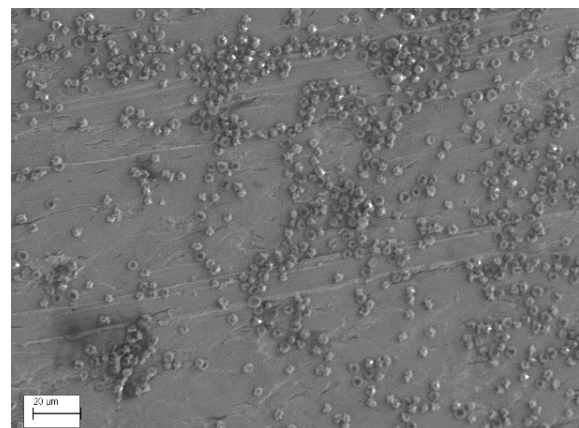
Figure 4.60: RBCs presence can be easily seen in the SEM images.

Sample 9 (non-electrical connection)

As can be seen in Figure 4.61, extensive numbers of RBCs were attracted onto the sample without electrical connection. Images with different magnification from the inner surface evidenced that RBCs did not change their shape during the experiments.



Magnification ×530: High coverage of RBCs

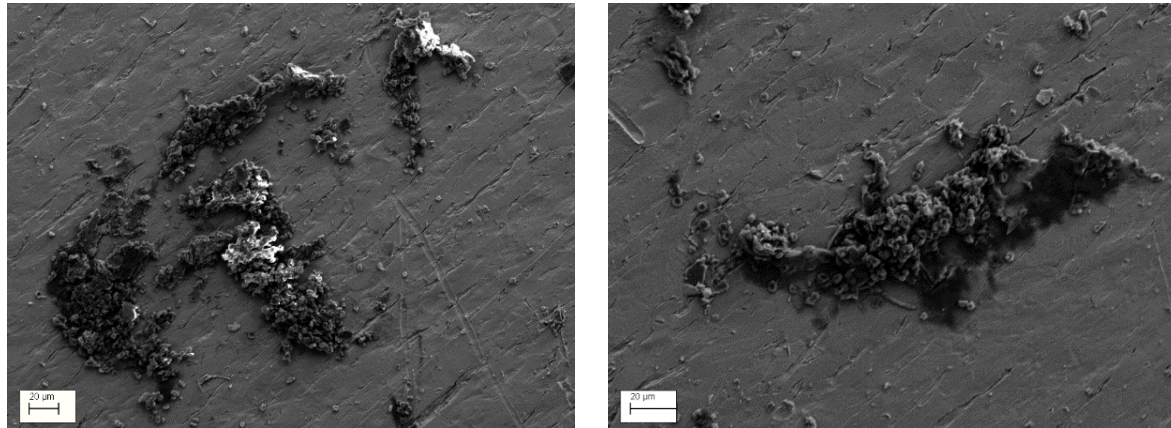


Magnification ×1.25k: Considerable presence of RBCs

Figure 4.61: SEM images illustrate full coverage of the surface of the stents by presence of quiet number of RBCs.

Sample 10 (27 mV)

Formation of RBCs' aggregations could be easily noticed on the surface of this stent (Figure 4.62). There were a number of RBCs' aggregations settling on the surface of the stent.



Magnification $\times 770$: Aggregations of RBCs

Magnification $\times 1.25k$: RBCs' clog

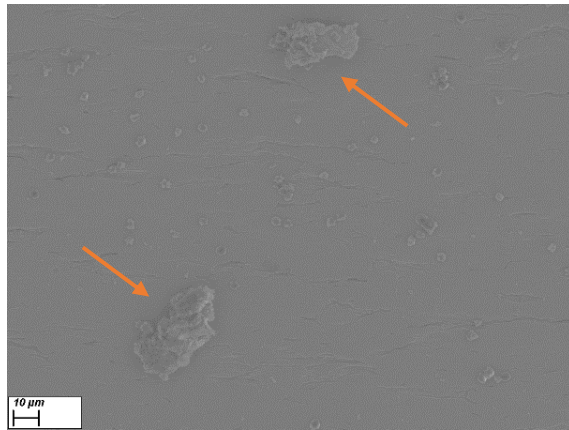
Figure 4.62: SEM images presents the formation of aggregations of RBCs

4.8.4 Applied Direct Current on Bare Stent with Extra Endothelial Cells

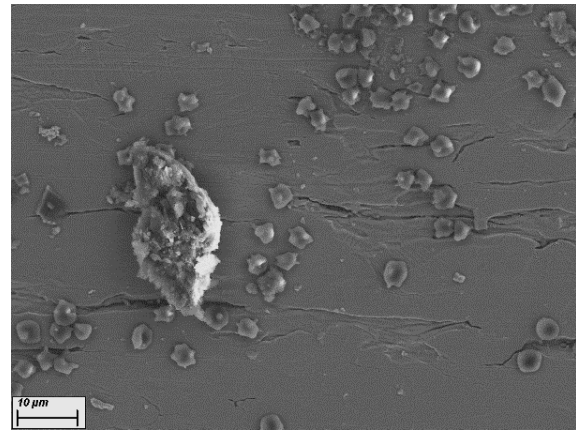
Due to the relatively low numbers of endothelial cells in the sheep blood used for experiments, human coronary artery endothelial cells were obtained and added to the sheep blood in an attempt to approximate endothelial cells that occur in conditions of vascular occlusive disease (coronary artery), in humans. Approximately 0.5M cells were added to the sheep blood, the experimental conditions and equipment remained identical in all other respects. SEM pictures were taken from the surface of the stents of after the experiment.

Sample 1 (1 V)

The stent underwent 1 V demonstrated the potential to attract endothelial cells among RBCs on its surface. Endothelial cells are shown with coloured arrows in Figure 4.63.



Magnification $\times 1.34k$: Incidence of endothelial cells besides RBCs

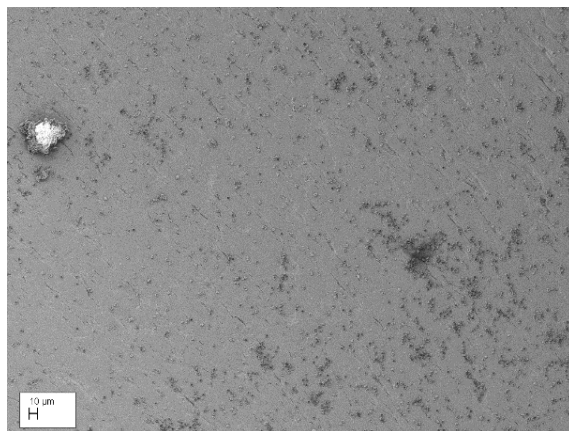


Magnification $\times 3.15k$: Presence of endothelial cell

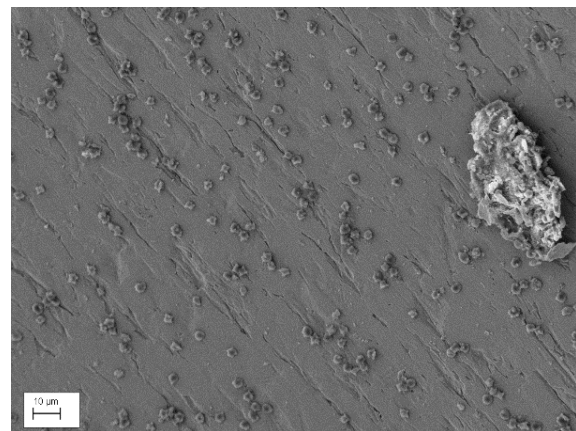
Figure 4.63: Incidence of endothelial cells and RBCs on the surface

Sample 2 (1 V)

As can be seen in Figure 4.64, quite a number of RBCs settled on the surface under application of 1V. It can be noticed that some RBCs had irregular morphologies which might be due to either the electrical charge or an impact of some components in the cells' flask which were added separately to the blood.



Magnification $\times 450$: Distribution of RBCs

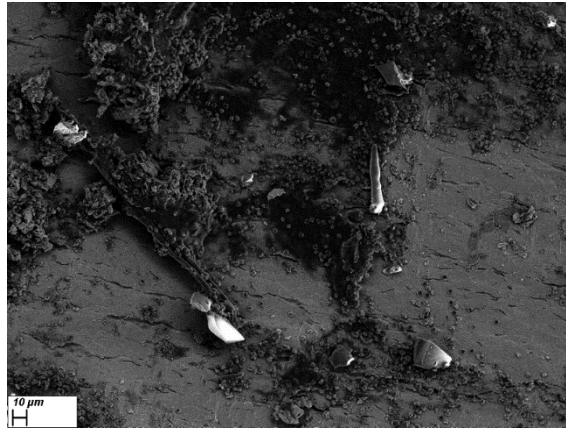


Magnification $\times 1.40k$: Widespread RBCs on the surface

Figure 4.64: Presence of numbers of RBCs on the surface

Sample 3 (non-electrical connection)

As can be seen in Figure 4.65, RBCs settled on any objects that were on the surface. Most of RBCs attached to other objects rather than remaining on the stents surface.



Magnification $\times 730$: Presence RBCs

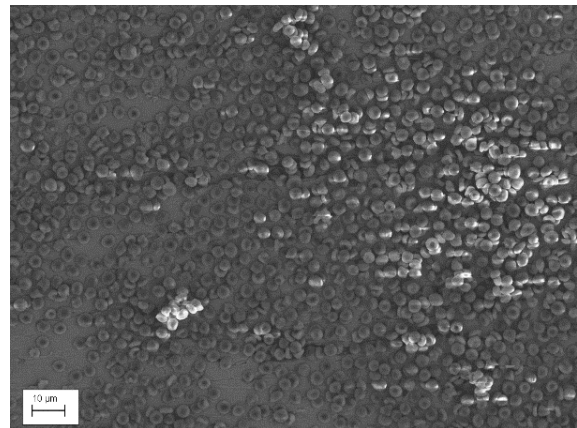
Figure 4.65: SEM pictures showed RBCs attached to objects on the surface

Sample 4 (27 mV)

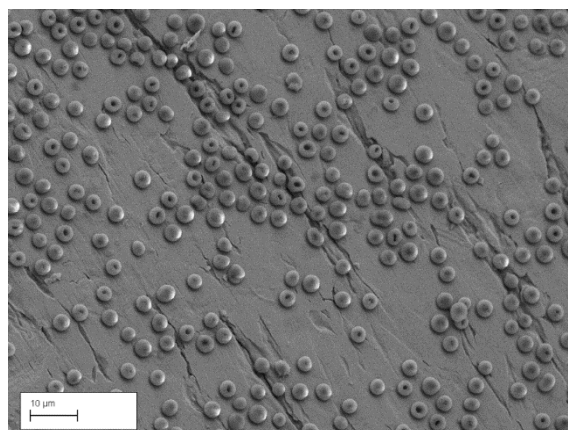
As it can be seen in Figure 4.66, quite a number of RBCs distributed on the surface. They covered the surface in both forms of even distribution and lump formation. RBCs morphology looked normal and healthy.



Magnification $\times 1.20k$: Presence of RBCs



Magnification $\times 1.70k$: Early clog formation of RBCs

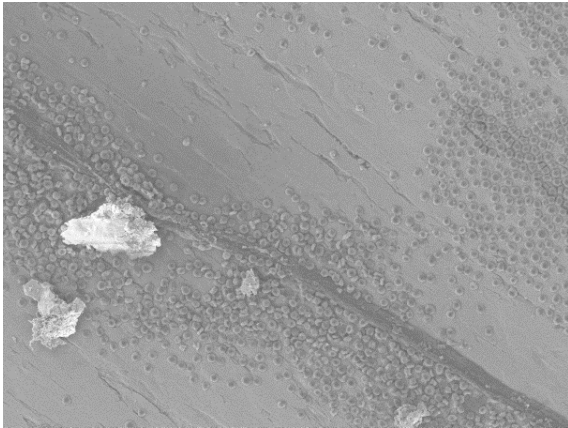


Magnification $\times 2.50k$: Incidence of RBCs

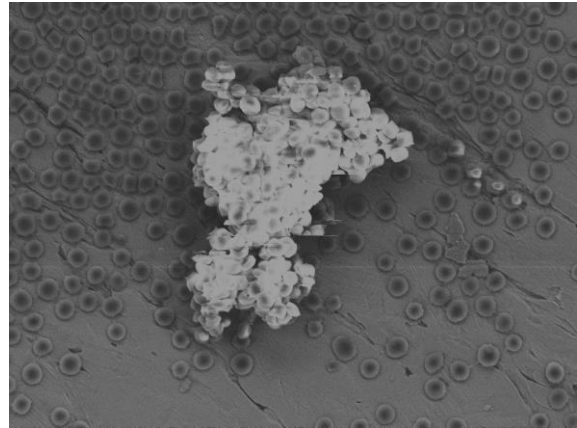
Figure 4.66: SEM images showed widespread RBCs

Sample 5 (1 V)

Figure 4.67 showed the coverage of the stent's surface by remaining of RBCs on it. Regular RBCs formed a single evenly distributed layer on the surface.



Magnification $\times 1.10k$: Occurrence of RBCs

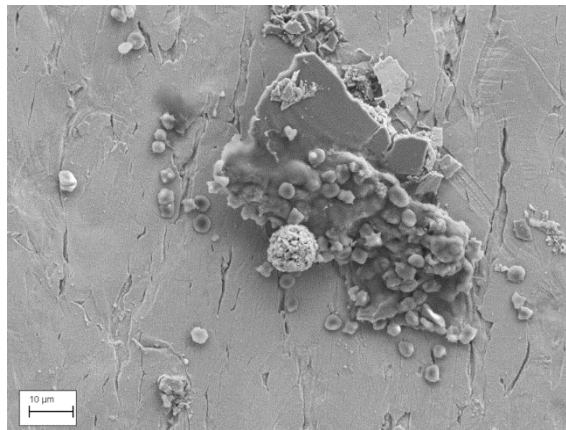


Magnification $\times 2.50$: Occurrence of RBCs

Figure 4.67: SEM images showed remaining of RBCs on the surface

Sample 6 (non-electrical connection)

As can be seen in Figure 4.68, a number of RBCs settled on the substances that were on the stent's surface,

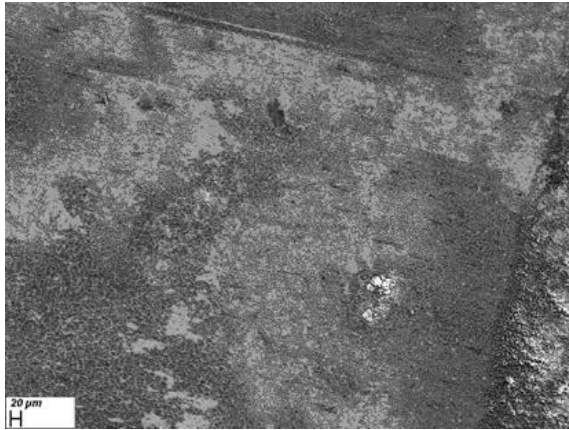


Magnification $\times 2.50k$: RBCs settled on the object

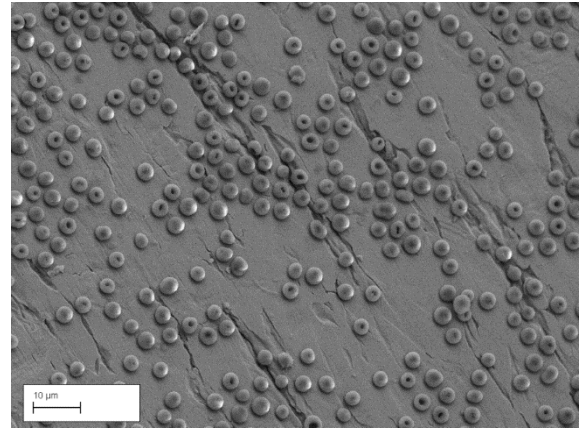
Figure 4.68: SEM image illustrated the attachment of RBCs on the item

Sample 7 (27 mV)

SEM images demonstrated the massive exhibition of RBCs in both forms of single even distributed layer and aggregations (Figure 4.69). RBCs' morphology looked biconcave and circular. RBCs covered the entirely surface of the stent with some rare uncovered regions.



Magnification $\times 270$: Extensive RBCs presence

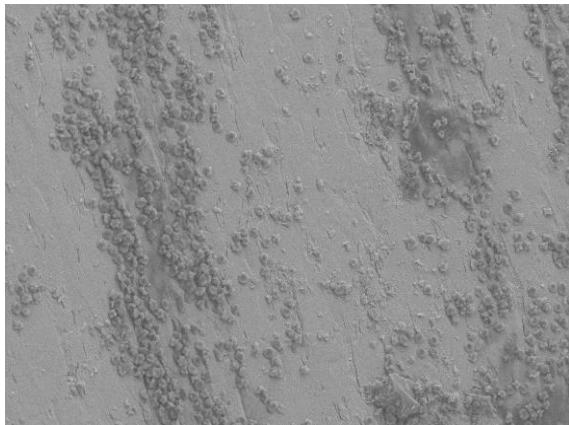


Magnification $\times 2.50k$: Healthy RBCs' presence

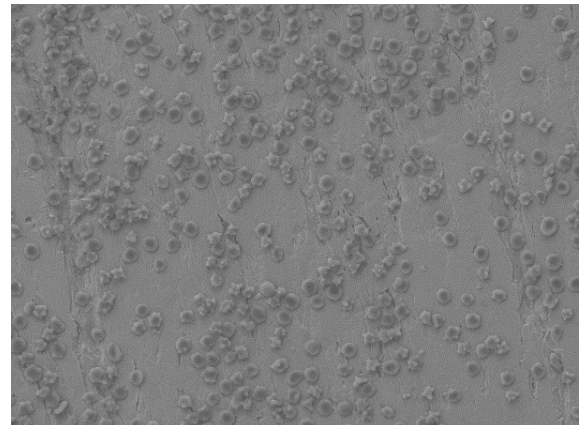
Figure 4.69: Widespread existence of RBCs in the form of single layer and aggregations

Sample 8 (1 V)

Similar to other stents with the same amount of electrical charge, significant number of RBCs settled on the surface of this stent. Figure 4.70 shows the remaining RBCs.



Magnification $\times 767$

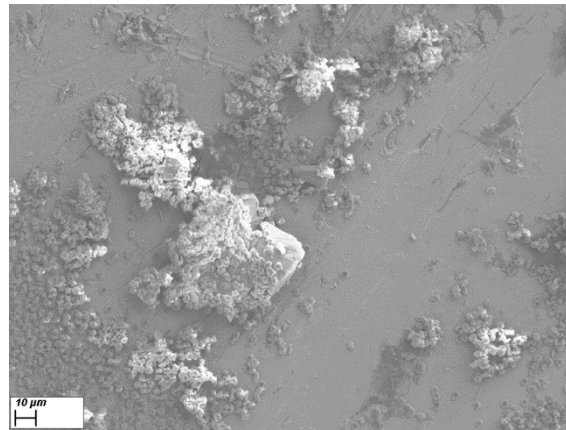


Magnification $\times 1.95$: Considerable attraction of RBCs

Figure 4.70: High coverage of RBCs on the surface

Sample 9 (non-electrical connection)

Figure 4.70 showed the presence of RBCs among substances on the surface of the stent. Rarely, RBCs in this sample settled on the bare surface of the stent. Similarly, this happened for other two samples with the same amount of electrical connection.

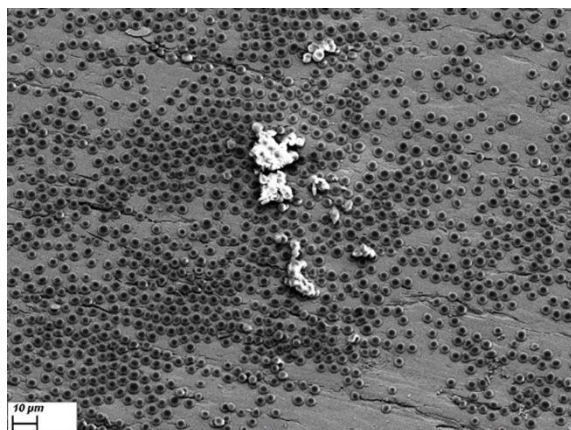


Magnification $\times 1.00k$

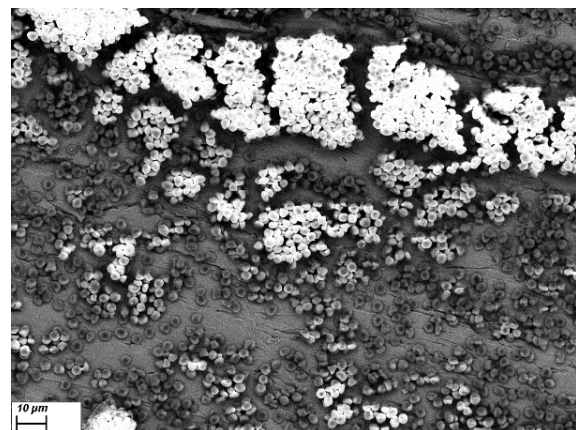
Figure 4.71: Trapped RBCs among substances on the surface

Sample 10 (27 mV)

As can be seen in Figure 4.72, a number of RBCs settled on the stent in the form of single layers and aggregations. RBCs seemed normal and ideal. This result looked the same as other samples with similar electrical charging.



Magnification $\times 1.25k$: Single layer RBCs occurrence



Magnification $\times 1.55k$: RBCs aggregations formation

Figure 4.72: SEM images showed the attraction of RBCs in form of single layers and aggregations

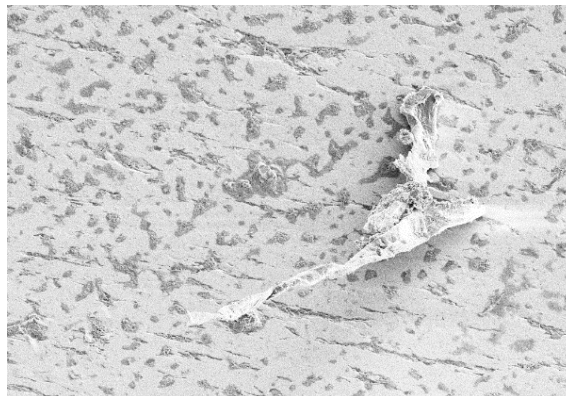
4.8.5 Applied Direct Current on Bare Stent with Extra Oxygen with Old Blood

These series of experiments were undertaken using sheep blood which was kept for four months. Significant differences were noticed between this experiment and the rest of the experiments. Oxygen flow was provided during the experiment to demonstrate whether oxygen had the potential to influence cells' electrical attraction or not. The rationale for these experiments was an attempt to refresh depleted and static oxygen content in the blood as it is *ex-vivo* and does not have the benefit of natural gaseous exchange occurring in the living organism.

Due to lack of information from SEM images from the samples of this experiment, only one picture per sample is presented. In addition, the presentations of the SEM pictures are different in this section because there were not any specific explanations for SEM images due to any specific or desired items not being attracted onto the surfaces.

The following SEM images including Figure 4.73 for Sample 1 (1 V), Figure 4.73 for Sample 2 (1 V), Figure 4.74 for Sample 3 (non-electrical connection) , Figure 4.76 for Sample 4 (27 mV), Figure 4.77 for Sample 5 (1 V), Figure 4.78 for Sample 6 (non-electrical connection), Figure 4.79 for Sample 7 (27 mV), Figure 4.80 for Sample 8 (1 V), Figure 4.81 for Sample 9 (non-electrical connection) and Figure 4.82 for Sample 10 (27 mV).

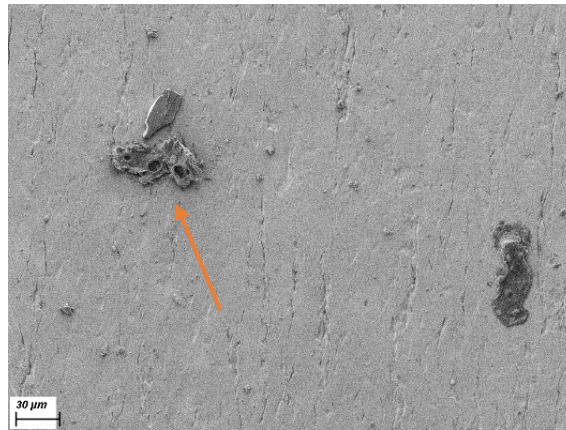
Sample 1 (1 V)



Magnification $\times 1.00k$

Figure 4.73: Presence of an endothelial cell

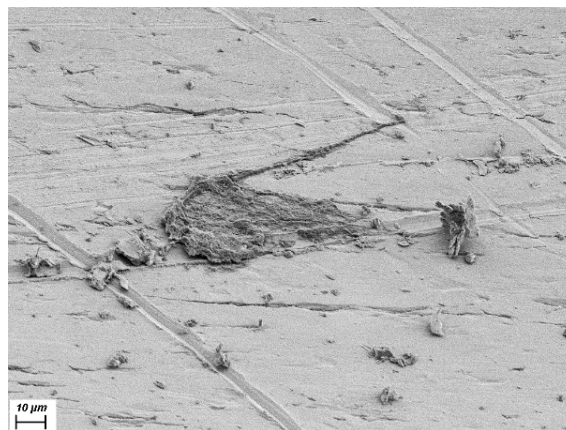
Sample 2 (1 V)



Magnification ×750

Figure 4.74: An endothelial cell pointed with a coloured arrow

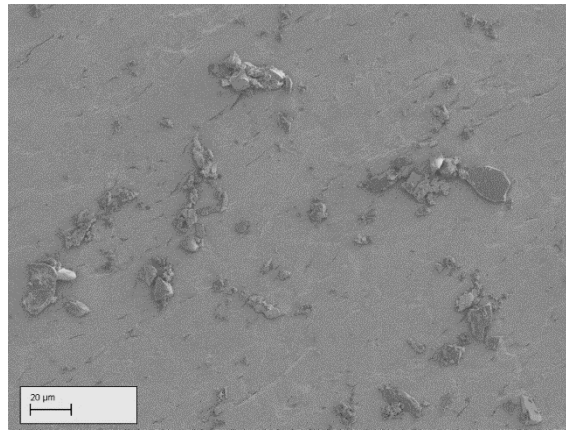
Sample 3 (non-electrical connection)



Magnification ×1.50k

Figure 4.75: A biological item on the surface

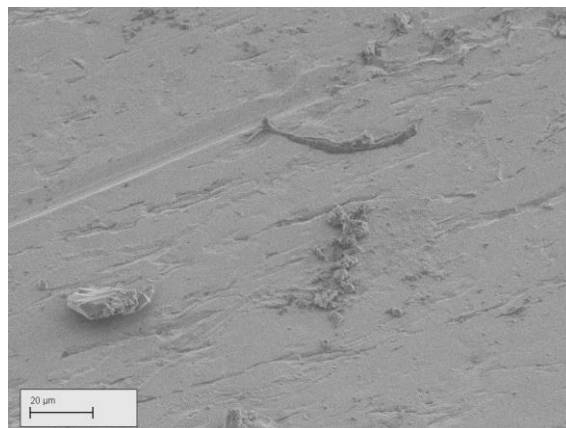
Sample 4 (27 mV)



Magnification ×1.00k

Figure 4.76: Focused image from the surface of the stent

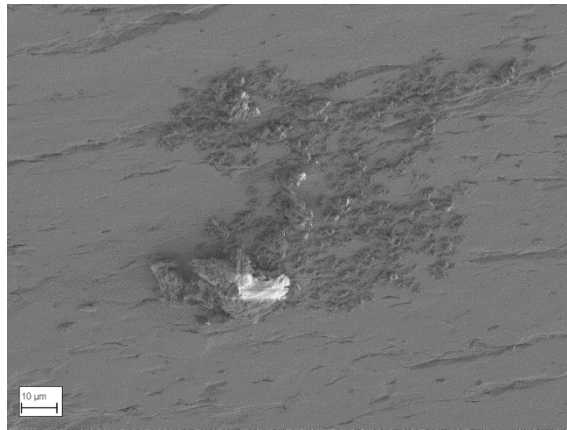
Sample 5 (1 V)



Magnification ×1.50k

Figure 4.77: Attachments of biological objects on the surface

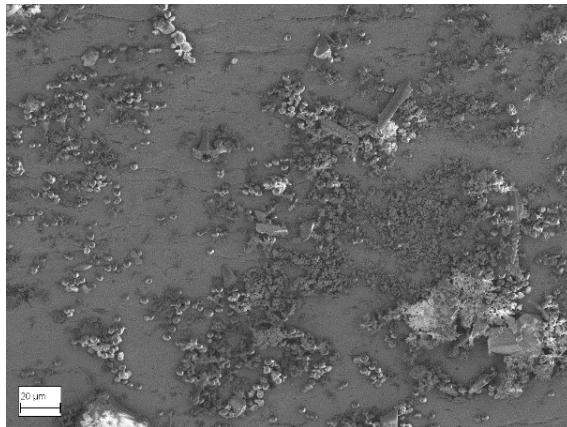
Sample 6 (non-electrical connection)



Magnification ×1.80k

Figure 4.78: Presence of biological items on the surface area

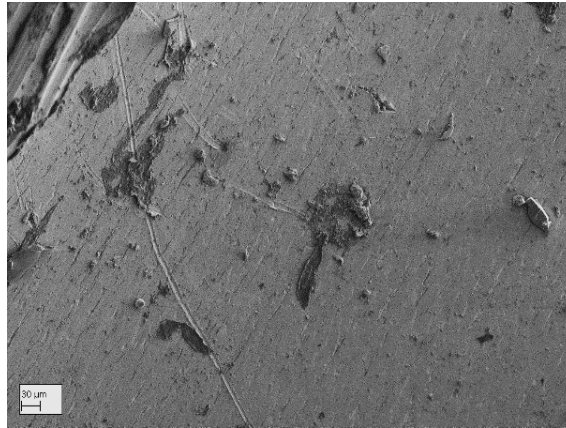
Sample 7 (27 mV)



Magnification ×1.00k

Figure 4.79: Accumulation of biological objects

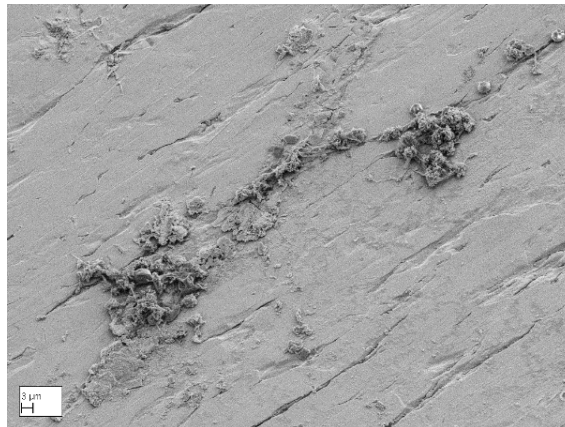
Sample 8 (1 V)



Magnification ×332

Figure 4.80: Existence of biological items

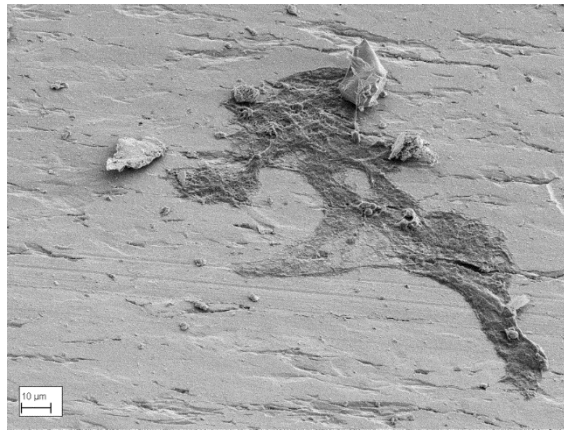
Sample 9 (non-electrical connection)



Magnification ×2.00k

Figure 4.81: Adherence of biological objects on the surface

Sample 10 (27 mV)



Magnification $\times 1.50k$

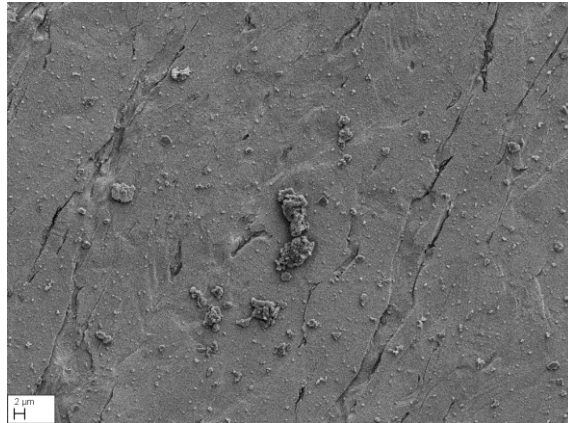
Figure 4.82: Presence of a biological item

4.8.6 Applied Direct Current on Bare Stent with Extra Oxygen

In this series of the experiments, oxygen flow was inserted to the blood tank to determine the impact of extra oxygen in attraction of blood components. As most of the samples with similar applied voltage demonstrated similar results and also because of time limitation, only 5 samples were examined in these experiments.

Sample 1 (27 mV)

As can be seen in Figure 4.83, there were not any particular items attracted onto the surface of this stent that underwent 27 mV. Most areas of this stent were clear without even the adherence of any specific items.

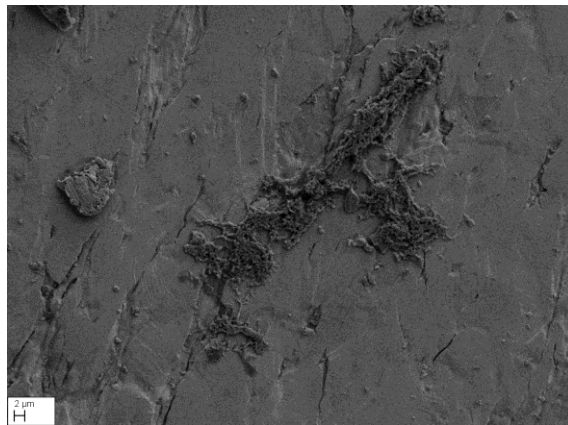


Magnification ×2.00k

Figure 4.83: SEM images illustrates the surface without adherence of any particular objects

Sample 2 (1 V)

Figure 4.84 presents that this amount of electrical field did not cause migrations of any specific items onto the surface of the stent.

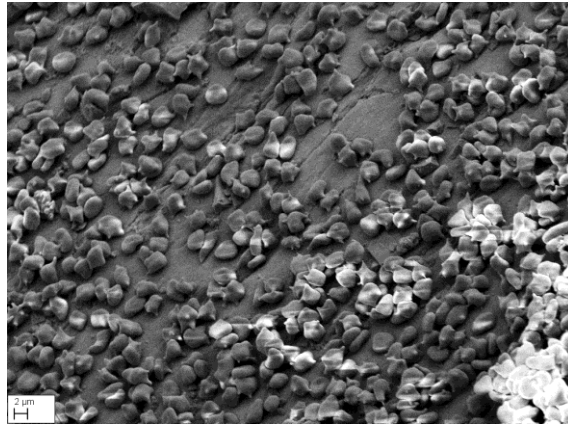


Magnification ×2.00k

Figure 4.84: SEM picture shows adherence of a biological item on the surface

Sample 3 (non-electrical connection)

SEM image from the stent without electrical charging (Figure 4.85) demonstrates coverage of some segments of the surface with presence of RBCs. RBCs presented on the stent forming either aggregations or monolayer in some areas.



Magnification ×2.50k

Figure 4.85: Accumulation of RBCs on the surface

Sample 4 (27 mV)

As can be seen in Figure 4.86, the surface of the stent, unexpectedly, did not contain any particular objects on its surface.

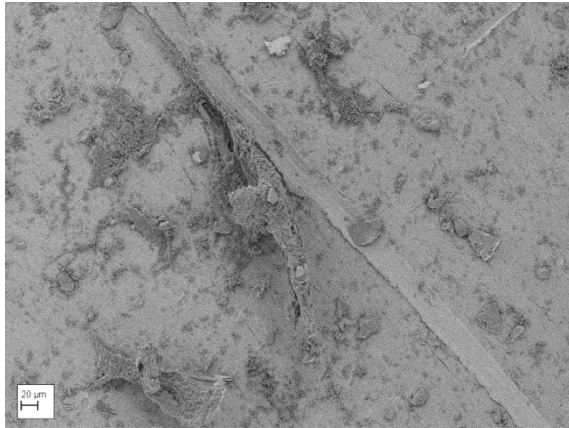


Magnification ×1.00k

Figure 4.86: Empty surface of the stent without presence of any items

Sample 5 (1 V)

Figure 4.87 illustrates several images of the stent under application of 1 V that caused adherence of unknown objects on the surface of the stents.



Magnification ×437



Magnification ×437

Figure 4.87: SEM pictures showed attraction of biological objects on the stent's surface

4.8.7 Applied Pulsed Direct Current on Bare Stent

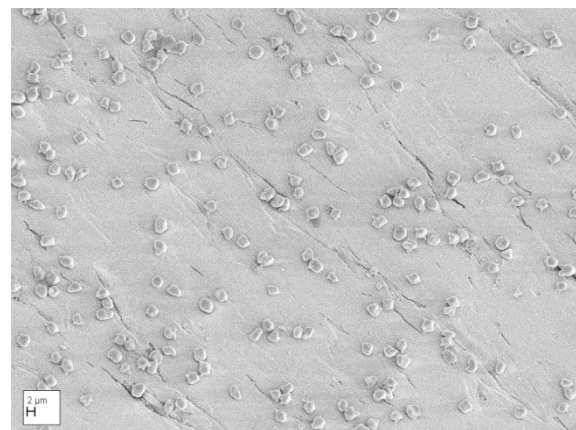
As mentioned in section 4.8.6, only 5 stents underwent this experiment. The differentiating factor here is the voltage applied on the stents was pulsed direct current with square wave frequency of 100 Hz. As a matter of fact, the electrical charge levels remained the same and only type of electricity was different.

Sample 1 (27 mV)

As can be seen in Figure 4.88, RBCs fully covered some areas of the stent under application of 27 mV. RBCs made monolayers on this stent.

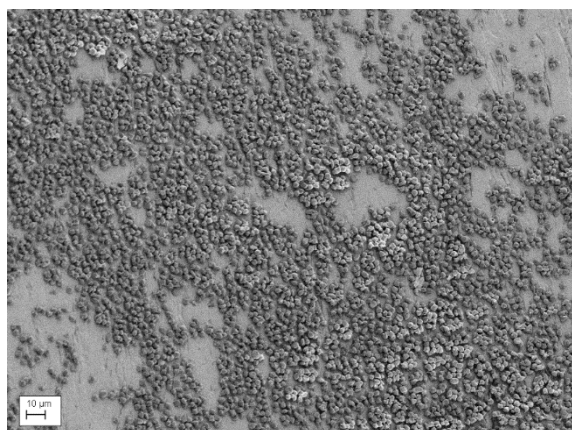


Magnification ×1.00k

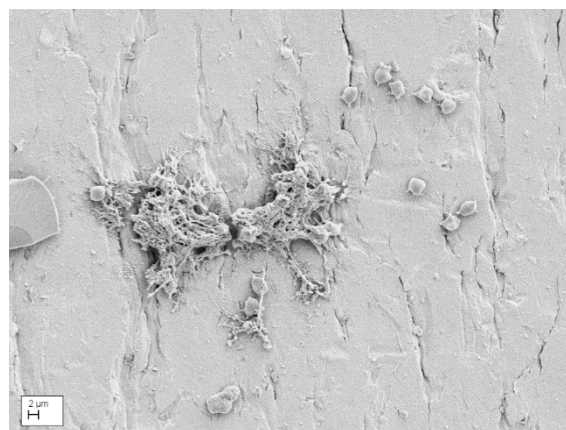


Magnification ×2.00k

Figure 4.88: Adherence of huge number of RBCs on the surface of the stent



Magnification ×1.00k

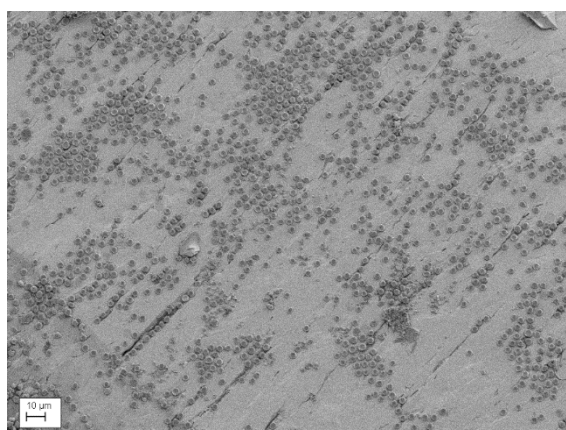


Magnification ×2.70k

Figure 4.91: Presence of RBCs plus attraction of a cell

Sample 5 (1 V)

Figure 4.92 showed attraction of a number of RBCs on the surface of the stent.



Magnification ×1.00k

Figure 4.92: Attraction of RBCs on the surface of the stent

4.9 Section Summary

The results in this chapter contain electrodes experiments which provide electrochemical measurements and images from the surface of the electrodes using SEM and AFM. The electrode experiment were designed to offset galvanic effect when placing electrodes in an electrolyte solution (cell media) and to ensure sufficient accuracy when attempting to directly measure cell membrane potential and polarisation status. The next parts of this chapter show the results of cell membrane potential, using three different techniques: direct touching method, di-electrophoresis and zeta potential method. In the next section, the influence of an applied

electrical field on the cells is shown. Finally, the last section illustrates the effect of applied electrical potentials relating to migration and morphology of cells onto the stent's surface.

As previously obtained results are presented in this chapter, the next chapter, therefore, moves on to discuss the results in this chapter and offers a hypothesis for the obtained results.

Chapter 5 Discussion

5.1 Introduction

With a historical perspective and as previously discussed, different stent types still cause negative outcomes. BMS's have a high rate of restenosis, an incidence of approximately 30% of cases has been reported (Her and Shin, 2018). The first generation of DES's significantly reduced the restenosis rates but resulted in late thrombosis (Tada *et al.*, 2013b). The use of antithrombotic therapies further reduced the risk of stent thrombosis, but increased bleeding rates. The second generation DES's reduced the risk of late stent thrombosis, but it resulted in incomplete endothelial coverage occurred, which led to very late thrombosis (Finn *et al.*, 2007b; Nishimoto *et al.*, 2017; Torrado *et al.*, 2018). Therefore, a procedure, which may facilitate appropriate vascular remodeling and a consequent reduction in the incidence of very late stent thrombosis, is possible by enabling the migration of vascular endothelial cells onto the blood contact surfaces of the stent. The technique suggested for these desirable migratory dynamics, is by the use of electrotaxis.

As implants made from synthetic materials in the human body are recognised as foreign objects, therefore specific local cells can be inhibited from residing on them; there is no particular impetus or influence for this residency. It has been suggested that using electrical fields on implants can be effective in migration of cells towards the implants. Prior studies have shown migration of cells under application of external electrical fields toward the cathode or the anode depending on the pattern and amount of direct current electric fields. For effective migration of cells, accurate cell membrane potential values are needed to determine optimum conditions for specific cell types. Thus, several techniques were used and their results were compared. It was then predicted that cells can migrate under appropriate applied electrical fields.

5.2 Electrode Experiments

In this research, instead of using a reference electrode, which is commonly used in other electrochemical measurement experiments, two electrodes, a commercially pure titanium and stainless steel alloy-grade 304, were immersed for a duration of 8 minutes into different water based solutions. Electrochemical potential measurements and topographical changes on the

surface of the electrodes were investigated to illustrate either corrosion or passivation of a metal.

The results of these experiments showed that the potentials tended towards more positive voltages which shows the tendency of electrodes to form a passivation layer which means slower corrosion (Figure 5.1). This matter can be linked to the nature of 304 stainless steel electrode which is known as a metal with good corrosion resistance against a wide range of solutions. This ascending trend could be seen in five results of experiments with deionized water, distilled water, 0.9% saline and 3 results of experiments with tap water. In all experiments, the first curves had less negative potentials which showed consistently, after repeating the experiments, more passivation layers formed on the electrodes causing increasing negative potentials. It can be also noted that only in 0.9% saline, due to its ionic content compared to other solutions in this study, the curves showed both a greater positive and negative with variation in potential. In the rest of the experiments, as there were less free ions in the solutions, the curves on the graphs are smooth. SEM images did not show a significant changes in surface texture. However, AFM studies did show a change in RMS values indicating that the SEM did not have the resolution to detect subtle changes. By increasing the magnification in the SEM to give higher resolution results in a significant reduced area on the sample examined which would have resulted in non-representative peak- to-trough data.

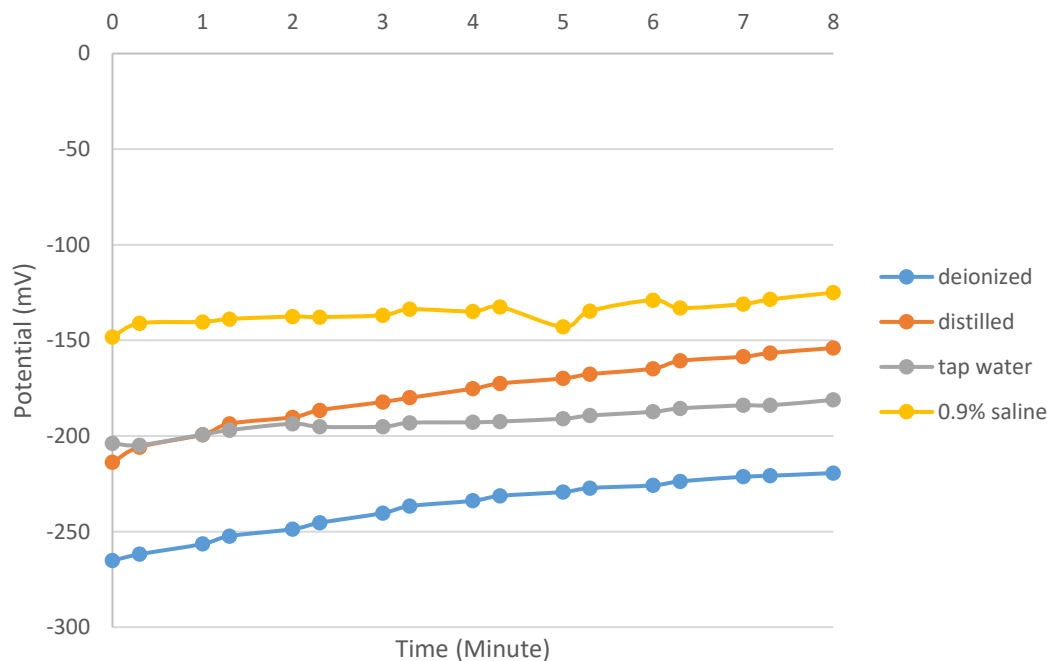


Figure 5.1: Comparison of average potential measurements of electrodes

A possible explanation for these findings might be that both electrodes are considered as less active metals, thus they cannot readily release ions as much as electrochemically active metals, causing significant differences in potential difference measurements. Even using those less active metals might have shown different results in more active ionic solutions. It is possible to hypothesise that the duration of immersing the electrodes in the solutions was relatively short, leading to incomplete passivation layer formation. If the duration was longer, the results may differ. The SEM images show furrows on the surface of the electrodes similar to those pictured on other SEM images of stents used in mimicked artery experiments. Other researchers have shown that this surface topography has an effect on the adhesion of cells (Govindarajan and Shandas, 2014; Tan, Muhamad and Abdullah, 2017). The corrosion rate of the sample electrode metal was not measured in these experiments as this would be normally be ascertained by incremental mass-loss measurements and would be likely to be of the order of 10^{-5} to 10^{-6} grams and difficult to measure: furthermore, the nature of this present study is to examine resistance/impedance characteristics of the electrodes which is impacted much more by passivation effects.

5.3 Direct Microelectrode Method

In this novel approach, the aim was to determine cell membrane potentials without rupturing the cell cytoplasm which would have a catastrophic effect on the cell activity and subsequent membrane potentials. Cells were cultured in two different conditions; full cell coverage in which the petri dish was covered completely by cells and half-cell coverage in which only one side of the petri dish was fully covered by cells. For a better evaluation of the obtained results, the mean \pm SD of three voltage measurements at 0 hour, 2 hours and 10 hours are shown in Figure 5.2, Figure 5.3, Figure 5.4 and Figure 5.5.

Figure 5.2 and Figure 5.3 show full and half cultured petri dishes of endothelial cells, respectively. In both figures, the measurements after 2 hours had the most negative potential measurements. The most obvious finding is that the standard deviations for measurements in the half cultured petri dish is less than the full cultured petri dish. The reason for this happening is that the fuller cell section had the potential to give more than one cell reading due to the proximity of many more cells were in contact with both the cathode and anode.

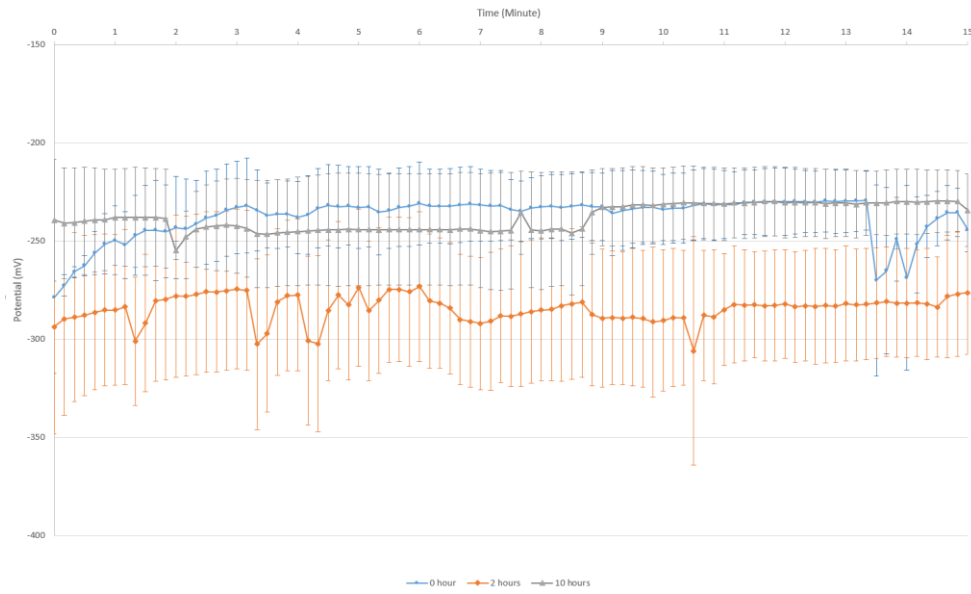


Figure 5.2: $MEAN \pm SD$ ($n=3$) of each measurement of complete cultured petri dish of human coronary artery endothelial cells (blue, orange and grey spots present 0 hour, 2 hours and 10 hours, respectively)

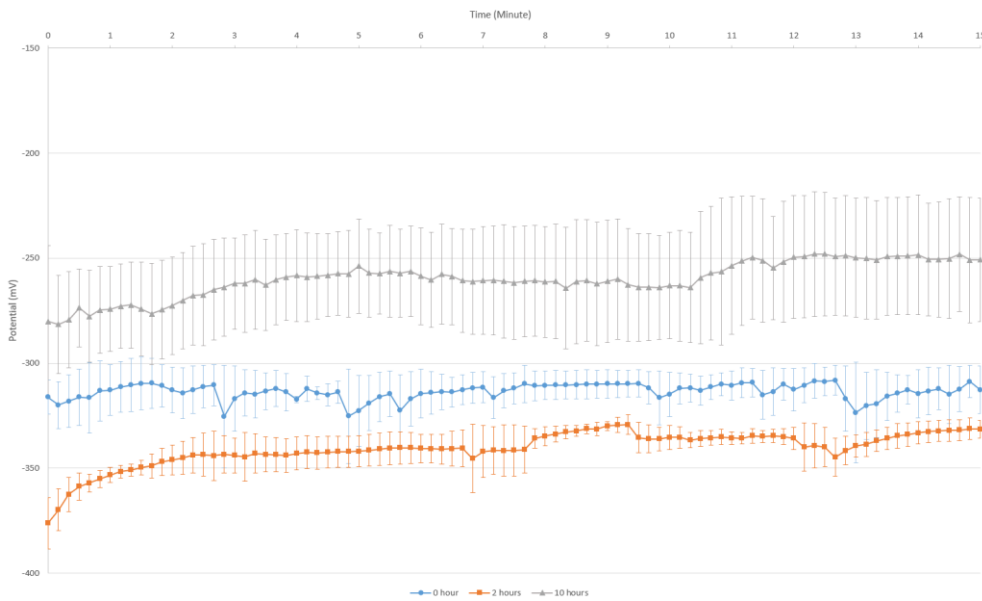


Figure 5.3: $MEAN \pm SD$ ($n=3$) of each measurement of half cultured petri dish of human coronary artery endothelial cells (blue, orange and grey spots present 0 hour, 2 hours and 10 hours, respectively)

The obtained results from human coronary artery endothelial cells is shown in Table 5.1:

Table 5.1: Determined human coronary artery endothelial cell membrane potentials

	0 hour	2 hours	10 hours
Complete cell cultured (mV)	-31.14 ± 19.19	-15.35 ± 35.60	31.03 ± 22.93
Half cell cultured (mV)	-44.43 ± 10.04	-71.62 ± 6.60	9.14 ± 25.53

The value that is equal to -44.43 ± 10.04 mV in the above table is considered as human coronary artery endothelial cell membrane potential that was determined using the direct microelectrode method. It is likely that ionic and oxygen concentration plus cycling of temperature will have an effect on cell membrane potential data. Therefore, it is considered that the above reading is the most significant.

Similarly to endothelial cells measurements, potential measurements of osteoblast cells had lower standard deviations in half cultured petri dish (Figure 5.4 and Figure 5.5).

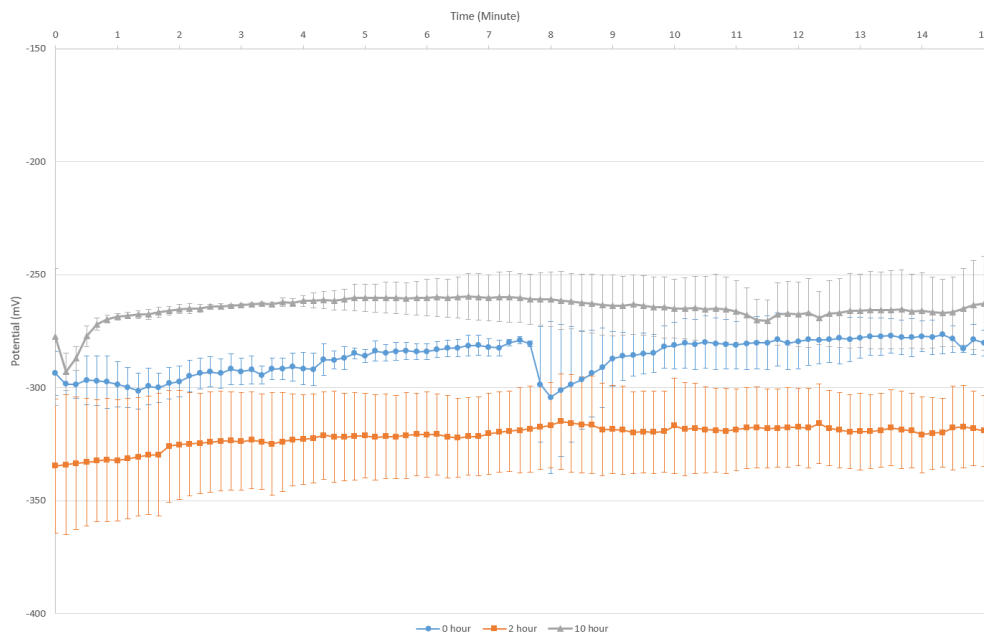


Figure 5.4: MEAN±SD (n=3) of each measurement of complete cultured petri dish of human osteoblast cells (blue, orange and grey spots present 0 hour, 2 hours and 10 hours, respectively)



Figure 5.5: MEAN±SD (n=3) of each measurement of half cultured petri dish of human osteoblast cells (blue, orange and grey spots present 0 hour, 2 hours and 10 hours, respectively)

The obtained results from human osteoblast cells is shown in Table 5.2:

Table 5.2: Determined human osteoblast cell membrane potentials

	0 hour	2 hours	10 hours
Complete cell cultured (mV)	-17.49 ± 8.67	-52.39 ± 20.03	4.22 ± 9.73
Half cell cultured (mV)	-52.6 ± 17.21	-103.42 ± 11.42	-18.64 ± 30.54

Human osteoblast cell membrane potential was determined using the direct microelectrode method and found to be 52.6 ± 17.21 mV. The value of -18.64 ± 30.54 mV showed that the osteoblast cells were entering the senescence phase and completing their viable life. The electrical values were still negative, but trending towards the positive, compared to 0 hour and 2 hours readings. This was also seen in the previous graphs and charts.

A complete graph containing both forms of complete and half-cell coverage of cells are presented in Figure 5.6 for both cell lines. The recorded potentials for full cultured petri dishes of endothelial cells are less negative than the half cultured petri dishes of cells. Thus, it can be understood that the half cultured petri dish resulted in more accurate data. It was clearly seen that the half cell cultured dishes show more variations. (Figure 5.6: a). A possible explanation for this is may be because of touching of the microelectrode tip to an aggregation of cells that

caused a decrease in the measured potentials. The potential measurements of human coronary artery endothelial cells illustrated a trend, compared with osteoblast cell potential measurements, which does not show any trend (Figure 5.6: b).

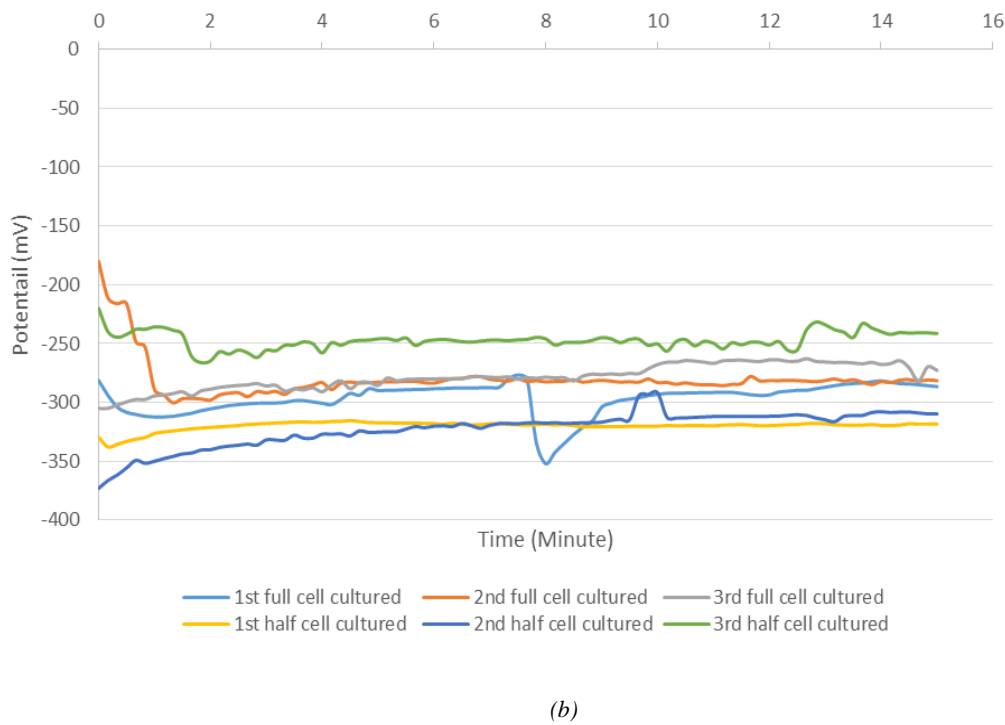
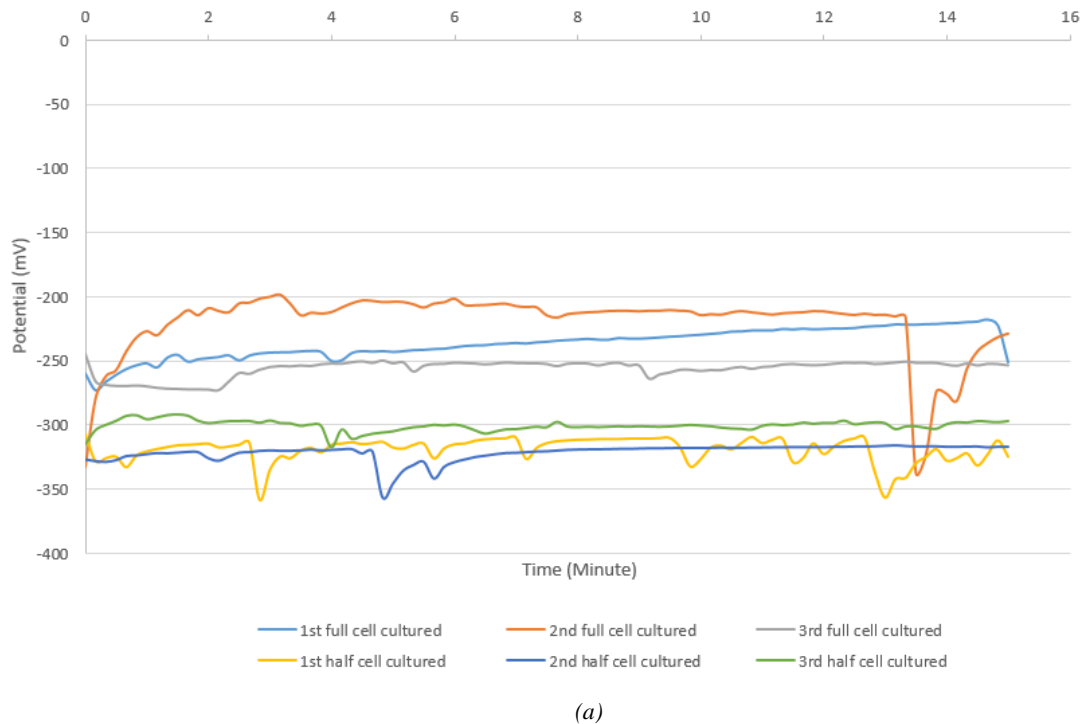


Figure 5.6: Comparison of human coronary artery endothelial cells (a) and human osteoblast cells (b) potential measurements in both full and half cell cultured in 0 hour

In both cell lines, measurements in half cultured petri dishes have smaller error bars, which shows less variation in cell membrane potential. Also, in both cell lines, the 2nd measurements after 2 hours have the most negative potentials. It can thus be suggested the reason may be because of cell proliferation between the 1st and the 2nd experiments. In addition, in all experiments, the 3rd measurements after 10 hours have the most positive potentials which might be due to cells were senescent.

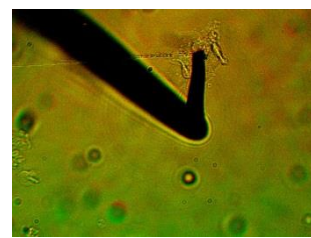
The results of these experiments were influenced by several factors. The first challenge was control of the tip of the microelectrode (the tip of the microelectrode tapers to $\sim 1 \mu\text{m}$). As cells were adherent to the bottom of the petri dishes and the microelectrode had a 2D, (x-y) view, the tip of microelectrode was difficult to control the pressure applied which could have an impact on the voltage recordings. Moreover, the microelectrode tip was bent which added difficulty to touch the cells membrane. In addition, this bending caused a shadow when it was inserted to the petri dish. As it can be seen in Figure 5.7, on many occasions the apparent tip visualized in the microscope, was merely the shadow of the tip.



(e) Tip of microelectrode, magnification $\times 80$



(f) Tip of microelectrode, magnification $\times 200$



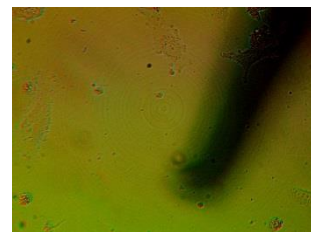
(g) Tip of microelectrode, magnification $\times 500$



(h) Shadow of microelectrode's tip, magnification $\times 80$



(i) Shadow of microelectrode's tip, magnification $\times 200$



(j) Shadow of microelectrode's tip, magnification $\times 500$

Figure 5.7: Comparison of observation of the microelectrode's tip and its shadow during experiments in three different magnifications $\times 80$, $\times 200$ and $\times 500$

5.4 Di-electrophoresis Method

Di-electrophoresis properties of vascular endothelial cells in a specific cell culturing media were measured by a machine developed expressly for these electrophoretic properties,

manufactured by 3D DEP Technology Ltd. The results of these measurements are shown in Figure 4.42.

5.5 Zeta Potential Method

Zeta potential results have suggested that cell membrane potentials in both human coronary artery endothelial cells and human osteoblast cells are close to each while measurements in DEP are dispersed in a large range. This fact can be easily noted from Figure 4.43 in which error bars for DEP measurements are ± 4.43 mV and ± 6.07 mV for human coronary artery endothelial cells and human osteoblast cells, respectively. While error bars for measurements in CCM for both types of cells are less than 1.50 mV. A possible explanation for this might be dependent on DEP components which result in greater scattered potential measurements. DEP media is made of 5.8% (w/v) sucrose plus 0.3% (w/v) dextrose buffer (Gascoyne *et al.*, 1997). It may be that the amount of sucrose and dextrose affect the zeta potential measurements.

Although zeta potential values for human coronary artery endothelial cells (in CCM: -9.76 ± 0.18 and in DEP: -21.53 ± 4.43) and human osteoblast cells (in CCM: -10.39 ± 1.32 and in DEP: -13.58 ± 6.07) are very different from each other for each type of cell line, their mean values are lower than previously reported by other researchers. The membrane potential of human endothelial cell was reported 51.6 ± 4.9 mV for micro vessels (HE and Curry, 1995) and 23.6 ± 5.5 mV for human umbilical vein (Vargas *et al.*, 1994). Human osteoblast cell membrane potential was reported -38.1 ± 2.5 mV (Hughes *et al.*, 2006) and -60 mV (Pangalos *et al.*, 2011). As (Bondar *et al.*, 2012; Ayala-Torres *et al.*, 2014) reported previously, zeta potential values are cell surface charges that are dependent on composition of a cell's cytoplasm and the physiological condition of cell. The reasons for the difference in reported values, may be due different methods that have been used and different physiological condition of cells.

5.6 Comparison of Different Methods of Cell Membrane Potential Measurements

Human coronary artery endothelial membrane potential was -44.43 ± 10.04 mV, determined using direct microelectrode method. While the measured potential using zeta potential method was -9.76 ± 0.18 mV. There is a noticeable difference between two measured value which may be related to the way that the technique was performed. Another possible explanation for this might be that in the zeta potential method, the surface charge of the cells were examined, while

in direct touching method, the microelectrode had direct point-contact with the cell. This difference can be also noted in potential measurements of human osteoblast cells. The determined potentials for human osteoblast cells were -52.6 ± 17.21 mV and -10.39 ± 1.32 mV using direct microelectrode method and zeta potential method, respectively. The obtained results can be seen in Table 5.3:

Table 5.3: Comparison of determined cell membrane potentials using different methods

Cell lines	Direct microelectrode method	Zeta potential method
Human coronary artery endothelial cells (mV)	-44.43 ± 10.04	-9.76 ± 0.18
Human osteoblast cells (mV)	-52.6 ± 17.21	-10.39 ± 1.32

5.7 Electrophoresis Method

The electrophoresis method was performed with slight changes using a sterilized custom cuvette in which cells were directly cultured (See 3.4.5). In reviewing the literature, no data was found on using electrophoresis method for cells. The method is commonly used for separation of DNA and protein and measurement of bacteria movements (Wilson *et al.*, 2001). Cells were cultured directly on the surface of the cuvette because transferring cells from the petri dish to the cuvette needs some physical or chemical actions. In physical cell detaching, a scraper is used, which can cause a physical damage to cells; in chemical cell detaching using trypsin-EDTA, cells might be affected chemically. In the electrophoresis method, after applying electrical charges on two gold electrodes incorporated in the cuvette, the movements of cells was observed directly through an inverted microscope.

The results from the short term application of DC, illustrated different patterns. Most of the changes were common between different amounts of applied DC. The results obtained from high range of applied DC, showed that applying DC at more than 1000 mV did not show noticeable movements of cells. However, a number of cells became shorter, expanded or orientated in different directions. Only slight changes can be seen in cells under application of 1500, 2000 and 3000 mV in a period of 15 minutes. Application of 30 mV only caused contraction or expansion of cells after 15 minutes. Various applied DC using 100, 200, 300 and 400 mV, resulted in movements of cells in different directions and other physical changes, including stretching, becoming thinner and smaller. Noteworthy to mention that 500 mV did not cause significant changes in the position of cells in period of 15 minutes.

The results obtained from the long term experiment; some cells showed contraction using 1000 mV. However, other trends such as displacement in various directions could be seen. The results from 30 mV applied DC for a longer period of time had the potential to cause changes and movements of cells. Although changes among cells showed variation, nevertheless, there were also similarities. Importantly, this level of electrical charge led to displacements of cells in different directions. Despite insignificant changes and movements under the application of 500 mV for the period of 15 minutes, in the long term with the same level of the charge, cells moved and expanded in a period of 3 hours. Although the cells moved randomly, they all enlarged, when compared to the beginning of the experiment.

The results of high range applied DC showed ineffectiveness in regard to movement, when applying of more than 1000 mV DC. As most cells membrane potentials are less than 100 mV, it can be understood why higher voltage did not have a great influence on cell displacements. Although results for 1000 mV for the short term showed negligible changes, more changes have been seen in at 1000 mV in the longer term. The results of 400 mV and 500 mV indicated changes mostly in dimension of cells in the short term. The most active applied DC levels were observed at 30, 100, 200 and 300 mV and resulted in significant changes in cells.

The most obvious finding was that the impact of the long term applied DC was more effective than the short term. Although impact of the long term applied DC only, could be noted at the beginning of the experiments, changes were more significant and notable than the short term applied DC. The differences between the long term and the short term of three different levels of DC is shown in Table 5.4. It can be said that cells under application of 30 mV had the most significant movements in the long term.

Table 5.4: Comparison of impact of long term and short term applied DC on cells

Amount of DC (mV)	Long term	Short term
30	1- Dislocation of cells 2- Various changes in cells dimensions	Mostly changes in size including contraction and expansion
500	1- Dislocation of cells 2- Expansion of cells	Negligible changes
1000	1- Dislocation of cells 2- Thinner in dimensions	Did not show particular changes expect few size changes

These experimental results have shown the impact of applied DC in cell migration and orientation. The study found that notable differences occurred between different levels of

applied electrical fields on cells. In addition, the duration of applied electrical field plays a critical role in movements of cells. What is surprising is that cells do move even when they are adherent to the surface. Based on this finding there is no need to use chemical or physical actions to detach cells from the surface of the cultured dish. However, it is obvious when cells are adherent to the surface, it takes more time to migrate. Thus, the migration of cells needs a longer period more than 15 minutes under application of an electrical field. However, the cells did not look active and healthy after 2-3 hours after placing the cuvette in the open air at temperature 25°C. If the whole experiment was conducted in an incubator, it may show different results. More interestingly, the results have shown that higher applied DC levels are unable to cause migration of cells. Possibly, higher electrical fields give shocks to cells that do not show measurable changes. The corollary of these findings indicated that if applied electrical fields are close to the cell membrane voltage, then movements and geometric changes can occur. As cells were cultured directly in the cuvette, there is a possibility that that material of the cuvette (acrylic) plays a role on the movement of cells. Other factors such as temperature, pH and ionic strength of the medium will also influence the migration and orientation of cells.

5.8 Mimicked Artery Experiments

A mimicked artery experiments tried to show whether coverage of vascular endothelial cells onto the surface of the stents was achievable by applying DCEF, or not. Obtained results are discussed and analysed as follows:

Results from applied DC on bare stents showed that:

Three stents (number 3, 6 and 9) with different positions in the manifold (Left and Right orientation) having different blood flow were considered as control samples, by not making any electrical connection. As can be seen from SEM images of these stent surfaces, considerable numbers of RBCs settled on them. It's also noticed that RBCs remained healthy during the experiment because there were no apparent changes in their morphologies. The stents undergoing 27 mV showed different results that may possibly be due to the different positions of stents in the manifold. Although positions of stents did not influence in the surface of stents with no electrical connection, it may impact stents when they were connected to small electrical charges. SEM images from stents number 4, 7 and 10 showed different results, possibly linked to the level of blood flow. Stents number 4 and 7 had better blood flows rather than the stent 10 which was far right in the manifold with less blood flow during the experiment.

However, stents number 4 and 7 which had sufficient blood flow, had dissimilar results from each other. Stent number 4 had a number of single layer RBCs on its surface, while stent number 7 possessed vast numbers of RBC aggregations beside single layer RBCs on the surface. On the other hand, stent number 10 had only RBCs aggregations on its surface. Aggregation formation is not a suitable behaviour because it is a pre-thrombosis stage and undesirable when treating patients with stents. Stents number 1, 2, 5 and 8, which had 1V applied during the experiment, presented roughly the same results. As a matter of fact, different levels of blood flow due to their positions did not significantly influence in the results. Stents number 1 and 4 interestingly had endothelial cells besides normal RBCs occurrence on the surface, whereas stent number 2 possessed endothelial cells plus extensive RBCs presence. On the other hand, stent number 8 had only dispersed RBCs on its surface. Before observation of SEM images, it was expected that stents number 5 and 8 would show important results which turned out to be almost the opposite after observing the results. Although stents number 1 and 2 placements were far left with lower than normal blood flow, their results were satisfactory and positive.

Results from applied DC on bare stent with extra endothelial cells showed that:

Stents number 3, 6 and 9, without electrical connections, displayed no particular cells on their surfaces. As a matter of fact, few aggregations of RBCs found were only on and around the areas with extraneous focal points. On the other hand, these stents could not attract any particular items on their surface without any electrical charging, which is as expected. Three stents (number 4, 7 and 10) demonstrated the same results in this series of experiment. This amount of electrical charging (27 mV) showed the potential in attraction of healthy RBCs in both forms of single layer and aggregation. Importantly, the position of the stents (two in middle and one in the far right of the manifold) did not affect the results. Noticeably, this level of electrical charging is not suitable in cases that are struggling with thrombus formations due to this degree of electricity leading to pre-thrombosis. The stents which underwent 1 V showed approximately the same results. The differences between the results can be linked to the position of stents and their level of blood flow. The first two samples (stent number 1 and 2) demonstrated the same results. Both of these stents attracted endothelial cells between regular and irregular shaped RBCs. These two stents caused attraction of only few RBCs. Commonly, these samples had the same blood flow level due to their positions being far left in the manifold.

Stent number 5 which was in the centre of the manifold and had a good stream of blood, had the chance to cause migration of healthy RBCs which made layers and aggregations. SEM images from the surface of this sample proved that RBCs had regular shape. The last sample that was applied 1 V, was sample number 8 which also had a good blood stream and resulted in presence of quite a number of RBCs, mostly regular shape ones.

Results from applied direct current on a bare stent with extra oxygen with old blood showed that:

Due to long storage of sheep blood (~ five months) and as this type of blood does not contain added preservatives, the blood became di-oxygenated and lost some components such as red blood cells. Compared to other mimicked artery experiments with fresh sheep blood, there were not any particular objects adherent to the surface of the stents. Thus, this type of experiment was repeated with new sheep blood to keep consistency in the project and determine scientific results.

Results from applied DC on bare stent with extra oxygen showed that:

Stent number 3 (non-electrical connection) illustrated the incidence of RBCs in some segments in form of aggregations and spread layers. Stents 1 and 4, under application of 27 mV, did show attraction of objects on the surface of the stent. Despite good blood stream, there was not any specific items attached to the surface. Similar to stents undergoing 27 mV, stents number 2 and 5 connecting to 1 V resulted in no migration of cells onto the surface of the stents.

Results from applied pulsed DC on bare stent showed that:

SEM images from the stent number 3 (non-electrical connection) showed presence of RBCs in both forms of monolayer and aggregations. The stents undergoing 27 mV electrical charge demonstrated attraction of vast amounts of RBCs. Both stents 1 and 4 showed similar results which was high coverage of the surface with RBCs. Stents number 2 and 5, which underwent 1 V, showed that this level of electrical connection had the potential to attract RBCs. However, they acted differently in the number of RBCs migrating. Stent number 2 caused formation of

aggregations of RBCs and massive RBCs monolayer. Whereas, stent number 5 resulted in adherence of an average number of RBCs on the surface.

5.8.1 Comparison of Total Results of Mimicked Artery Experiments

At the end of mimicked artery experiment series, 40 stents were examined and underwent different levels of electrical potentials under various conditions. Although in some cases stents with the same applied electrical charges demonstrated different results, there were common patterns in the results of most of the stents with similar conditions.

It is noteworthy to mention that in the experiment under application of DC, the level of blood flow did not have an impact on migration of cells and the amount of 1 V acted satisfactorily in attraction of cells towards the stents' surfaces. However, the amount of 27 mV is much closer to the cell membranes' potential, it had lower potential in attraction of endothelial cells and unfortunately this charge provided pre-thrombosis conditions which are not ideal for patients suffering heart diseases. Obtained results from applied DC with extra human coronary artery endothelial cells, it can be said that stents with no applied electrical charge did not attract any specific components on their surface. Before running the experiment, it was expected that stent without electrical connections would not attract any specific items on their surface. As a matter of fact, the logic was that an electrical potential causes migration of cells and when there is no electrical potential, there is no migrated cells. Applied 27 mV on the samples again showed the potential for pre-clotting formations on the stents which is exactly reverse of the concept of applying electricity on the stents. These samples demonstrated the attraction of RBCs in both the form of a single layer and aggregation formation. Lastly, 1 V applied on the stents showed potential to attract a small number of endothelial cells among RBCs' migration. Adding more oxygen resulted in no changes in migration of cells. Indeed, the only stent which was not under application of electrical field, demonstrated the presence of RBCs as a single layer and group of aggregations. As a result, combination of applying small charges and adding oxygen did not cause migration of cells. Applying pulsed DC with square waveform about 100 Hz had the potential to attract some RBCs in forms of monolayer and aggregations. Different levels of electrical charge did not change the levels of migration of endothelial cells. However different frequencies with the same voltages of this electrical pattern might be more efficient in attraction of desired cells as the response of cells is dependant to the frequencies (Salter, Robb and Wright, 1997).

- DC vs pulsed DC

In comparison to the same experiments, with different waveform pattern, in both of the experiments, stents without electrical connections caused adherence of RBCs but in different forms. Monolayer of RBCs alongside aggregations can be seen in pulsed DC results, while linear DC forms layers of RBCs. Unlike non-electrical stents, stents with 27 mV resulted in single layers of RBCs in pulsed DC experiment. This level of charge caused aggregations of RBCs as well as even distribution of RBCs in the DC experiment. Stents with 1V, caused adherence of endothelial cells as well RBCs in DC experiment while they caused the presence of RBCs in the form of single layers or aggregations in pulsed DC experiment.

- Extra O₂ vs normal O₂

Comparing the same experiments with different levels of oxygen, stents with no electrical connections in extra O₂ experiment led to presence of RBCs in form of single layers and aggregations only in some area of the stent, while in normal (ambient) O₂ stents showed a large number of single RBCs on the surface. In normal O₂ experiment, 27 mV resulted in adherence of RBCs as monolayer and aggregations while 27 mV in extra O₂ did not attract specific items. Similar to 27 mV in extra O₂, 1V showed no potential to migration of cells onto the surface. However, 1V in normal O₂ caused migration of endothelial cells as well as RBCs occurrence.

- Extra endothelial cells vs normal endothelial cells

In comparison to the same experiments with increased endothelial cell numbers, stents which did not have electrical connections resulted in no attraction of cells in extra endothelial cells experiment and showed massive accumulation of RBCs in normal endothelial cells experiment. Interestingly, electrical level of 27 mV in both types of experiment caused formation of RBCs in the form of even distribution and aggregations. Like 27 mV, stents with 1 V almost showed approximately the same results. Adherence of endothelial cells as well as RBCs monolayers and aggregations can be seen in both type of the experiments.

Our results further support the idea of migration of cells by external DCEF as pointed previously in chapter2 (McCaig, Song and Rajnicek, 2009; Balint, Cassidy and Cartmell, 2013). However, some results did not support the overall hypothesis: one possibility is that the duration of the experiment was insufficient to cause adequate migration of endothelial cells. It can thus be suggested that using different frequencies of pulsed DC may have more effect in

cells attachment. It was seen the surface of the stents had some grooves or furrow-like features, which might influence the attraction of RBCs (as can be seen in 4.8). The results from adding extra endothelial cells might be effected by the components in the flask of human coronary artery endothelial cells. As this cells were adherent, they became detached using trypsin-EDTA. During the transportation of cells to the blood: cells floating in a tiny amount of cell medium and trypsin-EDTA, all together were added to the blood. Although the amount of cell medium and trypsin-EDTA were negligible, they might have an influence on the blood's components and the results. And the last hypothesis which might have an impact on the obtained results is in opening of the stents using the linear wrench and holder and internal expanding gripper: some stress and tension was applied to the stent, which possibly caused detachment or trauma of cells on the surface of the stents.

Unexpected results of mimicked artery experiments show sufficient potential of DC in the attraction of red blood cells onto the surface of the stents depending, to the amount of DC. What is surprising is that RBCs aggregation on the surface of the stents under different conditions. Aggregation formations is not a good result in the improvement of stents' outcomes. As a matter of fact the aggregation formation provides a convenient environment in the segment were a stent is placed for thrombus to rapidly form.

5.9 Summary

The present results are significant in at least three major respects. The first aspect is an introduction of a novel method (direct microelectrode method) in recording cells membrane potentials. Its results are different from di-electrophoresis and zeta potential method because di-electrophoresis and zeta potential results are obtained under the impact of electric fields. The second major aspect is improvements in electrophoresis method in which human cells are used instead of DNA and proteins. This developed electrophoresis shows migration of adherent cells and polarisation status. Similarly, mimicked artery experiments show RBCs and cells respond to applied electrical fields depending on the time and magnitude of the charge. Although applied electrical fields have been previously used with various cells for different purposes like wound healing, medial collateral ligament, cardiac tissue engineering and bone fracture healing processes, there is no evidence in the literature that illustrates the use of an electrical charge applied to a stent to induce the migration and translocation of human coronary artery endothelial cells, onto the stent (See Table 2.7). Applying information from human cells migration under influences of different pattern of electrical charges might cause acceleration

of wound healing and bone fracture healing process. Ito *et al.* (2007) reported that applying high voltage electrical field led to acceleration of medial collateral ligament. In addition, results from surface topography of stents showing furrows might be useful in other areas of tissue engineering for acceleration and migration of cells. However, results of electrodes experiments are not very encouraging. The combination of findings provides some support to target human cells using external electrical fields to migrate cells towards specific destination. Future research will be given in the next chapter.

Chapter 6 Conclusion and Future Work

In this thesis, techniques have been described and developed to explore the potential to induce vascular endothelial cells onto the blood contact surfaces of small vessel stents; of particular relevance are coronary artery stents. If endothelial cells can be made to inhabit a stent, well known post implantation effects, particularly restenosis could be reduced. To facilitate the migration of these cells, preliminary experiments were undertaken to confirm typical electrical properties and polarisation status of candidate cell lipid membranes. This work was necessary to ensure that specific cells could be attracted by the application of a biologically relevant voltage, oppositely polarised, using the body of electrically charged sample stents in a specially developed bio-mimic test facility. Measurements of human coronary artery endothelial cells and human osteoblast cells membrane potentials are presented and novel techniques to take these measurements, have been described. Determination of the optimum endothelial cells membrane potentials is therefore needed to ensure the most favourable conditions for the acceleration of re-endothelialisation of vascular stents. Migration of cells under applied external forces (electrotaxis) is well known in several clinical disciplines, for example wound healing and bone fracture repair and could provide a method to affect accelerated re-endothelialisation of vascular stents.

6.1 Summary

This research started by electrochemical measurements of a pair of electrodes; a commercially pure titanium and a stainless steel alloy-grade 304. Morphology and topography scanning was performed using SEM and AFM, respectively to determine the surface changes on metals after immersing to different solutions. The obtained results from electrochemical measurements did not show obvious trends in potential difference measurements of the electrodes after immersion. AFM images illustrated incomplete passivation formation probably due to the shortness of experiments. Results from SEM images showed that the immersing the electrodes in solution for a short duration did not cause significant changes in morphology of the metals.

The main goal of the current study was determination of human coronary artery endothelial and human osteoblast cells membrane potentials, which were -44.43 ± 10.04 mV and -52.6 ± 17.21 mV, respectively that were determined using direct microelectrode method. As the approach was a new technique, other methods were used to validate and compare the obtained results. Zeta potential method showed the potential of -9.76 ± 0.18 mV and -10.39 ± 1.32 mV

for human coronary artery endothelial cells and human osteoblast cells, respectively. The differences between obtained potentials were linked to the way the experiments were conducted. In direct microelectrode method, the cell membrane potential was recorded directly by touching the cell. However, in zeta potential technique, the potential of the cell was measured from the related velocity of cell movement under application of electrical fields.

The second major finding of this thesis was that adherent cells could migrate and had orientation changes under application of electrical fields. Using a new way to perform the electrophoresis method, confirmed that applied electrical fields had the potential to lead to migration of cells or changes in their orientation.

The final aim of this project was to investigate the rate of migration of endothelial cells to vascular stents, by means of a specific electrical charge applied to the stents and the consequent effect this had on endothelial cells. The bio-mimicked experiments were designed to investigate the effect of electrical stimulation of the cells to populate the stent samples. Results of applying DC illustrated limited adherence of endothelial cells on the surface of the stents suggesting that the cells showed a response to the electric fields. Experiments using added oxygen and additional endothelial cells did not show an enhanced response,

6.2 Research Contribution

The advantages of migration of human cells under the influence of electrical fields can be used in not only cardiovascular research, but also other research area including skin generation, tissue engineering and bone fractures. The obtained results from using an electrical current applied to stents showed sufficient potential on the migration of human cells which might reduce strongly negative complications after stents deployment. The significant contribution of this project to the research in this topic have opened a new focus on migration of human cells using electrical charges that could result in significant reduction in failure rates.

The second important contribution of this project was modification of electrophoresis method in which there was no need of transferring objects to the system. The modified electrophoresis cuvette reduced the errors from physical and chemical damages to cells and molecules.

Finally, unique membranes potential measurement of human coronary artery endothelial cells using direct-contact microelectrode method provided validated data that can be used for other purposes relating to coronary artery issues. This novel method showed a reliable and fast approach to measure cells membrane potential.

6.3 Limitations

The main limitation of this project was the use of stainless steel tube as the mimicked stent. It is clear that the stent design affects the wall shear stress, flow rate and fluid dynamic. Thus, the mimicked stent acts differently compared to a mesh tube stent. In addition, presence of the slit in the structure of the mimicked stent might affect the flow rate of the blood and it is unclear whether it causes a positive or negative effect on attraction of cells. More importantly, the endothelial cells were attracted to the mimicked stent which had more contact surface with the blood. However, it is unknown that using a real stent with less contact surface has the sufficient potential to attract endothelial cells.

The second major limitation was electrophoresis experiments were done out of the incubator. However, cells were active and viable at the initial hours of the experiments, their shapes and voltages changed after some hours. It is not clear yet if the experiments were performed in the incubator area, whether the results would differ.

6.4 Future work

The data and results obtained during the course of this research have given some positive results which have good potential to add to the scientific knowledge base, in an area that is somewhat undersubscribed. Confident gain be gained in making this statement because the extensive literature reviews that have been made in course of this thesis indicates a lack of research in regard to how the electrical properties of cells influence their overall dynamics. The obvious evidence in regard to all functions in human being, for example cognitive processes, metabolic processes, the senses, movements and other functional processes, are all electrically governed. Furthermore, cell-to-cell signaling mechanisms consist of electrochemical transactions, arguably, the electrical component predominates and warrants further investigation with potential benefits in many clinical areas.

A further study should assess the long-term effects of ionic solutions on metal electrodes. This would add greater precision in the measurement of cell membrane potential, albeit with the attendant difficulties of taking measurements *ex-vivo*.

The study of potential measurements using DEP method should be repeated two or three times more to give more accurate data. Because the DEP experiments were done in University of Surrey with collaboration of Prof. Michael P. Hughes and Dr. Fatima H. Labeed, there was limited opportunity to repeat the DEP experiments.

Further studies need to be carried out in order to validate the optimum applied DC by the electrophoresis method. Because the experiments were done in opened air, (compromising sterility) it is suggested to repeat the experiments varying DC power, within the confines of an incubator. In addition, changing the duration of the experiments, the environment, the pattern of DC and the material of electrophoresis cuvette could result in different findings, which will need investigating.

Further research would explore the optimum applied DC to the stent in bio-mimicked experiments. Not only level of applied DC could be studied, but also pulsed DC or other waveform DC could be explored. In addition, using real stents and human blood may have shown different results. The typical open mesh architecture of coronary artery stents, their reduced surface area and significant difference in hemodynamic performance, compared to the plain walled experimental stents, might influence the interaction of endothelial cells and the electrically induced migration. Ideally the next step, once the endothelial cell surface potential experiments have shown consistent results, would be to repeat these experiments *in vivo*, using animal models.

References

1. 3FX Medical Animation Digital Solutions (2012) *Arterial wall schematic*. Available at: <https://www.3fx.com/Our-Work/Illustration.aspx#prettyPhoto> (Accessed: 2017).
2. abm (2017) *Human Primary Osteoblasts*. Available at: <https://www.abmgood.com/PrimaryCells/primaryCells-dispOne.php?sn=60&csn=43&ssn=11860&dsn=12285&catanumber=T4015> (Accessed: 2017).
3. Adcock, D.M., Kressin, D.C. and Marlar, R.A. (1997) 'Effect of 3.2% vs 3.8% sodium citrate concentration on routine coagulation testing', *American Journal of Clinical Pathology*, 107(1), pp. 105-110.
4. Akagi, T., Kato, K., Hanamura, N., Kobayashi, M. and Ichiki, T. (2014) 'Evaluation of desialylation effect on zeta potential of extracellular vesicles secreted from human prostate cancer cells by on-chip microcapillary electrophoresis', *JAPANESE JOURNAL OF APPLIED PHYSICS*, 53(6), pp. 6. doi: 10.7567/JJAP.53.06JL01.
5. Akaike, N., Kanaide, H., Kuga, T., Nakamura, M., Sadoshima, J. and Tomoike, H. (1989) 'Low-voltage-activated calcium current in rat aorta smooth muscle cells in primary culture', *The Journal of physiology*, 416(1), pp. 141-160. doi: 10.1113/jphysiol.1989.sp017754.
6. Al Suwaidi, J., Berger, P.B. and Holmes Jr, D.R. (2000) 'Coronary artery stents', *Journal of the American Medical Association*, 284(14), pp. 1828-1836.
7. Al-Bazzaz, F.J. and Gailey, C. (2001) 'Ion transport by sheep distal airways in a miniature chamber', *American Journal of Physiology - Lung Cellular and Molecular Physiology*, 281(4), pp. L1028-L1034.
8. Armstrong, E.J., Maddox, T.M., Carey, E.P., Grunwald, G.K. and Shunk, K.A. (2014) *Mortality after presentation with stent thrombosis is associated with time from index percutaneous coronary intervention: A report from the VA CART program*.
9. Ashby, D.T., Dangas, G., Mehran, R. and Leon, M.B. (2002) 'Coronary artery stenting', *Catheterization and Cardiovascular Interventions*, 56(1), pp. 83-102. doi: 10.1002/ccd.10209.

10. Aull, F. (1967) 'Measurement of the electrical potential difference across the membrane of the ehrlich mouse ascites tumor cell', *Journal of cellular physiology*, 69(1), pp. 21-32. doi: 10.1002/jcp.1040690105.
11. Ayala-Torres, C., Hernández, N., Galeano, A., Novoa-Aponte, L. and Soto, C. (2014) 'Zeta potential as a measure of the surface charge of mycobacterial cells', *Annals of Microbiology*, 64(3), pp. 1189-1195. doi: 10.1007/s13213-013-0758-y.
12. Bai, H., McCaig, C.D., Forrester, J.V. and Zhao, M. (2004) 'DC Electric Fields Induce Distinct Preangiogenic Responses in Microvascular and Macrovascular Cells', *Arteriosclerosis, Thrombosis, and Vascular Biology: Journal of the American Heart Association*, 24(7), pp. 1234-1239. doi: 10.1161/01.ATV.0000131265.76828.8a.
13. Balint, R., Cassidy, N.J. and Cartmell, S.H. (2013) 'Electrical stimulation: a novel tool for tissue engineering', *Tissue engineering. Part B, Reviews*, 19(1), pp. 48.
14. Bedair, T.M., ElNaggar, M.A., Joung, Y.K. and Han, D.K. (2017) 'Recent advances to accelerate re-endothelialization for vascular stents', *Journal of Tissue Engineering*, 8, pp. 204173141773154. doi: 10.1177/2041731417731546.
15. Bhattacharjee, S. (2016) *DLS and zeta potential – What they are and what they are not?*.
16. Binggeli, R. and Cameron, I.L. (1980) 'Cellular potentials of normal and cancerous fibroblasts and hepatocytes', *Cancer research*, 40(6), pp. 1830.
17. Binggeli, R. and Weinstein, R.C. (1985) 'Deficits in elevating membrane potential of rat fibrosarcoma cells after cell contact', *Cancer research*, 45(1), pp. 235-241.
18. Bondar, O., Saifullina, D., Shakhmaeva, I., Mavlyutova, I. and Abdullin, T. (2012) 'Monitoring of the Zeta Potential of Human Cells upon Reduction in Their Viability and Interaction with Polymers', *ACTA NATURAE*, 4(1), pp. 78-81.
19. Bootman, M.D., Collins, T.J., Peppiatt, C.M., Prothero, L.S., MacKenzie, L., De Smet, P., Travers, M., Tovey, S.C., Seo, J.T., Berridge, M.J., Ciccolini, F. and Lipp, P. (2001) 'Calcium signalling—an overview', *Seminars in Cell and Developmental Biology*, 12(1), pp. 3-10. doi: 10.1006/scdb.2000.0211.
20. Borle, A.B. and Loveday, J. (1968) 'Effects of Temperature, Potassium, and Calcium on the Electrical Potential Difference in HeLa Cells', *Cancer research*, 28(12), pp. 2401-2405.

21. Bregestovski, P., Bakhramov, A., Danilov, S., Moldobaeva, A. and Takeda, K. (1988) 'Histamine-induced inward currents in cultured endothelial cells from human umbilical vein', *British journal of pharmacology*, 95(2), pp. 429-436. doi: 10.1111/j.1476-5381.1988.tb11663.x.
22. Britannica (2018) *Coronary stent*. Available at: <https://www.britannica.com/science/coronary-stent> (Accessed: 2017).
23. British Heart Foundation (2018) *Cardiovascular disease statics 2017*. Available at: <https://www.bhf.org.uk/what-we-do/our-research/heart-statistics/heart-statistics-publications/cardiovascular-disease-statistics-2017> (Accessed: 2017).
24. British Heart Foundation (2017a) *BHF CVD statics compendium-2017*. United Kingdom: British Heart Foundation. Available at: <https://www.bhf.org.uk/what-we-do/our-research/heart-statistics/heart-statistics-publications/cardiovascular-disease-statistics-2017> (Accessed: 2017).
25. British Heart Foundation (2017b) *CVD Statics- BHF UK fact sheet*. United Kingdom: British Heart Foundation. Available at: <https://www.bhf.org.uk/statistics> (Accessed: 2018).
26. British Heart Foundation (2015) *Cardiovascular disease statics, 2015*. United Kingdom: British Heart Foundation. Available at: <https://www.bhf.org.uk/information-support/publications/statistics/cvd-stats-2015> (Accessed: 2017).
27. Broche, L.M., Hoettges, K.F., Ogin, S.L., Kass, G.E.N. and Hughes, M.P. (2011) 'Rapid, automated measurement of dielectrophoretic forces using DEP-activated microwells', *Electrophoresis*, 32(17), pp. 2393-2399. doi: 10.1002/elps.201100063.
28. Brown, M.J. and Loew, L.M. (1994) 'Electric Field-Directed Fibroblast Locomotion Involves Cell Surface Molecular Reorganization and Is Calcium Independent', *The Journal of cell biology*, 127(1), pp. 117-128. doi: 10.1083/jcb.127.1.117.
29. Brust-Mascher, I. and Webb, W.W. (1998) *Calcium Waves Induced by Large Voltage Pulses in Fish Keratocytes*.
30. Byrne, R.A., Joner, M. and Kastrati, A. (2015) 'Stent thrombosis and restenosis: what have we learned and where are we going? The Andreas Grüntzig Lecture ESC 2014', *European heart journal*, 36(47), pp. 3320-3331. doi: 10.1093/eurheartj/ehv511.

31. Capodanno, D., Gori, T., Nef, H., Latib, A., Mehilli, J., Lesiak, M., Caramanno, G., Naber, C., Di Mario, C., Colombo, A., Capranzano, P., Wiebe, J., Araszkievicz, A., Geraci, S., Pyxaras, S., Mattesini, A., Naganuma, T., Münzel, T. and Tamburino, C. (2015) 'Percutaneous coronary intervention with everolimus-eluting bioresorbable vascular scaffolds in routine clinical practice: early and midterm outcomes from the European multicentre GHOST-EU registry', *EuroIntervention : journal of EuroPCR in collaboration with the Working Group on Interventional Cardiology of the European Society of Cardiology*, 10(10), pp. 1144-1153. doi: 10.4244/EIJY14M07_11.
32. Chang, P.C.T., Sulik, G.L., Soong, H.K. and Parkinson, W.C. (1996) 'Galvanotropic and galvanotaxic responses of corneal endothelial cells', *Journal of the Formosan Medical Association*, 95(8), pp. 623-627.
33. Chen, G. and Cheung, D.W. (1992) 'Characterization of Acetylcholine-Induced Membrane Hyperpolarization in Endothelial Cells', *Circulation research*, 70(2), pp. 257-263. doi: 10.1161/01.RES.70.2.257.
34. Chow, M., Turcotte, R., Lin, C. and Zhang, Y. (2014) 'Arterial Extracellular Matrix: A Mechanobiological Study of the Contributions and Interactions of Elastin and Collagen', *Biophysical journal*, 106(12), pp. 2684-2692. doi: 10.1016/j.bpj.2014.05.014.
35. Claessen, B.E., Henriques, J.P.S., Jaffer, F.A., Mehran, R., Piek, J.J. and Dangas, G.D. (2014) 'Stent Thrombosis', *JACC: Cardiovascular Interventions*, 7(10), pp. 1081-1092. doi: 10.1016/j.jcin.2014.05.016.
36. Colombo, A., Stankovic, G. and Moses, J.W. (2002a) 'Selection of coronary stents', *Journal of the American College of Cardiology*, 40(6), pp. 1021.
37. Colombo, A., Stankovic, G. and Moses, J.W. (2002b) 'Selection of coronary stents', *Journal of the American College of Cardiology*, 40(6), pp. 1021-1033. doi: 10.1016/S0735-1097(02)02123-X.
38. Cooper, G.M. (ed.) (2000) *The Cell: A Molecular Approach*. 2nd edn. Sunderland (MA): Sinauer Associates; Series number, .
39. Cooper, M.S. and Keller, R.E. (1984) 'Perpendicular Orientation and Directional Migration of Amphibian Neural Crest Cells in dc Electrical Fields', *Proceedings of the National Academy of Sciences of the United States of America*, 81(1), pp. 160-164. doi: 10.1073/pnas.81.1.160.

40. Cooper, M.S. and Schliwa, M. (1985) 'Electrical and ionic controls of tissue cell locomotion in DC electric fields', *Journal of neuroscience research*, 13(1-2), pp. 223-244. doi: 10.1002/jnr.490130116.
41. Cooper, M.S. and Schliwa, M. (1986) 'Motility of Cultured Fish Epidermal Cells in the Presence and Absence of Direct Current Electric Fields', *The Journal of cell biology*, 102(4), pp. 1384-1399. doi: 10.1083/jcb.102.4.1384.
42. Cutlip, D.E., Windecker, S., Mehran, R., Boam, A., Cohen, D.J., Van Es, G., Steg, P.G., Morel, M., Mauri, L., Vranckx, P., McFadden, E., Lansky, A., Hamon, M., Krucoff, M.W., Serruys, P.W., Acad Res Consortium, Academic Research Consortium and on behalf of the Academic Research Consortium (2007) 'Clinical end points in coronary stent trials: A case for standardized definitions', *Circulation*, 115(17), pp. 2344-2351. doi: 10.1161/CIRCULATIONAHA.106.685313.
43. Daut, J., Mehrke, G., Nees, S. and Newman, W.H. (1988) 'Passive electrical properties and electrogenic sodium transport of cultured guinea-pig coronary endothelial cells', *The Journal of physiology*, 402(1), pp. 237-254. doi: 10.1113/jphysiol.1988.sp017202.
44. DEP technology (2017) *3DEP Technology*. Available at: <http://deptechnology.com/the-deptechnology-3dep/> (Accessed: 2017).
45. Deuffic-Burban, S., Delarocque-Astagneau, E., Abiteboul, D., Bouvet, E. and Yazdanpanah, Y. (2011) *Blood-borne viruses in health care workers: Prevention and management*.
46. Djamgoz, M.B.A., Mycielska, M., Madeja, Z., Fraser, S.P. and Korohoda, W. (2001) 'Directional movement of rat prostate cancer cells in direct-current electric field: Involvement of voltage-gated Na⁺ channel activity', *Journal of cell science*, 114(14), pp. 2697-2705.
47. DLVO Theory (2017) *DLVO Theory*. Available at: <https://imk209.wikispaces.com/TWL+DLVO+theory> (Accessed: 2017).
48. Dortch-Carnes, J., Van Scott, M.R. and Fedan, J.S. (1999) 'Changes in Smooth Muscle Tone During Osmotic Challenge in Relation to Epithelial Bioelectric Events in Guinea Pig Isolated Trachea', *Journal of Pharmacology and Experimental Therapeutics*, 289(2), pp. 911-917.

49. Drug Development (2018) *A section of an artery showing the formation of an atherosclerotic plaque*. Available at: <https://www.drugdevelopment-technology.com/projects/cardiobook/attachment/cardiobook3/> (Accessed: 2017).
50. Dubé, J., Rochette-Drouin, O., Lévesque, P., Gauvin, R., Roberge, C.J., Auger, F.A., Goulet, D., Bourdages, M., Plante, M., Moulin, V.J. and Germain, L. (2012) 'Human keratinocytes respond to direct current stimulation by increasing intracellular calcium: Preferential response of poorly differentiated cells', *Journal of cellular physiology*, 227(6), pp. 2660-2667. doi: 10.1002/jcp.23008.
51. Elitas, M., Dhar, N., Schneider, K., Valero, A., Braschler, T., McKinney, J.D. and Renaud, P. (2017) 'Dielectrophoresis as a single cell characterization method for bacteria', *Biomedical Physics & Engineering Express*, 3(1), pp. 15005. doi: 10.1088/2057-1976/3/1/015005.
52. EO Labs (2017) *DSC – Defibrinated Sheep Blood*. Available at: <http://www.eolabs.com/product/dsc-defibrinated-sheep-blood-10ml/> (Accessed: 2018).
53. Erickson, C.A. and Nuccitelli, R. (1984) 'Embryonic Fibroblast Motility and Orientation Can Be Influenced by Physiological Electric Fields', *The Journal of cell biology*, 98(1), pp. 296-307. doi: 10.1083/jcb.98.1.296.
54. Farb, A., Sangiorgi, G., Carter, A.J., Walley, V.M., Edwards, W.D., Schwartz, R.S. and Virmani, R. (1999) 'Pathology of acute and chronic coronary stenting in humans', *Circulation*, 99(1), pp. 44-52. doi: 10.1161/01.CIR.99.1.44.
55. Farboud, B., Nuccitelli, R., Schwab, I.R. and ISSEROFF, R.R. (2000) 'DC Electric Fields Induce Rapid Directional Migration in Cultured Human Corneal Epithelial Cells', *Experimental eye research*, 70(5), pp. 667-673. doi: 10.1006/exer.2000.0830.
56. Fardy, P.S., Yanowitz, F.G. and Wilson, P.K. (1988) *Cardiac rehabilitation, adult fitness, and exercise testing*. 2nd edn. Philadelphia: Lea & Febiger.
57. Ferrier, J., Ross, S.M., Kanehisa, J. and Aubin, J.E. (1986) 'Osteoclasts and osteoblasts migrate in opposite directions in response to a constant electrical field', *Journal of cellular physiology*, 129(3), pp. 283-288. doi: 10.1002/jcp.1041290303.
58. Finegold, J.A., Asaria, P. and Francis, D.P. (2013) 'Mortality from ischaemic heart disease by country, region, and age: Statistics from World Health Organisation and United

- Nations', *International journal of cardiology*, 168(2), pp. 934-945. doi: 10.1016/j.ijcard.2012.10.046.
59. Finn, A.V., Joner, M., Nakazawa, G., Kolodgie, F., Newell, J., John, M.C., Gold, H.K. and Virmani, R. (2007a) 'Pathological correlates of late drug-eluting stent thrombosis: Strut coverage as a marker of endothelialization', *Circulation*, 115(18), pp. 2435-2441. doi: 10.1161/CIRCULATIONAHA.107.693739.
60. Finn, A.V., Nakazawa, G., Joner, M., Kolodgie, F.D., Mont, E.K., Gold, H.K. and Virmani, R. (2007b) 'Vascular Responses to Drug Eluting Stents: Importance of Delayed Healing', *Arteriosclerosis, Thrombosis, and Vascular Biology*, 27(7), pp. 1500-1510. doi: 10.1161/ATVBAHA.107.144220.
61. Fox, K., Prof, Ford, I., Prof, Steg, P.G., Prof, Tendera, M., Prof, Robertson, M., BSc, Ferrari, R., Prof, BEAUTIFUL Investigators and BEAUTIFUL investigators (2008) 'Heart rate as a prognostic risk factor in patients with coronary artery disease and left-ventricular systolic dysfunction (BEAUTIFUL): a subgroup analysis of a randomised controlled trial', *Lancet, The*, 372(9641), pp. 817-821. doi: 10.1016/S0140-6736(08)61171-X.
62. Garg, S. and Serruys, P.W. (2010) 'Coronary stents: Looking forward', *Journal of the American College of Cardiology*, 56(10), pp. S43-S78. doi: 10.1016/j.jacc.2010.06.008.
63. Gascoyne, P.R.C., Wang, X., Huang, Y. and Becker, F.F. (1997) 'Dielectrophoretic separation of cancer cells from blood', *IEEE Transactions on Industry Applications*, 33(3), pp. 670-678. doi: 10.1109/28.585856.
64. Goel, S., Raj, S., Sharma, A., Gidwani, U., Frankel, R. and Shani, J. (2017) 'Bioresorbable Coronary Scaffolds: Current State of Evidence', *European Medical Journal Cardiology*, 5(1), pp. 53-61.
65. Govindarajan, T. and Shandas, R. (2014) 'A survey of surface modification techniques for next-generation shape memory polymer stent devices', *Polymers*, 6(9), pp. 2309-2331. doi: 10.3390/polym6092309.
66. Grahn, J.C., Reilly, D.A., Nuccitelli, R.L. and Isseroff, R.R. (2003) 'Melanocytes do not migrate directionally in physiological DC electric fields', *Wound Repair and Regeneration*, 11(1), pp. 64-70. doi: 10.1046/j.1524-475X.2003.11110.x.

67. Gruler, H. (1993) 'Directed cell movement: A biophysical analysis', *Blood cells*, 19(1), pp. 91-113.
68. Guo, A., Song, B., Reid, B., Gu, Y., Forrester, J.V., Jahoda, C.A.B. and Zhao, M. (2010) 'Effects of Physiological Electric Fields on Migration of Human Dermal Fibroblasts', *Journal of Investigative Dermatology*, 130(9), pp. 2320-2327. doi: 10.1038/jid.2010.96.
69. Haltiwanger, S. (2003) *The electrical properties of cancer cells. pulsed technologies: From the archives of Jimmie Holman & Paul Dorneanu.*
70. Hansson, G.K. (2005) 'Mechanisms of disease: Inflammation, atherosclerosis, and coronary artery disease', *New England Journal of Medicine*, 352(16), pp. 1626-1695. doi: 10.1056/NEJMra043430.
71. Harder, D.R., Harder, D.R., Sperelakis, N. and Sperelakis, N. (1978) 'Membrane electrical properties of vascular smooth muscle from the guinea pig superior mesenteric artery', *Pflügers Archiv European Journal of Physiology*, 378(2), pp. 111-119. doi: 10.1007/BF00584443.
72. HE, P. and Curry, F.E. (1995) 'Measurement of Membrane Potential of Endothelial Cells in Single Perfused Microvessels', *Microvascular Research*, (50), pp. 183-198.
73. Her, A. and Shin, E. (2018) 'Current Management of In-Stent Restenosis', *KOREAN CIRCULATION JOURNAL*, 48(5), pp. 337-349. doi: 10.4070/kcj.2018.0103.
74. Hodgkin, A.L. and Katz, B. (1949) 'The effect of sodium ions on the electrical activity of the giant axon of the squid', *The Journal of physiology*, 108(1), pp. 37-77. doi: 10.1113/jphysiol.1949.sp004310.
75. Hoettges, K.F., Hübner, Y., Broche, L.M., Ogin, S.L., Kass, G.E.N. and Hughes, M.P. (2008) 'Dielectrophoresis-activated multiwell plate for label-free high-throughput drug assessment', *Analytical Chemistry*, 80(6), pp. 2063-2068. doi: 10.1021/ac702083g.
76. Holmes, D.R., Kereiakes, D.J., Garg, S., Serruys, P.W., Dehmer, G.J., Ellis, S.G., Williams, D.O., Kimura, T. and Moliterno, D.J. (2010) *Stent Thrombosis.*
77. Hughes, S., Magnay, J., Foreman, M., Publicover, S.J., Dobson, J.P. and El Haj, A.J. (2006) 'Expression of the mechanosensitive 2PK+ channel TREK-1 in human osteoblasts', *Journal of cellular physiology*, 206(3), pp. 738-748. doi: 10.1002/jcp.20536.

78. Ismail, A., Hughes, M., Mulhall, H., Oreffo, R. and Labeed, F. (2015) 'Characterization of human skeletal stem and bone cell populations using dielectrophoresis: Dielectrophoretic properties of skeletal populations', *Journal of Tissue Engineering and Regenerative Medicine*, 9(2), pp. 162-168. doi: 10.1002/term.1629.
79. Ito, M., Murase, K., Tanaka, S. and Matsushita, T. (2007) 'Promotion of Medial Collateral Ligament Healing Using a High-Voltage Electrical Field', *Journal of Orthopaedic Surgery*, 15(1), pp. 22-26. doi: 10.1177/230949900701500106.
80. Jaffe, R. and Strauss, B.H. (2007) *Late and Very Late Thrombosis of Drug-Eluting Stents: Evolving Concepts and Perspectives*.
81. Jeudy, J., Waite, S. and Chen, J.J. (2015) *Imaging of coronary revascularisation*. Available at: <https://clinicalgate.com/imaging-of-coronary-revascularization-coronary-stents-and-bypass-grafts/> (Accessed: 2017).
82. Jones, D.B. and West, R. (1995) *Cardiac rehabilitation*. London: BMJ Publishing.
83. Julian, D.G., Cowan, J.C. and McLenachan, J.M. (1998) *Cardiology*. 7th edn. New York; Edinburgh: W.B. Saunders Co.
84. Khalifa, Y.S.E., Eisa, K.M., Bary, M.A., Hossam Eldin M.M. Ismail and Taha, A.M. (2018) 'Short term outcome of coronary artery bypass graft surgery: Evaluation of recently established cardiac center', *Journal of the Egyptian Society of Cardio-Thoracic Surgery*, 26(1), pp. 24-29. doi: 10.1016/j.jescts.2017.12.003.
85. Klomp, M., Beijik, M.A.M., Damman, P., Woudstra, P., Koch, K.T., TijssenI, J.G.P. and De Winter, R.J. (2011) 'Three-Year Clinical Follow-Up of an Unselected Patient Population Treated with the Genous Endothelial Progenitor Cell Capturing Stent: THREE-YEAR FOLLOW-UP AFTER GENOUS STENT TREATMENT', *Journal of interventional cardiology*, 24(5), pp. 442-449. doi: 10.1111/j.1540-8183.2011.00665.x.
86. Krasopoulos, G. (2013) *Bypass (CABG)*. Available at: <http://www.cardiosurgeon.co.uk/treatment-guide/bypass-cabg/> (Accessed: 2017).
87. Lahmer, T., Messer, M., Rasch, S., Beitz, A., Schnappauf, C., Schmid, R. and Huber, W. (2015) 'Sustained low-efficiency dialysis with regional citrate anticoagulation in medical intensive care unit patients with liver failure: A prospective study', *Journal of critical care*, 30(5), pp. 1096-1100. doi: 10.1016/j.jcrc.2015.06.006.

88. Laskey, R.E., Adams, D.J., Johns, A., Rubanyi, G.M. and Breemen, C.v. (1990) 'Membrane potential and Na(+)-K+ pump activity modulate resting and bradykinin-stimulated changes in cytosolic free calcium in cultured endothelial cells from bovine atria', *Journal of Biological Chemistry*, 265(5), pp. 2613-2619.
89. Lešer, V., Drobne, D., Pipan, Ž, Milani, M. and Tatti, F. (2009) 'Comparison of different preparation methods of biological samples for FIB milling and SEM investigation', *Journal of microscopy*, 233(2), pp. 309-319. doi: 10.1111/j.1365-2818.2009.03121.x.
90. Levick, J.R. (2010) *An introduction to cardiovascular physiology*. 5th edn. London: Hodder Arnold.
91. Leybaert, L. and Sanderson, M.J. (2012) 'Intercellular Ca(2+) waves: mechanisms and function', *Physiological Reviews*, 92(3), pp. 1359.
92. Li, L., El-Hayek, Y.H., Liu, B., Chen, Y., Gomez, E., Wu, X., Ning, K., Li, L., Chang, N., Zhang, L., Wang, Z., Hu, X. and Wan, Q. (2008) 'Direct-Current Electrical Field Guides Neuronal Stem/Progenitor Cell Migration', *Stem cells*, 26(8), pp. 2193-2200. doi: 10.1634/stemcells.2007-1022.
93. Li, X. and Kolega, J. (2002) 'Effects of direct current electric fields on cell migration and actin filament distribution in bovine vascular endothelial cells', *Journal of vascular research*, 39(5), pp. 391-404. doi: 10.1159/000064517.
94. Lin, K., Edelman, E.R., Strichartz, G. and Lilly, L.S. (2011) 'Basic cardiac structure and function', in Lilly, L.S. (ed.) *Pathophysiology of heart disease*. 5th, International edn. London; Baltimore, MD: Lippincott Williams & Wilkins, pp. 1-9.
95. Little, B., Little, B., Wagner, P., Wagner, P., Ray, R., Ray, R., Pope, R., Pope, R., Scheetz, R. and Scheetz, R. (1991) 'Biofilms: An ESEM evaluation of artifacts introduced during SEM preparation', *Journal of industrial microbiology*, 8(4), pp. 213-221; 222. doi: 10.1007/BF01576058.
96. Lonza (2017) *Clonetics™ Endothelial Cell System: Technical Information & Instructions*. USA: Lonza Walkersville. Available at: <https://www.google.co.uk/url?sa=t&rct=j&q=&esrc=s&source=web&cd=1&ved=0ahUKEwi azqL7hJLcAhXBfMAKHR5YDAkQFggoMAA&url=https%3A%2F%2Flonza.picturepark.com%2FWebsite%2F%3FAction%3DdownloadAsset%26AssetId%3D29423&usq=AOvVaw OiKr1VmnM-h8u89yfkqGM> (Accessed: 2017).

97. Louis, K.S. and Siegel, A.C. (2011) 'Cell viability analysis using trypan blue: manual and automated methods', in Stoddart, M.J. (ed.) *Mamalian cell viability*. first edn. United States: Humana Press, pp. 7-12.
98. Lückhoff, A., Luckhoff, A., Busse, R. and Busse, R. (1990) 'Activators of potassium channels enhance calcium influx into endothelial cells as a consequence of potassium currents', *Naunyn-Schmiedeberg's archives of pharmacology*, 342(1), pp. 94-99. doi: 10.1007/BF00178979.
99. Mahabadi, S., Labeed, F.H. and Hughes, M.P. (2015) 'Effects of cell detachment methods on the dielectric properties of adherent and suspension cells', *Electrophoresis*, 36(13), pp. 1493-1498. doi: 10.1002/elps.201500022.
100. Majesky, M.W., Dong, X.R., Hoglund, V., Mahoney, J., William M. and Daum, G. (2011) 'The Adventitia: A Dynamic Interface Containing Resident Progenitor Cells', *Arteriosclerosis, Thrombosis, and Vascular Biology*, 31(7), pp. 1530-1539. doi: 10.1161/ATVBAHA.110.221549.
101. Maktari, A. (2015) *Drug-eluting coronary stent presentation with revision*. Available at: <https://www.slideshare.net/AymenMaktari/drugeluting-coronary-stent-presentation-with-revisions> (Accessed: 2017).
102. Malvern Panalytical Ltd (2018) *Zetasizer range*. Available at: <https://www.malvernpanalytical.com/en/support/product-support/zetasizer-range/index.html> (Accessed: 2017).
103. Mann, K.G., Whelihan, M.F., Butenas, S. and Orfeo, T. (2007) 'Citrate anticoagulation and the dynamics of thrombin generation', *Journal of Thrombosis and Haemostasis*, 5(10), pp. 2055-2061. doi: 10.1111/j.1538-7836.2007.02710.x.
104. Marchenko, S.M. and Sage, S.O. (1993) 'Electrical properties of resting and acetylcholine-stimulated endothelium in intact rat aorta', *The Journal of physiology*, 462(1), pp. 735-751. doi: 10.1113/jphysiol.1993.sp019579.
105. Martin, D.M. and Boyle, F.J. (2011) 'Drug-eluting stents for coronary artery disease: A review', *Medical Engineering and Physics*, 33(2), pp. 148-163. doi: 10.1016/j.medengphy.2010.10.009.

106. McCaig, C.D., Song, B. and Rajnicek, A.M. (2009) 'Electrical dimensions in cell science', *Journal of cell science*, 122(23), pp. 4267-4276. doi: 10.1242/jcs.023564.
107. Mehrke, G., Pohl, U. and Daut, J. (1991) 'Effects of vasoactive agonists on the membrane potential of cultured bovine aortic and guinea-pig coronary endothelium', *The Journal of physiology*, 439(1), pp. 277-299. doi: 10.1113/jphysiol.1991.sp018667.
108. Monchi, M. (2017) 'Citrate pathophysiology and metabolism', *Transfusion and Apheresis Science*, 56(1), pp. 28-30. doi: 10.1016/j.transci.2016.12.013.
109. Moran, P. and Coats, B. (2012) 'Biological Sample Preparation for SEM Imaging of Porcine Retina', *Microscopy Today*, 20(2), pp. 28-31. doi: 10.1017/S1551929511001374.
110. Mudau, M., Genis, A., Lochner, A. and Strijdom, H. (2012) 'Endothelial dysfunction: The early predictor of atherosclerosis', *Cardiovascular Journal of Africa*, 23(4), pp. 222-231. doi: 10.5830/CVJA-2011-068.
111. Mycielska, M.E. and Djamgoz, M.B.A. (2004) 'Cellular mechanisms of direct-current electric field effects: Galvanotaxis and metastatic disease', *Journal of cell science*, 117(9), pp. 1631-1639. doi: 10.1242/jcs.01125.
112. Nakano, M., Yahagi, K., Otsuka, F., Sakakura, K., Finn, A., Kutys, R., Ladich, E., Fowler, D., Joner, M. and Virmani, R. (2014) 'Causes of Early Stent Thrombosis in Patients Presenting With Acute Coronary Syndrome An Ex Vivo Human Autopsy Study', *Journal of the American College of Cardiology*, 63(23), pp. 2510-2520. doi: 10.1016/j.jacc.2014.02.607.
113. Nakashima, M., Mombouli, J., Taylor, A.A. and Vanhoutte, P.M. (1993) 'Endothelium-dependent hyperpolarization caused by bradykinin in human coronary arteries', *Journal of Clinical Investigation*, 92(6), pp. 2867-2871. doi: 10.1172/JCI116907.
114. National Physical Laboratory (2017) *Bimetallic Corrosion*. National Physical Laboratory: National Physical Laboratory. Available at: http://www.google.co.uk/url?sa=t&rct=j&q=&esrc=s&source=web&cd=14&ved=0ahUKEwjqs4-0gZLcAhUUTsAKHST_BdkQFghtMA0&url=http%3A%2F%2Fwww.npl.co.uk%2Fupload%2Fpdf%2Fbimetallic_20071105114556.pdf&usg=AOvVaw2D3Uqb9fibZHW0E0DAcdt- (Accessed: 2017).

115. Nishimoto, Y., Ueda, Y., Sugihara, R., Murakami, A., Ueno, K., Takeda, Y., Hirata, A., Kashiwase, K., Higuchi, Y. and Yasumura, Y. (2017) 'Comparison of angioscopic findings among second-generation drug-eluting stents', *Journal of cardiology*, 70(3-4), pp. 297-302. doi: 10.1016/j.jjcc.2016.11.012.
116. Nishimura, K.Y., Isseroff, R.R. and Nucciteili, R. (1996) 'Human keratinocytes migrate to the negative pole in direct current electric fields comparable to those measured in mammalian wounds', *Journal of cell science*, 109(1), pp. 199-207.
117. Nuccitelli, R. and Smart, T. (1989) 'Extracellular Calcium Levels Strongly Influence Neural Crest Cell Galvanotaxis', *BIOLOGICAL BULLETIN*, 176(2), pp. 130-135.
118. Office for National Statistics (2016) *Deaths registered in England and Wales (Series DR): 2015*. Available at: <https://www.ons.gov.uk/releases/deathsregisteredinenglandandwalesseriesdr2013> (Accessed: 2017).
119. Ogden, D. and Stanfield, P. (2011) 'Patch clamp techniques for single channel and whole-cell recording', pp. 53-75.
120. Okada, Y., Sato, T. and Inouye, A. (1975) 'Effects of potassium-ions and sodium ions on membrane potential cells in rat duodenum ', *Biochimica et biophysica acta*, 413(1), pp. 104-115.
121. Olschewski, A., Olschewski, H., Brau, M.E., Hempelmann, G., Vogel, W. and Safronov, B.V. (2001) 'Basic Electrical Properties of In situ Endothelial Cells of Small Pulmonary Arteries during Postnatal Development', *American Journal of Respiratory Cell and Molecular Biology*, 25(3), pp. 285-290.
122. Orida, N. and Feldman, J.D. (1982) 'Directional protrusive pseudopodial activity and motility in macrophages induced by extracellular electric fields', *Cell motility*, 2(3), pp. 243.
123. Overholt, J.L., Ficker, E., Yang, T., Shams, H., Bright, G.R. and Prabhakar, N.R. (2000) 'HERG-Like Potassium Current Regulates the Resting Membrane Potential in Glomus Cells of the Rabbit Carotid Body', *Journal of neurophysiology*, 83(3), pp. 1150-1157.
124. Pang, J.H., Farhatnia, Y., Godarzi, F., Tan, A., Rajadas, J., Cousins, B.G. and Seifalian, A.M. (2015) 'In situ Endothelialization: Bioengineering Considerations to Translation', *Small*, 11(47), pp. 6248-6264. doi: 10.1002/sml.201402579.

125. Pangalos, M., Bintig, W., Schlingmann, B., Feyerabend, F., Witte, F., Begandt, D., Heisterkamp, A. and Ngezahayo, A. (2011) 'Action potentials in primary osteoblasts and in the MG-63 osteoblast-like cell line', *Journal of Bioenergetics and Biomembranes*, 43(3), pp. 311-322. doi: 10.1007/s10863-011-9354-7.
126. particle sciences (2012) *An overview of the zeta potential*. particle sciences. Available at: <http://www.particlesciences.com/news/technical-briefs/2012/overview-of-zeta-potential.html> (Accessed: 2012).
127. Patel, N. and Poo, M. (1984) 'Perturbation of the direction of neurite growth by pulsed and focal electric fields', *Journal of Neuroscience*, 4(12), pp. 2939-2947.
128. Pekker, M. and Shneider, M.N. (2014) 'The surface charge of a cell lipid membrane', . doi: 10.4172/2161-0398.1000177.
129. Perret, S., Cantereau, A., Audin, J., Dufy, B. and Georgescauld, D. (1999) *Interplay between Ca²⁺ release and Ca²⁺ influx underlies localized hyperpolarization-induced [Ca²⁺]_i waves in prostatic cells*.
130. Perski, A., Feleke, E., Anderson, G., Samad, B.A., Westerlund, H., Ericsson, C. and Rehnqvist, N. (1998) 'Emotional distress before coronary bypass grafting limits the benefits of surgery', *American Heart Journal*, 136(3), pp. 510-517. doi: 10.1016/S0002-8703(98)70229-7.
131. PhysiologyWeb, (2014) *Introduction- Resting Membrane Potential*. Available at: http://www.physiologyweb.com/lecture_notes/resting_membrane_potential/resting_membrane_potential_introduction.html (Accessed: 2016).
132. Pislaru, S.V., Harbuzariu, A., Gulati, R., Witt, T., Sandhu, G.S., Sandhu, N.P. and Simari, R.D. (2006) 'Magnetically Targeted Endothelial Cell Localization in Stented Vessels', *Journal of the American College of Cardiology*, 48(9), pp. 1839-1845. doi: 10.1016/j.jacc.2006.06.069.
133. Pliquet, U., Joshi, R.P., Sridhara, V. and Schoenbach, K.H. (2007) *High electrical field effects on cell membranes*.
134. Pollack, G.H. (2015) 'Cell electrical properties: reconsidering the origin of the electrical potential: Cell electrical properties', *Cell biology international*, 39(3), pp. 237-242. doi: 10.1002/cbin.10382.

135. Polyak, B., Fishbein, I., Chorny, M., Alferiev, I., Williams, D., Yellen, B., Friedman, G. and Levy, R.J. (2008) 'High Field Gradient Targeting of Magnetic Nanoparticle-Loaded Endothelial Cells to the Surfaces of Steel Stents', *Proceedings of the National Academy of Sciences of the United States of America*, 105(2), pp. 698-703. doi: 10.1073/pnas.0708338105.
136. Polymax (2016) *Technical Specification for platinum cured silicon tubing*. UK: Polymax. Available at: <https://www.polymax.co.uk/silicone-tubing> (Accessed: 2016).
137. Poo, M.M. (1981) 'In SITU Electrophoresis of Membrane Components', *Annual Review of Biophysics and Bioengineering*, 10(1), pp. 245-276. doi: 10.1146/annurev.bb.10.060181.001333.
138. Quorum Technologies (2008) *SC7640 Auto/Manual High Resolution Sputter Coater*. Quorum Technologies Ltd. Available at: https://www.google.co.uk/url?sa=t&rct=j&q=&esrc=s&source=web&cd=1&ved=0ahUKEwjnr5y0g5LcAhWkKsAKHUT1BS8QFghLMAA&url=https%3A%2F%2Fwww.quorumtech.com%2F_assets_%2Fpdf%2FManuals%2FOM-SC7640-Issue-3.pdf&usg=AOvVaw0242BBP_19Q0hZKaBjpvlr (Accessed: 2017).
139. Quorum Technologies (2002) *Sputter Coating*. UK: Quorum Technologies Ltd. Available at: http://www.google.co.uk/url?sa=t&rct=j&q=&esrc=s&source=web&cd=1&ved=0ahUKEwjM1IrPg5LcAhXDfMAKHeElAgAQFggtMAA&url=http%3A%2F%2Fwww.iitk.ac.in%2Fmeesa%2FSEM%2Fcoater_manual_technical.pdf&usg=AOvVaw15CT6-UkdxQbolwE4h0sSq (Accessed: 2017).
140. Rapp, B., De Boisfleury-Chevance, A. and Gruler, H. (1988) 'Galvanotaxis of human granulocytes. Dose-response curve', *European Biophysics Journal*, 16(5), pp. 313-319. doi: 10.1007/BF00254068.
141. Reejhsinghani, R. and Lotfi, A.S. (2015) 'Prevention of stent thrombosis: challenges and solutions', *Vascular health and risk management*, 11, pp. 93-106. doi: 10.2147/VHRM.S43357.
142. Revest, P.A., Jones, H.C. and Joan Abbott, N. (1994) 'Transendothelial electrical potential across pial vessels in anaesthetised rats: a study of ion permeability and transport at

the blood-brain barrier', *Brain research*, 652(1), pp. 76-82. doi: 10.1016/0006-8993(94)90319-0.

143. Rose, R.C. and Schultz, S.G. (1971) 'Studies on the electrical potential profile across rabbit ileum. Effects of sugars and amino acids on transmural and transmucosal electrical potential differences', *The Journal of general physiology*, 57(6), pp. 639-663. doi: 10.1085/jgp.57.6.639.

144. Ross, R. (1999) 'Mechanisms of disease - Atherosclerosis - An inflammatory disease', *NEW ENGLAND JOURNAL OF MEDICINE*, 340(2), pp. 115-126.

145. Russell, F.M., S. S. N. Biribo, Selvaraj, G., Oppedisano, F., Warren, S., Seduadua, A., Mulholland, E.K. and Carapetis, J.R. (2006) 'As a Bacterial Culture Medium, Citrated Sheep Blood Agar Is a Practical Alternative to Citrated Human Blood Agar in Laboratories of Developing Countries', *Journal of clinical microbiology*, 44(9), pp. 3346-3351. doi: 10.1128/JCM.02631-05.

146. Rutala, W.A. and Weber, D.J. (2004) 'Disinfection and Sterilization in Health Care Facilities: What Clinicians Need to Know', *Clinical Infectious Diseases*, 39(5), pp. 702-709. doi: 10.1086/423182.

147. Rutala, W.,A., Weber, D.,J. and the Healthcare Infection Control Practices Advisory Committee (HICPAC) (2008) *Guidelines for disinfection and sterilization in healthcare facilities*. U.S. department of health and human sciences: Centers for disease control and prevention. Available at: <https://stacks.cdc.gov/view/cdc/11560> (Accessed: 2017).

148. Salopek, B., Krasic, D. and Filipovic, S. (1992) 'Measurmenta and application of zeta potential', *Rudarsko-geolosko-naftni zbornik*, 4, pp. 147-151.

149. Salter, D.M., Robb, J.E. and Wright, M.O. (1997) 'Electrophysiological responses of human bone cells to mechanical stimulation: Evidence for specific integrin function in mechanotransduction', *Journal of Bone and Mineral Research*, 12(7), pp. 1133-1141. doi: 10.1359/jbmr.1997.12.7.1133.

150. Secemsky, E., Matteau, A., Yeh, R., Steg, P., Camenzind, E., Wijns, W., McFadden, E., Mauri, L. and PROTECT Trial Investigators (2015) 'Comparison of Short- and Long-Term Cardiac Mortality in Early Versus Late Stent Thrombosis (from Pooled PROTECT Trials)', *AMERICAN JOURNAL OF CARDIOLOGY*, 115(12), pp. 1678-1684. doi: 10.1016/j.amjcard.2015.03.010.

151. Segal, S.S. and Beny, J.L. (1992) 'Intracellular recording and dye transfer in arterioles during blood flow control', *AJP - Heart and Circulatory Physiology*, 263(1), pp. H1-H7.
152. Sharma, N.R. and Davis, M.J. (1994) 'Mechanism of substance P-induced hyperpolarization of porcine coronary artery endothelial cells', *AJP - Heart and Circulatory Physiology*, 266(1), pp. H156-H164.
153. Sheridan, D.M., Isseroff, R.R. and Nuccitelli, R. (1996) 'Imposition of a Physiologic DC Electric Field Alters the Migratory Response of Human Keratinocytes on Extracellular Matrix Molecules', *Journal of Investigative Dermatology*, 106(4), pp. 642-646. doi: 10.1111/1523-1747.ep12345456.
154. Simard, T., Hibbert, B., Ramirez, F., Froeschl, M., Chen, Y. and O'Brien, E. (2014) 'The Evolution of Coronary Stents: A Brief Review', *CANADIAN JOURNAL OF CARDIOLOGY*, 30(1), pp. 35-45. doi: 10.1016/j.cjca.2013.09.012.
155. Solenoid (2017) *Pinch Solenoid Valve: 3/2- NC (Normally Closed)- NO (Normally Open)*. Italy: Solenoid. Available at: <http://www.sirai.com/dgssearch/search.php?q=s306> (Accessed: 2017).
156. Sommer, P. and Armstrong, E.J. (2015) 'Stent Thrombosis: Current Management and Outcomes', *Current Treatment Options in Cardiovascular Medicine*, 17(3), pp. 1-12. doi: 10.1007/s11936-015-0365-2.
157. Stefani, E. and Cerejido, M. (1983) 'Electrical properties of cultured epithelioid cells (MDCK)', *Journal of Membrane Biology*, 73(2), pp. 177-184. doi: 10.1007/BF01870440.
158. Strom, J.B. and Libby, P. (2011) 'Atherosclerosis', in Lilly, L.S. (ed.) *Pathophysiology of heart disease*. 5th, International edn. London; Baltimore, MD: Lippincott Williams & Wilkins, pp. 113-134.
159. Stump, R.F. and Robinson, K.R. (1983) 'Xenopus Neural Crest Cell Migration in an Applied Electrical Field', *The Journal of cell biology*, 97(4), pp. 1226-1233. doi: 10.1083/jcb.97.4.1226.
160. Sulik, G.L., Sulik, G.L., Soong, H.K., Soong, H.K., Chang, P.C.T., Chang, P.C.T., Parkinson, W.C., Parkinson, W.C., Elner, S.G., Elner, S.G., Elner, V.M. and Elner, V.M. (1992) 'Effects of steady electric fields on human retinal pigment epithelial cell orientation

and migration in culture', *Acta Ophthalmologica*, 70(1), pp. 115-122. doi: 10.1111/j.1755-3768.1992.tb02102.x.

161. Sundelacruz, S., Levin, M. and Kaplan, D.L. (2009) 'Role of membrane potential in the regulation of cell proliferation and differentiation', *Stem Cell Reviews and Reports*, 5(3), pp. 231-246. doi: 10.1007/s12015-009-9080-2.

162. Szatkowski, M., Mycielska, M., Knowles, R., Kho, A.- and Djamgoz, M.B.A. (2000) 'Electrophysiological recordings from the rat prostate gland in vitro: identified single-cell and transepithelial (lumen) potentials', *BJU international*, 86(9), pp. 1068-1075. doi: 10.1046/j.1464-410x.2000.00889.x.

163. Tada, T., Byrne, R., Simunovic, I., King, L., Cassese, S., Joner, M., Fusaro, M., Schneider, S., Schulz, S., Ibrahim, T., Ott, I., Massberg, S., Laugwitz, K. and Kastrati, A. (2013a) 'Risk of Stent Thrombosis Among Bare-Metal Stents, First-Generation Drug-Eluting Stents, and Second-Generation Drug-Eluting Stents Results From a Registry of 18,334 Patients', *JACC-CARDIOVASCULAR INTERVENTIONS*, 6(12), pp. 1267-1274. doi: 10.1016/j.jcin.2013.06.015.

164. Tada, T., Byrne, R.A., Simunovic, I., King, L.A., Cassese, S., Joner, M., Fusaro, M., Schneider, S., Schulz, S., Ibrahim, T., Ott, I., Massberg, S., Laugwitz, K. and Kastrati, A. (2013b) 'Risk of stent thrombosis among bare-metal stents, first-generation drug-eluting stents, and second-generation drug-eluting stents: Results from a registry of 18,334 patients', *JACC: Cardiovascular Interventions*, 6(12), pp. 1267-1274. doi: 10.1016/j.jcin.2013.06.015.

165. Tan, C.H., Muhamad, N. and Abdullah, M.M.A.B. (2017) *Surface Topographical Modification of Coronary Stent: A Review*. pp. 12031.

166. Tang, H., Wang, Q., Wang, X., Zhou, J., Zhu, M., Qiao, T., Liu, C., Mao, C. and Zhou, M. (2016) 'Effect of a Novel Stent on Re-Endothelialization, Platelet Adhesion, and Neointimal Formation', *Journal of Atherosclerosis and Thrombosis*, 23(1), pp. 67-80. doi: 10.5551/jat.31062.

167. Tarantola, A., Abiteboul, D. and Rachline, A. (2006) *Infection risks following accidental exposure to blood or body fluids in health care workers: A review of pathogens transmitted in published cases*.

168. Texas Heart Institute (2017) *Heart anatomy*. Available at: <https://www.texasheart.org/heart-health/heart-information-center/topics/heart-anatomy/> (Accessed: 2017).
169. The Center for Prevention Heart Attack and Stroke (2016) *What is Atherosclerosis?* Available at: <http://www.thecenterforprevention.com/what-is-atherosclerosis/> (Accessed: 2017).
170. Toro, L., Gonzalez-Robles, A. and Stefani, E. (1986) 'Electrical properties and morphology of single vascular smooth muscle cells in culture', *American Journal of Physiology - Cell Physiology*, 251(5), pp. 763-773.
171. Torrado, J., Buckley, L., Durán, A., Trujillo, P., Toldo, S., Valle Raleigh, J., Abbate, A., Biondi-Zoccai, G. and Guzmán, L.A. (2018) *Restenosis, Stent Thrombosis, and Bleeding Complications: Navigating Between Scylla and Charybdis*.
172. Trivedi, D.P., Hallock, K.J. and Bergethon, P.R. (2013) 'Electric fields caused by blood flow modulate vascular endothelial electrophysiology and nitric oxide production', *Bioelectromagnetics*, 34(1), pp. 22-30. doi: 10.1002/bem.21741.
173. U.S. Food & Drug Administration (2016) *Submission and review of sterility information in premarket notification (510(k)) submissions for devices labeled as sterile*. USA: U.S. Department of health and human sciences ,Food & Drug Administration, center for devices and radiological health, center for biological evaluation and research. Available at: [https://google2.fda.gov/search?q=Submission+and+Review+of+Sterility+Information+in+Premarket+Notification+%28510\(k\)%28%29%29+Submissions+for+Devices+Labeled+as+Sterile&client=FDAgov&site=FDAgov&lr=&proxystylesheet=FDAgov&requiredfields=-archive%3AYes&output=xml_no_dtd&getfields=*](https://google2.fda.gov/search?q=Submission+and+Review+of+Sterility+Information+in+Premarket+Notification+%28510(k)%28%29%29+Submissions+for+Devices+Labeled+as+Sterile&client=FDAgov&site=FDAgov&lr=&proxystylesheet=FDAgov&requiredfields=-archive%3AYes&output=xml_no_dtd&getfields=*) (Accessed: 01/2016).
174. University of Birmingham (2014) *Health and Safety Guidance: Work with human body fluids and tissues*. Birmingham: University of Birmingham. Available at: https://www.google.co.uk/url?sa=t&rct=j&q=&esrc=s&source=web&cd=1&ved=0ahUKEwjdmIylgJLcAhVPNMAKHezuDh8QFggoMAA&url=https%3A%2F%2Fintranet.birmingham.ac.uk%2Fhr%2Fdocuments%2Fpublic%2Fhsu%2Fhsuguidance%2FGuidance-on-work-with-human-body-fluids-and-tissue.pdf&usq=AOvVaw2k5V0s_V5B_UcqVQS8K5_Z (Accessed: 2017).

175. University Surgical vascular (2017) *Angioplasty and Stenting*, Available at: <http://www.gasurgery.com/treatment-options/angioplasty-and-stenting/> (Accessed: 2017).
176. Updegraff, E. (2017) *What is Resting Membrane Potential?* Available at: <http://www.wisegeek.org/what-is-resting-membrane-potential.htm> (Accessed: 2016).
177. Vargas, F.F., Vargas, F.F., Caviedes, P.F., Caviedes, P.F., Grant, D.S. and Grant, D.S. (1994) 'Electrophysiological characteristics of cultured human umbilical vein endothelial cells', *Microvascular research*, 47(2), pp. 153-165. doi: 10.1006/mvre.1994.1012.
178. Veitinger, S. (2018) *The patch-clamp technique*. Available at: <https://www.leica-microsystems.com/science-lab/the-patch-clamp-technique/> (Accessed: 2017).
179. Voets, T., Droogmans, G. and Nilius, B. (1996) 'Membrane currents and the resting membrane potential in cultured bovine pulmonary artery endothelial cells', *The Journal of physiology*, 497(Pt 1), pp. 95-107. doi: 10.1113/jphysiol.1996.sp021752.
180. von der Weid, P.Y. and Beny, J.L. (1992) 'Effect of Ca²⁺ ionophores on membrane potential of pig coronary artery endothelial cells', *AJP - Heart and Circulatory Physiology*, 262(6), pp. H1823-H1831.
181. Wang, E. and Zhao, M. (2010) 'Regulation of tissue repair and regeneration by electric fields', *Chinese Journal of Traumatology (English Edition)*, 13(1), pp. 55-61. doi: <http://dx.doi.org/10.3760/cma.j.issn.1008-1275.2010.01.011>.
182. Wang, E., Zhao, M., Forrester, J.V. and MCCaig, C.D. (2000) 'Re-orientation and Faster, Directed Migration of Lens Epithelial Cells in a Physiological Electric Field', *Experimental eye research*, 71(1), pp. 91-98. doi: 10.1006/exer.2000.0858.
183. Wang, J., Jin, X., Huang, Y., Ran, X., Luo, D., Yang, D., Jia, D., Zhang, K., Tong, J., Deng, X. and Wang, G. (2018) 'Endovascular stent-induced alterations in host artery mechanical environments and their roles in stent restenosis and late thrombosis', *Regenerative Biomaterials*, 5(3), pp. 177-187. doi: 10.1093/rb/rby006.
184. Watanabe, H., Morimoto, T., Shiomi, H., Natsuaki, M., Kawai, K., Kozuma, K., Igarashi, K., Kadota, K., Tanabe, K., Morino, Y., Hibi, K., Akasaka, T., Abe, M., Suwa, S., Muramatsu, T., Kobayashi, M., Dai, K., Nakao, K., Tarutani, Y., Fujii, K., Kimura, T., RESET and NEXT Investigators and the RESET and NEXT Investigators (2018) 'Impact of Angiographic Residual Stenosis on Clinical Outcomes After New-Generation Drug-Eluting

- Stents Implantation: Insights From a Pooled Analysis of the RESET and NEXT Trials', *Journal of the American Heart Association*, 7(13), pp. e008718. doi: 10.1161/JAHA.118.008718.
185. Weid, P.Y.v.d. and Helden, D.F.V. (1997) 'Functional electrical properties of the endothelium in lymphatic vessels of the guinea-pig mesentery', *The Journal of physiology*, 504(Pt 2), pp. 439-451. doi: 10.1111/j.1469-7793.1997.439be.x.
186. Weiner, B., B., Tscharnuter, W., W. and Fairhurst, D. (1993) *Zeta potential: A new Approach.* , Winnipeg, Manitoba, Canada. 8-12 September.
187. Werkum, J.W.v., Heestermans, A.A., Zomer, A.C., Kelder, J.C., Suttorp, M.J., Rensing, B.J., Koolen, J.J., Brueren, B.R., Dambrink, J.H., Hautvast, R.W., Verheugt, F.W.A. and Berg, J.M.t. (2009) 'Predictors of coronary stent thrombosis: the Dutch Stent Thrombosis Registry', *Journal of the American College of Cardiology*, 53(16), pp. 1399-1409. doi: 10.1016/j.jacc.2008.12.055.
188. Wilson, W.W., Wade, M.M., Holman, S.C. and Champlin, F.R. (2001) 'Status of methods for assessing bacterial cell surface charge properties based on zeta potential measurements', *Journal of Microbiological Methods*, 43(3), pp. 153-164. doi: 10.1016/S0167-7012(00)00224-4.
189. Woodrough, R.E., Canti, G. and Watson, B.W. (1975) 'Electrical potential difference between basal cell carcinoma, benign inflammatory lesions and normal tissue', *The British journal of dermatology*, 92(1), pp. 1.
190. World Health Organization (2018) *Cardiovascular diseases (CVDs)*. Available at: [http://www.who.int/news-room/fact-sheets/detail/cardiovascular-diseases-\(cvds\)](http://www.who.int/news-room/fact-sheets/detail/cardiovascular-diseases-(cvds)) (Accessed: 2017).
191. World Health Organization (2007) *The top ten causes of death*. World Health Organization. Available at: <http://www.who.int/> (Accessed: 2017).
192. Yamamoto, Y., Klemm, M.F., Edwards, F.R. and Suzuki, H. (2001) 'Intercellular electrical communication among smooth muscle and endothelial cells in guinea-pig mesenteric arterioles', *The Journal of physiology*, 535(1), pp. 181-195. doi: 10.1111/j.1469-7793.2001.00181.x.

193. Yang, M. and Brackenbury, W.J. (2013) 'Membrane potential and cancer progression', *Frontiers in Physiology*, 4, pp. 185. doi: 10.3389/fphys.2013.00185.
194. Yao, L., Shanley, L., McCaig, C. and Zhao, M. (2008) 'Small applied electric fields guide migration of hippocampal neurons', *Journal of cellular physiology*, 216(2), pp. 527-535. doi: 10.1002/jcp.21431.
195. Yeh, E., Pinsky, B.A., Banaei, N. and Baron, E.J. (2009) 'Hair sheep blood, citrated or defibrinated, fulfills all requirements of blood agar for diagnostic microbiology laboratory tests', *PLoS ONE*, 4(7), pp. e6141. doi: 10.1371/journal.pone.0006141.
196. Ypey, D.L. and DeFelice, L.J. (2007) 'The patch-clamp technique explained and exercised with use of simple electrical equivalent circuits', in DeFelice, L.J. (ed.) *Electrical properties of cells* USA: Plenum Press Book, pp. 3-6.
197. Zhao, M., Agius-Fernandez, A., Forrester, J. and McCaig, C. (1996) 'Directed migration of corneal epithelial sheets in physiological electric fields', *Investigative ophthalmology & visual science*, 37(13), pp. 2548-2558.
198. Zhao, M., Bai, H., Wang, E., Forrester, J.V. and McCaig, C.D. (2004) 'Electrical stimulation directly induces pre-angiogenic responses in vascular endothelial cells by signaling through VEGF receptors', *Journal of cell science*, 117(3), pp. 397-405. doi: 10.1242/jcs.00868.
199. Zhao, M., Forrester, J.V. and McCaig, C.D. (1999) 'A Small, Physiological Electric Field Orients Cell Division', *Proceedings of the National Academy of Sciences of the United States of America*, 96(9), pp. 4942-4946. doi: 10.1073/pnas.96.9.4942.
200. Zhao, Z., Watt, C., Karystinou, A., Roelofs, A.J., McCaig, C.D., Gibson, I.R. and De Bari, C. (2011) 'Directed migration of human bone marrow mesenchymal stem cells in a physiological direct current electric field', *European Cells and Materials*, 22, pp. 344-358.
201. Zhao, Z., Zhao, M., Qin, L., Reid, B., Pu, J. and Hara, T. (2012) 'Directing migration of endothelial progenitor cells with applied DC electric fields', *Stem Cell Research*, 8(1), pp. 38-48. doi: 10.1016/j.scr.2011.08.001.

Appendix A: Electrochemical Measurement Data

Deionized water

Table 1.A

Time (Min)	1 st (mV)	2 nd (mV)	3 rd (mV)	4 th (mV)	5 th (mV)
0	-210	-307.5	-295.6	-253.1	-259.6
0.3	-207	-303.9	-289.4	-249.7	-259.2
1	-199	-298	-289.6	-243.5	-252.3
1.3	-193.5	-291.9	-285.8	-238.3	-252.1
2	-190	-288.4	-283.6	-231.5	-250.1
2.3	-190	-279.9	-279.7	-228.6	-248.8
3	-180.6	-273	-275.7	-225	-247.2
3.3	-177.3	-268.6	-272	-221.1	-244.2
4	-175.9	-265.2	-269	-217.8	-241.5
4.3	-172.4	-263.2	-267.2	-214.3	-239.6
5	-171.7	-260.8	-264.8	-211.1	-237.9
5.3	-170.6	-258.7	-262.6	-208.2	-236
6	-170	-257.7	-261.4	-205.7	-234.3
6.3	-166.4	-255.8	-260.1	-203.5	-232.8
7	-160	-254.3	-258.9	-201.2	-232.2
7.3	-162.3	-252.6	-257.7	-198.9	-232.5
8	-160	-251	-256.8	-196.9	-232.1

Distilled water

Table 2.A

Time (Min)	1 st (mV)	2 nd (mV)	3 rd (mV)	4 th (mV)	5 th (mV)
0	-70	-317.4	-276.1	-228.3	-177
0.3	-59.6	-311.1	-274.4	-217.6	-166.3
1	-55.8	-304.8	-264.1	-211	-160.7
1.3	-51.4	-302.6	-263.2	-193.5	-157
2	-49.8	-297.2	-260	-189.7	-154.3
2.3	-46.6	-291	-255.7	-187.5	-151.8
3	-40.2	-285.2	-251.4	-184.9	-149.3
3.3	-37.8	-281.8	-246.8	-182.6	-150.8
4	-33.7	-278.6	-243.1	-178.8	-142
4.3	-30	-276.1	-239.4	-177.5	-139.7
5	-28.1	-273.8	-235.9	-173.9	-137.8
5.3	-26.79	-271.6	-233	-169.9	-137.1
6	-21.1	-269.6	-230.7	-166.7	-135.7
6.3	-14.2	-267.8	-224.4	-162.8	-134.3

7	-10.3	-265.7	-222.8	-160.9	-133
7.3	-8.4	-263.8	-221.4	-157.3	-132
8	-4.6	-262.3	-219.6	-152.1	-131.4

Tap water

Table 3.A

Time (Min)	1 st (mV)	2 nd (mV)	3 rd (mV)	4 th (mV)	5 th (mV)
0	-60	-161.2	-210.8	-276.7	-310.6
0.3	-80	-157.3	-207.6	-265.4	-313.6
1	-80	-150.1	-204.1	-247	-315.1
1.3	-80	-146.8	-201.6	-240.5	-315.6
2	-70	-144.1	-203.6	-234.8	-315.4
2.3	-70	-142.3	-209.9	-238.9	-314.9
3	-60	-139.1	-221.6	-240.7	-314.2
3.3	-60	-134.4	-215.2	-242.7	-313.1
4	-60	-133.3	-214.9	-244.4	-311.7
4.3	-60	-131.9	-215.4	-245	-309.8
5	-60	-129.2	-216.1	-242.3	-307.2
5.3	-60	-127.4	-216.6	-238.8	-303.9
6	-60	-125.3	-217	-233.7	-300.5
6.3	-60	-123.5	-217.4	-229.2	-297.7
7	-60	-121.8	-217.9	-225.5	-294.7
7.3	-60	-120	-218.3	-221.8	-299.7
8	-60	-118.1	-218.9	-218.7	-289.7

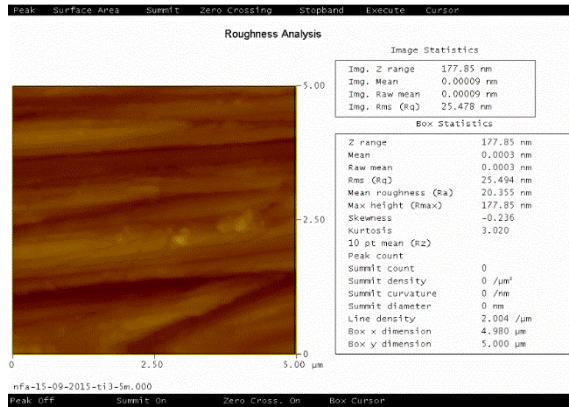
0.9% saline

Table 4.A

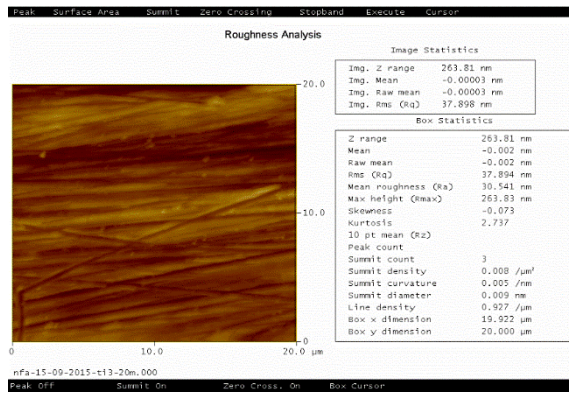
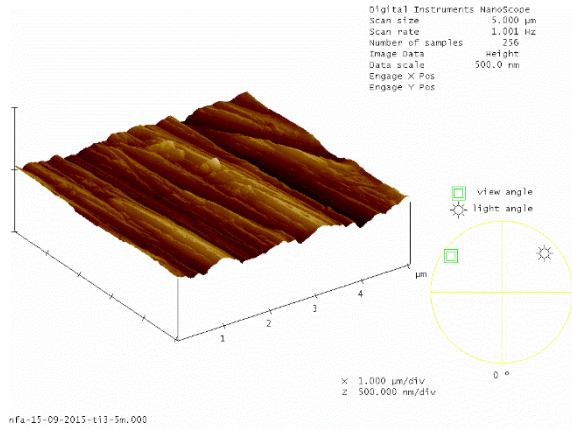
Time (Min)	1 st (mV)	2 nd (mV)	3 rd (mV)	4 th (mV)	5 th (mV)
0	-69.24	-199.2	-150.2	-117.9	-204.8
0.3	-53.27	-177.7	-160.7	-119.2	-194.6
1	-80.1	-186.5	-142.3	-112.1	-180.6
1.3	-63.71	-176	-136.6	-120.2	-197.5
2	-73.12	-160.1	-150.8	-113.2	-190.5
2.3	-60.11	-157.9	-168	-136	-167
3	-64.7	-153.6	-163	-122.1	-180.7
3.3	-48.3	-154	-147	-120.7	-198.7
4	-37.36	-177.5	-144.2	-125.8	-189.3
4.3	-40.55	-172.9	-136.3	-127.8	-184.9
5	-51.08	-185.9	-172	-121.1	-184.3
5.3	-48.69	-187.2	-158.7	-115.6	-163.3
6	-42.41	-164.3	-141.5	-116.7	-179.9
6.3	-57.8	-168.9	-139	-117	-182.5

7	-48.01	-171.7	-137.7	-115.1	-182.3
7.3	-42.5	-172.9	-135.3	-117.5	-174.5
8	-38.7	-171.5	-130.9	-113	-170.9

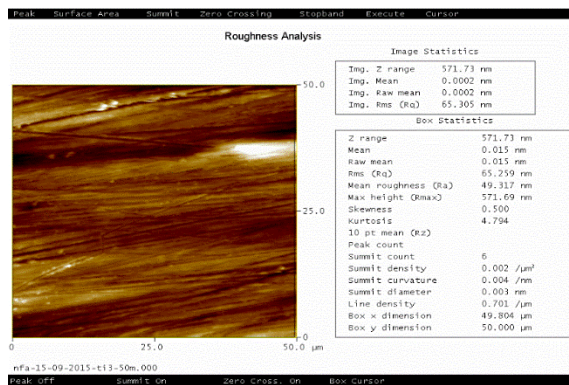
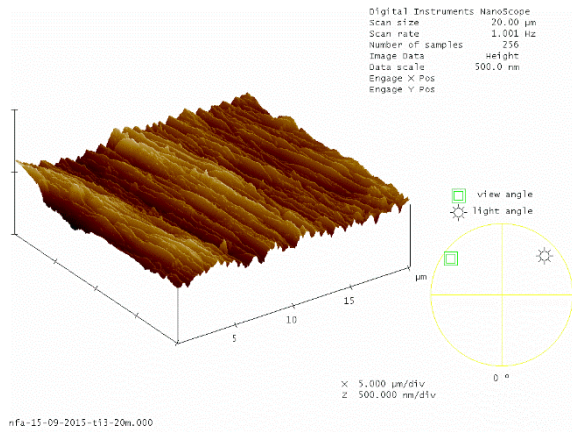
Appendix B: AFM Data



5 μm



20 μm



50 μm

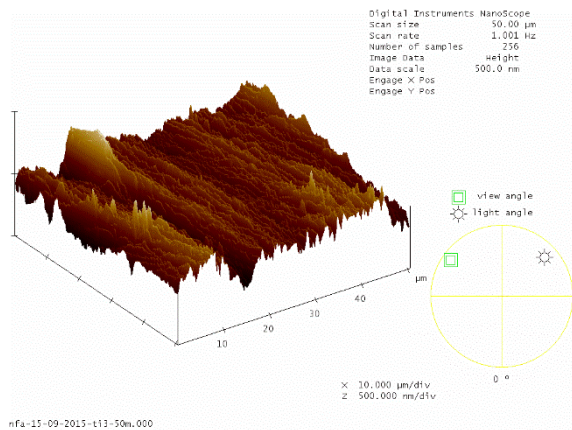
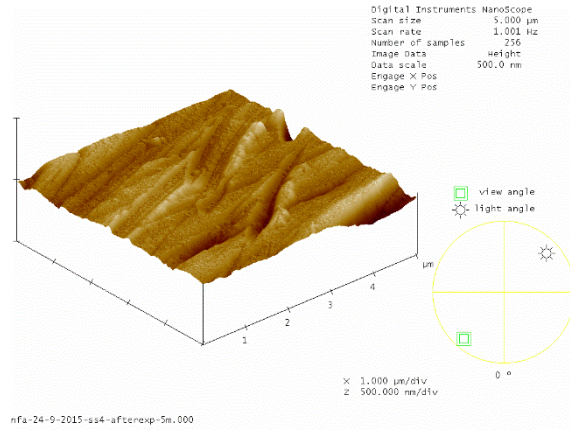
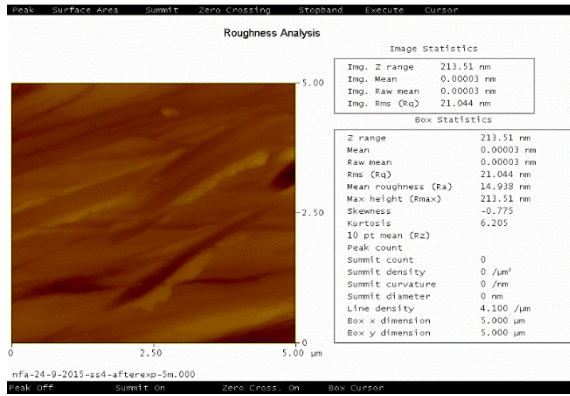
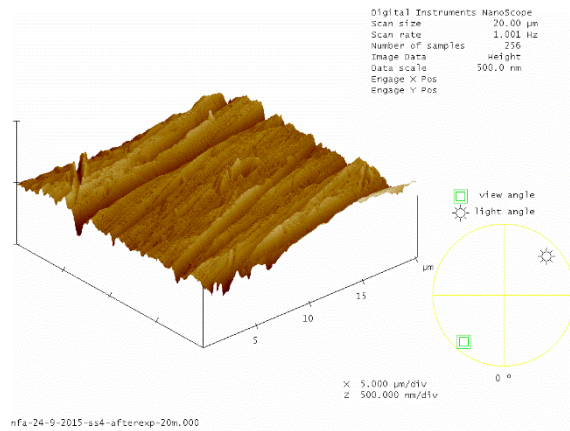
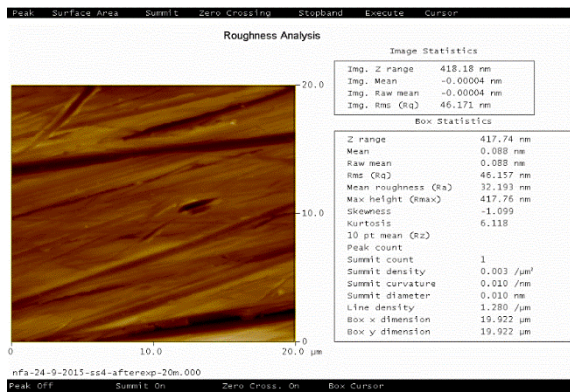


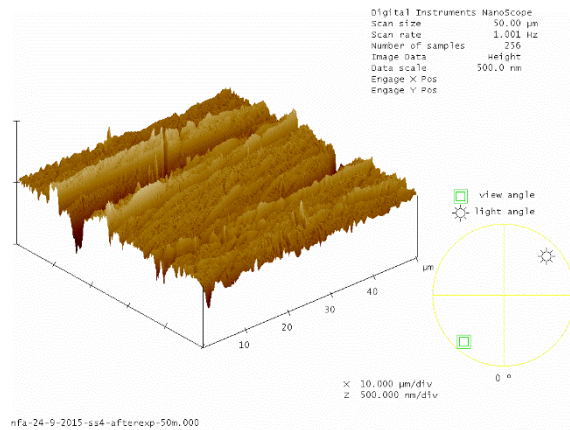
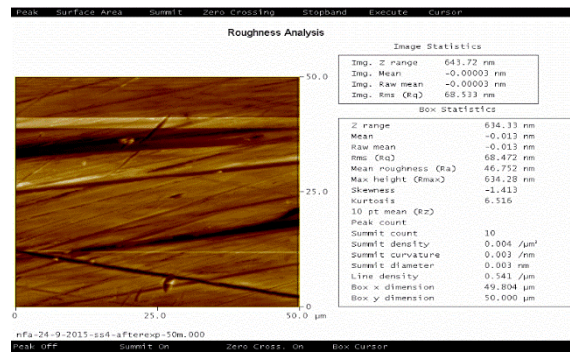
Figure 1.B: After polishing (Stainless steel; controlled sample)



5 μm

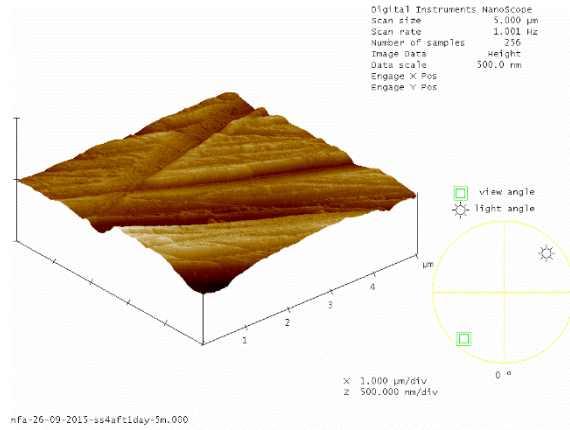
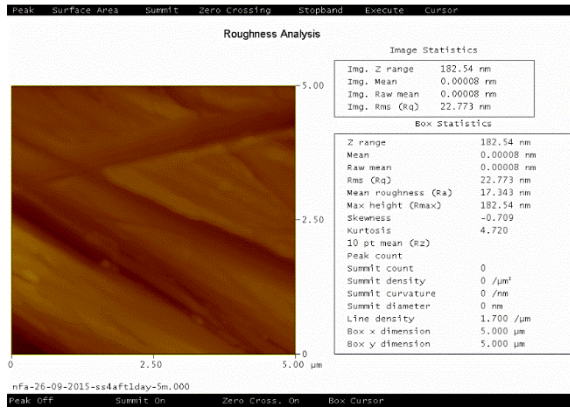


20 μm

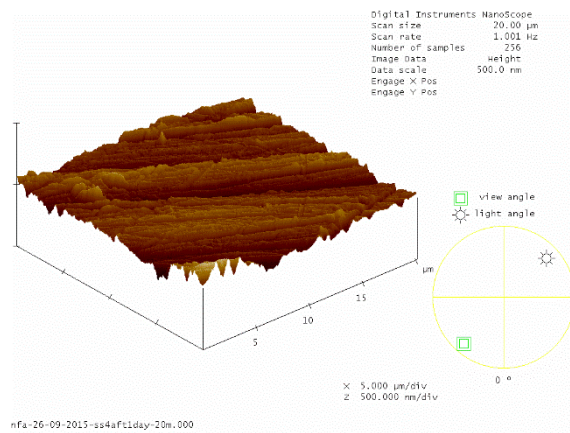
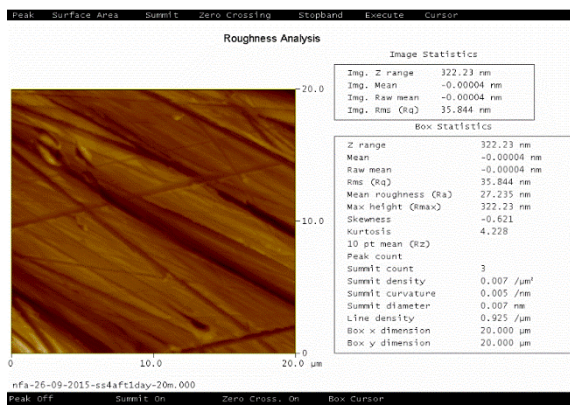


50 μm

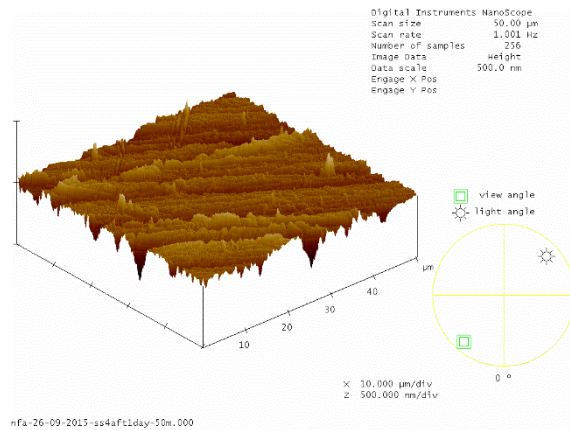
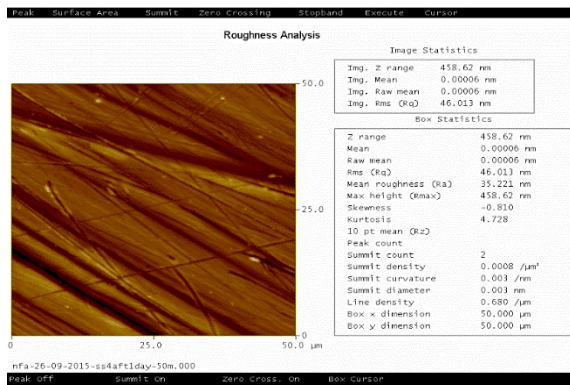
Figure 2.B: After the experiment (Stainless steel; controlled sample)



5 μm

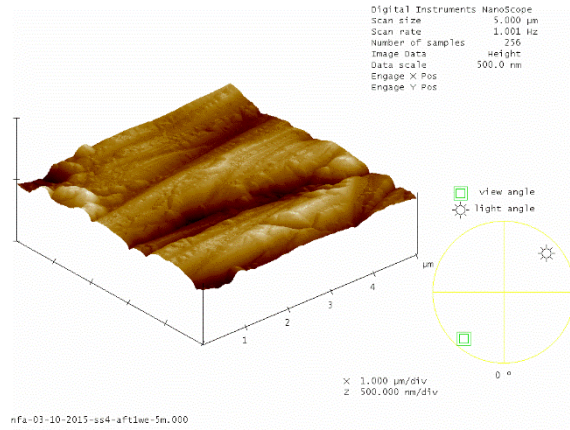
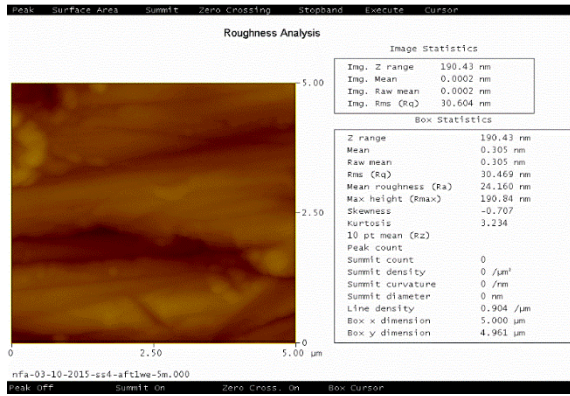


20 μm

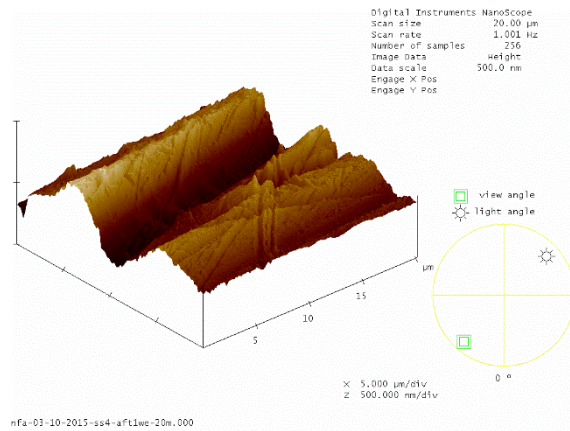
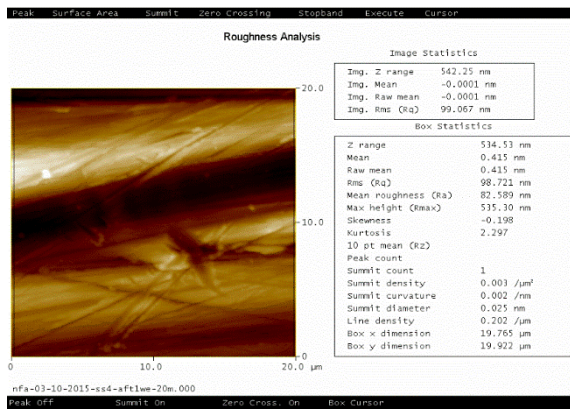


50 μm

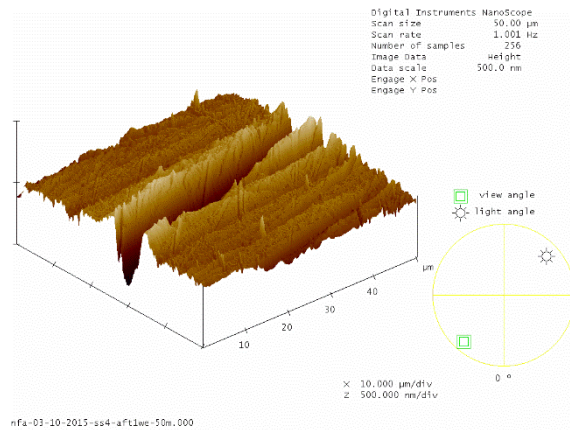
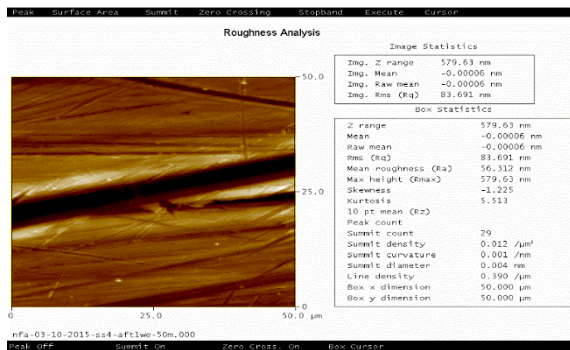
Figure 3.B: 1 day after the experiment (Stainless steel; controlled sample)



5 μm

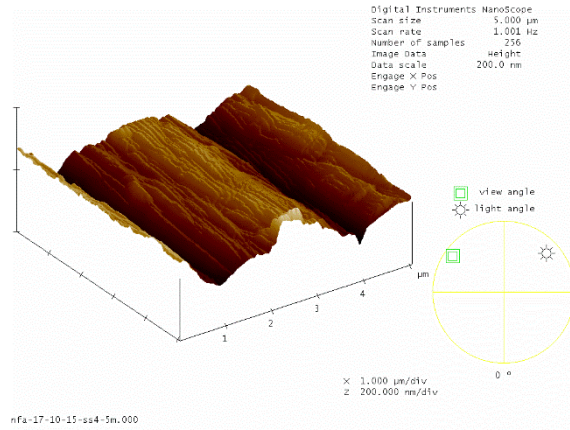
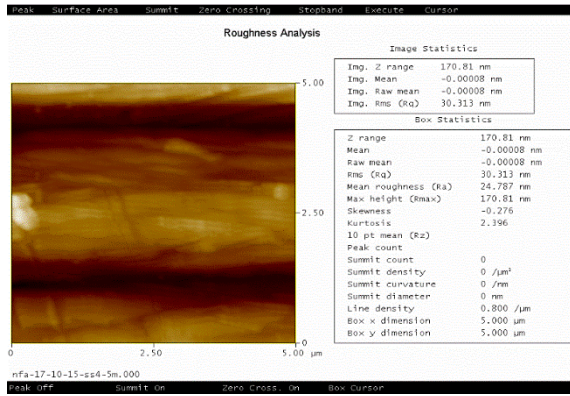


20 μm

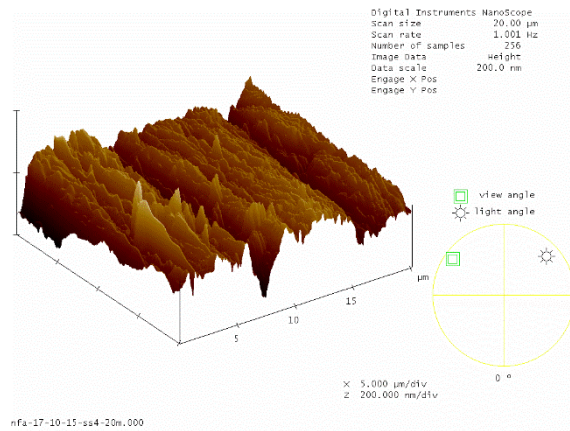
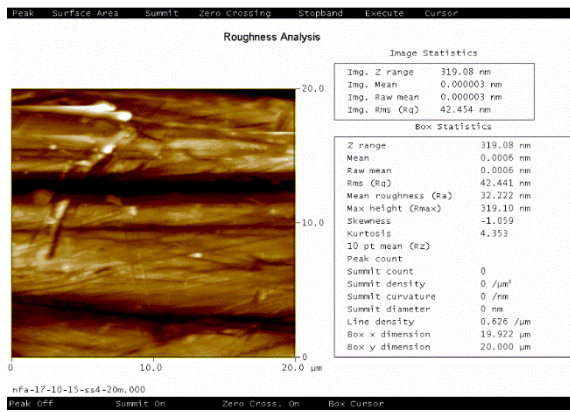


50 μm

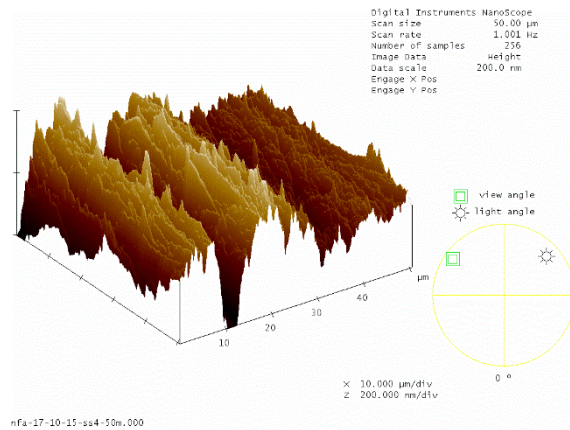
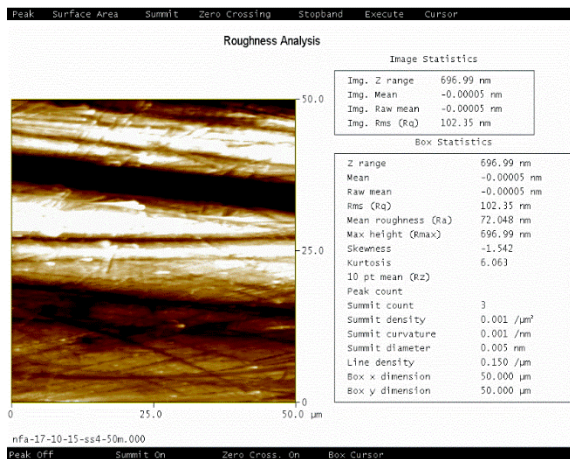
Figure 4.B: 1 week after the experiment (Stainless steel; controlled sample)



5 μm

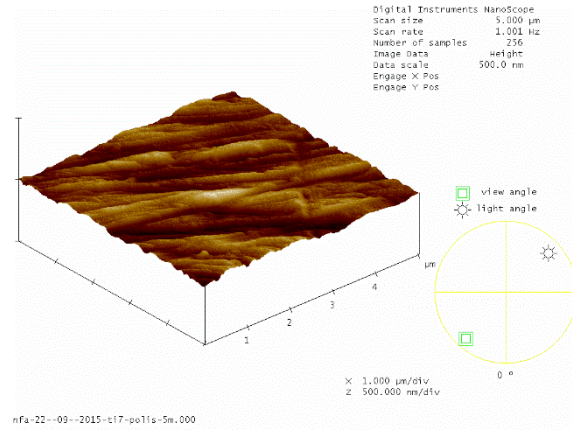
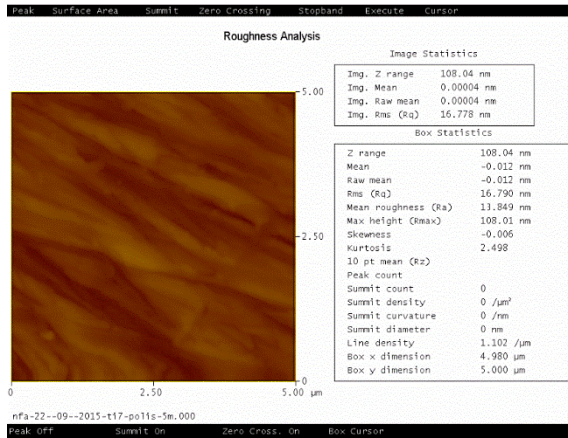


20 μm

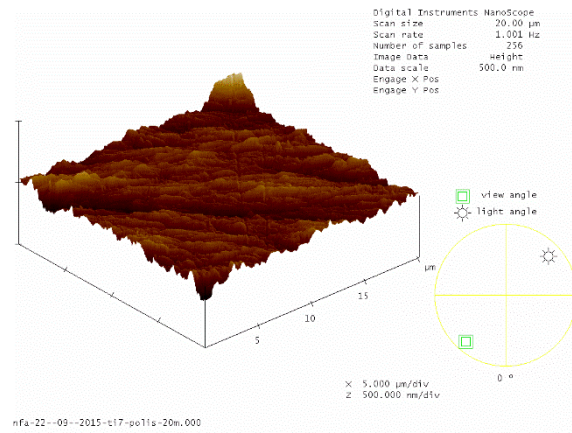
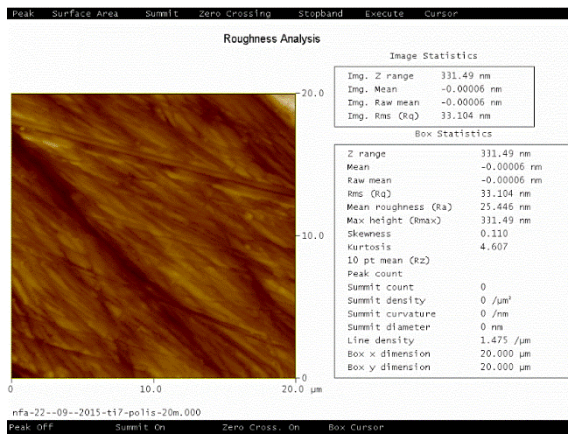


50 μm

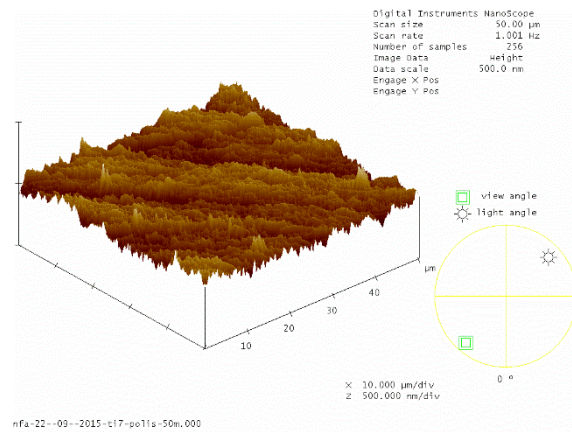
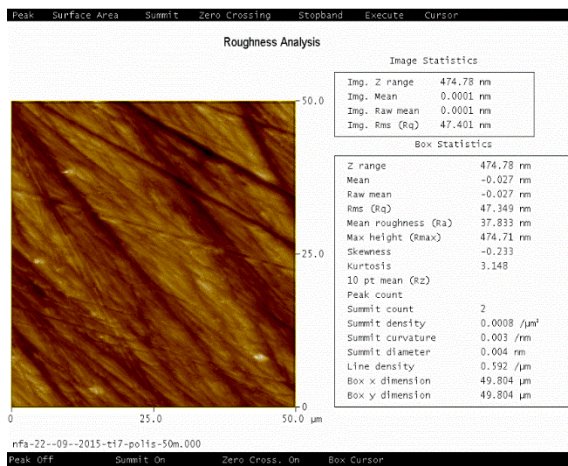
Figure 5.B: 2 weeks after the experiment (Stainless steel; controlled sample)



5 μm

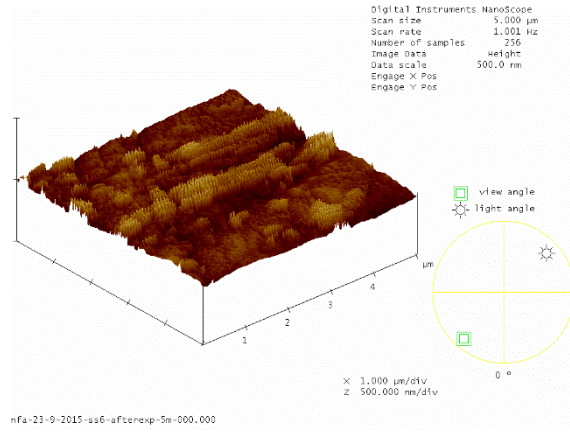
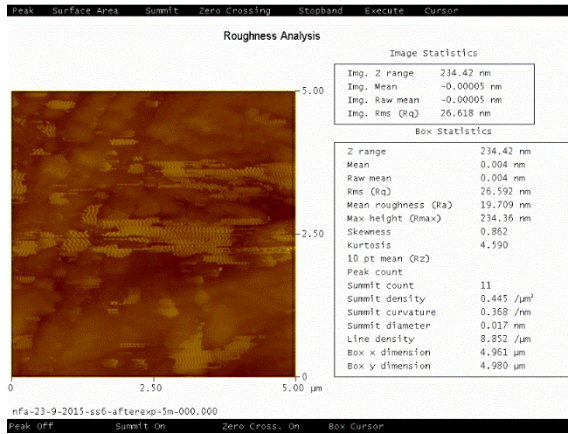


20 μm

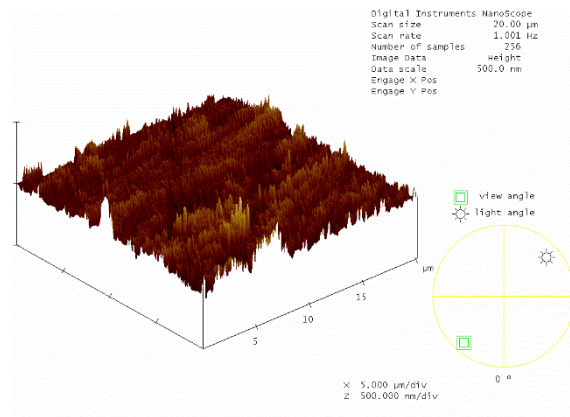
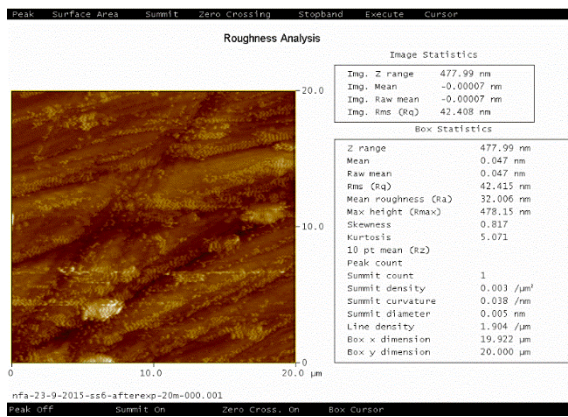


50 μm

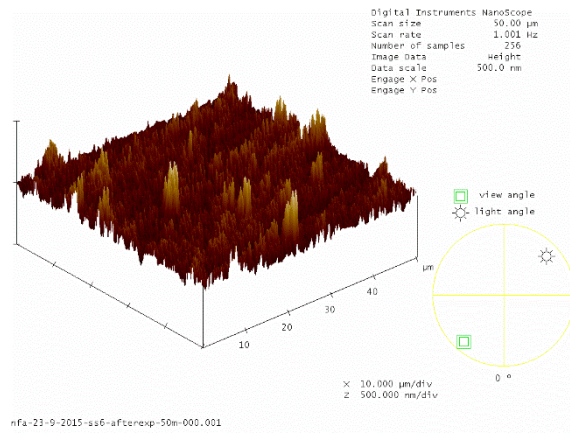
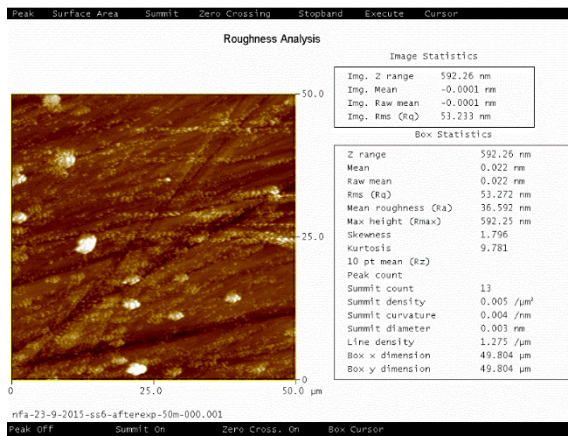
Figure 6.B: After polishing (Stainless steel; distilled water sample)



5 μm

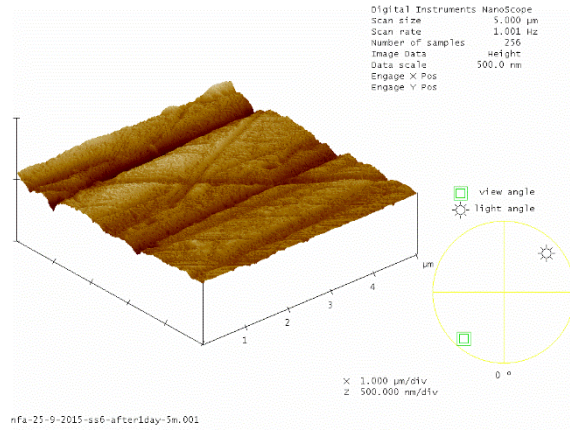
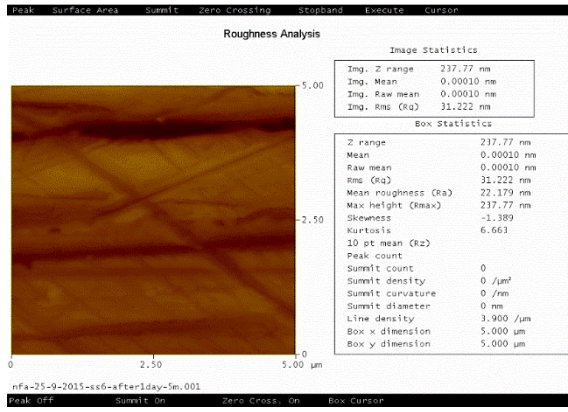


20 μm

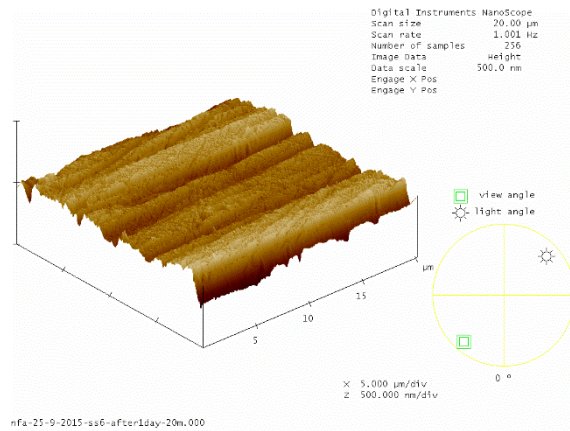
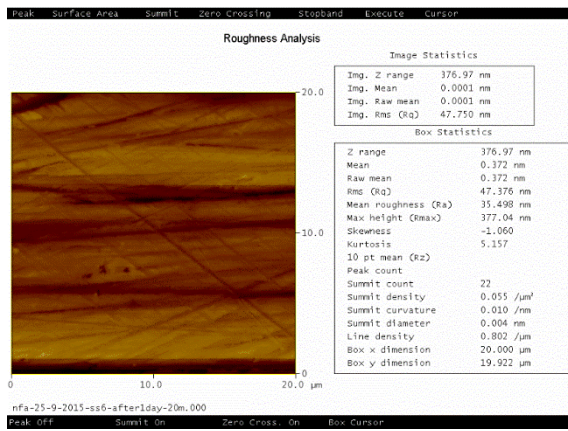


50 μm

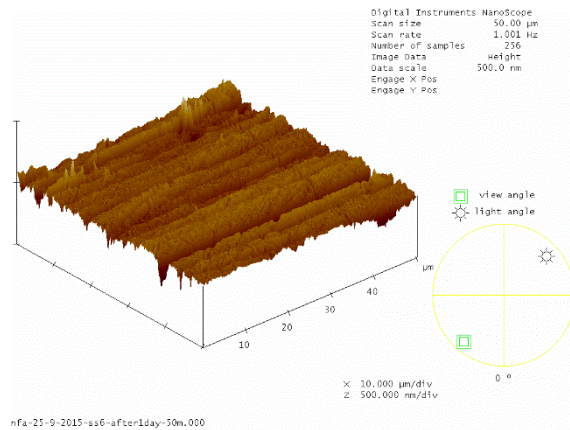
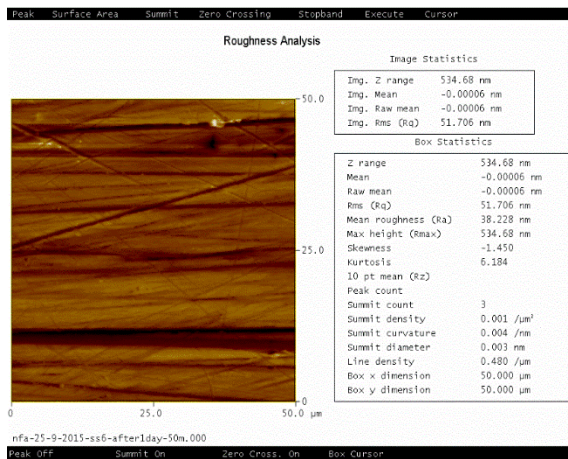
Figure 7.B: After experiment (Stainless steel; distilled water sample)



5 µm

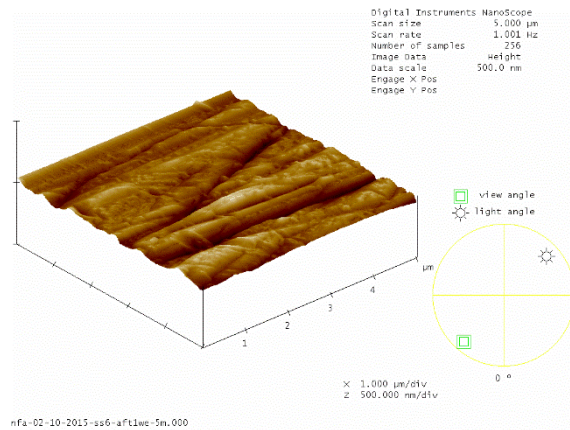
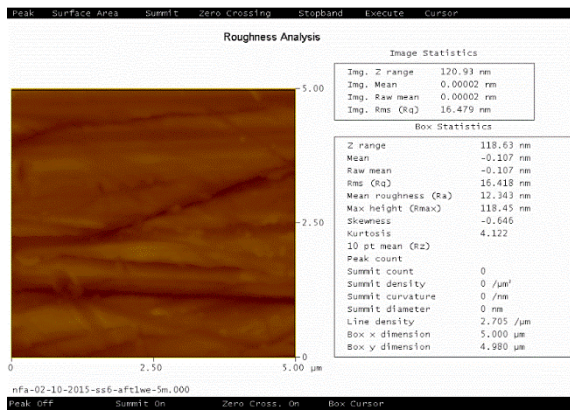


20 µm

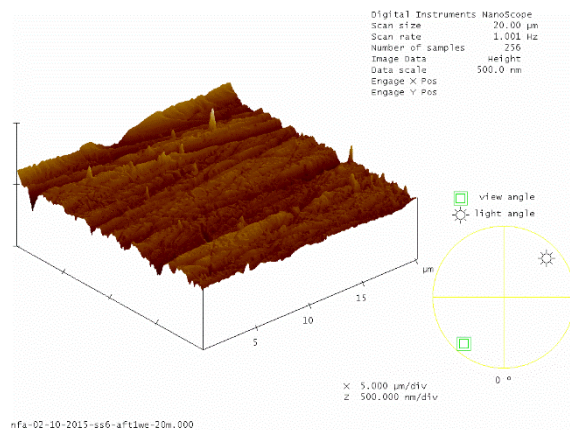
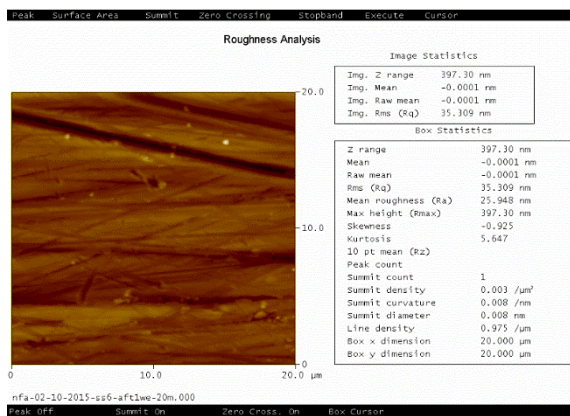


50 µm

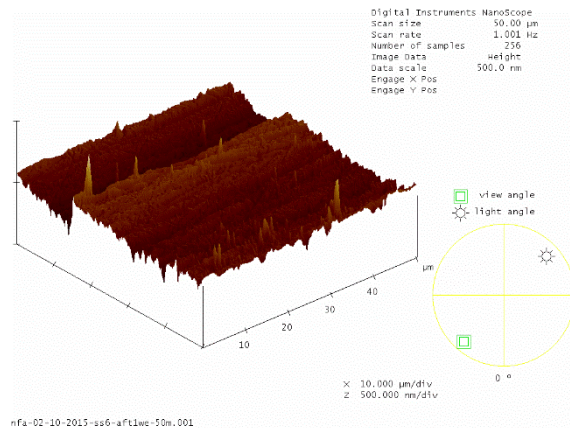
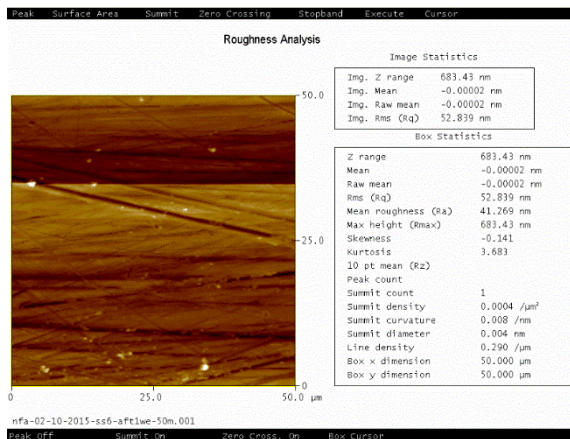
Figure 8.B: 1 day after the experiment (Stainless steel; distilled water sample)



5 μm

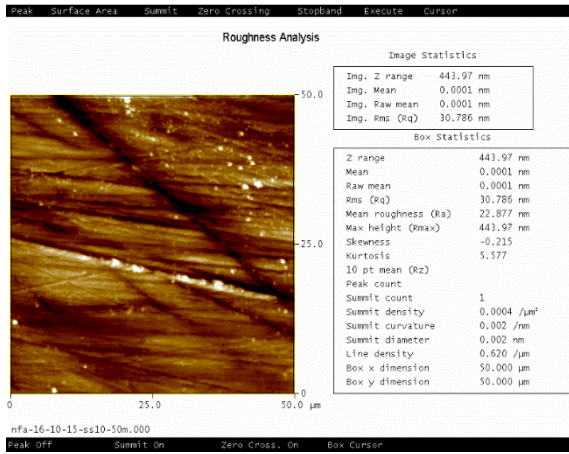


20 μm

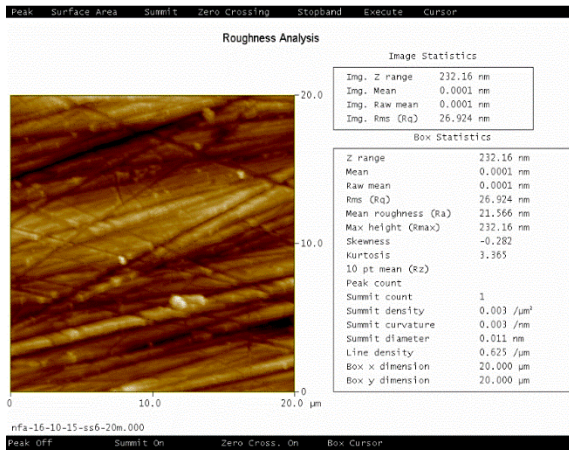
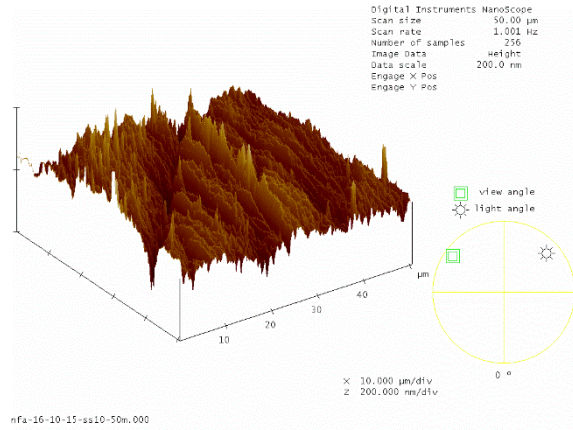


50 μm

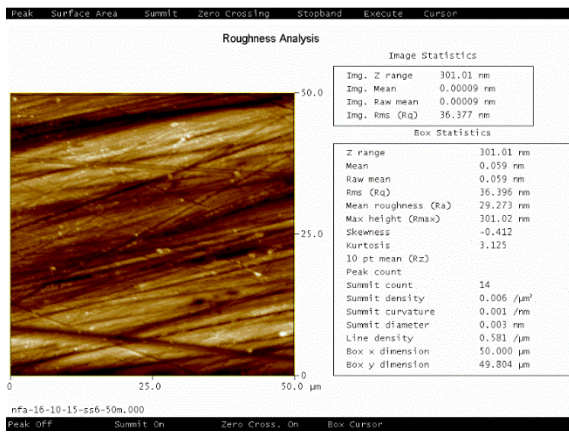
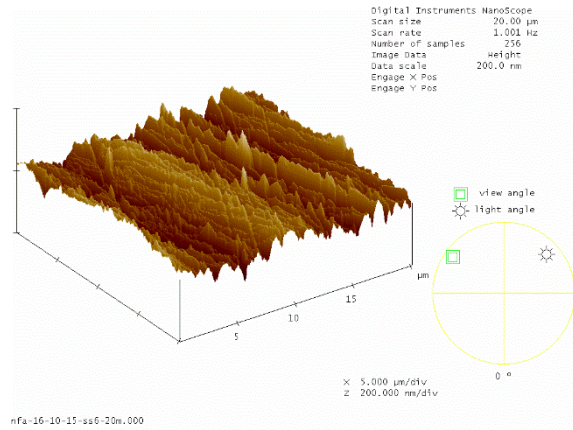
Figure 9.B: 1 week after the experiment (Stainless steel; distilled water sample)



5 μm



20 μm



50 μm

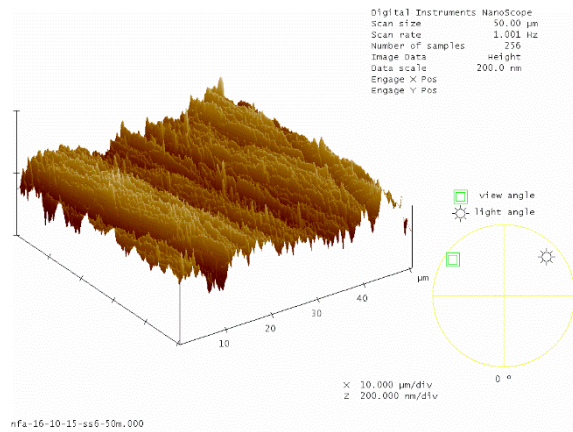
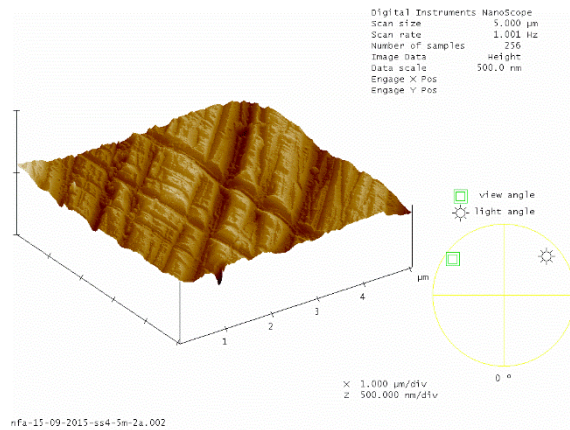
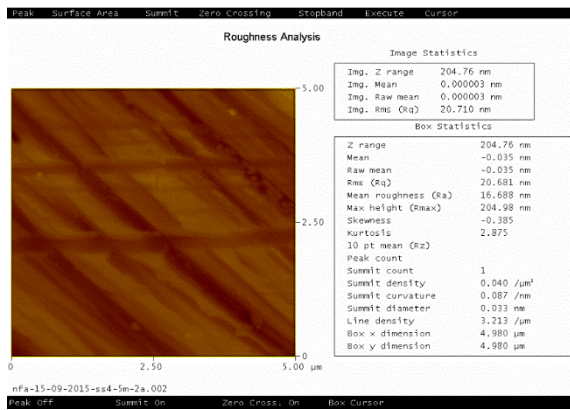
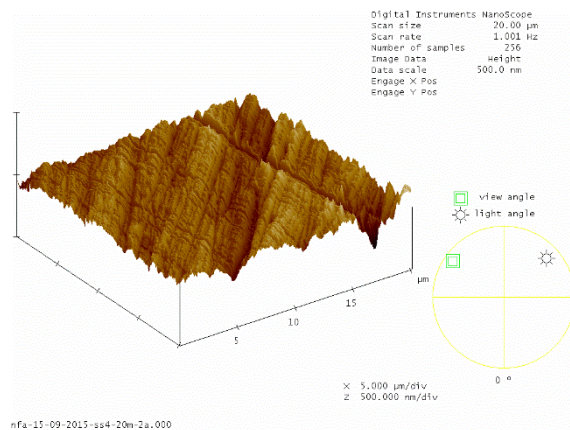
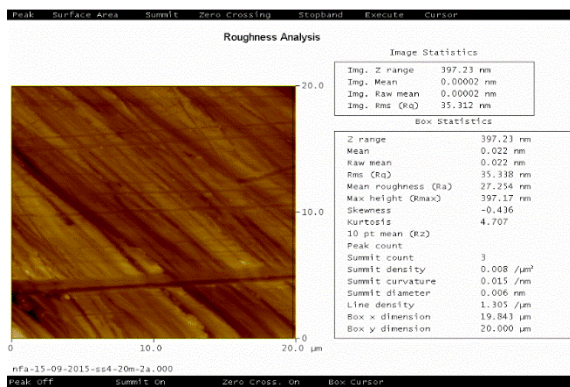


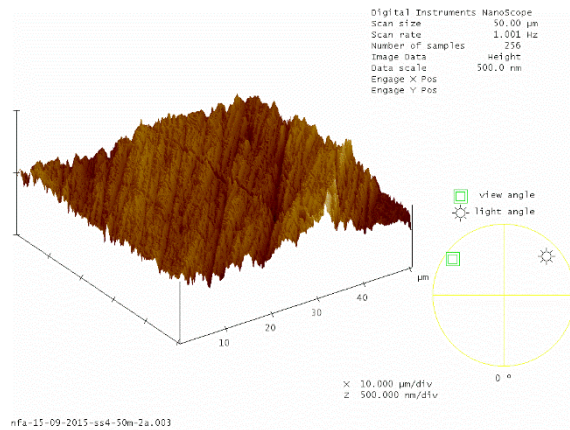
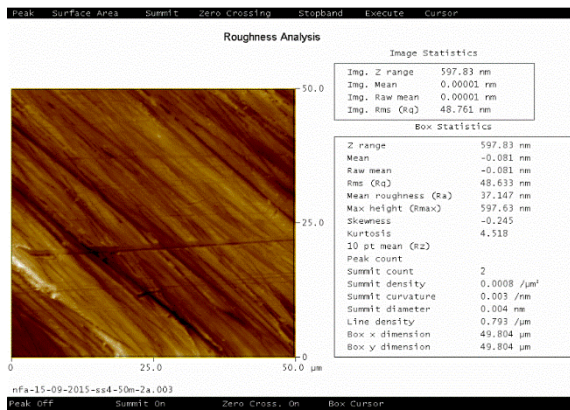
Figure 10.B: 2 weeks after the experiment (Stainless steel; distilled water sample)



5 μm

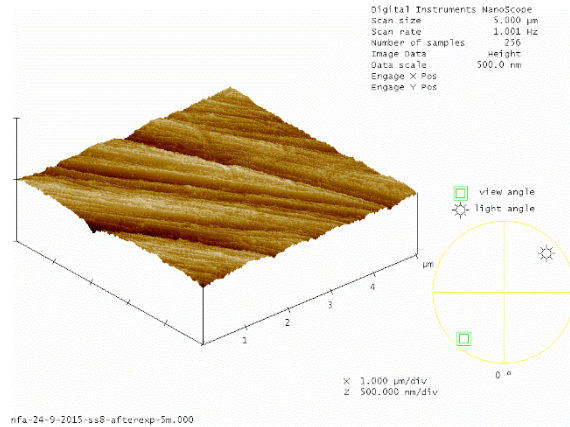
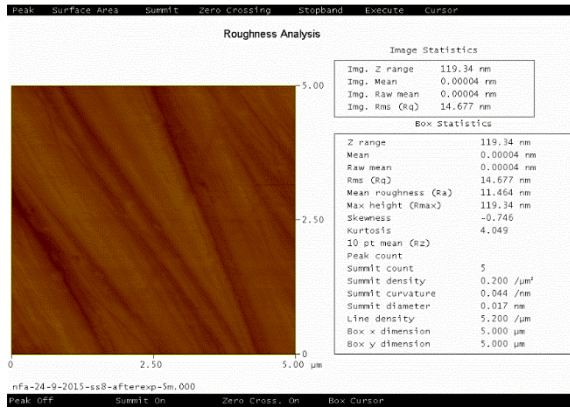


20 μm

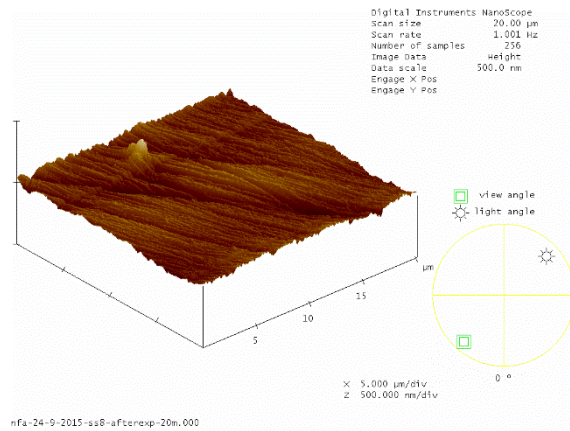
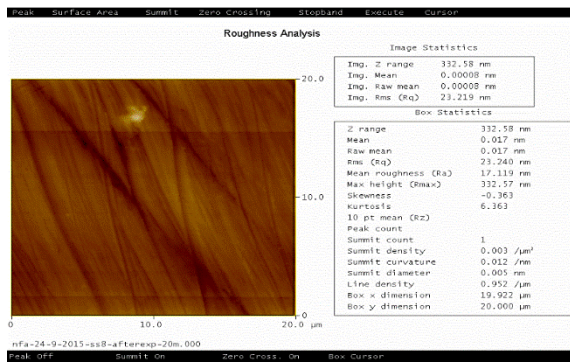


50 μm

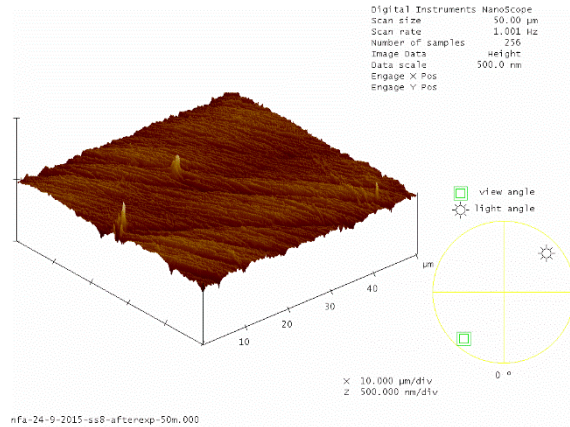
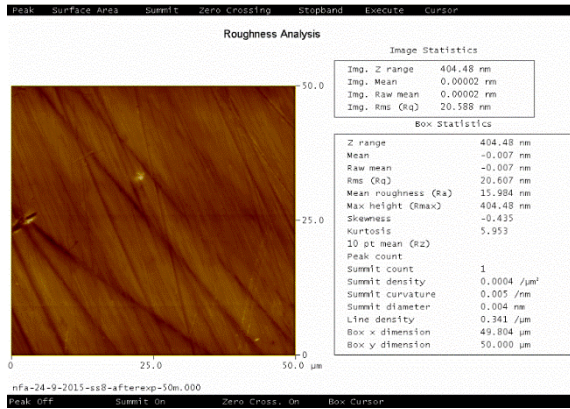
Figure 11.B: After polishing (Stainless steel; deionized water sample)



5 µm

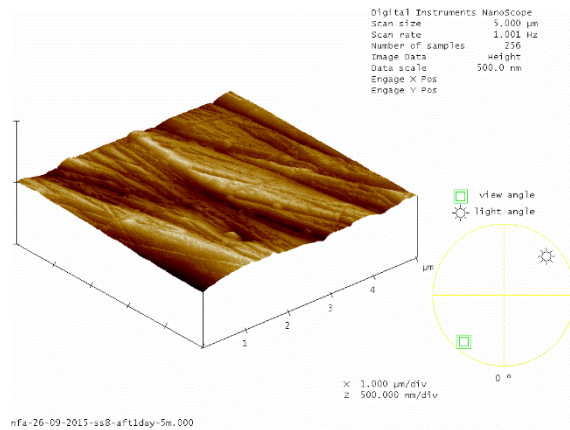
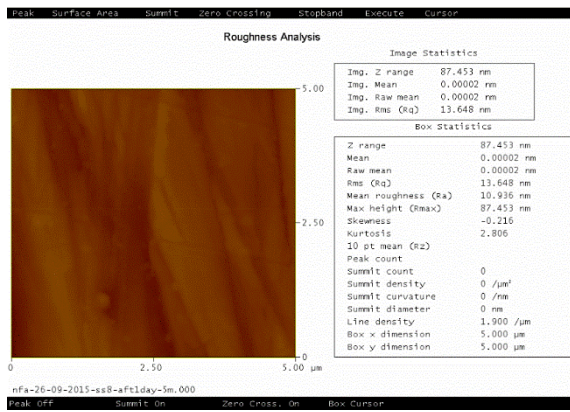


20 µm

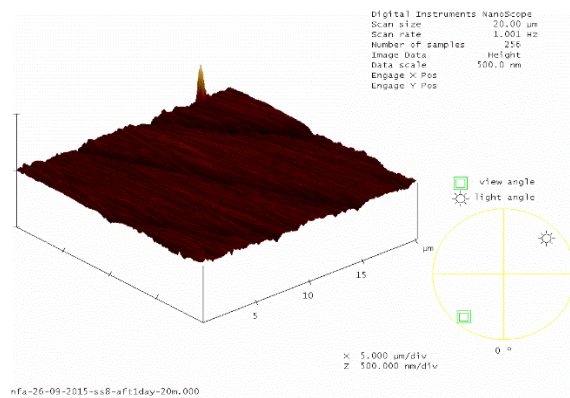
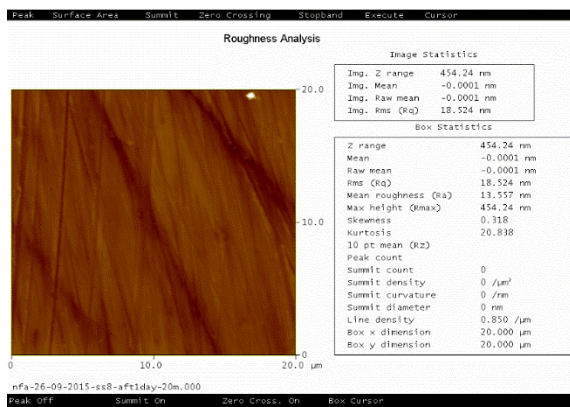


50 µm

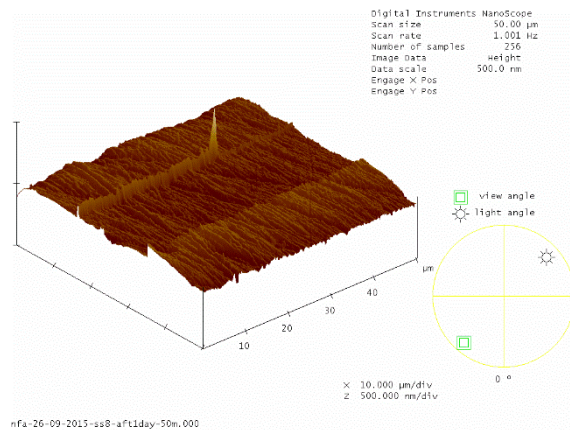
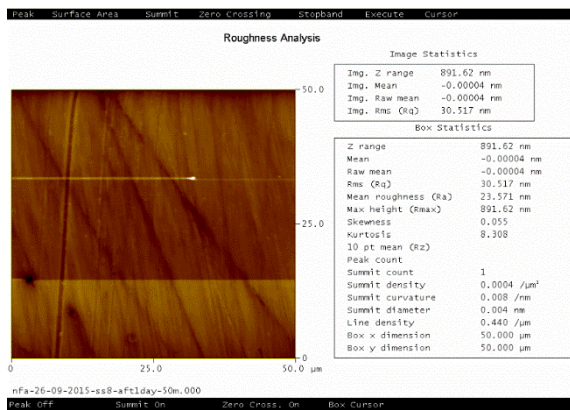
Figure 12.B: After the experiment (Stainless steel; deionized water sample)



5 μm

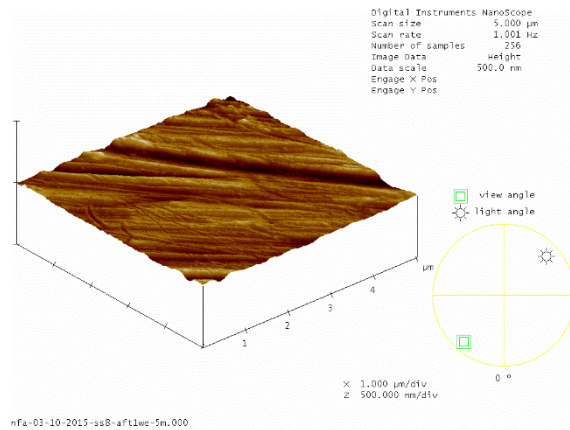
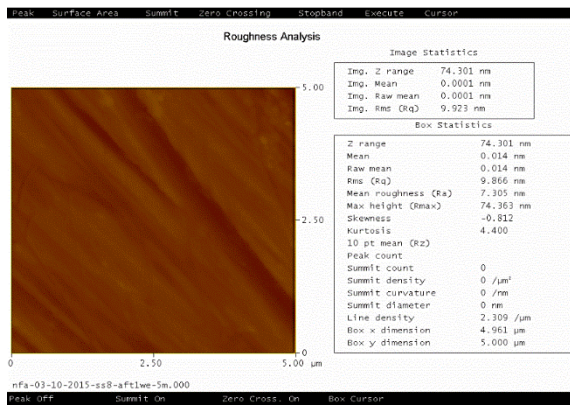


20 μm

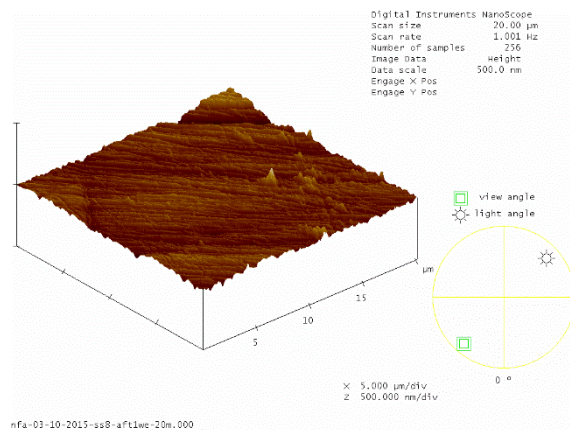
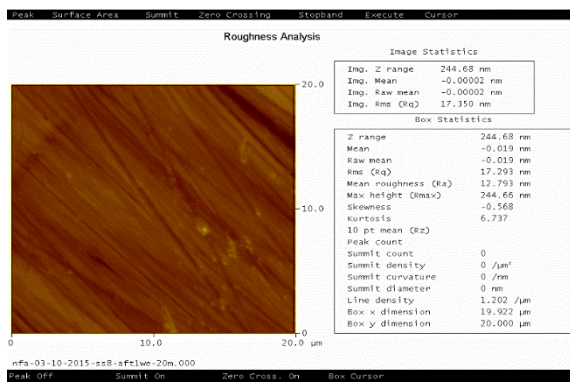


50 μm

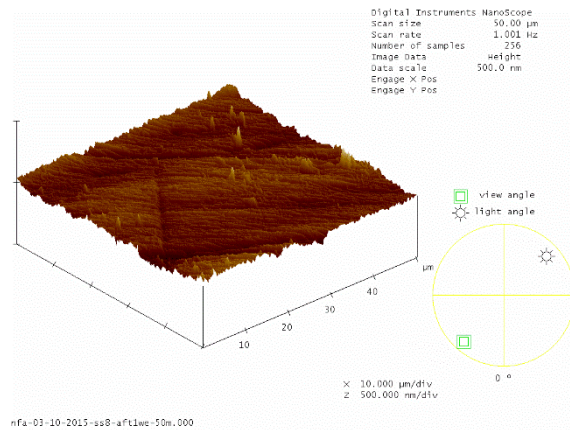
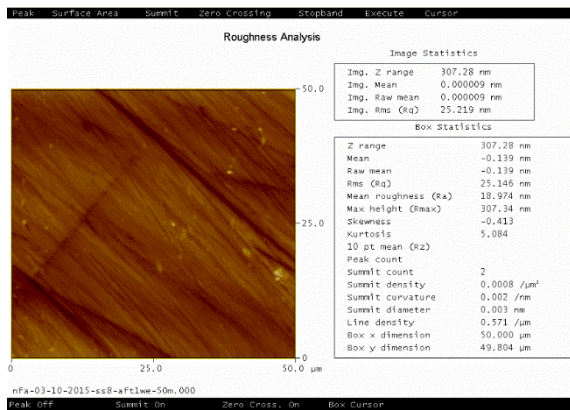
Figure 13.B: 1 day after the experiment (Stainless steel; deionized water sample)



5 μm

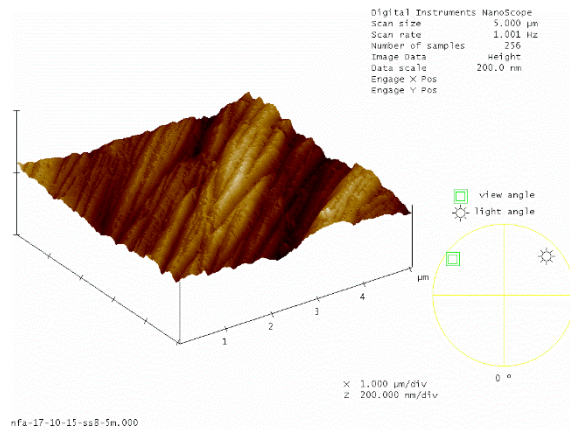
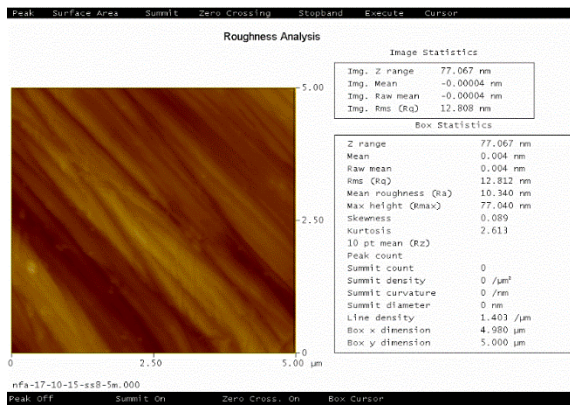


20 μm

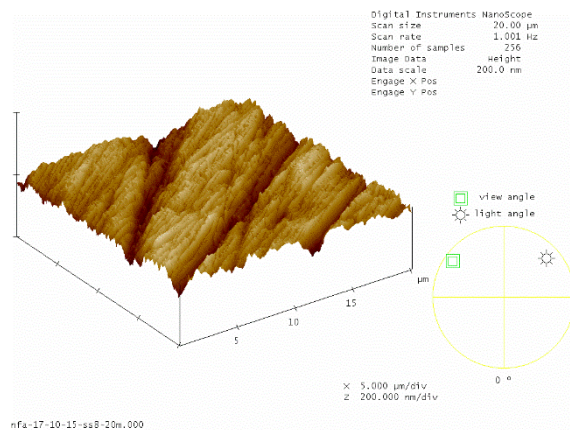
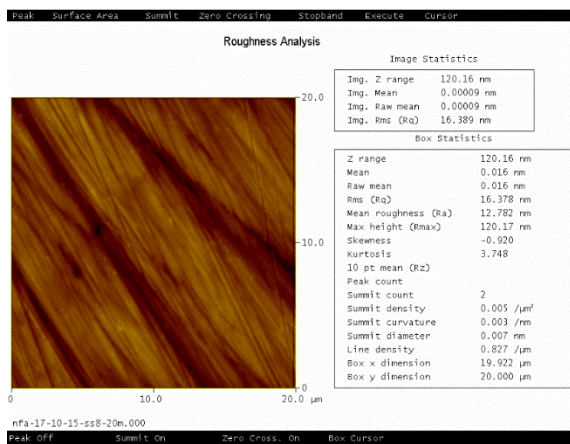


50 μm

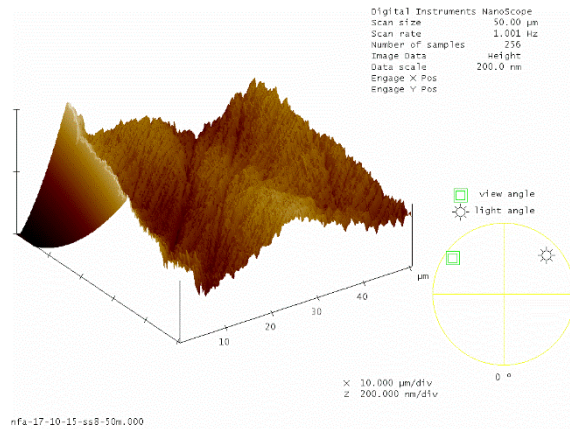
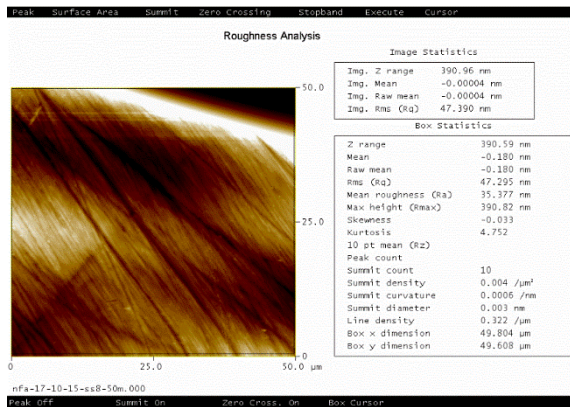
Figure 14.B: 1 week after the experiment (Stainless steel; deionized water sample)



5 μm

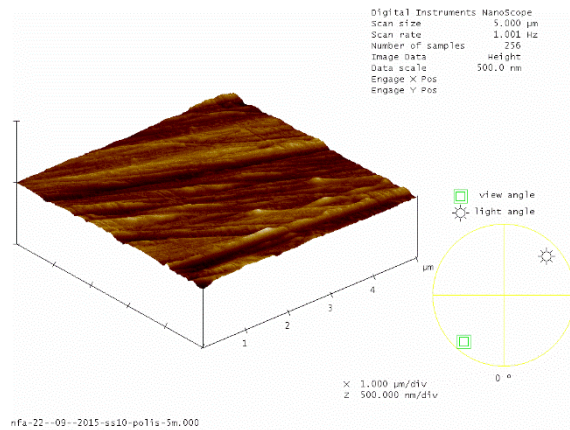
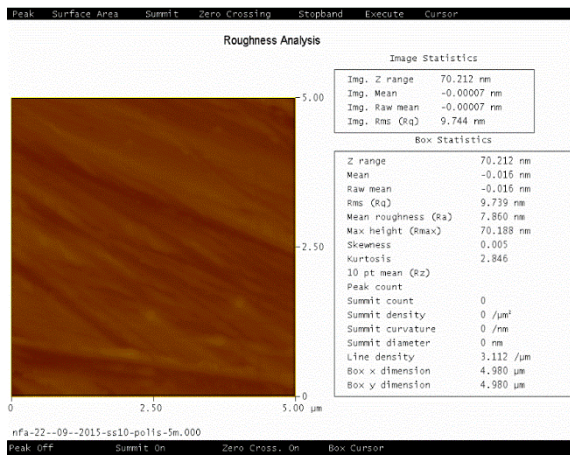


20 μm

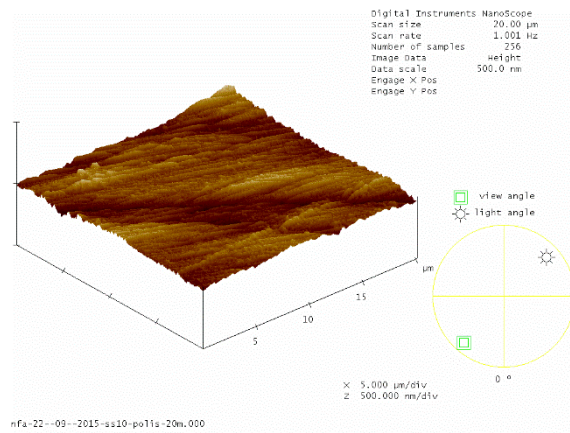
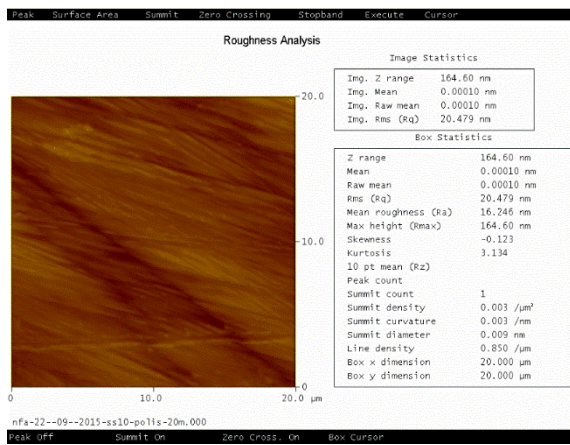


50 μm

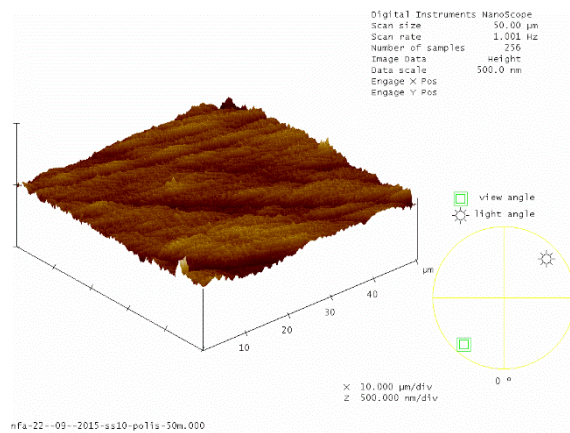
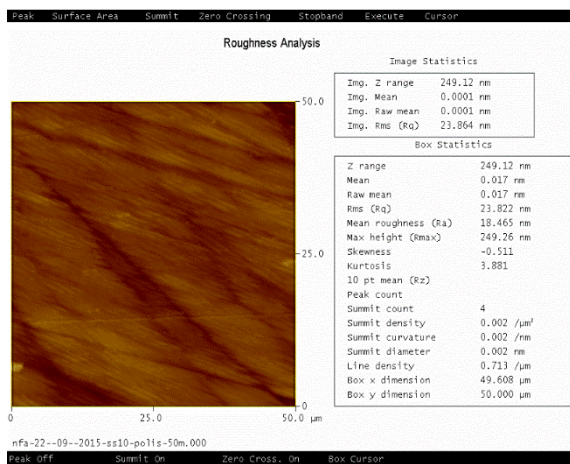
Figure 15.B: 2 weeks after the experiment (Stainless steel; deionized water sample)



5 μm

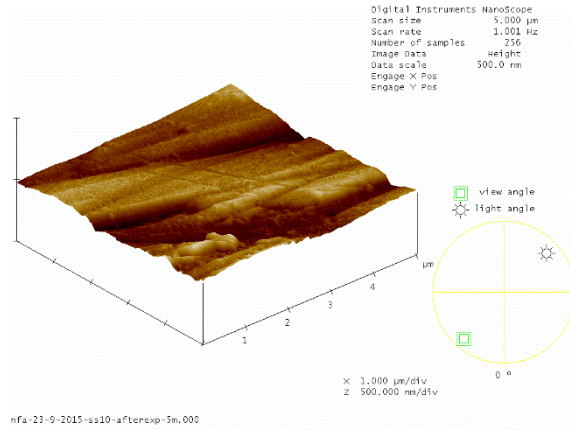
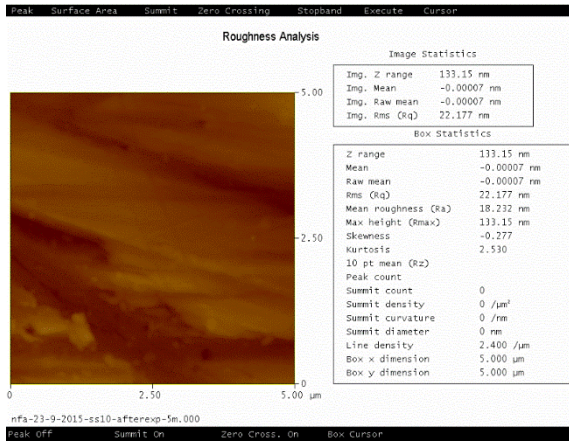


20 μm

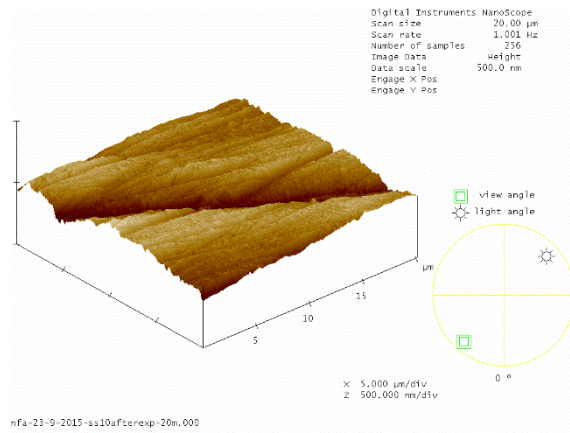
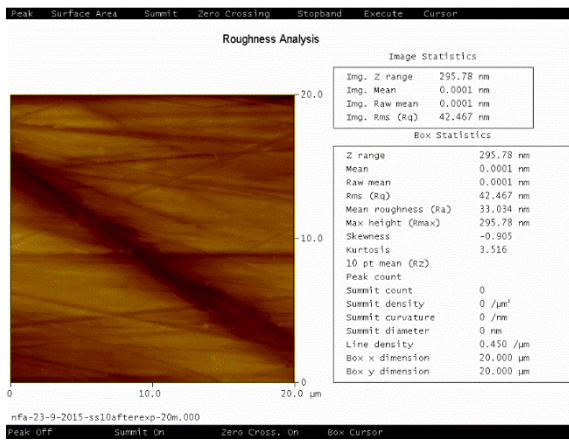


50 μm

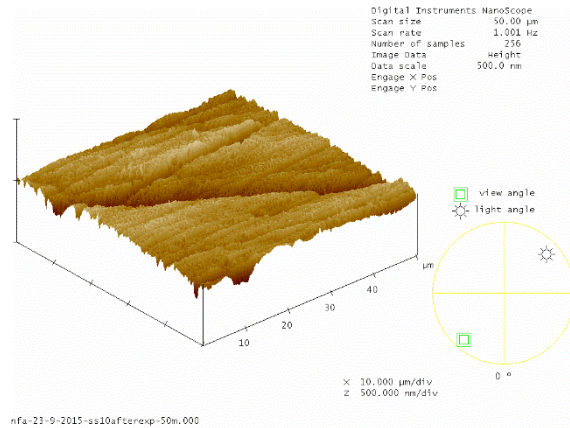
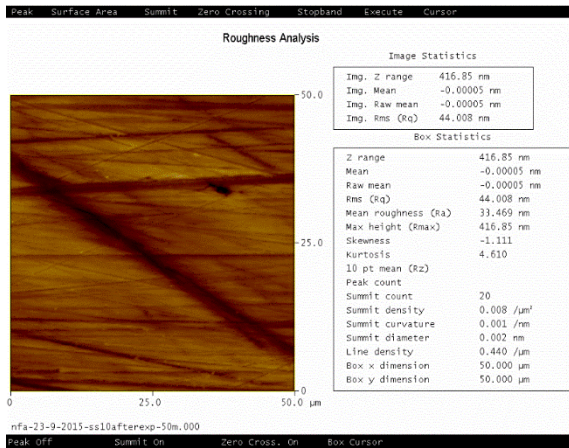
Figure 16.B: After polishing (Stainless steel; tap water sample)



5 μm

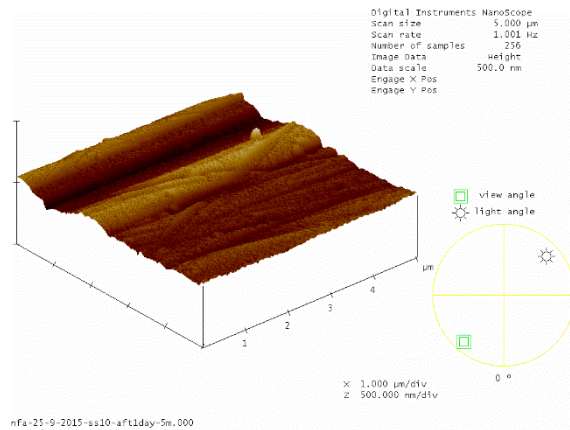
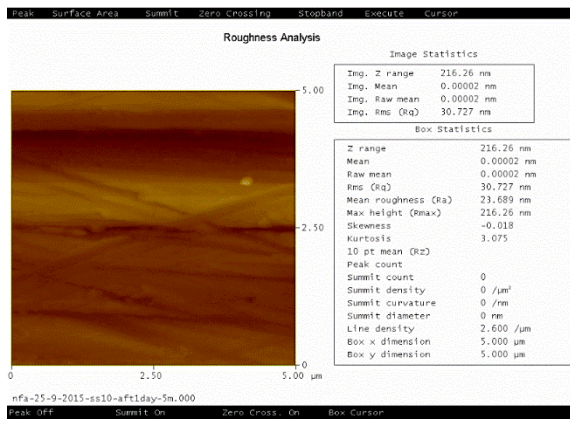


20 μm

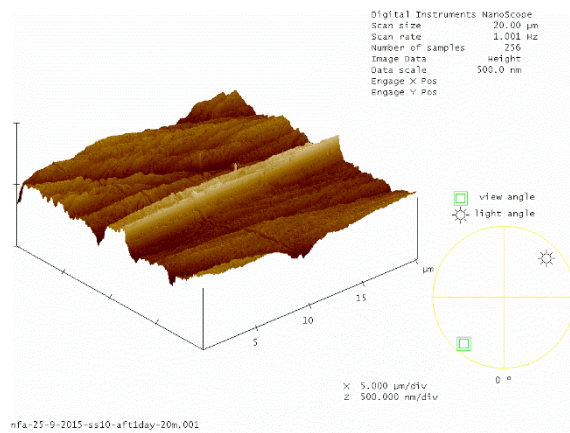
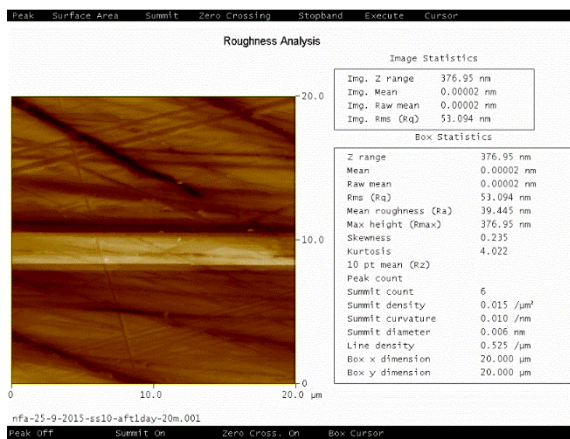


50 μm

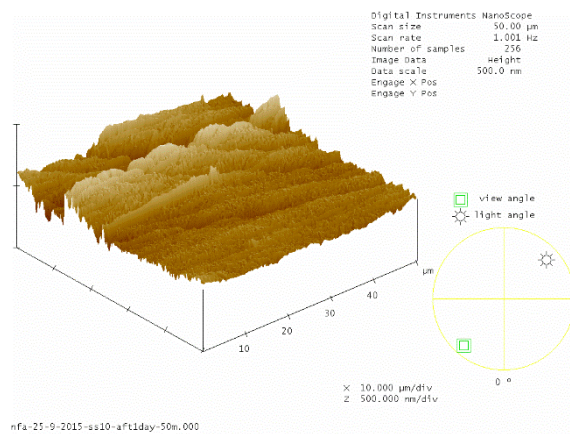
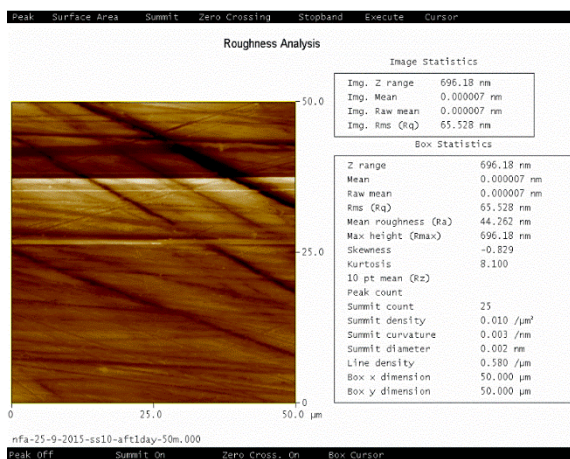
Figure 17.B: After the experiment (Stainless steel; tap water sample)



5 μm

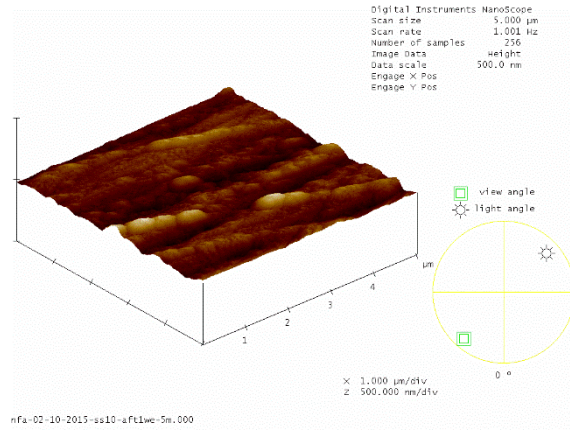
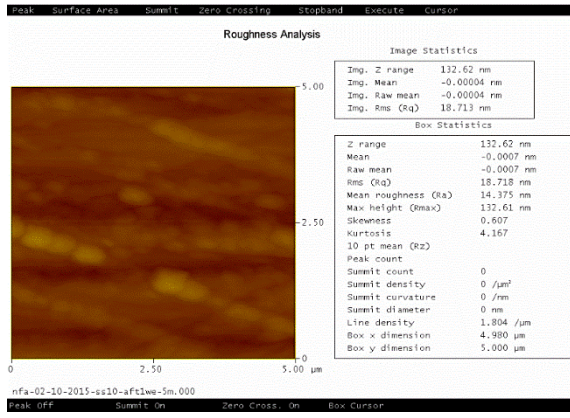


20 μm

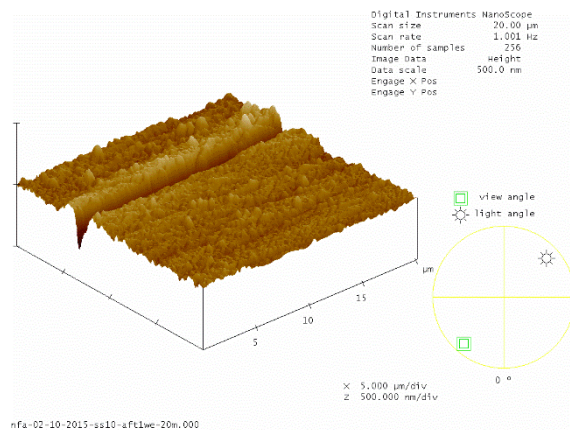
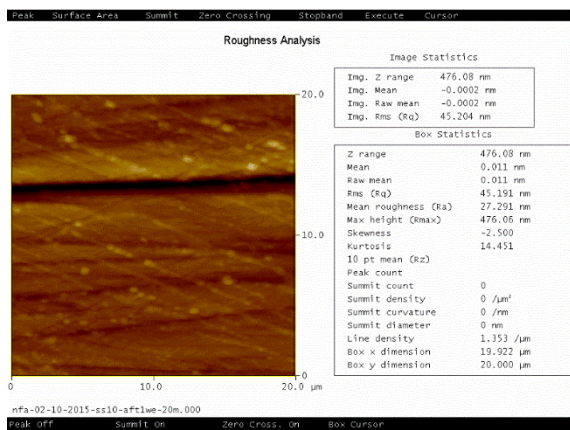


50 μm

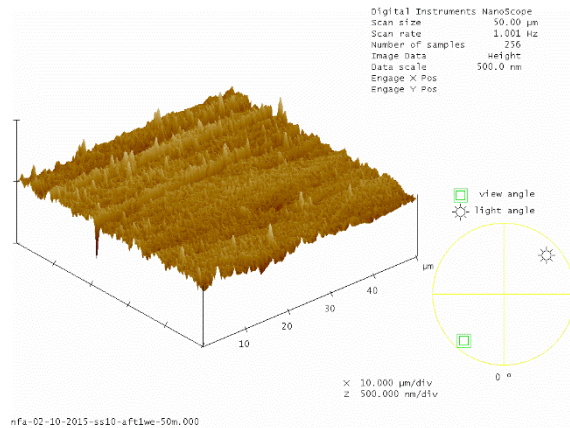
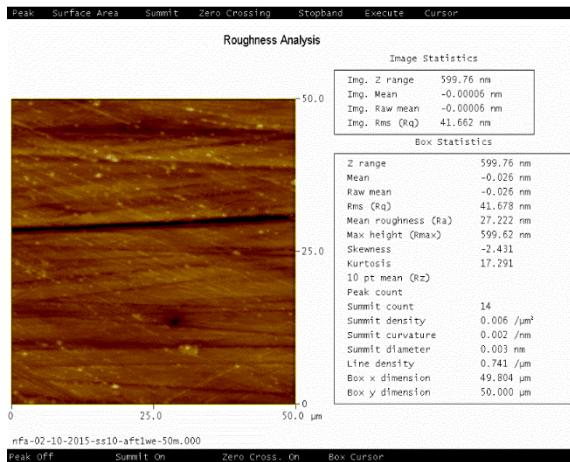
Figure 18.B: 1 day after the experiment (Stainless steel; tap water sample)



5 μm

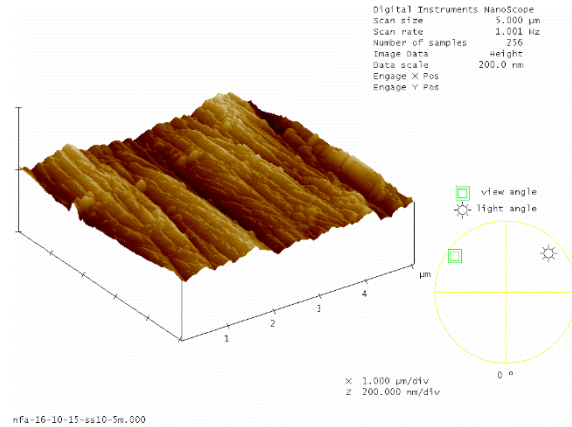
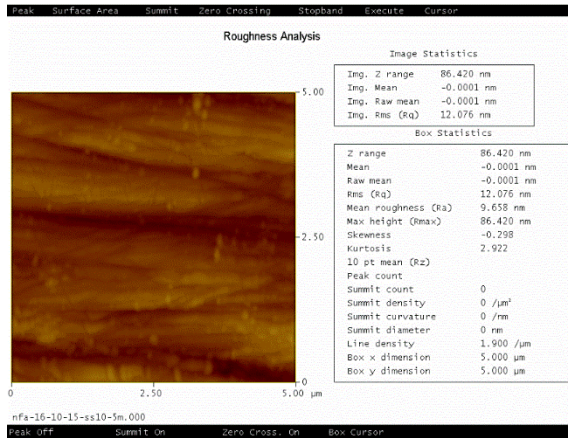


20 μm

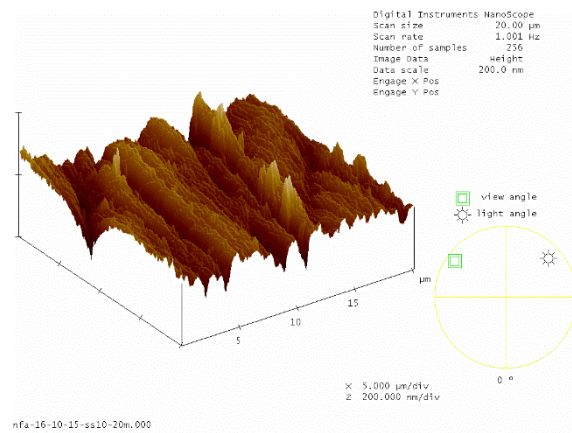
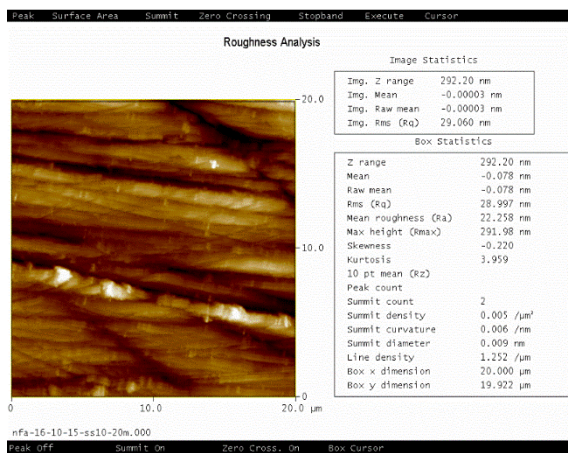


50 μm

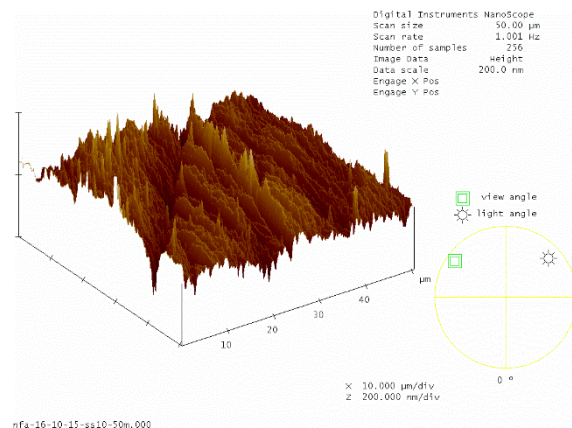
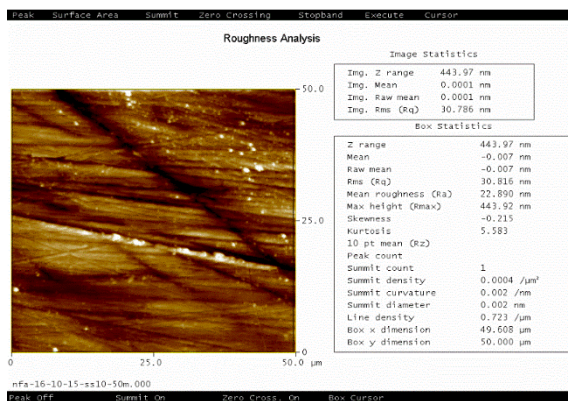
Figure 19.B: 1 week after the experiment (Stainless steel; tap water sample)



5 μm

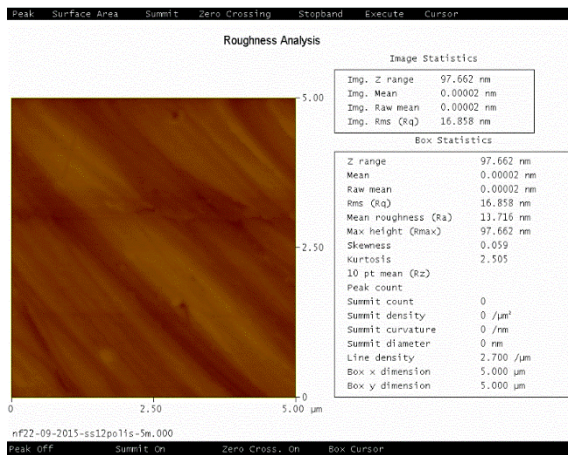


20 μm

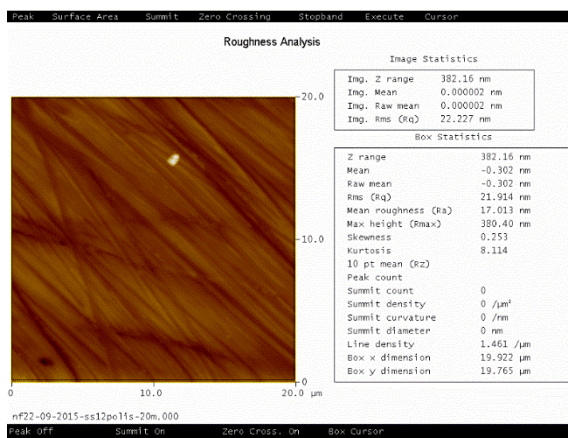
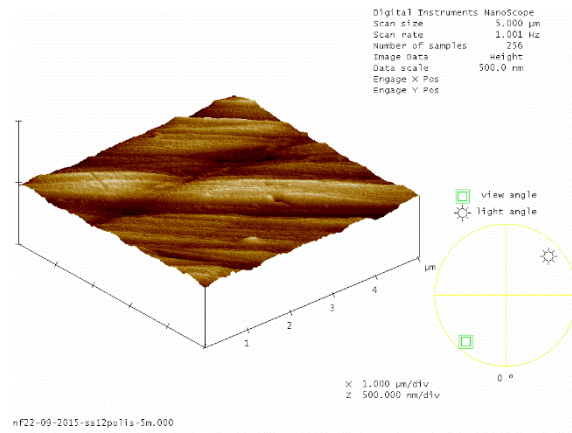


50 μm

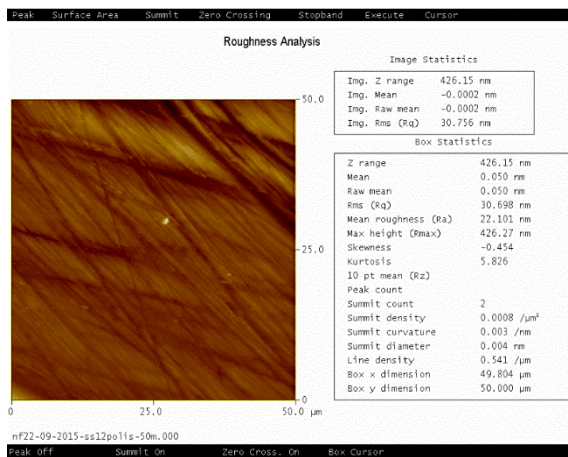
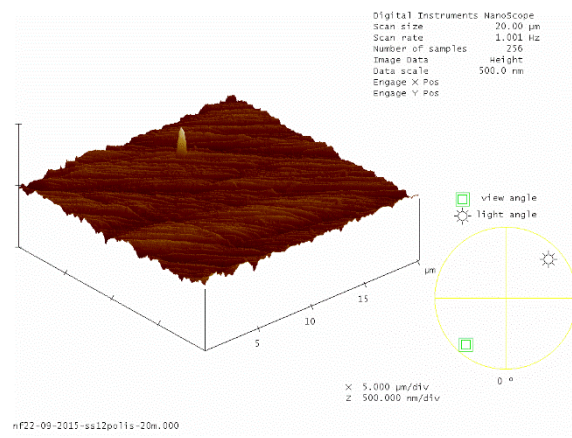
Figure 20.B: 2 weeks after the experiment (Stainless steel; tap water sample)



5 μm



20 μm



50 μm

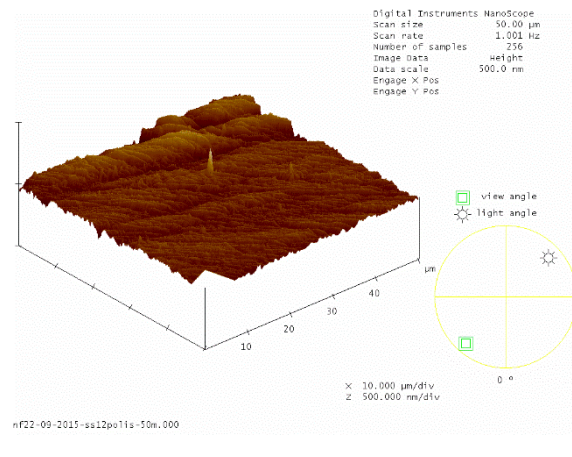
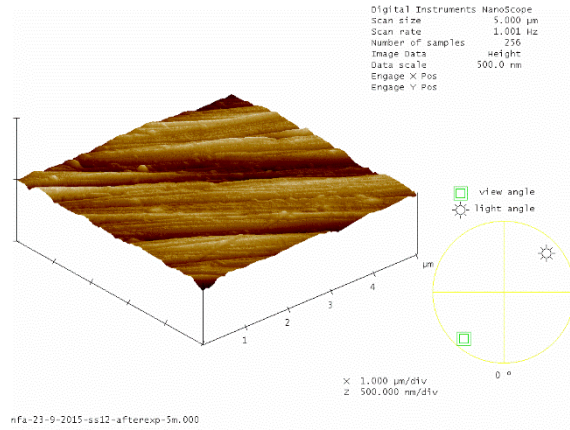
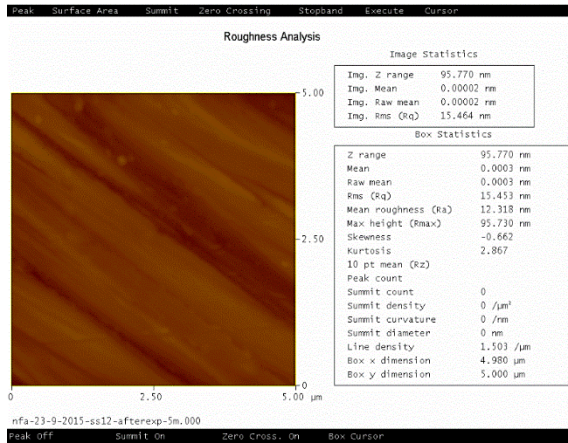
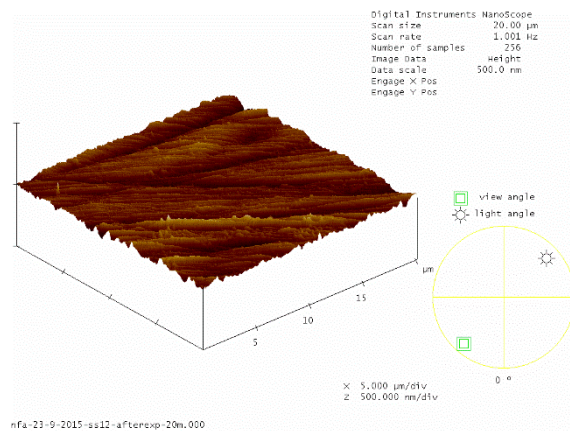
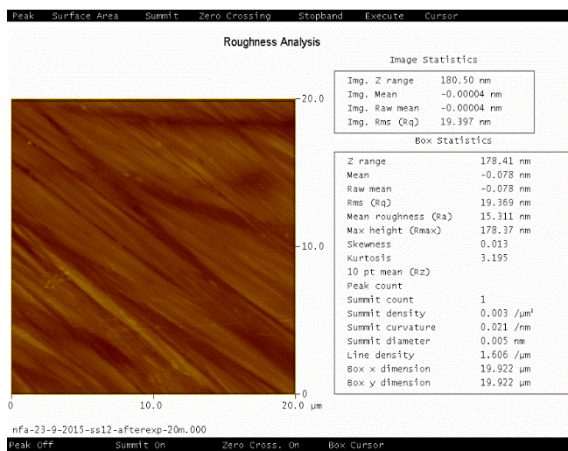


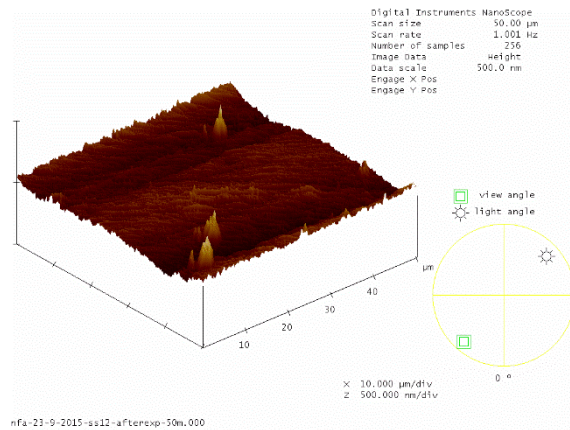
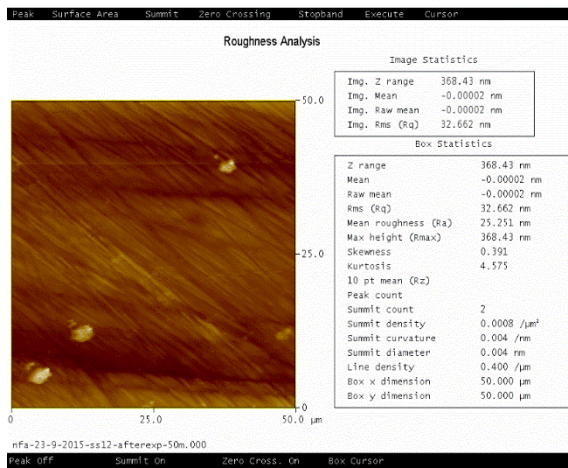
Figure 21.B: After polishing (Stainless steel;0.9% saline sample)



5 μm

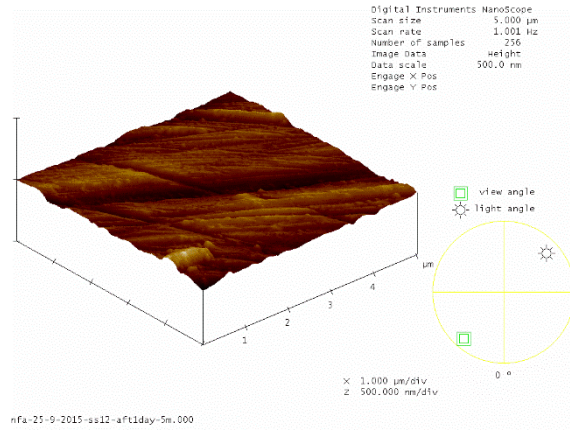
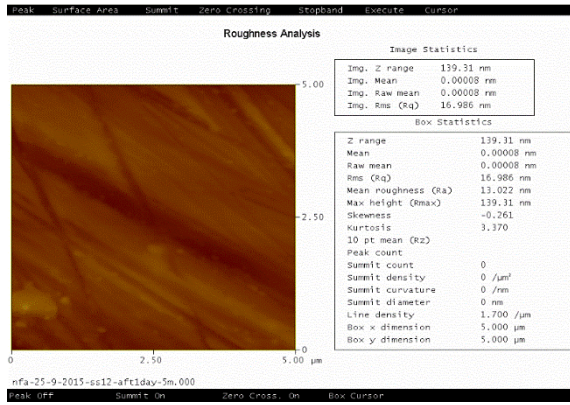


20 μm

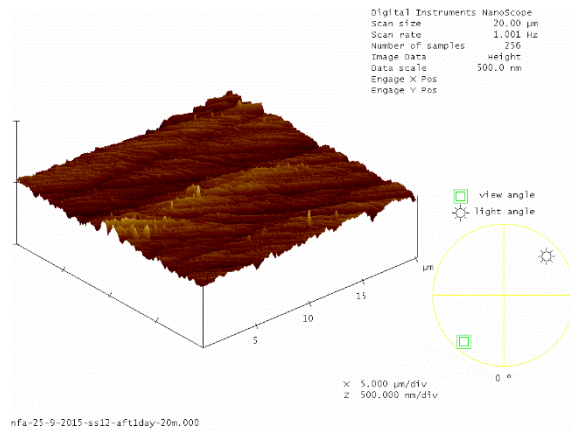
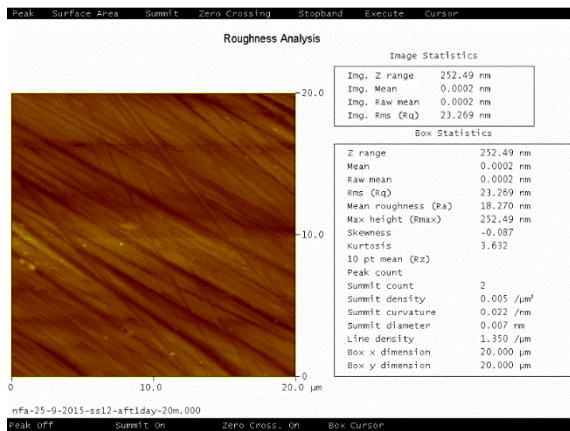


50 μm

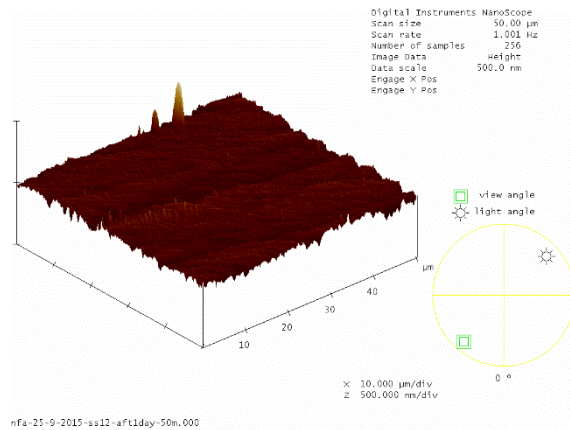
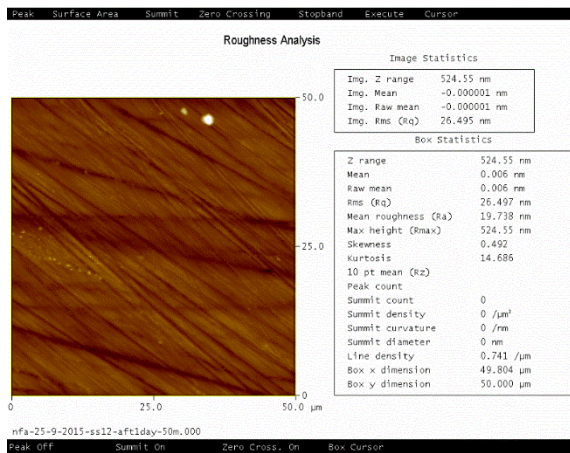
Figure 22.B: After the experiment (Stainless steel;0.9% saline sample)



5 μm

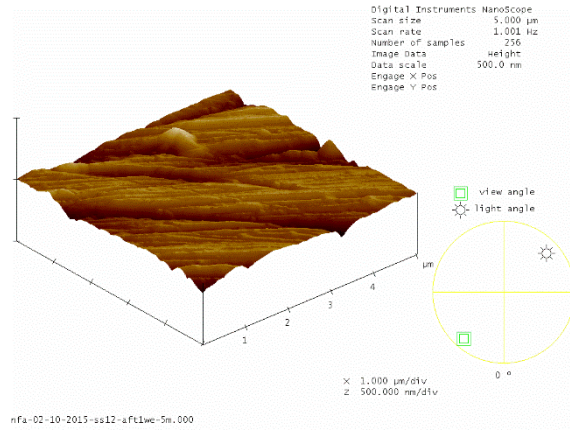
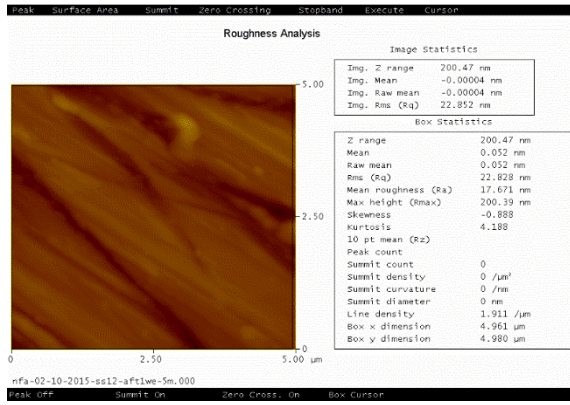


20 μm

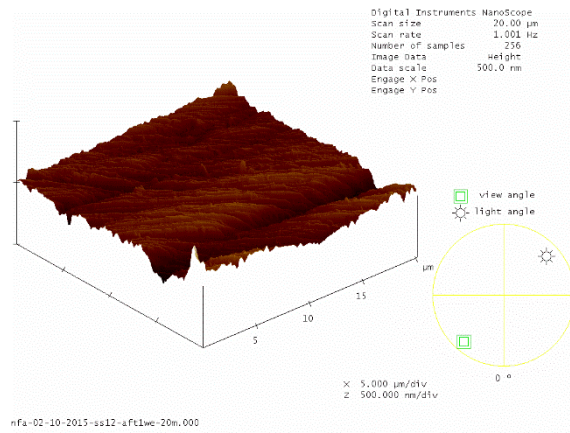
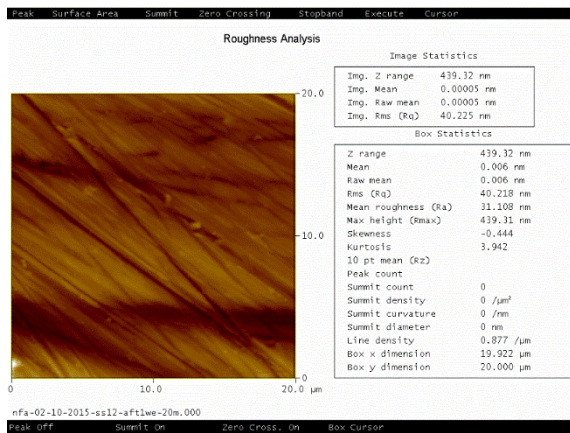


50 μm

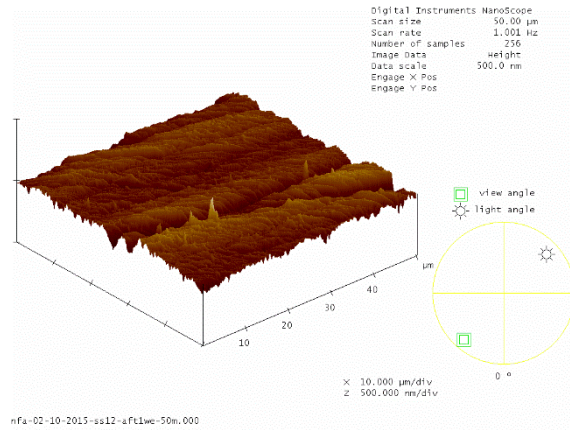
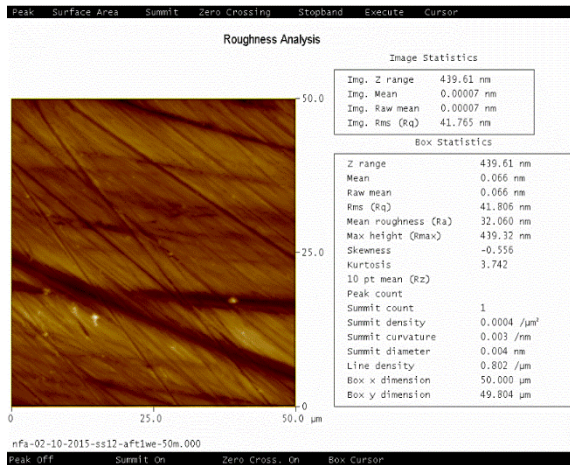
Figure 23.B: 1 day after the experiment (Stainless steel;0.9% saline sample)



5 μm

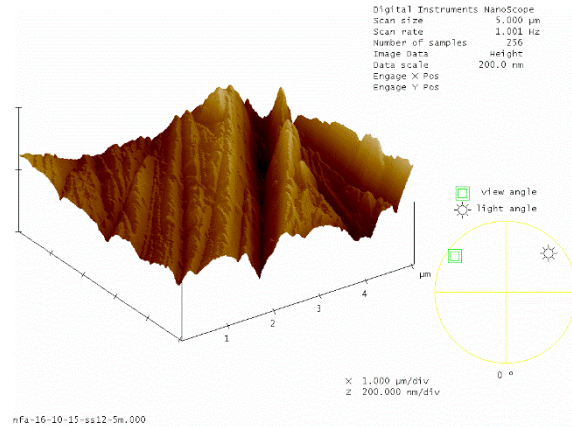
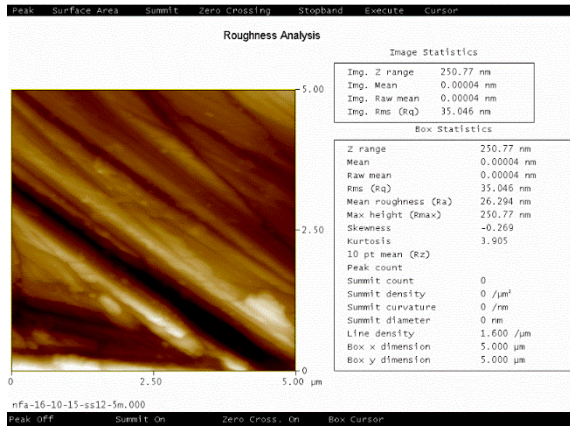


20 μm

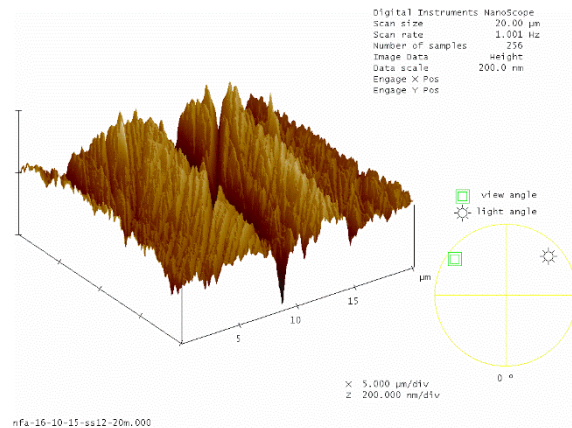
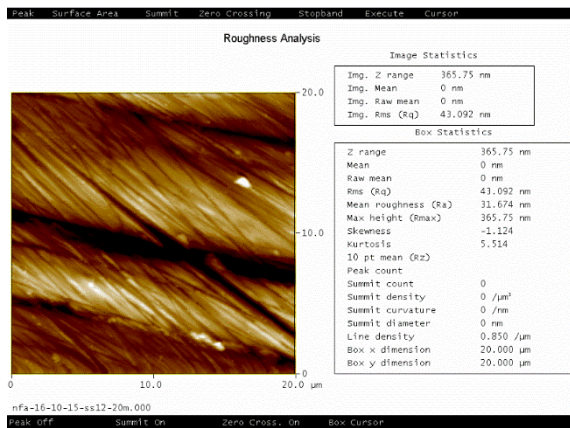


50 μm

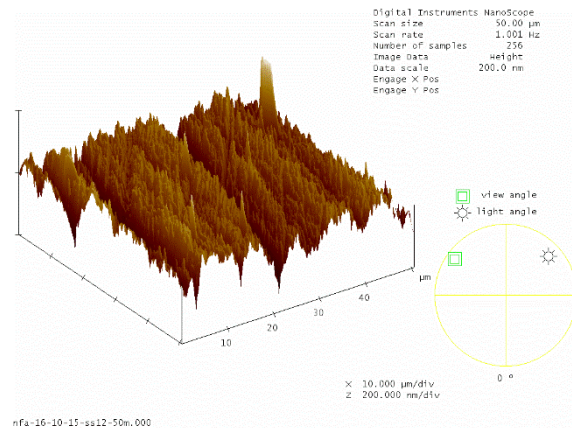
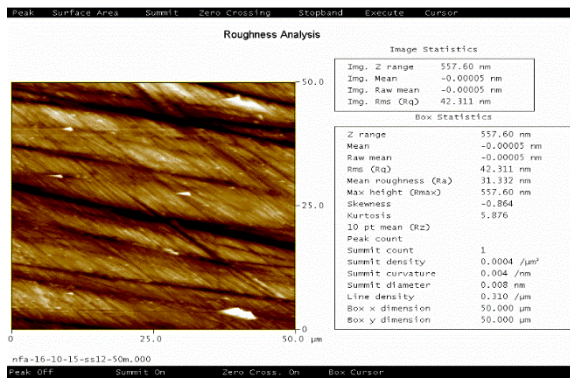
Figure 24.B: 1 week after the experiment (Stainless steel;0.9% saline sample)



5 μm

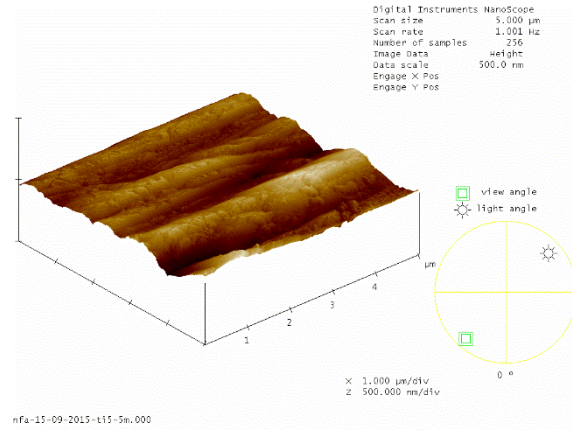
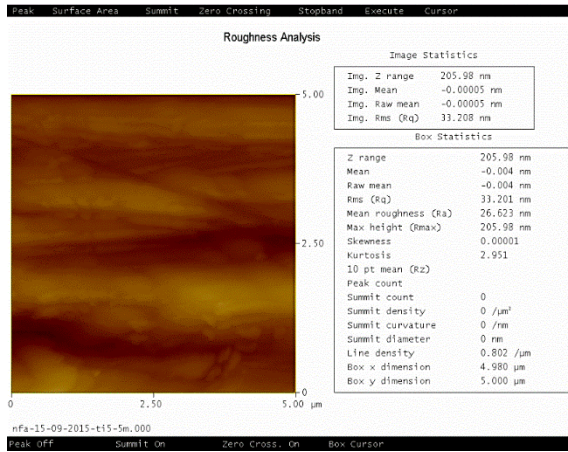


20 μm

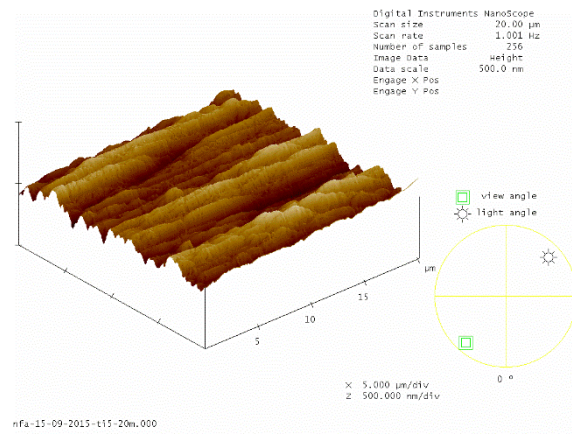
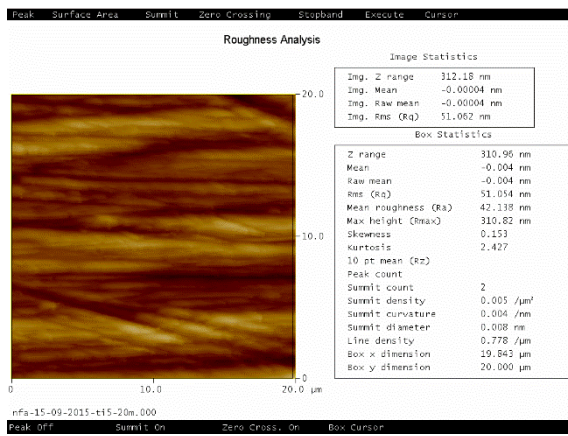


50 μm

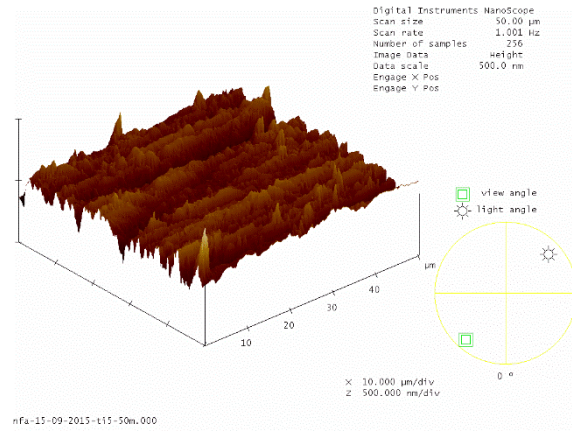
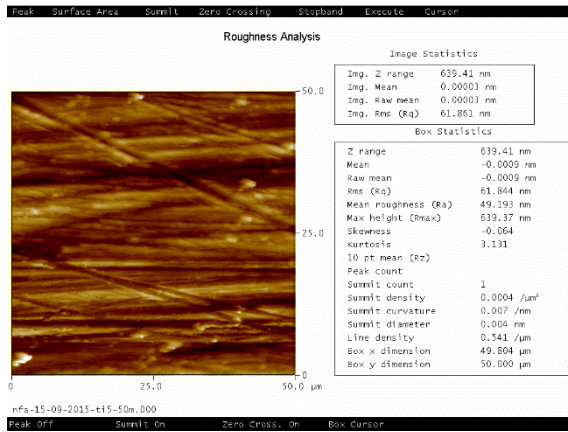
Figure 25.B: 2 weeks after the experiment (Stainless steel;0.9% saline sample)



5 μm

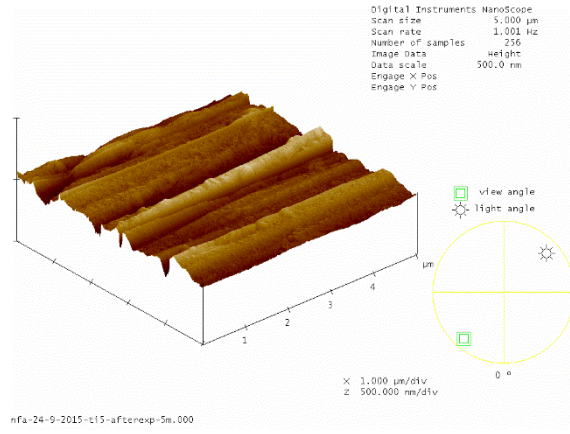
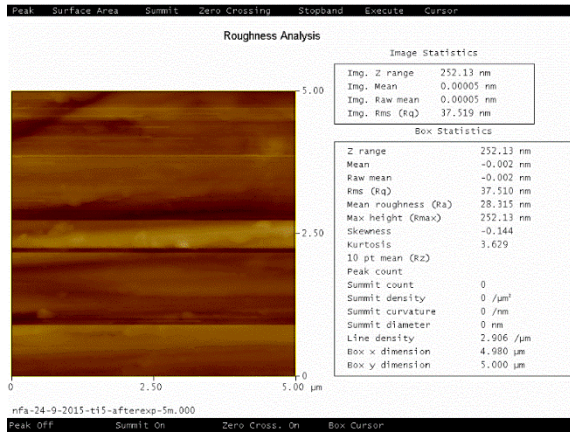


20 μm

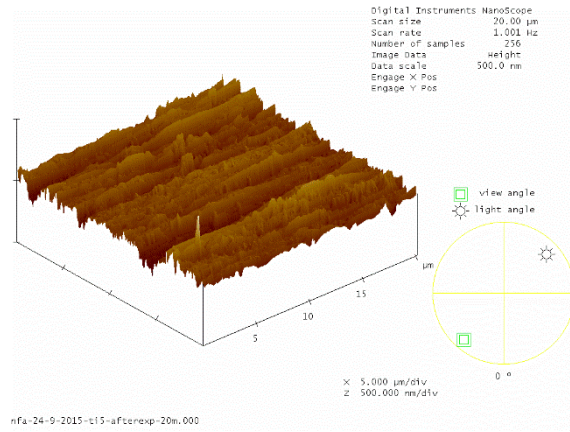
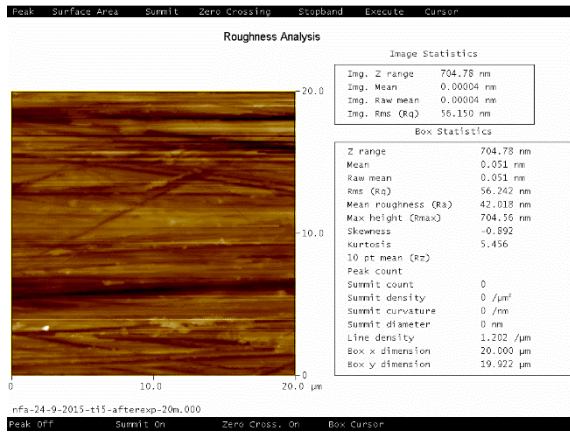


50 μm

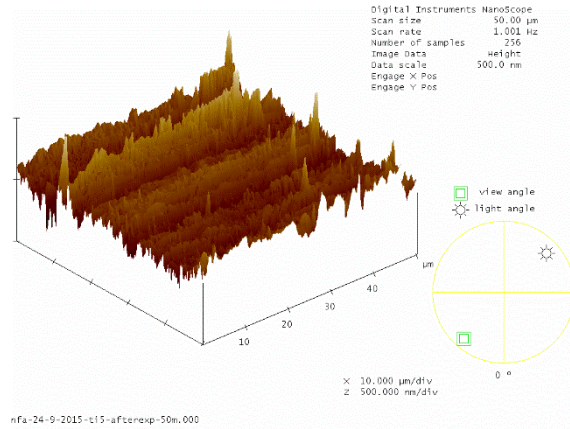
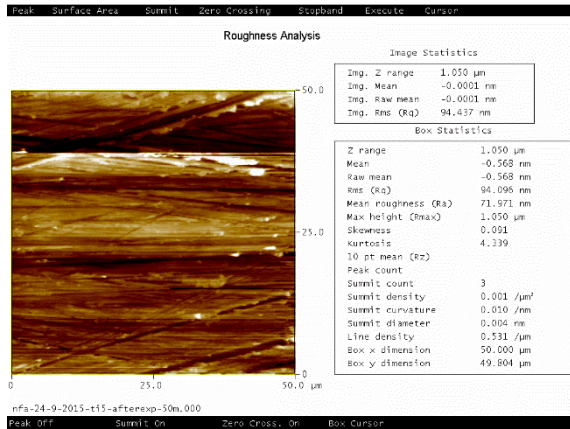
Figure 26.B: After polishing (Titanium; controlled sample)



5 μm

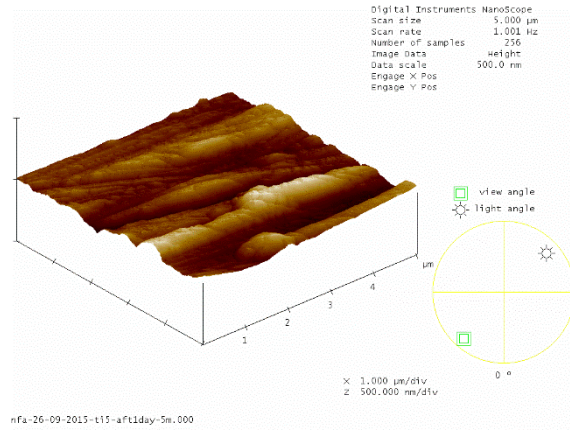
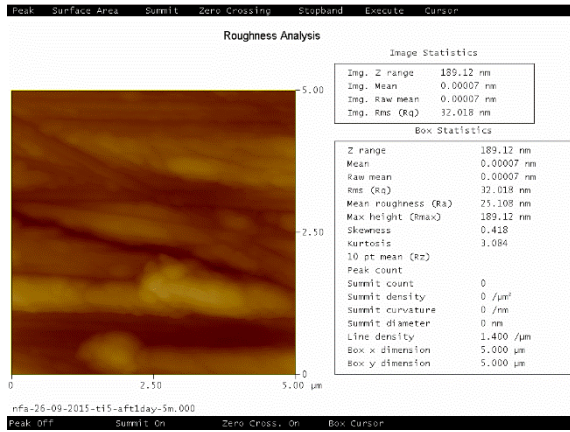


20 μm

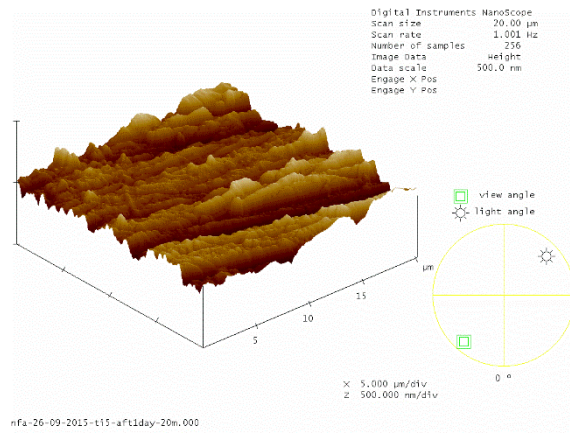
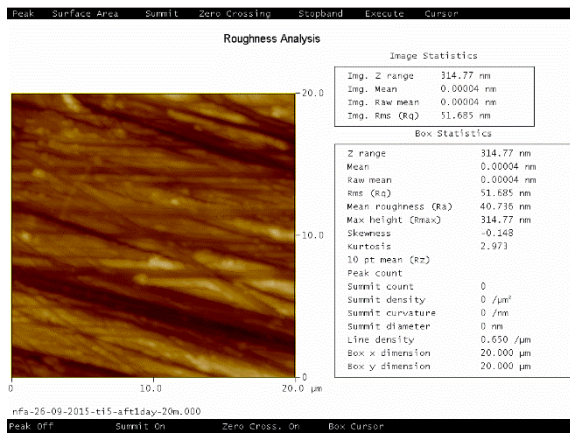


50 μm

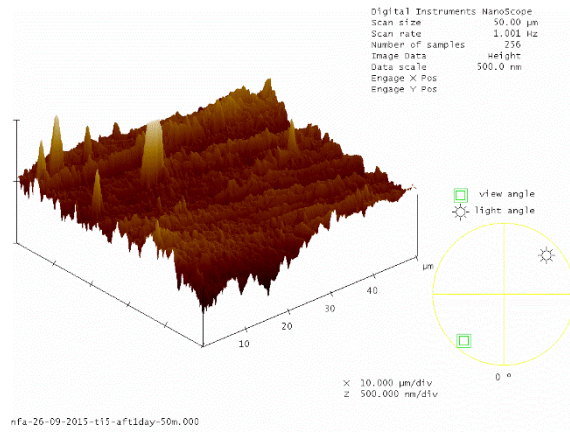
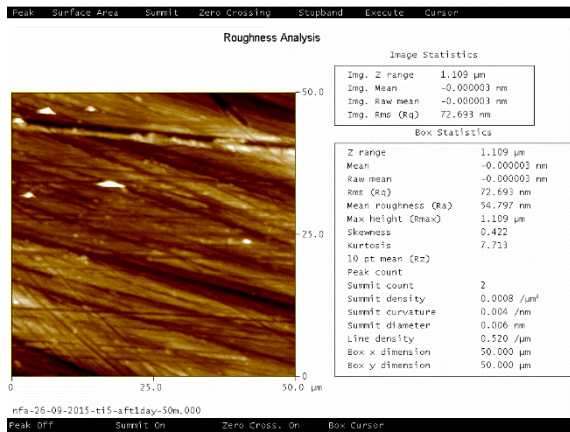
Figure 27.B: After the experiment (Titanium; controlled sample)



5 μm

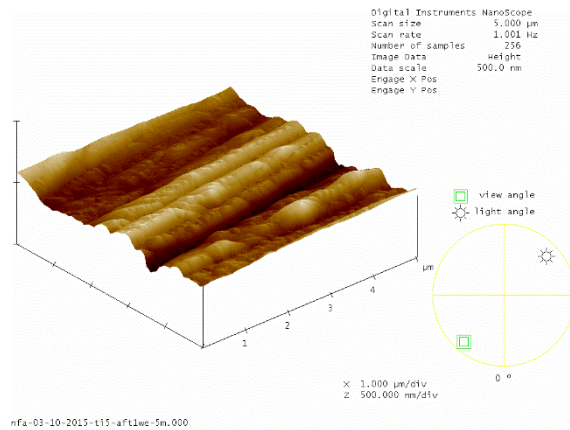
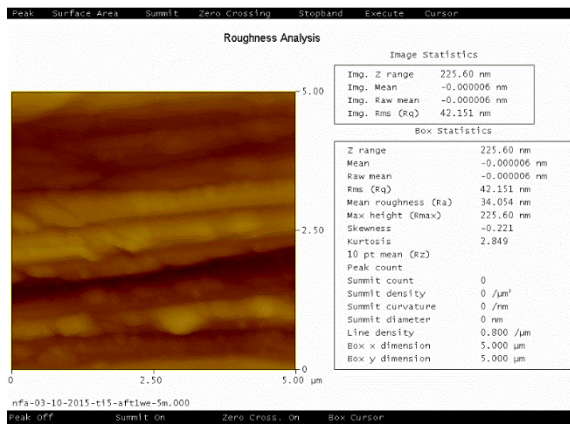


20 μm

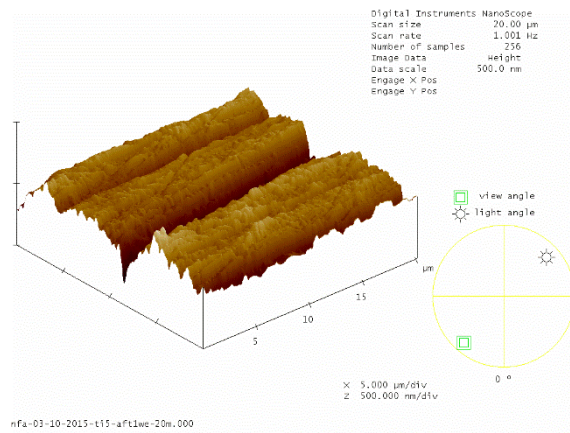
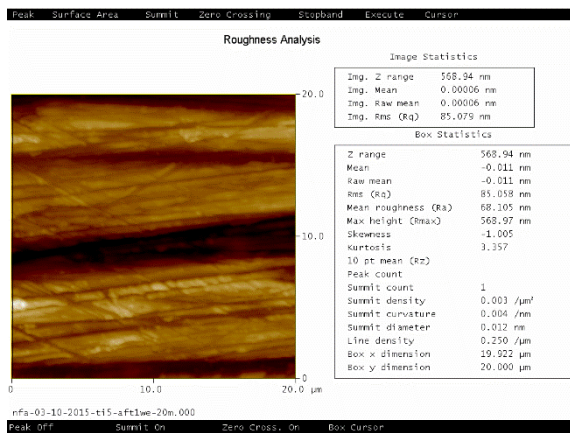


50 μm

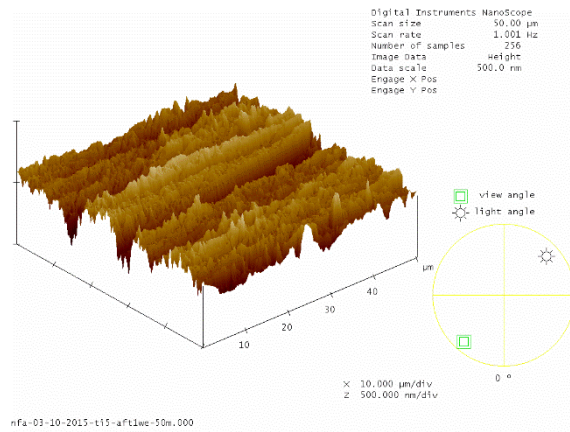
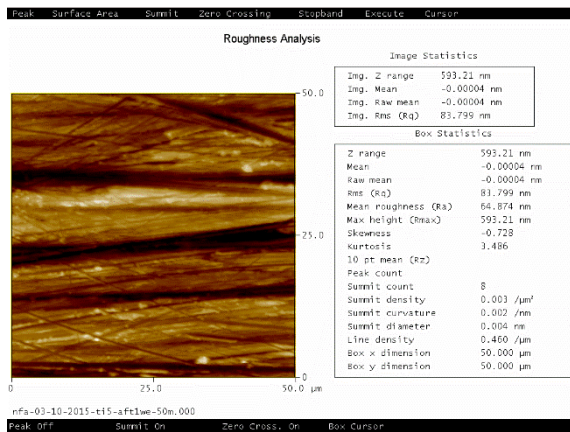
Figure 28.B: 1 day after the experiment (Titanium; controlled sample)



5 μm

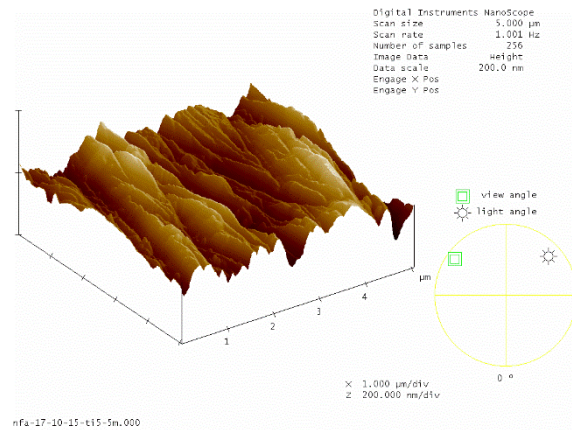
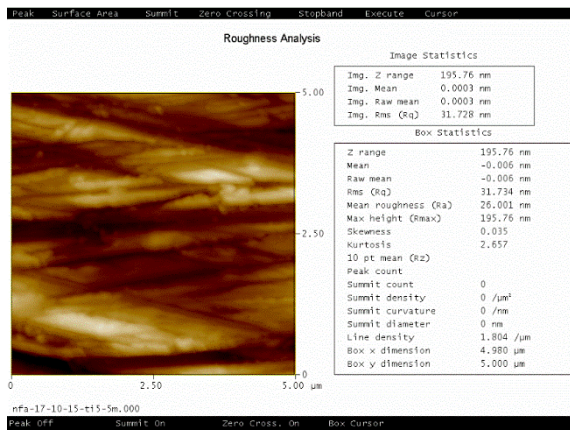


20 μm

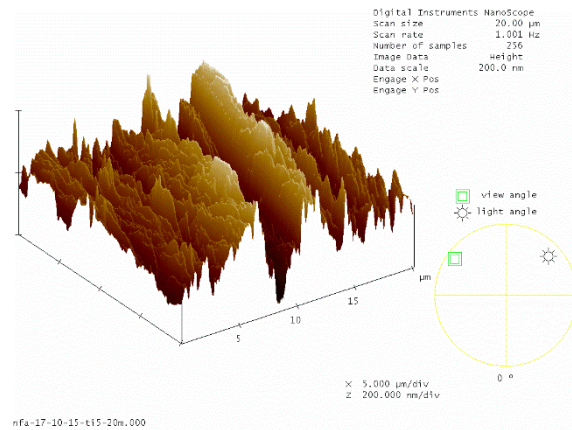
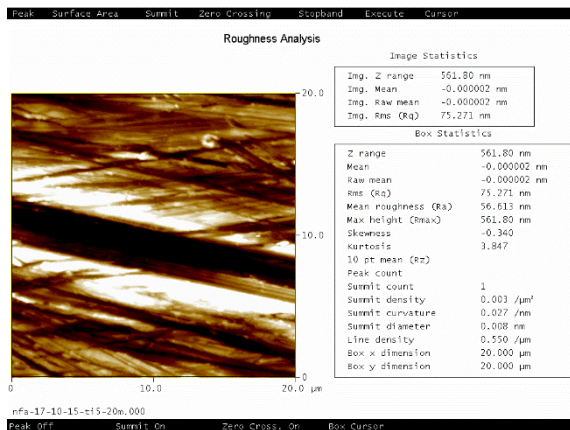


50 μm

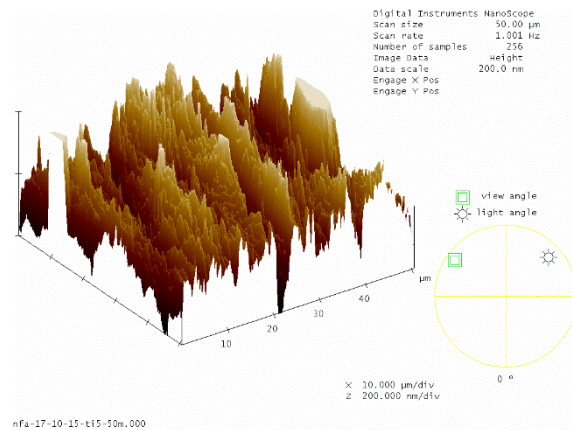
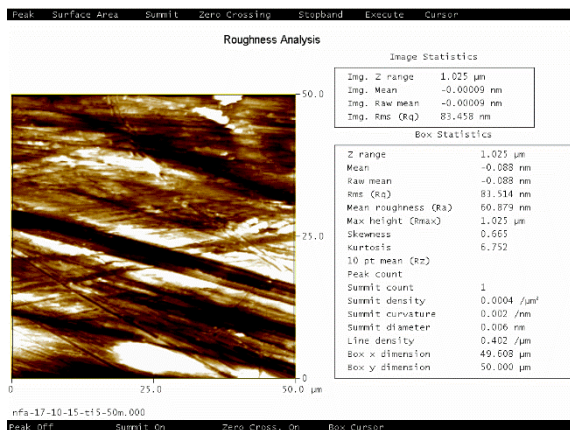
Figure 29.B: 1 week after the experiment (Titanium; controlled sample)



5 μm

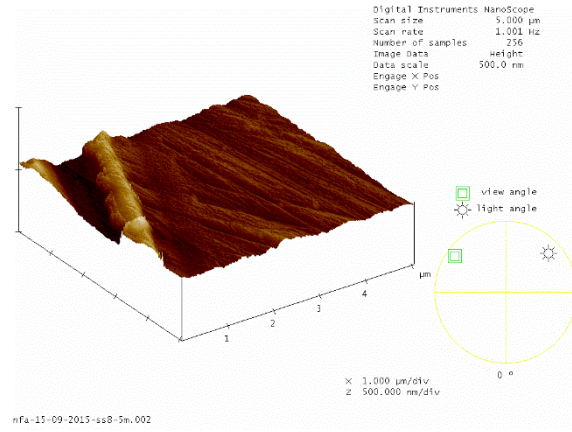
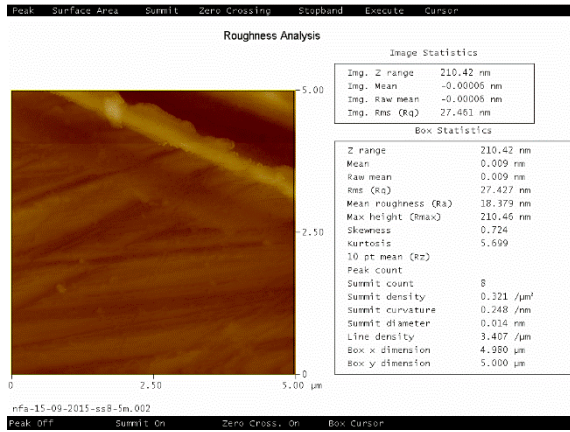


20 μm

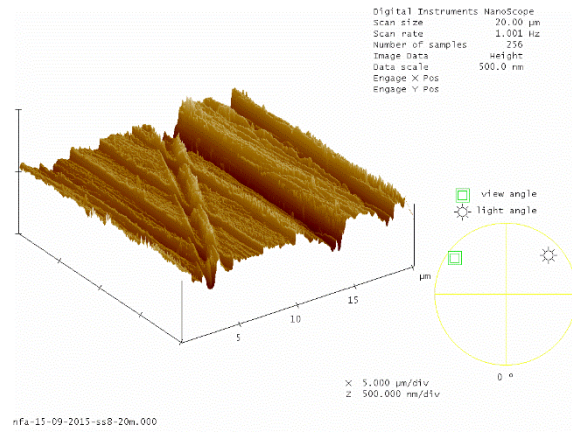
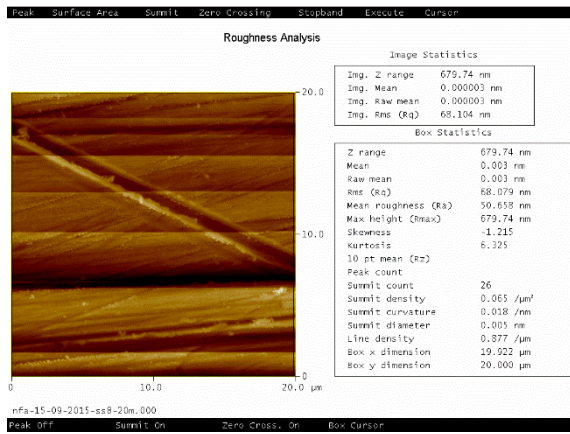


50 μm

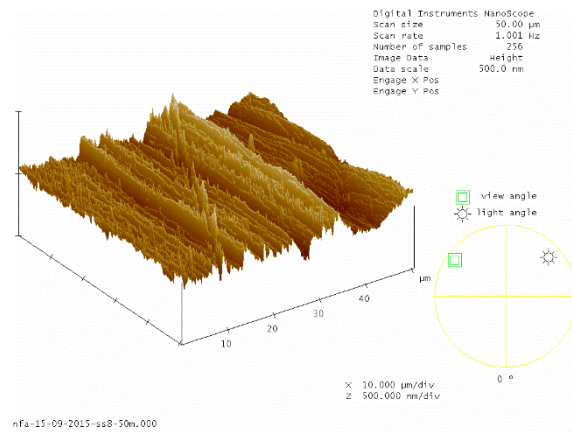
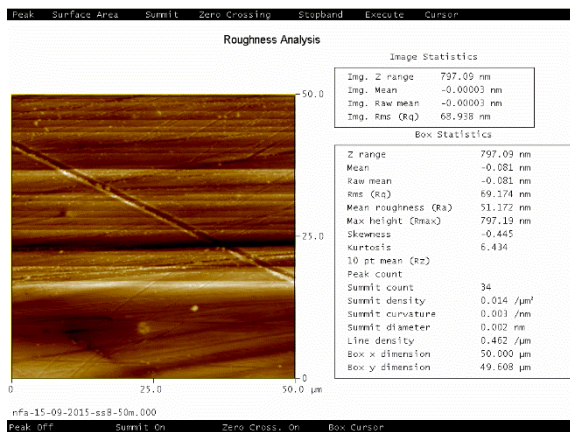
Figure 30.B: 2 weeks after the experiment (Titanium; controlled sample)



5 μm

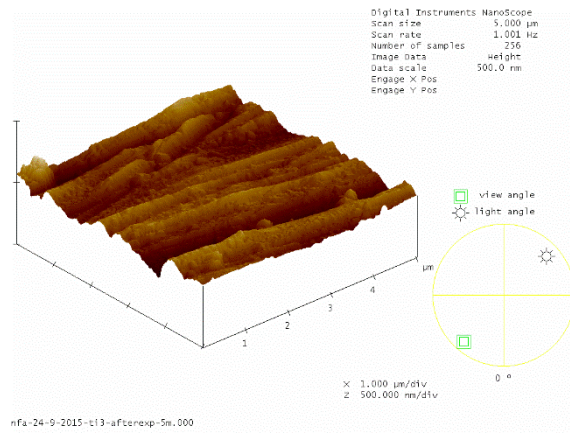
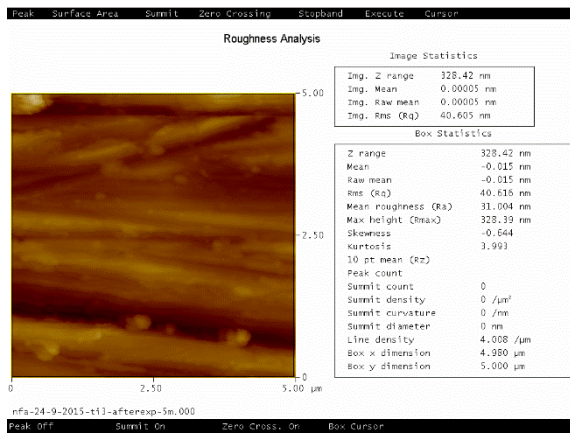


20 μm

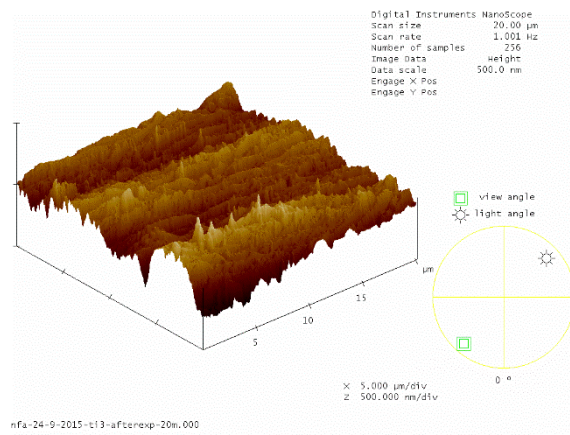
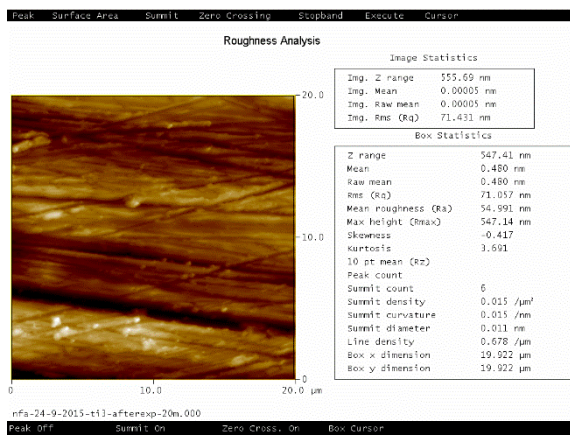


50 μm

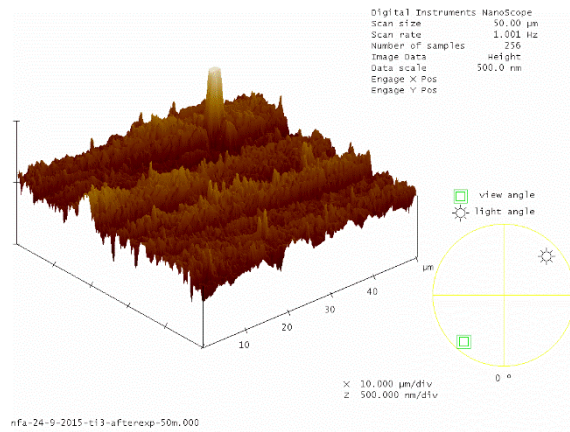
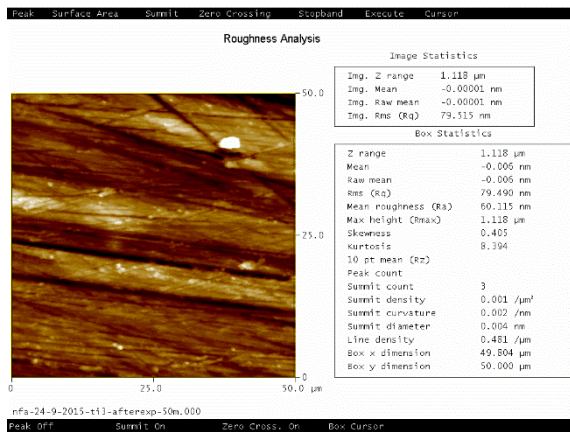
Figure 31.B: After polishing (Titanium; deionized water sample)



5 μm

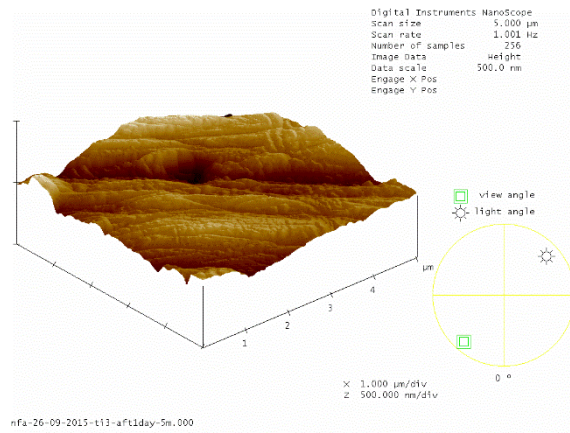
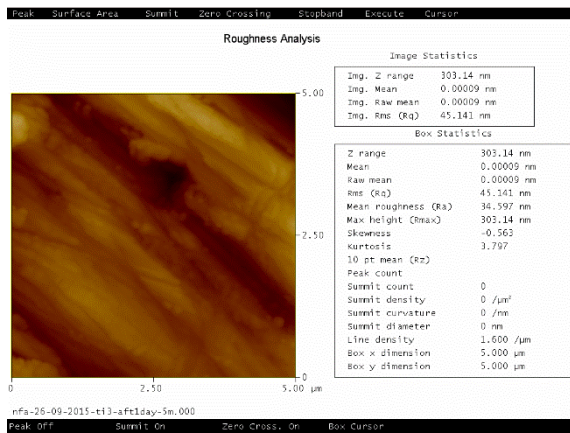


20 μm

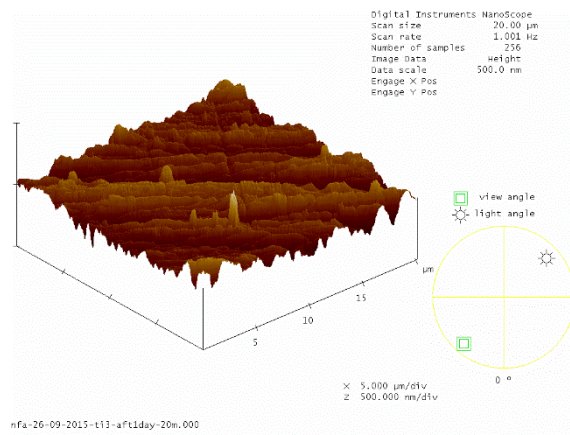
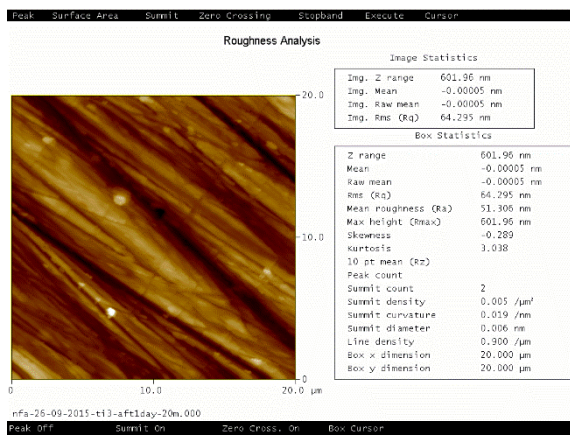


50 μm

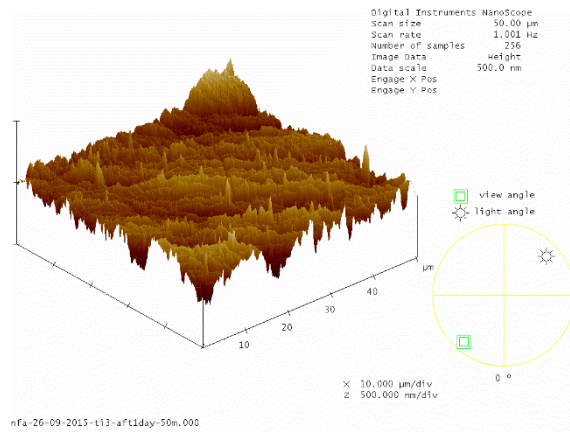
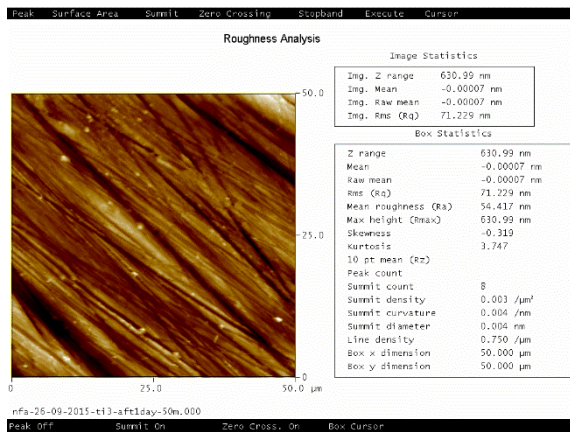
Figure 32.B: After the experiment (Titanium; deionized water sample)



5 μm

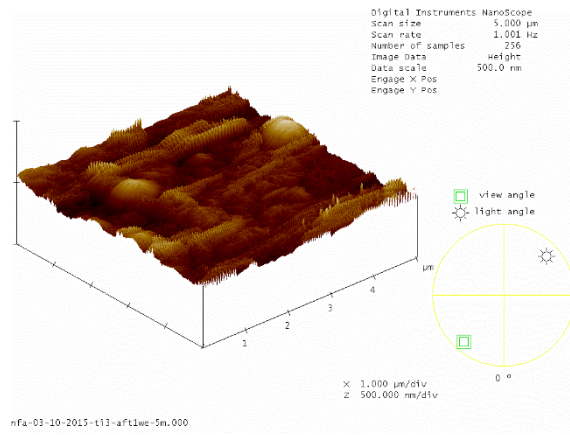
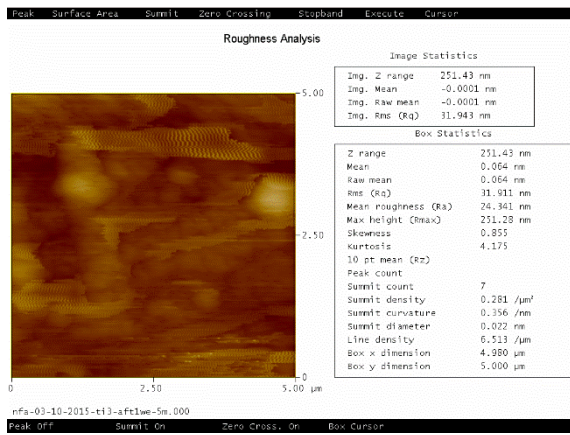


20 μm

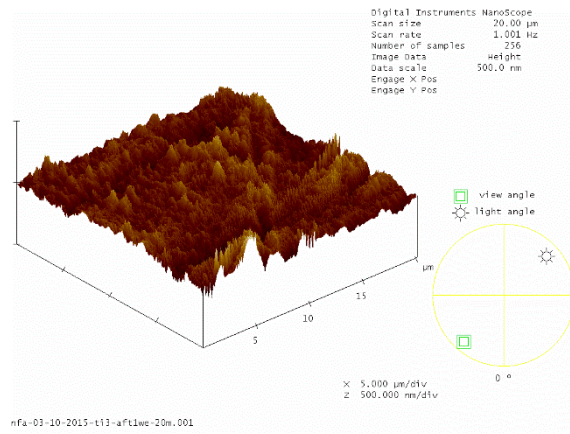
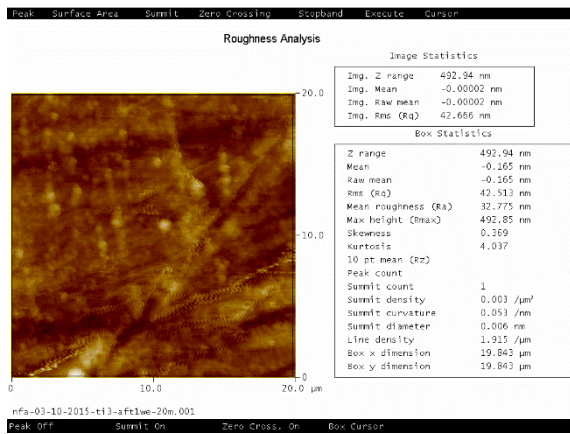


50 μm

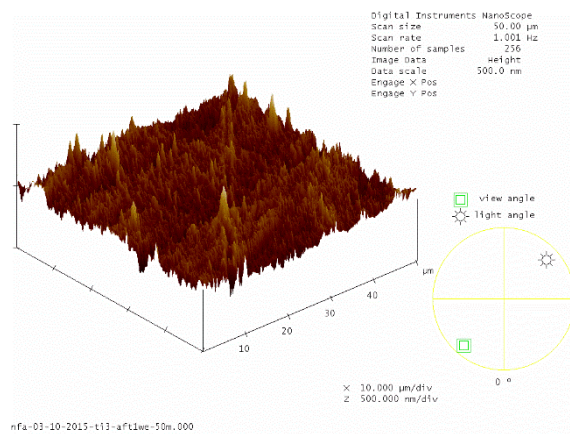
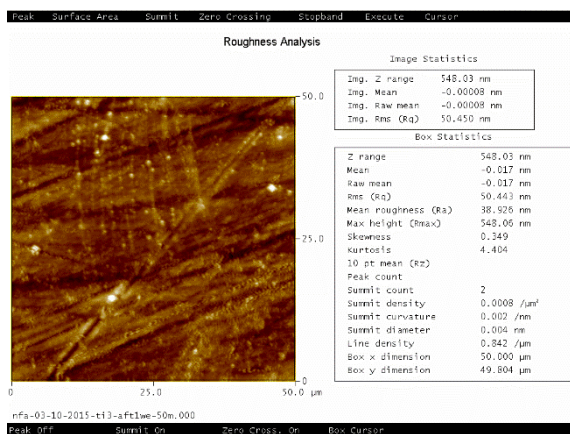
Figure 33.B: 1 day after the experiment (Titanium; deionized water sample)



5 μm

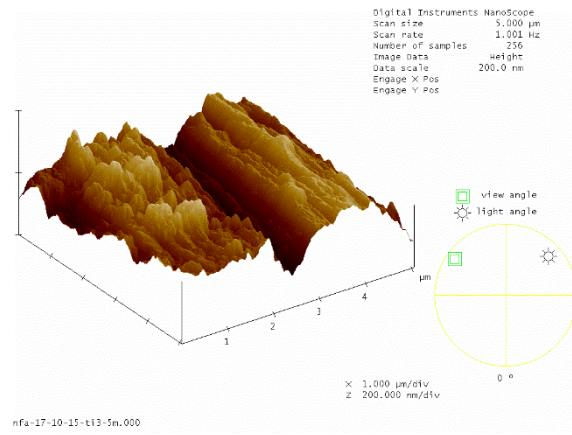
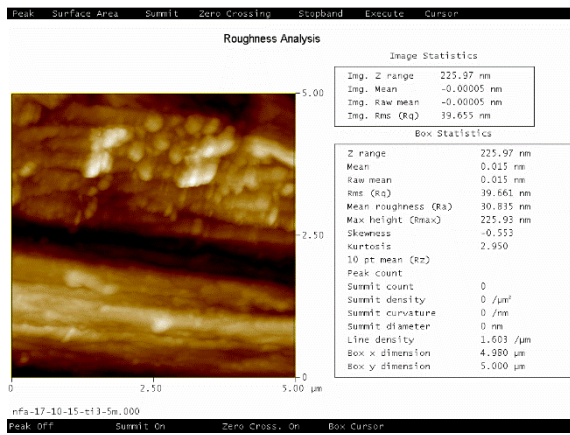


20 μm

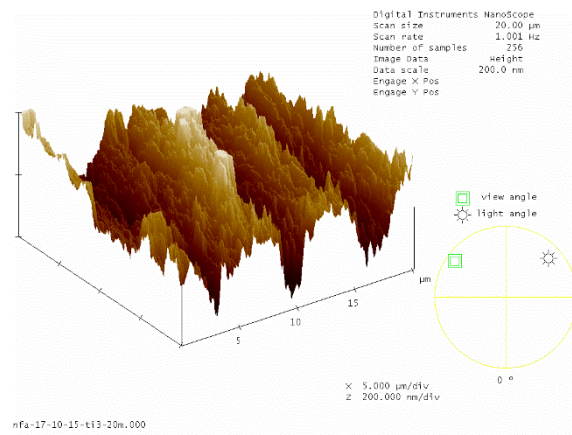
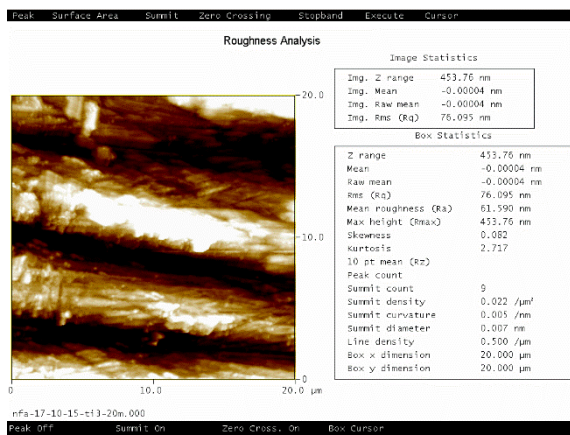


50 μm

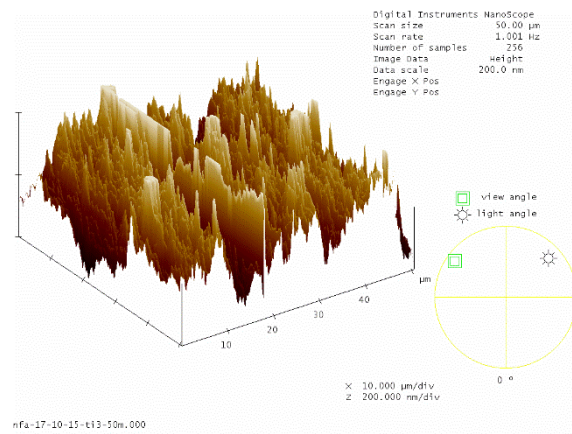
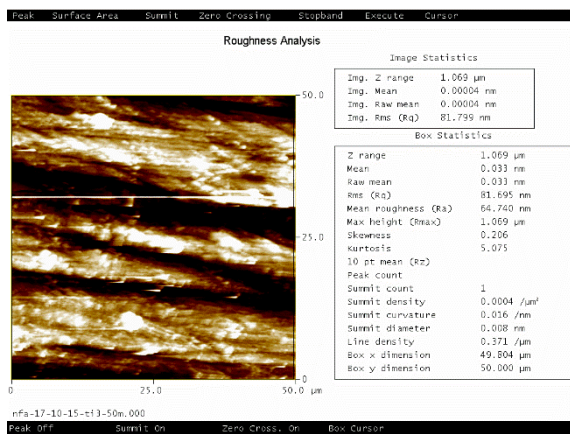
Figure 34.B: 1 week after the experiment (Titanium; deionized water sample)



5 μm

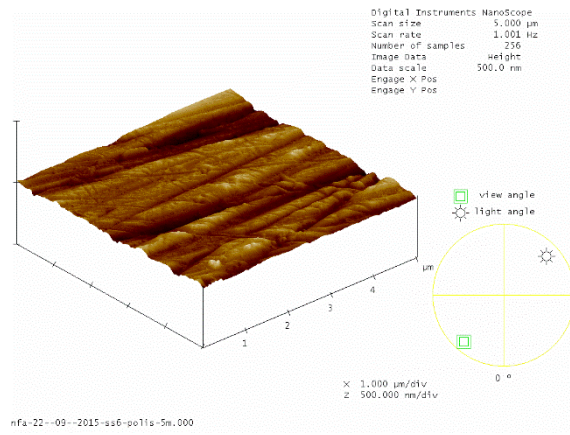
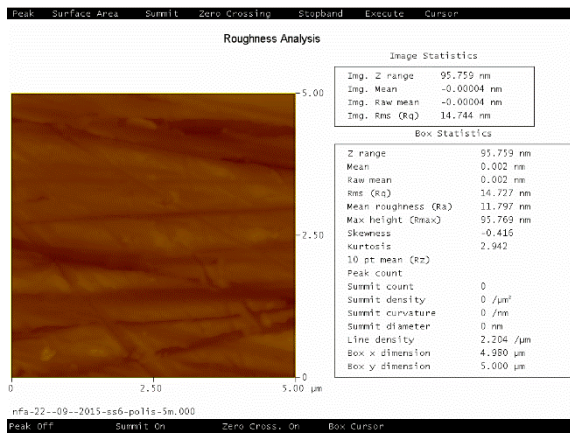


20 μm

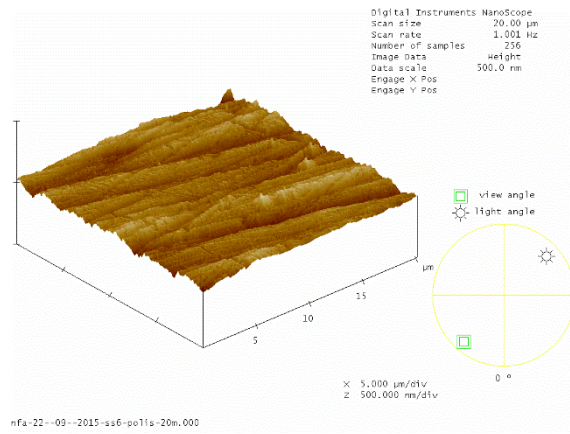
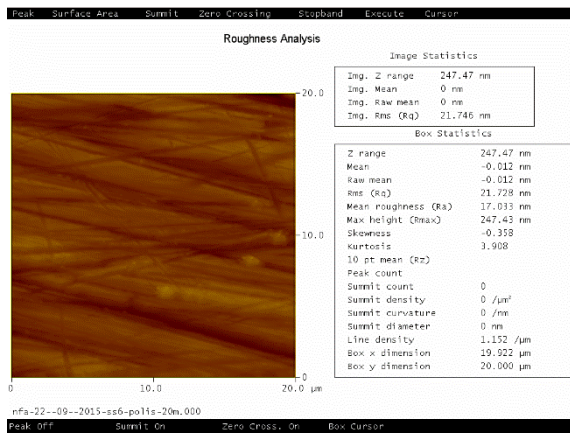


50 μm

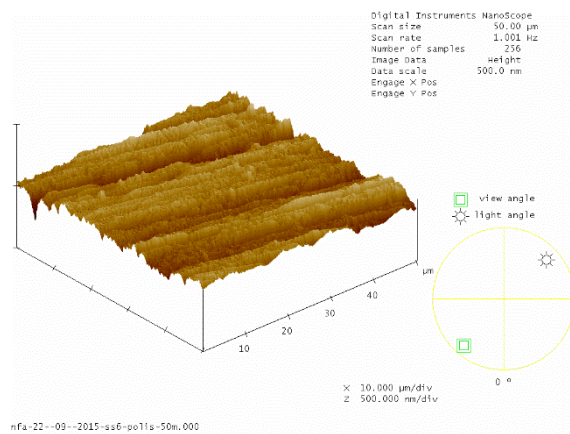
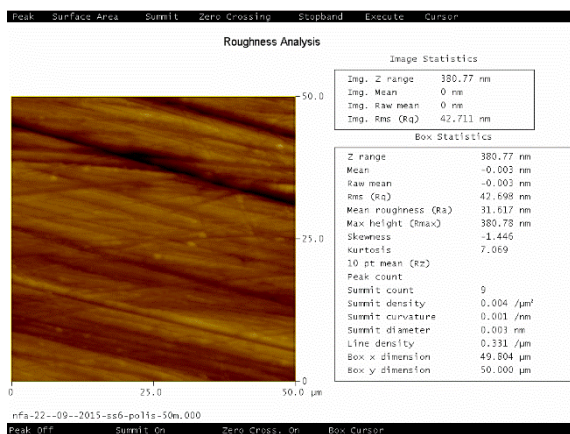
Figure 35.B: 2 weeks after the experiment (Titanium; deionized water sample)



5 μm

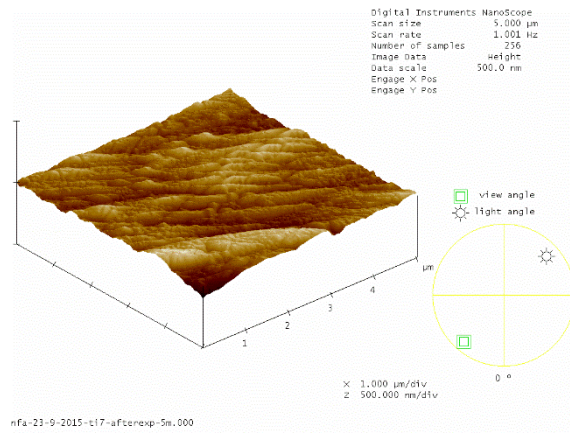
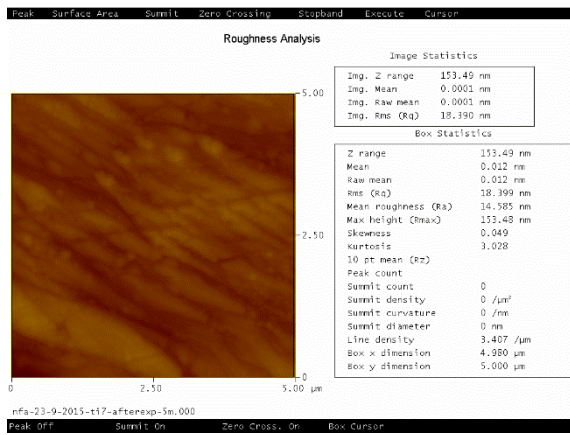


20 μm

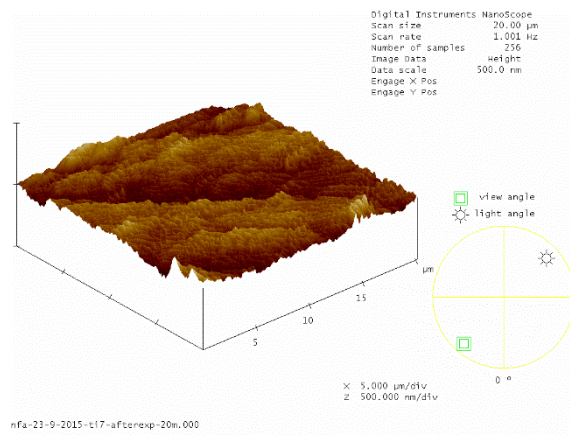
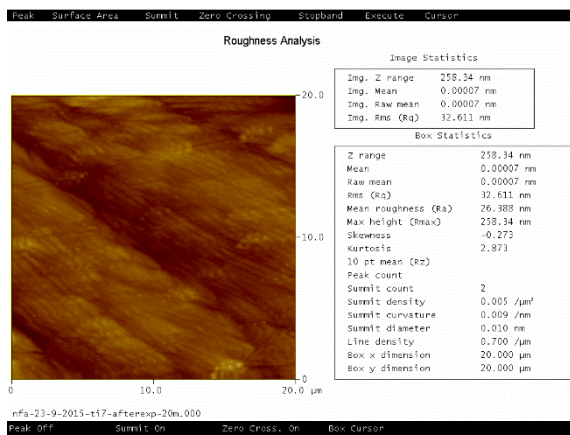


50 μm

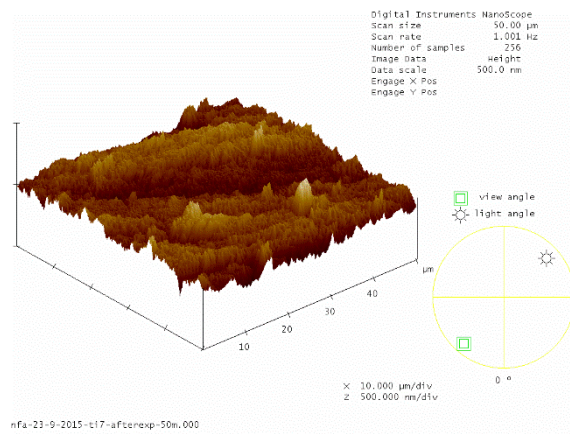
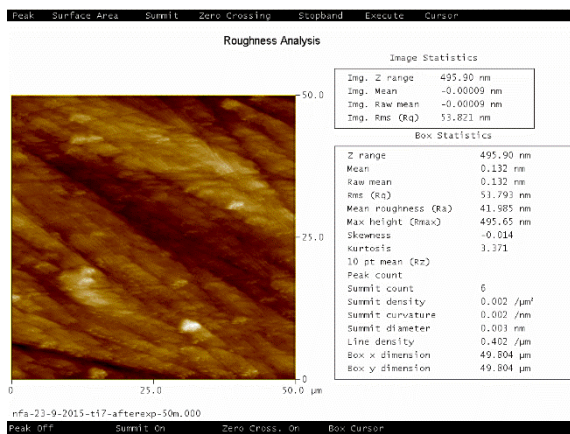
Figure 36.B: After polishing (Titanium; distilled water sample)



5 μm

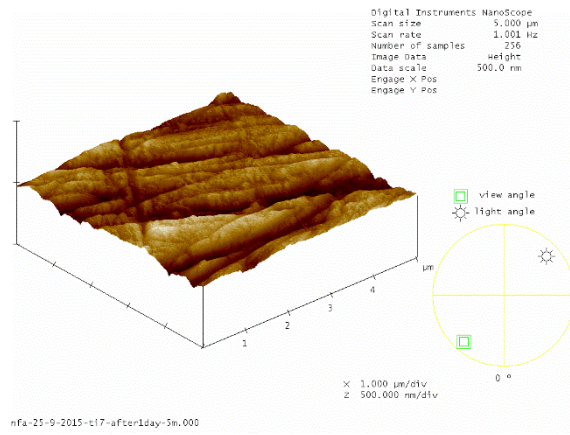
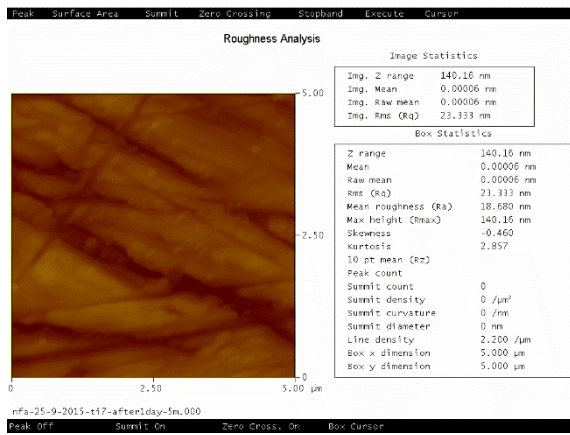


20 μm

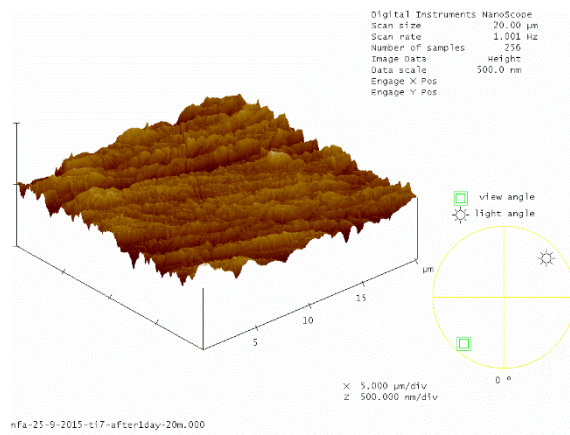
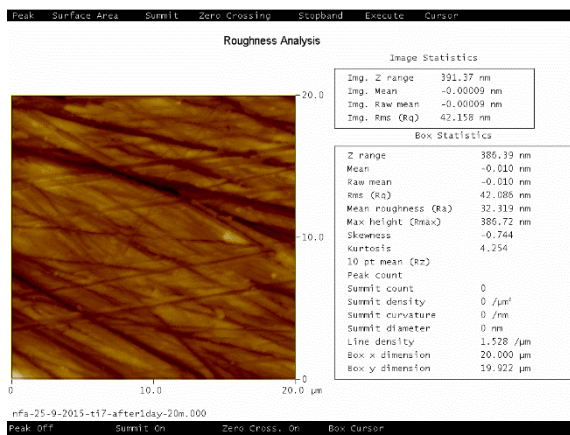


50 μm

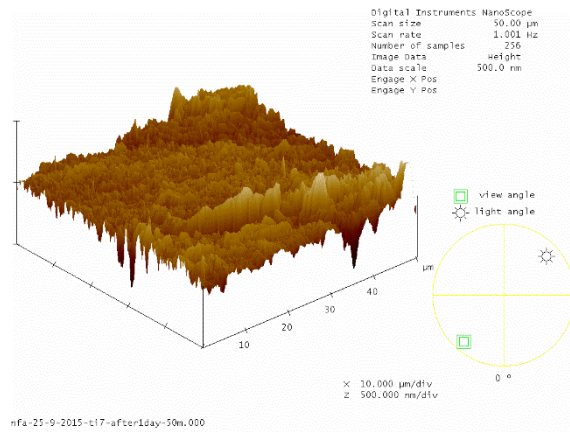
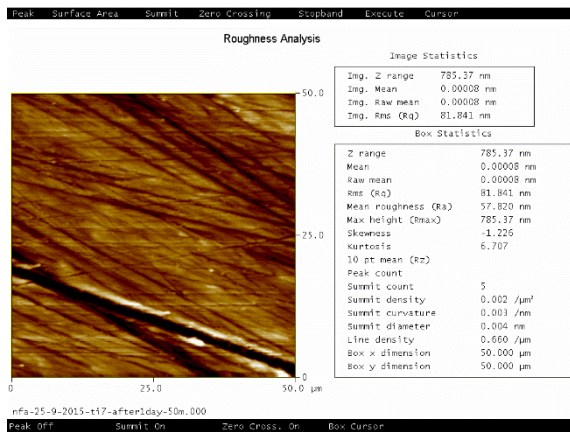
Figure 37.B: After the experiment (Titanium; distilled water sample)



5 μm

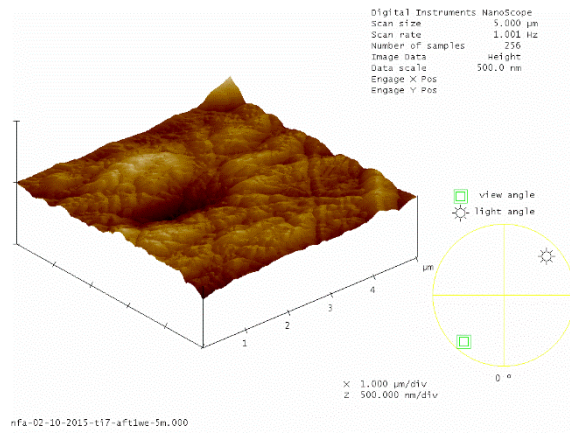
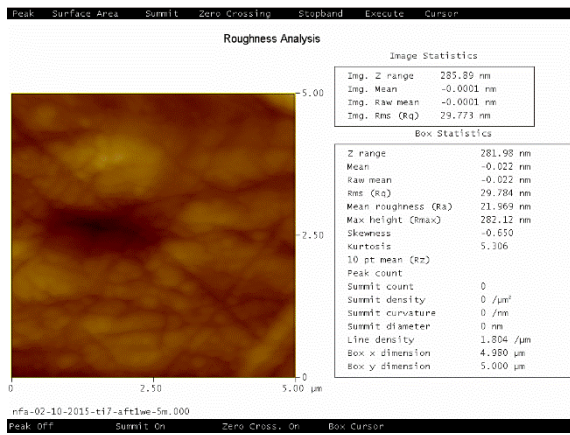


20 μm

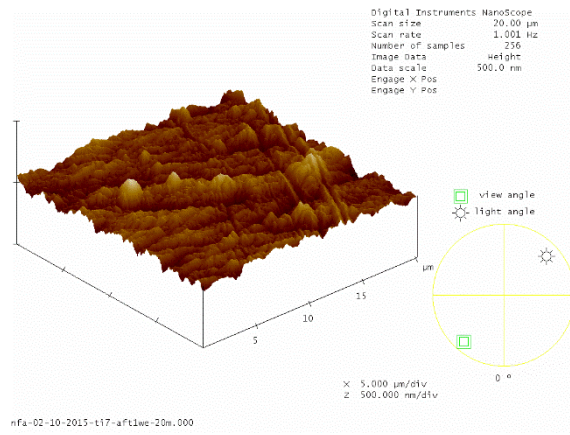
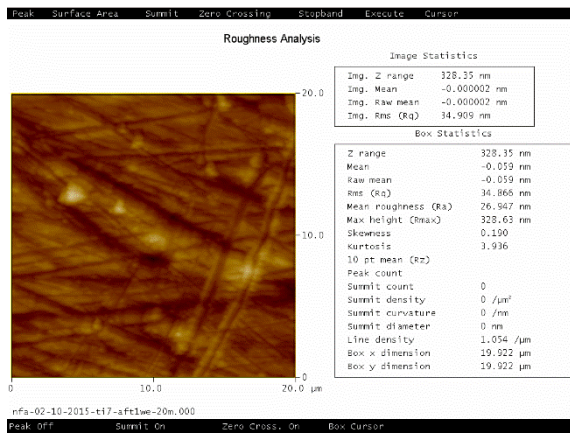


50 μm

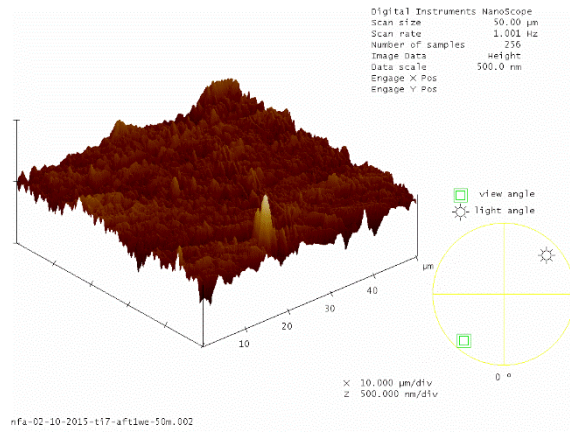
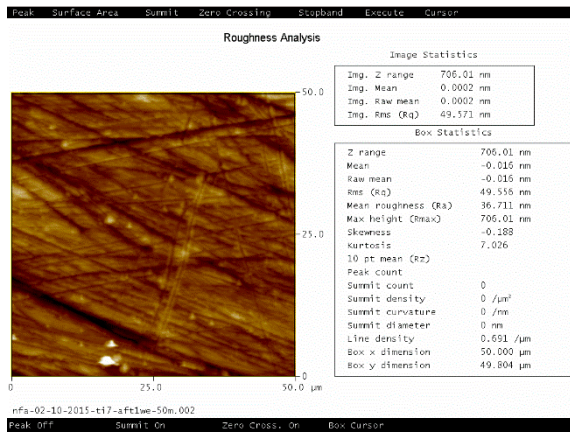
Figure 38.B: 1 day after the experiment (Titanium; distilled water sample)



5 μm

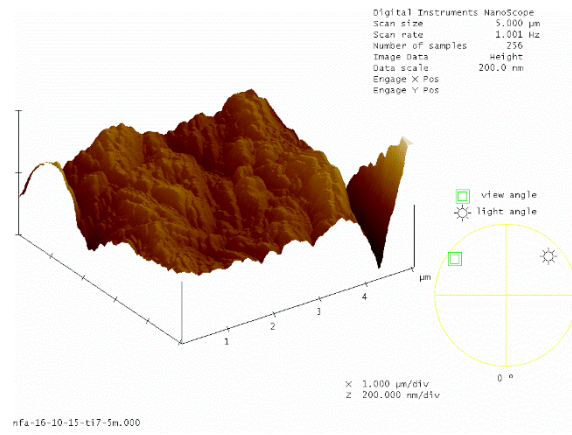
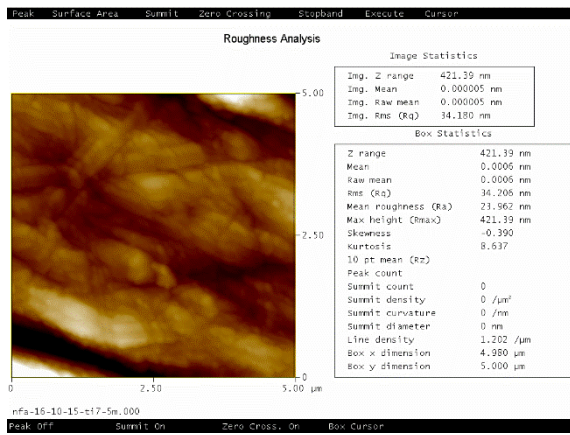


20 μm

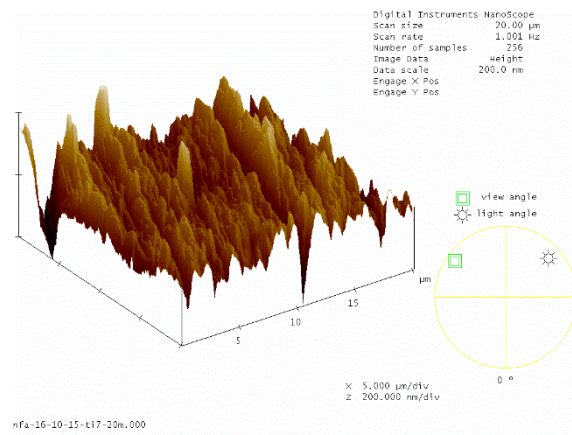
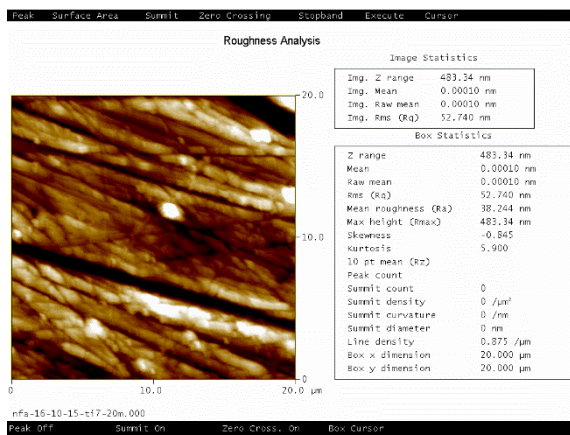


50 μm

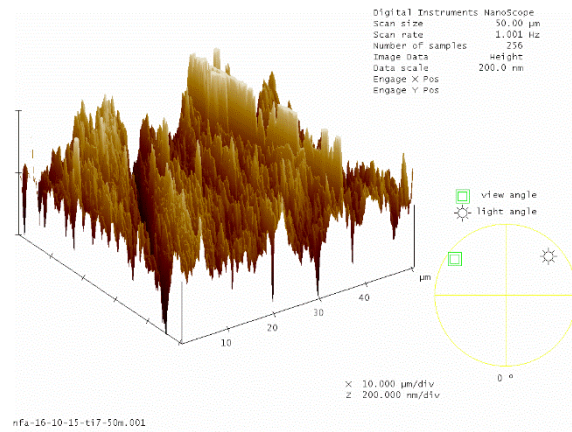
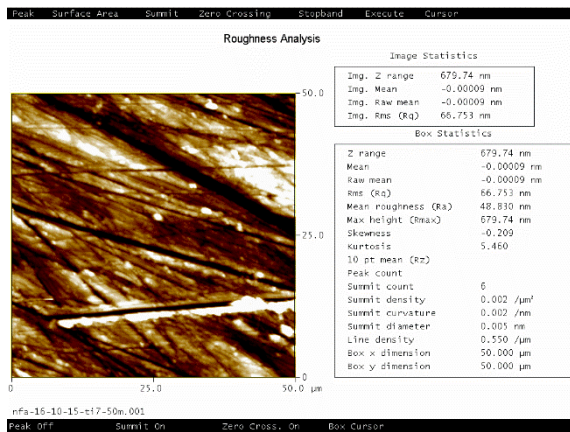
Figure 39.B: 1 week after the experiment (Titanium; distilled water sample)



5 µm

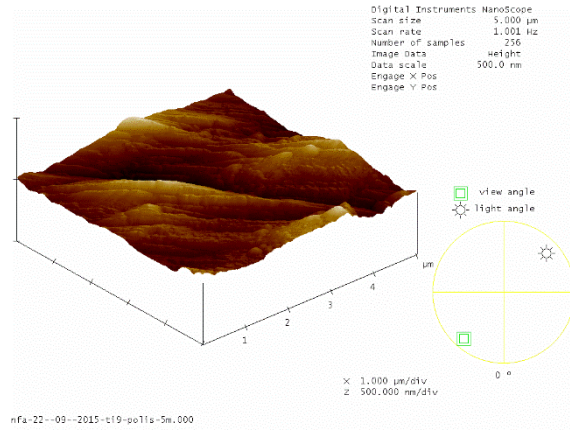
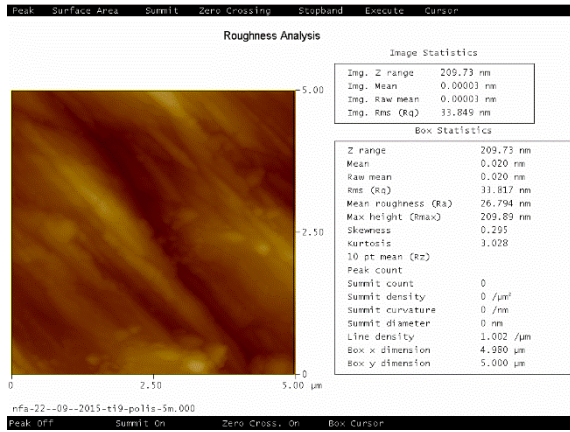


20 µm

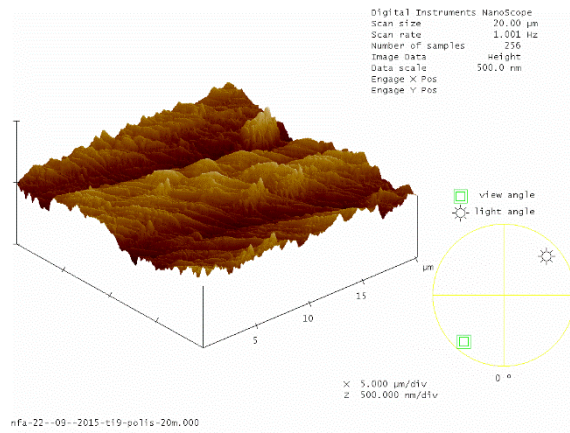
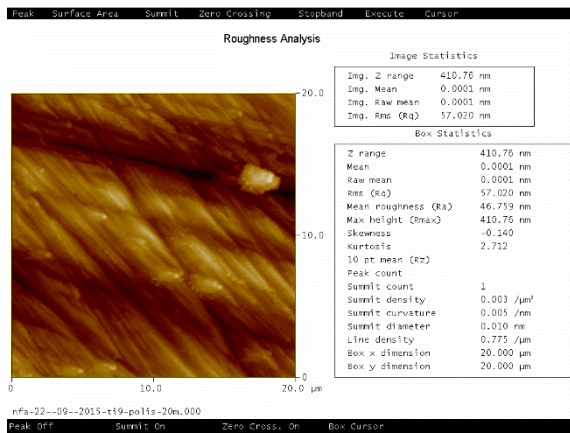


50 µm

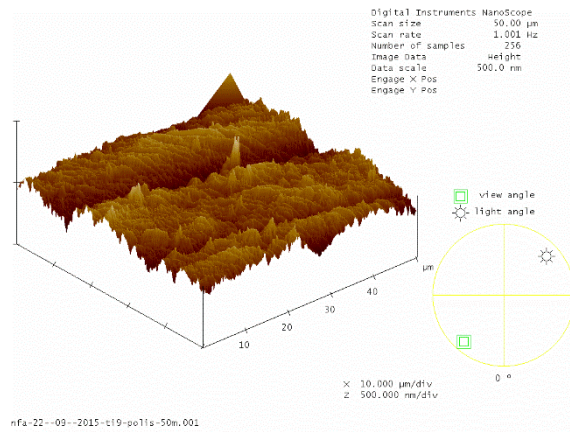
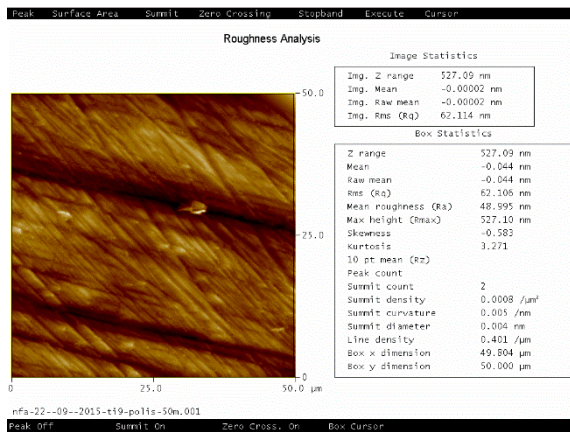
Figure 40.B: 2 weeks after the experiment (Titanium; distilled water sample)



5 μm

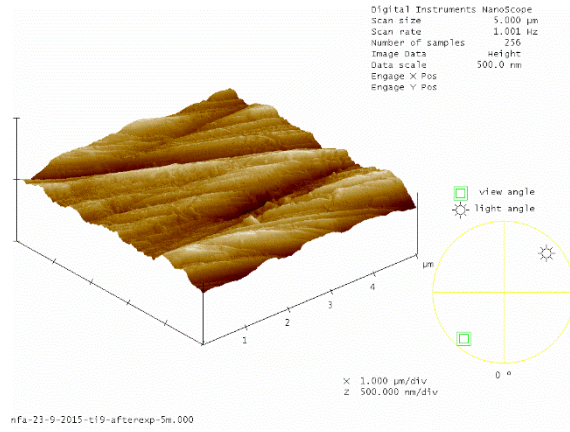
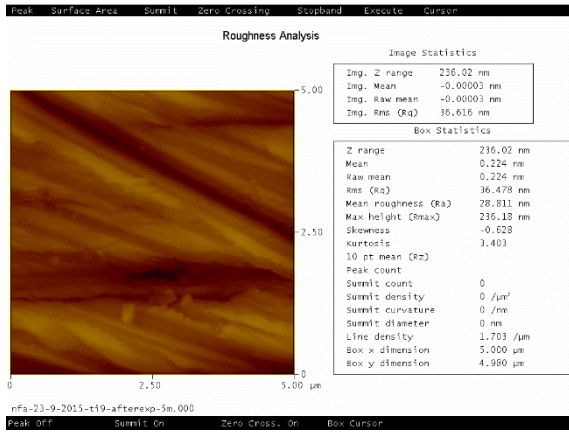


20 μm

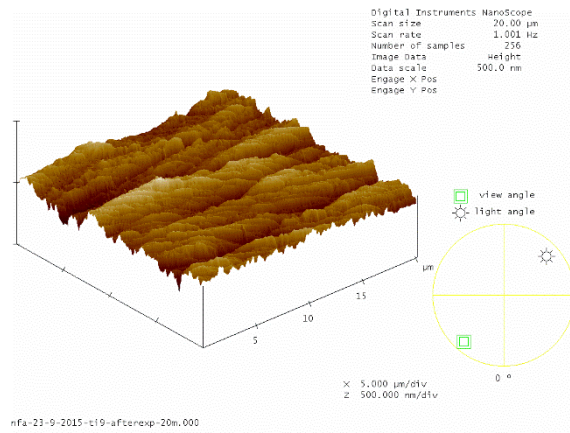
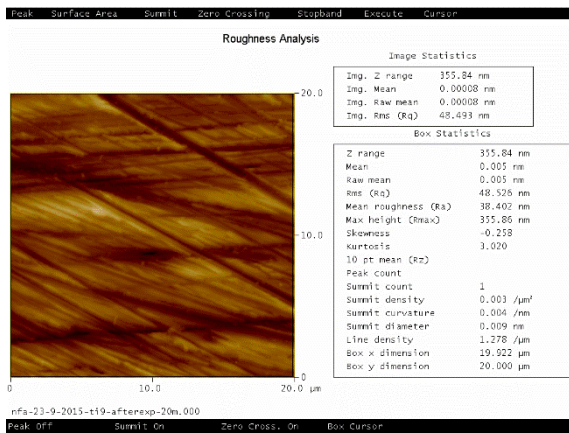


50 μm

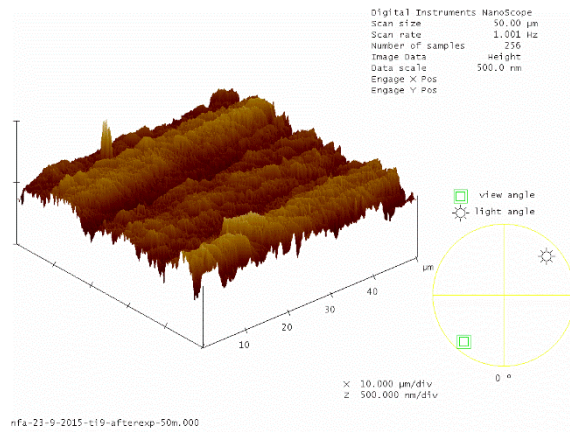
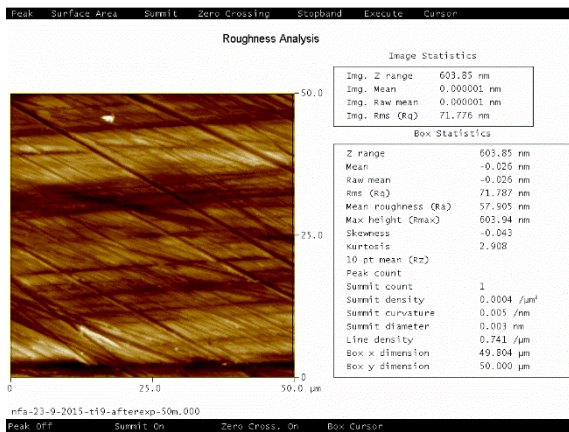
Figure 41.B: After polishing (Titanium; Tap water sample)



5 µm

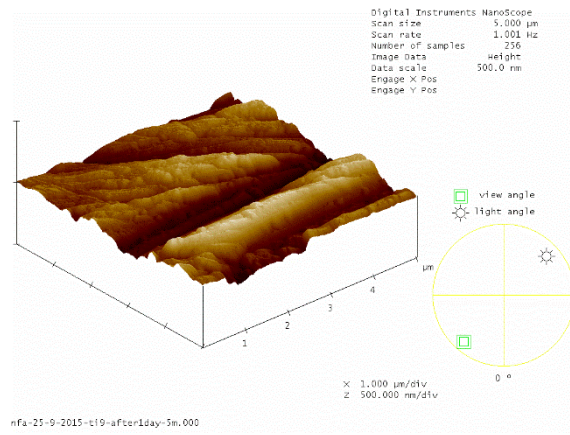
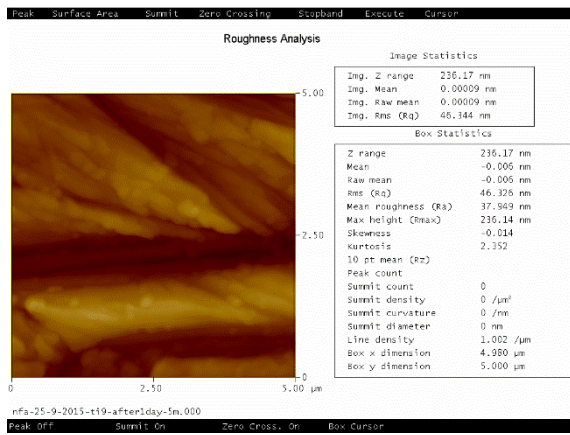


20 µm

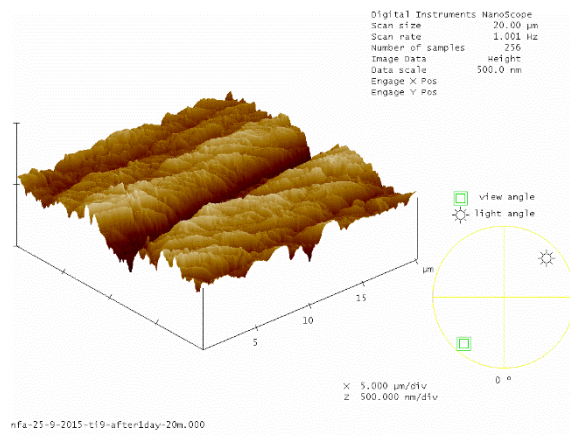
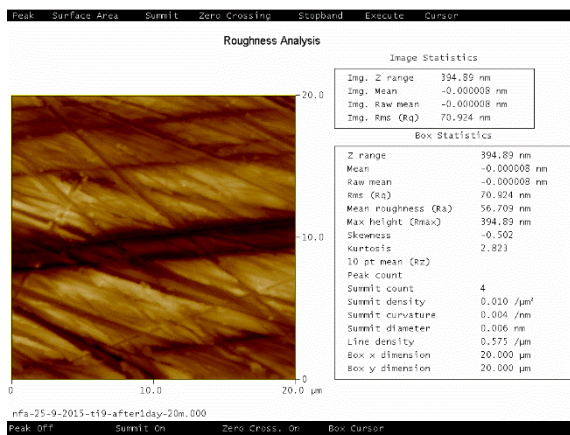


50 µm

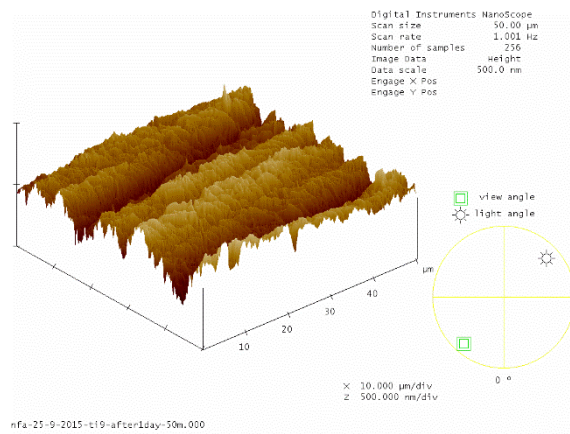
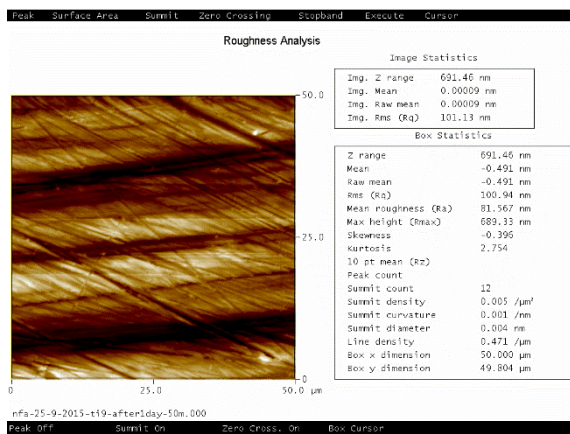
Figure 42.B: After the experiment (Titanium; Tap water sample)



5 μm

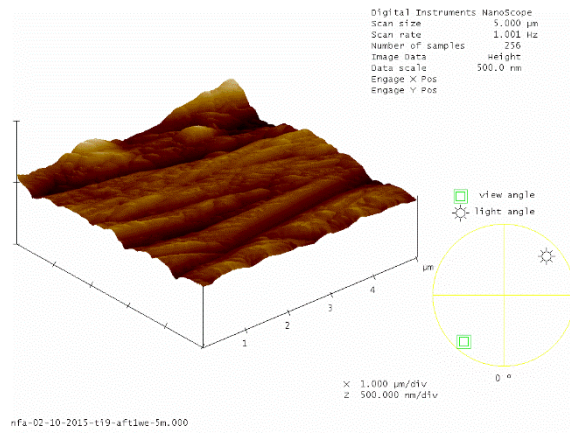
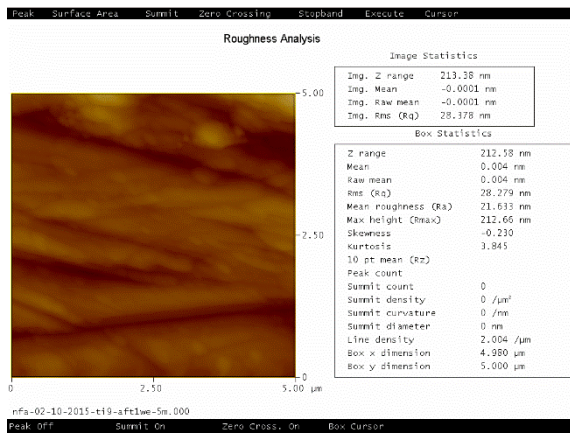


20 μm

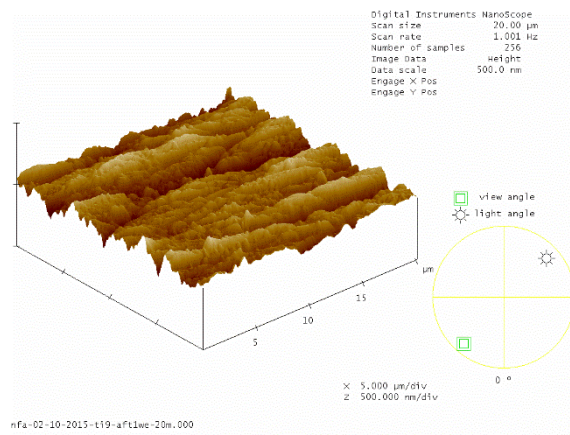
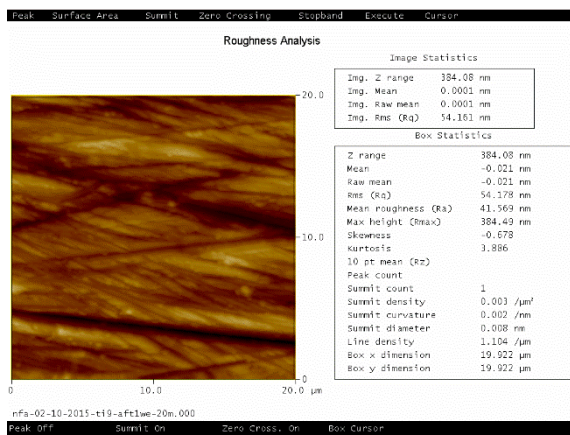


50 μm

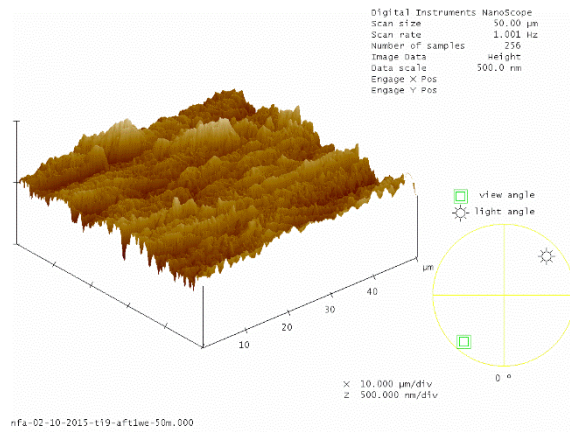
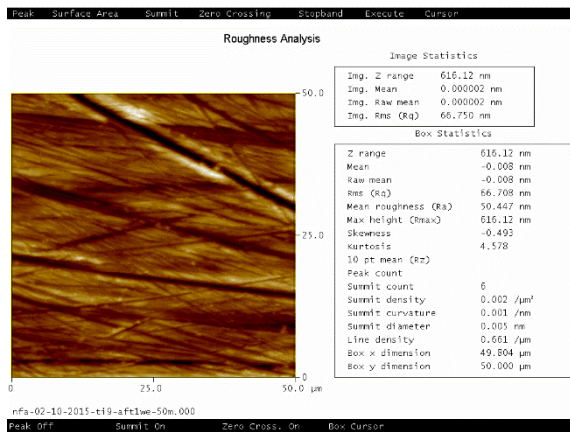
Figure 43.B: 1 day after the experiment (Titanium; Tap water sample)



5 μm

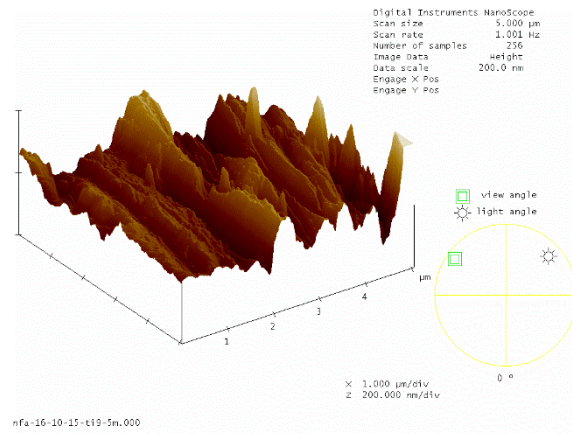
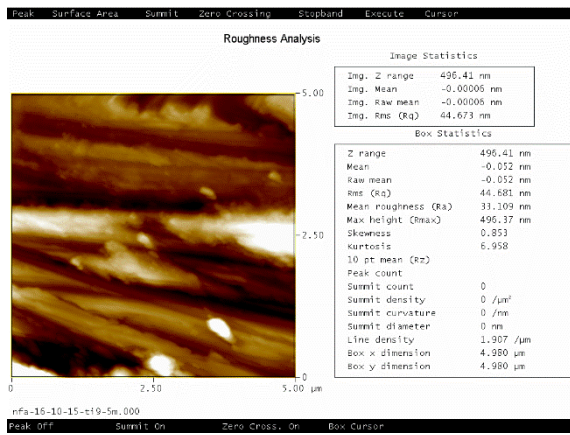


20 μm

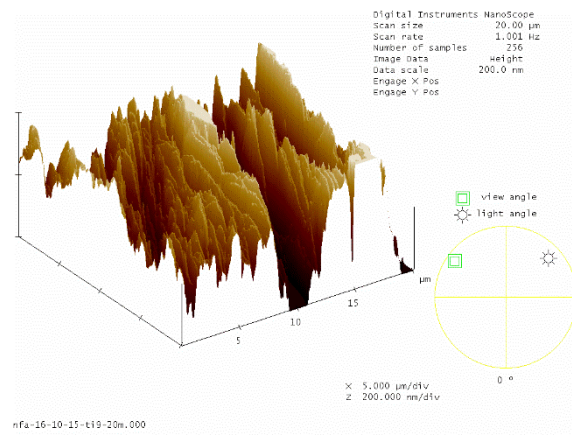
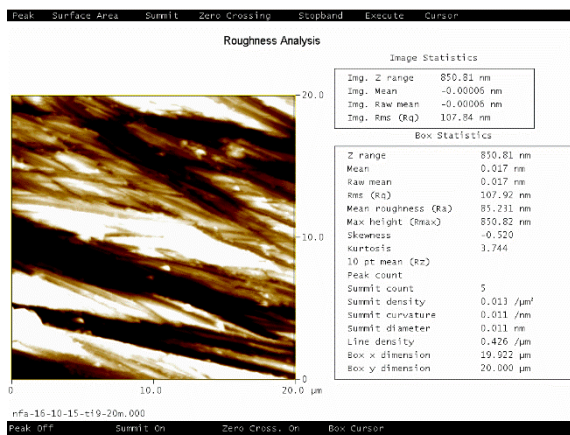


50 μm

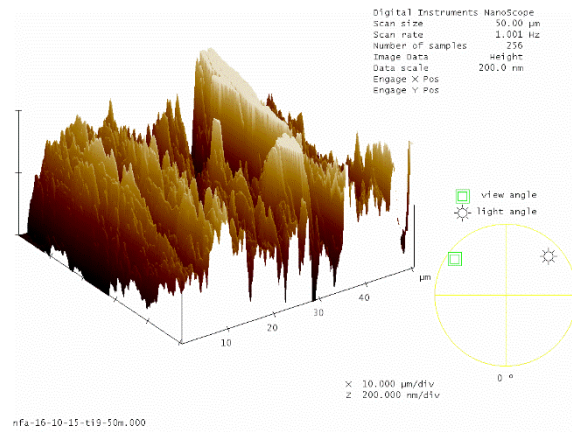
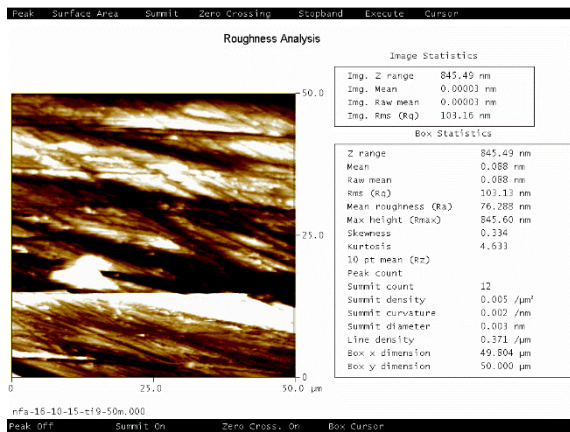
Figure 44.B: 1 week after the experiment (Titanium; Tap water sample)



5 µm

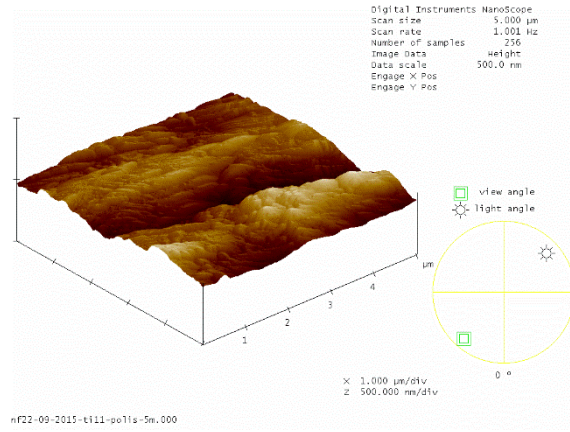
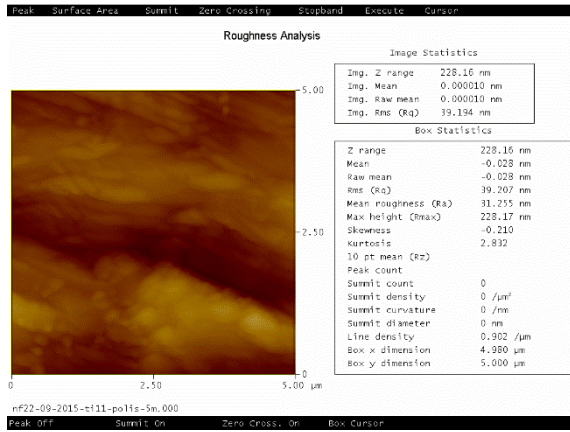


20 µm

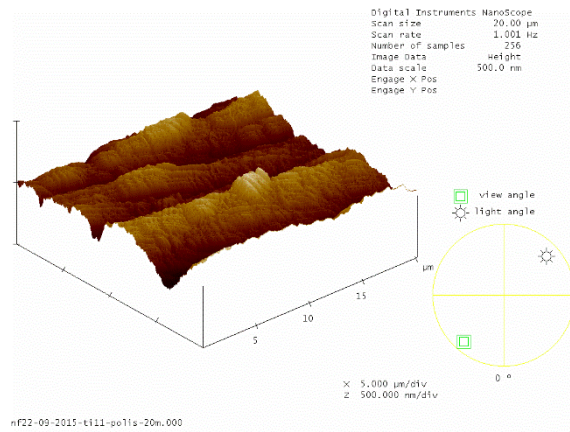
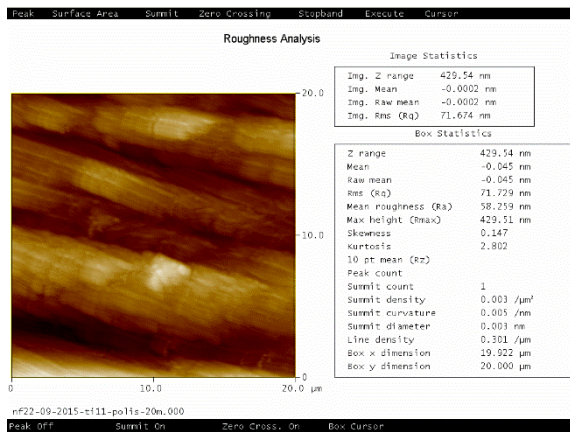


50 µm

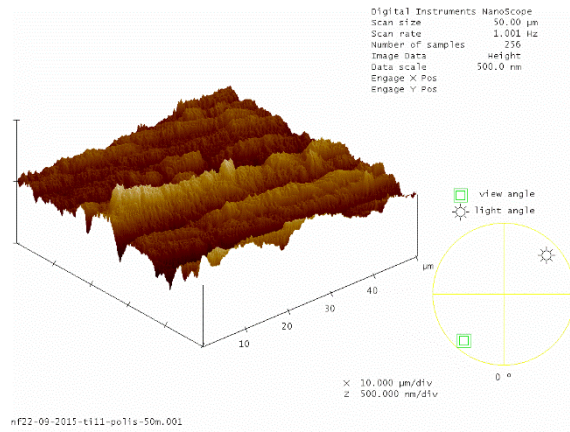
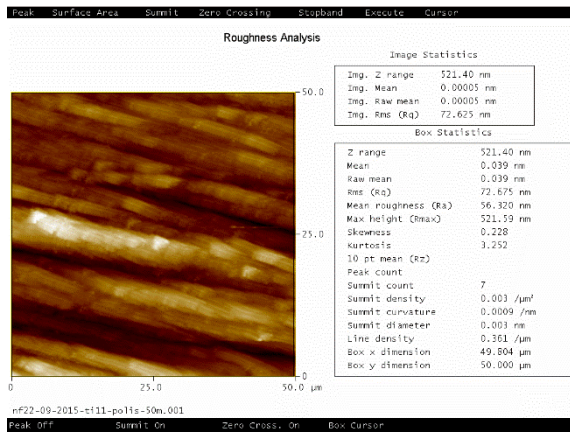
Figure 45.B: 2 weeks after the experiment (Titanium; Tap water sample)



5 μm

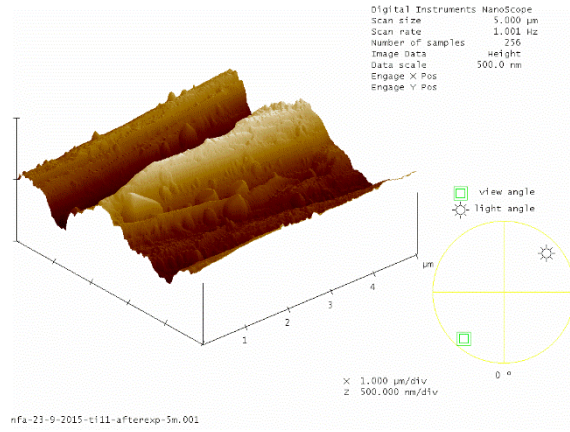
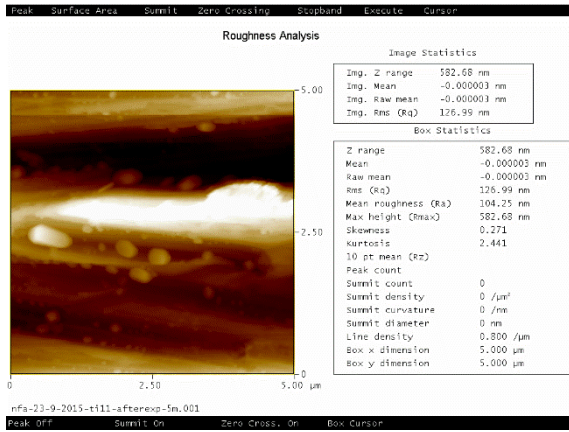


20 μm

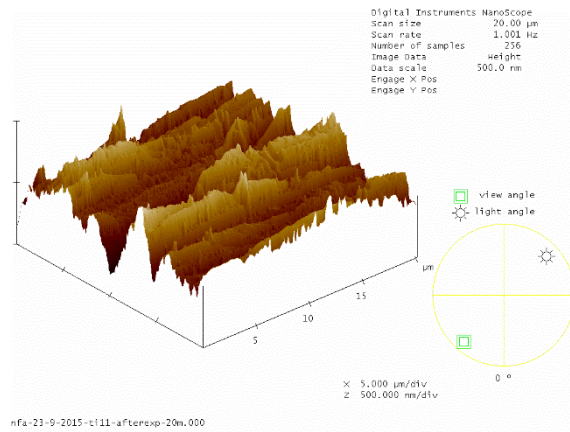
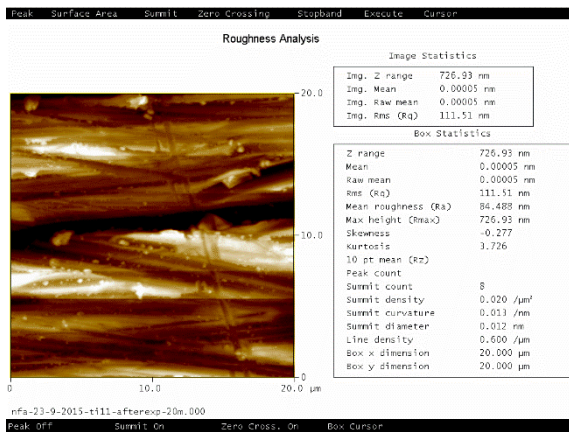


50 μm

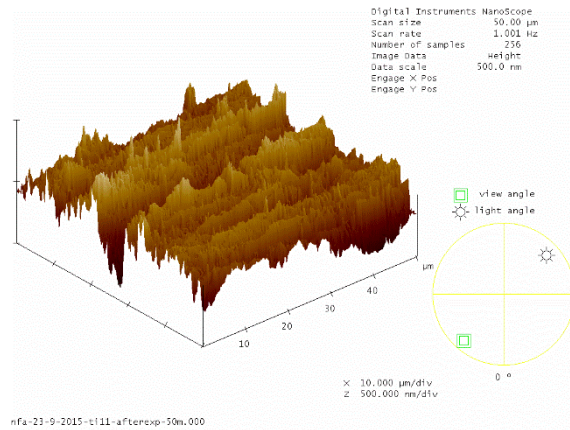
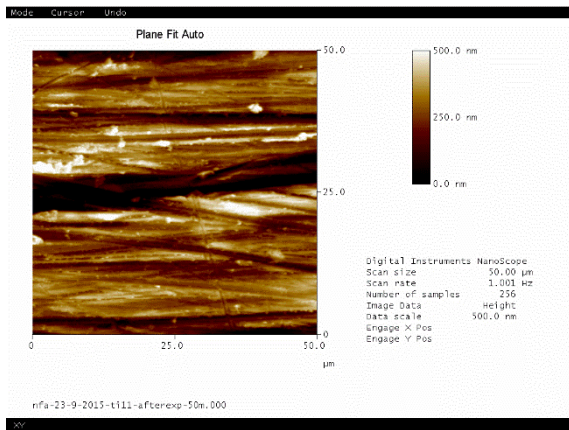
Figure 46.B: After polishing (Titanium; 0.9% saline sample)



5 µm

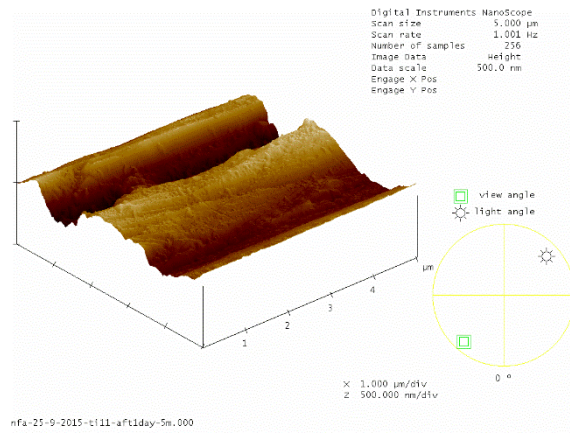
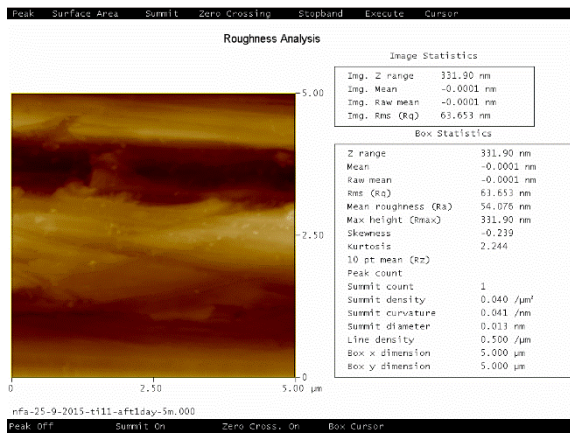


20 µm

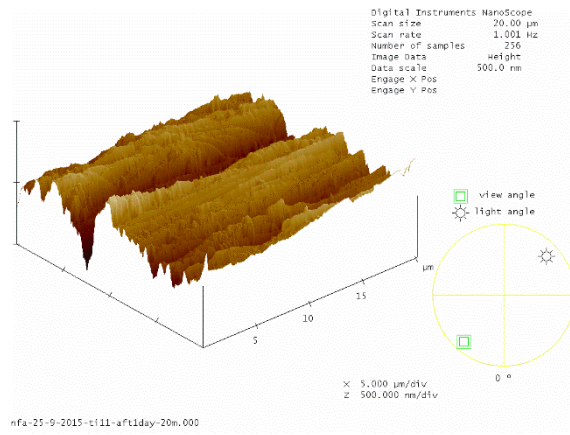
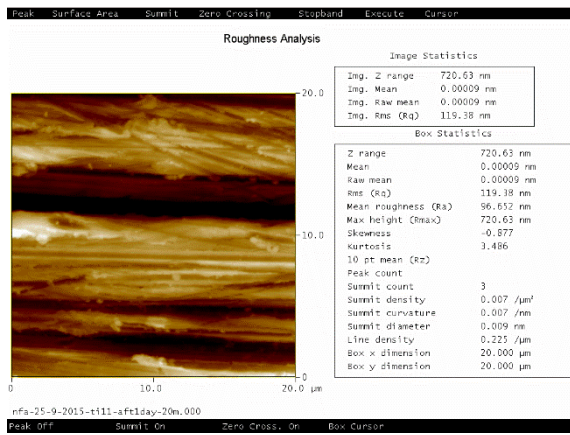


50 µm

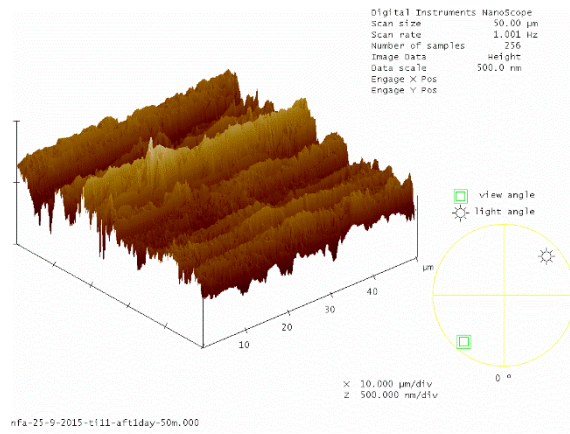
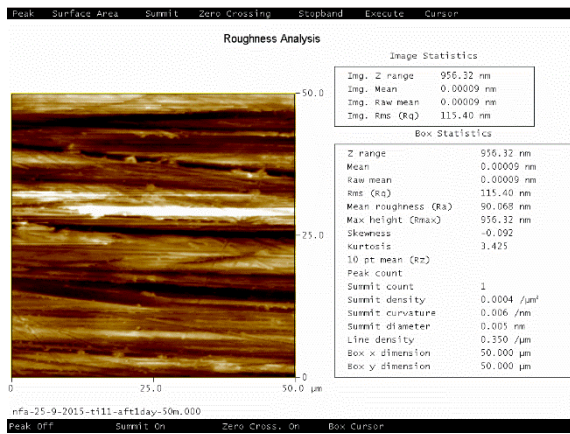
Figure 47.B: After the experiment (Titanium; 0.9% saline sample)



5 μm

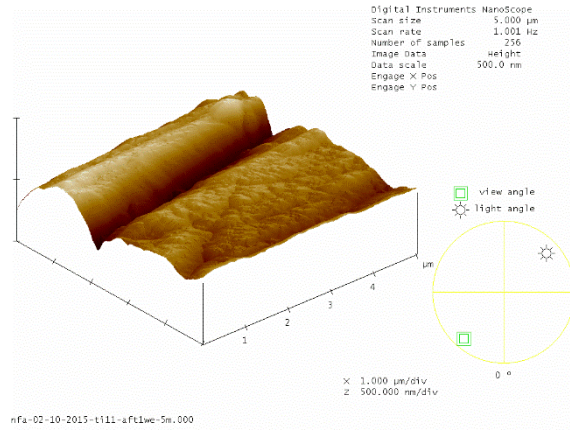
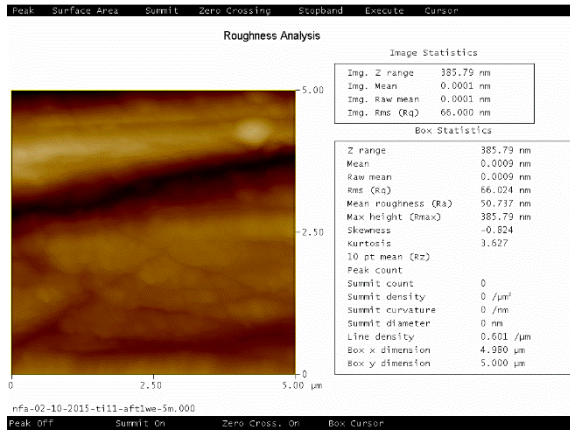


20 μm

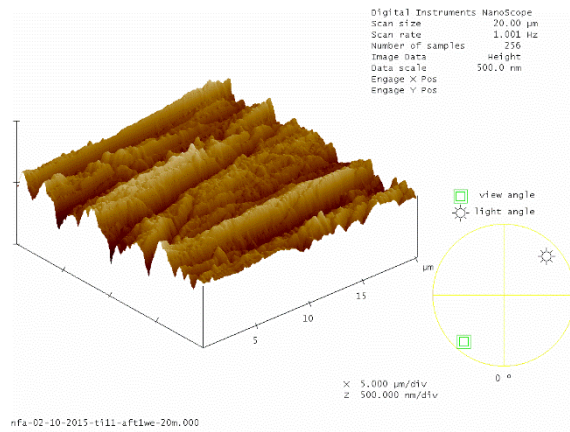
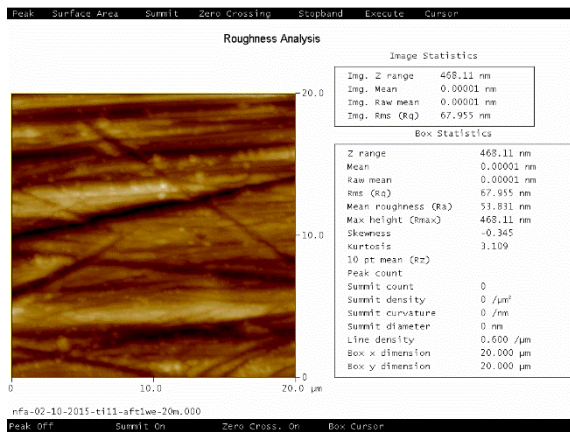


50 μm

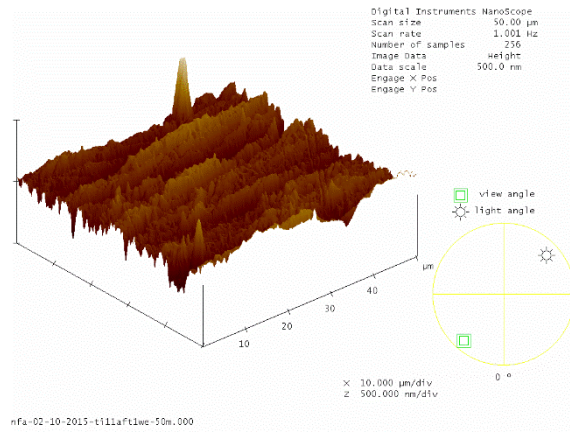
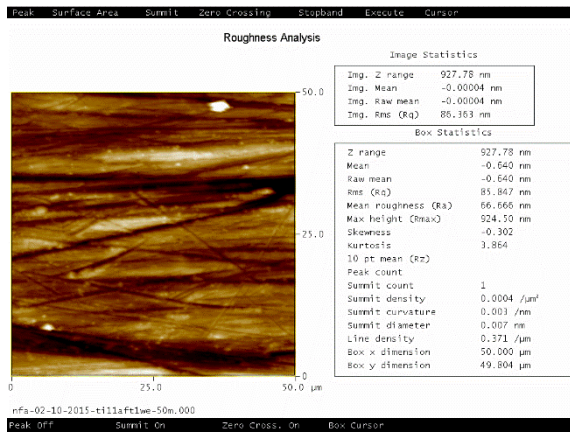
Figure 48.B: 1 day after the experiment (Titanium; 0.9% saline sample)



5 μm

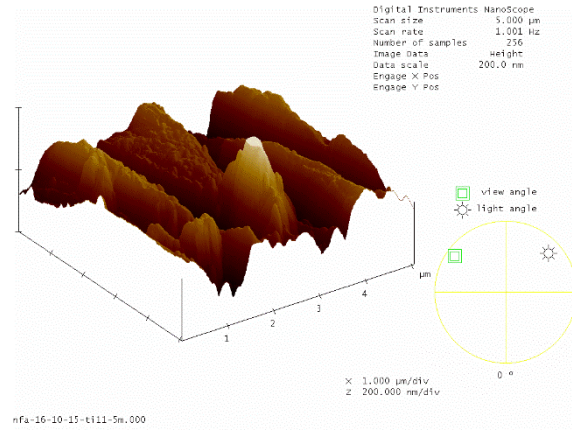
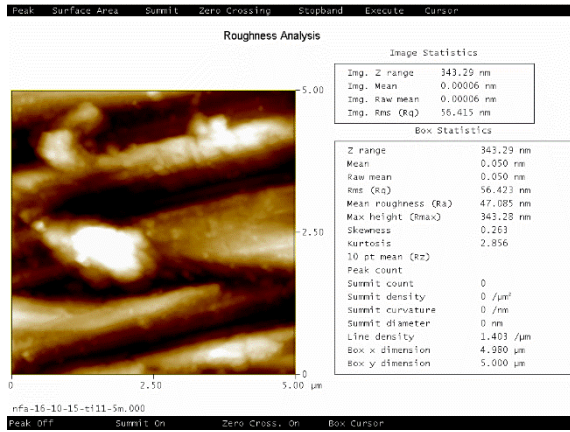


20 μm

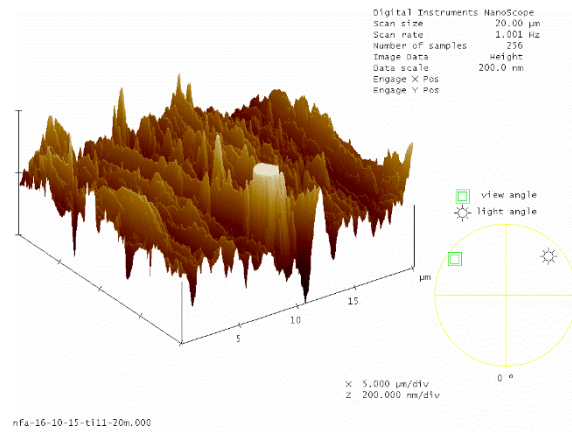
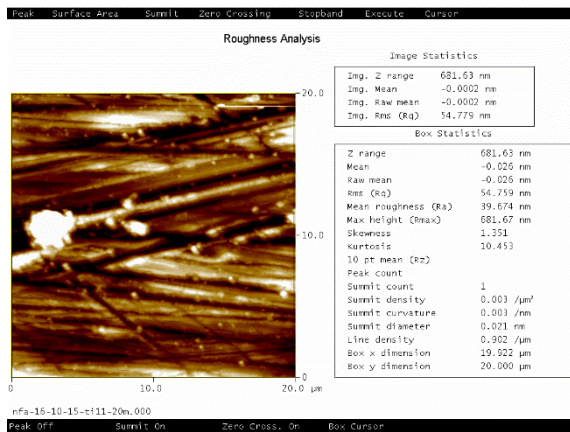


50 μm

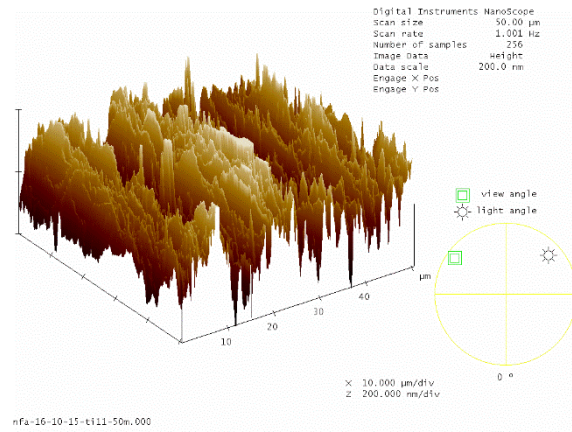
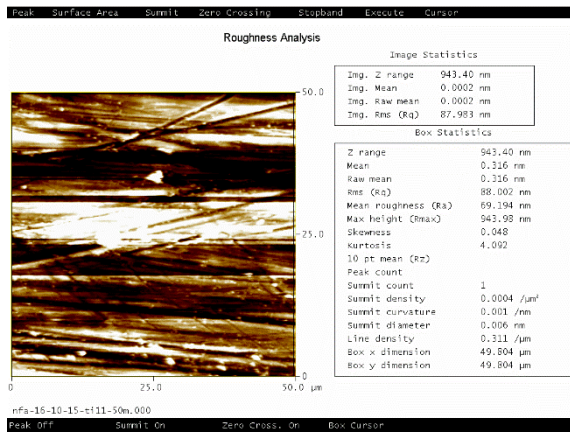
Figure 49.B: 1 week after the experiment (Titanium; 0.9% saline sample)



5 μm



20 μm



50 μm

Figure 50.B: 2 weeks after the experiment (Titanium; 0.9% saline sample)

Appendix C: Direct Microelectrode Method Data

- Cell growth medium

Table 1.C

Time (minute)	Human Coronary Artery Endothelial Cell Growth Medium (mV)	Human Osteoblast Cell Growth Medium (mV)
0	-269.6	-293
0.2	-266.5	-291.5
0.4	-265.2	-291.1
0.6	-269.2	-290.3
0.8	-268	-288.3
1	-266.5	-287.2
1.16	-265.7	-287.8
1.33	-266.6	-287.9
1.5	-268.7	-286.8
1.66	-269.8	-285.9
1.83	-269.3	-286.1
2	-267.4	-286.4
2.16	-268.9	-285.7
2.33	-270.6	-285.7
2.5	-269.1	-285.4
2.66	-268.6	-285.2
2.83	-268.7	-285.9
3	-268.4	-285.4
3.16	-269.7	-285.2
3.33	-268	-285.3
3.5	-266.1	-285
3.66	-267.8	-284.9
3.83	-270	-284.8
4	-267.8	-285.2
4.16	-267.8	-285
4.33	-269.6	-285.4
4.5	-268.4	-285.6
4.66	-269.6	-285.9
4.83	-268.5	-285.9
5	-267.2	-286.1
5.16	-269.5	-285.6
5.33	-270.7	-286.3
5.5	-269.8	-285.7
5.66	-269.1	-285.4
5.83	-270.1	-285.6
6	-269.7	-285.7

6.16	-269.1	-285.4
6.33	-269.8	-285.8
6.5	-269.9	-285.7
6.66	-270.4	-285.8
6.83	-271.1	-285.9
7	-271.3	-286.1
7.16	-269.9	-285.9
7.33	-269	-286
7.5	-269.7	-285.9
7.66	-269.6	-285.9
7.83	-270.7	-285.8
8	-270.7	-285.7
8.16	-270.9	-286
8.33	-271.5	-286
8.5	-269.4	-285.9
8.66	-269.7	-285.7
8.83	-270.4	-285.8
9	-270.7	-285.7
9.16	-270.7	-286.1
9.33	-268.4	-286.1
9.5	-268.7	-286.1
9.66	-268.9	-286.4
9.83	-269.5	-286.8
10	-268.8	-286.9

- Complete cultured human endothelial cells

Table 2.C

Time (minute)	1 st (mV)			2 nd (mV)			3 rd (mV)		
	0 hour	2 hours	10 hours	0 hour	2 hours	10 hours	0 hour	2 hours	10 hours
0	-260.1	-221.1	-214	-332.4	-307.2	-221.1	-244.2	-352.6	-283
0.16	-273	-227.5	-201.9	-279.3	-294.7	-254	-265.8	-347	-267.2
0.33	-266.5	-237.8	-201.3	-262	-285.5	-258.8	-268.5	-343.2	-262
0.5	-261.1	-243.4	-201.2	-257.2	-278.2	-258.4	-269.4	-341.9	-259.8
0.66	-256.6	-246.2	-201.8	-242.5	-272.5	-258.3	-269.5	-340.2	-257.7
0.83	-253.7	-247.9	-202.6	-231.7	-269	-257.1	-269.1	-338.5	-257.8
1	-252.2	-250.8	-203.2	-226.9	-266	-256.2	-269.8	-338.5	-254.5
1.16	-255.3	-249.4	-202.9	-230	-262.2	-255.4	-270.9	-338.9	-255.6
1.33	-247.8	-304.1	-202	-221.9	-259.6	-255.2	-271.6	-339.5	-256.5
1.5	-245.6	-278.4	-202.1	-216.2	-257.3	-254.8	-271.8	-339.6	-256.8
1.66	-250.9	-249.7	-202.8	-210.5	-253.3	-254.5	-272.1	-338.3	-256.6
1.83	-249	-252.1	-202.9	-214.3	-248.8	-254.1	-272.1	-338	-258.7

2	-248.1	-249.2	-249.5	-208.9	-248.6	-253.7	-272.3	-336.4	-261.1
2.16	-247.3	-250	-229.8	-211.1	-248.9	-253.1	-272.8	-335.6	-260.5
2.33	-246	-252	-217.3	-212.1	-244.7	-252.7	-265.9	-334.9	-262
2.5	-249.9	-251.4	-213	-205.2	-242.7	-252.5	-259.2	-333.4	-262.9
2.66	-246.2	-251.8	-210.6	-204.6	-242.4	-251.8	-259.9	-333.6	-264.3
2.83	-244.5	-251.6	-209.5	-201.5	-242.1	-250.9	-256.6	-332.4	-265
3	-243.8	-250.3	-209.4	-200.1	-241.5	-250.7	-254.5	-331.9	-266.7
3.16	-243.6	-251.9	-210.1	-198.4	-241.1	-250.8	-253.7	-332.3	-269.8
3.33	-243.5	-335.3	-210.1	-205.6	-241	-252.6	-254	-331.3	-276.2
3.5	-242.9	-319	-210.3	-214.5	-240.8	-252.8	-253.3	-331.5	-276.1
3.66	-242.6	-271.8	-209.8	-212.5	-240.5	-252.3	-253.7	-330.7	-275.3
3.83	-243.3	-262.1	-209.4	-213.1	-240.8	-252	-252.3	-330.4	-275.1
4	-250.3	-260.8	-208.5	-212	-240.7	-251.6	-251.7	-331	-275.4
4.16	-249.8	-332.3	-208	-208.4	-239.8	-251.4	-251.9	-330.3	-275
4.33	-244.2	-337.6	-207.2	-205.1	-239	-251.2	-250.7	-330.2	-274.8
4.5	-242.7	-286	-206.5	-202.9	-241	-251.2	-250	-328.8	-275.2
4.66	-243.1	-263.3	-206.2	-203.2	-240.4	-250.9	-251.2	-329	-275.7
4.83	-242.7	-282.3	-206.1	-204.2	-235.9	-250.6	-249.4	-329.3	-275.3
5	-243.3	-256.8	-206.1	-203.9	-235.3	-250.6	-251.6	-329	-275.5
5.16	-242.8	-289.5	-206.7	-204.1	-240.2	-250.4	-250.8	-327	-275.5
5.33	-241.9	-264.8	-206.9	-205.9	-244.4	-250.6	-258.1	-331.4	-275.3
5.5	-241.7	-251.8	-206.6	-208.4	-245.3	-250.4	-253.5	-326.9	-275.3
5.66	-241.1	-257.1	-206.8	-205.3	-240.8	-250.2	-252.1	-326	-275.4
5.83	-240.8	-256.7	-206.8	-204.3	-242	-250.1	-252	-328.7	-275.4
6	-239.8	-251.3	-206.8	-201.5	-241.3	-250.2	-251.1	-326.8	-275.5
6.16	-238.7	-251.6	-206.7	-206.5	-261.6	-250.2	-251.4	-328.4	-275.3
6.33	-238.3	-251.2	-206.6	-206.7	-265.8	-250.2	-251.7	-327.9	-275.5
6.5	-238.1	-252.3	-206.7	-206.4	-269.7	-250.3	-252.4	-330.7	-275.7
6.66	-237.2	-250.1	-206.4	-205.8	-288.3	-249.1	-251.8	-331.5	-275.8
6.83	-236.9	-250.4	-206.2	-205.4	-290.6	-249.5	-251	-332.2	-275.5
7	-236.4	-249.3	-206.5	-207.3	-295.1	-250.6	-251.4	-331.6	-276.9
7.16	-236.8	-249.8	-206.2	-208	-287.4	-250.8	-251.5	-335.5	-278.3
7.33	-235.9	-250.4	-205.7	-208.2	-281.1	-250.8	-251.6	-332.9	-278.4
7.5	-235.4	-250.8	-205.5	-214.5	-277.7	-250.9	-252.1	-336.6	-277.7
7.66	-234.6	-249.8	-205.5	-216.2	-274.5	-250.8	-253.8	-337.3	-250.1
7.83	-234.1	-250.3	-205.4	-213.6	-271.6	-250.7	-251.9	-335.9	-276.7
8	-233.7	-249.7	-205.6	-212.7	-271	-250.7	-251.6	-334.6	-278.2
8.16	-233.2	-250.5	-205.3	-212.1	-269.2	-250.8	-251.7	-334.9	-275.8
8.33	-233.8	-248.8	-205.5	-211.8	-263.3	-250.5	-253.2	-336.9	-275.2
8.5	-233.9	-249.6	-205.6	-211.1	-260.5	-250.2	-251.8	-336	-282
8.66	-232.6	-249.4	-205.4	-210.9	-259.1	-249.9	-251.2	-335	-275.9
8.83	-233	-249.5	-205	-211	-276.6	-249.6	-253.3	-336.2	-251.3
9	-233.1	-251.5	-205.2	-211.3	-280.3	-249.6	-253.2	-336	-243.6
9.16	-232.6	-252.7	-205	-210.9	-279.9	-249.4	-263.7	-334.4	-243.5

9.33	-232.1	-253.5	-204.6	-210.9	-279.5	-249.2	-260.4	-334.9	-243.7
9.5	-231.5	-251.6	-204.3	-210.4	-279.2	-248.4	-258.8	-335.8	-242
9.66	-231.1	-252.8	-204.4	-210.9	-279.3	-248.5	-256.7	-336.6	-241.5
9.83	-230.5	-252	-205.4	-211.4	-278.8	-249.1	-256.7	-342.9	-240.9
10	-230	-253.2	-205.9	-214.3	-279.1	-249.1	-257.6	-339.1	-238.8
10.16	-229.3	-252.2	-205.2	-213.6	-278.2	-249.1	-256.9	-336.5	-238.7
10.33	-228.7	-253.7	-204.7	-214	-278	-248.9	-257	-335.8	-237.6
10.5	-227.6	-253.4	-204.7	-212.2	-277.4	-248.7	-255.4	-387.1	-238.4
10.66	-227.4	-254	-205.2	-211.2	-276.8	-248.6	-254.5	-332.9	-238.8
10.83	-226.7	-253.9	-205.2	-212.2	-277	-248.4	-255.9	-335.1	-238.8
11	-226.6	-254.6	-205.5	-213	-277.3	-248.3	-254.5	-323	-239.8
11.16	-226.7	-248.5	-205.9	-213.9	-277.2	-248	-254	-321.2	-237.7
11.33	-225.5	-251.2	-205.7	-212.9	-276.8	-247.9	-252.5	-320.2	-238.4
11.5	-225.9	-252.8	-205.5	-212.4	-276.4	-247.7	-252.1	-318.3	-237.8
11.66	-225.3	-252.8	-205.6	-212.1	-276.1	-247.8	-252.8	-320.2	-236.2
11.83	-225.8	-252.2	-205.6	-211.2	-275.8	-247.7	-253.1	-320.3	-235.9
12	-225.5	-251.9	-205.5	-211.4	-275.4	-247.6	-252.8	-318.9	-238.3
12.16	-225.2	-254	-205.7	-212.5	-275	-247.4	-251.9	-321.4	-238
12.33	-225.1	-253.4	-206.6	-213.4	-274.5	-247.4	-251.2	-321	-237.2
12.5	-224.8	-252.3	-206.6	-214.2	-274.3	-247.4	-251.3	-323.2	-236.9
12.66	-223.8	-252.1	-206.3	-213.2	-274.2	-247.3	-251.2	-322.2	-239.3
12.83	-223.3	-253.5	-207	-214.2	-274.1	-247.2	-252.1	-321.7	-237.9
13	-223	-250.3	-207.3	-214	-274.1	-247.2	-251.7	-320.9	-237.4
13.16	-222	-252.6	-207.4	-215.4	-274.2	-247.1	-251	-320.8	-239.3
13.33	-222.1	-252	-207.9	-215.8	-274.1	-246.9	-250.2	-320.2	-236.8
13.5	-222.2	-251.7	-208.4	-336.9	-273.8	-247	-251.1	-319.2	-236.4
13.66	-221.8	-250.9	-207.9	-322.6	-273.6	-247.1	-251.2	-318.2	-236.2
13.83	-221.7	-253	-207.4	-273.9	-273.2	-247	-251.3	-318.6	-235
14	-221.1	-252.5	-207.5	-275.6	-273	-246.9	-252.6	-319.3	-235.5
14.16	-220.9	-253.5	-207.4	-281.1	-272.9	-246.7	-253.5	-318.2	-236.2
14.33	-220.2	-252.9	-208	-255.8	-272.5	-246.4	-251.7	-320.4	-235.5
14.5	-219.8	-259.5	-208.1	-242.6	-272.4	-246.3	-253.2	-318.9	-234.5
14.66	-218.3	-243.3	-208.2	-236.2	-272.1	-246.1	-252	-319	-234.4
14.83	-222.8	-240.8	-208.4	-231.5	-271.8	-245.8	-252.2	-318.4	-235.1
15	-251.3	-240.3	-208.3	-228.7	-271.6	-245.6	-253.1	-317.1	-248.9



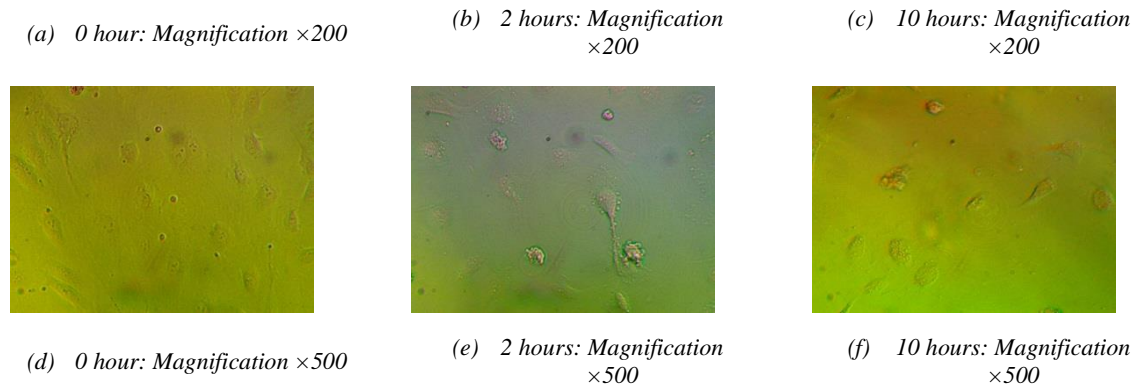


Figure 1.C: Human coronary artery endothelial cells in different timing and magnifications for the 2nd experiment

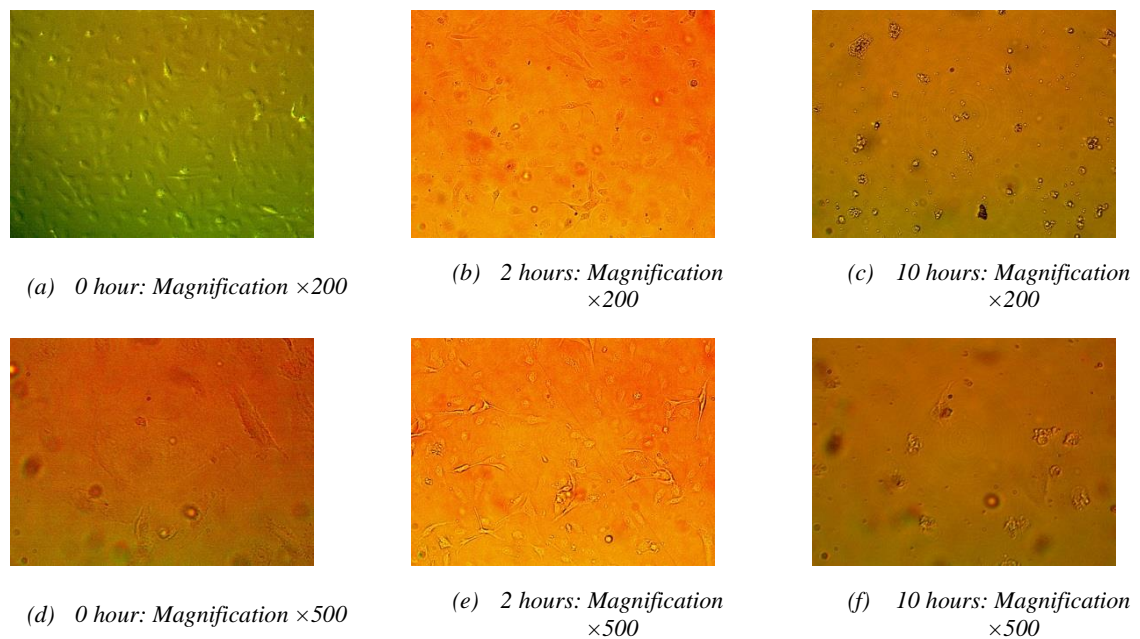


Figure 2.C: Human coronary artery endothelial cells in different timing and magnifications for the 3rd experiment

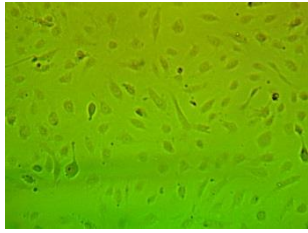
- Half cultured human endothelial cells

Table 3.C

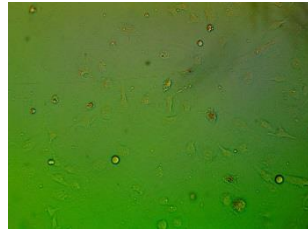
Time (minute)	1 st (mV)			2 nd (mV)			3 rd (mV)		
	0 hour	2 hours	10 hours	0 hour	2 hours	10 hours	0 hour	2 hours	10 hours
0	-306.7	-376.1	-299.8	-326.5	-391.2	-229.4	-315.3	-361.4	-311.1
0.16	-327.8	-370.1	-306.7	-327.8	-381.8	-250.3	-304.3	-357.5	-287.3
0.33	-325.5	-364.2	-304.7	-328.4	-371.6	-249.2	-300.3	-351.8	-284.2
0.5	-324.3	-360.4	-289.4	-327	-365.7	-247.5	-297.2	-350.1	-284.2
0.66	-332.4	-357.8	-294.2	-323.8	-362	-246.9	-293.3	-351.5	-292

0.83	-323.3	-355.8	-292.3	-323.3	-359.6	-245.7	-292.8	-350	-286
1	-320.2	-354.6	-291.3	-322.3	-356.9	-245.6	-295.9	-348.2	-285.6
1.16	-318.3	-353.9	-288.7	-321.4	-353.5	-244.4	-294.4	-347.3	-285.4
1.33	-316.8	-353.9	-290	-321.6	-351.8	-243.5	-292.7	-347	-283.5
1.5	-315.5	-354.2	-291.9	-321.1	-349.2	-242.7	-292.2	-345.7	-288
1.66	-315.1	-356.7	-290.3	-320.5	-346.5	-242.5	-293.1	-343.4	-296.8
1.83	-314.6	-356.2	-283.2	-320.7	-343.8	-242.2	-297.1	-341	-298.1
2	-314.2	-356	-277.2	-325.5	-341.6	-242.1	-298.9	-340.6	-298.5
2.16	-317.1	-356.2	-270.9	-327.5	-339.6	-241.7	-298.1	-339.6	-297.8
2.33	-316.4	-355.9	-264.3	-324.2	-337.6	-240.9	-297.4	-338	-298.2
2.5	-315.1	-357.9	-261	-321.1	-336	-241.5	-297.3	-336.7	-299.8
2.66	-313.5	-360.6	-254.8	-320.7	-335.7	-242.2	-297.2	-336.1	-297.9
2.83	-357.8	-355.8	-252.8	-319.7	-339.1	-242.2	-298.6	-335.4	-296.3
3	-334.6	-354.9	-251.4	-319.3	-342.3	-242.3	-296.9	-334.6	-292.2
3.16	-324.2	-360.6	-252.3	-319.6	-340	-239.7	-298.8	-333.2	-294
3.33	-325.5	-355.2	-249	-319.6	-341.3	-238.8	-299.1	-332.3	-293
3.5	-319.7	-354.7	-257.3	-319.3	-341	-239.3	-301	-334.6	-291.5
3.66	-317.4	-354.6	-251.5	-318.7	-341	-239.4	-300	-335.3	-289.7
3.83	-321	-354.7	-250.2	-319.3	-341.7	-239	-301.1	-335.5	-287.6
4	-315.1	-353.6	-246.8	-318.9	-340.3	-239.2	-317.8	-335.1	-288.9
4.16	-314.1	-353.1	-251.1	-318.5	-339.6	-238.1	-303.9	-334.5	-287.9
4.33	-313.1	-353.4	-251.4	-318.3	-339.3	-238.2	-311.2	-335.6	-286.2
4.5	-314.6	-352.9	-251.4	-321.8	-338.3	-237.9	-308.9	-335.9	-284.8
4.66	-313.8	-352.6	-250.2	-320.2	-338.8	-237.4	-307.2	-335.1	-284.5
4.83	-312.8	-352.4	-249	-356.7	-338.2	-237.4	-306.2	-335.7	-285.9
5	-317.2	-352.2	-237.8	-345.6	-338	-238	-305.3	-335.6	-285.4
5.16	-318.1	-352	-247.5	-335.4	-337.7	-237.5	-303.5	-334.7	-286.2
5.33	-315.2	-351.7	-250.6	-330.9	-337.4	-237.6	-302.1	-333.8	-283.6
5.5	-314.1	-351.4	-245.9	-328.3	-337.1	-236.3	-301.5	-333	-286.6
5.66	-325.7	-350.9	-249.1	-341.6	-336.8	-236.5	-300.2	-333.1	-285.9
5.83	-317.9	-350.6	-246.8	-332.3	-337	-235.9	-300.8	-333.4	-286.2
6	-314.7	-350.2	-248.5	-328.6	-336.5	-236.8	-300	-335.1	-290.5
6.16	-314.1	-350.4	-253.3	-326.5	-336.4	-236.8	-301.6	-335.6	-290.8
6.33	-311.9	-351.1	-247.6	-324.6	-336.4	-234.7	-304.5	-335.3	-290.6
6.5	-310.8	-352.2	-250.6	-323.5	-336.1	-235.7	-307.1	-333.8	-289.9
6.66	-310.3	-352.7	-252.2	-322.3	-335.7	-235.9	-305.4	-333	-294
6.83	-310	-368.4	-251.8	-321.4	-335.7	-236.1	-303.8	-332.2	-295.3
7	-309.5	-359.3	-248.7	-321.2	-335.5	-236.8	-303.6	-331.3	-296.3
7.16	-326	-357.3	-248.7	-320.7	-335.3	-236.3	-302.6	-332	-296.4
7.33	-317.6	-358.6	-248.5	-320.2	-335.2	-235.9	-301.7	-331	-298.6
7.5	-313.8	-358.6	-251.2	-320	-334.8	-235.4	-302.1	-331	-298.5
7.66	-312.3	-356.8	-249.7	-319.4	-335	-235.8	-297.9	-331.8	-297.6
7.83	-311.6	-341.9	-248.9	-318.9	-334.6	-235.8	-301.6	-330.9	-297.3
8	-311.1	-340.2	-250.2	-318.6	-334.7	-235.9	-302.1	-329.3	-297.8

8.16	-311	-337.9	-247.9	-318.5	-334.5	-236	-301.7	-328.8	-299.2
8.33	-310.7	-335.8	-252.1	-318.4	-334.3	-236.4	-302	-328.3	-304.3
8.5	-310.7	-333.9	-249.3	-318.3	-334.2	-232.2	-301.7	-328.7	-301.8
8.66	-310.6	-331.9	-249.5	-318.1	-333.6	-232.1	-301.4	-328.2	-300.2
8.83	-310.3	-330.3	-251.8	-318.1	-335.6	-232.5	-301.7	-328.1	-302.2
9	-310.3	-328.1	-249	-317.8	-332.8	-233	-301.3	-328.6	-301.1
9.16	-310.3	-325.8	-246.1	-317.6	-334.4	-233.7	-301.6	-328.2	-299.8
9.33	-309.9	-324	-254.4	-317.6	-335.3	-234.8	-301.8	-328.4	-298.8
9.5	-309.8	-344.7	-257.3	-317.5	-334.8	-236.3	-301.5	-326.8	-298
9.66	-317	-345	-257.7	-317.3	-333.7	-236.1	-300.9	-329.4	-297.5
9.83	-331.9	-343.6	-258.7	-317.4	-334.6	-236.6	-300.3	-330	-296.6
10	-326.4	-342.9	-255.3	-317.4	-333.8	-236.6	-300.8	-329.4	-297.2
10.16	-317.2	-342.4	-253.4	-317.3	-333.7	-236.7	-301.4	-330	-299.3
10.33	-315.7	-341.8	-255	-317.1	-333.8	-237.3	-302.4	-334.5	-299.7
10.5	-318.7	-341.1	-256.1	-317.3	-333.1	-222.4	-303.1	-333.5	-299.2
10.66	-313.6	-340.6	-252.1	-317.2	-332.9	-220.8	-303.4	-333.4	-298.3
10.83	-309	-340.3	-252.6	-317.1	-332.8	-215.5	-304	-332.2	-301
11	-313.8	-339.8	-250.8	-317	-332.4	-214.8	-301.1	-334.7	-295
11.16	-311.2	-339.4	-251.5	-316.9	-333.5	-213.6	-299.9	-334.3	-288.7
11.33	-310.4	-339.4	-250.4	-316.8	-332.8	-213.4	-300.5	-331.7	-285
11.5	-328.5	-339.1	-253.7	-316.7	-332.8	-214	-300	-332.8	-285.6
11.66	-325.4	-338.9	-254.7	-316.7	-332.6	-224.4	-298.5	-332.4	-284.8
11.83	-314	-340.4	-258.2	-316.7	-332.1	-213.5	-299.4	-332.6	-283.4
12	-322.3	-343.2	-254.9	-316.7	-332.3	-211.1	-298.7	-332	-282.4
12.16	-316.5	-356.3	-254	-316.5	-332.3	-211.5	-298.8	-331.2	-282.2
12.33	-312	-354.3	-252.1	-316.4	-332	-209.8	-297	-331.5	-282.2
12.5	-310.2	-353.1	-253.1	-316.2	-332.2	-209.7	-299.8	-334.5	-281.3
12.66	-309.5	-349.8	-254.9	-316.2	-332.1	-212.6	-298.9	-352.4	-280.3
12.83	-336.4	-348.2	-256.9	-316	-332.3	-210.2	-298.3	-344.5	-279.2
13	-356.1	-345.5	-255.8	-315.6	-332.7	-212.3	-299	-340	-281.1
13.16	-341.8	-346.5	-255	-315.3	-332.7	-212.3	-303.6	-336.8	-282.8
13.33	-340.7	-344.2	-255.7	-315.8	-333.4	-214	-301.5	-333.2	-282.7
13.5	-329.4	-343.1	-253.2	-316.2	-332.8	-212.8	-301.4	-331.5	-281.4
13.66	-324.4	-342.5	-255	-316.1	-332.7	-212.1	-302.6	-328.7	-279.9
13.83	-318.5	-341.2	-255.3	-316.1	-332.8	-211.7	-303.3	-327.8	-279.5
14	-327.4	-339.8	-255.7	-316.4	-332.8	-210.4	-299.7	-327	-279
14.16	-325.4	-338.8	-256.9	-316.4	-332.7	-215	-298.2	-326.4	-279.7
14.33	-321.8	-338.1	-258.8	-316.3	-332.7	-213.5	-298.5	-326.1	-279.5
14.5	-331.1	-338.1	-257.8	-316.2	-332.4	-212.2	-297.3	-325.5	-280.6
14.66	-322.5	-337.5	-253.3	-316.9	-332.6	-212.4	-297.7	-325.5	-278.7
14.83	-311.7	-336.6	-255.9	-316.4	-332.8	-212.1	-298.2	-324.2	-284.6
15	-324.3	-335.8	-255.1	-316.4	-332.6	-212.7	-297.3	-325.9	-284.4



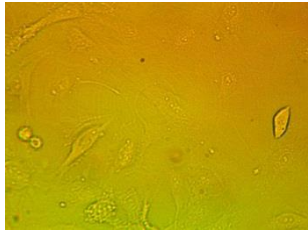
(a) 0 hour: Magnification $\times 200$



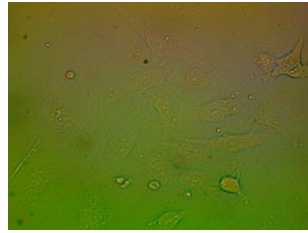
(b) 2 hours: Magnification $\times 200$



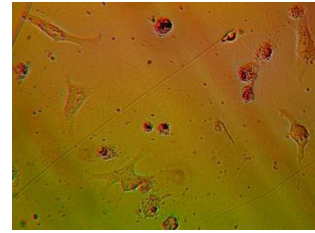
(c) 10 hours: Magnification $\times 200$



(d) 0 hour: Magnification $\times 500$

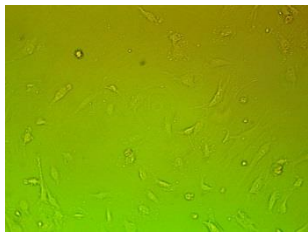


(e) 2 hours: Magnification $\times 500$

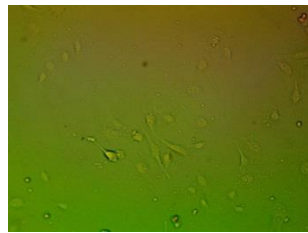


(f) 10 hours: Magnification $\times 500$

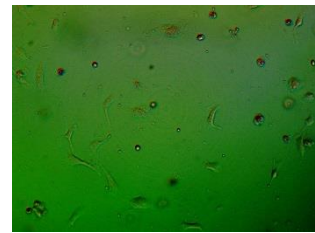
Figure 3.C: Half cultured petri dish of human coronary artery endothelial cells for the 1st experiment



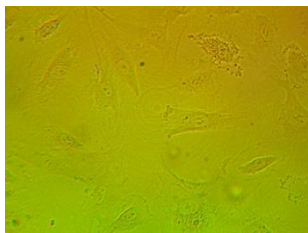
(a) 0 hour: Magnification $\times 200$



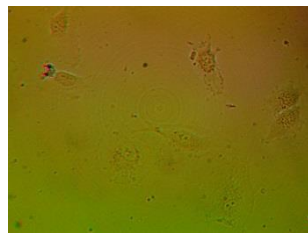
(b) 2 hours: Magnification $\times 200$



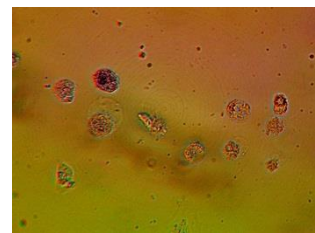
(c) 10 hours: Magnification $\times 200$



(d) 0 hour: Magnification $\times 500$



(e) 2 hours: Magnification $\times 500$



(f) 10 hours: Magnification $\times 500$

Figure 4.C: Half cultured petri dish of human coronary artery endothelial cells for the 2nd experiment

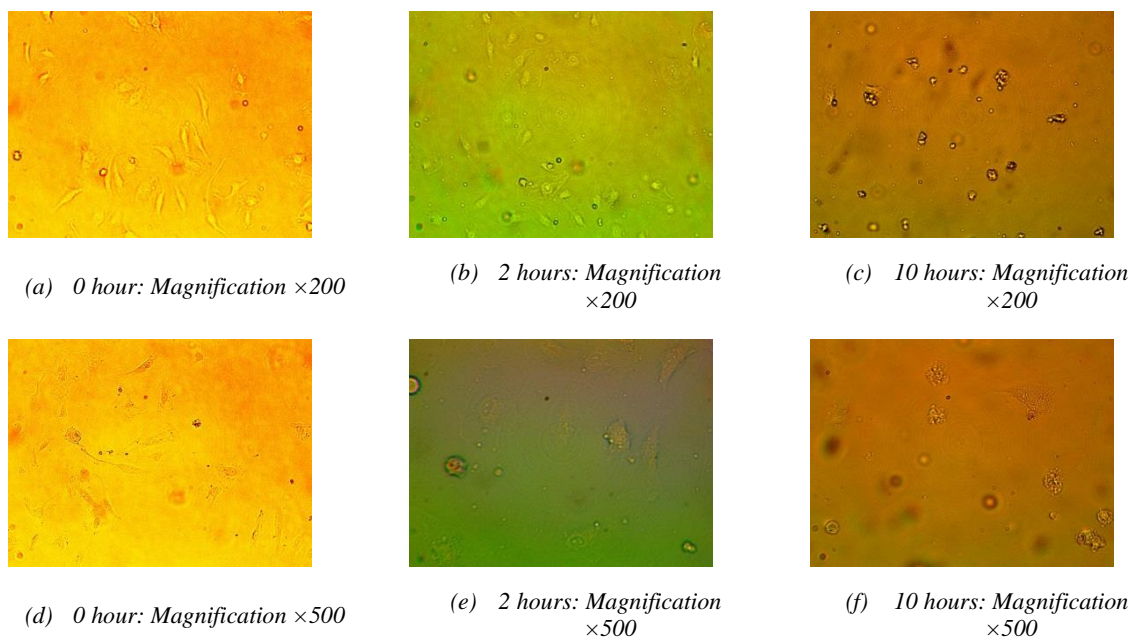


Figure 5.C: Half cultured petri dish of human coronary artery endothelial cells for the 3rd experiment

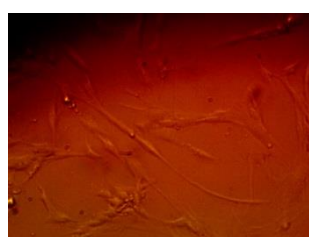
- Complete cultured human osteoblast cells

Table 4.C

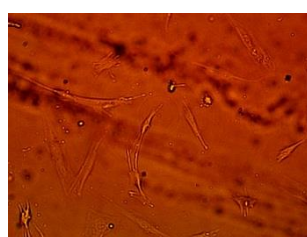
Time (minute)	1 st (mV)			2 nd (mV)			3 rd (mV)		
	0 hour	2 hours	10 hours	0 hour	2 hours	10 hours	0 hour	2 hours	10 hours
0	-281.2	-301.7	-256.1	-294.77	-328.7	-256.1	-305	-320.3	-373.5
0.16	-293.9	-303.8	-287.2	-296.3	-321.9	-287.2	-305	-304.5	-376.5
0.33	-303.8	-305.9	-283.4	-289.9	-320.5	-283.4	-302.1	-294.3	-374.2
0.5	-308.4	-307.4	-273.9	-282.2	-319.2	-273.9	-299.5	-283.6	-372.4
0.66	-310.1	-308.7	-269.9	-283.4	-317.9	-269.9	-297.4	-275.6	-370.3
0.83	-311.7	-309.2	-268.4	-283.4	-316.4	-268.4	-297.4	-272.1	-370.3
1	-312.3	-310	-267.5	-289.1	-316.5	-267.5	-294.3	-270.5	-370
1.16	-312.3	-309.6	-267	-293.6	-315.7	-267	-293.7	-270	-369
1.33	-311.7	-309.9	-266.4	-300.3	-314.4	-266.4	-292.4	-270.2	-367.4
1.5	-310.4	-309.8	-265.8	-296.8	-313.1	-265.8	-290.9	-270.5	-366.8
1.66	-309.1	-309.5	-265.1	-296.5	-311.4	-265.1	-294.5	-269.8	-367.9
1.83	-306.9	-305.7	-264.5	-297	-311	-264.5	-290.1	-268.8	-360.8
2	-305.4	-306.1	-263.7	-297.9	-310.3	-263.7	-288.7	-268	-359.4
2.16	-304	-308.1	-263.5	-293.5	-309.5	-263.5	-287.1	-268.2	-357.3
2.33	-302.6	-308.9	-263.7	-292.1	-308.9	-263.7	-286.2	-267.3	-356.2
2.5	-301.7	-309	-263.3	-291.6	-307.8	-263.3	-285.5	-265.9	-355.6
2.66	-301.1	-308.4	-263.1	-295	-307.8	-263.1	-285	-265.5	-354.9
2.83	-300.6	-309.3	-263.1	-290.7	-307.1	-263.1	-283.9	-264.5	-354.2
3	-300.5	-310	-263	-291.8	-306.9	-263	-286	-263.9	-354.3

3.16	-300.4	-310.6	-263.3	-290.5	-305.6	-263.3	-285.3	-262.4	-353.3
3.33	-299.9	-311.6	-263.4	-293.1	-306.7	-263.4	-290.3	-261.7	-353.7
3.5	-298.4	-311.9	-263.7	-288.4	-306.1	-263.7	-288.3	-261.7	-356.8
3.66	-298.4	-312.4	-263.4	-287.2	-304.8	-263.4	-289.3	-259.3	-354.8
3.83	-299.5	-312.8	-263.6	-285.3	-304.7	-263.6	-287.5	-259.7	-351.3
4	-300.6	-313.3	-263.4	-283.1	-304.7	-263.4	-290.9	-258.1	-350.6
4.16	-301.8	-313.4	-263.8	-288.9	-304	-263.8	-285.1	-256.5	-349.7
4.33	-297.4	-310.9	-263.9	-283.6	-304.1	-263.9	-281.6	-255.6	-348.4
4.5	-292.2	-311	-264.3	-282.7	-304.3	-264.3	-288.2	-255.4	-349.8
4.66	-293.9	-311.6	-264.2	-283.4	-305.1	-264.2	-283	-254.4	-349.1
4.83	-288.3	-311.7	-264.3	-283.3	-304	-264.3	-282.8	-251.9	-348.6
5	-289.8	-312.3	-264.5	-282.7	-304.2	-264.5	-285.4	-251.6	-347.2
5.16	-289.6	-313.3	-264.8	-282.4	-304.2	-264.8	-279.2	-251.4	-348.3
5.33	-289.5	-313.7	-264.9	-282.5	-303.6	-264.9	-281.5	-250.5	-347.3
5.5	-289.2	-314	-265.2	-282	-304	-265.2	-280.4	-250.5	-347.3
5.66	-288.9	-314	-265.5	-281.9	-302.2	-265.5	-280.1	-250.5	-347.1
5.83	-288.8	-313.2	-265.6	-283.2	-302.9	-265.6	-280.1	-249.8	-346
6	-288.3	-313.4	-265.9	-283.6	-302.2	-265.9	-280	-248.6	-346.7
6.16	-288.1	-314	-265.9	-281.5	-302.9	-265.9	-279.7	-248.2	-345.2
6.33	-287.8	-314.7	-266.3	-279.9	-303.7	-266.3	-279.9	-248.3	-346.6
6.5	-287.7	-315.4	-266.4	-279.8	-305.1	-266.4	-279.5	-247.3	-346.2
6.66	-287.8	-315.2	-266.8	-278	-304.4	-266.8	-278.2	-245.1	-345
6.83	-287.5	-313.4	-267.1	-278	-305.6	-267.1	-278	-245.3	-345.9
7	-287.3	-311.1	-267.3	-280.3	-304.6	-267.3	-278.5	-245.7	-345.4
7.16	-287.1	-309.2	-267.5	-281.1	-304.8	-267.5	-278.8	-244.4	-344.8
7.33	-280	-307.7	-267.7	-281.7	-305.6	-267.7	-278.2	-243.8	-344.4
7.5	-276.7	-306.3	-267.9	-279.9	-304.7	-267.9	-280.3	-244.9	-345.5
7.66	-280.5	-304.6	-268.6	-282.1	-304.9	-268.6	-278.8	-245.1	-345.1
7.83	-334.7	-306.5	-268.9	-281.5	-301.8	-268.9	-279.4	-244.3	-343.9
8	-352	-307.5	-269.5	-282.5	-299.5	-269.5	-278.4	-243.9	-343
8.16	-342.3	-308.8	-270.4	-282	-292.9	-270.4	-279.1	-243.2	-343.2
8.33	-334.7	-310.5	-270.3	-281.9	-292.4	-270.3	-278.9	-244.4	-344.3
8.5	-327.2	-313.3	-271.4	-280.8	-291.9	-271.4	-281.7	-244.6	-344
8.66	-320.9	-315.2	-272.1	-282.7	-290.7	-272.1	-277.5	-244.4	-343.5
8.83	-315.7	-316.7	-272.8	-281.7	-294.5	-272.8	-275.9	-244.7	-344.4
9	-304	-317.3	-273.2	-281.1	-295.1	-273.2	-276.3	-244.6	-342.9
9.16	-300.6	-318.3	-273	-281.8	-294.9	-273	-275.6	-245.1	-342.8
9.33	-298.2	-318.7	-272.5	-282.7	-298.2	-272.5	-276.3	-244.5	-342.7
9.5	-297.1	-318.3	-272.9	-282.3	-297.9	-272.9	-275.2	-244.9	-342.5
9.66	-295.9	-318.2	-273.6	-282.8	-298.2	-273.6	-275.5	-245.4	-342.8
9.83	-294.1	-318.9	-274.1	-280	-297.7	-274.1	-271.4	-245.2	-341.5
10	-293.1	-319.4	-274.3	-283.1	-289.8	-274.3	-267.7	-246.7	-341.2
10.16	-292.2	-319.7	-274.5	-282.9	-292.5	-274.5	-265.8	-245.8	-342.9
10.33	-292.1	-319.9	-274.8	-284.5	-292.5	-274.8	-265.8	-244.7	-341.6

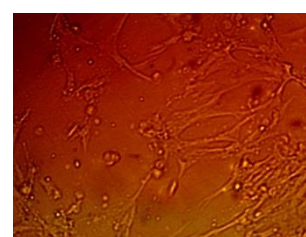
10.5	-292	-320.1	-275.4	-283.3	-294.5	-275.4	-264.3	-244.7	-341
10.66	-291.8	-319	-275.7	-284.6	-296.1	-275.7	-264.8	-243.5	-341.4
10.83	-291.6	-318.6	-275.7	-284.9	-296.4	-275.7	-265.7	-244.9	-342.4
11	-291.5	-316.4	-276	-285	-297.6	-276	-266.8	-247	-341.7
11.16	-291.3	-314.8	-276.3	-285.7	-297.5	-276.3	-264.5	-250.8	-341.2
11.33	-291.4	-314.5	-276.8	-284.6	-297.1	-276.8	-264.2	-256.8	-341
11.5	-292.3	-314.9	-277.1	-284	-298.5	-277.1	-264	-257.3	-340.7
11.66	-293.4	-314.8	-277.2	-277.9	-298.5	-277.2	-264.7	-247.9	-340.6
11.83	-294	-312.9	-277.1	-281.7	-298.7	-277.1	-265.2	-247.2	-341
12	-293.6	-312.3	-277.5	-281.3	-299.3	-277.5	-263.7	-247.4	-340.6
12.16	-291.1	-314	-277.7	-281.4	-298.3	-277.7	-263.7	-245.5	-341
12.33	-290.4	-309.8	-277.5	-281.2	-298	-277.5	-265	-252.3	-339.9
12.5	-289.6	-314.7	-277.5	-281.4	-299.2	-277.5	-264.9	-246.7	-339.8
12.66	-289.6	-315.7	-277.6	-281.8	-299.9	-277.6	-262.8	-245.5	-340.6
12.83	-288.2	-317.2	-277.6	-282.3	-300.7	-277.6	-265.1	-242.5	-340.4
13	-287	-318.5	-277.5	-281.3	-299	-277.5	-265.6	-243.1	-340.7
13.16	-285.7	-318	-277.7	-280	-300	-277.7	-266.1	-241.4	-340.1
13.33	-284.5	-317.4	-277.7	-281.7	-299.6	-277.7	-265.8	-241.7	-339.7
13.5	-283.9	-317.2	-277.7	-280.6	-297.5	-277.7	-266.4	-241.1	-338.7
13.66	-283.4	-317.5	-277.6	-282.7	-298.2	-277.6	-267.1	-240.5	-340.1
13.83	-282.5	-317.9	-277.7	-284.7	-299.2	-277.7	-265.9	-242.9	-339.8
14	-281.6	-321.3	-277.8	-282.3	-300.1	-277.8	-267.7	-242.2	-341.1
14.16	-282.8	-317.6	-277.7	-283.1	-302	-277.7	-267	-244.5	-340.8
14.33	-283.9	-317.5	-277.4	-281	-302.4	-277.4	-264.4	-245.8	-339.8
14.5	-284.2	-317.6	-277.4	-280.6	-295.1	-277.4	-270.5	-244.4	-340.5
14.66	-284.9	-317.7	-277.4	-281.8	-294.6	-277.4	-281.6	-239.7	-339.4
14.83	-285.7	-317.3	-277.4	-280.8	-298.3	-277.4	-269.7	-235.6	-338.7
15	-286.5	-315.6	-277.4	-281.4	-301.9	-277.4	-272.6	-233.2	-339.8



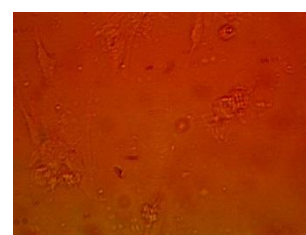
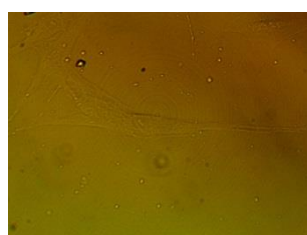
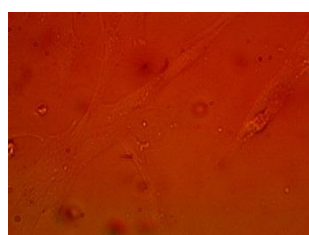
(a) 0 hour: Magnification $\times 200$



(b) 2 hours: Magnification $\times 200$



(c) 10 hours: Magnification $\times 200$

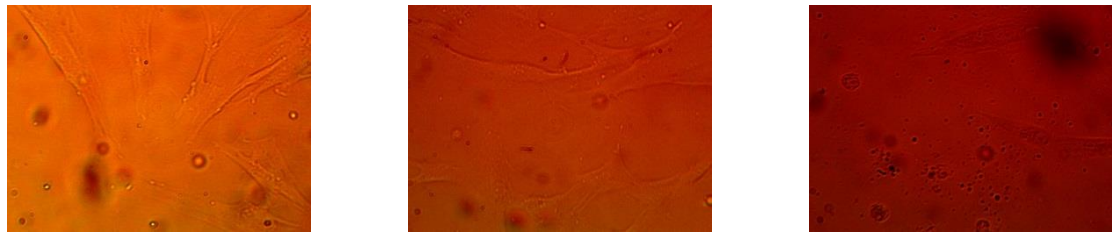


(d) 0 hour: Magnification $\times 500$ (e) 2 hours: Magnification $\times 500$ (f) 10 hours: Magnification $\times 500$

Figure 6.C: Cultured human osteoblast cells for direct microelectrode method for the 2nd experiment



(a) 0 hour: Magnification $\times 200$ (b) 2 hours: Magnification $\times 200$ (c) 10 hours: Magnification $\times 200$



(d) 0 hour: Magnification $\times 500$ (e) 2 hours: Magnification $\times 500$ (f) 10 hours: Magnification $\times 500$

Figure 7.C: Cultured human osteoblast cells for direct microelectrode method for the 3rd experiment

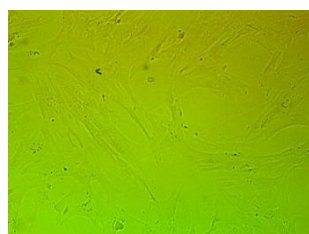
- Half cultured human osteoblast cells

Table 5.C

Time (minute)	1 st (mV)			2 nd (mV)			3 rd (mV)		
	0 hour	2 hours	10 hours	0 hour	2 hours	10 hours	0 hour	2 hours	10 hours
0	-329.4	-414.4	-370.5	-373	-417.7	-337.5	-219.9	-343.3	-388.7
0.16	-337.8	-413.7	-365.1	-366.3	-407.6	-333.8	-239.8	-329.6	-385.5
0.33	-335.5	-410.6	-357.3	-361.6	-403.7	-331.7	-244.6	-326.3	-384.4
0.5	-333.1	-407.2	-354.7	-355.6	-397.6	-322.6	-242.2	-323.5	-381.4
0.66	-331.1	-404.8	-352	-349.1	-392.8	-320	-237.8	-322.3	-379.4
0.83	-329.7	-403.2	-352.1	-351.7	-391.5	-318.2	-237.8	-322.1	-376.6
1	-326.3	-402	-353.9	-349.9	-389.3	-315.2	-235.8	-320.2	-374.3
1.16	-325	-402.2	-351.5	-347.7	-380.3	-314	-236.2	-319.6	-373
1.33	-324.1	-397.2	-350.2	-345.8	-397.1	-311.7	-238.6	-317.9	-371.7
1.5	-323.2	-397.1	-348.1	-343.7	-395.5	-310.6	-242.1	-316.8	-370.5
1.66	-322.3	-395.5	-350.4	-342.9	-395.9	-305.9	-261	-315.5	-371.1
1.83	-321.7	-395	-348.1	-340.4	-389.5	-304.4	-266.1	-314.2	-370.8
2	-321.1	-394.2	-346.9	-340.1	-387.5	-301.9	-264.7	-313.6	-369.1
2.16	-320.6	-393.5	-347.4	-338.1	-386.4	-299.7	-256.9	-312.4	-367.6
2.33	-320.1	-393.2	-347.1	-337	-384.8	-300.5	-258.9	-310.6	-366.1

2.5	-319.5	-393.3	-346.4	-336.3	-383.7	-301.9	-255.4	-311.9	-364.5
2.66	-318.7	-392.8	-347	-335.3	-383.4	-299.8	-257.8	-314.1	-364
2.83	-318.3	-392.7	-343.9	-336.3	-384.2	-296.6	-261.8	-315	-364
3	-317.8	-392.2	-345.1	-331.7	-382.7	-297.2	-255.5	-316.3	-364.7
3.16	-317.4	-391.5	-343.1	-331.8	-381.5	-297.4	-256.1	-314.5	-364
3.33	-317	-391.1	-343	-332.1	-380.1	-299.1	-251.4	-314.3	-364.6
3.5	-316.7	-391.4	-341.7	-327.7	-380.2	-297.1	-251.2	-311	-362.8
3.66	-316.4	-389.6	-343.2	-330.3	-379.3	-296.1	-248.5	-314.8	-361.1
3.83	-316.9	-389.8	-343.4	-330.3	-379	-296.6	-250	-308.8	-360.1
4	-316.7	-389.9	-342.8	-326.9	-378.4	-296	-257.8	-309.7	-360.4
4.16	-316.1	-389.6	-341.4	-327	-379.2	-292.5	-249.2	-310.8	-360.1
4.33	-316.1	-389.8	-339.3	-326.6	-378.6	-293.7	-251.3	-304.9	-361.9
4.5	-315.3	-389.7	-339	-328.4	-377.8	-292.7	-248.2	-301.4	-359.9
4.66	-316.1	-388.6	-338.7	-324.1	-377.2	-294.1	-247.2	-301.5	-358.1
4.83	-317	-387.8	-340	-325.4	-377.1	-292.5	-247	-300.4	-358.7
5	-317.2	-388	-338.9	-325.2	-376	-294.4	-245.9	-301.6	-358.3
5.16	-317.3	-387.8	-342	-324.8	-372.3	-291.3	-245.7	-299.5	-356.5
5.33	-317.5	-387.3	-342.4	-324.8	-377.8	-290.6	-247.3	-298.7	-357.8
5.5	-317.5	-386.9	-341.7	-322.5	-376.4	-288.8	-245.1	-297.1	-357.7
5.66	-317.5	-387.8	-341.9	-320.4	-375	-289.2	-251.5	-298.9	-355.7
5.83	-317.7	-387.3	-343.2	-321.4	-374.7	-290.3	-248	-297.7	-356.7
6	-317.9	-387.2	-341.5	-320.1	-374.2	-291.3	-246.9	-297.2	-356.3
6.16	-318.5	-386.3	-340.4	-319.8	-374	-293.1	-246.3	-297.1	-354.8
6.33	-317.6	-386.9	-342.1	-320.4	-372.7	-291.3	-247.2	-296.3	-354
6.5	-318.6	-386.6	-339.6	-317.8	-373.2	-292.7	-248.3	-296	-353
6.66	-319.1	-386.8	-339.7	-319.7	-373.1	-288.8	-248.7	-293.7	-354.1
6.83	-318.8	-385.3	-340.6	-321.9	-372.8	-288.7	-247.8	-295.1	-354.2
7	-318	-385.7	-338.4	-319.4	-372.9	-289.5	-247	-296.1	-353.8
7.16	-318.1	-386	-339.2	-317.9	-371.9	-289.3	-247	-294.6	-353
7.33	-318.5	-385.6	-339	-317.8	-371.9	-286.6	-247.5	-294.5	-353
7.5	-318.9	-385.7	-338.7	-318	-371.9	-286.9	-246.7	-295.9	-353.1
7.66	-319.2	-385.4	-338.6	-317.3	-371	-288.5	-246.4	-297.6	-352.9
7.83	-318.8	-384.9	-340.3	-317.1	-370.8	-289.6	-244.7	-296.5	-352.9
8	-318.5	-385.5	-348.9	-317.6	-371	-287.9	-245.9	-293.6	-352.2
8.16	-319.2	-385.2	-339.5	-317.1	-370.5	-288.3	-251.2	-296.5	-351.8
8.33	-318.7	-385.5	-320.6	-317.8	-371.2	-287.2	-249	-293.3	-353.1
8.5	-319.7	-386	-337.7	-317.6	-370.6	-287.9	-248.9	-292.8	-353.5
8.66	-320.7	-385.3	-341.1	-317.3	-370.6	-286.5	-248.7	-293	-353.2
8.83	-320.5	-384.6	-343.4	-317.1	-369.3	-288.1	-247.1	-292	-352.7
9	-320.6	-384	-345.1	-316.7	-369	-288.1	-244.9	-290.9	-352.4
9.16	-320.6	-384	-337.7	-315.1	-370.4	-287.7	-245.8	-291.7	-352.4
9.33	-320.4	-383.9	-337.7	-314.2	-370.5	-288.5	-249.1	-293.2	-352.2
9.5	-320.3	-384	-335	-314.7	-369.5	-286.6	-246.4	-292	-352
9.66	-320.3	-382.8	-334.7	-294.2	-369.5	-286.4	-246.2	-292.9	-352.1

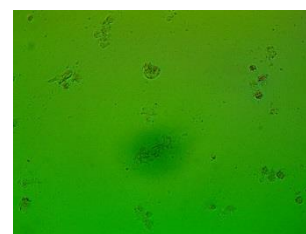
9.83	-320.3	-383.8	-331.7	-293.2	-369.2	-286.9	-251.5	-290.6	-352.2
10	-320.2	-379.7	-334.6	-291.7	-368.8	-290.3	-250.3	-293	-352.1
10.16	-319.4	-376.8	-330.4	-312.4	-368.4	-289.2	-256.4	-292	-352
10.33	-319.8	-376.4	-333.3	-313.2	-368.1	-287	-248.2	-292.1	-352.2
10.5	-319.6	-376.3	-344.5	-313.1	-367.8	-288.8	-246.5	-289.9	-351.4
10.66	-319.6	-377.4	-341.7	-312.6	-368.6	-288.6	-251.8	-292.2	-351.9
10.83	-319.6	-377.2	-341.1	-312.3	-365.7	-288.1	-248	-291.6	-351.6
11	-319.8	-376.1	-336.7	-311.9	-365.5	-289.9	-249.6	-291.3	-352.3
11.16	-319.2	-374.1	-338	-311.8	-365.7	-294	-254.5	-291.1	-352.1
11.33	-319	-373.6	-334.4	-311.8	-366.3	-291	-249.2	-292.2	-351.5
11.5	-318.7	-372.2	-331.6	-311.8	-365	-289.2	-251	-292.2	-351.4
11.66	-319.2	-373.5	-333.1	-311.8	-365.6	-287.6	-248.7	-289.4	-351.3
11.83	-319.7	-373.8	-332.7	-311.9	-366.3	-293	-248.9	-291.2	-351
12	-319.6	-372.9	-332	-311.7	-357.9	-293.6	-251.2	-290.6	-351.1
12.16	-319.3	-372	-329.5	-311.6	-359.6	-294.8	-248.1	-293.3	-351
12.33	-318.8	-372.9	-329.5	-310.9	-359.9	-296.4	-255.7	-292.5	-351.3
12.5	-318.6	-372.6	-328	-310.3	-361.5	-295.4	-255.3	-291.7	-351.2
12.66	-317.9	-371.5	-332.6	-311	-361.1	-295.7	-238.2	-293	-351.4
12.83	-317.7	-371.3	-337.5	-313.2	-364.1	-295.9	-231.7	-293.9	-351.3
13	-318	-371.8	-340.4	-314.7	-362.1	-296.3	-234	-293.9	-351.1
13.16	-318.9	-371.5	-341.8	-316.3	-362.6	-294.8	-238.1	-292	-350.8
13.33	-319.2	-371.4	-341.1	-311.7	-362.5	-294.5	-240.3	-292.1	-350
13.5	-319.3	-372.6	-342.5	-311.2	-361.5	-295	-244.8	-292.6	-351
13.66	-319.2	-376	-342.1	-311	-363.7	-296.5	-232.9	-292.6	-350.9
13.83	-318.7	-375.8	-343	-308.5	-362.8	-295.3	-236.7	-290.6	-350.6
14	-319.4	-375.6	-342.3	-307.8	-363.3	-296.2	-239.8	-292.4	-350.2
14.16	-319.4	-376.2	-344.6	-308.5	-364.6	-296.3	-242.1	-292	-350
14.33	-319.2	-375.9	-347.3	-308.2	-362.8	-298.9	-240.5	-292.3	-349.9
14.5	-318	-375.8	-349.8	-308.1	-363.5	-296.3	-241.1	-293.3	-350.4
14.66	-318.4	-375.8	-347.6	-308.9	-362.2	-297.5	-240.7	-292.1	-350.1
14.83	-318.4	-376.4	-345.8	-309.6	-363.4	-296.8	-240.8	-291.5	-349.8
15	-318.4	-376	-346.7	-309.7	-362.7	-296.7	-241.4	-292.7	-349.5



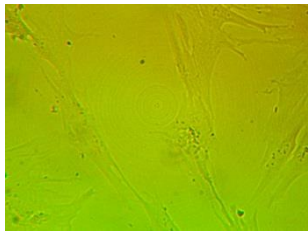
(a) 0 hour: Magnification $\times 200$



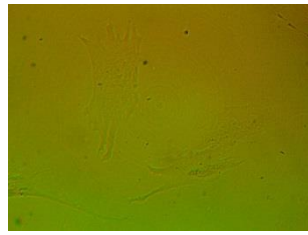
(b) 2 hours: Magnification $\times 200$



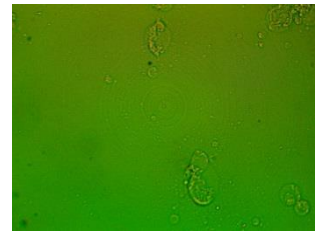
(c) 10 hours: Magnification $\times 200$



(d) 0 hour: Magnification $\times 500$

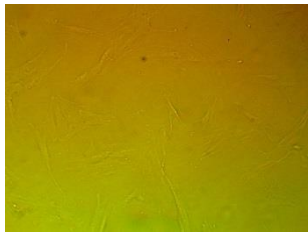


(e) 2 hours: Magnification $\times 500$



(f) 10 hours: Magnification $\times 500$

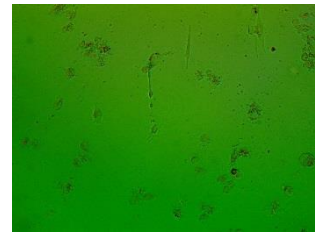
Figure 8.C: Half cultured petri dish of human osteoblast cells for the 1st experiment



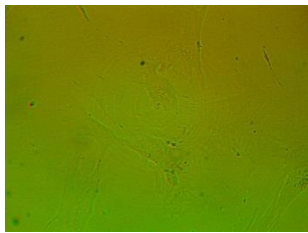
(a) 0 hour: Magnification $\times 200$



(b) 2 hours: Magnification $\times 200$



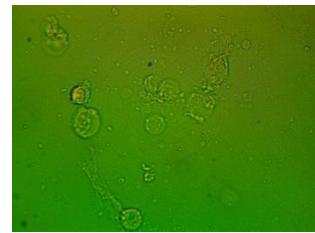
(c) 10 hours: Magnification $\times 200$



(d) 0 hour: Magnification $\times 500$



(e) 2 hours: Magnification $\times 500$



(f) 10 hours: Magnification $\times 500$

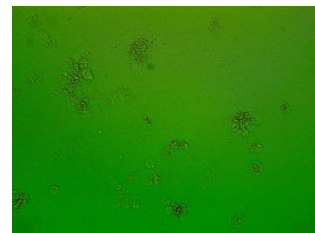
Figure 9.C: Half cultured petri dish of human osteoblast cells for the 2nd experiment



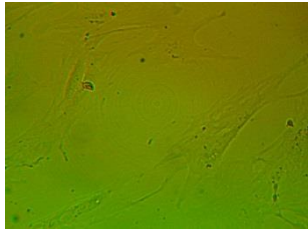
(a) 0 hour: Magnification $\times 200$



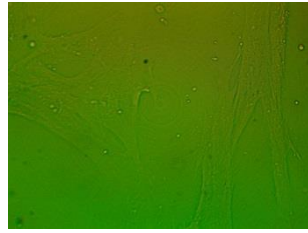
(b) 2 hours: Magnification $\times 200$



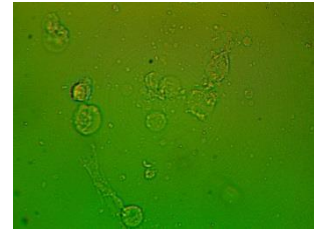
(c) 10 hours: Magnification $\times 200$



(d) 0 hour: Magnification $\times 500$



(e) 2 hours: Magnification $\times 500$

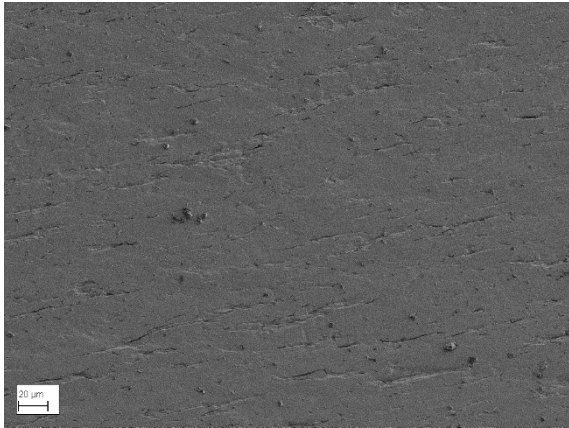


(f) 10 hours: Magnification $\times 500$

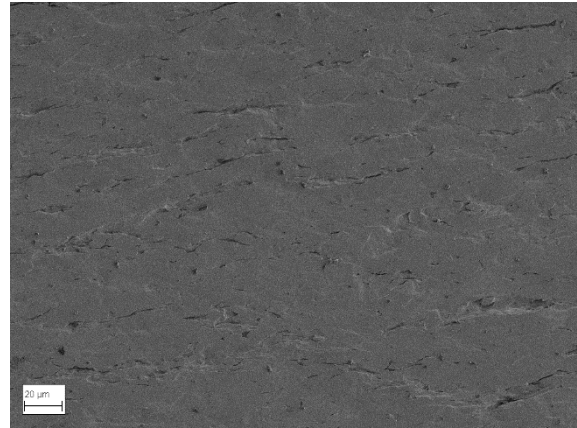
Figure 10.C: Half cultured petri dish of human osteoblast cells for the 3rd experiment

Appendix D: Mimicked Artery SEM Images

- Bare Stent



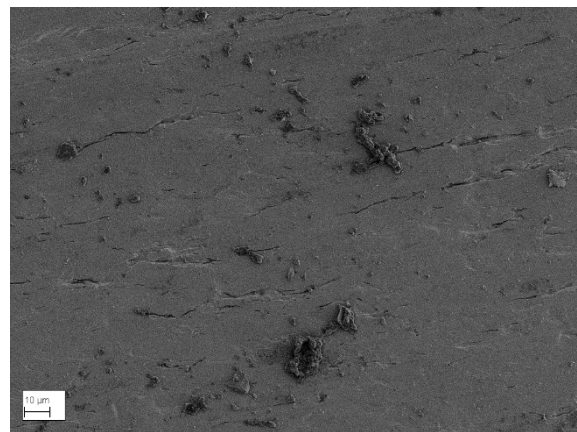
Magnification ×775



Magnification ×994



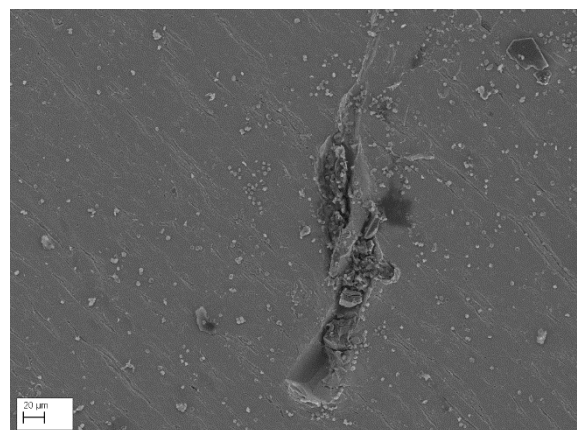
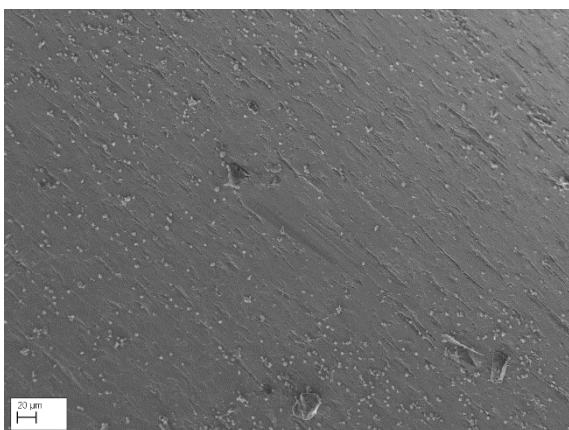
Magnification ×1k



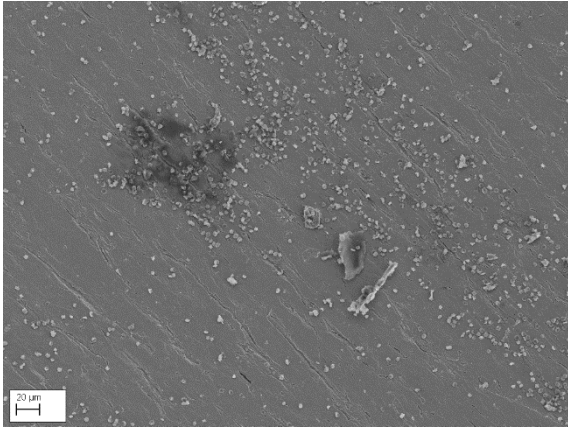
Magnification ×1.33k

Figure D.1: Bare Stent

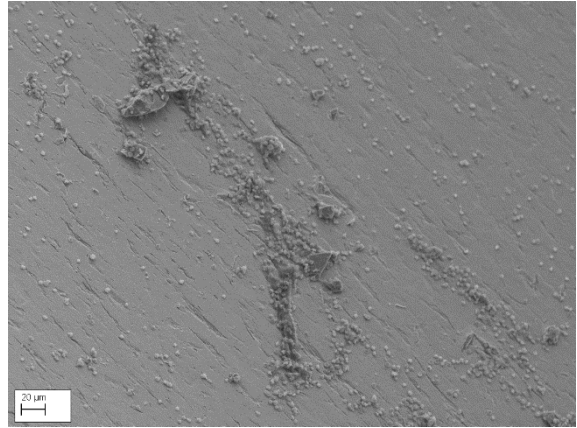
- Applied Direct Current on Bare Stent



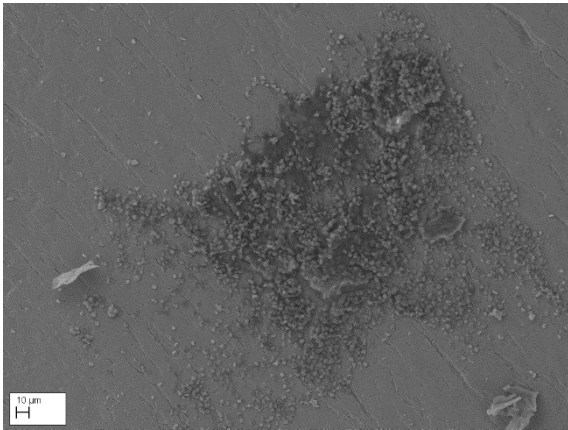
Magnification ×500



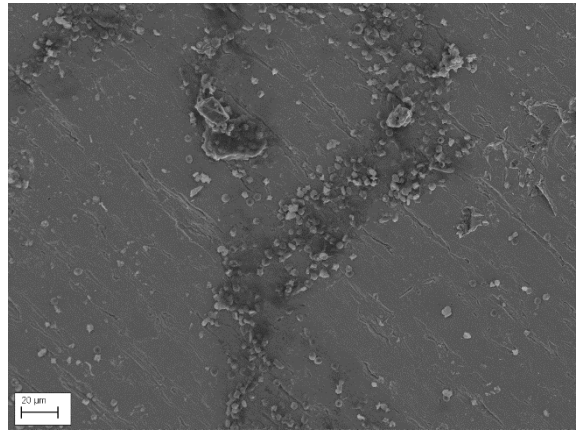
Magnification ×600



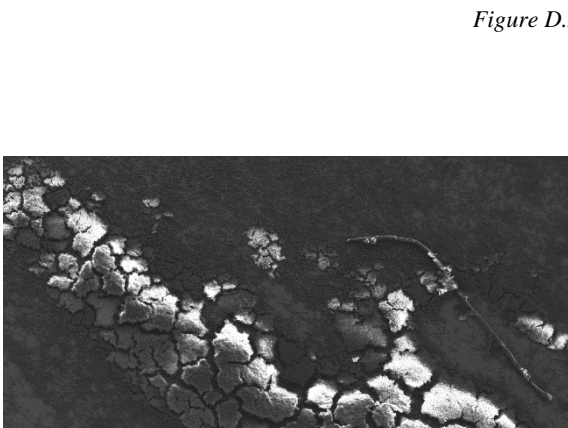
Magnification ×612



Magnification ×635



Magnification ×675



Magnification ×963

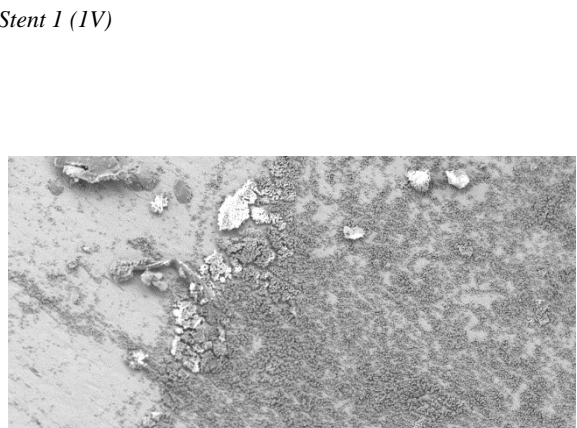
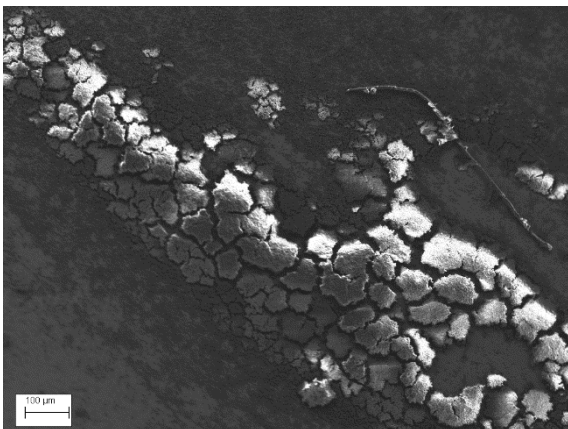
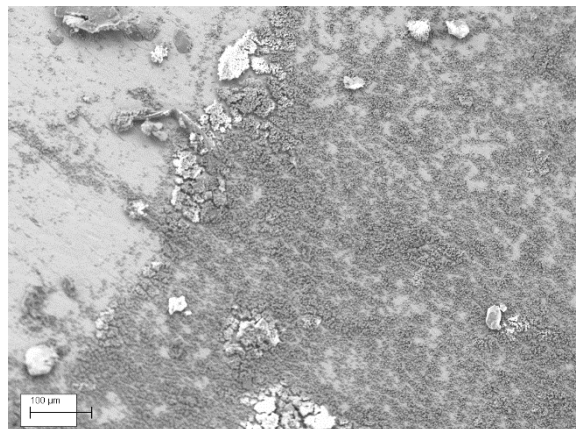


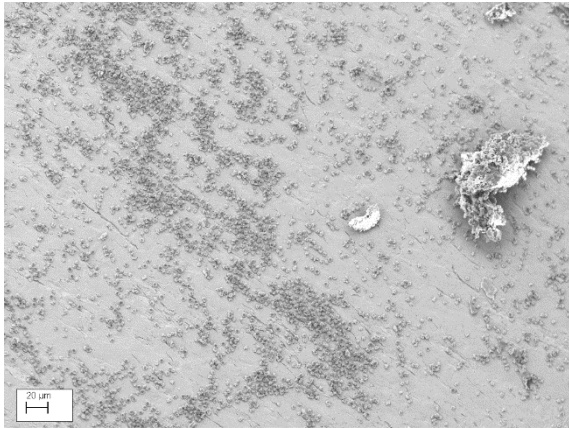
Figure D.2: Stent 1 (IV)



Magnification ×230



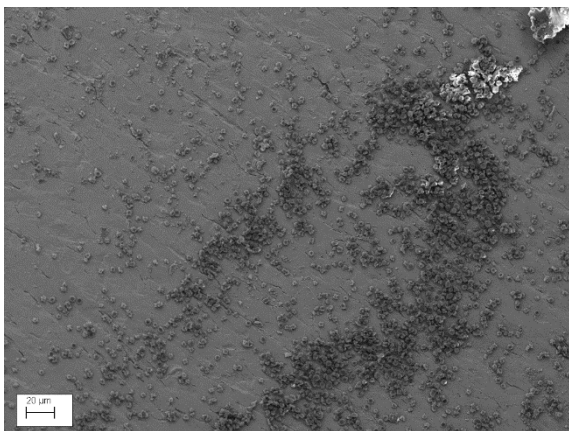
Magnification ×326



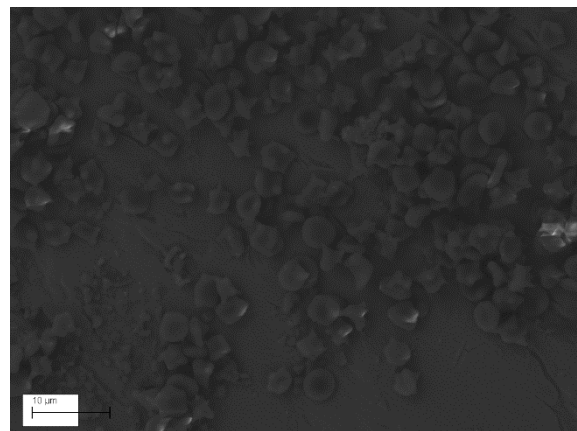
Magnification ×547



Magnification ×646

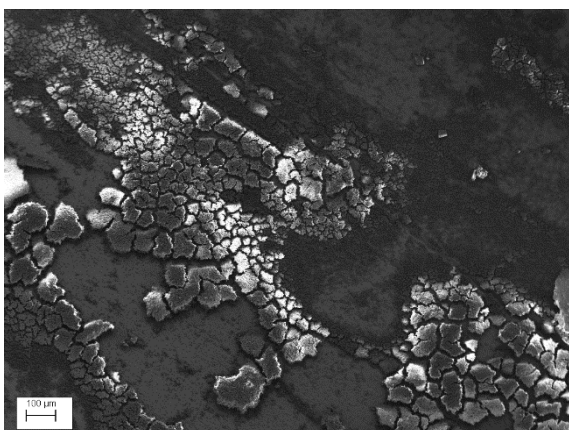


Magnification ×747

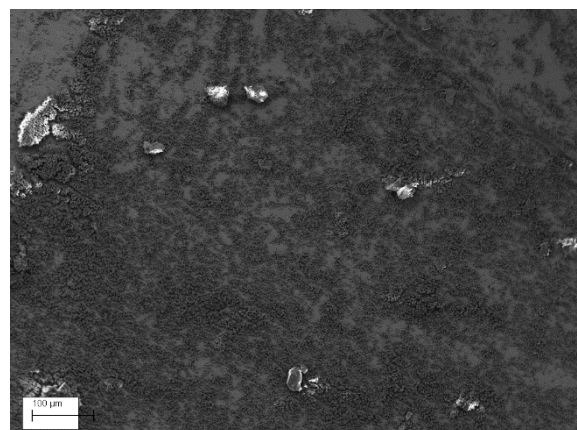


Magnification ×4.11

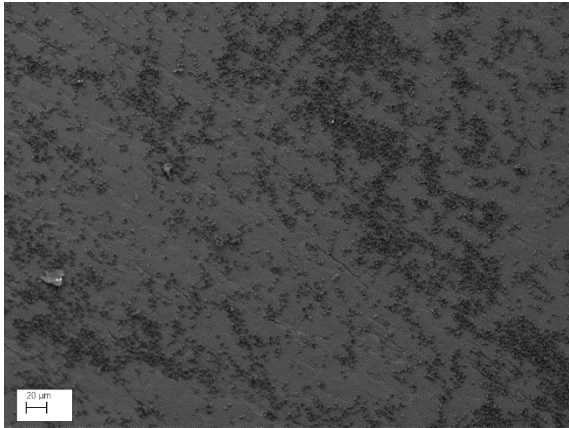
Figure D.3: Stent 2 (IV)



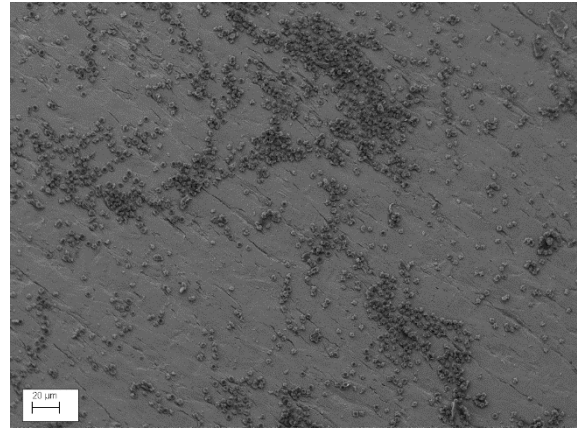
Magnification ×154



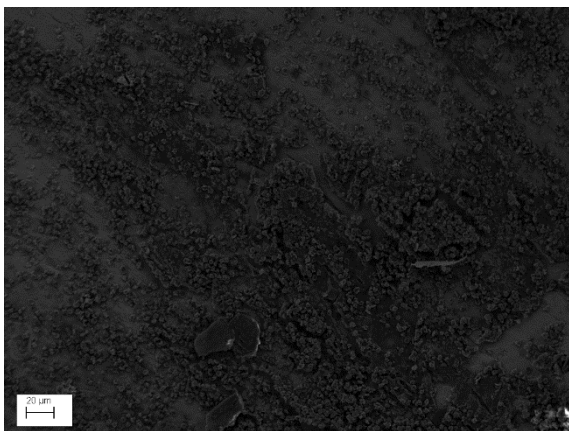
Magnification ×324



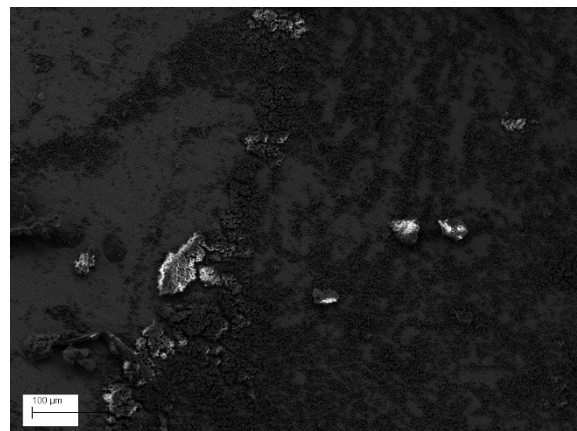
Magnification ×549



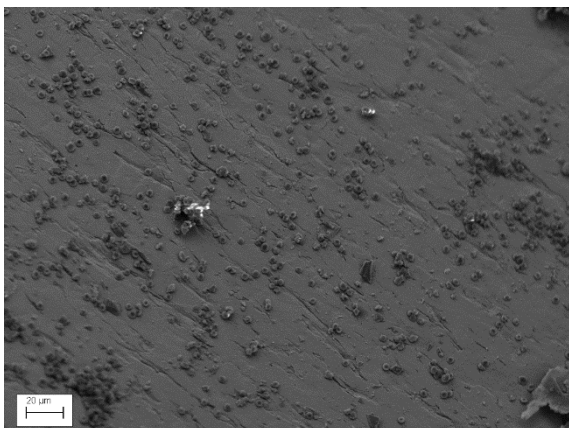
Magnification ×722



Magnification ×730



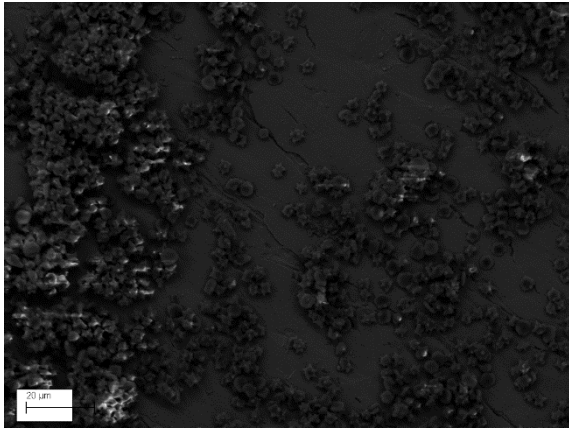
Magnification ×402



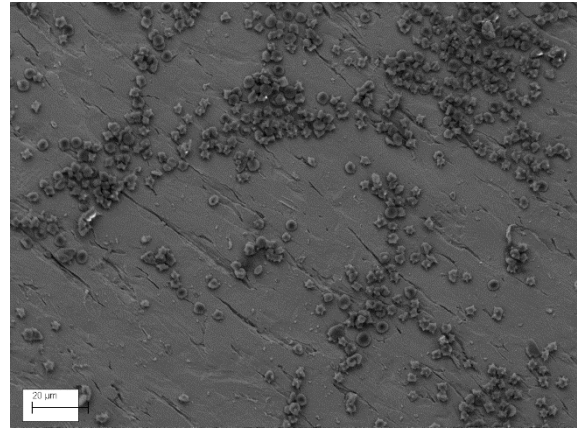
Magnification ×983



Magnification ×1.26k

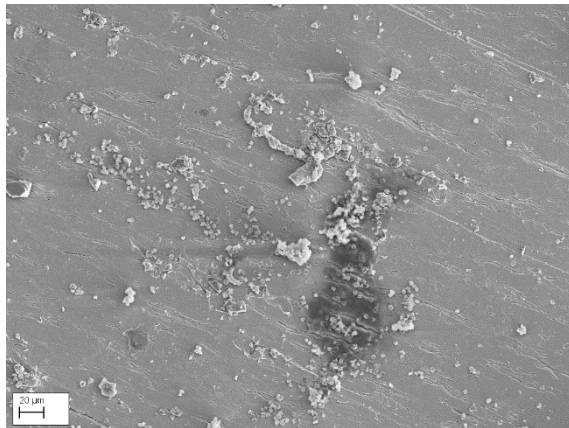


Magnification ×1.86k

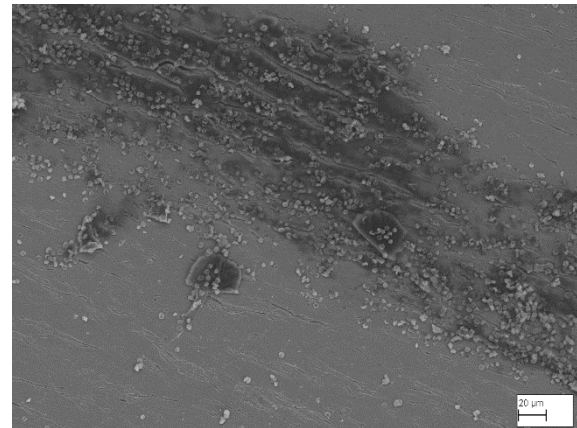


Magnification ×1.48

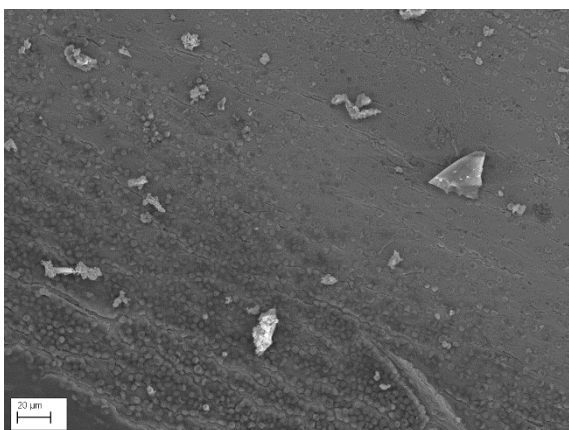
Figure D.4: Stent 3 (0V)



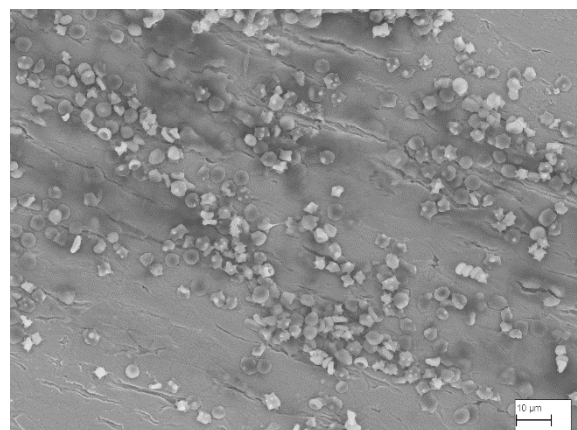
Magnification ×651



Magnification ×729

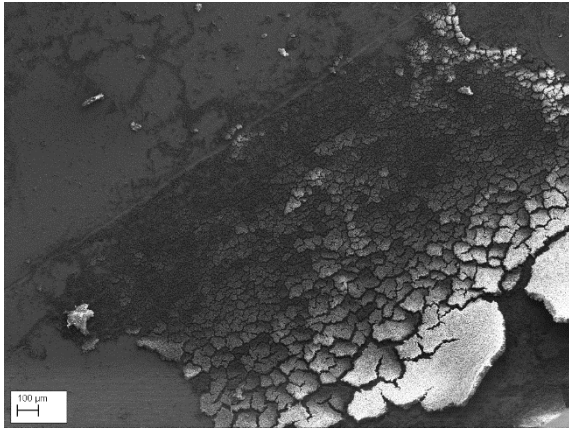


Magnification ×885

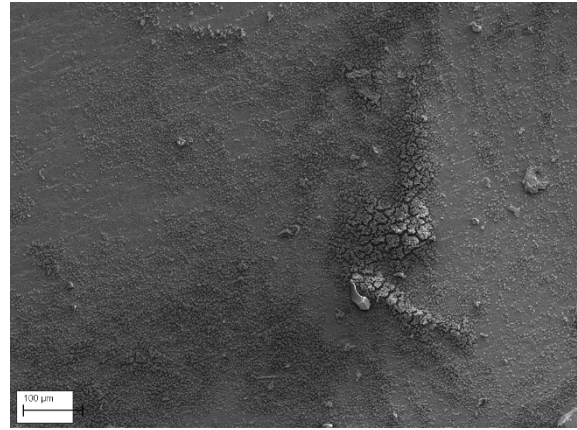


Magnification ×1.86k

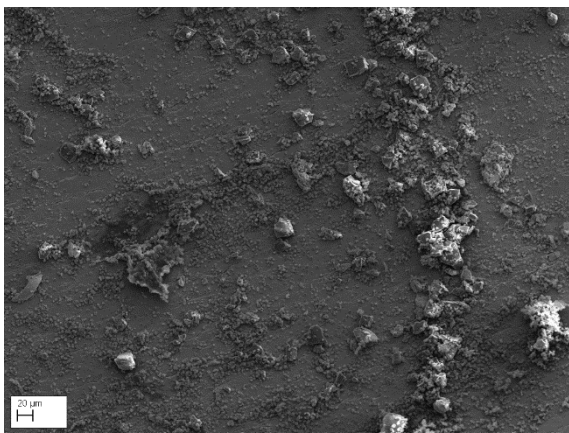
Figure D.5: Stent 4 (27mV)



Magnification ×126



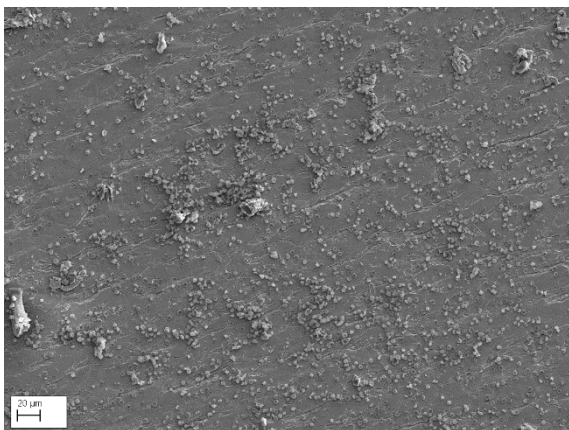
Magnification ×313



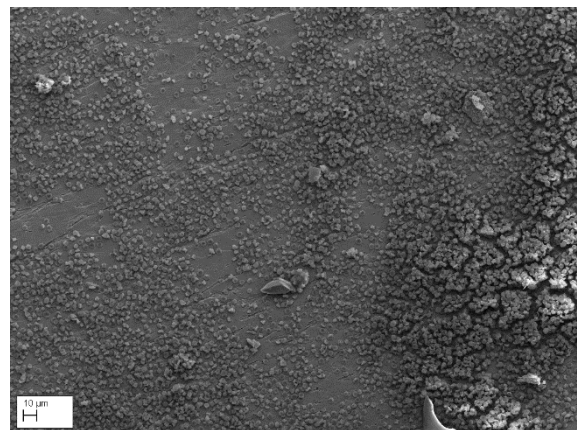
Magnification ×412



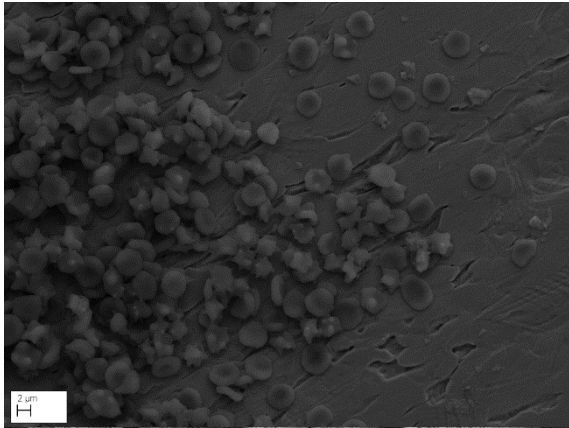
Magnification ×432



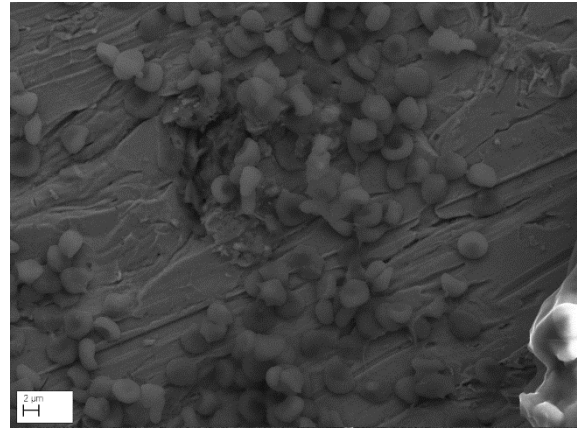
Magnification ×601



Magnification ×698

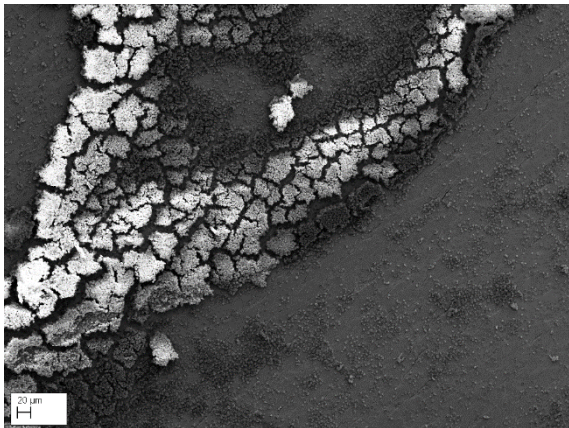


Magnification ×3.5k

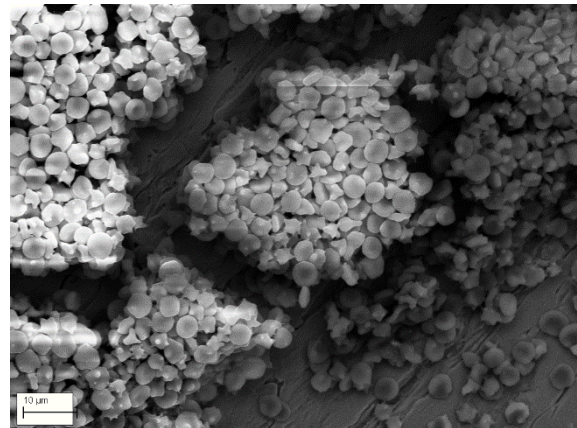


Magnification ×4.10

Figure D.6: Stent 4 (0V)

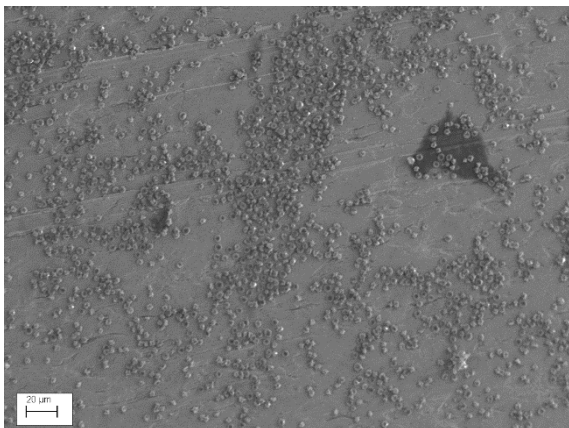


Magnification ×346

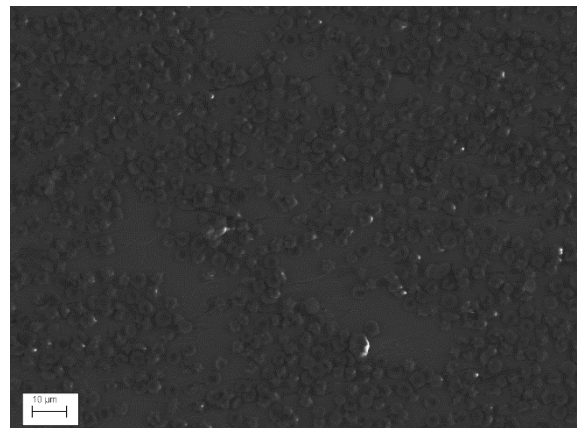


Magnification ×2.38k

Figure D.7: Stent 5 (1V)



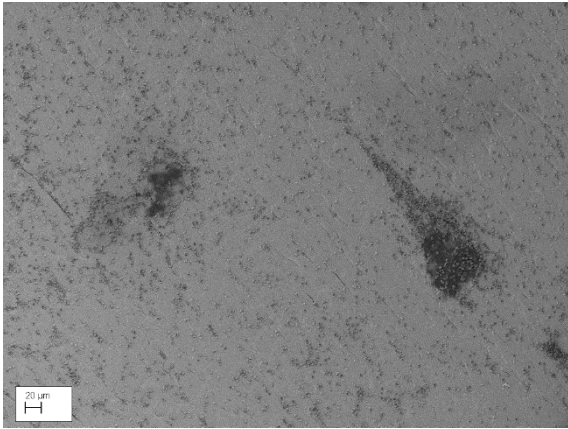
Magnification ×824



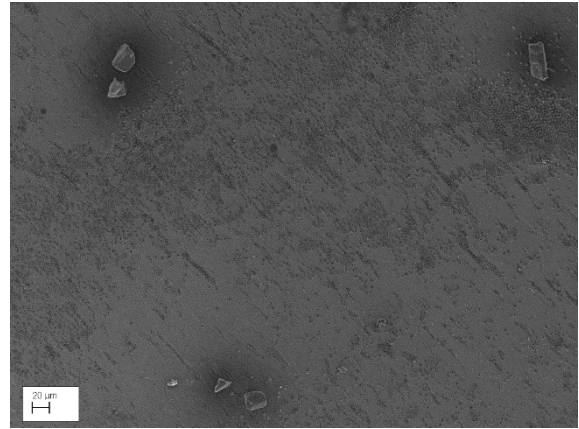
Magnification ×1.82k

Figure D.8: Stent 6 (0V)

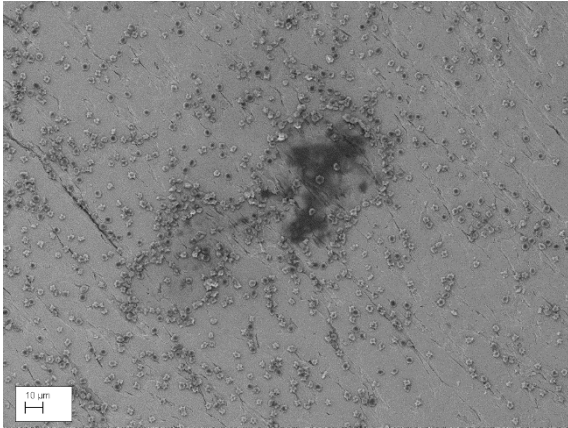
- Applied Direct Current on Bare Stent with Extra Endothelial Cells



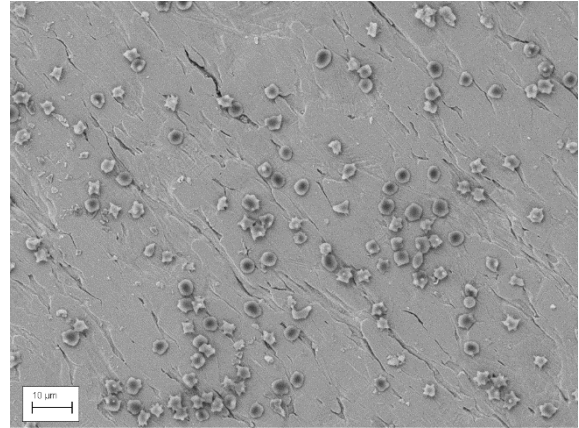
Magnification $\times 418$



Magnification $\times 453$

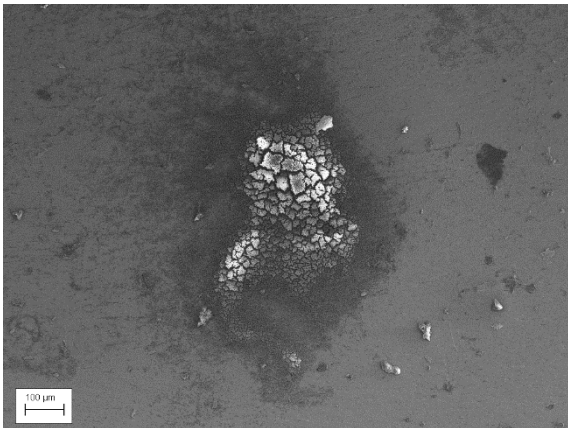


Magnification $\times 1k$

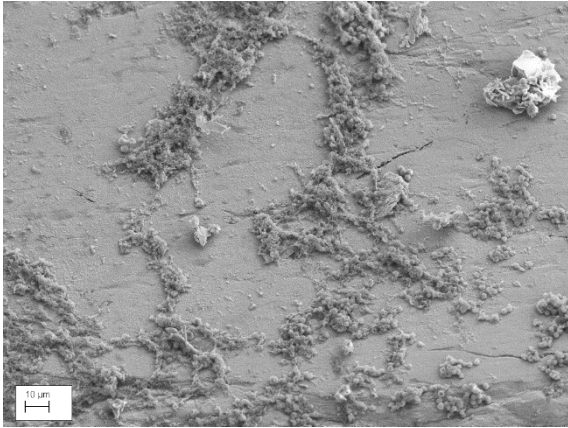


Magnification $\times 2.10$

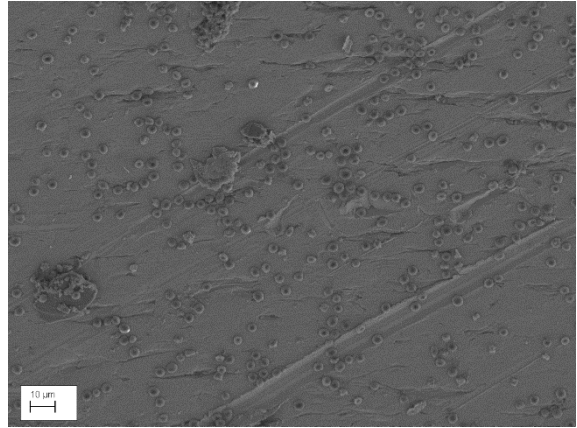
Figure D.9: Stent 1 (IV)



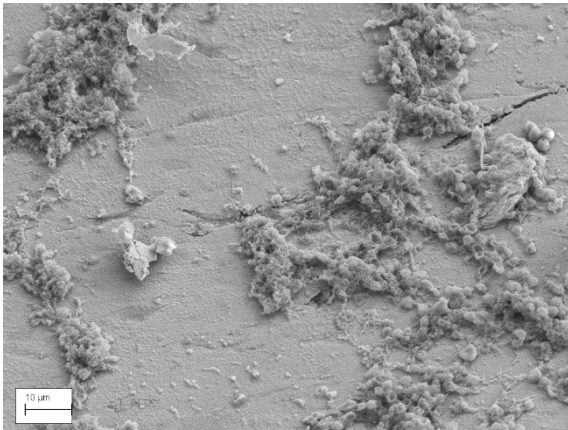
Magnification ×200



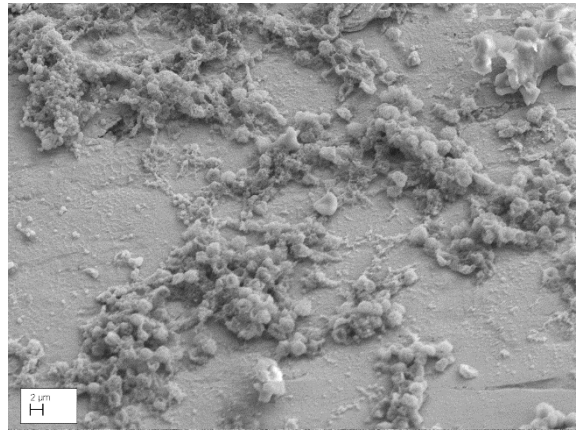
Magnification ×340



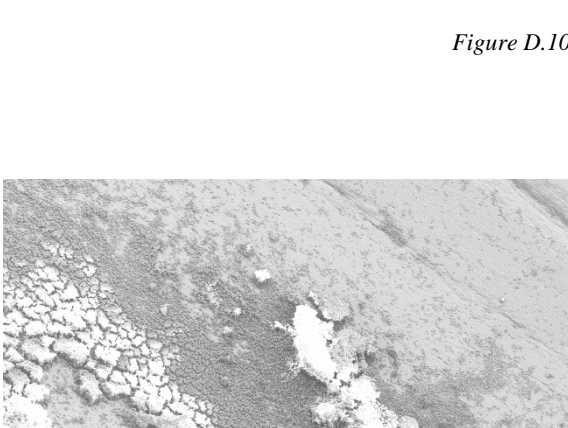
Magnification ×1.25k



Magnification ×1.31k



Magnification ×2.54k



Magnification ×3.40k

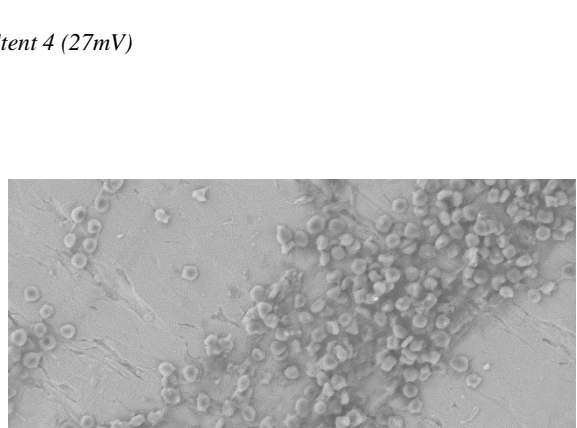


Figure D.10: Stent 4 (27mV)

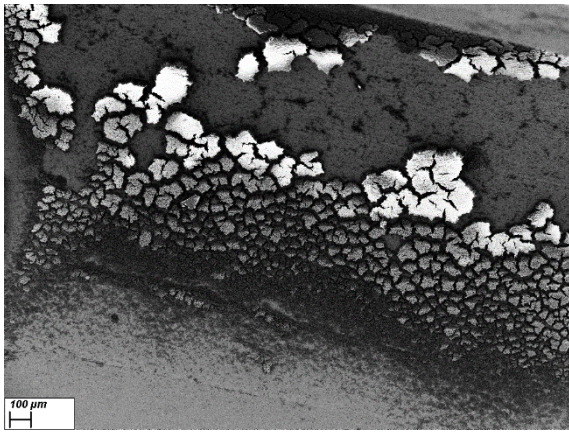
Magnification ×300



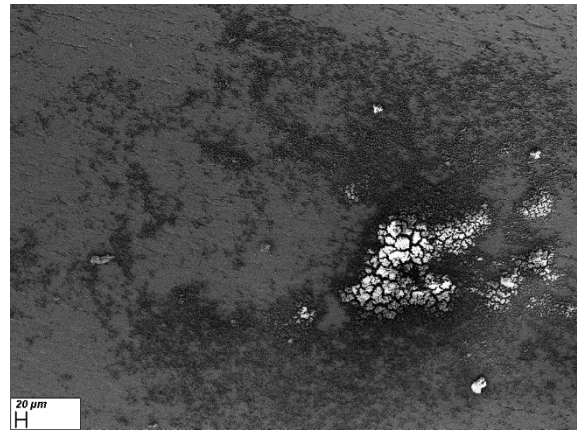
Magnification ×2.23k



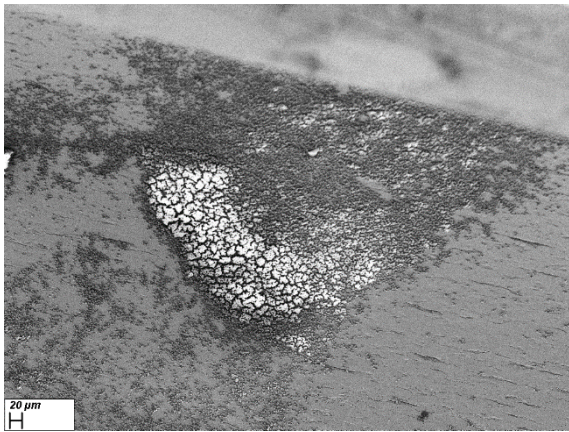
Figure D.10: Stent 5 (1V)



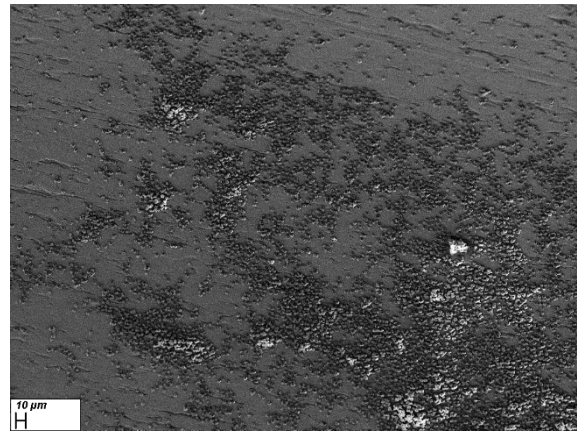
Magnification ×113



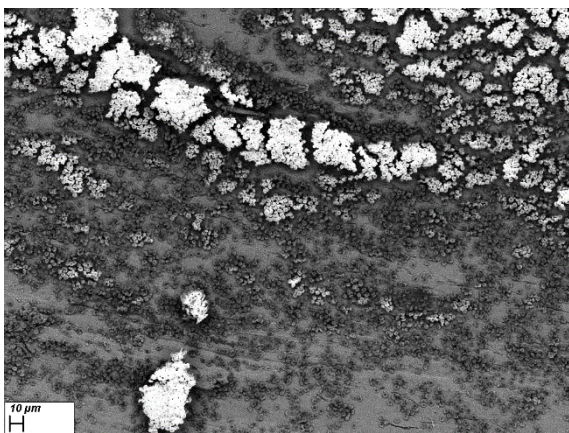
Magnification ×275



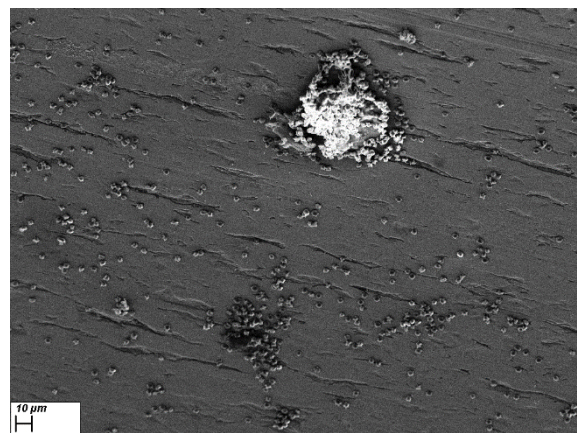
Magnification ×320



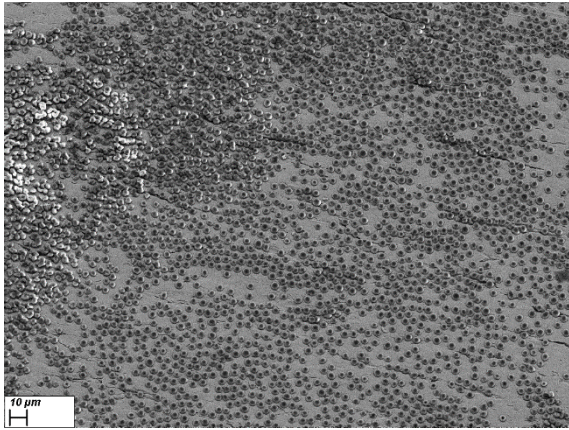
Magnification ×535



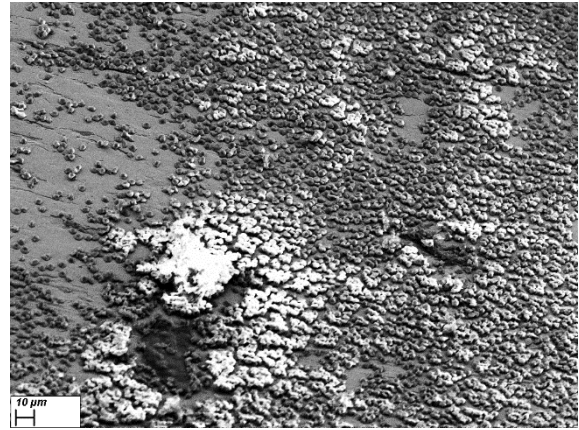
Magnification ×700



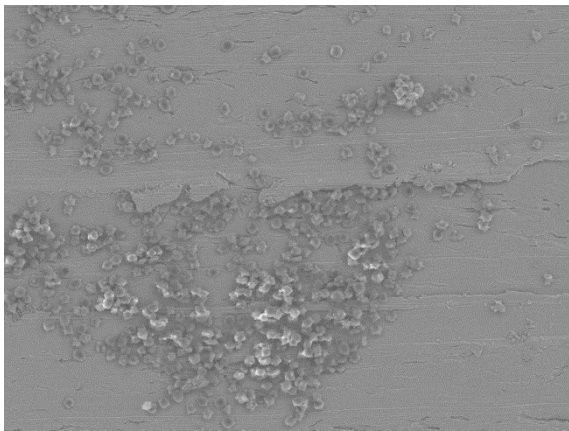
Magnification ×842



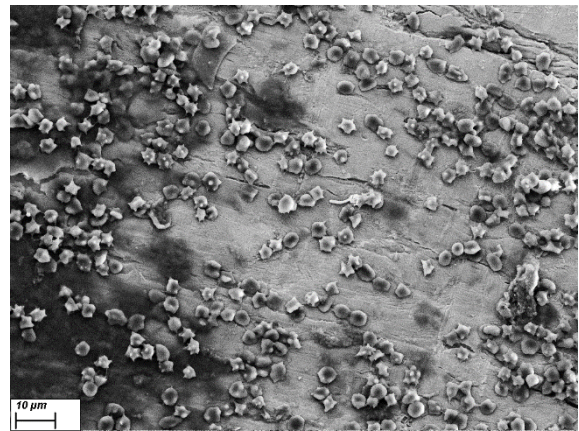
Magnification ×900



Magnification ×964

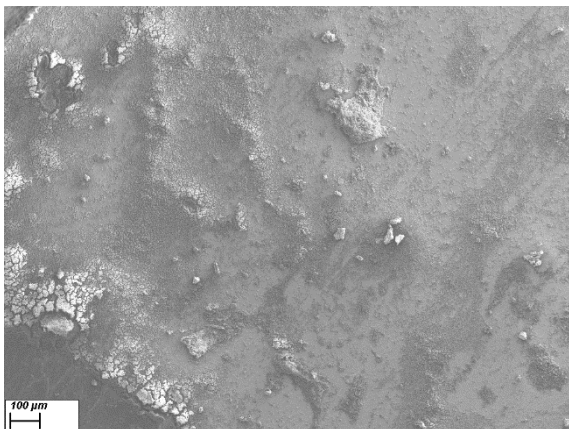


Magnification ×1.61k

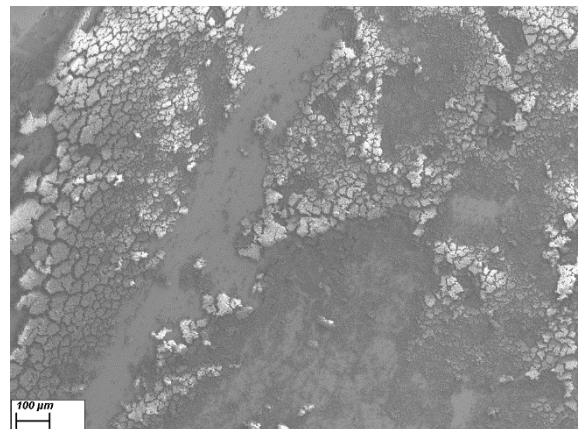


Magnification ×2k

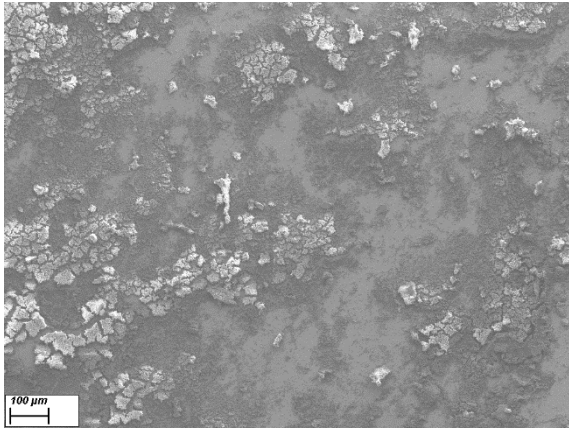
Figure D.11: Stent 6 (27mV)



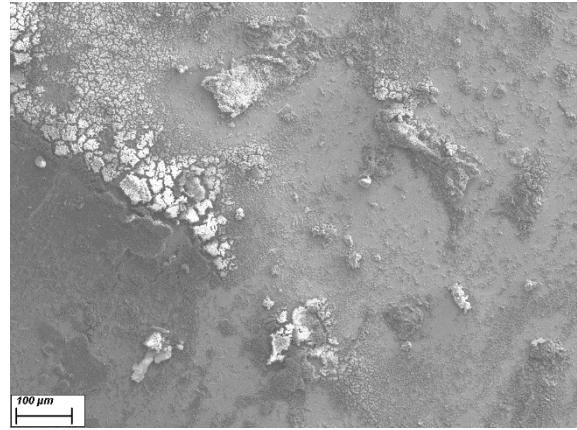
Magnification ×156



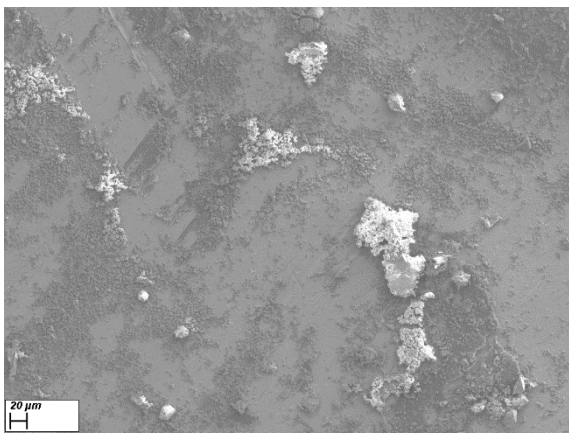
Magnification ×176



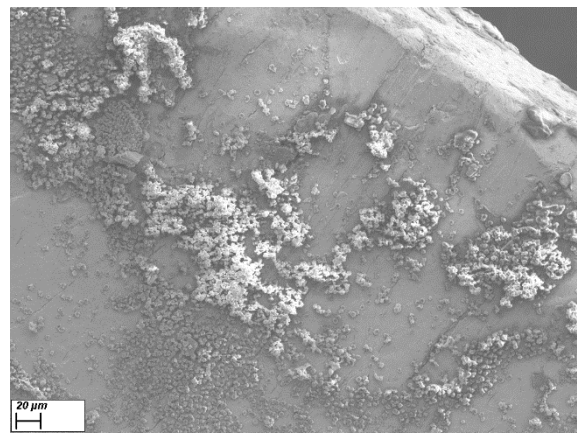
Magnification ×200



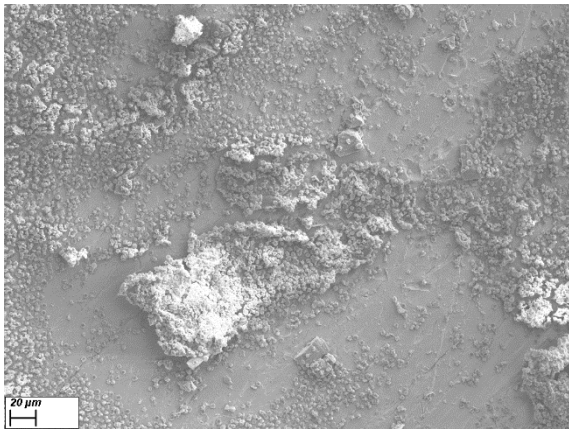
Magnification ×300



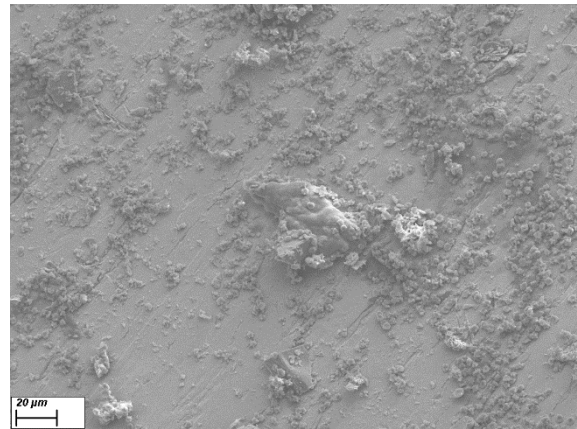
Magnification ×433



Magnification ×640

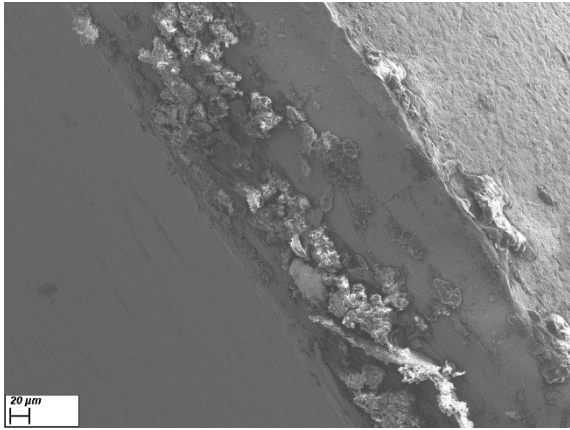


Magnification ×677

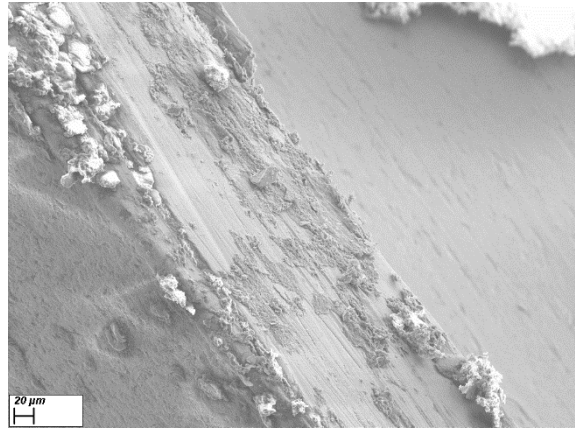


Magnification ×1k

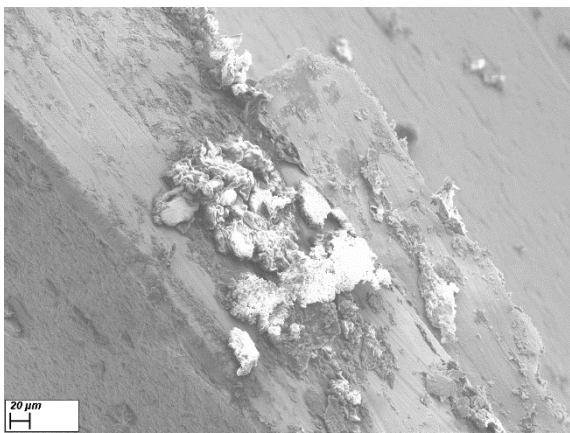
Figure D.11: Stent 7 (OV)



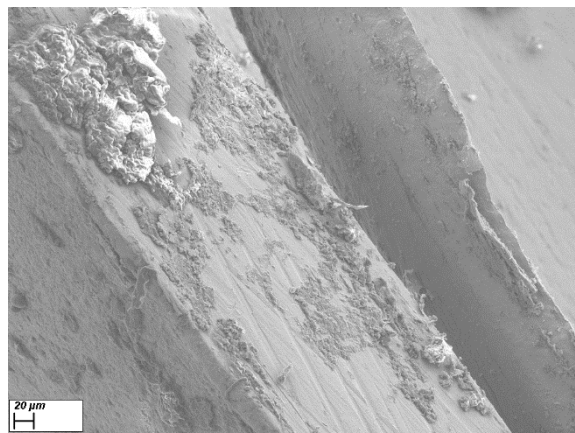
Magnification ×500



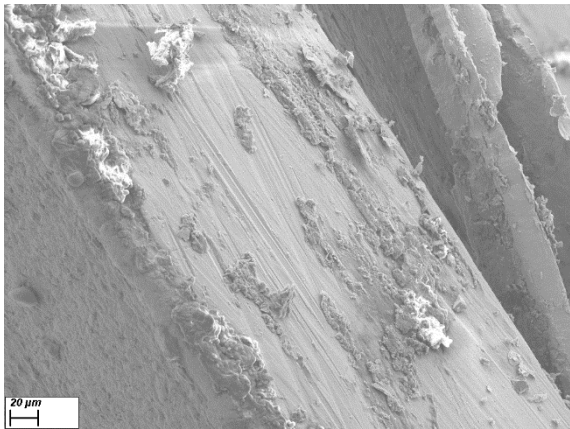
Magnification ×510



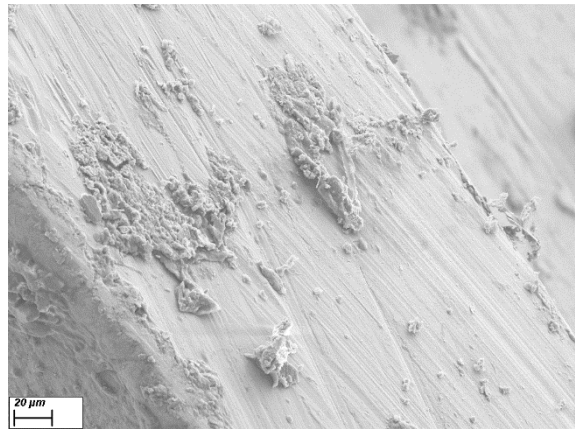
Magnification ×510



Magnification ×510



Magnification ×730



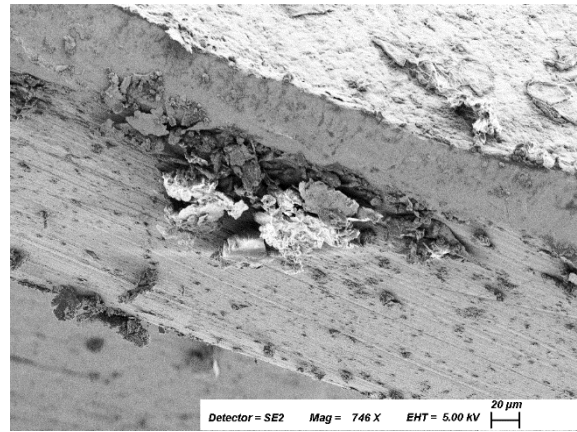
Magnification ×1k

Figure D.12: Stent 8 (27mV)

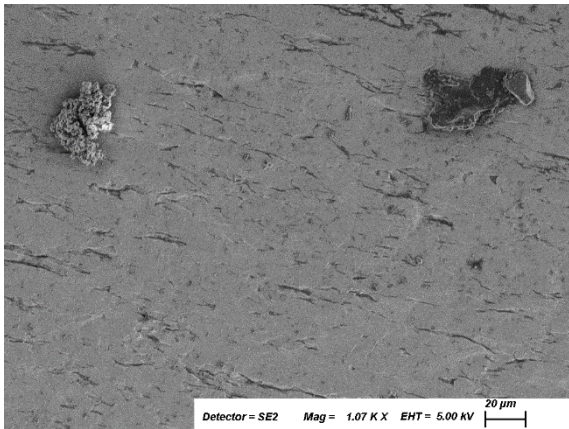
- Applied Direct Current on Bare Stent with Extra Oxygen with Old Blood



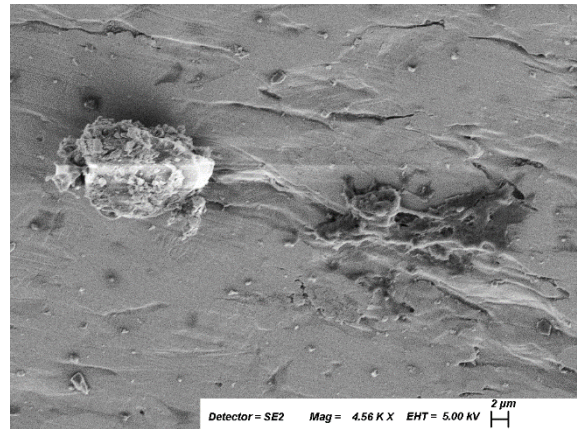
Magnification ×529



Magnification ×746



Magnification ×1k



Magnification ×4.56k

Figure D.13: Stent 1 (1V)



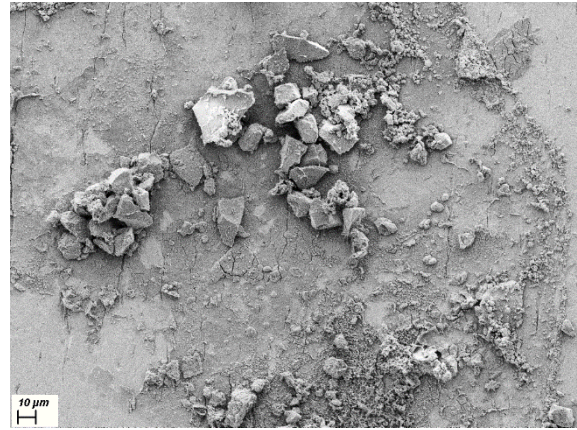
Magnification ×343



Magnification ×581



Magnification ×840



Magnification ×947



Magnification ×1.04k

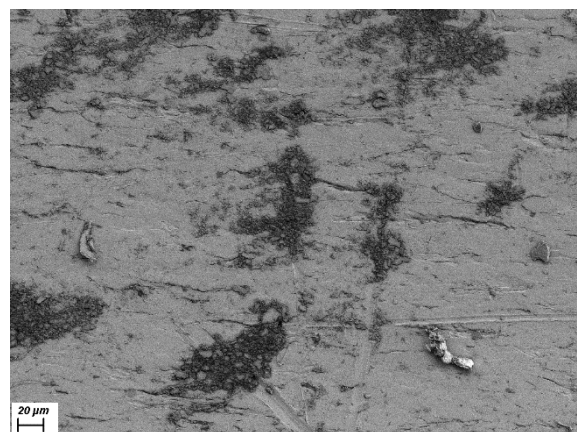


Magnification ×1.30k

Figure D.14: Stent 2 (IV)



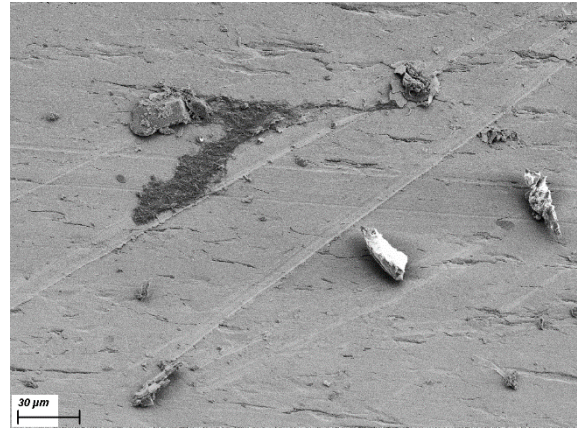
Magnification ×573



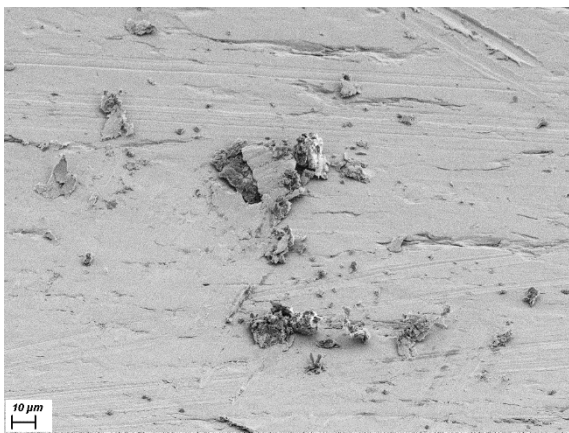
Magnification ×674



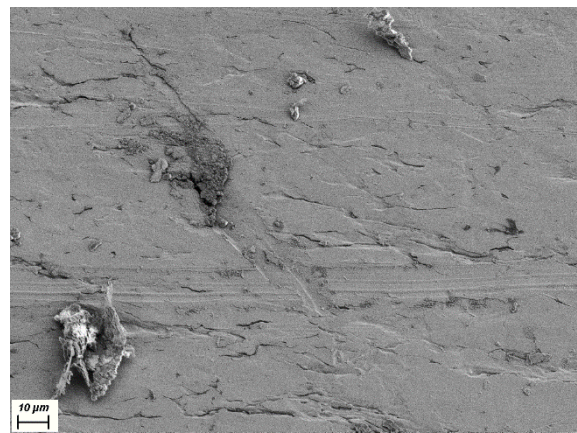
Magnification ×875



Magnification ×1.08k



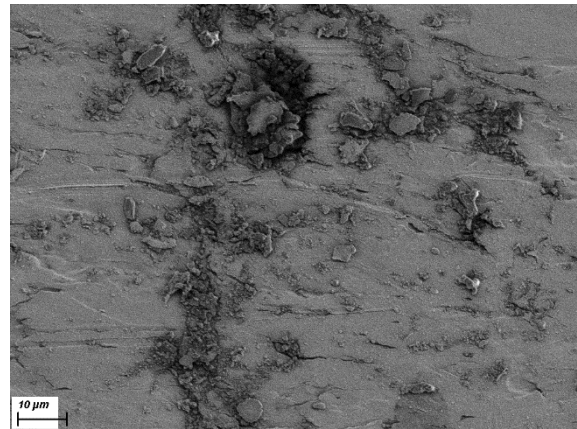
Magnification ×1.22k



Magnification ×1.60k

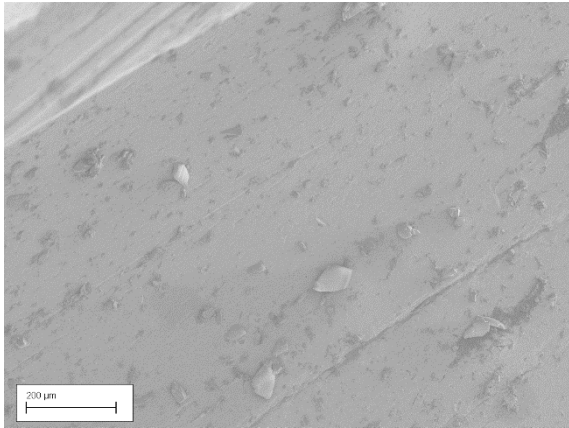


Magnification ×1.96k

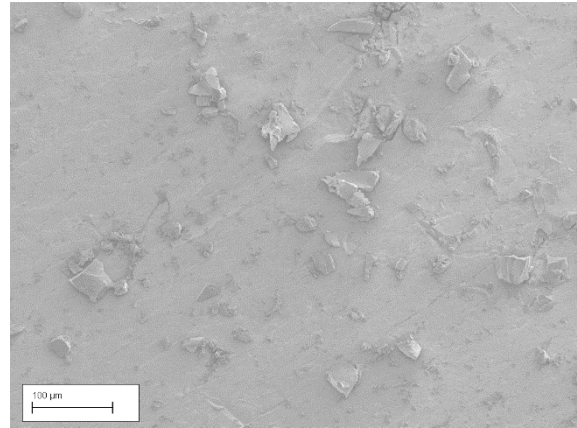


Magnification ×2.58k

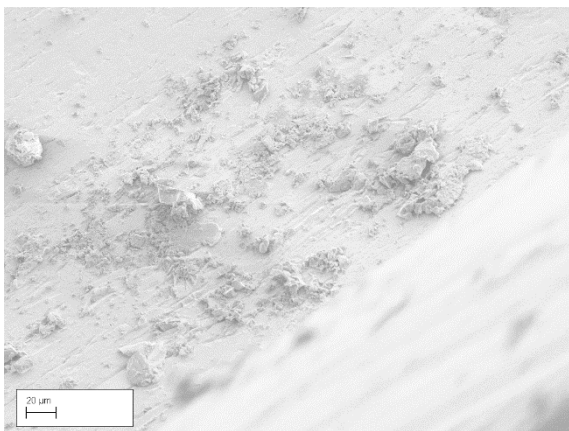
Figure D.15: Stent 3 (OV)



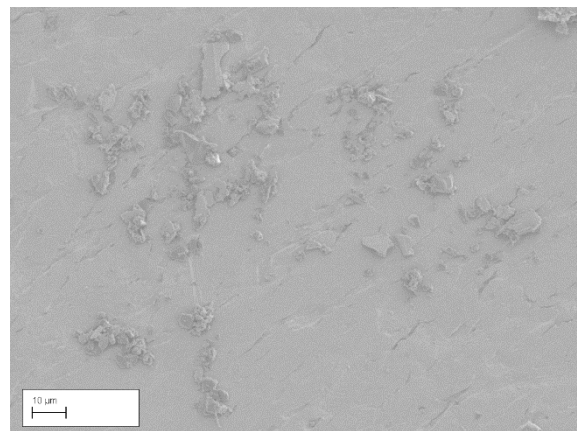
Magnification ×237



Magnification ×425

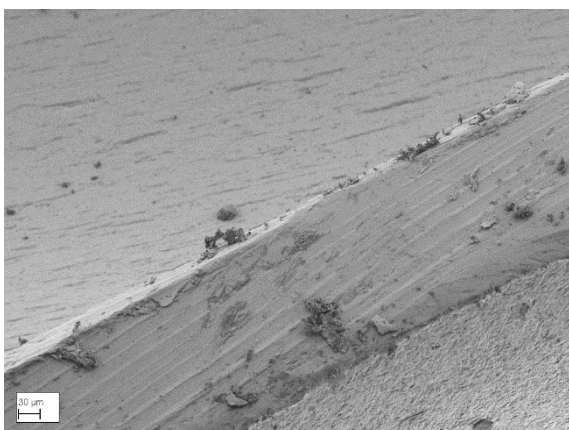


Magnification ×788

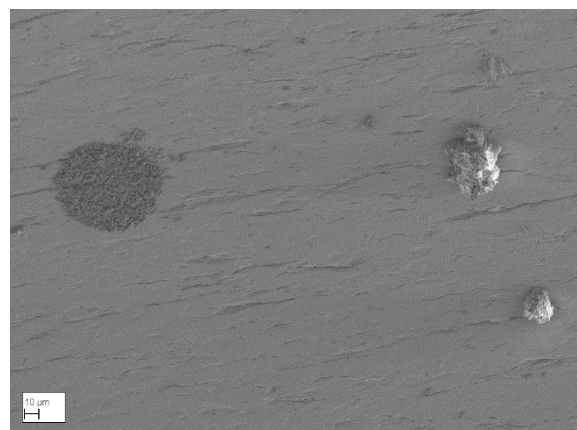


Magnification ×1.80k

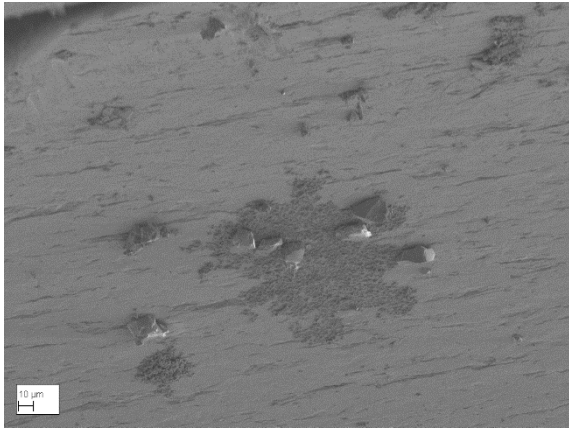
Figure D.16: Stent 4 (27mV)



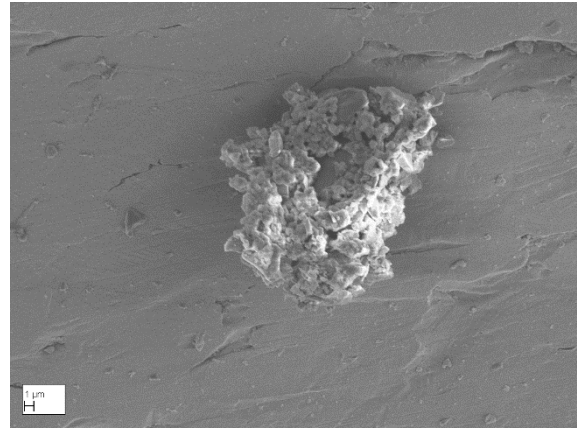
Magnification ×380



Magnification ×749

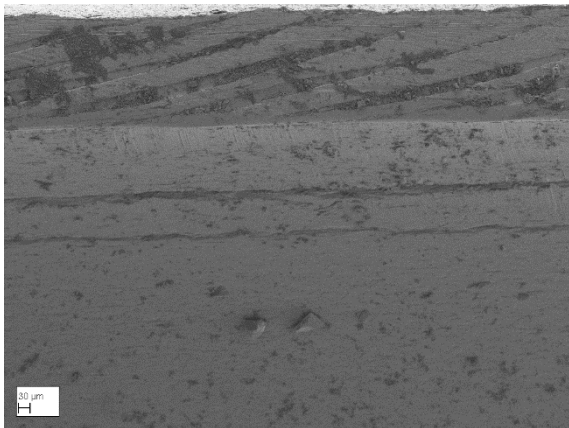


Magnification ×781

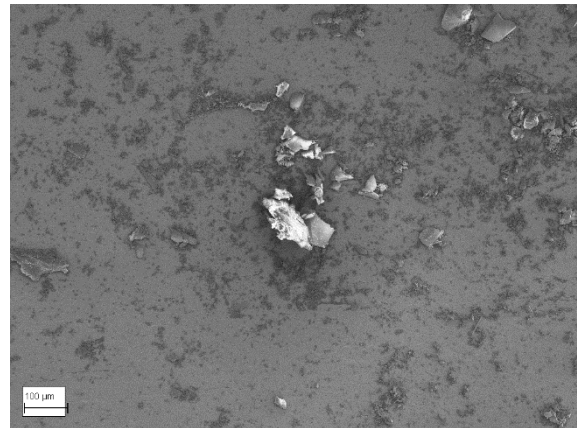


Magnification ×4.29k

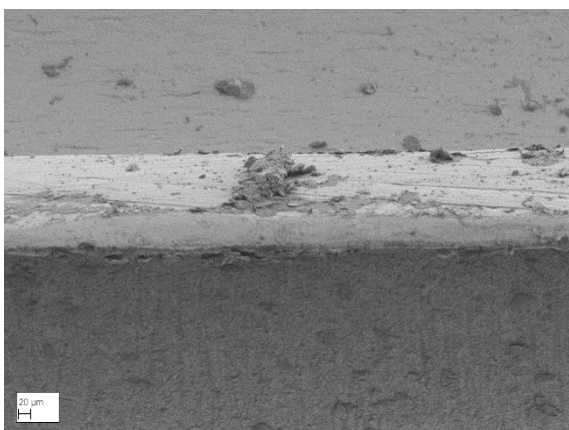
Figure D.17: Stent 5 (0V)



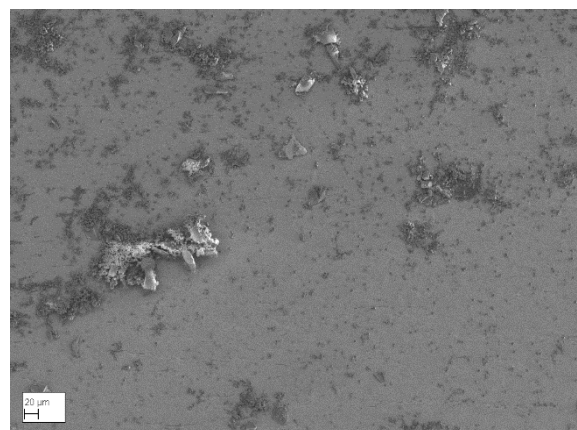
Magnification ×202



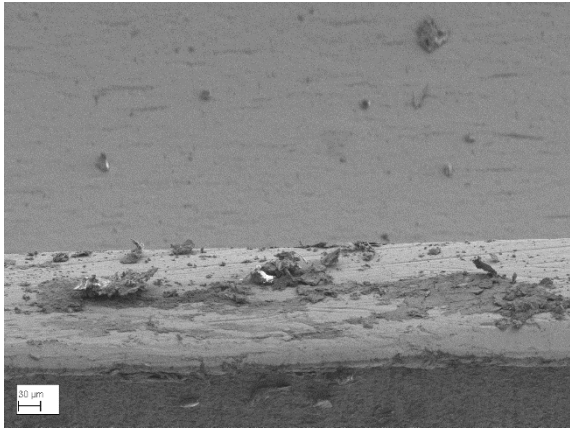
Magnification ×230



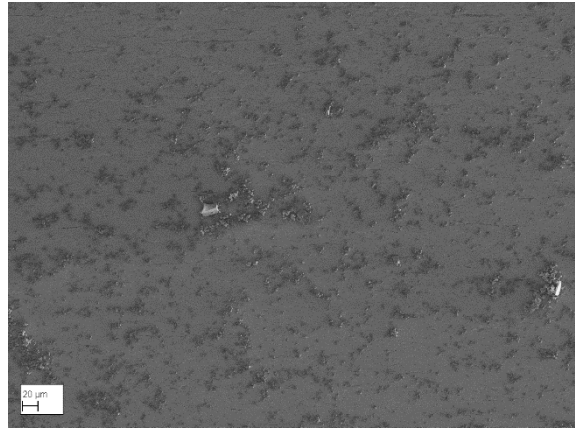
Magnification ×325



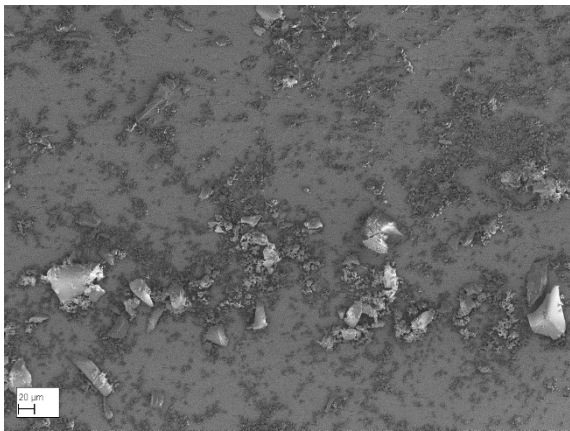
Magnification ×359



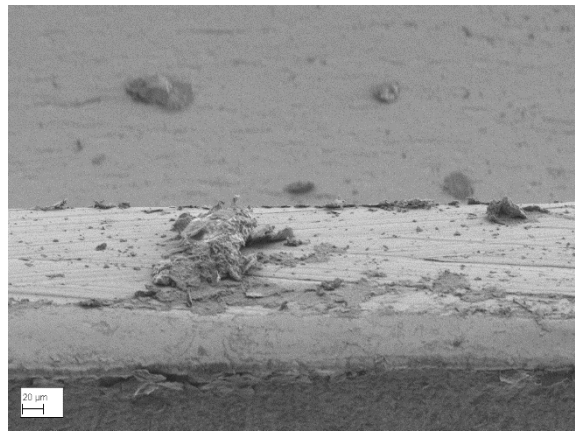
Magnification ×389



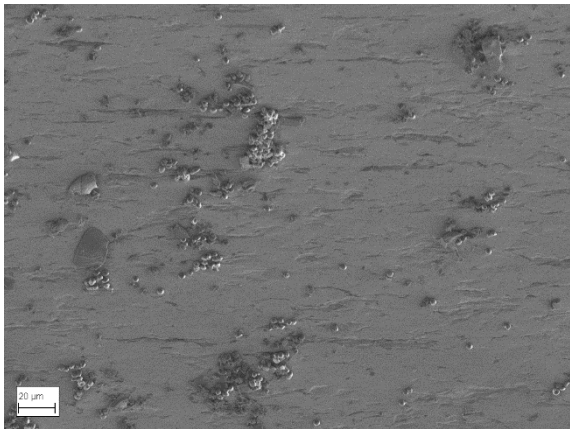
Magnification ×406



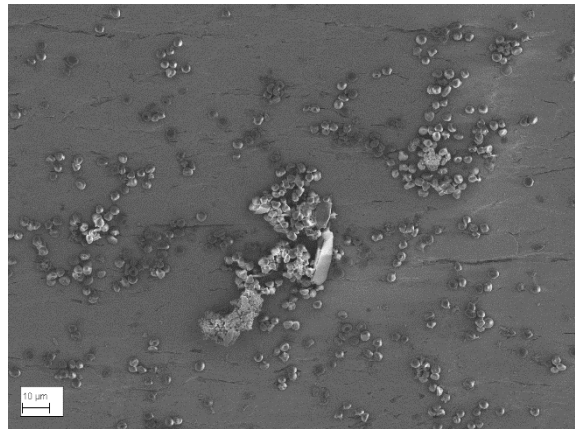
Magnification ×430



Magnification ×556



Magnification ×968

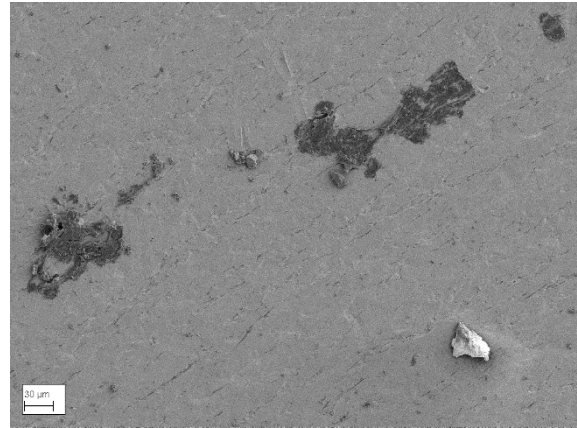


Magnification ×1.44k

Figure D.18: Stent 6 (27mV)



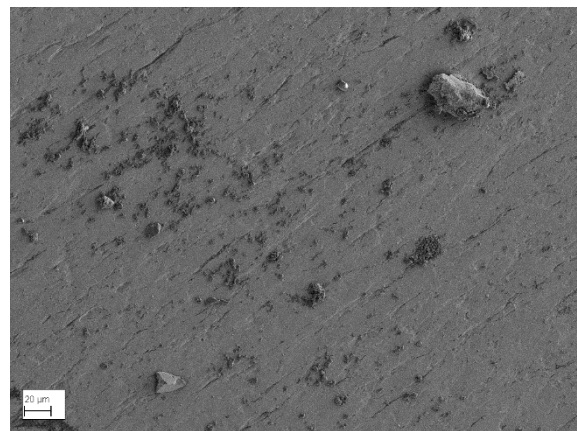
Magnification ×400



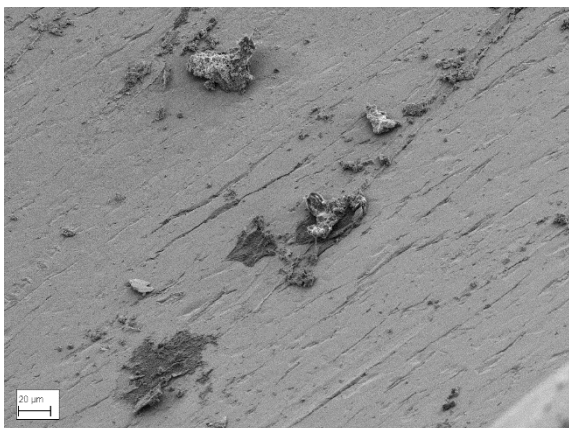
Magnification ×500



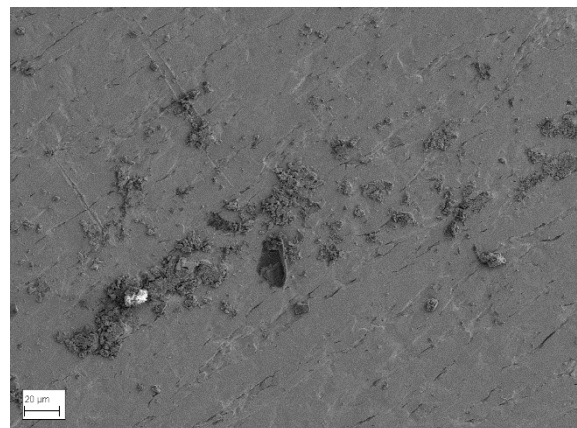
Magnification ×540



Magnification ×700



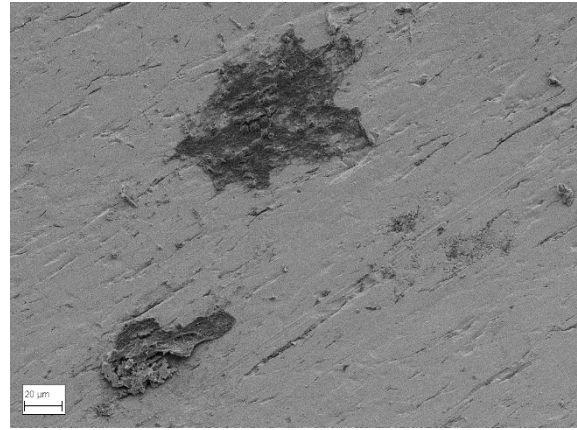
Magnification ×851



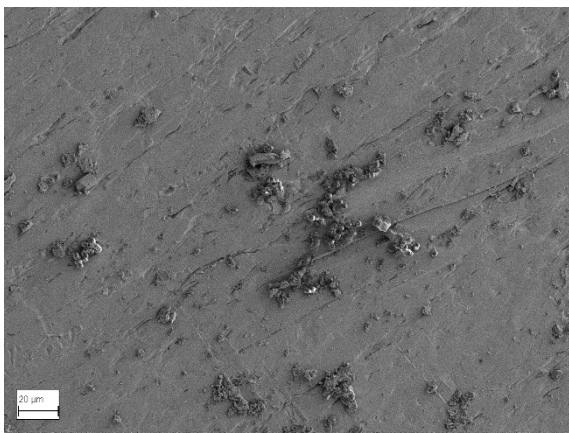
Magnification ×928



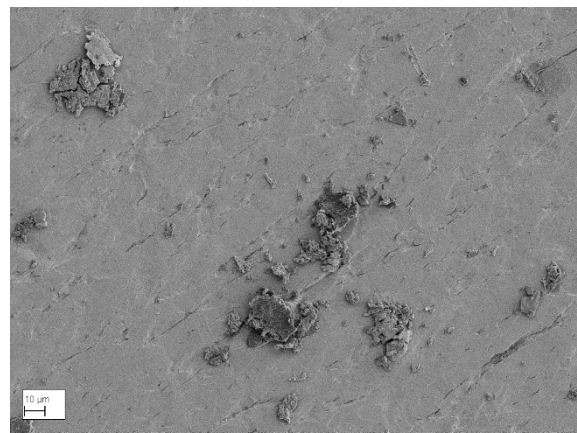
Magnification ×950



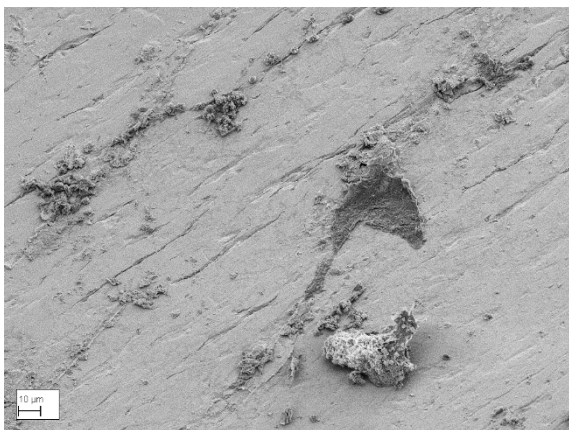
Magnification ×1k



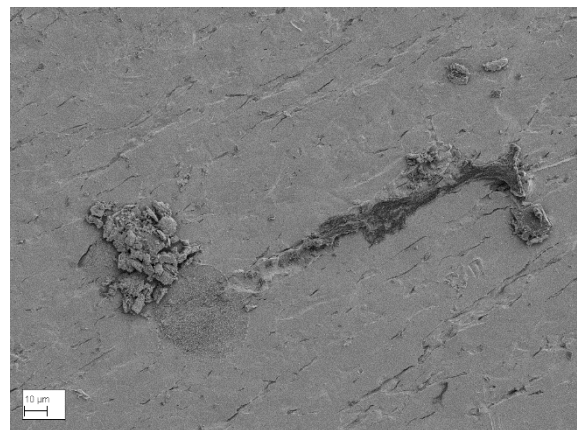
Magnification ×1k



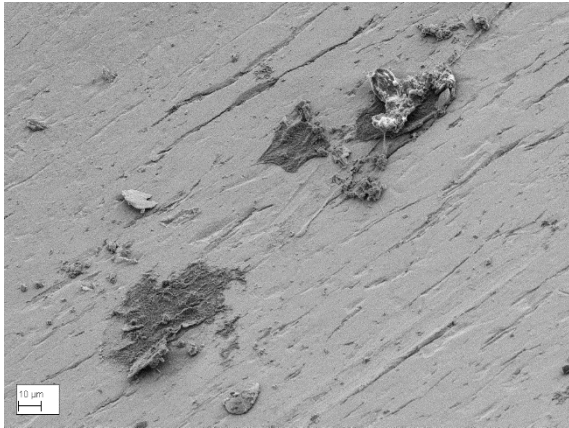
Magnification ×1.08k



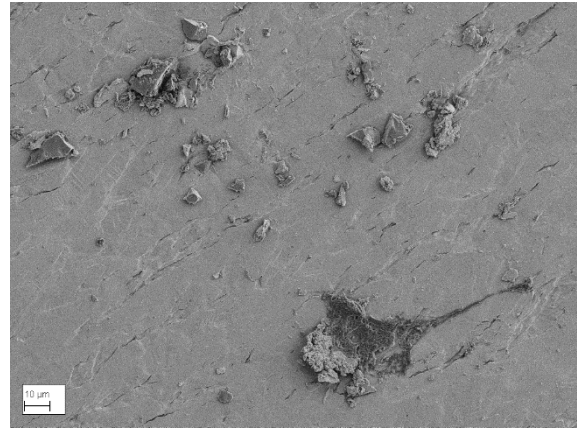
Magnification ×1.17k



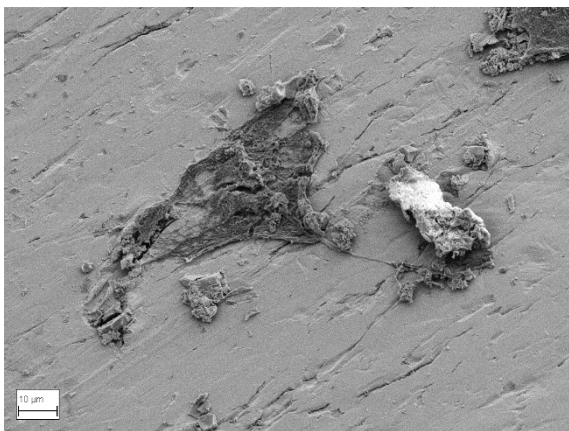
Magnification ×1.19k



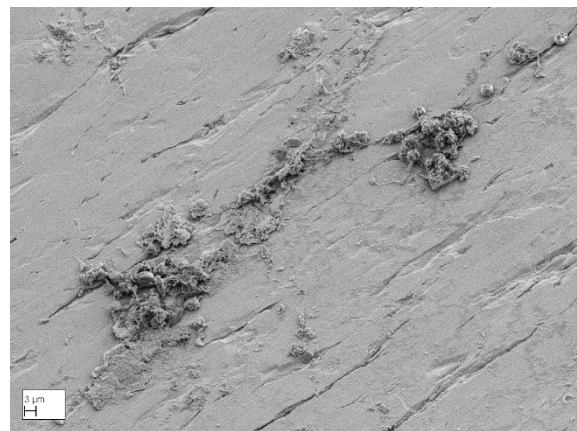
Magnification ×1.19k



Magnification ×1.35k

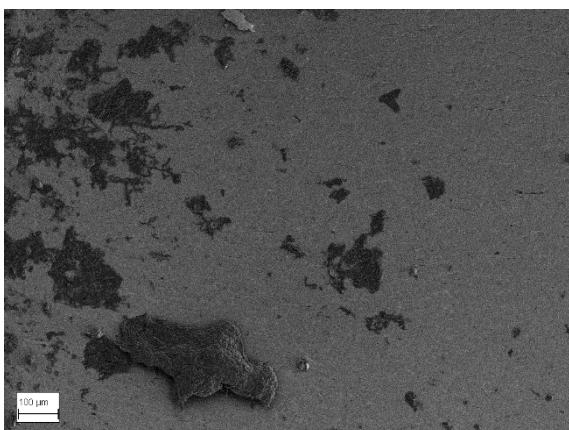


Magnification ×2.06k

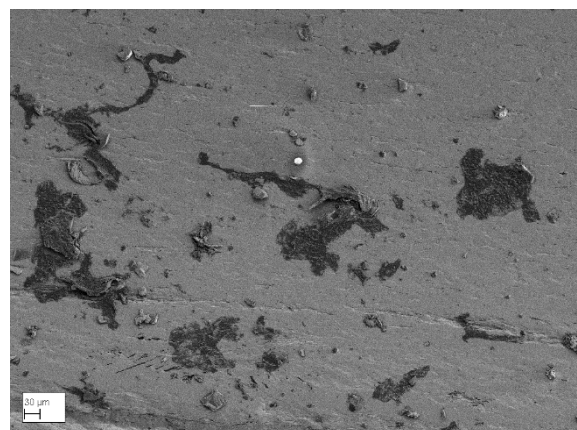


Magnification ×2.06k

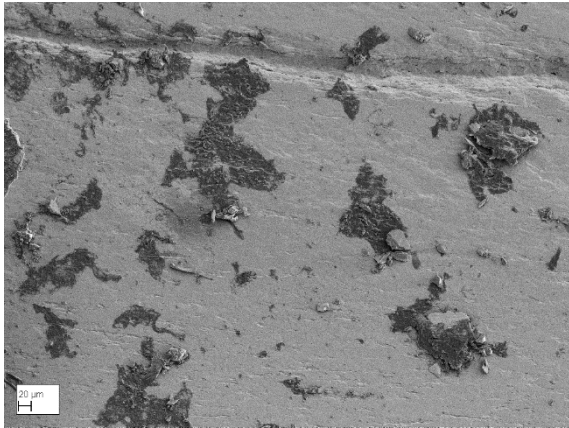
Figure D.19: Stent 7 (0V)



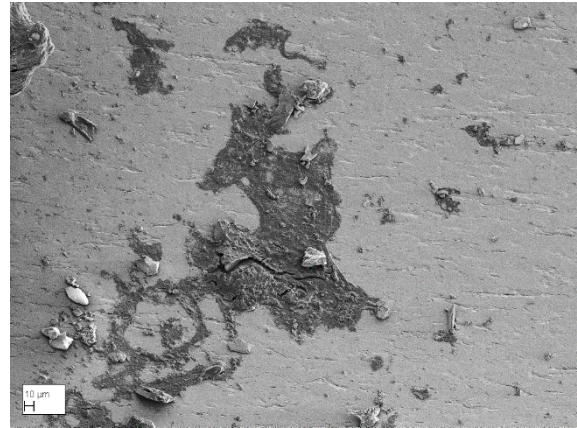
Magnification ×210



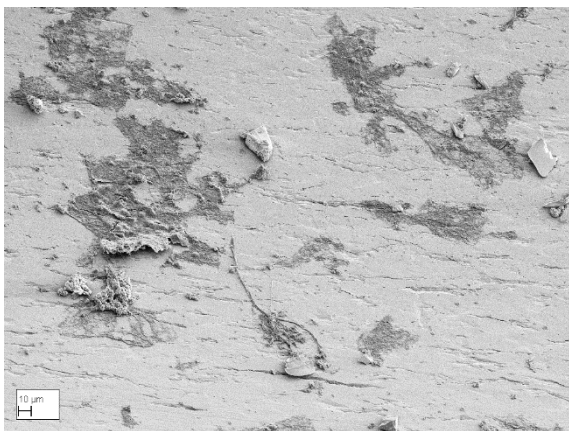
Magnification ×271



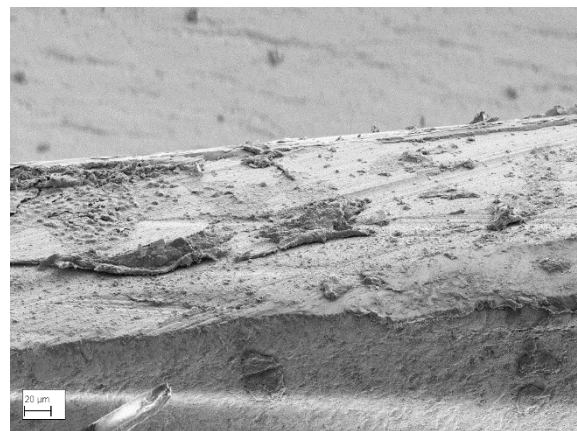
Magnification ×340



Magnification ×485



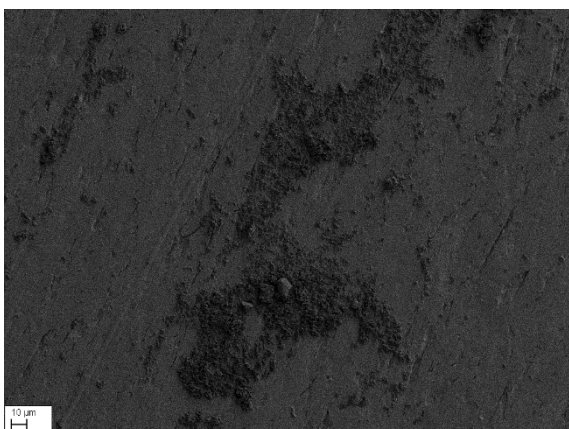
Magnification ×648



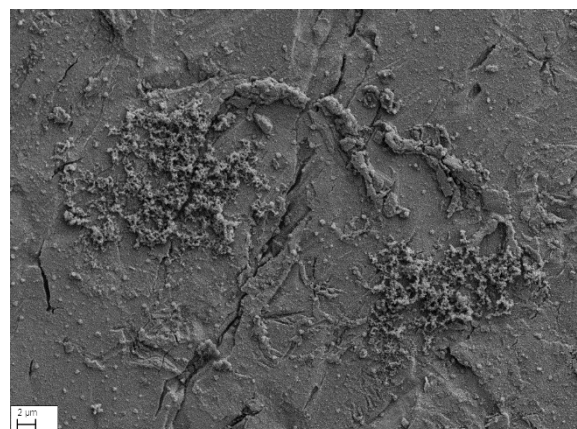
Magnification ×700

Figure D.20: Stent 8 (27mV)

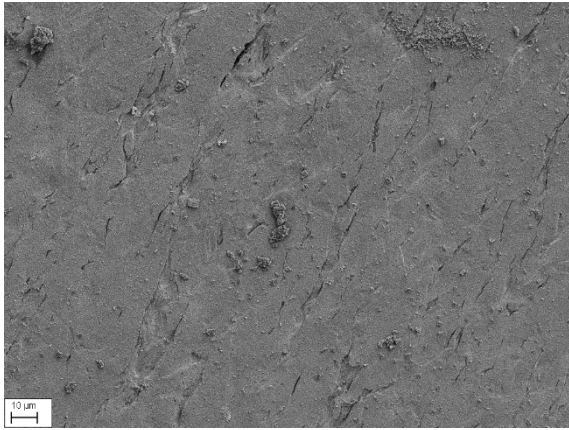
- Applied Direct Current on Bare Stent with Extra Oxygen



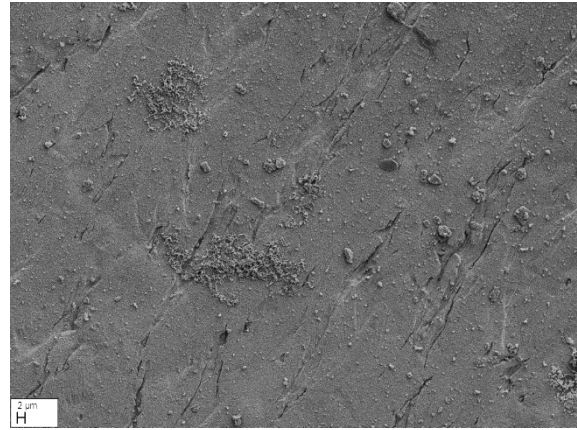
Magnification ×600



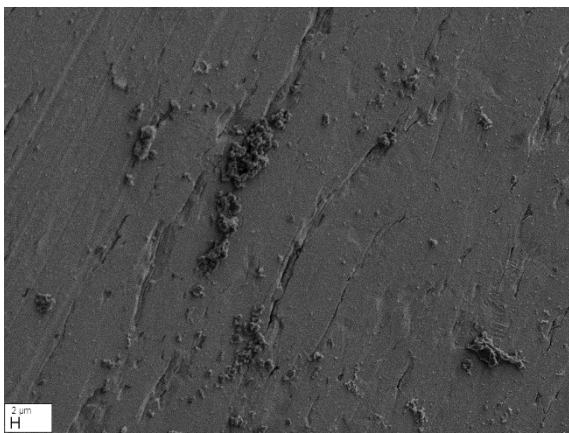
Magnification ×3.5k



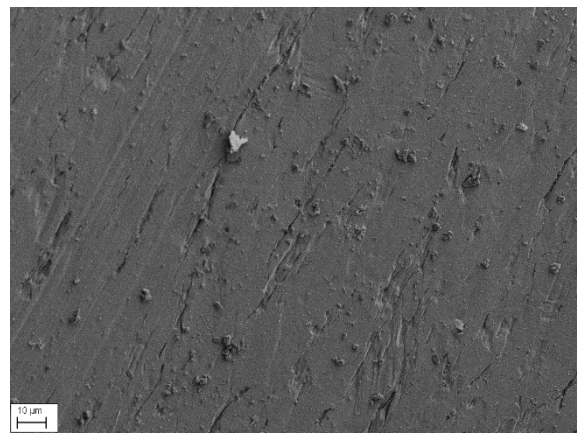
Magnification ×1k



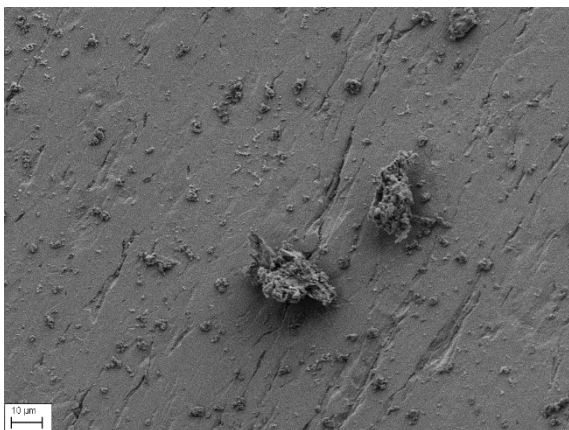
Magnification ×1.5k



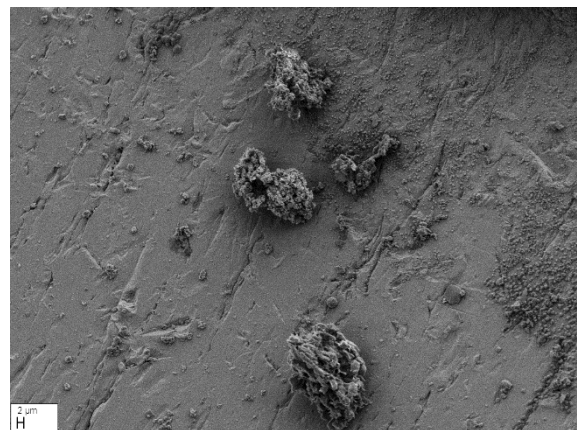
Magnification ×1.5k



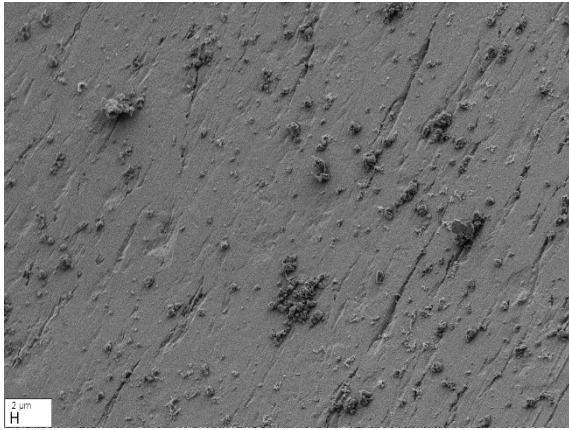
Magnification ×1.10k



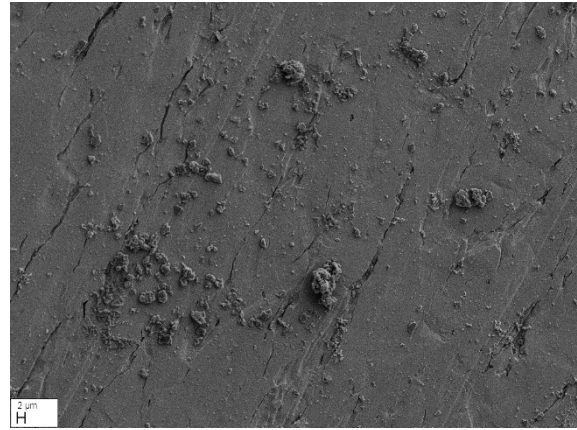
Magnification ×1.19k



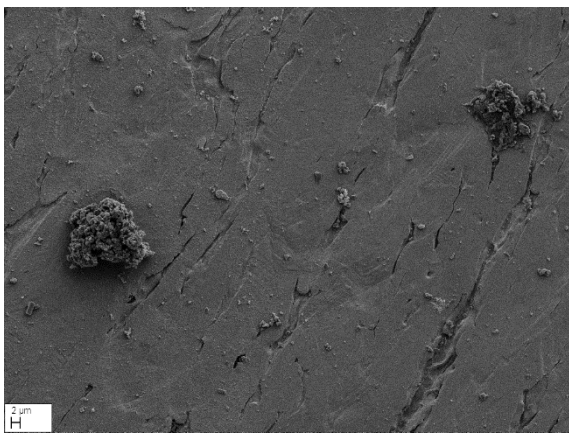
Magnification ×1.22k



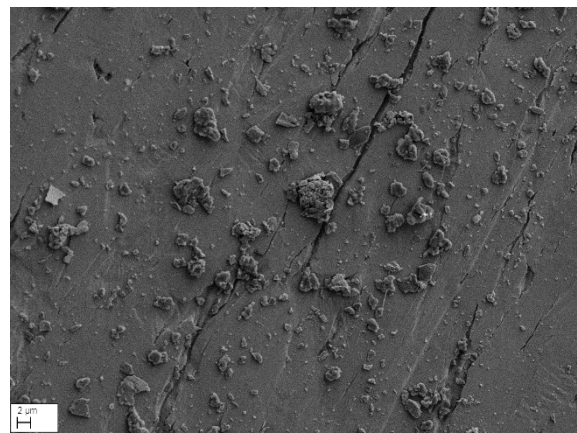
Magnification ×1.23k



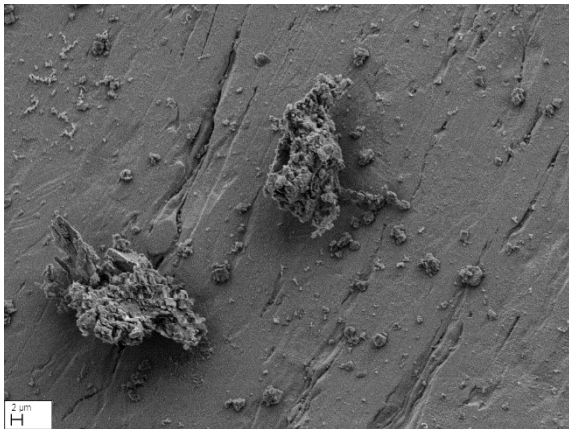
Magnification ×1.50



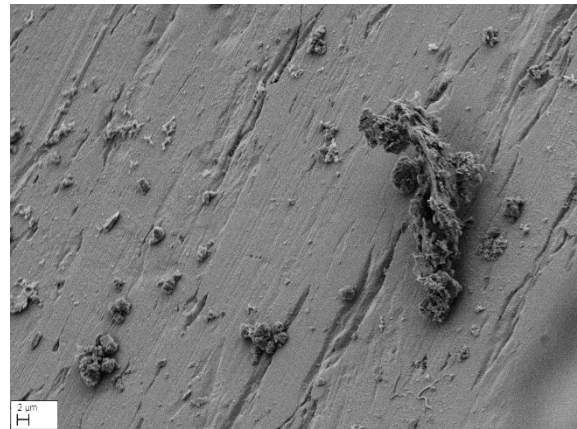
Magnification ×1.66k



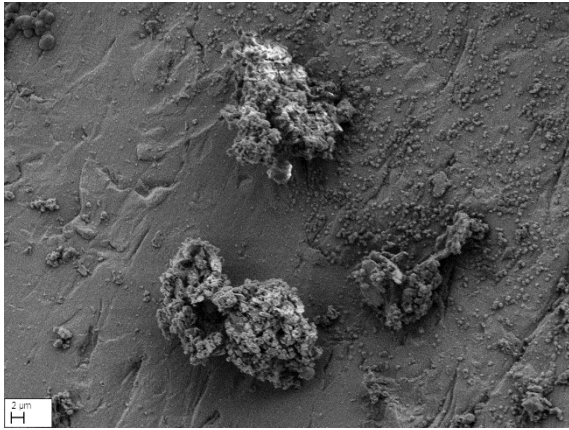
Magnification ×2.50k



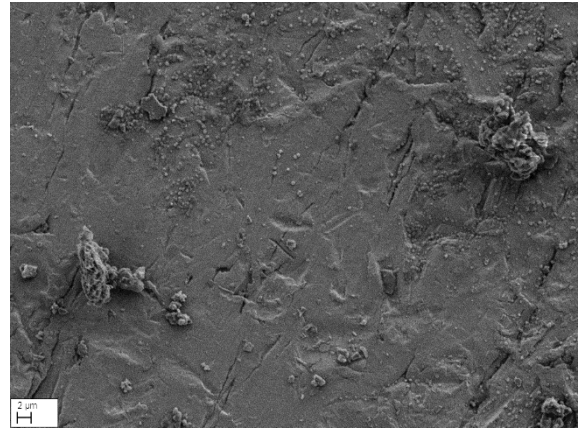
Magnification ×2.10k



Magnification ×2.25k

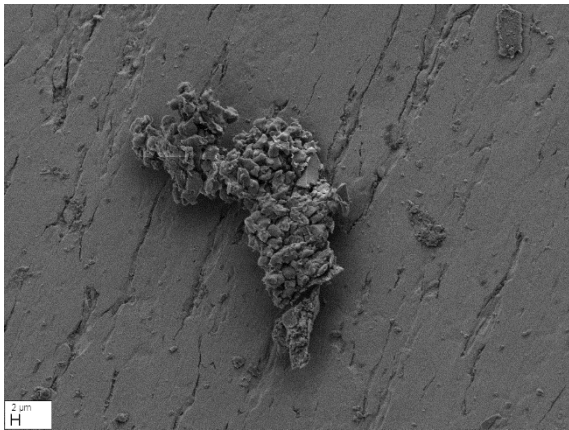


Magnification ×2.41k

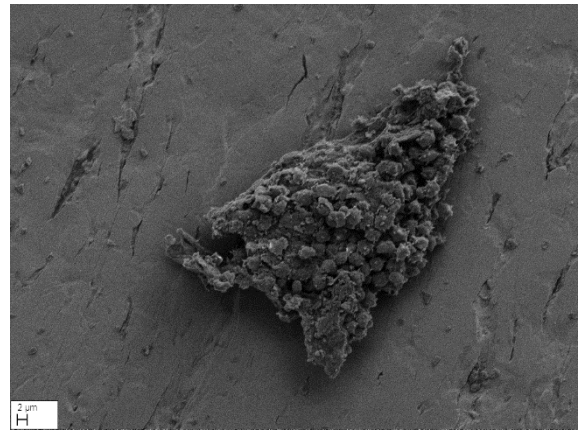


Magnification ×2.63k

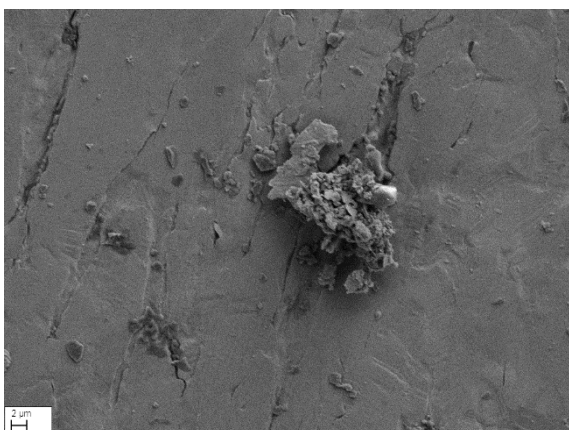
Figure D.21: Stent 1 (27mV)



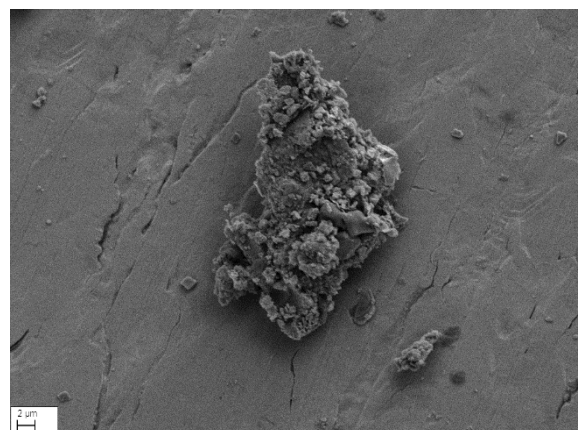
Magnification ×1.60k



Magnification ×1.90k

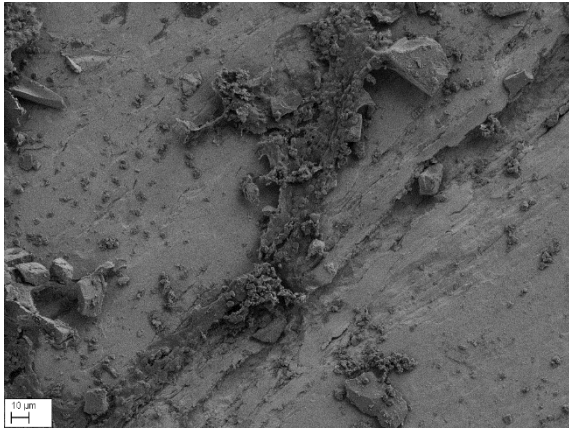


Magnification ×3k

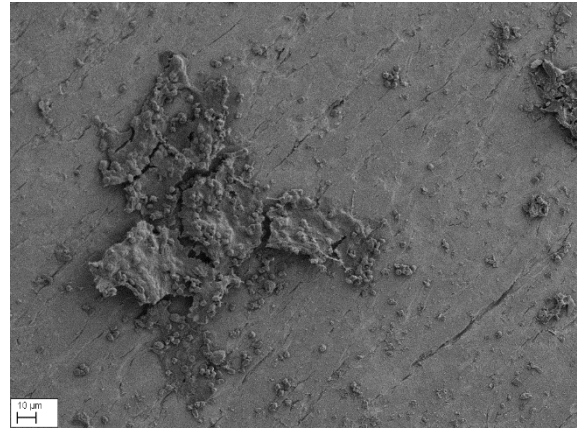


Magnification ×3.38k

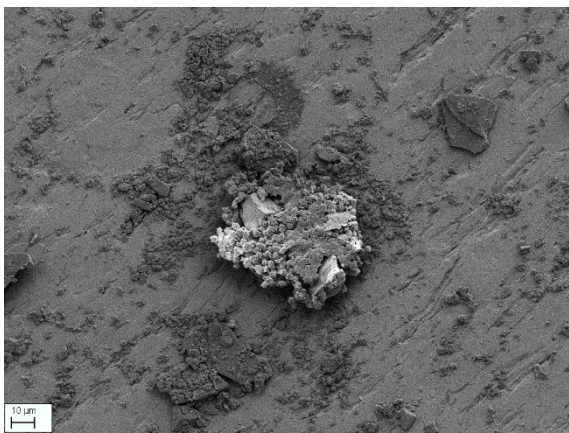
Figure D.22: Stent 2 (1V)



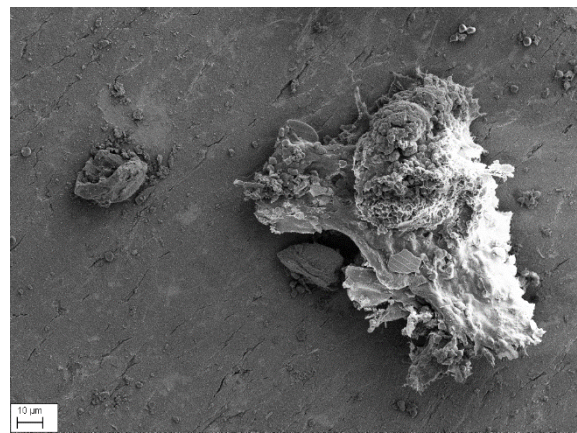
Magnification ×672



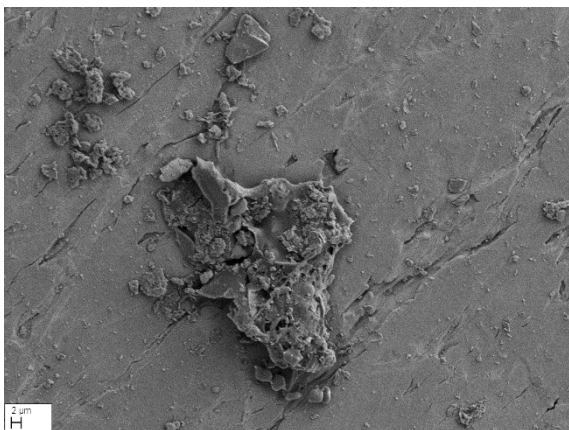
Magnification ×713



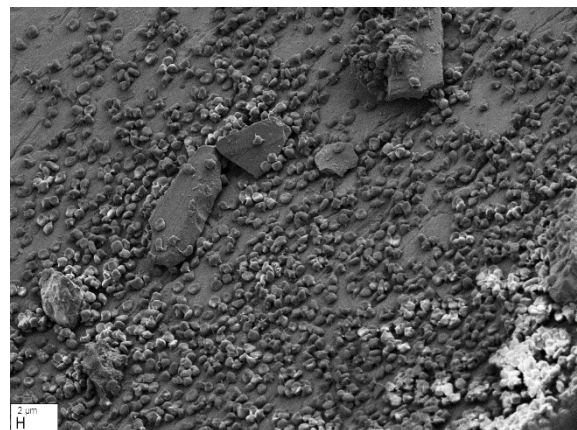
Magnification ×881



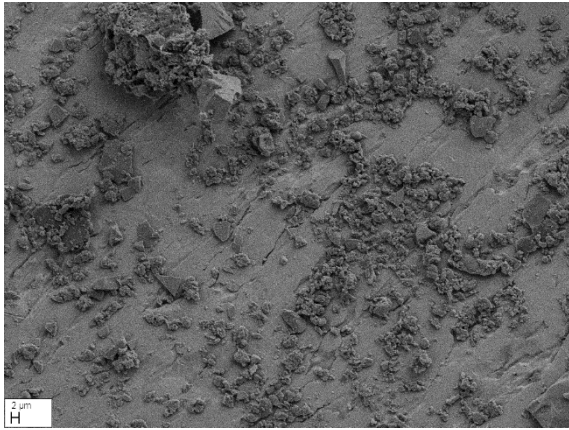
Magnification ×961



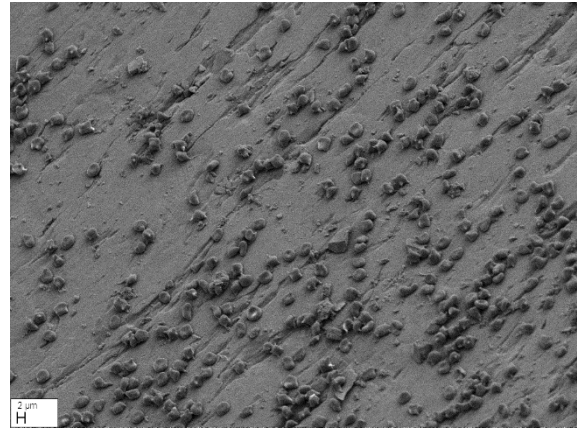
Magnification ×1.20k



Magnification ×1.24k

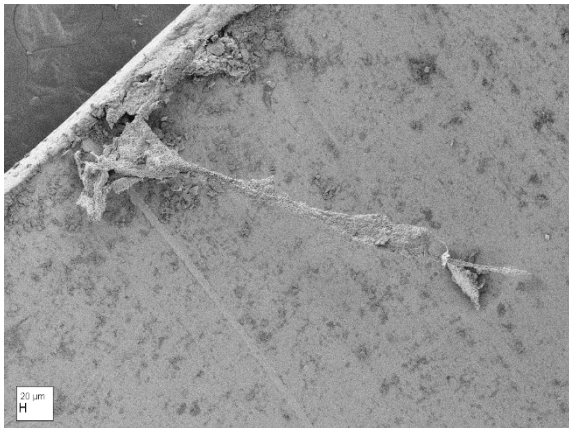


Magnification ×1.48k



Magnification ×1.5k

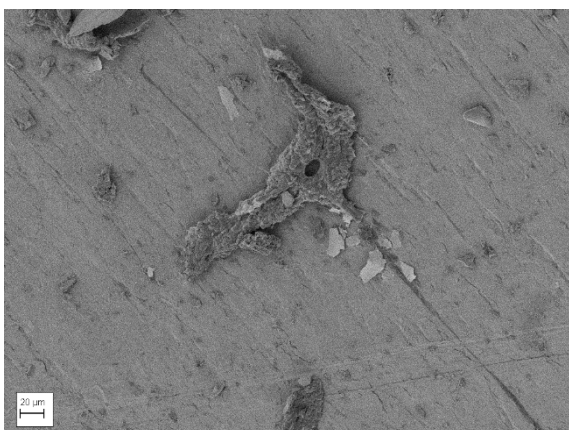
Figure D.23: Stent 3 (0V)



Magnification ×150



Magnification ×580



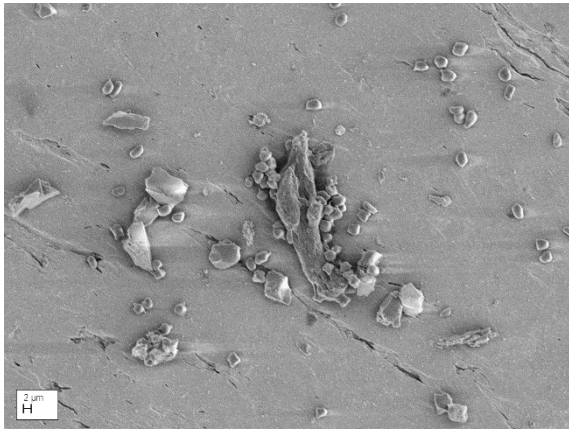
Magnification ×630



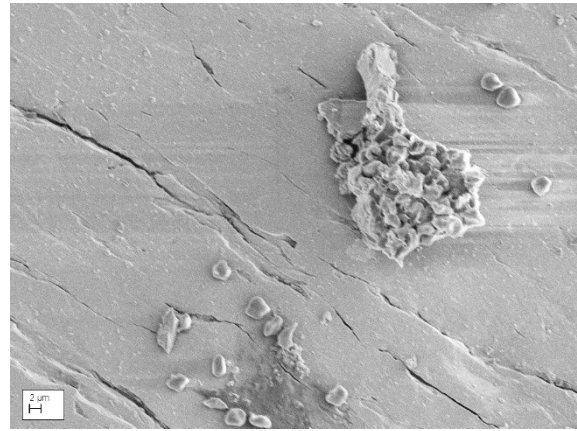
Magnification ×740

Figure D.24: Stent 4 (1V)

- Applied Pulsed Direct Current on Bare Stent

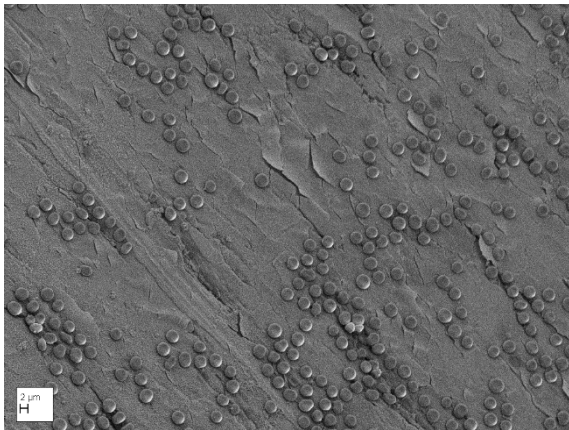


Magnification $\times 2k$



Magnification $\times 3k$

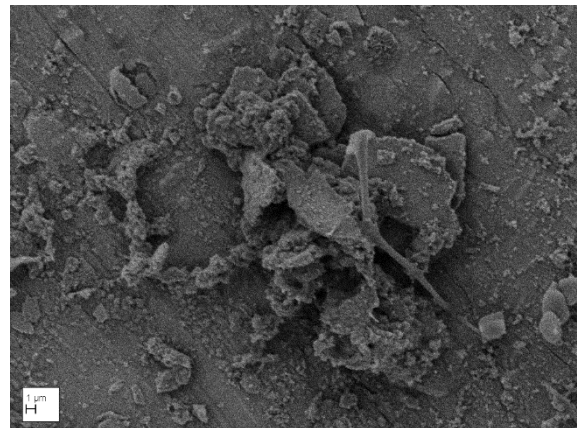
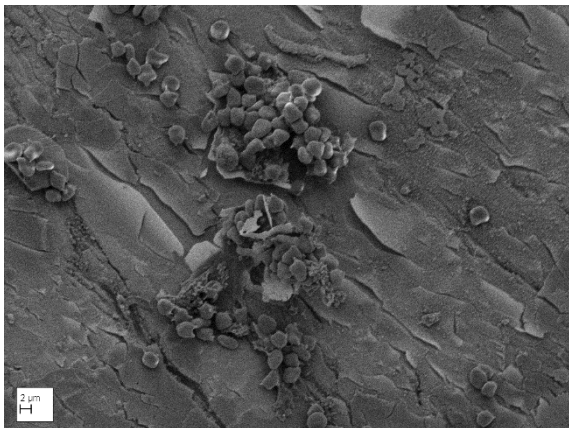
Figure D.25: Stent 1 (27mV)



Magnification $\times 2k$



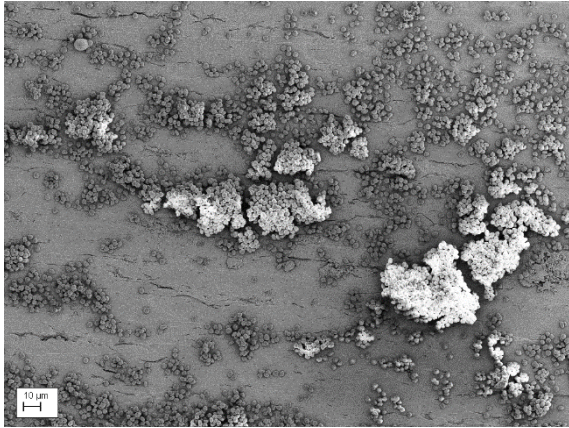
Magnification $\times 2.5k$



Magnification ×3k

Magnification ×5k

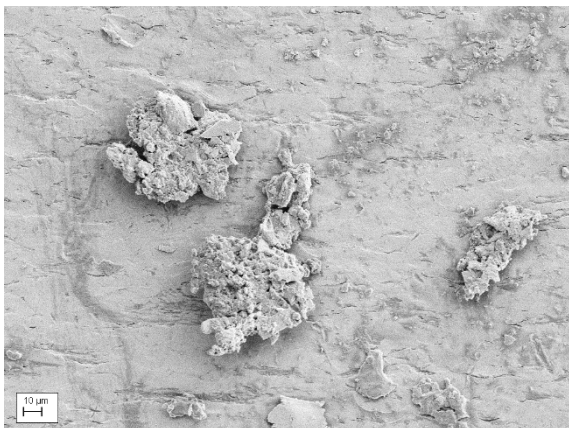
Figure D.26: Stent 2 (IV)



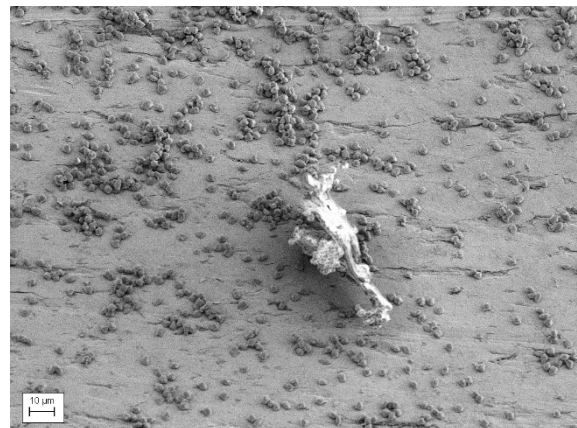
Magnification ×900



Magnification ×950



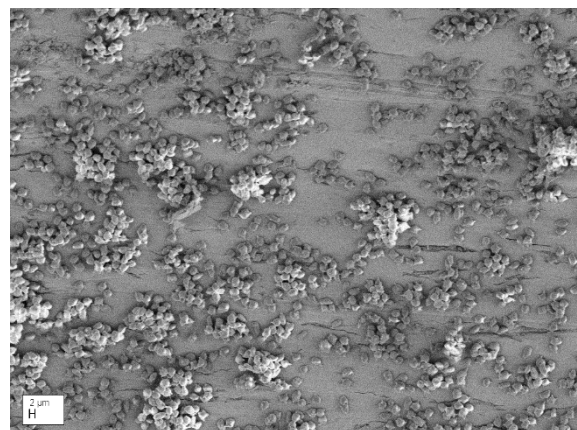
Magnification ×1k



Magnification ×1.32k



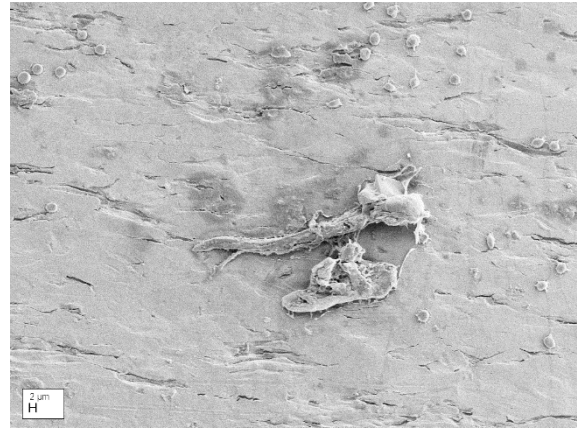
Magnification ×1.5k



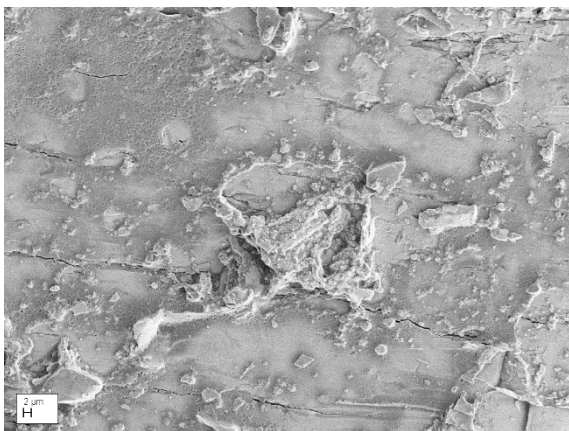
Magnification ×1.5k



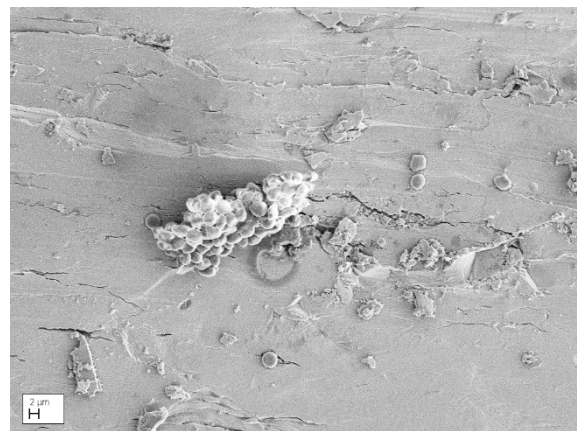
Magnification ×1.64k



Magnification ×1.70k

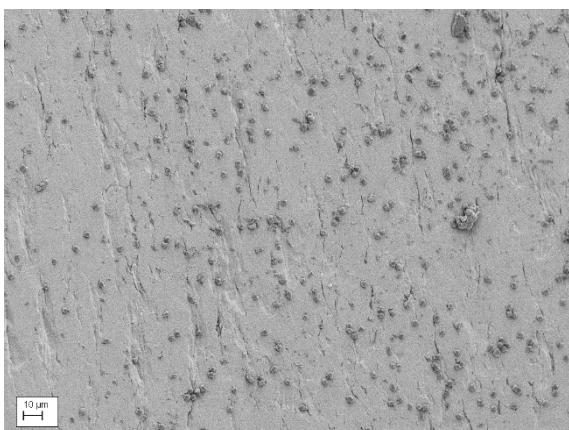


Magnification ×2k

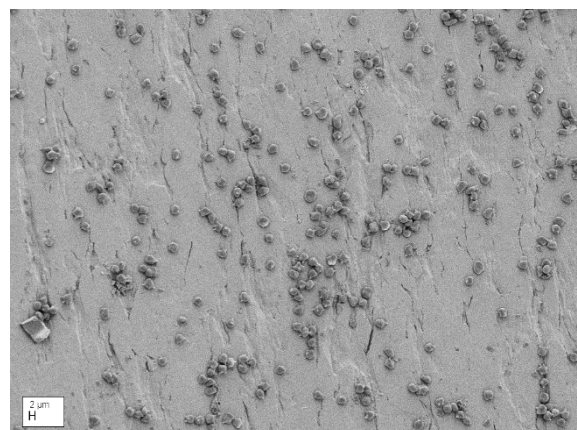


Magnification ×2.50k

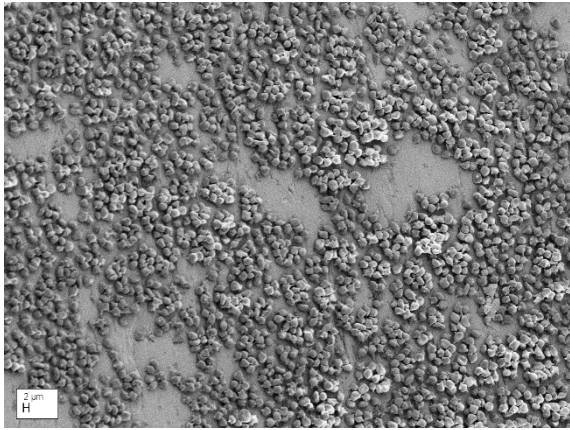
Figure D.27: Stent 3 (0V)



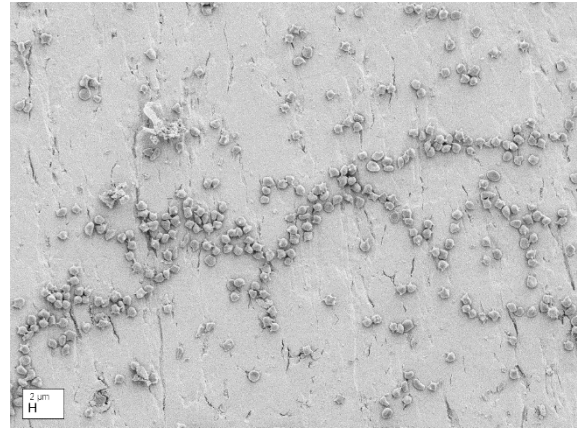
Magnification ×1k



Magnification ×1.50k

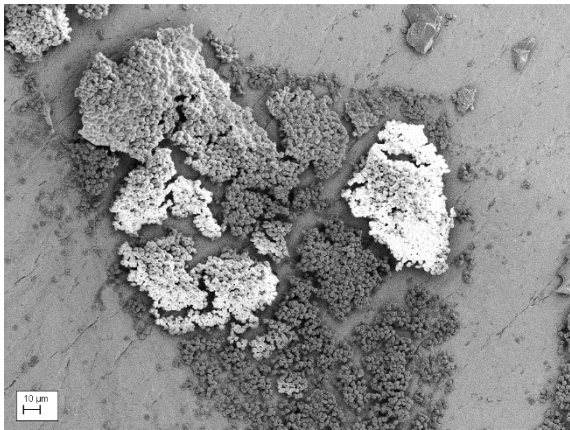


Magnification $\times 1.50k$



Magnification $\times 1.50k$

Figure D.28: Stent 4 (27mV)



Magnification $\times 886$



Magnification $\times 1k$

Figure D.29: Stent 5 (1V)

Appendix E: Publication

Electric Stents: A Novel Approach for Endothelisation of Small Vessel Stents.

N. Faridamin¹, A. Anson², M. Hughes³, A.J. Reynolds²

1. Brunel University London, College of Engineering Design and Physical Science, Kingston Lane Uxbridge, UB8 3PH. UK
2. Brunel University London, The Experimental Techniques Centre, Kingston Lane Uxbridge, UB8 3PH. UK
3. University of Surrey, Centre for Biomedical Engineering, Guildford, Surrey GU2 7HX

Abstract

Small vessel stents have become a common treatment for coronary artery occlusive disease. The treatment consists of dilating the stent using an angioplasty balloon at the vascular site, where a blockage or restriction has occurred and the aim is to reinstates arterial patency

A deficit of blood to the heart muscles, can present as angina, leading to a potential myocardial infarct with associated morbidities. Deployment of the stent inside the affected coronary artery facilitates dilation and physical support the diseased vessel lumen allowing normal blood flow to resume. However, as the stent is a foreign object, consisting of synthetic materials and the rigours of its physical placement and changes in local blood flow conditions, it can elicit immune system reactions, which in turn may lead to thrombus, neointimal hyperplasia and/or vascular spasm, which may then result in re-blockage of the vessel, referred to as in-stent restenosis.

The objective of this current research is to explore the potential of re-endothelisation of small vessel stents to reduce potential restenosis, by the application of an electrical field directly onto the stent to invoke specific cell migration (vascular endothelial cells) towards and onto the stents surfaces. This can be facilitated by exploiting the potential difference seen across the cells lipid membrane, with particular reference to the polar nature of this electrical field. Depending upon the cell activity, the external surface of the lipid membrane is predominantly

negative; if the stent is positively charged, an attraction and subsequent adherence of the negatively-going cells onto the positively charged stent can occur.

To demonstrate and understand the electrically induced cell migration phenomena, a bio-mimic system consisting of a number stented coronary arteries was constructed. The experimental stents had electrical connection, plus no electrical connections (control): ovine blood was circulated through the mimic arteries and stents, under standardised physiological conditions, approximating pressure, temperature and pulsatility. Stent surfaces were then examined using electron microscopy to determine cell numbers and adherency. In addition, further instrumentation was developed, to confirm polarisation status and lipid membrane voltage profile of human coronary artery vascular endothelial cells, using electrophoretic techniques.

Other Publications

1. Oral presentation at 11th International Congress on Coronary Artery Disease, Florence, Italy
2. Poster presentation at Brunel Three Minute Thesis, Brunel University London, UK
3. Poster presentation at Medical Engineering Centres Annual Meetings and Bioengineering 14, Imperial College London, UK
4. Poster presentation at Brunel Graduate School, Brunel University London, UK